Report No. FAA-RD-75-127

MEASUREMENT OF THE TRAILING VORTEX SYSTEMS OF LARGE TRANSPORT AIRCRAFT, USING TOWER FLY-BY AND FLOW VISUALIZATION (SUMMARY, COMPARISON AND APPLICATION)

Leo J. Garodz
David M. Lawrence
Nelson J. Miller

JANUARY 1976

FINAL REPORT

Prepared for

U. S. DEPARTMENT OF TRANSPORTATION
FEDERAL AVIATION ADMINISTRATION
Systems Research & Development Service
Washington, D. C. 20590

NOTICE

This document is disseminated under the sponsorship of the Department of Transportation in the interest of information exchange. The United States Government assumes no liability for its contents or use thereof.

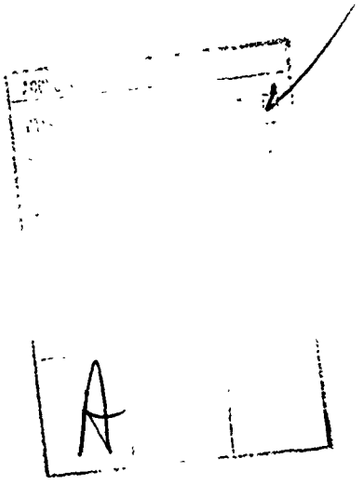

Technical Report Documentation Page

1. Report No.	2. Government Accession No.	3. Recipient's Catalog No.
FAA-RD-75-127		

4. Title and Subtitle	5. Report Date
MEASUREMENT OF THE TRAILING VORTEX SYSTEMS OF LARGE TRANSPORT AIRCRAFT, USING TOWER FLY-BY AND FLOW VISUALIZATION (SUMMARY, COMPARISON AND APPLICATION)	January 1976
	6. Performing Organization Code
7. Author(s) Leo J. Garodz, David M. Lawrence and Nelson J. Miller	8. Performing Organization Report No. FAA-NA-75-3
9. Performing Organization Name and Address Federal Aviation Administration National Aviation Facilities Experimental Center Atlantic City, New Jersey 08405	10. Work Unit No. (TRAIS)
	11. Contract or Grant No. 214-531-070
12. Sponsoring Agency Name and Address U.S. Department of Transportation Federal Aviation Administration Systems Research and Development Service Washington, D.C. 20590	13. Type of Report and Period Covered Final Rept. April 1971—November 1973
	14. Sponsoring Agency Code

15. Supplementary Notes

16. Abstract

Full-scale flight test investigations have been made of the characteristics, persistence and movement of the trailing vortices generated by propeller and jet transport aircraft. The tests were performed by the National Aviation Facilities Experimental Center (NAFEC), Atlantic City, New Jersey, during the period 1970-1973, using tower fly-by and vortex flow visualization. The results are summarized and comparisons made of the vortices of the Douglas DC10, DC9, and DC7; Boeing 747, 727, and 707; Lockheed C5A, C141, and L1011; and the Convair 880 aircraft. Vortex mathematical models and decay mechanisms are discussed and their effects (upset potential) on encountering aircraft are investigated for possible air traffic control application.

17. Key Words	18. Distribution Statement
Wake Turbulence Trailing Vortices Hot-Film Anemometry Full-Scale Flight Tests	Document is available to the public through the National Technical Information Service, Springfield, Virginia 22151

19. Security Classif. (of this report)	20. Security Classif. (of this page)	21. No. of Pages	22. Price
Unclassified	Unclassified	160	

Form DOT F 1700.7 (8-72) Reproduction of completed page authorized

240 550

TABLE OF CONTENTS

TABLE OF CONTENTS (continued)

Page

APPENDICES

LIST OF ILLUSTRATIONS

LIST OF ILLUSTRATIONS (continued)

LIST OF ILLUSTRATIONS (continued)

LIST OF TABLES

LIST OF SYMBOLS

b_f	Wingspan of following airplane.
b_g	Wingspan of generating airplane.
$\bar{c}$	Mean chord.
Hp	Pressure altitude.
r	Radius.
r_c	Core radius.
S	Wing area.
s	Wing semispan.
t	Time elapsed since vortex generated.
t*	Time to vortex breakup.
T_ℓ	Time to linking.
V_θ	Tangential velocity within vortex.
V_{θ_o}	Tangential velocity within vortex at time zero.
V	True airspeed.
V_∞	Speed of undisturbed stream.
W	Airplane gross weight.
y	Spanwise station.
$\bar{y}$	Spanwise station of centroid of vorticity distribution.
$\bar{y}\ (y_1)$	Spanwise station of centroid of vorticity distribution outboard of station y_1.
z	Longitudinal distance separating generator and following aircraft.

LIST OF GREEK SYMBOLS

Γ	Circulation or strength of vortex.
Γ_c	Circulation at vortex core radius.
Γ_o	Circulation at time zero.
δ_f	Flap deflection.
$\epsilon^{1/3}$	Atmospheric turbulent dissipation rate.
η	Dimensionless spanwise coordinate (= y ÷ b/2)
ν	Kinematic viscosity, $\mu \div \rho$
ρ	Ambient air density.
ϕ	Angular coordinate defining spanwise station η, $\eta = \cos \phi$. ($-1 \leq \eta \leq 1$)

INTRODUCTION

PURPOSE.

The work described in this report was performed to gain information on the vortex wake characteristics of a representative group of large transport airplanes, to aid in the development of improved terminal-area air-traffic control procedures based on considerations of the vortex-wake phenomenon.

BACKGROUND.

It was determined early in 1970 that there was a need to investigate further the vortex wake characteristics of large jet transport airplanes in conditions representative of terminal area operations. An investigation was conducted as a joint operation involving the Federal Aviation Administration (FAA) National Aviation Facilities Experimental Center (NAFEC), the National Aeronautics and Space Administration (NASA), the Boeing Company, and the United States Air Force. The airplanes involved, flight test techniques used, and results obtained are described in references 1, 2, and 3.

NAFEC's part in that operation included the acquisition of quantitative data on the Boeing 707, 727, and 747; McDonnell-Douglas DC8 and DC9; and the Lockheed C5A, using tower fly-by and flow visualization. At the time of these early tests, a very limited number of sensors was available for the measurement of vortex airflow velocities. However, in view of the then-accepted theory of trailing vortices of fixed-wing airplanes (reference 4), namely that the vortex core diameter is initially equal to 15 percent of the wingspan, the available instrumentation appeared to suffice for achieving the objective of the planned tests. It was subsequently shown in reference 5 and in other literature (including those individual reports forming the basis of this summary report) that the vortex core diameter is frequently much smaller, especially in clean configurations, and the need for further testing, using closer sensor spacing, became apparent. Accordingly, further tower fly-by tests were run, using 1-foot sensor spacing on the following airplanes: Boeing 707, 727, and 747; Lockheed C141, C5A, and L1011; McDonnell-Douglas DC9 and DC10; and Convair 880. Tests were also run on the Douglas DC7 using 4-foot sensor spacing. Flow visualization was also employed, using aircraft- and tower-mounted smoke generators. These tests have been reported individually (references 6 through 13), covering the airplanes listed (with the exception of the Lockheed C141 and C5A, on which only unpublished material exists). In the course of preparing these individual reports, certain trends, apparently attributable to airplane design features, emerged. This report identifies and discusses these trends and presents the principal findings of the entire test series. It also proposes an approach to improving aircraft separation criteria based on considerations of the vortex phenomenon as identified in these tests.

The report is divided into three parts under the following general headings:

1. Characteristics of the vortex wake as a function of aircraft type and flight configuration.

2. Possible effect on a second aircraft encountering the wake.

3. Application of knowledge gained to development of improved separation criteria.

DISCUSSION

TEST AIRPLANES.

Three-view drawings and aircraft specifications are presented in appendix A, grouped according to design configuration as follows:

Group I

Boeing 747 and 707
Convair 880

Airplanes of this group are characterized by low wing, low horizontal tail, four wing-mounted engines in forward-slung under-wing pods and swept-back wing planform.

Group II

Lockheed C5A and C141

Airplanes of this group are characterized by high wing, T-tail, four wing-mounted engines in forward-slung underwing pods and swept-back wing planform. The military operational requirements of these two airplanes (short field, lower minimum control speeds) are reflected in the reduced wing sweep-back angle and more inboard mounting of the engines, as compared with Group I airplanes

Group III

Lockheed L1011
McDonnell-Douglas DC10

These airplanes are characterized by low wing, low-horizontal tail, two wing-mounted engines in forward-slung, under-wing pods, a third engine at the base of the vertical tail, and swept-back wing. Aside from the mounting and ducting of the central engine, these two airplanes are very similar in general appearance.

Group IV

Boeing 727
McDonnell-Douglas, Series 10

These airplanes are characterized by low wing, T-tail, engines mounted at the rear of fuselage, swept-back wing. They differ in that the B727 mounts a third engine at the base of the vertical tail, and the DC9 wing planform reflects a short-field operational requirement (reduced sweep-back angle and higher aspect ratio).

Group V

Douglas DC7

This airplane is a conventional unswept, high aspect ratio, low-wing, propeller-driven design.

The above five groups of airplanes represent a natural classification, as it has been believed for some time that major design variables such as wing planform, engine location and empennage configuration, exert a strong influence on the structure of the airplane wake over great downstream distances. One of the findings of this vortex flight test program is that this is so.

The most obvious differences between Group I and Group II are in the wing and horizontal tail location. Group I airplanes have lower aspect ratio wings than those of Group II (approximately 6-7, compared with 7-8 in Group II), and the wing sweep-back angle is approximately 10° less in Group II. Trailing-edge flaps in Group I airplanes are in two segments per side, with a large cut-out in line with the inboard engine. On Group II airplanes, the flaps are essentially unbroken over their span. Finally, the spanwise location of the engines is noticeably different between the two groups. Engines are closer inboard on Group II airplanes. All the differences cited between the two Boeing commercial transports and the two Lockheed military transports reflect the different operational requirements of the two classes of airplane. These differences are potentially significant in how they affect the development of the aircraft wake.

Group III airplanes are so similar in appearance that it seems unlikely there would be any detectable differences between their wakes. The general specifications (appendix A) show that wing planform parameters differ but slightly, and that leading- and trailing-edge high-lift devices and lateral controls are generally similar. The relative location of wings, engines and horizontal tail are likewise very similar, and the only readily apparent difference is in the mounting and ducting of the central engine (see figures A-6 and A-7 in appendix A). This single feature, especially since it only affects the height of that engine's efflux relative to the rest of the wake, would not be expected to cause any detectable difference in downstream wake development.

Airplanes of Group IV have these major features: "clean wing," aft-mounted engines, and T-tail. However, the wing planforms, as defined by sweep-back angle and aspect ratio are somewhat different, as also are the leading- and trailing-edge high-lift devices (no leading-edge devices on DC9 series 10; large cutout between inboard and outboard flap sections of B727, no cutout on DC9). It is thus possible that these should be considered as two separate classes.

Group V, the Douglas DC7 stands on its own, being the sole representative of the conventional high aspect ratio, unswept wing, propeller-driven class of airplane.

MATHEMATICAL REPRESENTATION OF THE VORTEX

The mathematical modeling of trailing vortices has been attempted many times with varying degrees of success. One of the methods that has been applied frequently is that of reference 4, which is based on an equality between the induced drag (drag due to lift) and the kinetic energy per unit length of wake. The latter is computed assuming a potential-flow velocity distribution, and integrating the energy over the cross section of the wake. While the upper limit of integration causes no problems even though the integration is carried out to infinity (this is not true of a single isolated vortex, but is true for any combination of vortices, the strengths of which sum algebraically to zero), the lower limit, without modification, yields an infinity, since the velocity at the core of the potential-flow vortex increases indefinitely as the radius is reduced. The resolution of this is also the basis of the estimate of vortex core diameter. It is postulated that at a certain radius, known as the core radius, the tangential velocity reaches a peak, and at smaller radii, instead of continuing to increase as the reciprocal of the radius, it decreases linearly to zero at zero radius. From physical considerations, it has to do something approaching this, since the tangential velocity must approach zero with the radius in order to avoid infinite accelerations. The transition from the inverse form of velocity distribution to linear is assumed to be instantaneous. With this solidly rotating core, the total summation of energy in the plane normal to the aircraft flightpath is now finite and the resulting energy expression can readily be solved for the vortex core radius and the associated peak tangential velocity. The method is a rather indirect approach to the determination of core radius, and its weakness is the assumption that potential flow exists outside the vortex cores. It has been found that the vortex core diameters yielded by this approach are often very much larger than those measured in flight and that the peak tangential velocities are correspondingly smaller.

Another approach to the problem of wake vortex rollup is presented in reference 14. According to Betz, the circulation Γ_1, at a given station η_1,

along the span of an elliptically-loaded wing, appears at a radius in the rolled-up vortex sheet given by:

$$\left(\frac{r_1}{b/2}\right)^2 = \left(\frac{\phi_1 - \sin\phi_1 \cos\phi_1}{2\sin\phi_1}\right)^2 \qquad (1)$$

where $\cos\phi_1 = \eta_1$

and $\sin\phi_1 = \sqrt{1-\eta_1^2}$

Some simplification of this expression is possible at the wingtip (ϕ = zero) and at the root ($\phi = \pi/2$).

To a third order of approximation,

$$\phi - 1/2 \sin 2\phi = \frac{2\phi^3}{3}$$

Therefore, for small ϕ,

$$\frac{r}{b/2} = \frac{\phi^2}{3} = \frac{\sin^2\phi}{3}$$

but

$$\sin^2\phi = 1-\eta^2$$

$$\therefore \frac{r}{b/2} = \frac{1}{3}\left(1-\eta^2\right)$$

or $$3r\frac{b}{2} = \left(\frac{b}{2} + y\right)\left(\frac{b}{2} - y\right)$$

So when ϕ is small, and

$$\frac{y}{b/2} = \cos\phi \rightarrow 1$$

or

$$3r\frac{b}{2} = b\left(\frac{b}{2} - y\right)$$

or $$r = \frac{2}{3}\left(\frac{b}{2} - y\right) \qquad (2)$$

In words, the radius at which the circulation at a station near the tip appears in the rolled-up vortex is equal to two-thirds of the distance between that station and the tip. The consequences of equation (1) in terms of the variation of tangential velocity as radius is reduced indefinitely can be evaluated simply enough. We have for the elliptically-loaded wing,

$$\frac{r}{b/2} = \frac{\phi - 1/2 \sin 2\phi}{2 \sin \phi}$$

and

$$\Gamma = \Gamma_o \sqrt{1-\eta^2}$$

so

$$V_\theta = \frac{\Gamma_o \sqrt{1-\eta^2}}{2\pi r}$$

$$= \frac{\Gamma_o}{2\pi} \frac{4\sqrt{1-\eta^2} \sin \phi}{b(\phi - 1/2 \sin 2\phi)}$$

$$\therefore V_\theta = \frac{2\Gamma_o}{\pi b} \frac{\sin^2 \phi}{\phi - 1/2 \sin 2\phi}$$

$$\doteq \frac{3\Gamma_o}{\pi b \phi} \text{ when } \phi \to \text{zero.} \qquad (3)$$

Thus, by this formulation, V_θ tends to infinity as the radius is reduced. It does, however, provide an indication of how V_θ at a given ϕ varies with median circulation, Γ_o, and wingspan, b. It is still interesting too, to evaluate the tangential velocities and radii obtained as η approaches unity. Consider a hypothetical large airplane with elliptical lift distribution, having the following weight, span, and airspeed:

W = 500,000 pounds
b = 200 feet
V = 250 ft/s
Then Γ_o = 5,350 ft^2/s (median circulation)
Take η = .99
Then ϕ = Arccos .99
= .1415 radian
and V_θ = 180 ft/s
r_c = .67 feet

The corresponding figures for η = .98 are:

V_θ = 127 ft/s
r_c = 1.3 feet

These figures are certainly of the right order of magnitude for the case considered, cf reference 6, figure C-7 in appendix C of that report, for example.

The Betz formulation of reference 14 is restricted to wings having an elliptical lift distribution, and it takes no account of energy lost in the boundary layer and its influence on velocity distribution in the rolled-up vortex. Certain other types of lift distribution, expressible in terms of conic sections, polynomial equations or simple trigonometric functions may be analyzed for vortex rollup, following the pattern set by Betz; however, this is rather restrictive and a more general method capable of handling any possible lift distribution is required, because not all lift distributions yield a simple rollup into two oppositely rotating tip vortices. Irregularities in the lift distribution can result in more than a single vortex-pair being generated at the wing trailing-edge. The conditions for this are presented in reference 15, some results of which are quoted: The first is that the radius in the rolled-up vortex at which the circulation is equal to the circulation at a given spanwise station y_1, is equal to the distance from that station y_1, to the centroid of the $d\Gamma(y)/dy$ distribution outboard of y_1, to the tip.
The statement is illustrated by figure 1.

In the lower sketch, $\bar{y}\ (y_1)$ is the centroid of the distribution of $d\Gamma(y)/dy$ outboard of y_1.

then $$\bar{y}(y_1)-y_1 = r \tag{4}$$

where r is the radius at which the circulation $\Gamma\ (r)$ is equal to Γ_1.

Betz' work laid down the following invariant, to be maintained from start to finish of the rollup process:

$$\int_{y_1}^{b/2} \frac{d\Gamma(y)}{dy}\, y\, dy = \bar{y}(y_1)\ \Gamma(y_1) \tag{5}$$

In words, this says that the first moment of the vorticity shed between point y_1, and the wingtip, with respect to the plane of symmetry, y=o, is equal to the circulation Γ_1, at y_1, in the lift distribution, multiplied by the distance $\bar{y}(y_1)$.

From equation (5), we have

$$\frac{d\Gamma(y)}{dy}\, y\, dy = \Gamma(y)\, d\bar{y} + \bar{y}\, d\Gamma(y)$$

or

$$\frac{d\Gamma(y)}{dy}\,(y-\bar{y}) = \Gamma(y)\,\frac{d\bar{y}}{dy}$$

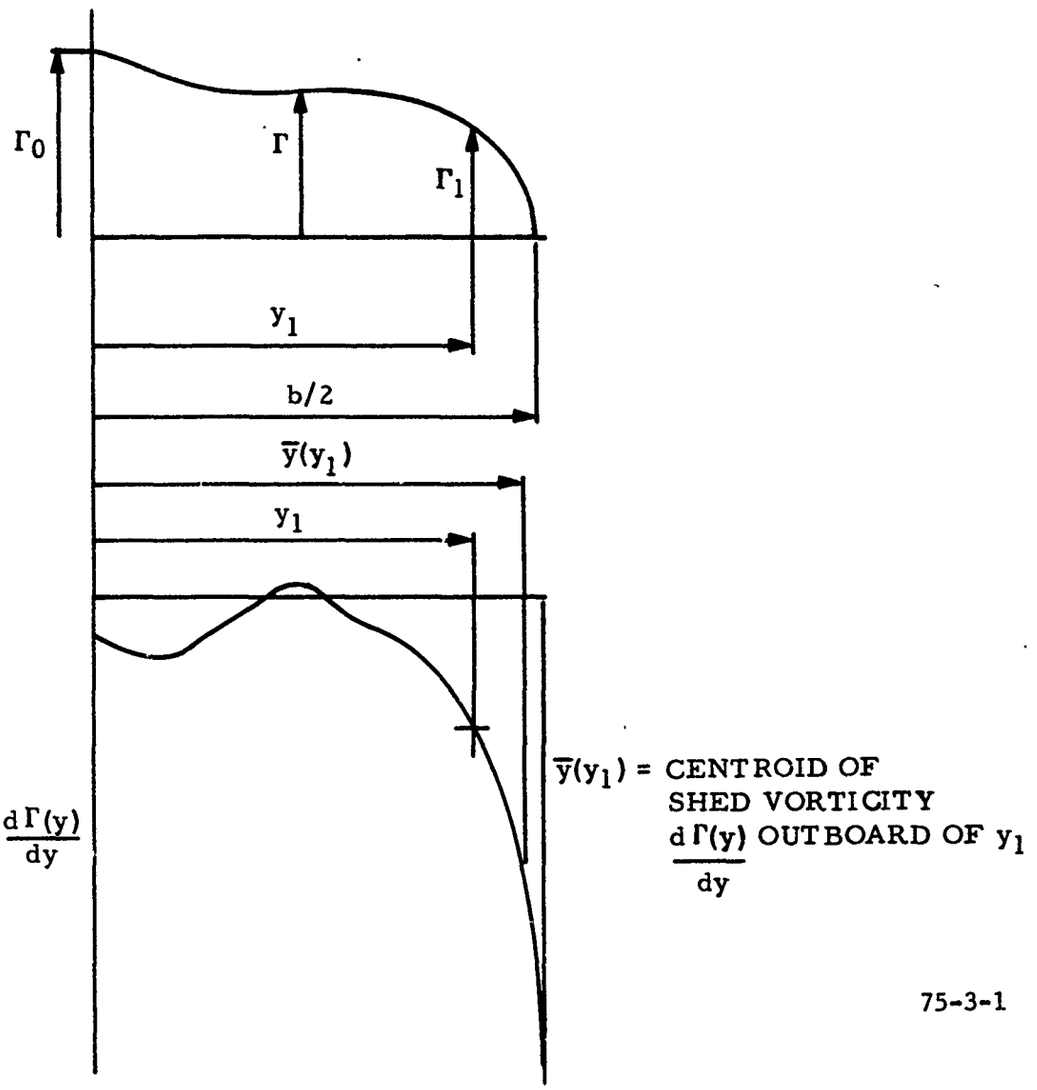

FIGURE 1. DEFINITION OF TERMS IN MODIFIED BETZ ROLLUP ANALYSIS

and

$$\frac{d\bar{y}}{dy} = \frac{\frac{d\Gamma(y)}{dy}(y-\bar{y})}{\Gamma(y)} \tag{6}$$

From equation (4)

$$\frac{dr}{dy} = \frac{d\bar{y}}{dy} - 1$$

$$= \frac{y-\bar{y}}{\Gamma}\frac{d\Gamma}{dy} - 1 \tag{7}$$

Now, a simple rollup implies that the shed vorticity from the extreme tip appears at the center of the vortex, and that as the station of interest is moved inboard, the associated radius in the rolled-up vortex increases. Failure to maintain this would mean that more than a single value of circulation would appear at certain values of the radius, which is clearly impossible. Thus from equation (7), we have the condition that

$$\frac{y-\bar{y}}{\Gamma}\frac{d\Gamma}{dy} < 1 \tag{8}$$

or

$$-\frac{d\Gamma}{dy} < \frac{\Gamma}{\bar{y}-y}$$

since $d\Gamma/dy$ is usually negative in the right half plane and $\bar{y}>y$.

A simple physical interpretation of equation (8) is shown in figure 2.

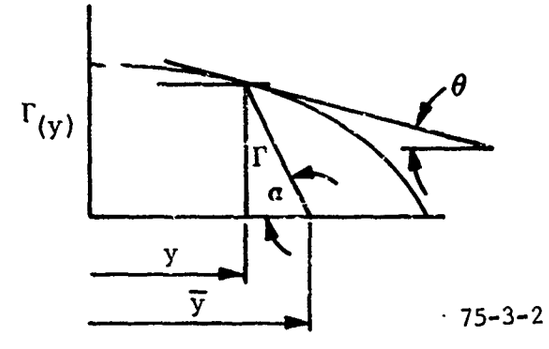

FIGURE 2. CONDITION FOR SIMPLE ROLLUP OF VORTEX SHEET ($\alpha>\theta$)

The quantity $\Gamma/\bar{y}-y$ is the tangent of the angle α. This is required to be larger than $-d\Gamma/dy$ which is the tangent of the angle θ. Not all lift distributions realize this condition and, when this happens, more than one vortex per semispan is produced in the rollup process. The calculation of the rollup of the shed vorticity from any arbitrary spanwise lift distribution, with any number of shed vortex pairs, is fully described in reference 15. Some results, using the tower fly-by data, have been presented and the ability of the method (which is something of a "cookbook" procedure when critically examined) to account for measured tangential velocity data is surprisingly good, in view of the assumptions inherent in the method.

Another approach to the determination of the peak tangential velocity is also presented in reference 15. By equation (4)

$$r = \bar{y}-y$$

Over the last increment of span dy, we have

$$d\Gamma = \left(\frac{d\Gamma}{dy}\right)_{b/2} dy$$

Since over the vanishingly small interval dy, the gradient $d\Gamma/dy$ is held constant, the centroid of this increment in the distribution is at the mid-point. Thus

$$\bar{y} = y+1/2\ dy$$

and

$$r = 1/2\ dy$$

and

$$\therefore\ 2\pi(1/2)dy\ V_\theta = \frac{d\Gamma}{dy}\,dy \qquad (9)$$

$$V_\theta = \frac{1}{\pi}\left(\frac{d\Gamma}{dy}\right)_{b/2}$$

For many lift distributions, including the elliptical, $d\Gamma/dy$ at the tip is theoretically infinite, and V_θ, therefore, indeterminate. Equation (9) does, however, indicate that V_θ is sensitive to the rate at which the circulation in the immediate vicinity of the tip diminishes to zero.

Another approach to the determination of the peak tangential velocity and of the core radius is that of reference 16. According to this, the tangential velocity at a radius r is given by

$$V_\theta = \frac{\Gamma_o}{2\pi r}\left(1 - e^{-r^2/4\nu t}\right) \qquad (10)$$

where

ν = Coefficient of viscosity
t = Elapsed time since generation of vortex
Γ_o = Circulation at zero viscosity

On the basis of this model, certain deductions can be made with respect to core radius and peak tangential velocity. Differentiating V_θ with respect to r.

$$\frac{dV_\theta}{dr} = \frac{-\Gamma_o}{2\pi r^2}\left(1 - e^{-r^2/4\nu t}\right) + \frac{\Gamma}{2\pi r}\frac{d}{dr}\left(1 - e^{-r^2/4\nu t}\right)$$

$$= \frac{\Gamma_o}{2\pi}\left(\frac{-i}{r^2} + e^{-r^2/4\nu t}\left[\frac{1}{r^2} + \frac{1}{2\nu t}\right]\right)$$

When V_θ is a maximum,

$$e^{-r^2/4\nu t}\left[\frac{1}{r^2} + \frac{1}{2\nu t}\right] = \frac{1}{r^2}$$

or

$$e^{r^2/4\nu t} = 1 + \frac{r^2}{2\nu t}$$

or

$$\frac{r^2}{4\nu t} = \ell n\left(1 + \frac{r^2}{2\nu t}\right)$$

Solving this numerically,

$$\frac{r_c^2}{4\nu t} = 1.26 \qquad (11)$$

This defines the conditions under which the tangential velocity V_θ is a maximum. If we identify the corresponding radius as r_c, core radius, we can write

$$V_{\theta_{max}} = \frac{\Gamma_o}{2\pi r_c}\left(1 - e^{-1.26}\right)$$

$$= \frac{.716\ \Gamma_o}{2\pi r_c} \qquad (12)$$

In other words, the core circulation is related to the potential flow circulation by

$$\Gamma_c = .716\ \Gamma_o \qquad (13)$$

Thus, just because of the form of equation (10), with no reference to actual values of r, ν, or t, it has been possible to show that the core radius circulation is a fixed proportion of the potential flow value, that would exist in the absence of viscosity.

From equation (11), it follows that

$$r_c = \sqrt{5.04\ \nu.t}^{1/2} \tag{14}$$

and from equation (12), it follows that

$$V_{\theta_{max}} \propto t^{-1/2} \tag{15}$$

This formulation of Lamb's is discussed in reference 17, including an objection that has been raised concerning it; namely, that in the case of a single vortex, an infinite amount of kinetic energy is associated with it. This is not true when there are two or more vortices whose strengths sum algebraically to zero.

The decay law for the peak velocity $V_{\theta_{max}}$ has been the subject of considerable investigation. Work cited in reference 18 indicated, on theoretical grounds, that the peak velocity would decay as $t^{-1/2}$, and experimental data which supports this is also cited. The experimental work of reference 5 concludes that the peak velocity decays according to

$$\frac{V_\theta}{V_{\theta_o}} = \left(1 + .0065\ \frac{z}{c}\right)^{-1/2} \tag{16}$$

where

V_θ = Peak velocity

V_{θ_o} = Peak velocity at instant of vortex generation

z = Distance downstream from generating aircraft

$\bar{c}$ = Aircraft mean chord

At a true airspeed of 150 knots say, the value of z at the end of a minute is 15,000 feet and with a mean chord of 20 feet, the quantity $.0065\ z/\bar{c}$ comes out to be 4.9. Thus as z increases beyond 15,000 feet, equation (16) approaches $(.0065\ z/\bar{c})^{-1/2}$, which is proportional to $t^{-1/2}$. Neither reference 5, nor reference 18 indicates any mechanism by which the core radius circulation diminishes with time, but rather, they indicate that the radius itself increases as $t^{1/2}$, which with the above law for the decay of the core radius tangential velocity, results in a constant value of core radius circulation.

It was remarked earlier that the Betz formulation for the rollup of the trailing vortex sheet had been shown to give good results in the near wake. One of the assumptions made in Betz' original formulation (reference 14) is that the vorticity from each wing rolls up into an axisymmetric line vortex of finite radius, which implies that there is no mutual interference between the members of the vortex pair. Application of the Betz invariants to the elliptic lift distribution results in a pair of trailing vortices which are separated by a distance of $\pi b/4$ when rolled up, and whose radius is $\pi b/8$. Thus, the vortices are tangential to each other and some justification is required for the assumption of no mutual interference. While this is evidently possible in the early life of the wake, since the formulation yields acceptable results, this state of affairs cannot last indefinitely because the expansion of the vortex core must ultimately render the assumption of no mutual interference invalid.

The discussion so far has dealt mostly with the question of peak tangential velocity and the associated core radius. As a practical matter, the peak tangential velocity in a vortex is a difficult quantity to determine, especially if the vortex core is small and the local velocity gradients correspondingly large. Since the anemometry is necessarily not continuous across the vortex, but is placed at regular intervals (1 foot in most cases of interest in this report), the absolute peak velocity is usually not sensed, though if the error is large because of a small core diameter, it indicates a very large velocity gradient and thus means that the radial interval over which the peak velocity is present is small, and, therefore, of diminished importance in calculating the upset potential of an airplane encountering that vortex.

Determination of the vortex core radius is more certain. The interpretation of the sensor velocity time histories, collectively, to yield the velocity distribution taken vertically through the vortex at the time that it is in the line of the sensors has been discussed in references 6 and 13. The time of interest can be identified by the peaking of the velocities, and the velocities at the individual sensors are assumed to be horizontal, either into or away from the tower. The resolution of the ambiguity of the data (sensors yield no directional information) is made from considerations of the axisymmetry of the flow, and the fact that the data usually shows when aerodynamic interference is present, thus indicating when a measured velocity is into the tower (downwind) or away from the tower (upwind).

The velocity distributions obtained are presented as an appendix of each individual report, references 6 through 13, and a selection has been made from the data on the airplanes in the study group. These data are presented in appendix B of this report.

The question now arises as to the distribution of velocity within the vortex. Evidently, from considerations of the rollup mechanism as described in references 14 and 15, the initial distribution of tangential velocity is determined by the spanwise lift distribution. The application of the modified Betz procedure to the analysis of the data has not been attempted because of the time involved, and because, from an operational point of view, it is questionable whether any useful purpose would be served by pursuing the analysis in that

much detail. It has been shown to yield acceptable results for relatively short-term development of the vortices, but it has already been pointed out that the assumptions of no mutual interference and of the confinement of the vorticity within finite radii cannot be expected to hold good indefinitely. An alternative approach to the problem of vortex velocity distribution is presented in reference 19, which warrants careful study. Prior to its appearance, a single analysis (reference 20) existed, treating the line vortex in turbulent flow. The result obtained was similar to that obtained in laminar flow (reference 16), with the kinematic viscosity replaced or supplemented by an "eddy viscosity" term, the magnitude of which is proportional to the strength of the line vortex, which itself is just equal to the median circulation of the generating wing. Experimental data, however, showed a discrepancy over a significant portion of the velocity profile, between laminar flow vortices calculated on the basis of the "effective viscosity" and experimental (turbulent) vortices, indicating that the "effective viscosity" approach is incorrect. Reference 19 suggests that the reason for this failure lies in the fact that the mechanisms of laminar and turbulent vortices are quite different, to the extent that a turbulent flow can be quite independent of viscosity.

Following along the lines set forth by Prandtl, Von Karman, and Taylor in reference 21, for example, in which a universal logarithmic velocity distribution law is developed for turbulent flows in rectangular channels, at Reynolds' Numbers large enough that the turbulent shearing stresses are dominant and laminar friction exerts little influence, reference 19 presents an analysis in which it is shown that the ideas that led to the aforementioned logarithmic velocity distribution law could, with suitable modification be applied to the circulating motion that occurs in a vortex. The result of the analysis is the now well-known Hoffman-Joubert logarithmic circulation distribution

$$\frac{\Gamma}{\Gamma_c} = 1 + \ell n \frac{r}{r_c} \tag{17}$$

where

Γ = Circulation at radius r

Γ_c = Circulation at core radius r_c

It is evident by inspection of equation (17) that it cannot apply over the whole range of r, since setting r equal either to zero or a very large number both lead to impossible results. Within the vortex core itself, something close to solid body rotation takes place, in which case the circulation is proportional to the square of the radius, and a transition takes place to the logarithmic distribution as 'r' approaches 'r_c.' At some large value of r, equation (17) again ceases to apply, since the circulation cannot grow indefinitely. Physically, the failure of equation (17) at large r means that the turbulent shear stresses are becoming very small, and hence, the condition of applicability of equation (17) is no longer being met; namely, that the turbulent shear stresses be large compared with those due to the kinematic viscosity ν.

APPLICATION TO EXPERIMENTAL RESULTS

Appendix B of this report is a selection of vortex tangential velocity distributions for the airplanes in the study group. For each airplane, the distributions are grouped by flight configuration and vortex age. Selecting the core radius r_c, and the associated tangential velocity V_θ (r_c), solely on the basis of of yielding a good fit to the velocity distribution data (in other words, making no attempt to determine what these should be on the basis of airplane type, flight configuration or flight condition), a velocity distribution of the form of equation (17) was calculated for each plot. Examining these plots in their natural grouping, the following observations can be made:

BOEING 747 AIRPLANE (REFERENCE 6).

TAKEOFF CONFIGURATION. (All references to configuration refer to airplane geometrical configuration, and do not include power setting, which in most cases is that for level flight at nominal airspeed of test run.) The vortex cores are uniformly small in diameter; $2r_c$ is estimated to be 1 to 2 feet. The associated peak tangential velocity used in obtaining the curve fit was 140 feet per second (ft/s) in each case. The entire group of takeoff vortices analyzed for this airplane is presented in figures C-1 through C-115 (appendix C) of the referenced report. The peak-recorded velocities (which are uncorrected for wind) range between 48 and 165 ft/s, but since this quantity is an isolated point and uncorrected for wind, it is not used in determining V_θ (r_c) used in the plots. However, as figure 17, page 25, of reference 6 indicates, 140 ft/s is a representative value.

The age of the vortices has a bearing on the quality of fit to the data that is obtained with the Hoffman-Joubert circulation distribution equation.

The initial distribution, according to the Betz formulation, is determined by the spanwise lift distribution or more correctly the spanwise rate-of-change of the lift distribution. The logarithmic distribution has been shown to be a universal equilibrium distribution for a turbulent line vortex, and when the initial velocity distribution within the vortex differs from the logarithmic, then some unspecified interval of time must elapse before the the equilibrium state is reached. For the B747, the takeoff flap setting is 10°, and it is unlikely that the resulting lift distribution yields more than one major vortex pair. The degree to which this is rolled up, the magnitude of the ground effect, and the time elapsed since rollup determine the extent to which the velocity distribution differs from the logarithmic. The takeoff vortex velocity distributions of figures B-1 through B-4 (appendix B) are for relatively short-age vortices, and it is evident from these, especially the first three (11, 13, and 17 seconds) that the vortex structure has not reached its equilibrium state. The discrepancy is much less in the fourth vortex (26 seconds), though there is evidence there too that the rollup process is not complete.

It should be noted that in all four cases, the better data fit was unexpectedly obtained in that part of the vortex in which the tangential velocity is against the relative wind; i.e., where the data is more likely to be subject to aerodynamic interference. This is the case in the upper half of the downwind vortex and the lower part of the upwind vortex. It should be noted too that all four vortices reached the tower at a height above the ground approximately equal to a semispan of the generating airplane. This puts them within the height range of ground effect, especially so since the ambient windspeed (measured at the 140-foot level) was quite high (approximately 10 miles per hour (mi/h)), and therefore, the vortices were subject to wind shear. Notwithstanding these considerations however, the vortex cores are all small and the velocity distributions are reasonably well described by the logarithmic law.

HOLDING CONFIGURATION. The flap setting in this configuration is 1.0°, an apparently insignificant amount of deflection, which nonetheless is important since it is combined with a chord extension. The resulting lift distribution is less likely to produce secondary vortices than that for takeoff. Although these vortices (figures B-5 through B-8) are also of short age (10-21 seconds), they consistently conformed to the logarithmic velocity distribution, showing a better fit than was obtained in takeoff configuration. Some discrepancies (not minor in figure B-6) are apparent in the "downwind" portion of the vortex (tangential velocity additive to wind), though these are not as marked as in takeoff configuration. The resulting vortex core diameters are uniformly small again, and the value of V_θ (r_c) yielding a good fit was again found to be 140 ft/s, though this is low compared with the peak-recorded tangential velocities found for this configuration, figure 18, reference 6.

Some comment on core radius circulation is in order here. It is evident that in the flight configurations employing small or zero flap deflections, the vortex core diameters are of the same order of magnitude as the spacing between sensors (1 foot), and are, therefore, subject to large (percentage) errors. In such a vortex, the velocity gradients are extremely high (within the core itself, they may be as high as 2 to 300 ft/s per foot), and therefore, the chances of measuring the true peak velocity on a given run are small. The result of these uncertainties is that core radius circulation is probably larger than measured in many cases.

LANDING CONFIGURATION. It is immediately apparent (figures B-9 through B-12) that the tangential velocity distribution in the landing configuration (flap angle = 25°) is quite different, in terms of peak velocity and vortex core radius, from that found in takeoff and holding configurations. Vortex ages represented range from 11 to 27 seconds, peak velocities from 60 to 73 ft/s and core radii from 8 to 16 feet. Now according to the Milne-Thomson formulation (reference 22), the vortex core radius is given by:

$$r_c = .0855 \text{ X span of generating wing}$$

and

$$V_{\theta_{max}} = \frac{4}{\pi} \frac{W}{\rho V_D} \frac{1}{2\pi r_c} \qquad (18)$$

The preceding results are predicated on an elliptical lift distribution. Inserting the following numbers (representative of Boeing 747 in landing configuration):

W = 500,000 pounds

b = 200 feet

V = 250 ft/s, true airspeed

we obtain

r_c = 17.1 feet

$V_{\theta_{max}}$ = 50 ft/s

Thus, the Milne-Thomson formulation has led to a result that is certainly of the same order of magnitude as the measured result obtained in a flight configuration that produces a far from elliptical lift distribution. This must surely be regarded as a fortuitous result, however.

What is of interest here is the fact that an increase in flap angle from 10° (takeoff) to 25° (landing) has resulted in such a large change in the parameters describing the trailing vortices, especially when the first 10° resulted in little detectable change other than the production of a lower peak tangential velocity, compare figures 17 and 18, reference 6.

Qualitatively, deployment of flaps to the landing position would be expected to result in more energy appearing in the wake because of the higher induced drag associated with the irregular lift distribution, heavily loaded inboard and lightly loaded outboard. At the same time, the higher profile drag of the wing in this condition results in high energy losses in a thicker boundary layer, a fact which may account for the reduced velocities within the core and the much reduced peak tangential velocity and larger core. To account for the higher overall energy coincidental with the lower velocities within the core, one would again expect to find the core diameters much larger, and the tangential velocities external to the core to diminish with radius much more slowly. This is the result found, as is shown in figures B-9 through B-12, appendix B of this report. It certainly appears that the flow is less well organized in this landing configuration data, and this may well be true and be the reason for the more rapid degeneration of the wake that is believed to occur in the flapped configurations. However, in the early stages of wake development, as represented by figures B-1, B-6, and B-9, which are 11-second vortices in takeoff, holding, and landing configurations, respectively, the landing vortex, which maintains quite high tangential velocities (30 to 40 ft/s) out to large radii (50 feet), probably constitutes a more severe hazard to an encountering airplane than do those vortices characterized by a much higher peak velocity associated with a very tight core and subsequent rapid fall-off in velocity exterior to the core.

BOEING 707 AIRPLANE (REFEKENCE 7).

On the basis of previous arguments, citing the general similarities between the B747 and B707 wing designs, the vortices generated by the latter airplane would be expected to produce tangential velocity distributions geometrically similar to those found in the B747 vortices. A selection of B707 vortex velocity distributions is presented in figures B-13 through B-18 in appendix B of this report, and the complete set is presented in appendix B of reference 7. The peak-recorded velocities (uncorrected for wind) are presented in figures 5, 6, 7, and 8 of reference 7 and in the next section of this report. For comparison purposes, the absolute peak values for the two airplanes, plus the Convair 880, are presented in table 1.

TABLE 1. ABSOLUTE PEAK VELOCITIES, FT/S, FOR THREE FLIGHT CONFIGURATIONS, B747, B707 AND CV880

	Airplane Configuration					
	Takeoff		Holding		Landing	
Airplane	δ_f (Degrees)	$V_{\theta max}$ (ft/s)	δ_f (Degrees)	$V_{\theta max}$ (ft/s)	δ_f (Degrees)	$V_{\theta max}$ (ft/s)
B747	10	165	1	260	25	150
B707	14	110	0	200	40	110
CV880	22	108	0	150	55	106

TAKEOFF CONFIGURATION. Turning now to the velocity distributions of figures B-13 and B-14, the takeoff configuration ($\delta_f = 14°$) shows a tendency towards a small core diameter, but probably on account of the larger flap angle employed on the B707 at takeoff, the vortices are not as tight as was found with the B747. Comparing figures B-13A and B-14A, as a case in point, it seems that at this flap angle (i.e., 14°), the core diameter may be large or small, with the associated low or high core-radius tangential velocity. The tight core condition can evidently persist to quite long vortex ages (figure B-14B), or the larger core condition may appear quite early (figure B-14A). Whether the transition from the small core condition to the larger is aircraft-related, or whether it is induced by the experimental setup, is an important question that cannot be answered yet, but it is as well to mention that in this particular situation, or in any other situation where trailing vortices are subject to measurement using an instrumented tower, the tower itself has an undetermined effect on the phenomenon being measured.

HOLDING CONFIGURATION (δ_f = ZERO). Four representative velocity distributions (ages 24 to 60 seconds) are shown in figures B-15 and B-16.

The vortex core diameters are uniformly small (up to 2 feet at 60 seconds vortex age) and the peak velocities range from approximately 100 to 200 ft/s. The vortices are evidently fully developed, as the scatter in the data is small for this kind of experiment, and the logarithmic distribution law yields a good fit to the data points. The vortices struck the tower at heights between 50 and 105 feet (airplane wingspan = 145 feet approximately), three of them at heights less than 70 feet, or less than a semispan. Nonetheless, it is not apparent that proximity to the ground has had any marked effect on this group of vortices. The complete set of velocity distributions for this configuration is presented in figures B-10 through B-32 of reference 7, and these figures constitute one of the most consistent sets of data obtained in the entire vortex test program.

LANDING CONFIGURATION. The greater complexity of the lift distribution in this configuration is expected to lead to longer times to vortex rollup and development of the equilibrium velocity distribution. Figures B-33 through B-64 of reference 7 bear this out, the velocity distributions obtained being ragged and untidy, with evidence that secondary vortices are complicating the picture (without going through the modified Betz analysis of reference 15, it is reasonably certain that the B707 lift distribution in the landing configuration violates the condition necessary for simple direct rollup of the vortex sheet into a single vortex pair). The trend toward larger core diameters and very definitely lower peak velocities is unmistakable, and as indicated in table 1, the absolute peak velocity is little more than half that found in the flaps-up configuration.

CONVAIR 880 AIRPLANE (REFERENCE 8).

The velocity distributions for this airplane follow the pattern set by the other airplanes in Group I; namely, that larger flap deflections are associated with larger core diameters and reduced peak velocities.

TAKEOFF CONFIGURATION ($\delta_f = 22°$). Four representative velocity distributions are presented in figures B-19 through B-22 of this report. They indicate that core diameters may be as large as 18 feet, but as is seen in figure B-22, the diameter may also be quite small. This apparent ambiguity was also noted on the Boeing 707 in takeoff configuration ($\delta_f = 14°$), but not on the Boeing 747, which uses a flap angle of 10° for takeoff. For the entire group of test runs on the CV880, covering three separate periods of testing, the range of peak velocities recorded in the takeoff configuration is 20 to 110 feet per second. The extreme low values are attributable to the wider sensor spacing (4 feet) used during the first test period. Only three of the total of 79 data points exceeded a value of 85 ft/s.

HOLDING CONFIGURATION (δ_f = ZERO). Figures B-23 through B-26 show that this configuration yields consistently small vortex core diameters (1 to 2 feet), a result also found for the other airplanes in this group. Such small core diameters, especially in combination with wide sensor spacing, produce great scatter in the data, the peak-recorded velocities being spread fairly evenly between limits of 20 and 150 feet per second.

LANDING CONFIGURATION (δ_f = 55°). Vortex data in this configuration is limited to 33 data points, only one of which (106 ft/s) exceeds 85 ft/s, the rest being scattered between 20 and 85 ft/s. Vortex core diameters tend to be large (>10 feet), but an unexpectedly small value (5 feet) was found on one run (figure B-22).

In summary, the three airplanes in this group, as expected, exhibit generally similar characteristics, and it appears that the Hoffman-Joubert logarithmic velocity distribution gives a close approximation to the velocity distributions found on all three airplanes in all flight configurations tested.

LOCKHEED C141 AIRPLANE (UNPUBLISHED DATA).

A limited amount of vortex flight testing was performed on this airplane because of the short time for which it was available and the unfavorable wind conditions existing at that time. Twenty-four test runs were made (takeoff, 8; holding, 6; and landing, 10) in winds as high as 39 ft/s. For all but runs 3-7 and 21-24 (i.e., 9 runs of the total of 24), the meteorological recording equipment malfunctioned and no wind data was obtained for runs 1 and 2, and 8-20. Spot readings on backup equipment located at 140 feet indicate however that the windspeed was high. The gross weight of the airplane during the 24 test runs was between 218,200 and 186,000 pounds, very low weights for this airplane which has a maximum takeoff gross weight (MTOGW) of 316,000 pounds. By configuration, the equivalent airspeeds and flap settings during these tests were:

	Takeoff	Holding	Landing
EAS, Knots	110 - 120	200 - 210	113 - 125
Flap Setting (Percent Full)	75	0	100

The span loading at the median weight was 1,260 pounds per foot (lb/ft) (202,000 pounds ÷ 160 feet), which is very nearly the value that was obtained on the Boeing 727, for example. A plot of peak-recorded velocity versus vortex age is presented in the next section, and figures B-31 through B-36 present six representative vortex tangential velocity distributions (two per configuration, one upwind and one downwind). Only three peak velocities (of a total of 43 recognized) exceeded 100 ft/s. The highest values (up to 140 ft/s) were recorded in the holding (flaps zero, gear up) configuration, and the lowest in landing (none greater than 74 ft/s). In the takeoff configuration, peak velocities were scarcely greater (none greater than 78 ft/s) than those in landing. The above tabulation shows that the takeoff flap setting for this airplane is quite large, 75 percent of the maximum. Peak velocity has been found to vary with flight configuration on other airplanes (Boeing 707 and 747) and the results found on the C141 are quite consistent, in terms of their variation with flap setting, though the absolute values are low.

In view of the extremely high winds that were blowing during the C141 vortex tests (up to 39 ft/s, when 5-10 ft/s would be desired), it is unsafe to draw conclusions on this limited sample of data. The span loading was comparable to that computed for the Boeing 727 (reference 11) and significantly lower than those computed for the Boeing 707 (reference 7, span loading 1,320-1,810 lb/ft), even allowing for the disparity in span loading, the peak velocities recorded for the C141 are low, and the reason for this is probably wind shear, a factor that is particularly important in this group of tests because of the unusually high winds (with greater flexibility of timing, the tests on this airplane would have been delayed until a more suitable windspeed occurred) and the large size of the airplane (span 160 feet; cf tower height 140 feet) exceeded only by the Boeing 747 and the Lockheed C5A.

Until further tests on this airplane are performed, at more representative gross weights and in the presence of much less wind shear, the true vortex tangential velocity distribution is a matter of conjecture. The general form of the distributions in figures B-31, B-32, and B-35, B-36 is typical of what was found on this airplane, and like that found on the other airplanes discussed in this report, is described by the logarithmic relationship deduced by Hoffman and Joubert (reference 19). In figures B-33 and B-34, the profiles have not developed along the visual lines. In the 'upwind' half of the vortex (i.e., that half of the vortex in which the tangential velocity opposes the wind), a very different kind of flow is apparent--one in which the peak velocities have evidently been clipped. In the other half of the vortex--'downwind' half, the velocity distribution is still not very close to the logarithmic--it falls off more rapidly than usual from the peak value.

LOCKHEED C5A AIRPLANE (UNPUBLISHED DATA).

Thirty-three vortex test runs were made with this, the largest airplane in the study group. As with the C141 vortex tests, weather conditions were less than ideal, but the limited availability of the airplane precluded postponement in anticipation of better conditions. At all times, the wind was extremely light, approaching a dead calm. As a result of this, despite the proximity of the airplane to the tower on the majority of the test runs, no vortex reached the tower in less than 45 seconds, some taking more than 90 seconds. All vortices intercepted were "downwind" or first vortices. The "upwind" (second) vortices under the conditions prevailing were not expected to drift towards the tower and none did.

Of the 33 runs, 11 were made in takeoff configuration (δ_f = 16°, gear down); 8 in holding configuration (δ_f = 0°, gear up); and 14 in landing configuration (δ_f = 40°, gear down). Airplane gross weight was between 513,000 pounds and 460,000 (W/b = 2,310 and 2,070 lb/ft). The equivalent airspeeds during these tests, by configuration, were as follows:

	Takeoff	Holding	Landing
EAS, Knots	130 - 140	190 - 200	118 - 126

Characteristically, the highest peak tangential velocities were recorded in the holding configuration, though these values were low, considering the high span loading. In the other two configurations, peak tangential velocities were scattered between 40 and 75 ft/s.

As with the C141 vortex results, though for different reasons, no conclusions should be drawn from the data so far presented. Ground effect in this instance is probably considerable on account of the extreme size of the airplane. The important dimensions in a test of this kind are tower height (140 feet), airplane wingspan (222 feet) and airplane altitude (above ground level (AGL)) abeam of the tower (204-288 feet). A 115 ft/s velocity at 98 seconds was recorded on one run. That such a high velocity should still exist at all 98 seconds after the passage of the airplane, is indication enough that under better wind conditions, using a tower the height of which more closely approximated the wingspan of the airplane (at least that), the true envelope of peak velocities would be very different from that suggested by the data presented in the next section (outside of the 115 ft/s--98 seconds point mentioned). Having regard for the results of reference 6, in which low age vortices (10 to 15 seconds) produced peak velocities greater than 200 ft/s (one of 270 ft/s), but no data is presented after 80 seconds (final point is actually 71 ft/s at 78 seconds), the present data, without a careful consideration of the extremely limiting conditions under which it was gathered, could be dangerously misleading. Elsewhere in this report, qualitative arguments have been put forward in an attempt to account for differences caused by flap deployment, in the wake of a particular airplane. These differences were particularly noticeable on the Boeing 707 and 747. The Lockheed C5A (and C141) differ from these in several important respects, which might be expected to influence the basic wake and the way in which it is affected by flap deployment. The high-wing configuration, with the unbroken top surface that it presents, yields a better lift "carry-over" than the low-wing configuration. The flap configuration does not feature the cut-out behind the inboard engines found on the two Boeing airplanes, mainly because the high-wing configuration permits the engines to be mounted a greater distance below the wing itself, and the flap deflections are smaller. Reference 7 shows that on the Boeing 707 airplane in the landing configuration, the level of engine thrust influences the vortex core diameter and peak tangential velocity--in that configuration, the efflux of the outboard engine evidently becomes entrained in the center of the vortex springing from the end of the flap. A lower relative location of the engine, such as is possible on high wing airplanes (despite the considerable negative dihedral that is apparent when the airplane is at rest on the ground), would change this picture somewhat and less of the high-energy efflux would be entrained in the vortex center. Add to these factors the higher aspect ratio of the C5A wing, the reduced sweepback (approximately 10° less than on the B747) and the more inboard location of all four engines, and it is apparent that the C5A wake does not necessarily develop according to the same pattern as does the wake of the B747. In the absence of further measurements, it must be assumed that the C5A generates a more severe and larger wake than does the Boeing 747.

Representative tangential velocity distributions for the three configurations tested are presented in figures B-37 through B-42. The peak recorded velocities for the C141 and C5A by configuration are presented in table 2.

TABLE 2. ABSOLUTE PEAK VELOCITIES FOR THREE FLIGHT CONFIGURATIONS, C141 AND C5A AIRPLANES

	Airplane Configuration					
	Takeoff		Holding		Landing	
Airplane	δ_f (Degrees)	$V_{\theta_{max}}$ (ft/s)	δ_f (Degrees)	$V_{\theta_{max}}$ (ft/s)	δ_f (Degrees)	$V_{\theta_{max}}$ (ft/s)
C141	30	78	0	140	40	74
C5A	16	73	0	115	40	67

LOCKHEED L1011 AIRPLANE (REFERENCE 9).

Representative tangential velocity distributions are presented in figures B-43 through B-54, as follows:

TAKEOFF CONFIGURATION (δ_f = 10°). The vortex core diameters are uniformly small ($2\ r_c \cong 2$ feet). This is consistent with what was found on the Boeing 747 which also uses a 10-degree flap setting at takeoff. The wing-mounted engines of the L1011 airplane are mounted at 44 percent of the semispan, while the outboard flap segment terminates at 77 percent semispan. It is questionable then, whether the small flap setting used in this flight configuration causes the development of a separate and distinct flap vortex. The expected wake development, therefore, is a rapid rollup into two vortices, very little different in velocity distribution from those generated in the flaps-up configuration. Certainly, the velocity distributions of figures B-43 through B-46 are near-perfect examples of the logarithmic form of velocity distribution. The peak velocities, which are extremely localized, as evidenced by the very tight cores formed, vary between limits of 135 and 225 ft/s.

TAKEOFF/APPROACH CONFIGURATION (δ_f = 25°). As its name implies, this is an intermediate configuration, using a flap setting midway between the normal settings for takeoff landing (i.e., 10° and 42°). The tangential velocity distributions (figures B-47 through B-50) are characterized by a somewhat larger core diameter ($2\ r_c \cong 4$ feet), and correspondingly smaller peak velocity (range of values, 105 to 135 ft/s), though there are not enough data points to determine what the upper bound might eventually be. As with the takeoff configuration, the form of the velocity distribution is logarithmic as described by the Hoffman-Joubert equation.

LANDING CONFIGURATION ($\delta_f = 42°$). Four typical velocity distributions in this configuration are presented in figures B-51 through B-54. The vortex core diameters are uniformly small ($2r_c \cong 2 - 4$ feet) and the peak velocities fall between 80 and 125 feet per second. The velocity distributions are again of the logarithmic form.

The trailing vortices of the L1011 airplane are like those of the Boeing 727 and the McDonnell-Douglas DC9 in that they are characterized by an apparent insensitivity to airplane flight configuration--that is to say, regardless of the flap setting, the vortices were consistently of small core diameter and high peak velocity. This is in contrast to the situation found on certain airplanes with four wing-mounted engines (Group I, for example), whose wake is strongly affected by flap configuration. It now seems very evident, in light of the L1011 results, that the outboard engine efflux of the Group I airplanes strongly influences the velocity distribution of the vortices springing from the end of the flap, when the latter is at a large deflection. The L1011 engines are not situated at the termination of the flaps, but are in the location occupied by the inboard engines of four-engined airplanes. If the airplane could be flown with the inboard flap segments at a large deflection, and the outboard segments neutral, this would place the engines at the flap termination and it would then be instructive to see if a separate flap vortex (as opposed to a wingtip vortex) developed, and if the vortex core was large in diameter and the peak velocity correspondingly smaller.

McDONNELL-DOUGLAS DC10, SERIES 10, AIRPLANE (REFERENCE 10).

Six representative velocity distributions are presented in figures B-55 through B-60. Predictably, they are very similar to those of the trailing vortices produced by the L1011 airplane.

TAKEOFF CONFIGURATION ($\delta_f = 10°$). Vortex core diameters are 1 to 2 feet and the highest peak velocity 184 feet per second. Velocity distribution follows the logarithmic equation.

LANDING CONFIGURATION ($\delta_f = 35°$). As was found with the L1011 airplane (which uses a 42-degree flap angle in landing configuration), the vortex core diameters were not greatly affected by the full deployment of the flap. Vortex core diameters remained small (1.5 to 5.0 feet). The highest peak-recorded velocity was 160 ft/s.

The general remarks made concerning the L1011 are equally applicable to the DC10, since there has been no indication that the difference in the mounting of the central engine (which is the only immediately apparent external difference between the two airplanes) materially affects the development of the wake in any airplane flight configuration.

The peak recorded velocities, for the L1011 and DC10, by configuration are outlined in table 3.

TABLE 3. ABSOLUTE PEAK VELOCITIES FOR FOUR FLIGHT CONFIGURATIONS, L1011 and DC10 AIRPLANES

	Airplane Configuration							
	Takeof		Cruise		T/O-Approach		Landing	
Airplane	δ_f (Degrees)	$V_{\theta_{max}}$ (ft/s)	δ_f (Degrees)	$V_{\theta_{max}}$ (ft/s)	δ_f (Degrees)	$V_{\theta_{max}}$ (ft/s)	δ_f (Degrees)	$V_{\theta_{max}}$ (ft/s)
L1011*	10	225	0	125	25	135	42	125
DC10**	10	192	0	95	22	65	35	160

*Two data points only in cruise configuration.
**Two data points only in cruise, four in takeoff-approach.

BOEING 727, SERIES 100, AIRPLANE (REFERENCE 11).

The vortex tangential velocity distributions measured on this airplane (figures B-61 through B-64) are characterized by small core diameters in all three airplane flight configurations tested. The flap configuration of the B727 does not differ greatly from that of the B707, with which it was found that vortex peak velocity and core diameter were strongly influenced by the degree of flap deflection. Both airplanes employ triple-slotted chord-extending flaps arranged in two segments per side, with upper surface spoilers ahead of the flaps, inboard "high-speed" ailerons set between the inboard and outboard flap segments, and "low-speed" ailerons outboard. Because of this general similarity, it is suspected that the configuration sensitivity that is found in the B707 vortex velocity distributions, and is absent in the B727 vortices is attributable in some manner to the presence of engines, particularly the outboard engines, on the wing of the B707, and to their absence on the B727 wing. In reference 7, figure 13, it is shown that in the B707 vortex tests, a lower peak velocity occurs in the vortex adjacent to an outboard engine when that engine is producing its share of the total thrust required, and a higher peak velocity is found in that vortex when the engine is throttled back to flight idle. As has always been found, the higher peak velocity is associated with a smaller core diameter. A further step, not yet taken because it is not without an element of risk at low altitude and low airspeed, would be to throttle the engine back to an even lower level of thrust, down to zero net thrust, if this is possible.

Appendix A of reference 11 shows that the vortex core diameters were uniformly small (never greater than 3 to 4 feet) irrespective of the airplane flight configuration. During the time scale of the tests (vortex ages were from 5 to 120 seconds), the only detectable change in vortex structure was the decay of the peak tangential velocities.

McDONNELL-DOUGLAS DC9, SERIES 10, AIRPLANE (REFERENCE 12).

A limited number of data runs were made with this airplane in the takeoff configuration (9 out of 61) and the balance were made in the landing configuration. The corresponding flap angles were 20° (takeoff) and 50° (landing). It is quite apparent that as was found with the Boeing 727, the DC9 trailing vortices have consistently small diameter cores ($2r_c$ equals 1-2 feet) in both configurations tested. The only perceptible difference between configurations was in the magnitude of the peak velocities, as shown in the table 4.

TABLE 4. COMPARISON BY AIRPLANE TYPE AND FLIGHT CONFIGURATION OF PEAK TANGENTIAL VELOCITIES IN B727 AND DC9 WING TRAILING VORTICES

	Takeoff (ft/s)	Landing (ft/s)
DC9 min/max peak velocity	70 - 120	30 - 130
B727 min/max peak velocity	20 - 210	30 - 260

The corresponding span loadings and wing loadings are, approximately:

	Span Loading (W/b) (lb/ft)	Wing Loading (W/S) (lb/ft^2)
DC9	830	80
B727	1,220	78

This shows clearly enough that span loading governs the strength of the vortices independently of the wing loading, as is indicated by the basic expression

$$L = \rho V \bar{\Gamma} b$$

$$\bar{\Gamma} = \frac{1}{\rho V} \cdot \frac{W}{b} \qquad (19)$$

Figures B-65 through B-67 are a representative sample of DC9 vortex velocity distributions in takeoff and landing configurations. All six are of comparatively low age vortices, and there is some evidence of the presence of secondary vortices and incompletion of vortex rollup. The results obtained on this airplane are the least affected by ground effect in the whole program, simply because of the relatively small wingspan (less than 90 feet).

DOUGLAS DC7 AIRPLANE (REFERENCE 13).

All vortex measurements on this airplane were made using the 4-foot sensor spacing, and this has made the determination of the velocity distribution in the vortex more difficult and less certain. A large number of runs were made and the results are presented in appendices E and G of reference 13. The results may be summarized as follows:

Takeoff configuration (δ_f = 20°) produced the lowest peak velocities, with a range of values from 30 to 140 ft/s, with most points concentrated between 35 and 100 ft/s. The wide spacing of the instrumentation reduced the chances of intercepting the peak velocity, as in many cases the core diameter of the vortex appears to be less than 4 feet, while the maximum is about 8 feet.

In holding configuration (δ_f = zero), the range of peak velocities is 30 to 180 ft/s, with the majority of values between 30 and 100 ft/s. The vortex cores are uniformly small in diameter (2 to 5 feet), as would be expected in this clean configuration.

In landing configuration (δ_f = 40 or 50°), the range of peak velocities and their distribution between the limits do not differ from what was found in the holding configuration. Core diameters were also found not to differ significantly from the values found in that configuration.

SLIPSTREAM ROTATION. The propellers rotate clockwise (viewed along the line of flight), so that port-side propellers rotate with the adjacent tip vortex and the starboard-side propellers rotate against the adjacent tip vortex. It was found that in takeoff configuration only, this produced a marked effect on vortex peak velocities. When there is like-rotation of propeller and vortex, the peak velocities are scattered fairly evenly between limits of 35 and 135 ft/s. When propeller and vortex rotate in opposite senses (starboard wing), 41 out of 43 values of peak velocity fall between 35 and 65 ft/s. The remaining two values are still less than 90 ft/s.

TANGENTIAL VELOCITY DISTRIBUTION EXTERNAL TO CORE. The wide sensor spacing used in this particular group of vortex flight tests leaves too much uncertainty about the true peak velocity and the core diameter for any precise mathematical representation of the overall velocity distribution to be possible. It appears, however, from an inspection of the velocity distributions of appendix E of reference 13, that the logarithmic form used with considerable success on the other results would also describe quite well the DC7 trailing vortices. This is to be expected, as the other results, which cover a wide range of transport aircraft design configurations, tested in flaps up and flaps down conditions, are well described by the logarithmic distribution.

SUMMARY--VORTEX VELOCITY DISTRIBUTIONS.

Summarizing the findings on the velocity distributions of the vortices generated by the different groups of airplanes, the following observations may be made. The arrangement of the subject airplanes into groups characterized by

certain geometric characteristics appears to have been justified. One result expected was that airplanes having four wing-mounted engines would show the greatest configuration dependence, in terms of two parameters descriptive of the vortex (i.e., core diameter and peak velocity), and that airplanes with no wing-mounted engines would show the least. Thus, the former group (four wing-mounted engines) uniformly show large variations in vortex core diameter and peak velocity, as a function of flap setting--small flap settings are associated with small vortex core diameters and high peak velocities, while large flap settings are associated with large core diameters and much lower peak velocities--while the latter group (all engines fuselage-mounted) exhibit very little variation in core diameter and peak velocity -- as a function of flap setting. This result is illustrated in figures B-1 through B-30 and B-61 through B-67.

The C141 and C5A vortex data was gathered under unfavorable conditions--in the case of the C141, the winds were very high throughout the entire test series, while for the C5A tests, the winds were nearly calm. Thus, in neither case is the data completely comparable with that for Group I airplanes which was gathered under more favorable conditions. The C141 data for takeoff and landing none the less indicates that core radius increases with increasing flap angle--on this particular airplane, the takeoff flap setting is large, being 75 percent of the setting for landing (which is 40°), and thus there is only 10° difference between takeoff and landing. In both configurations, the vortex velocity distributions are qualitatively like those found for the low-wing four-engine airplanes of Group I, in landing configuration. Sensitivity to flap setting is also apparent in the C5A data, although the peak velocities are all low on account of the age of the vortices--a result of the near-calm conditions mentioned above.

Airplanes having no wing-mounted engines (B727 and DC9) or only two, mounted fairly close in toward the fuselage (L1011 and DC10) are represented in figures B-43 through B-67, which show that airplanes in either of these two categories consistently produce vortices with small diameter cores, regardless of fl setting.

Finally, regardless of airplane type or flight configuration, whenever a data run yields a well-developed vortex with a clearly distinguishable axi-symetric flow pattern, the resulting velocity distribution most frequently conformed to the logarithmic circulation distribution of reference 19. Some prime examples of this are given in appendix B, figures B-4, B-5, B-10, B-11 (B747); B-15, B-16, B-18 (B707); B-19, B-21, B-23, B-25, B-28 (CV880); B-32, B-35 (C141); B-42 (C5A); B-43 through B-54 (L1011); B-55 through B-60 (DC10); B-61 through B-64 (B727); and B-65 through B-67 (DC9).

VORTEX PERSISTENCE/DECAY (OPERATIONAL CONSIDERATIONS)

GENERAL.

Of concern to air traffic control (ATC) is the persistence of aircraft trailing vortices and their possible presence along aircraft flightpaths. Vortex characteristics may adversely affect the pilot's ability to operate his airplane safely in controlled airspace. Knowing the limits of this "hazardous" persistence, air traffic may be separated accordingly, to minimize the risk of an encounter.

The previous section discussed vortex characteristics and modeling as a function of aircraft type and flight configuration. This section discusses vortex decay.

Knowing the characteristics of the vortex flow field, that is the distribution of tangential velocity and its persistence, and the response of an encountering aircraft, one may then determine limits in terms of time or distance wherein the vortices are hazardous. This is the subject of discussion in the next section.

DETAILS OF APPROACH.

In this section, qualitative and quantitative data from full-scale flight test vortex measurements using tower fly-by and vortex flow visualization are examined. Major details of the test aircraft, configuration, weights, test procedures, instrumentation, and data acquisition are listed either in appendix A or in the references and, with certain exceptions, will not be repeated.

A desirable consideration in the analysis of vortex behavior is the correlation of vortex persistence and decay with the atmospheric conditions under which the tests were conducted.

Various parameters were considered for correlation of vortex persistence and decay mode with some index of atmospheric conditions. These indices were Richardson number (R_i), power spectral density analysis of atmospheric turbulence, wind direction/speed index (DSI), wind velocity, and atmospheric turbulent dissipation rate, $\epsilon^{1/3}$. Lack of time, certain data acquisition difficulties, and test aircraft availablity only permitted correlation of vortex persistence with ambient wind-speed and for the B727 tests with the atmospheric turbulent dissipation rate parameter.

The tower fly-by portion of the flight-test program originally called for gathering data for four different ambient wind ranges, 0-5, 6-10, and 11-15 and >15 knots, and data on the vertical temperature gradient over the span of the tower. The sensitivity of the Richardson number (R_i) to temperature gradients and, therefore, to the accuracy of temperature measurements, however, precluded use of this parameter because accuracy, unobtainable with the available instrumentation, was required at the five levels of temperature sensors on the 140-foot-high measurement tower.

For vortex investigations at altitude, using flow visualization, the only reliable detailed meteorological data was that gathered during the investigation of B727-200 vortices during climbout and turning flight. Otherwise, only pilot comments were available on the atmospheric turbulence, and these were necessarily subjective.

The limited availablility of aircraft for flight testing did not permit testing under a sufficiently wide range of atmospheric conditions, to permit relating vortex persistence to atmospheric conditions. For example, as mentioned earlier, the C5A tower fly-by tests were conducted under near-calm conditions whereas the C141 tests were performed in very high winds with speeds from 20 to 35 knots.

The tower fly-by technique for vortex investigations and the associated meteorological instrumentation has already been discussed in the various references. For the vortex flow-visualization tests with the B727-200, a Cessna 402 airplane was instrumented for the measurement of turbulence, temperature, relative humidity and windspeed and direction.

Because of: (1) the relatively small height of the test towers (200 feet at Idaho Falls and 100 and 140 feet at NAFEC); (2) inadequate theories for prediction of vortex settling; and (3) atmospheric stability, buoyancy and wind effects on vortex characteristics and transport, it would have been advantageous to equip all the test aircraft with a vortex flow visualization system. This was impractical, however, for reasons of cost and time, and only the B747 and B707 (for Idaho Falls tests) and the CV880 and B727-200 (for Edwards Air Force Base tests), were so equipped. The B727-100, was used for tower fly-by testing at NAFEC and Idaho Falls, while the B727-200, with a vortex flow visualization system, was used at Edwards Air Force Base.

For the first three aircraft, the vortex marking was accomplished by injecting CORVUS oil into the exhaust system of the outboard engines, with a resultant dense white smoke. The CV880 installation and operation is shown in figures 3 and 4.

For the B727-200 airplane, the modification was accomplished by the installation of CORVUS oil smoke generators, one at each wing tip (figures 5 and 6).

For the upper altitude flow-visualization tests, a K-38 aerial camera, mounted on three-axis gimbals was used. This camera has a 36-inch focal length lens and uses 9-inch aerial film. Each negative is 9 inches by 18 inches in size. The total angular field of view is 14° by 28°. Telescopes mounted on each side are boresighted near the leading edge of the film format and are used for tracking the aircraft as it passes overhead. Normally, a frame rate of 1 per 10 seconds was used. The vortex flow-visualization studies were conducted with the CV880 at NAFEC and the B727-200 at Edwards Air Force Base.

For the tower fly-by tests, flow-visualization was also provided by colored smoke grenades mounted at seven levels on the tower as shown in figure 7.

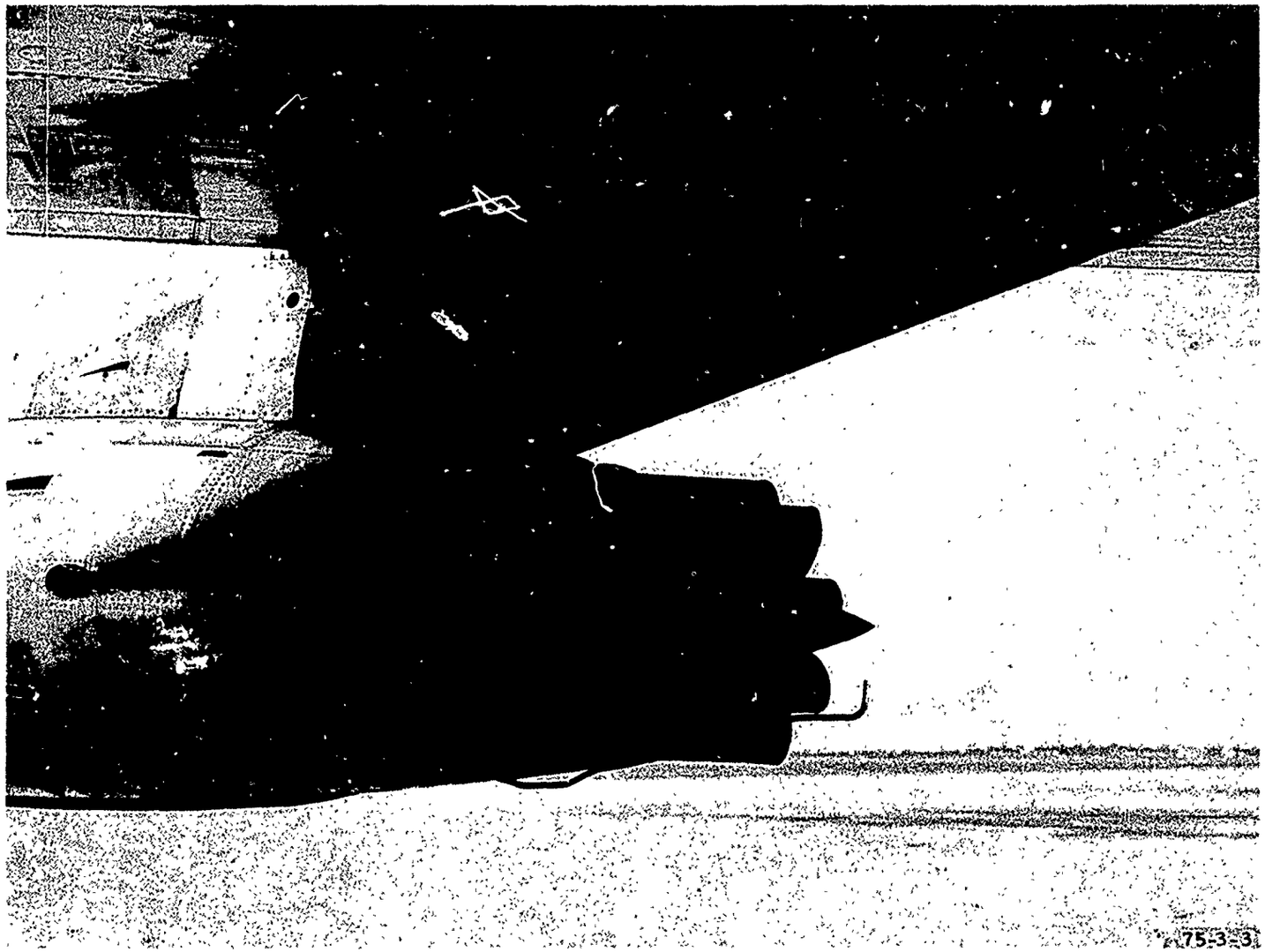

FIGURE 3. CV880 OUTBOARD ENGINE SMOKE OIL FLOW LINE FOR VORTEX MARKING

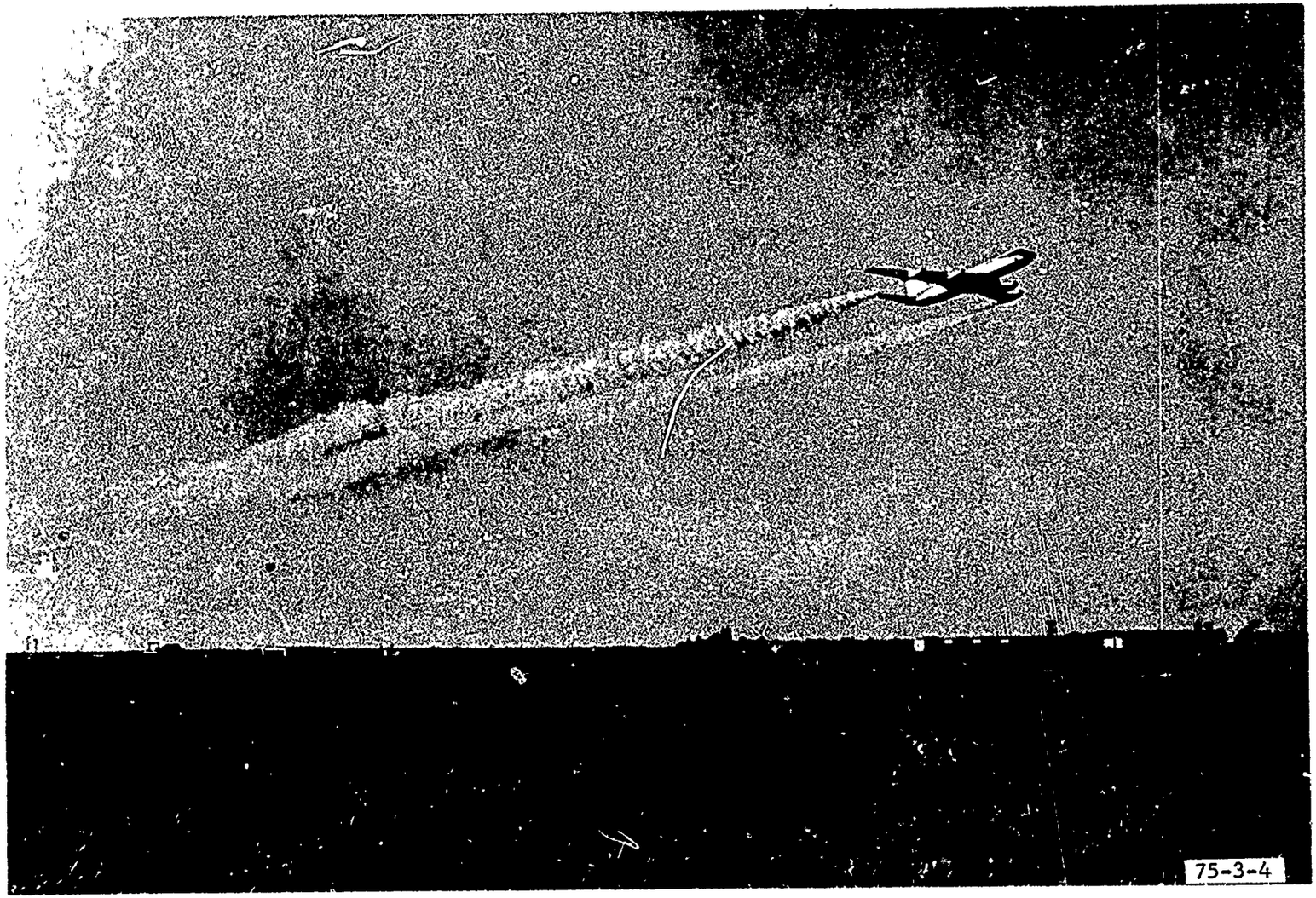

FIGURE 4. CORVUS OIL SMOKE GENERATOR IN OPERATION ON CV880

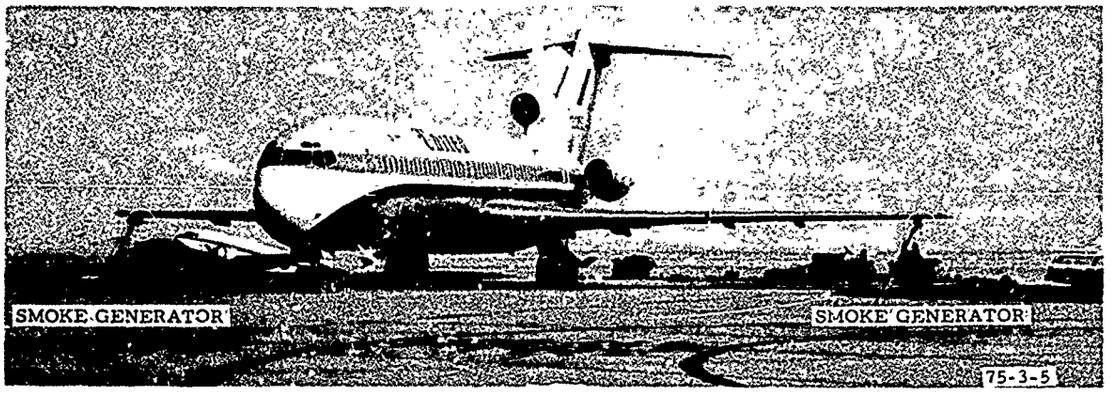

FIGURE 5. BOEING 727 FLIGHT TEST AIRCRAFT (MODIFIED WITH CORVUS OIL SMOKE GENERATORS)

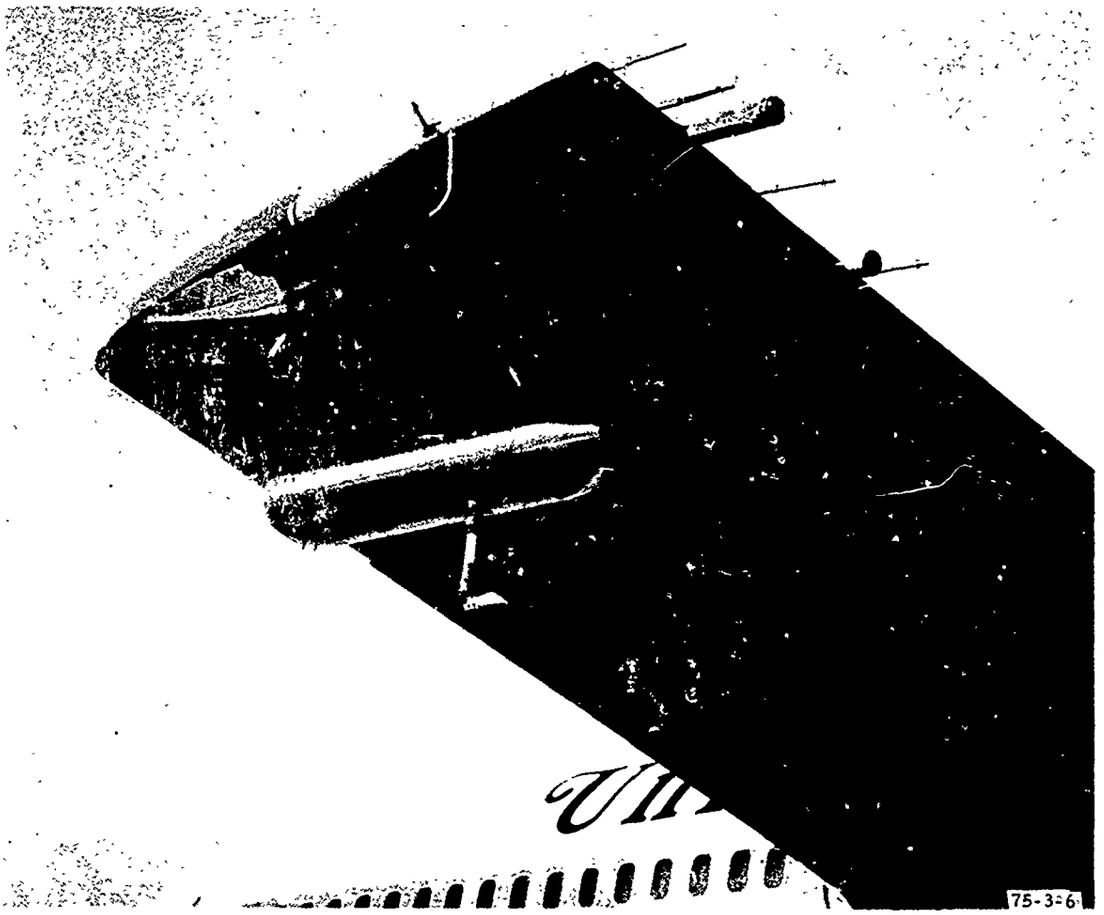

FIGURE 6. CLOSEUP OF CORVUS OIL SMOKE GENERATOR INSTALLED ON B727 WINGTIP

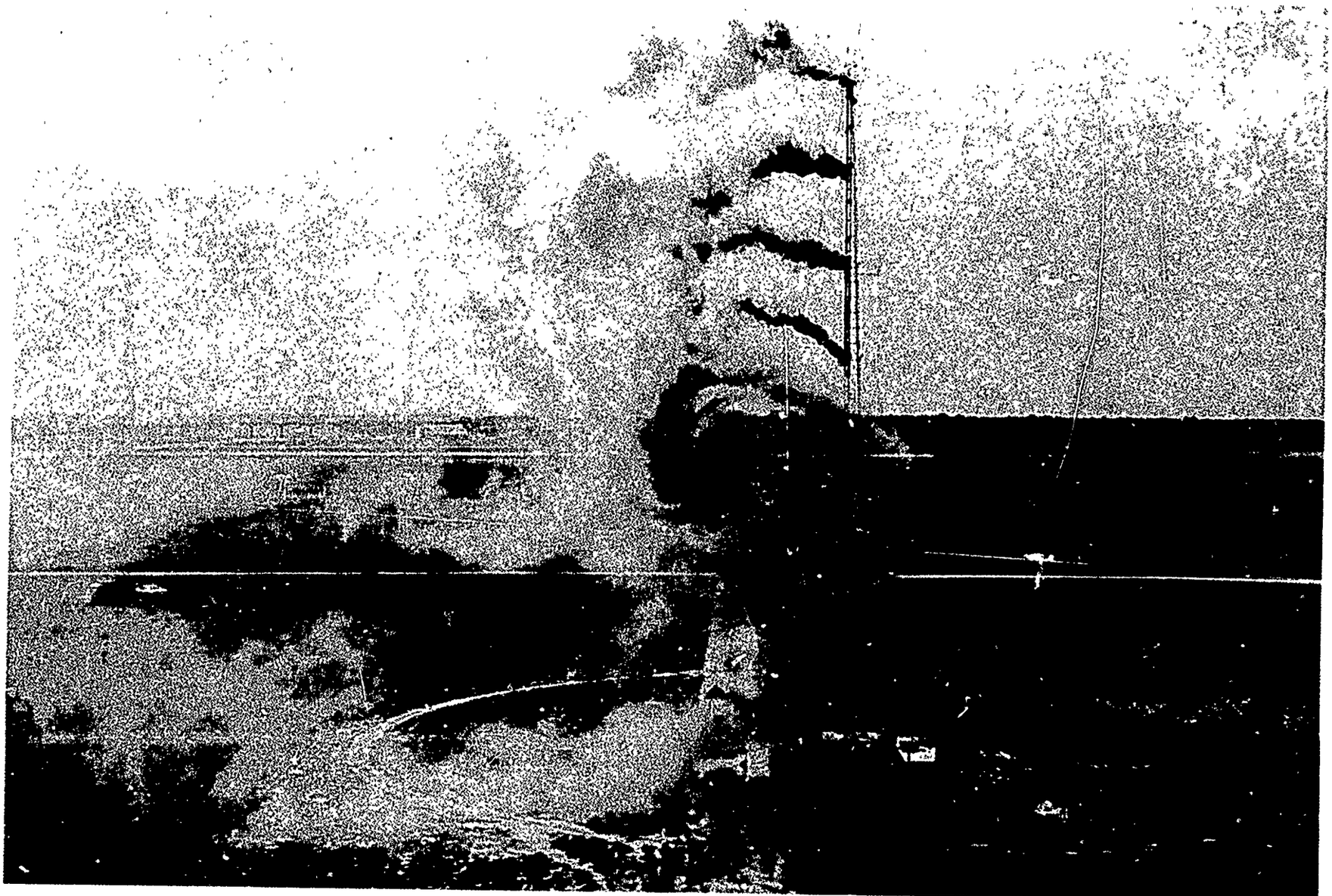

FIGURE 7. BOEING 747 WING VORTEX OUTLINED BY ENTRAINED SMOKE

TOWER FLY-BY DATA.

Summary plots of peak-recorded tangential velocity versus time are shown in figures 8 through 17. These plots show that vortex systems dissipate to insignificant tangential velocities by the time they are at most 120 seconds old. Nor were there any "orderly" vortex rotational flow fields after 90 to 120 seconds of vortex lifespan, the lifespan depending on aircraft model and configuration.

This upper limit for vortex age held regardless of aircraft model or configuration per model (including wing engines at idle thrust as for the B707 tests cited earlier). This was true for a variety of atmospheric conditions, including temperature inversion conditions and 180-degree wind shears within the 100- to 140-foot (NAFEC), 200-foot (Idaho Falls) height of the test towers. In addition, although a wide range of atmospheric conditions were not experienced during tests with any one aircraft, such can be said to be fairly true for the combination of all the aircraft tested. Accordingly, it is concluded that the vortices do not persist in hazardous form (as defined earlier and discussed in the next section) for longer than 2 minutes for any of the aircraft tested, regardless of configuration for flight within the earth's boundary layer.

Although quantitative data on vortex intensity cannot be obtained after tower passage, visually it was observed that the entrained colored smoke provided a good indication of the passage of the vortices as they passed through the tower, up to their complete dissipation by whatever mode. The B747 and L1011 vortices shown in figures 7 and 18 are typical examples of the vortex flow field.

Four major modes of vortex decay were observed during the tower fly-by tests. They have also been noted to occur during flight at higher altitudes, as discussed later. Two of them can be primarily attributed to vortex instability, the third to viscous dissipation, and the fourth to vortex interaction with the atmosphere.

CROW-INSTABILITY (SINUOUS MOVEMENT) ONSET, REFERENCE 23. The vortices undergo a sinusoidal instability with subsequent linking of the vortex pair, after which rapid disintegration of the vortex system occurs.

At times, the linking results in a series of vortex rings, but this is not always the case. This observation was possible with the NAFEC CV880 which had the dual CORVUS smoke oil vortex flow visualization system installed (figures 3 and 4), and when the test airplane was flown relatively high abeam of the tower, thus minimizing separation of the vortices due to ground effect. This instability is shown schematically in figures 19 and 20 and in flight, for the B747, in figure 21. The decay mechanism is discussed later in this report along with associated photographic coverage of the decay sequence at higher altitudes for the B747.

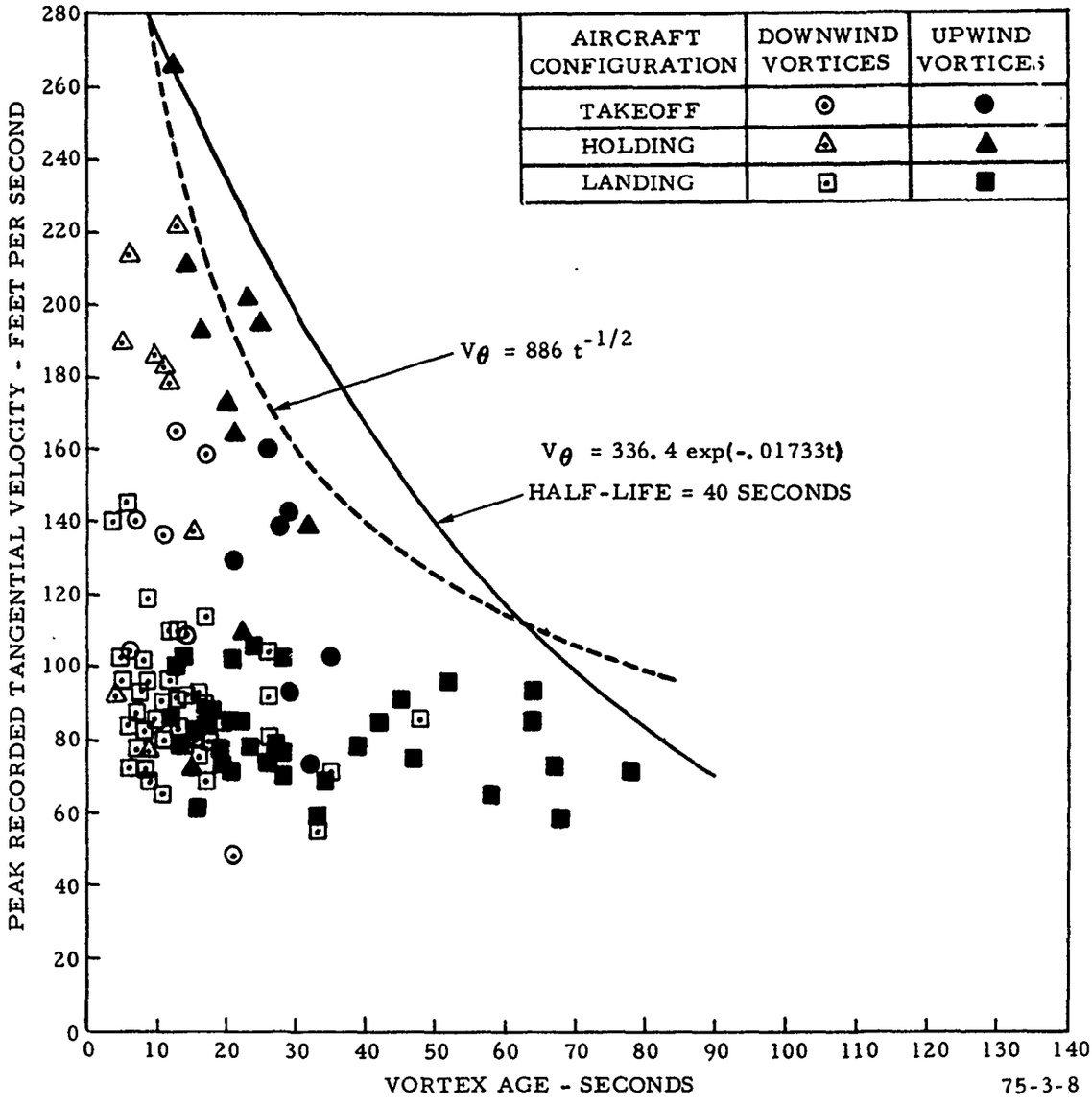

FIGURE 8. PEAK RECORDED TANGENTIAL VELOCITY VS. AGE (ALL CONFIGURATIONS--B747)

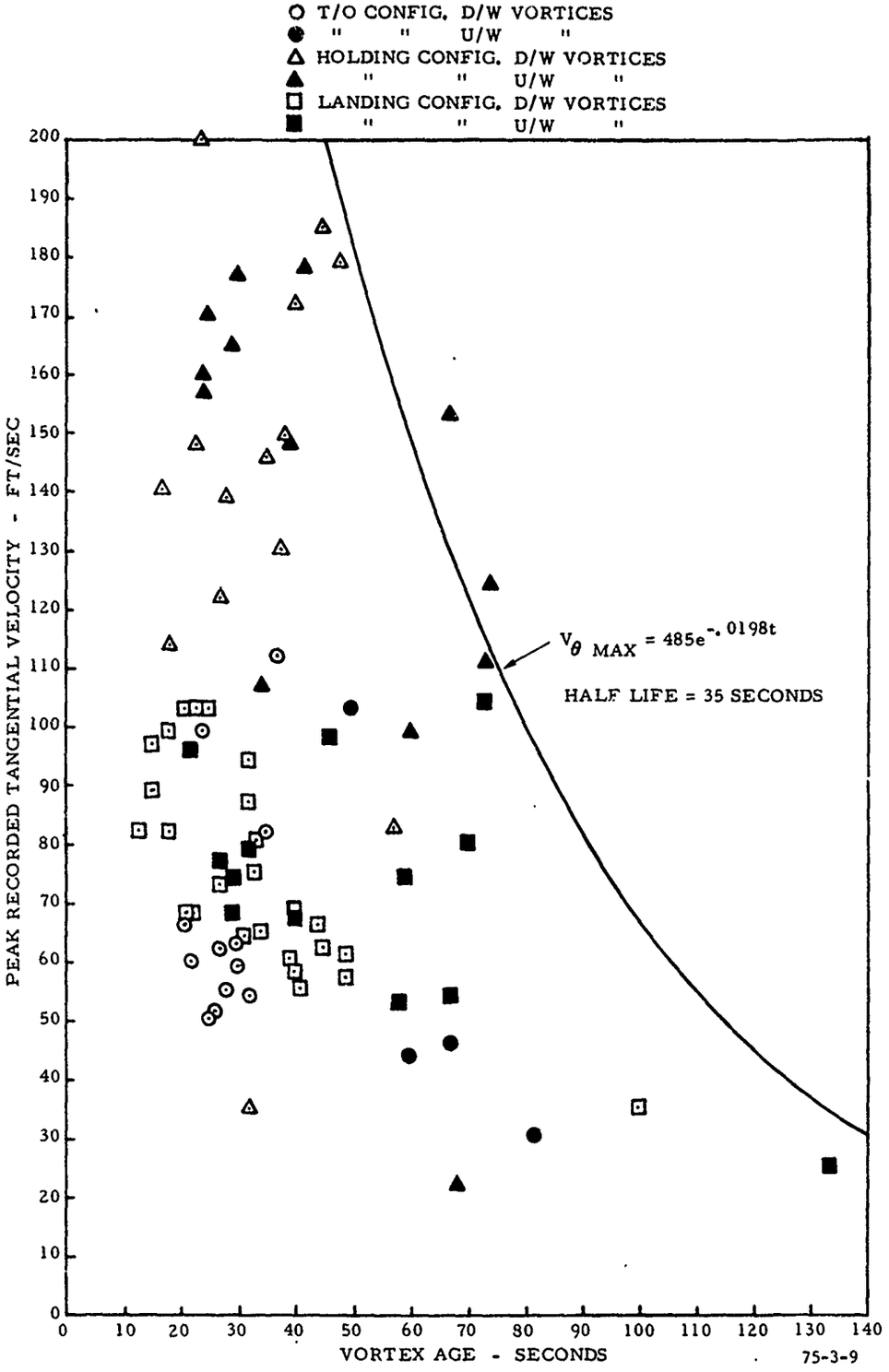

FIGURE 9. PEAK RECORDED TANGENTIAL VELOCITY VS. AGE (ALL CONFIGURATIONS--B707-320)

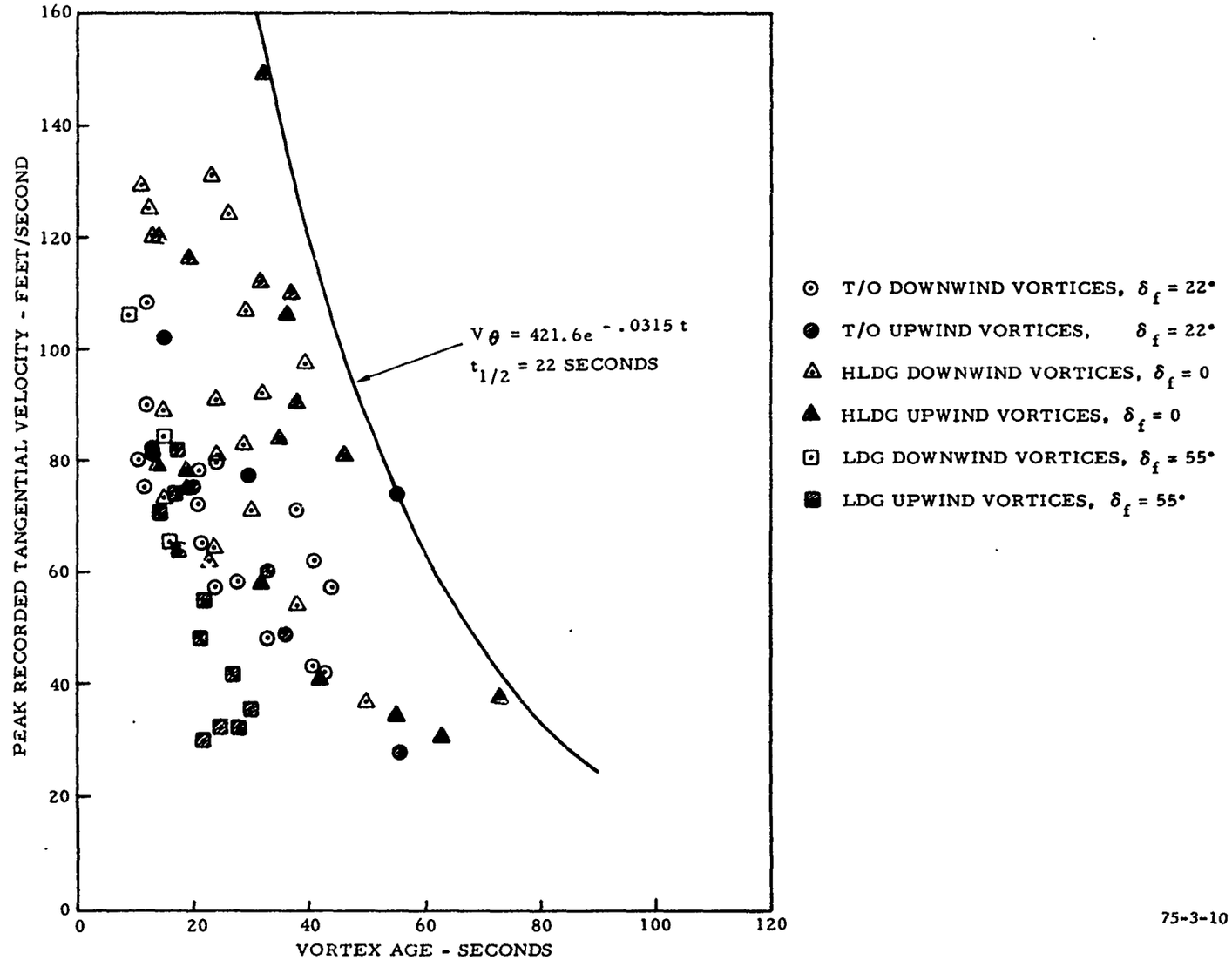

FIGURE 10. PEAK RECORDED TANGENTIAL VELOCITY VS. AGE (ALL CONFIGURATIONS--CV880)

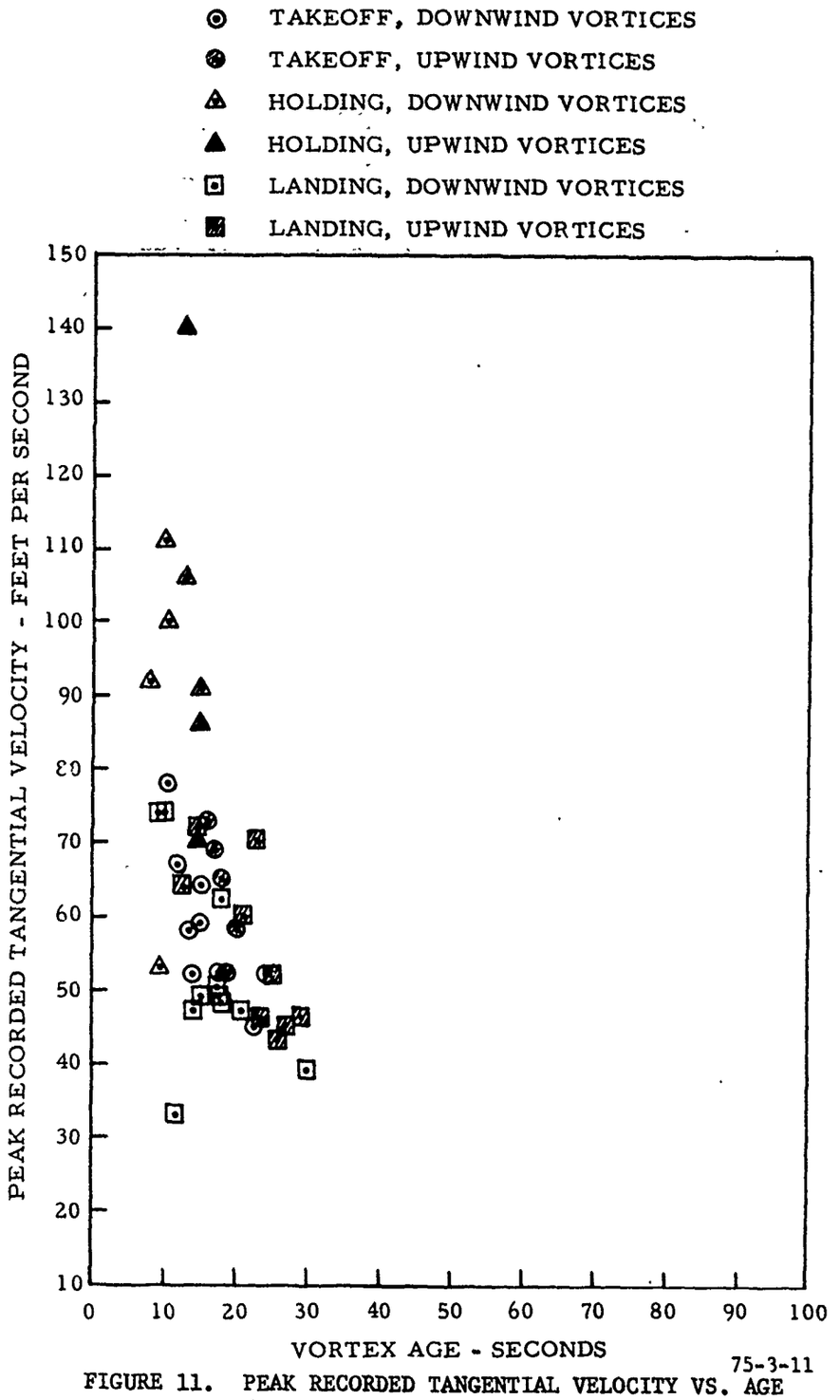

FIGURE 11. PEAK RECORDED TANGENTIAL VELOCITY VS. AGE (ALL CONFIGURATIONS--C141)

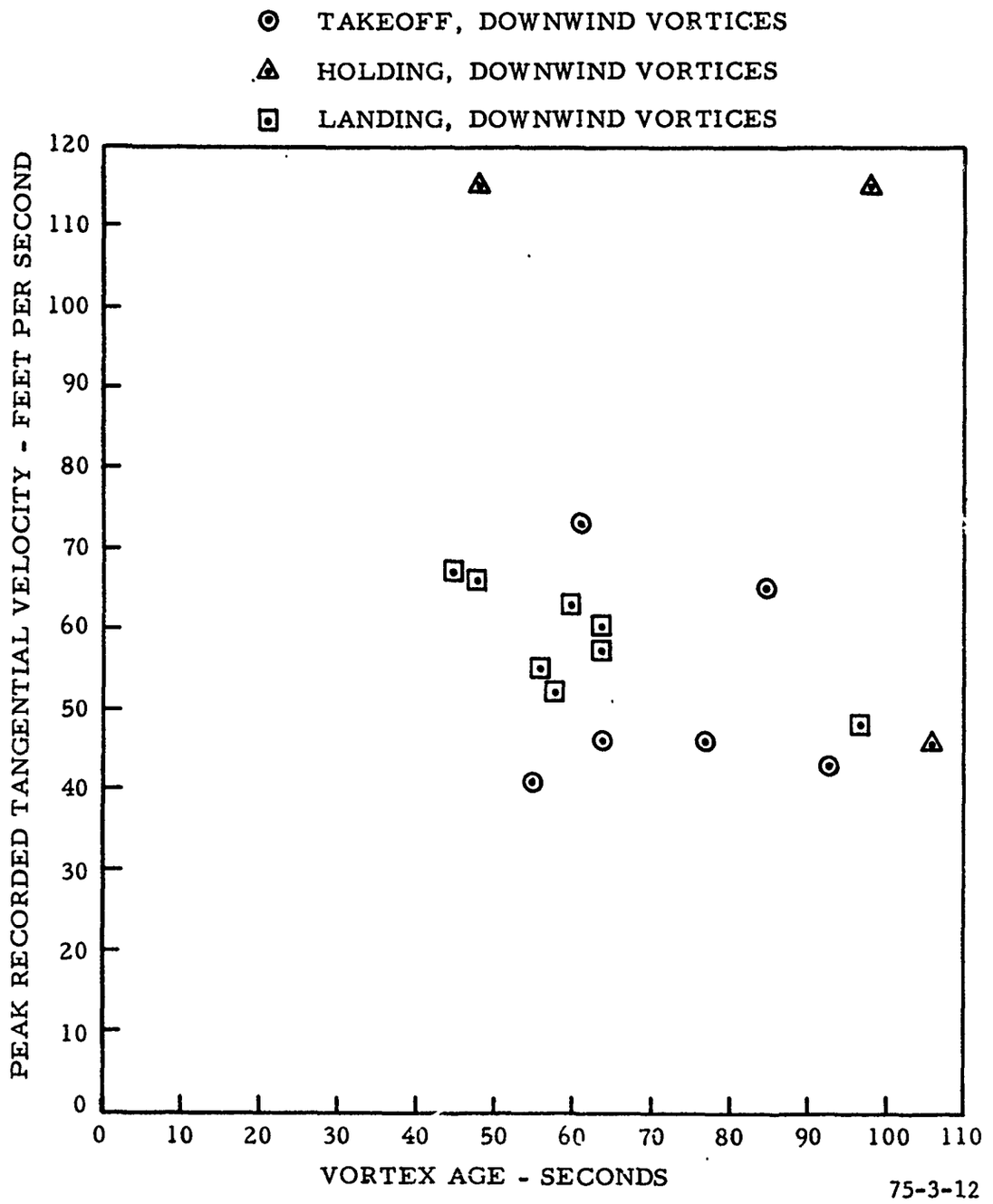

FIGURE 12. PEAK RECORDED TANGENTIAL VELOCITY VS. AGE (ALL CONFIGURATIONS--C5A)

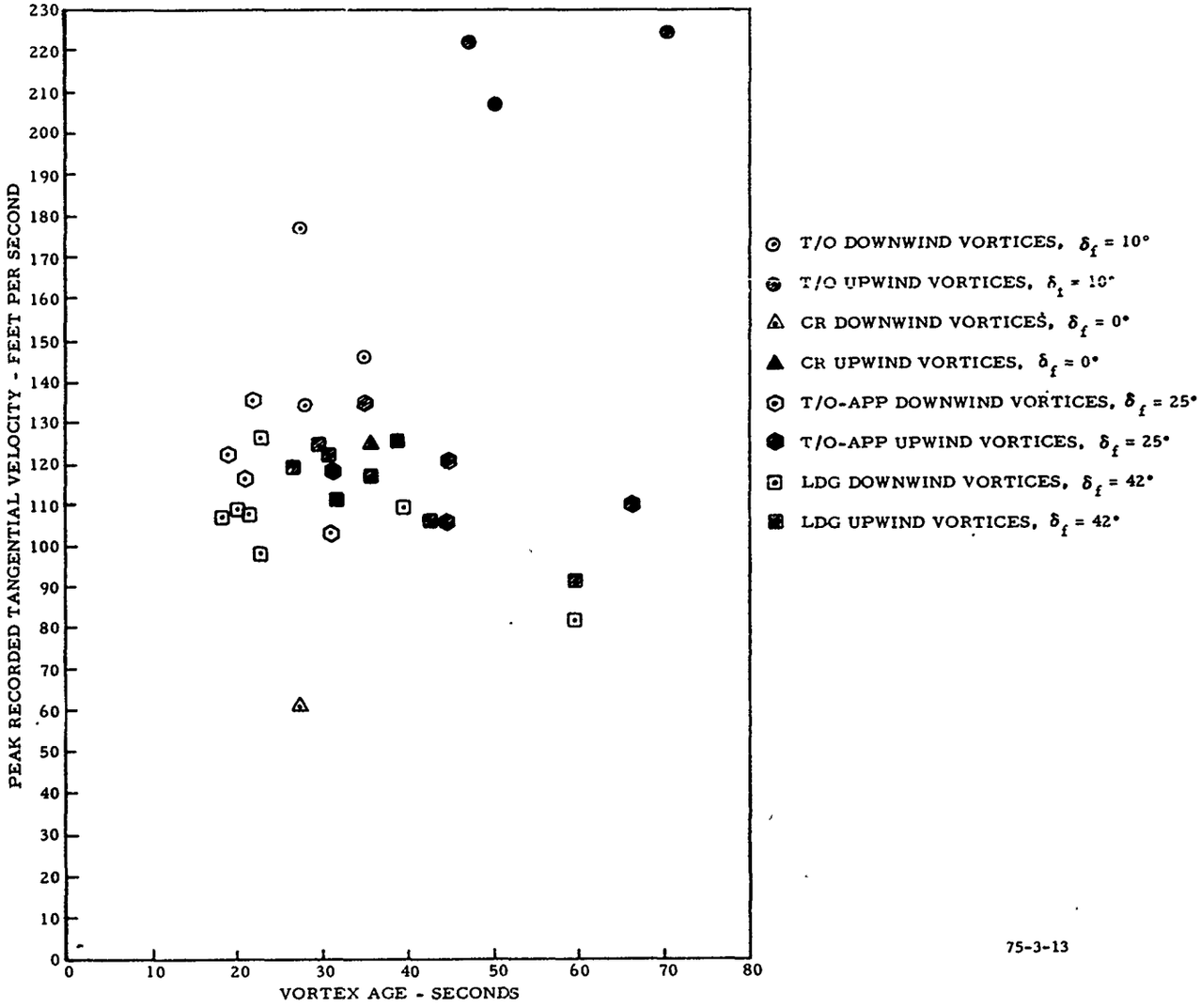

FIGURE 13. PEAK RECORDED TANGENTIAL VELOCITY VS. AGE (ALL CONFIGURATIONS—L1011)

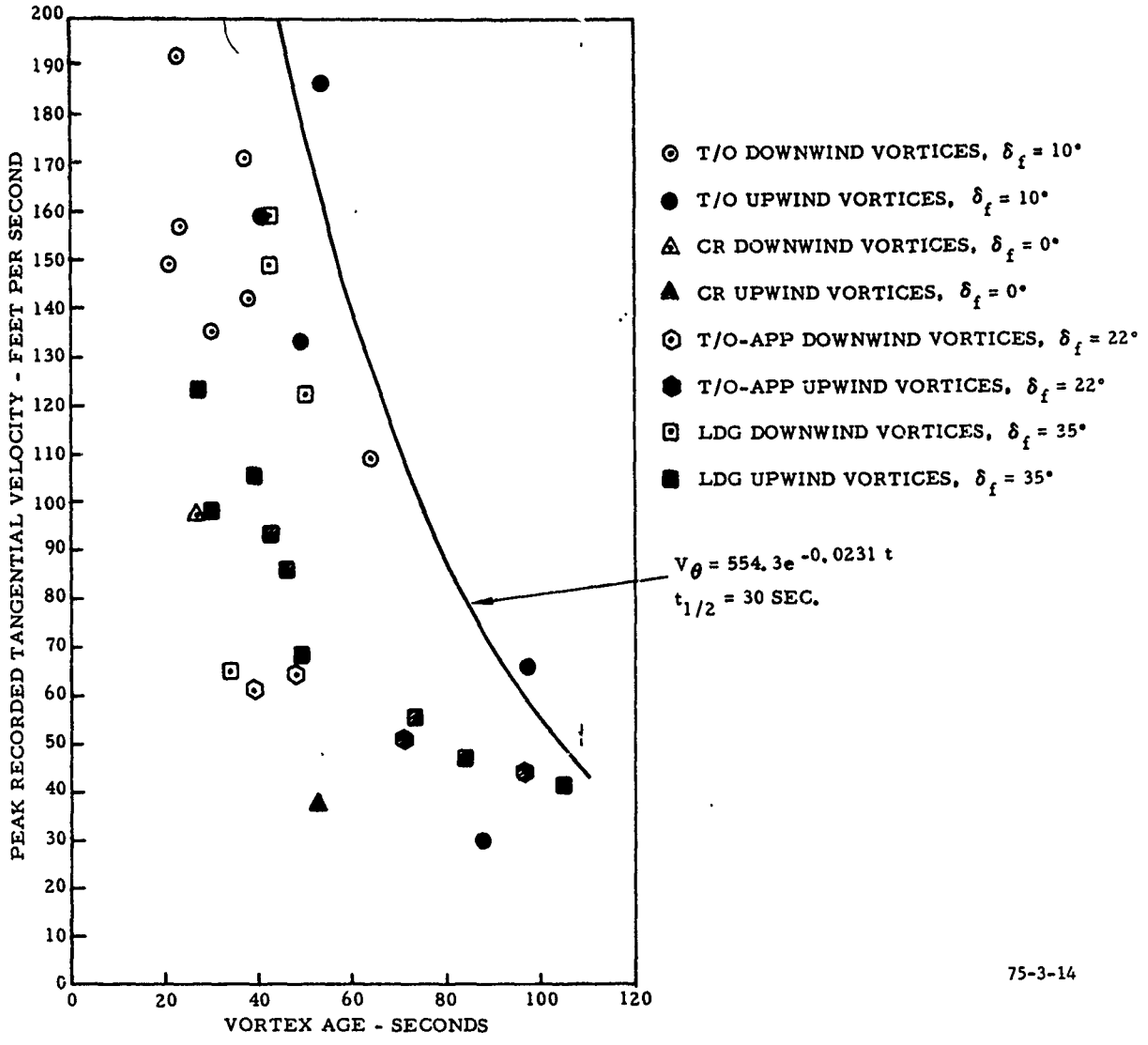

FIGURE 14. PEAK RECORDED TANGENTIAL VELOCITY VS. AGE (ALL CONFIGURATIONS—DC10)

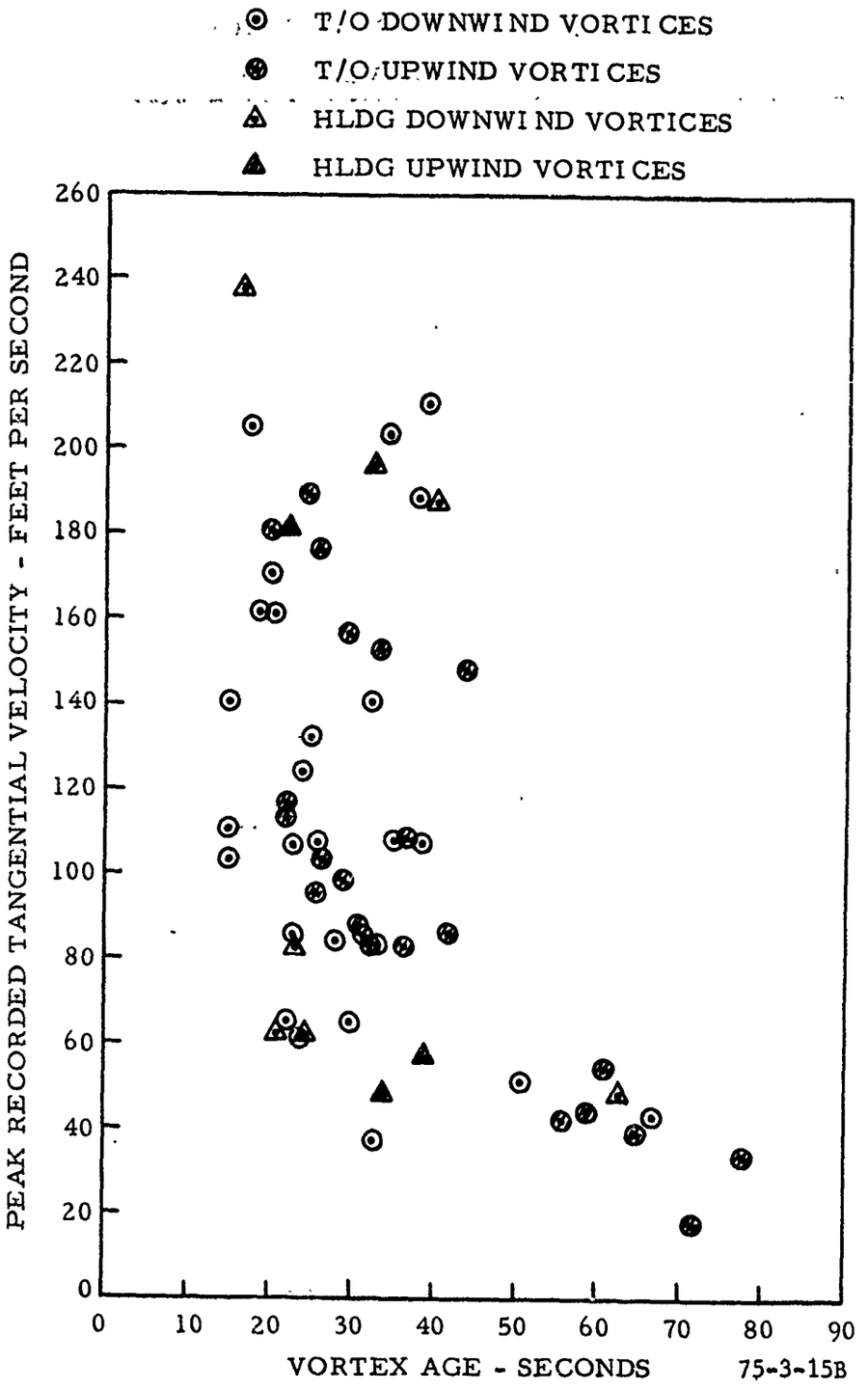

FIGURE 15A. PEAK RECORDED TANGENTIAL VELOCITY VS. AGE (TAKEOFF AND HOLDING CONFIGURATIONS--B727)

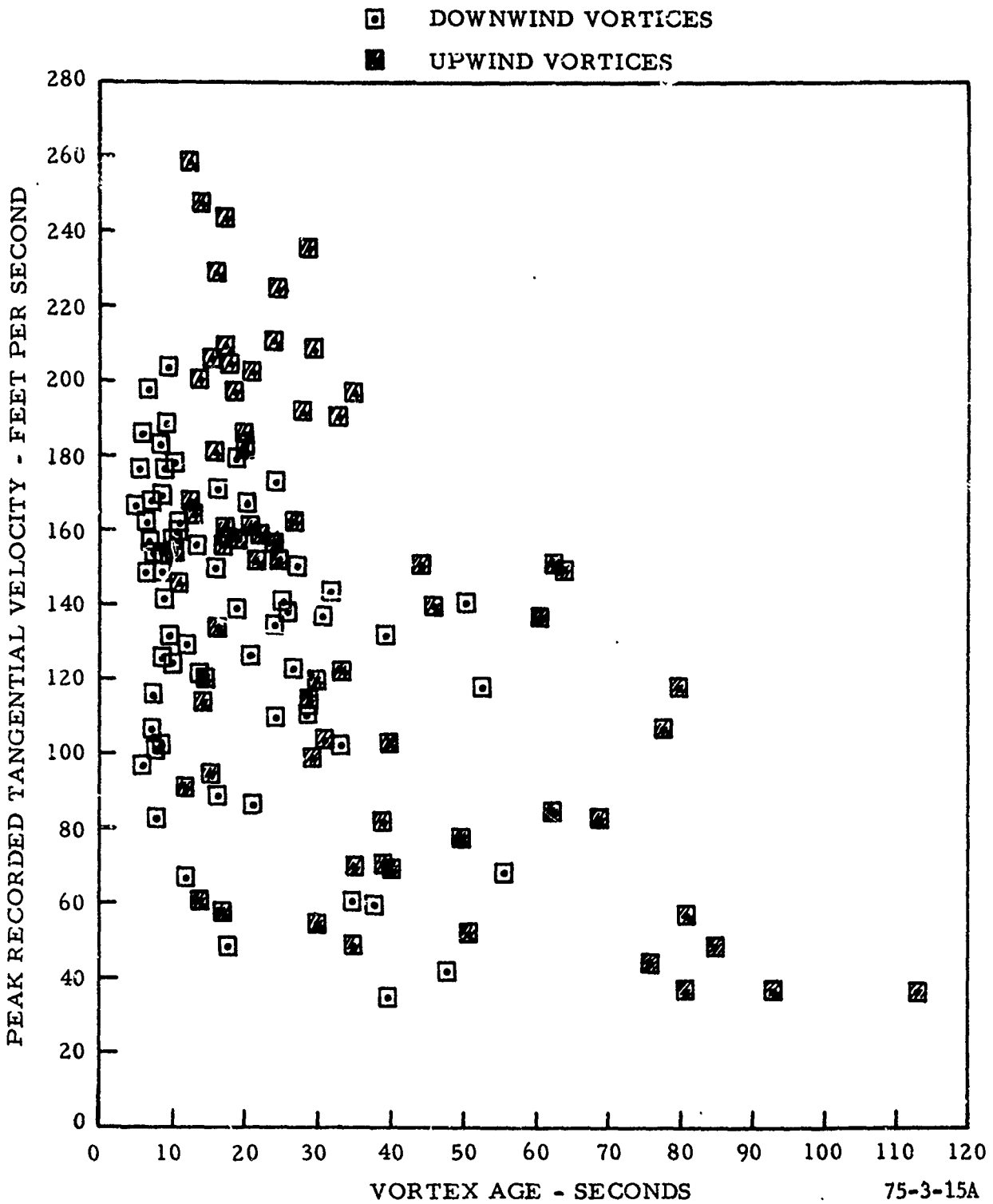

FIGURE 15B. PEAK RECORDED TANGENTIAL VELOCITY VS. AGE (LANDING CONFIGURATION--B727)

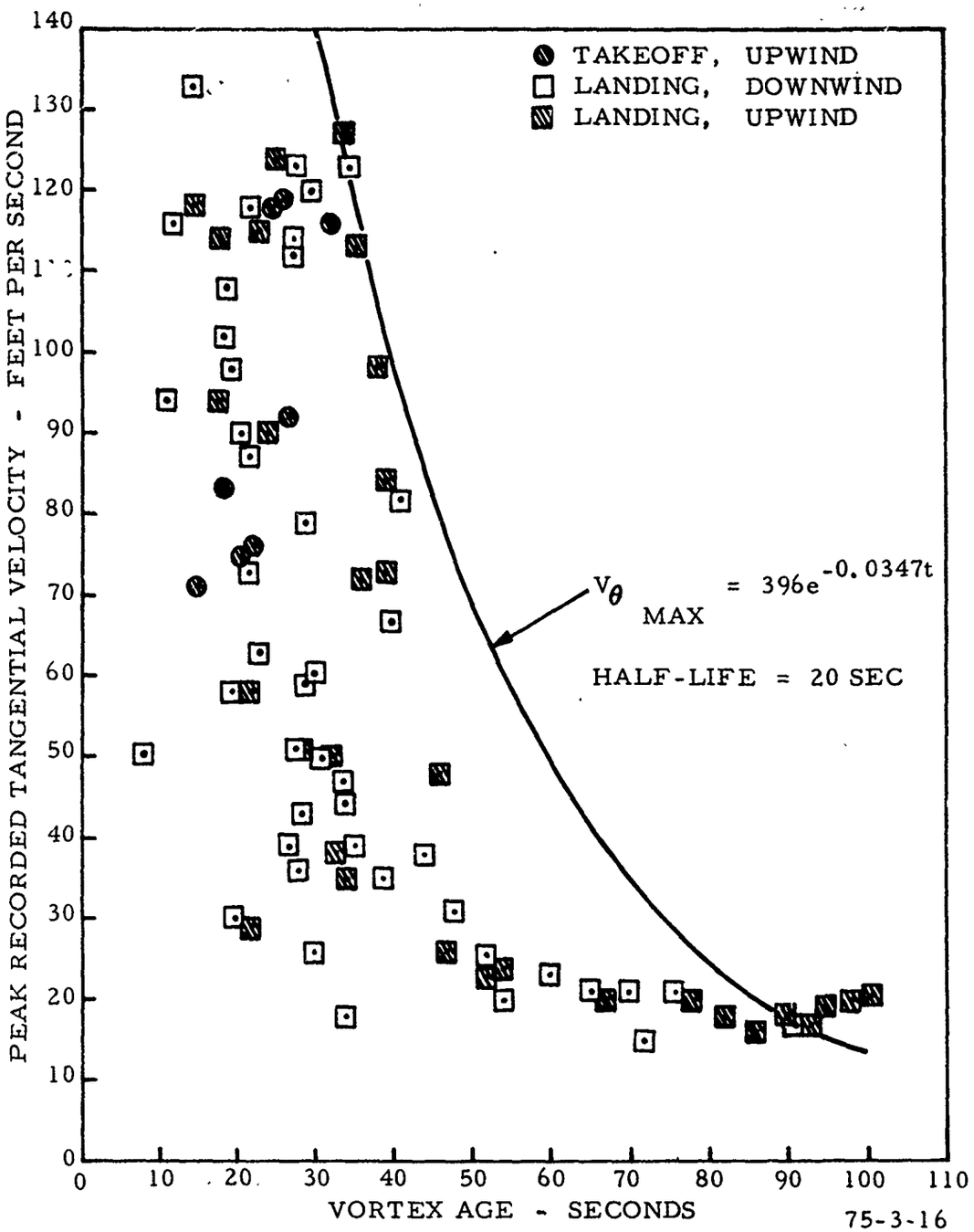

FIGURE 16. PEAK RECORDED TANGENTIAL VELOCITY VS. AGE (ALL CONFIGURATIONS--DC9 - SERIES 10)

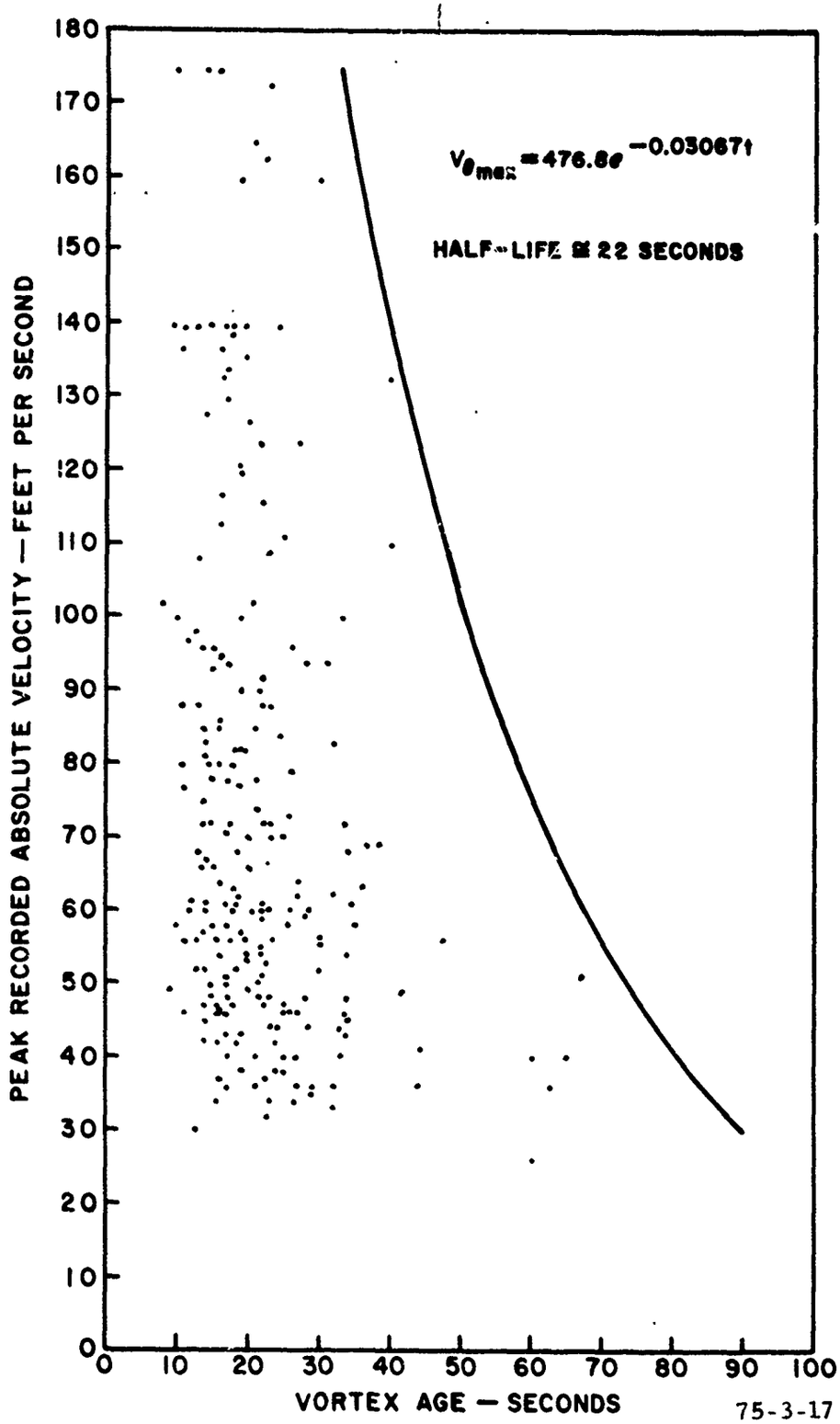

FIGURE 17. PEAK RECORDED TANGENTIAL VELOCITY VS. AGE (ALL CONFIGURATIONS—DC7)

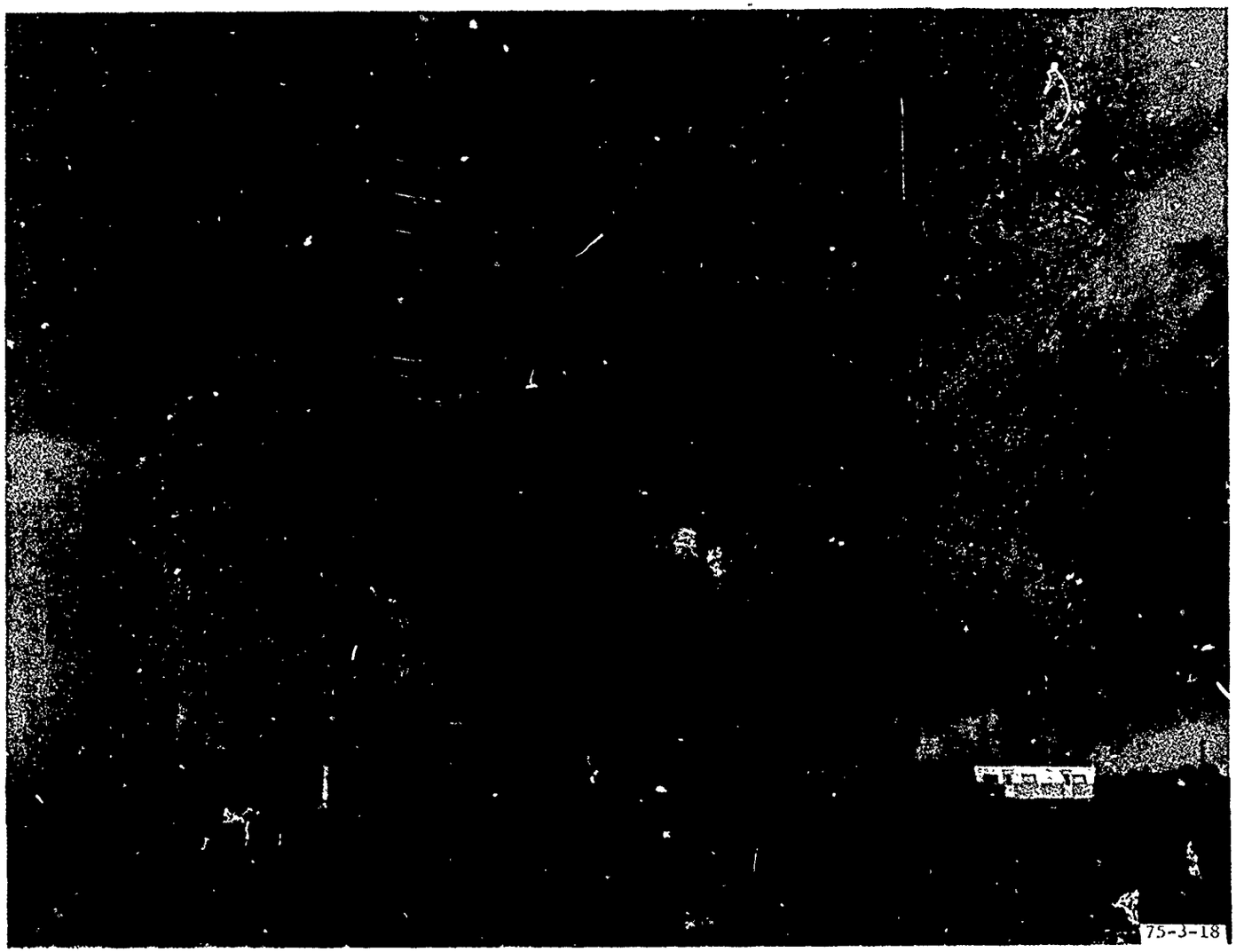

FIGURE 18. LOCKHEED L1011 PORT WING VORTEX SYSTEM AS OUTLINED BY VORTEX ENTRAINED SMOKE

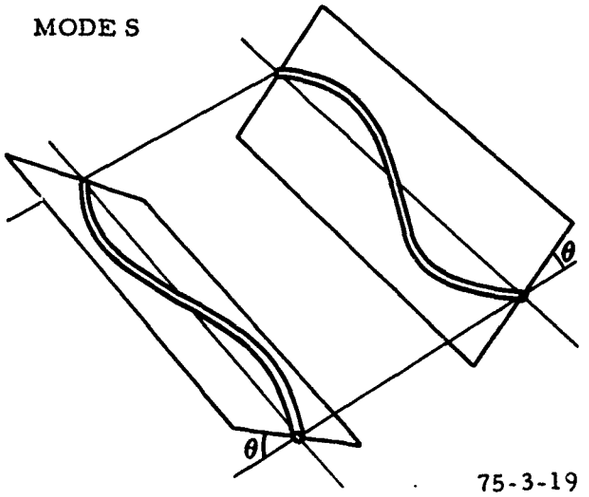

FIGURE 19. GENERAL SHAPE OF UNSTABLE "S" MODE IN MUTUAL INTERACTION INSTABILITY (AFTER CROW)

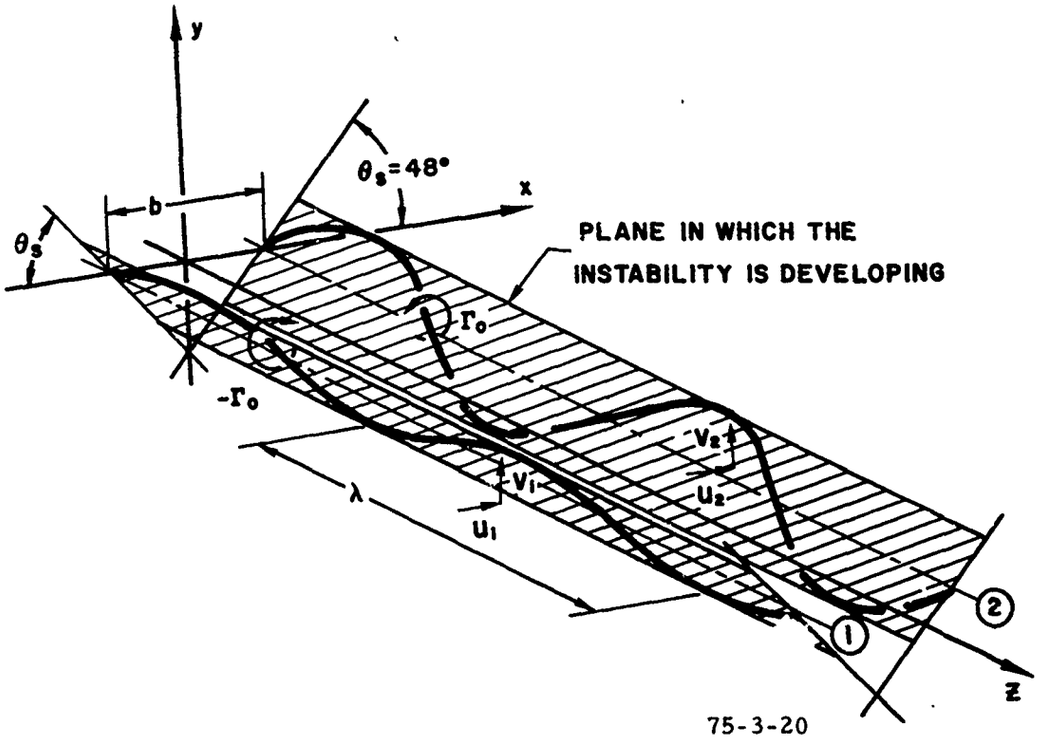

FIGURE 20. GEOMETRY OF THE OSCILLATING VORTEX PAIR

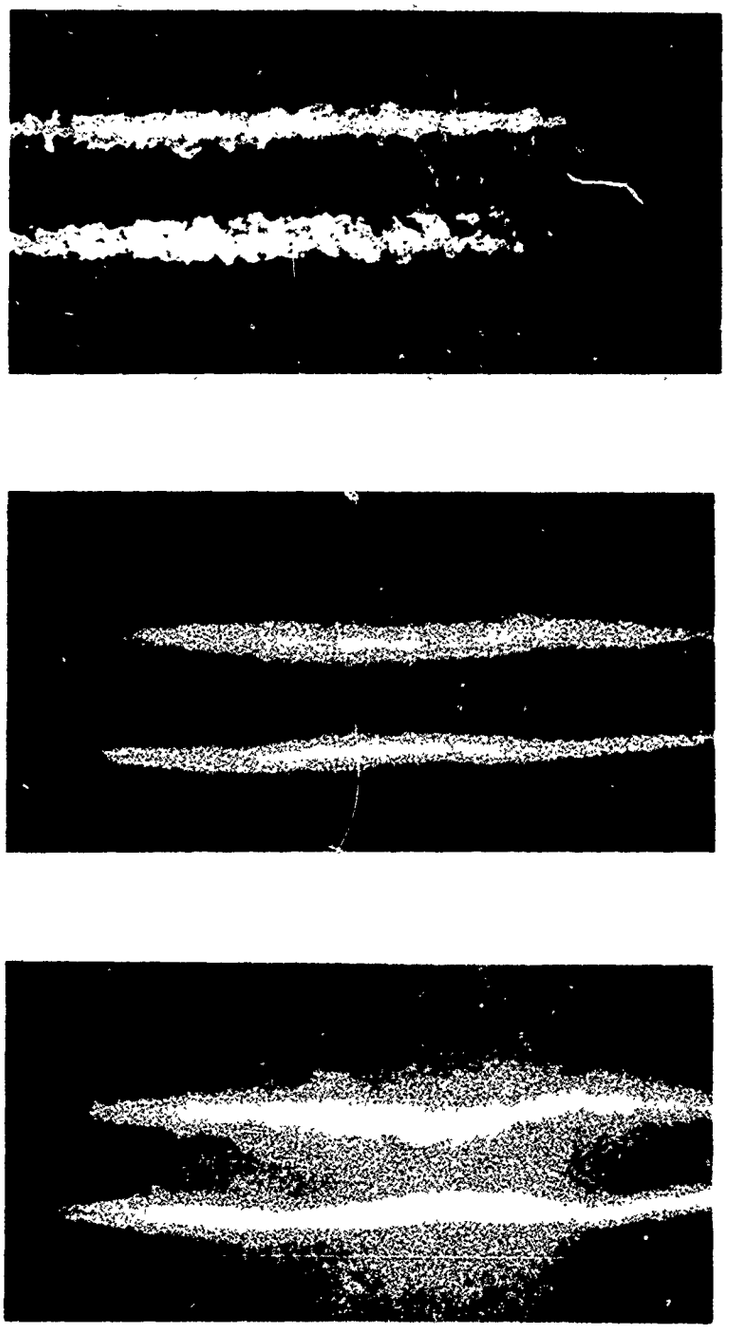

75-3-21A

NUMBERS IN PARENTHESIS ARE TIME IN SECONDS AFTER CV880 PASSED OVERHEAD.

FIGURE 21. B747 VORTEX DECAY AS OUTLINED BY CORVUS OIL (Sheet 1 of 2)

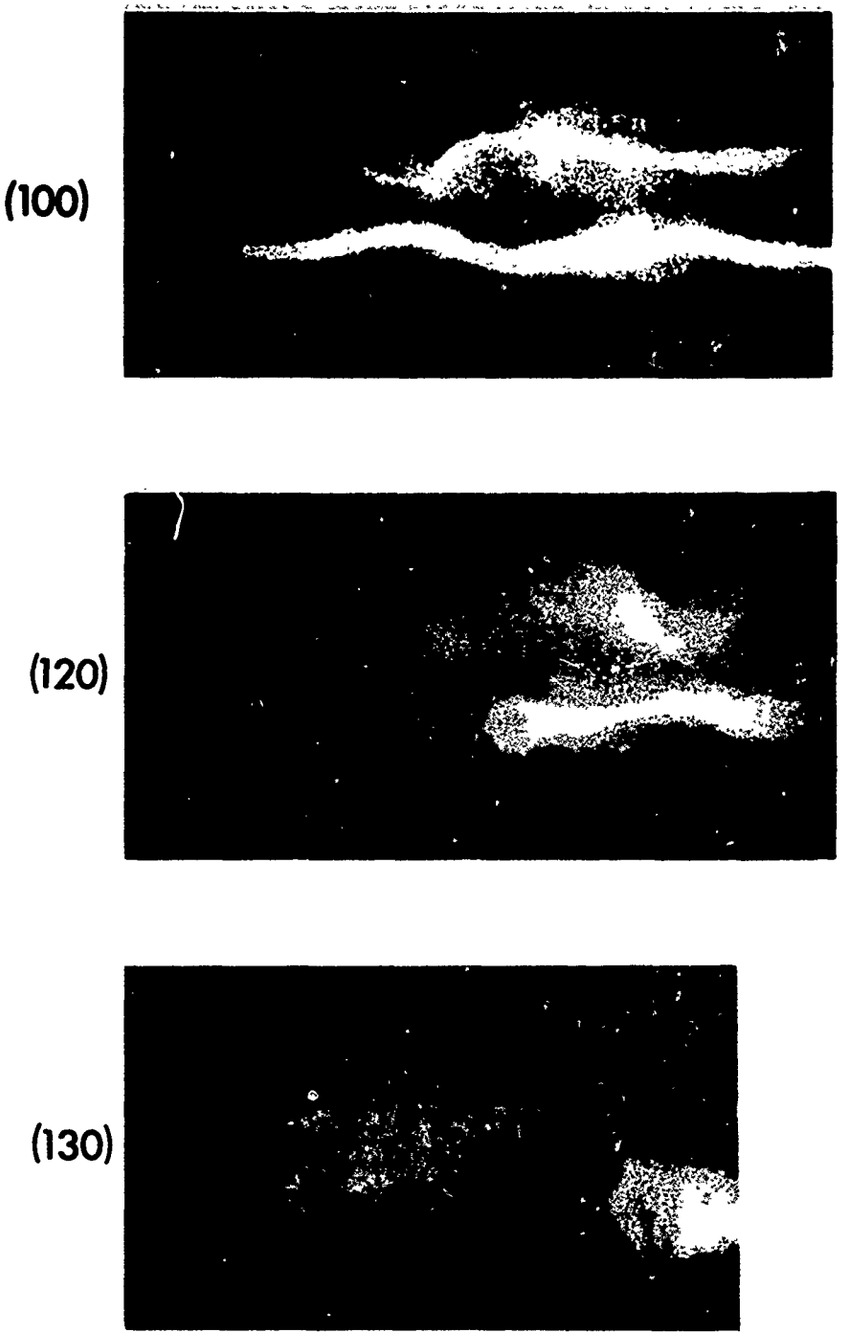

75-3-21B

NUMBERS IN PARENTHESIS ARE TIME IN SECONDS AFTER CV880 PASSED OVERHEAD.

FIGURE 21. B747 VORTEX DECAY AS OUTLINED BY CORVUS OIL (Sheet 2 of 2)

VORTEX CORE BREAKDOWN OR BURSTING. The "tubular-type" vortex structure was observed to grow slowly in diameter until it reached what appeared to be constant core diameter, e.g., about 5 to 8 feet for the L1011 in landing configuration, and lasted from 90 to just under 120 seconds for this airplane. At this time, it was noted that there occurred a sudden growth of core diameter followed by the development of a spiralling-type flow around the enlarged core cylinder and subsequent rapid core disintegration to random turbulence, in 2 to 5 seconds after appearance of the spiral flow. This was the predominant decay mode observed during the tower fly-by tests. An example of this type of breakdown is shown for the DC7 on the left side of figure 22 for the lower altitude flight tests and a good example is shown in figure 23 for the B727-200 for the higher altitude flight tests.

The possible contribution of the test tower to vortex dissipation, due to tower/vortex interaction, has always been of concern. The tower definitely disturbs the vortex tube to some extent and permits relatively higher pressure air to enter the vortex core. This interaction at times appears to accelerate vortex decay, primarily in the bursting mode. However, this has been found to be the exception rather than the rule. Some of the unusual cores and concentric tubular vortices noted with flow-visualization, as in figure 24 for example, for L1011 data run 11, are believed to be caused by tower interaction. In figure 25, however, for L1011 data run 6, this phenomenon is not observable.

Further justification for minimizing tower-induced effects on the vortices in analyses of the data was found in correlating visual observations reported in the references cited with those of Tombach, reference 24. In the tower fly-by tests, an axial flow appeared many times upon vortex tower passage. The axial flow or burst direction of travel varied; sometimes it was in the direction of flight, other times away, and in other instances, the flow was biaxial; Tombach observed the same type of phenonenon in his vortex flow visualization tests with a Cessna 170 wherein no towers were used.

VORTEX VISCOUS DISSIPATION. Apparent vortex viscous dissipation was noted on occasion wherein the vortex just gradually decayed due to turbulent diffusion or viscous shear.

VORTEX/ATMOSPHERIC INTERACTION. This type of decay is best described as a catchall for the many effects due to large-scale atmospheric patterns as they interact with the organized motion of the wake. Atmospheric turbulence, created by atmospheric instability or by shear flow, has a definite effect on the lifespan of the vortices, particularly the onset of vortex instability, either Crow-type or that due to bursting.

It might be said that another dissipative mode may be added and that is due to vortex/ground interaction, particularly where the ground has large-scale protuberances because certainly some surface structures, artificial or otherwise, can accelerate the decay of vortices. For example, on several occasions during the flight testing conducted at Idaho Falls (reference 1), it was observed that the vortices disintegrated (a burst-type mode) immediately after drifting through a series of telephone poles. However, the 200-foot tower did not

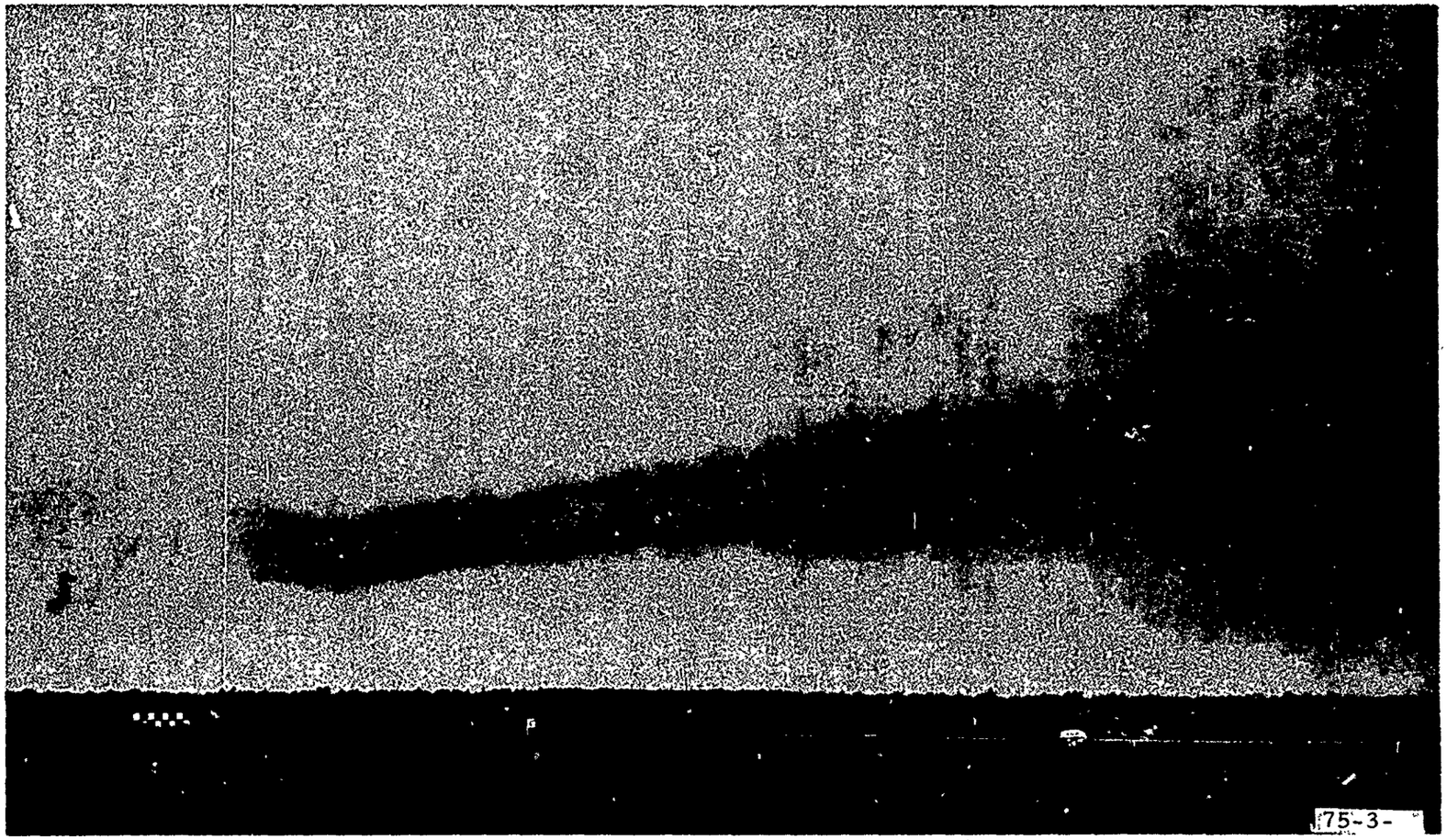

FIGURE 22. DOUGLAS DC7 AIRPLANE VORTEX DRIFTING ACROSS TEST SITE
(NOTE ONSET OF SPIRAL FLOW AND VORTEX BURSTING)

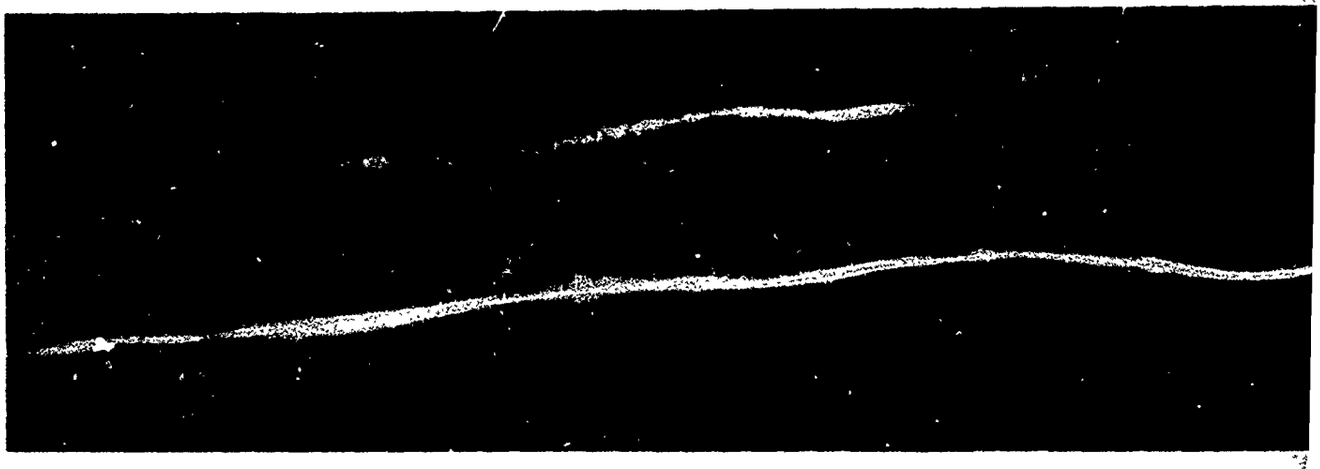

FIGURE 23. BREAKDOWN (BURSTING)

(BURSTING) OF ISOLATED WING VORTEX

2

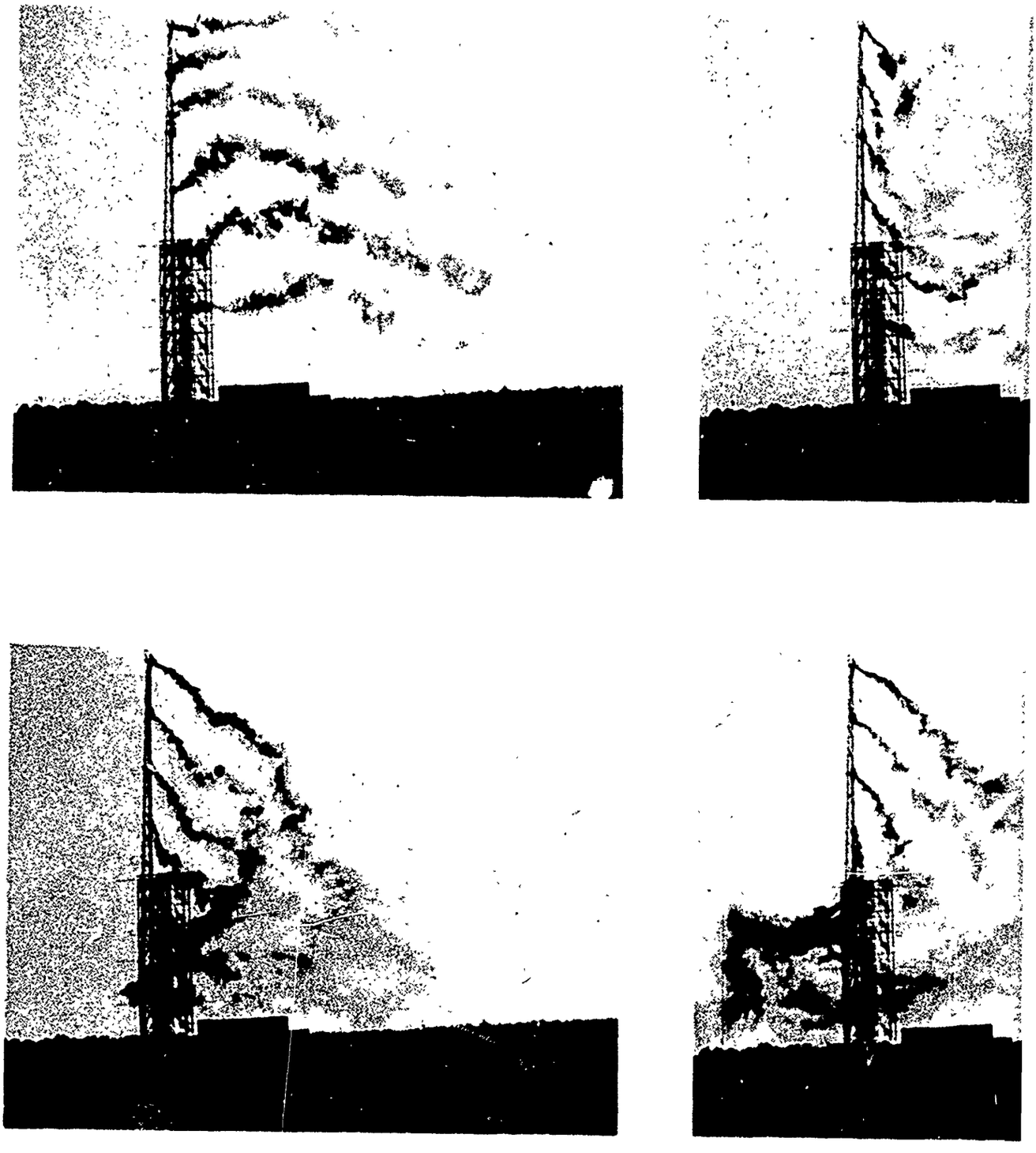

FIGURE 24. PHOTOGRAPHIC COVERAGE (16mm MOVIE) OF TAKEOFF/APPROACH CONFIGURATION δ_f = 25

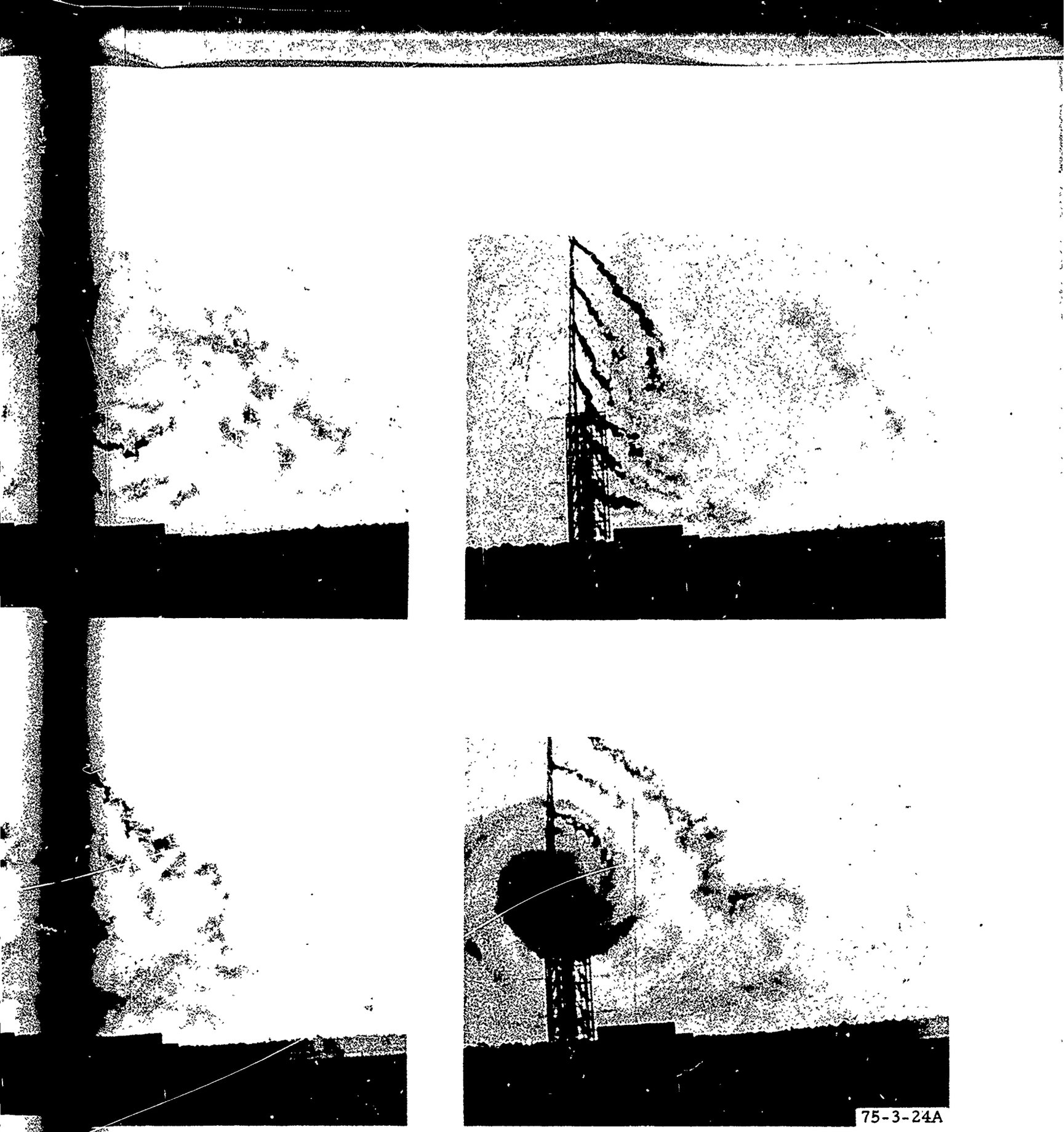

OF L
25°
(MOVIE) OF L1011 VORTICES FOR DATA RUN 11,
TION δ_f = 25° (Sheet 1 of 2)

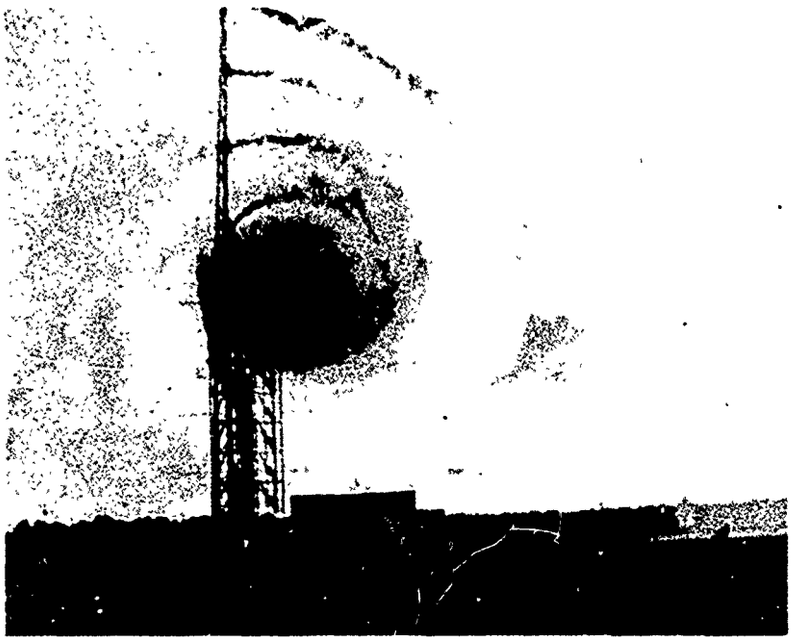

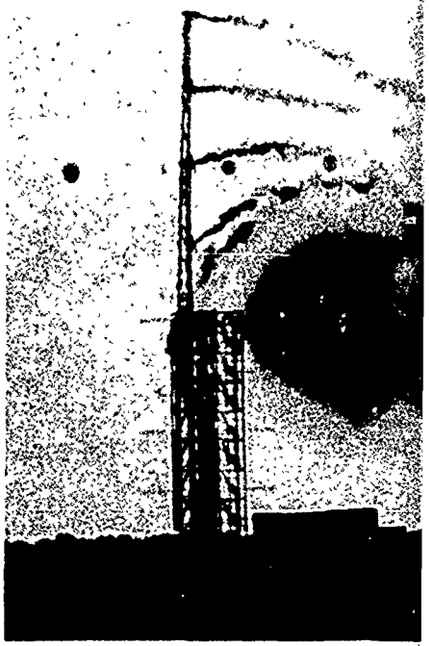

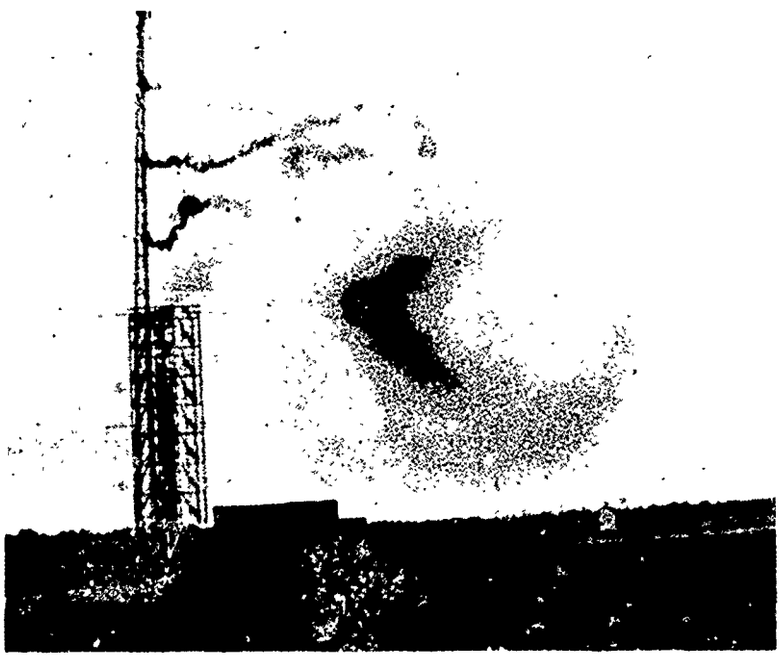

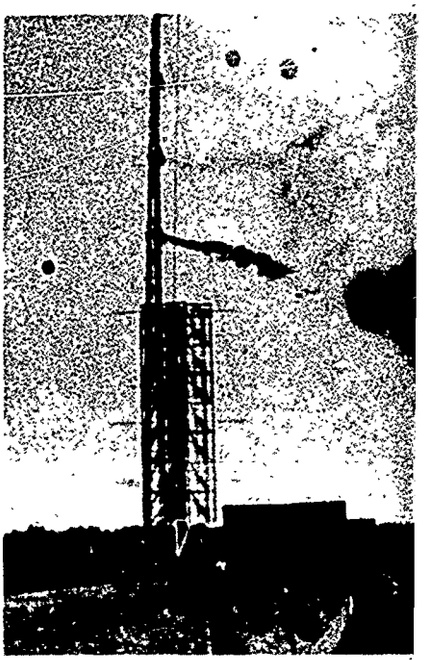

FIGURE 24. PHOTOGRAPHIC COVERAGE (16mm MOVIE) OF
TAKEOFF/APPROACH CONFIGURATION, δ_f =

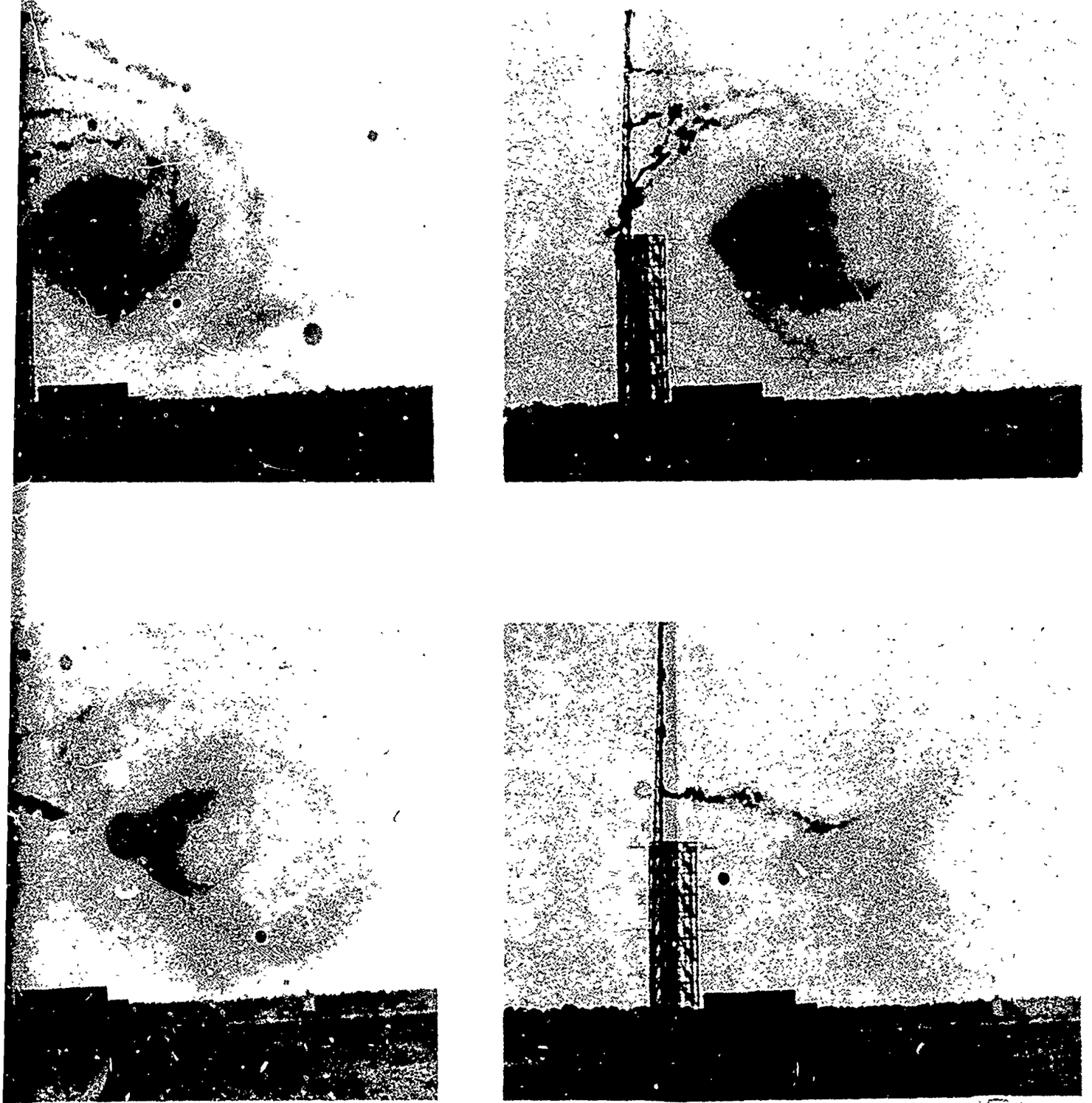

75-3-24B

(16mm MOVIE) OF L1011 VORTICES FOR DATA RUN 11,
GURATION, δ_f = 25° (Sheet 2 of 2)

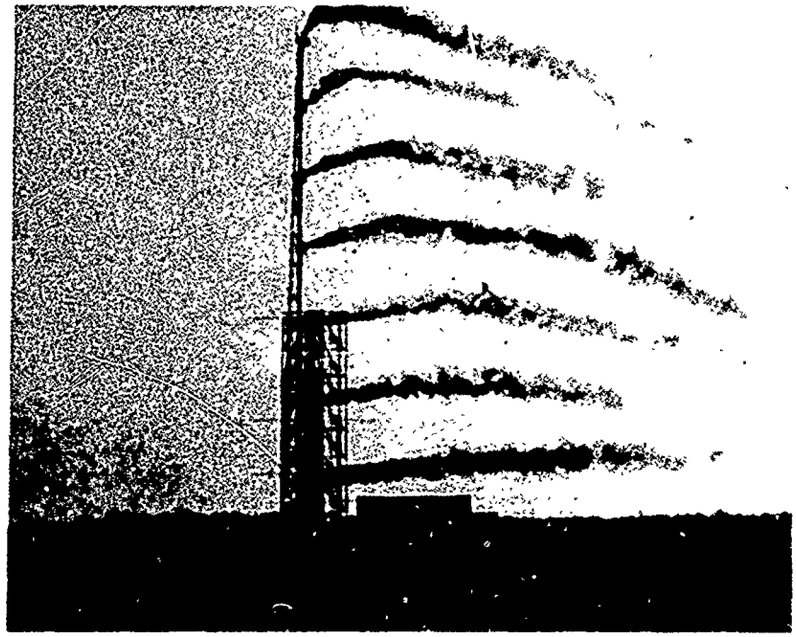

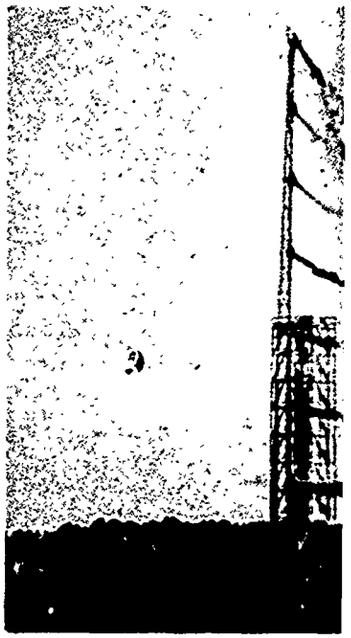

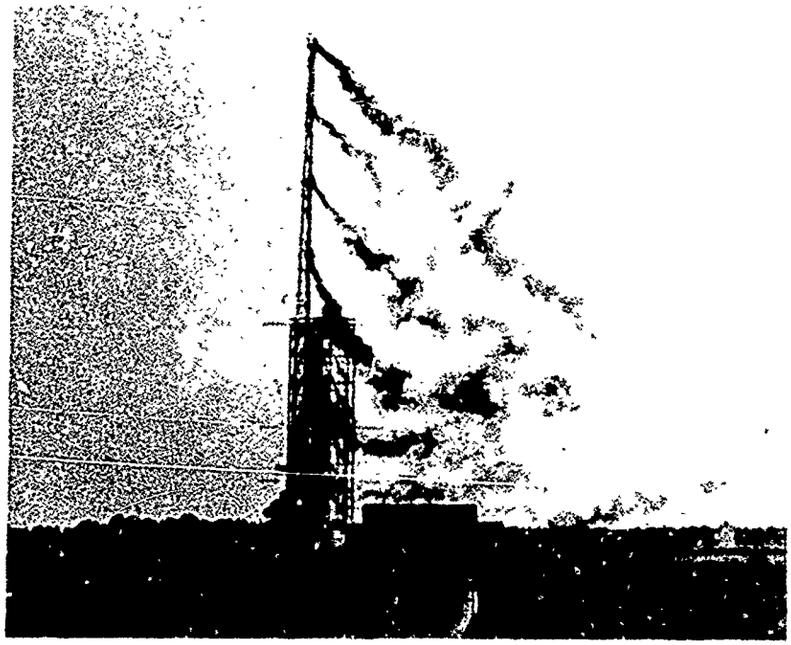

FIGURE 25. PHOTOGRAPHIC COVERAGE (16mm MOVIE) TAKEOFF/APPROACH CONFIGURATION, δ_f

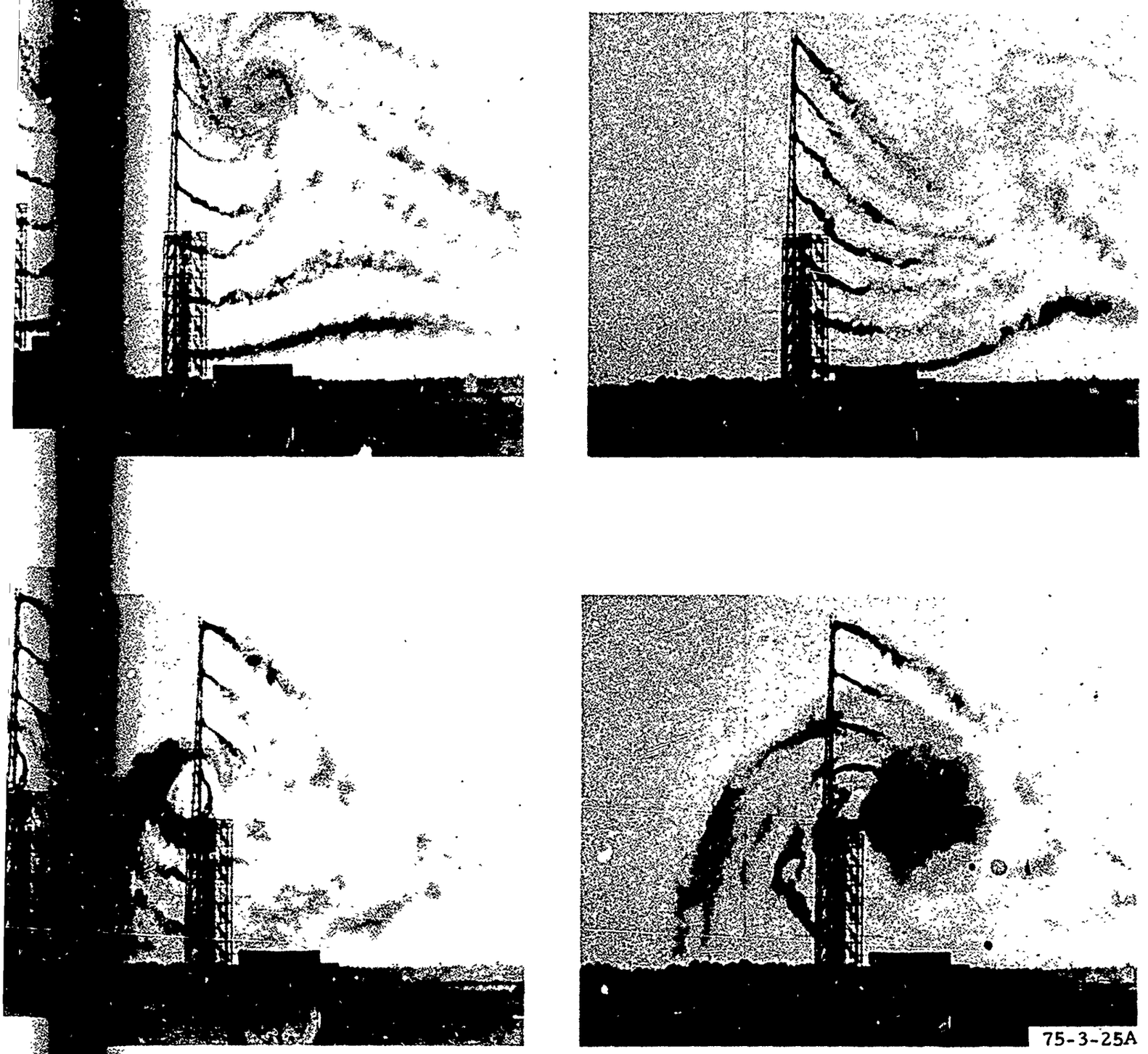

E) OF
δ_f =

6mm MOVIE) OF L1011 VORTICES FOR DATA RUN 6,
RATION, δ_f = 25° (Sheet 1 of 2)

2

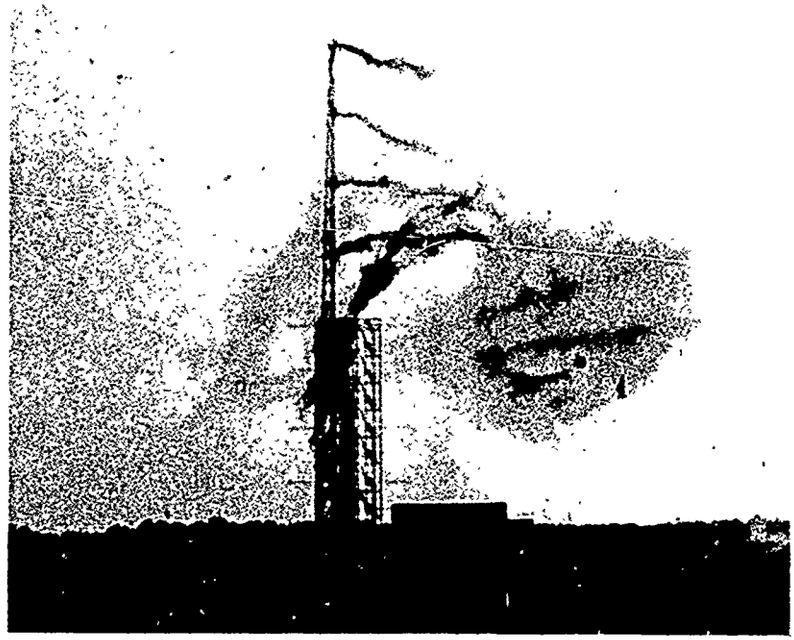

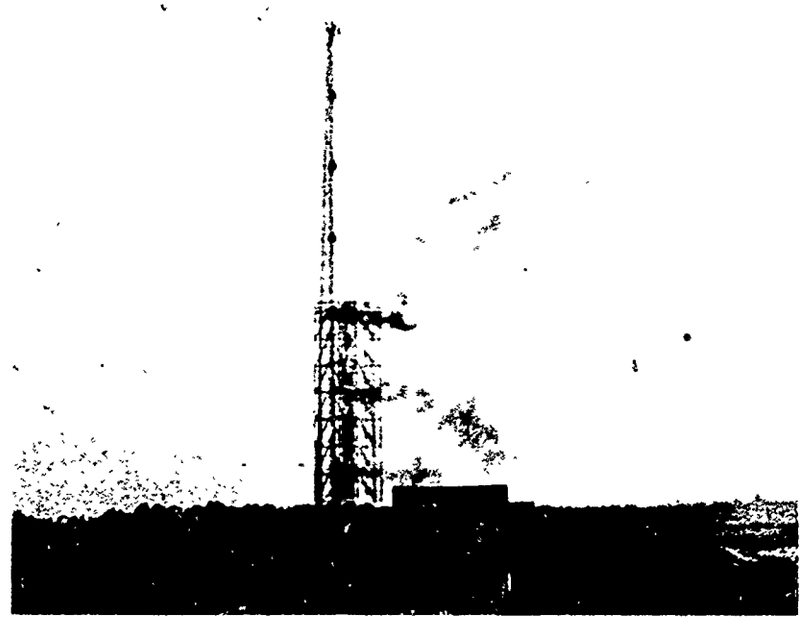

FIGURE 25. PHOTOGRAPHIC COVERAGE (16mm MOVIE) OF L101 TAKEOFF/APPROACH CONFIGURATION, $\delta_f = 25°$

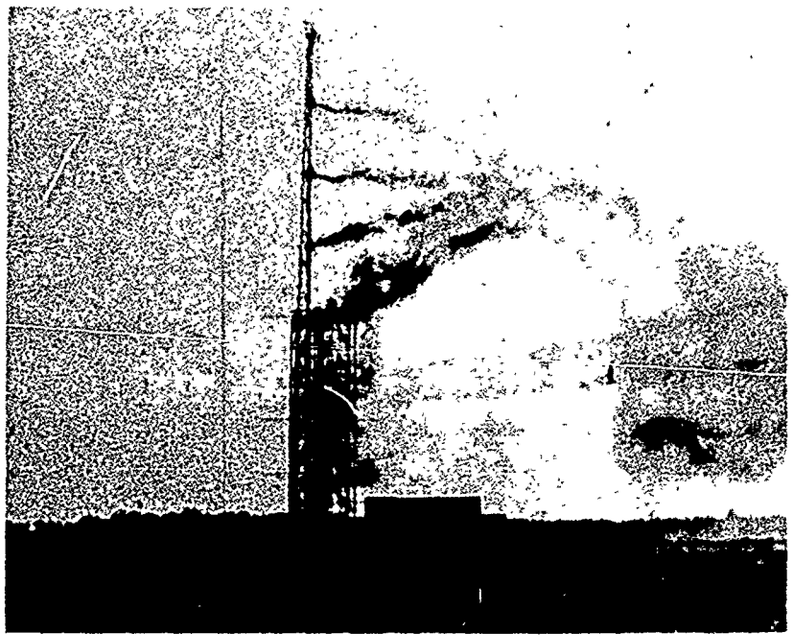

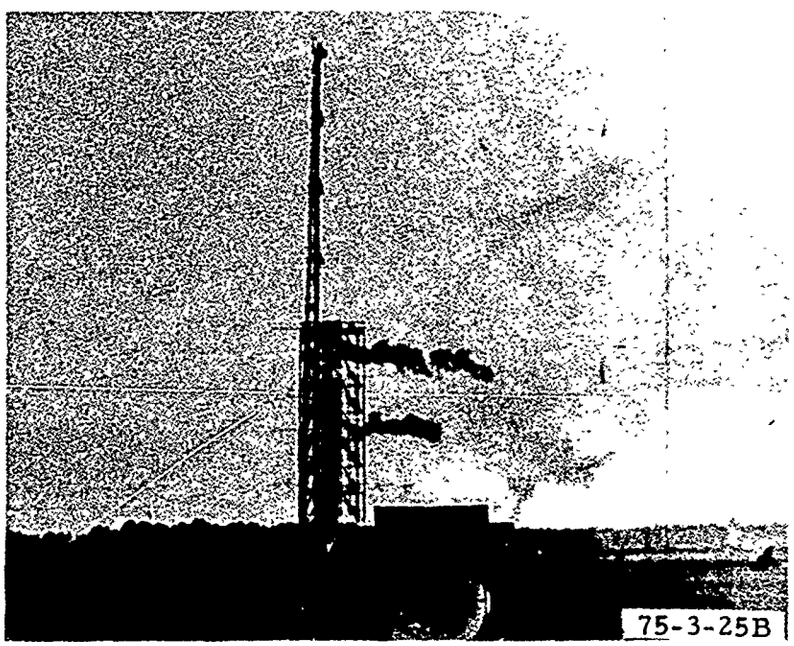

1011
° (S
OVIE) OF L1011 VORTICES FOR DATA RUN 6,
N, δ_f = 25° (Sheet 2 of 2)

appear to cause any instability onset upon tower passage. The vortices appeared laminar in nature until intercepting the poles. This type of effect appears to be age-dependent as well as terrain dependent. The earlier discussion on vortex-tower interaction also can fall into this category.

Finally, vortex/engine exhaust interaction should be considered as a possible decay mode or at least contributing to one of the four major modes described above. This suggestion is based upon the results of the B707 tower fly-by tests with one engine at idle thrust reported in reference 7 and, more recently, the results of in-flight probing of a B747 vortex system by a T-37 instrumented for measuring aircraft dynamic response due to vortex encounters, reference 25. The effects of decreasing jet engine thrust were evident as increasing vortex strength and/or life. In addition, the test pilots stated that outboard engines on the B747 airplane appeared to have a more alleviating influence on the vortices than the inboard pair. However, that study is still underway and will not be further discussed here.

For the recorded tower fly-by data, the envelopes defining the absolute peak tangential velocities for the aircraft tested were approximated by exponential equations of the form

$$V_{\theta_{max}} = A \exp(-kt) \tag{20}$$

where A and k are experimentally determined constants.

The vortex half-life and empirical curve fits using this form are summarized in table 5 (page 64). These boundaries and decay math models should not be used as an index of the hazard caused by the vortices of these particular aircraft because that can only be determined by superimposing the radial distribution of vortex tangential velocities, as long as an organized flow still exists, as a forcing function on the aircraft penetrating them, as discussed in the next section. Rather the boundaries do provide a relative indication of the persistence of vortices from one aircraft model with those from another, up to a point. The decay envelope math models do not account for variations in aircraft configuration, ground effect, crosswind, or head/tail wind, mainly because sufficient data were not acquired to perform this analysis in detail; nor do they account for vortex instability onset which, as stated earlier, was found to be the major mechanism contributing to vortex destruction. Thus, one must not attempt to extrapolate the vortex peak velocities to an indefinite age, particularly past 2 minutes because the vortices have already decayed to insignificant rotational velocity before this time or been destroyed primarily due to Crow-instability linking or, as was usually the case, due to vortex bursting. Conversely, the data should not be extrapolated to zero time inasmuch the equation does not define $V_{\theta_{max}}$ for t = zero. Thus, each empirical equation has an upper and lower time boundary between which it can serve a useful purposes.

It is pertinent to point out that the most persistent vortices were found to be the upwind vortices during crosswind conditions and, therefore, the envelopes, if anything, are very conservative inasmuch as they include primarily crosswind data.

TABLE 5. SUMMARY OF DATA ON PEAK VELOCITY DEGAY ENVELOPES (EMPIRICAL CURVES)

Group	Airplane	A	k	Half-Life (Seconds)	Range of Applicability (Seconds)	V_θ (ft/s)
I	B747	336.4	.0173	40	10 - 80	283 - 84
	B707	485	.0198	35	45 - 80	199 - 99
	CV880	421.6	.0315	22	30 - 90	164 - 25
II	C5A*					
	C141*					
III	L1011**					
	DC10	554.3	.0231	30	44 - 110	201 - 44
IV	B727	341.5	.0126	55	20 - 90	265 - 110
	DC9	396	.0347	20	30 - 90	140 - 17
V	DC7	476.8	.0307	22	35 - 70	163 - 56

Notes:

*Insufficient data to establish trend.
**Unexplained very high values (>200) at high times (47 - 70 seconds)

UPPER AIR VORTEX FLOW VISUALIZATION DATA.

These data are mostly qualitative but do provide a good insight into vortex decay modes and, in some cases, vortex transport. Although no quantitative data on intensity is obtainable using this technique, good quantitative results are possible on persistence. Some of the same conclusions were generally reached by Tombach, reference 24, and Chevalier, reference 26. They analyzed the vortices as visualized by smoke grenades mounted on a Cessna 170 (Tombach) and DeHavilland Beaver DHC2 and a Beechcraft T34F (Chevalier).

CV880 flight tests were conducted from 5,000 to 35,000 feet pressure altitudes, at NAFEC. The tests were conducted on several different days in landing, take-off, holding, and cruise configuration. The flap deflections were δ_f =55, 22, and zero degrees, respectively. In addition, the CV880 has wing spoilers mounted on the top outboard wing panels which are automatically deflected upward to an 8-degree null position whenever full landing flap deflection of 55° is selected and thus augment the conventional aileron lateral control system. The gross weight during the tests varied from approximately 140,000 to 165,000 pounds.

Referring to the K-38 photographs of figures C-1 through C-3, appendix C, for the CV880 in holding, takeoff, and landing configurations, respectively, one can distinctly see the decay modes and persistence of the vortex pair. Note that the vortices persist for 120, 100, and 90 seconds, respectively. The decrease in vortex age with increased landing flap deflection is readily apparent and correlates well with the tower fly-by test results as well as with upper altitude tests on other days and with other aircraft models as discussed later on herein.

For example, during flight tests conducted a year earlier, figure C-4, depicts the CV880 vortex pair for the takeoff configuration, Hp = 5,000 feet and clearly shows that the vortices tend to become unstable and disintegrate into segments in 90 seconds. The breakdown mode appears to be a combination of Crow instability linking, on the left side of figure C-4 (middle photo on sheet 1 of 3 and following page, sheet 2 of 3) and vortex bursting in the middle and the right-hand side of the same figure. Figure C-4 (see top of sheet 2 of 3) shows a DC7 flying in trail behind the CV880 and slightly below its vortex pair and can be used for scaling purposes on separation of the vortex pair if one so desires.

Another significant result, although the data is very limited, is that the time for vortex breakup, due to instability onset, was independent of altitude for the CV880 for the same configuration and the breakup mode was also the same. This is substantiated by figures C-1, C-5, and C-6 which depict the linking type of vortex instability onset with subsequent rapid breakdown.

The B727-200 flight tests (reference 27), in which vortex flow visualization was used, revealed substantially the same results on vortex persistence. First a series of level flight tests were conducted at approximately 600 feet AGL at Edwards Air Force Base (field elevation $\cong$ 2,300 feet) wherein the turbulence dissipation rate, ϵ, varied from approximately zero to 0.5. The B727 vortex decay mechanism was found to be primarily vortex bursting or breakdown. Linking was not observed for these test conditions. Colored video tape coverage was taken of these flyovers and is available at NAFEC for review.

A series of flight tests were also conducted in which the B727 was performing straightout and turning flight noise-abatement climbouts. K-38 camera photographs of the B727 vortex system are shown in figures C-7 and C-8 for B727 test flights 11-1 and 12-1, respectively. It can be observed that one wingtip vortex (port wing) flow appears more dense than the other. This is a result of modifying this smoke generator to produce a greater CORVUS oil flow rate and, therefore, a more conspicuous smoke trail.

The sequence of photographs for B727 flight 11-1 are for the airplane in the takeoff configuration, δ_f = 15°, starting a climbing left turn at approximately 6,000 feet AGL. A 30-degree bank angle was established above 3,000 feet AGL. Initiation of sinusoidal action by the vortex pair can be clearly seen at t = 20 seconds. Initiation of bursting, particularly of the port wing vortex, is seen at t = 30 seconds. Finally, at t = 50 seconds, we see an isolated port wing and rapid onset of axial flow just prior to the final destruction of the orderly flow of the vortex.

The sequence of photographs for B727 flight 12-1 are for the airplane in a climbing left turn, as before, with δ_f = zero degree. Some sinusoidal motion of the vortex pair is seen at t = 20 seconds. However, more dramatic and clearly evident is the onset of vortex bursting or breakdown at t = 40 seconds. Note the conical collapse of both vortices at 40< t <50 seconds of age. For both flights, the vortex persistence was approximately 60 seconds. For the second series of photographs, run 12-1, the vortex pair is apparently thinner and less conspicuous than for run 11-1. This is due to the clean configuration of the airplane and associated higher indicated airspeed which, for the same rate of flow of the smoke oil, would produce a less dense smoke trail. The somewhat ragged trail of the vortex pair for run 12-1 is attributed to the increase in atmospheric turbulence. The flight was performed later in the day during conditions of increased convective activity due to ground heating.

Prior to these B727 flight tests, there was some question of the vortices moving apart from each other while an airplane was in turning flight, to the point where there remained an "isolated" vortex, and supposedly longer than normal vortex persistence. However, such was not found to be the case for the vortices shed by the B727 while in climbing turns with bank angles up to 30°.

For correlation with atmospheric conditions, the meteorological data acquisition airplane, cited earlier, recorded values for the atmospheric turbulence dissipation rate $\varepsilon^{1/3}$ from 0.2 to 1.0 during the period of these flight tests (climbing flight) at altitudes of 4,500 to 5,000 feet AGL.

The correlation between these studies and those of others, e.g., Condit, reference 2, and Kerr and Dee, reference 28 on vortex persistence, particularly in airplane configurations representative of those used in terminal area operations is good.

MERGING OF VORTEX DECAY RESULTS.

Several schemes have been proposed for displaying vortex persistence as a function of various aircraft and/or atmospheric parameters. One such scheme is figure 26 taken from reference 2, along with CV880 and B727 data plotted thereon. It shows good agreement with regard to initial vortex breakup due to either linking or bursting, i.e., change from an orderly rotational flow to a random turbulent-type flow. Another scheme is shown in figure 27 taken from reference 29. This shows the time for vortex linking as a function of the parameter $\varepsilon^{1/3}$, cited earlier, for takeoff configuration. One can note the maximum time to linking for an $\varepsilon^{1/3}$ value of 0.1 which signifies the extreme low end of "negligible" atmospheric turbulence. This corresponds to the type of atmosphere under which the majority of the flight test investigations discussed herein were conducted; the C141 tower fly-by tests being a notable exception because of high winds. This also corresponds to the atmospheric conditions under which one would expect vortices to be most persistent. For the largest aircraft plotted thereon; i.e., the B747, the maximum time for linking is approximately 120 seconds for the above cited $\varepsilon^{1/3}$ value.

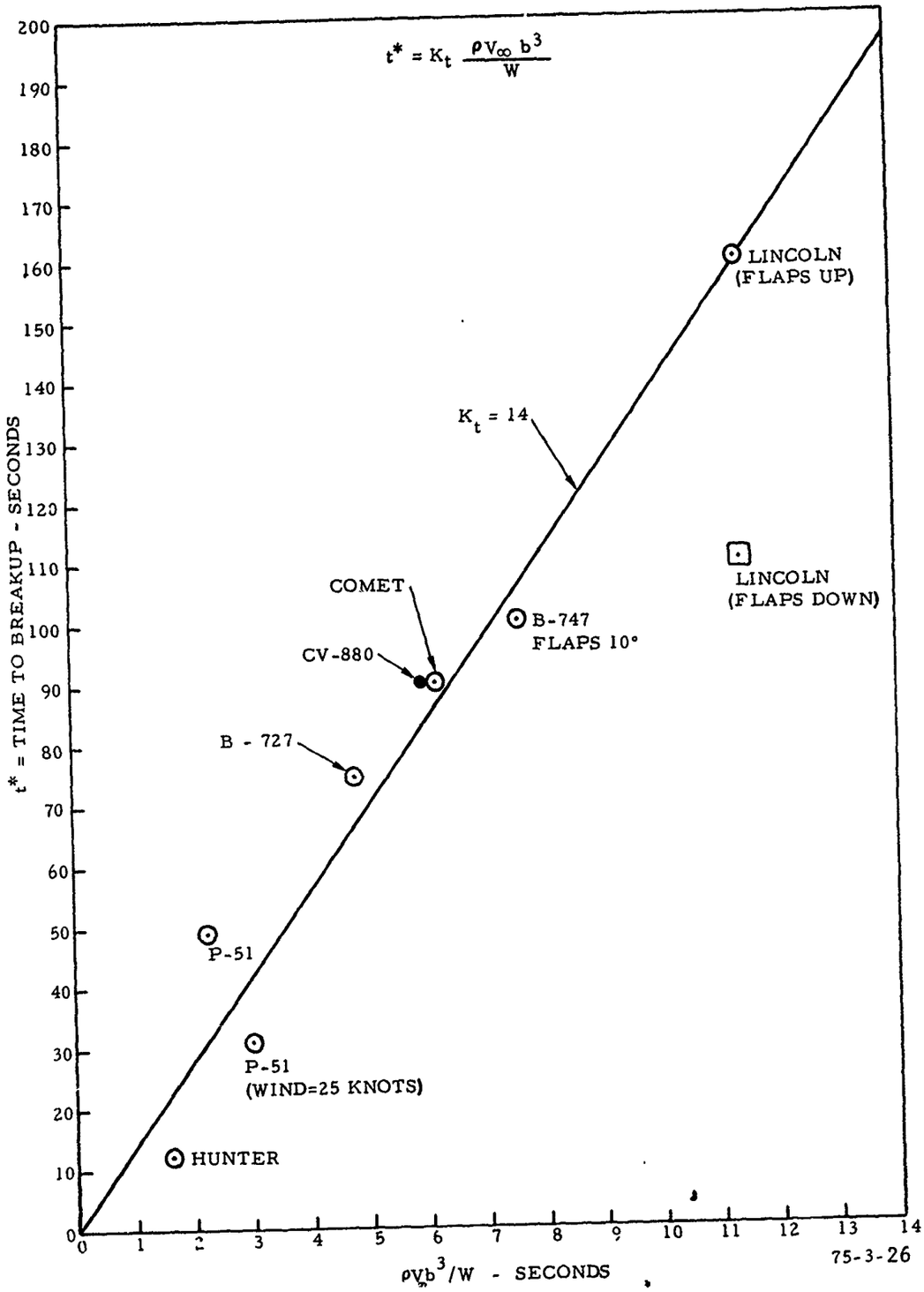

FIGURE 26. FLIGHT TEST DATA ON VORTEX WAKE BREAKUP

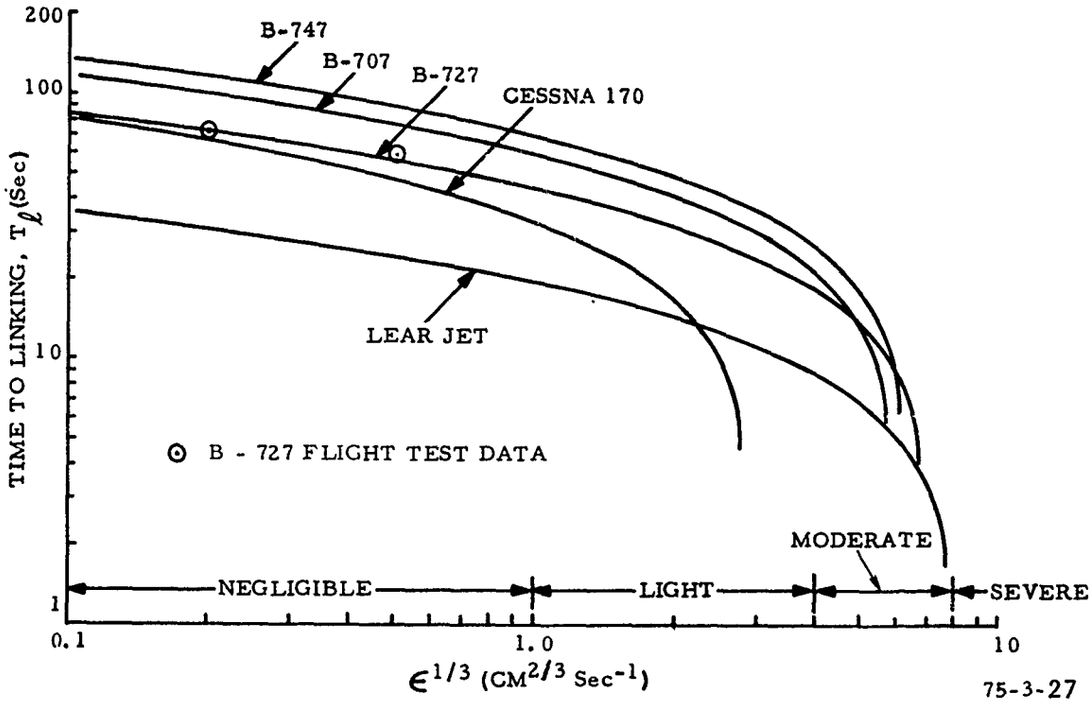

FIGURE 27. TIME TO VORTEX LINKING AS A FUNCTION OF ATMOSPHERIC TURBULENT DISSIPATION RATE $\epsilon^{1/3}$, FOR TAKEOFF CONFIGURATION

The B727 vortex persistence of 60 to 90 seconds noted during the flyovers, agrees with the time-to-linking vortex data shown thereon for the B727. Also shown are the CV880 data plotted against the subjective degree of turbulence provided by the pilots, as a numerical value for $\epsilon^{1/3}$ was not available for the flight tests with that airplane.

A third parameter correlation of vortex decay with atmospheric conditions is the ambient windspeed, particularly at the lower altitudes. For the tests using the tower fly-by technique, the majority of the flights were performed under crosswind conditions, and this may in certain instances be a disadvantage. Tower fly-by testing was started early in 1970, initially at Idaho Falls, and then continued at NAFEC. The flight tests were conducted under crosswind conditions in order to gather as much data as possible, particularly on vortex decay. It was believed at the time that a pair of vortices were similar in size and intensity in ground effect at identical ages, although their paths would be different. After a few tower fly-by tests, it became evident that the two vortices, "upwind" and "downwind," were somewhat different as was their persistence in close proximity to the ground. The upwind vortex was found to be more persistent, intense and to have a more orderly flow than the downwind one. A good example of this can be seen in figure 24 or 25 for the L1011 airplane.

Accordingly, it is not possible to arrive at any final conclusions on the differences between a vortex pair in a crosswind and one existing in a head or tail wind close to the ground. Comparing tower fly-by data acquired under crosswind conditions with the limited data acquired under parallel-to-wind flight tests leads to a preliminary conclusion that flightpaths perpendicular to the wind produce a more persistent vortex--the upwind vortex.

Within the earth's boundary layer, correlation of vortex persistence with windspeed without regard to direction may be useful because it is a rough index of the turbulence. The 1970 flight tests with the CV880, reference 8, using the tower fly-by technique revealed that an ambient windspeed (mostly crosswind) 3 to 7 mi/h appears to have the most pronounced effect in perpetuating the vortex tangential velocities as they move laterally over the ground within the first 100 feet above the ground for the takeoff and landing configurations.

Flight test investigations of aircraft dynamic response due to encounter of the trailing vortex wake generated by transport-type aircraft, conducted by the Royal Aircraft Establishment (RAE) in England, reference 28, and the Boeing Company, reference 2, revealed good correlation in vortex persistence with tower fly-by and upper altitude flow visualization studies for the generating aircraft in either takeoff or landing configuration. The persistence was based on the capability of the probe aircraft to be safely controlled, particularly in roll, while making a vortex encounter. In addition, visual observations were made on the preceding aircraft's vortex pair, as visualized by smoke, and "leveling off" and breaking up of the vortex pair was noted at about 2 minutes behind the generator. This would primarily be attributed to onset of rapid vortex breakup and dissipation which in turn results in cessation of interaction between the vortex pair.

A significant result of these probe flight tests was the effect of windspeed on the vortex lifespan. With zero wind, the trailing vortices remained laterally along the aircraft's flightpath and the turbulence level would be expected to be less. However, it was observed that as the windspeed increased, the turbulence increased, and the persistence and, therefore, the lateral movement of the vortices (under crosswind conditions) were diminished. Figure 28 (after McGowan, reference 30) shows a vortex persistence of 2 minutes for a 10-knot wind at the lower altitudes (less than 5,000 feet AGL). Superimposed on this plot are B747 (from reference 2), and CV880 data points. It is felt that the envelope is very conservative as the altitude is reduced, particularly for the downwind vortex in ground effect.

Using these data, the maximum possible displacement of the vortex due to crosswinds (and expected associated atmospheric turbulence) is shown in figure 29. It can be seen that for the conditions cited in the figure, the maximum lateral displacement of the vortex wake is approximately 0.35 miles for terminal area operations; i.e., low altitudes and aircraft configurations with some degree of landing flap deflection.

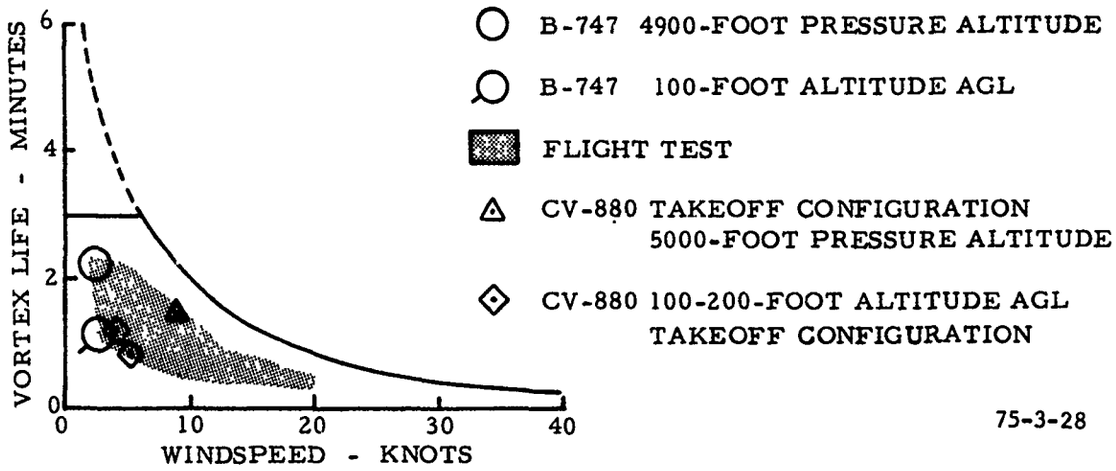

FIGURE 28. VORTEX PERSISTENCE AS A FUNCTION OF AMBIENT WINDSPEED AND HEIGHT ABOVE THE GROUND (FROM REFERENCE 30)

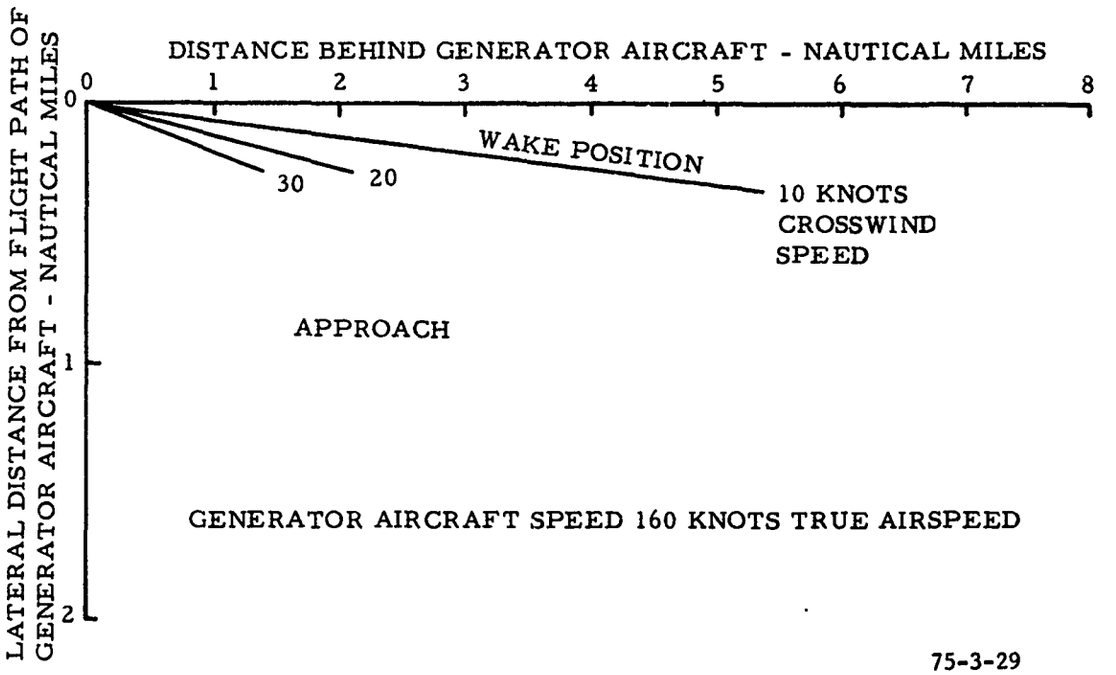

FIGURE 29. LATERAL DISPLACEMENT AND PERSISTENCE OF VORTEX WAKE DUE TO CROSSWIND

SUMMARY--VORTEX PERSISTENCE/DECAY.

The persistence (vortex age) of a trailing vortex system was analyzed in this section based on full-scale vortex flight-test results obtained by NAFEC and the results thereof correlated with those of other investigators using full-scale flight-test techniques. Vortex persistence means the longest age at which the vortex still exhibits come orderly rotational flow and/or is strong enough to adversely affect an encountering aircraft. Herein, we primarily considered those flight-test and atmospheric conditions which were conducive to permitting the most persistent vortices; namely, low ambient wind velocity, stable atmosphere, little or no turbulence. Not all of the atmospheric conditions which are considered to affect the lifespan of vortices in some way could be selectively or individually correlated with vortex decay because of lack of suitable data acquisition systems. These parameters would include windspeed, wind shear, atmospheric stability, and turbulence. However, in spite of the lack of an accurate knowledge of the atmospheric conditions existing at the time of the various flight tests cited, the correlation on vortex behavior between one set of tests and another is good.

VORTEX PENETRATION EFFECTS

DESCRIPTION OF SIMULATION.

To determine the effects of vortex encounter, one requires information on the following items:

1. Characteristics of the generating aircraft.
2. Nature of the vortex flow phenomenon.
3. Effect of atmospheric variables upon flow.
4. Characteristics of penetrating aircraft.

The formulation of the problem consists of calculating the vortex characteristics of a given aircraft using a selected vortex mathematical model. These characteristics, such as velocity as a function of space and time, are then used as inputs to the penetrating aircraft expressed in terms of its dynamic characteristics. The overall penetration problem has been treated very simply using developed expressions and simplified static moments and it has been handled in detailed form by considering comprehensive math modeling, along with complete penetrating aircraft response dynamics. A brief discussion of some of the previous methods used will be presented along with the analysis used in calculating penetration effects in this report.

Presented in an earlier section of this report is a discussion of the various mathematical models utilized in the past to describe vortex wake characteristics.

The following is a brief discussion of the various methods used to determine vortex penetration effects by following aircraft:

In the analysis, there are three basic types of vortex encounter considered; namely, (1) crosstrack penetration in which the following aircraft flightpath is perpendicular to the generating aircraft's flightpath. This type of encounter is analogous to a gust encounter in which the aircraft wing and tail surface is subjected to positive and negative "g" loadings varying with the type of vortex generated and spacing behind the generating aircraft, (2) along-track penetration, the following aircraft is flying a flightpath similar to that of the generating aircraft. In this case, the following aircraft is immersed in the downwash flow field of the trailing vortices causing an increased rate of sink, and (3) along-vortex-axis penetration, the following aircraft is flying down the axis of one of the generating aircraft's wingtip vortex. For this encounter, the penetrating aircraft is subjected to a rolling moment. In reality of course, the vortex penetrations are not made precisely as described above. Vortex encounters could be made at various angles with respect to the generating aircraft's flightpath. Also, the along-track penetrations could be made with the following aircraft's wing partially extending through the one vortex with the remaining wing subjected to the downwash flow field. Various investigators have modeled these encounters, starting with the simplest form of encounter through complete simulation accounting for variation of the aircraft flightpath through the vortex flow field.

The treatment of cross-track penetration is presented in the data by McGowan of reference 31. In that work, the Spreiter and Sacks theory (reference 4) is used to determine vortex characteristics. The normal load factor on an airplane traversing trailing vortices is calculated from consideration of the incrementally-induced angles of attack.

A solution of the Navier Stokes equations for vortex tangential velocity is used as a model of the flow field in reference 32.

$$V_\theta = \frac{\Gamma}{2\pi r}\left[1 - \exp\left(\frac{-r^2}{4\nu t}\right)\right] \tag{21}$$

In that reference work, a computer program was presented which accounted for cross-track penetration by calculating normal load factors as experienced similarly in gust encounters and also determined angle-of-attack changes during penetration.

A semi-empirical vortex model using logarithmic radius variation of circulatory strength was used in the development of vortex modeling in references 33 and 34.

$$\frac{V_\theta(r)}{V_\theta(r_c)} = \frac{1 + \ell n\left(\frac{r}{r_c}\right)}{\left(\frac{r}{r_c}\right)} \tag{22}$$

The rolling moment of the penetrating aircraft is then calculated by strip theory for penetration along the vortex core.

Evaluation of penetration effects in reference 35 utilizes an exponential form of induced velocity including eddy viscosity terms. In that work, the derivation is made for radial distance from vortex center at which an aircraft crossing the path of the vortex is in danger of being dragged by the induced vortex velocities into the vortex core. Combinations of wind-tunnel testing and strip theory have been used as in reference 36 to calculate lift and rolling moment of penetrating aircraft.

Flight-test data of actual aircraft penetration has been used as in references 37 through 39 to determine separation distance criteria. The development of vortex strength and persistence based on a modified analytic expression which used available flight data is presented in reference 39. The expression defining aircraft combinations capable of producing a vortex hazard to following aircraft was as follows:

$$\left(\frac{2Jb}{\pi^2}\right) < q\left[\frac{-C_{\ell_\delta}\ \delta_{max}}{C_{\ell_p}}\ \bar{b}\right] \qquad (23)$$

Where,

J = gross weight/b^2, lb/ft^2

q = dynamic pressure

C_{ℓ_δ} = lateral control effectiveness derivative

C_{ℓ_p} = roll damping derivative

$\bar{b}$ = wingspan of probe aircraft, feet

Results of this analysis will be discussed in a following section.

The work performed by Condit and Tracey, reported in reference 2, combines flight-test data of actual penetrations along with derivation of roll rate equations of an aircraft symmetrically encountering one of the trailing vortices. In that development, strip theory is used with an assumed logarithmic variation of circulation to determine rolling moment. The classical analysis of Betz (reference 14) has been developed by Donaldson et al. (references 15 and 40), where a vortex hazard is defined in terms of the pb/2V parameter.

Aircraft response is calculated in reference 41 as a result of penetration at a given angle with respect to the trailing vortex pair. The simulation, using modified lifting surface theory, determines excursions in pitch angle, pitching moment, and angle of attack as a result of the penetration. Further background and reference material pertaining to vortex penetration may be obtained from the descriptions presented in references 34, 39, 42, and 43.

A summary of the methods used to classify vortex penetrations and hazard definition is presented in table 6.

ROLLING MOMENT CALCULATION.

The method of calculating the rolling moments produced on an airplane encountering the vortex system generated by a preceding airplane is described herein, together with the assumption and limitations inherent in the method.

It is generally assumed that the worst form of encounter that an airplane may make with a trailing vortex system occurs when the airplane roll axis is coincident with the vortex axis of rotation. The initial response is in roll, though yaw will usually be present too; and a plausible index of the severity of the encounter is considered to be the steady roll rate that would be produced by the rotating air mass acting on the airplane, assuming that the ailerons are held neutral and that the roll axis remains coincident with the vortex axis. If this steady roll rate exceeds or approaches the roll rate that the ailerons are capable of producing in undisturbed air, then the encounter is considered hazardous. While this represents an oversimplification of the problem, it does nevertheless provide a basis for comparison between one encounter and another. It is also the basis of the roll equation developed by Boeing (reference 2), which was obtained from an application of simple rolling theory and classical vortex theory relating aircraft size, weight, and flight parameters to the strength of the trailing vortex.

In calculating the rolling moment produced on an airplane making such an encounter, the lift distribution on the wing is assumed to be the same as that produced by a vertical gust front, whose velocity distribution across the airplane span is the same as the tangential velocity distribution in the trailing vortex system of the lead airplane, as determined from the NAFEC tower tests. This approach excludes any lateral or longitudinal velocity components, which are of secondary importance.

The vertical gust distribution produces an asymmetric angle-of-attack distribution given by:

$$\Delta\alpha = \Delta v/V$$

where Δv = Vertical gust velocity induced by vortex.
V = True airspeed.

TABLE 6. VORTEX PENETRATION AND HAZARD DEFINITIONS

Ref.	Equation/Term of Hazard	Notes	Assumptions
47	$\dot{p}_v = \dot{p}_m - \dot{p}_a$	Response to given vortex strength.	Requires roll rate time constant.
	$\left(\frac{W/b}{\rho V_\infty}\right)_g + \left(b^2 p_a\right)_f$	Ability of aircraft to overcome vortex.	Need span lift.
	$K\left(\frac{W/b}{\rho V_\infty}\right)_g \Big/ \left(b^2 \tau \dot{p}_a\right)_f$	Empirical ability to overcome vortex.	Span lift, damping, planform.
34	$\frac{C_\ell}{C_{\ell_{\delta_a}}} \delta_a, \lvert p \rvert \Big/ p_{\delta_{max}}$	Ability to control aircraft in vortex.	Pilot assessment.
2	$\left(\frac{W/b}{\rho V_\infty}\right)_g \cdot \left(\frac{1}{b^2 p_a}\right)_f$	Critical area defined, roll control.	Difficult to measure for ATC.
48	$A_d = 2\pi \left(\frac{b_g}{4}\right)^2$	Critical span, rotational velocity.	Arbitrary definitions.
	$C_p = \frac{\Delta p}{\rho/2 V_\infty^2}$	Exceed wing tip velocity, pb/2 max.	
42	$C'_\ell = \ell n \frac{b/2a}{(b/a)(1+.00063\pi/\bar{C}C_L)^{1/2}}$	Symmetrical encounter.	Assumed velocity distribution.
44	$\phi > \pm 10°$	Constant circulation hazard defined $\phi > \pm 10°$.	Uncoupled eq. of motion.
49	$C''_{\ell_{ss}} > 0.1$	Rolling effectiveness.	Subject to ε analysis.
32	$\Delta n = \frac{\rho \, Up \, Vg \, C_{L\alpha}}{2 \, W/S}$	Sharp edge gust penetration.	Gust alleviation factor.

TABLE 6. VORTEX PENETRATION AND HAZARD DEFINITIONS (continued)

Ref.	Equation/Term of Hazard	Notes	Assumptions
38	$\lvert\dot{p}\rvert_{meas} \Big/ \lvert\dot{p}\rvert_{\delta_{max}}$	Inflight penetration data.	Location of vortex.
31	$n = 1 + \left(\frac{C_{L\alpha}}{W} q S\right)\left(\alpha_L + \alpha_r\right)$	Perpendicular penetration.	Spanwise loading constant.
35	$C_l = 0.013 \ln\left(51 b_f / b_g\right) \Big/ \left(b_f / b_g\right)$	Log vortex model.	Aileron effectiveness.
37	$r_{fatal} = \frac{200}{y}^{1/2}$	Danger of aircraft crossing path of vortex.	Pilot inputs.
45	p vs b_f/b_g	Summary of data.	

Definition of Symbols.

I.

a	Vortex core radius.
b	Airplane wingspan.
b_f	Wingspan--following aircraft.
b_g	Wingspan--generator aircraft.
C_l	Rolling moment coefficient (= R.M. $\div (1/2)\rho V^2 Sb$)
$C_{l\delta_a}$	Aileron rolling moment derivative $\partial C_l / \partial \delta a$, per radian
$C_{l_{ss}}$	Steady state rolling moment coefficient.
$\bar{c}$	Mean chord.
$C_{L\alpha}$	Lift coefficient.
C_L	Lift slope, per radian.
$\dot{p}a$	Applied roll acceleration of probe aircraft.
$\dot{p}m$	Measured roll acceleration of probe aircraft.

$\dot{p}_v$	Resultant roll acceleration in vortex.
p	Roll rate.
p_a	Available roll rate.
$p_{\delta max}$	Maximum available roll rate.
U_p	Up gust velocity.
V_g	True airspeed--generator aircraft.
V_∞	True airspeed--generator aircraft.
W	Airplane gross weight.
z	Downstream distance behind generator.

Suffixes: a = available c = critical f = following g = generator aircraft

II. Greek.

α_L	Wing angle of attack modified for aerodynamic lag.
α_r	Induced angle of attack due to airplane response.
δ_a	Aileron angle.
ρ	Density of the atmosphere.
τ	Roll time constant.
ϕ	Roll angle.

The change in angle of attack, distributed asymmetrically along the span, leads to an asymmetric lift distribution which is integrated across the span to determine the rolling moment. The steady roll rate that results is simply that at which the roll-damping moment just cancels the applied moment due to the asymmetric angle-of-attack distribution. The simple strip integration employed to determine the asymmetric lift yields a conservative answer, since the so-called induced angle of attack, due to the encountering airplane's own trailing vortex system is not accounted for. However, the method does yield quick answers and does form a valid basis for comparison between one encounter and another, so long as the airplane encountering the vortex has a wing of moderately large aspect ratio and slight to moderate sweepback. Figure 30 demonstrates how the tangential velocity from the tower data is applied to the wing to generate a rolling moment.

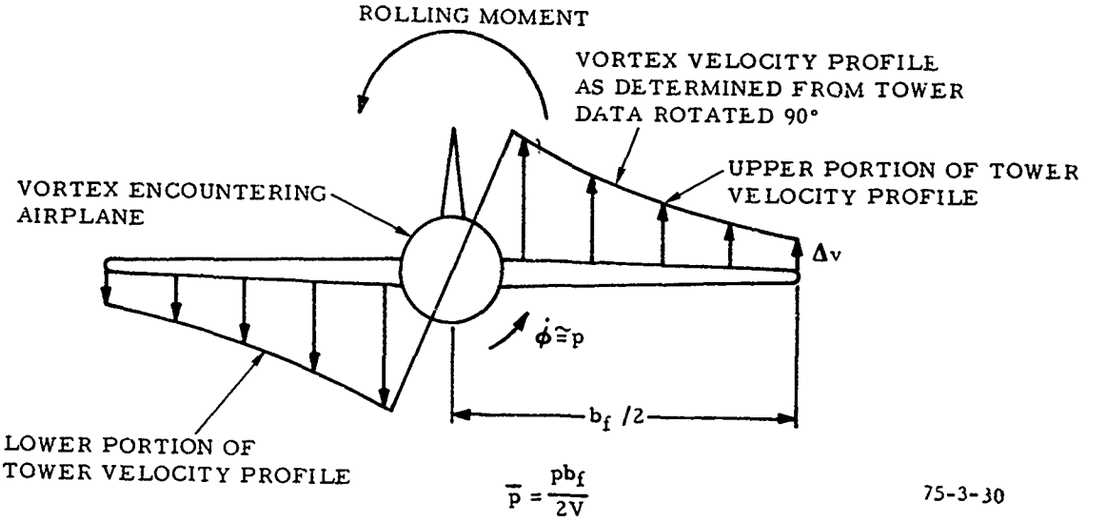

FIGURE 30. APPLICATION OF NAFEC VORTEX TOWER DATA ON FOLLOWING AIRCRAFT ROLLING MOMENT

This very simple criterion can yield no information on the subsequent motion that occurs when an airplane is disturbed in flight by the vortices generated by another. However, having regard for all the simplifying assumptions, if the steady roll rate so determined exceeds the airplane's roll-rate capability, especially at low altitude, there is little doubt that a more lengthy and detailed analysis would reveal that recovery from the upset would be difficult if not impossible.

As a result of modifying the reference 42 equations to include aircraft wing taper, as was developed previously, the non-dimensional roll-rate parameter, pb/2V or $\bar{p}$ is given by:

$$\bar{p} = \frac{12.7}{bV} \int_0^s V_\Theta(r) \left[\frac{r}{s} - \frac{r^2}{s^2} \quad (1-\lambda) \right] dr \qquad (24)$$

where

r = radius
s = semispan
λ = taper ratio

In order to perform computer calculations, the roll-rate equation was used in the following form:

$$\bar{p} = \chi \sum_{\eta=o}^{s} V_\theta(r) \left(\frac{r}{s}\right)\left[1 - \frac{r}{s}\left(1-\lambda\right)\right] \Delta r \tag{25}$$

The tangential velocity profiles obtained by tower fly-by were used in the evaluation of the roll-rate parameter. Standard summation techniques were used to solve equation (25). A complete description of the methods employed may be found in reference 46. In addition to roll rate, the angular momentum (AM) and the kinetic energy (KE) contained within the velocity profiles obtained from the tower data were calculated as follows:

$$AM = 2\pi\rho \int_{R_o}^{R^1} V_\theta(r) r^2 \, dr \tag{26}$$

$$KE = \pi\rho \int_{R_o}^{R^1} V_\theta^2(r) r \, dr \tag{27}$$

The angular momentum, kinetic energy, and roll rate parameter were not only calculated using the tower acquired velocity profiles, but also, a logarithmic model of velocity variation was used and values of AM, KE, and p were compared with the actual test data

$$V_\theta = V_\theta\ (r_c) \left[1 + \frac{\ell n\ (r/r_c)}{(r/r_c)}\right] \tag{28}$$

and

$$V_\theta\ (r_c) = 0.68\left[\frac{W}{qS}\ V\right]\left[\frac{1 + 0.00063Vt}{\bar{c}\left(\frac{W}{qS}\right)}\right]^{-1/2} \tag{29}$$

$$r_c = Co\ C_{\ell_o}\ (0.02) \left[1 + \frac{0.00063Vt}{\bar{c}\left(\frac{W}{qS}\right)} \right]^{1/2} \qquad (30)$$

RESULTS OF ROLL RATE DATA.

One method of specifying aircraft roll capability is given in terms of wingtip helix angle generated by a rolling maneuver. This angle is referred to as roll rate parameter, pb/2V or $\bar{p}$. The results of imposing the acquired tower velocity profiles upon various following aircraft to determine a degree of upset may be found in appendix D.

The resulting values of pb/2V are shown as a function of following to generating wingspan ratio, bf/bg. Each figure is presented for a different aircraft and configuration tested. In calculating pb/2V, it was assumed that the following aircraft had the same airspeed as the generating aircraft. The age of the vortex is determined from t_o, when the aircraft flight was at a point perpendicular to the line from the tower to the flightpath, to t_{final} when the vortex intercepted the tower.

Referring to figure 30, one can see a symmetrical velocity profile centered on the aircraft body longitudinal axis. In reality, the acquired tower velocity profiles include nonuniform effects such as ground effect, boundary layer profile, atmospheric conditions, ground surface irregularities, and tower interference. Each of these factors could cause the velocity profile to be nonsymmetrical. In order to utilize the real data as acquired and to apply results to the calculation of $\bar{p}$, the vortex was treated as two separate halves. The calculation then assumed that each half would contribute to the results independently. Figures 31 and 32 show the results of the calculations for the B727 and L1011 aircraft in takeoff configuration. For the same input conditions, the theoretical logarithmic model figure 31 shows the highest $\bar{p}$ for all values of bf/bg. When utilizing the lower portion of the velocity profile, results are slightly lower than the math model. Finally, the lowest values of $\bar{p}$ are obtained by using the upper portion of the velocity profile. It has been found that the lower portion of the profile in ground effect has been fuller, thus leading to a greater rolling moment on a following aircraft. In order to more realistically represent encounter conditions, figures in appendix D were calculated (and all other plots unless specified) using the upper portion of the velocity profiles. It was first expected that the roll-rate parameter would be a well-ordered function with bf/bg and vortex age as variables. However, the variability of test conditions (due to atmosphere, aircraft variables, wind variability) causes nonuniformities, as can be seen in appendix B. This was also noted in the scatter of data when plotting peak tangential velocity versus vortex age (see figures 8 through 17). In addition, since the vortex is not completely stabilized in the short range of ages tested (up to 60 seconds), rolling moments on following aircraft are affected more by a redistribution of velocity than by decay.

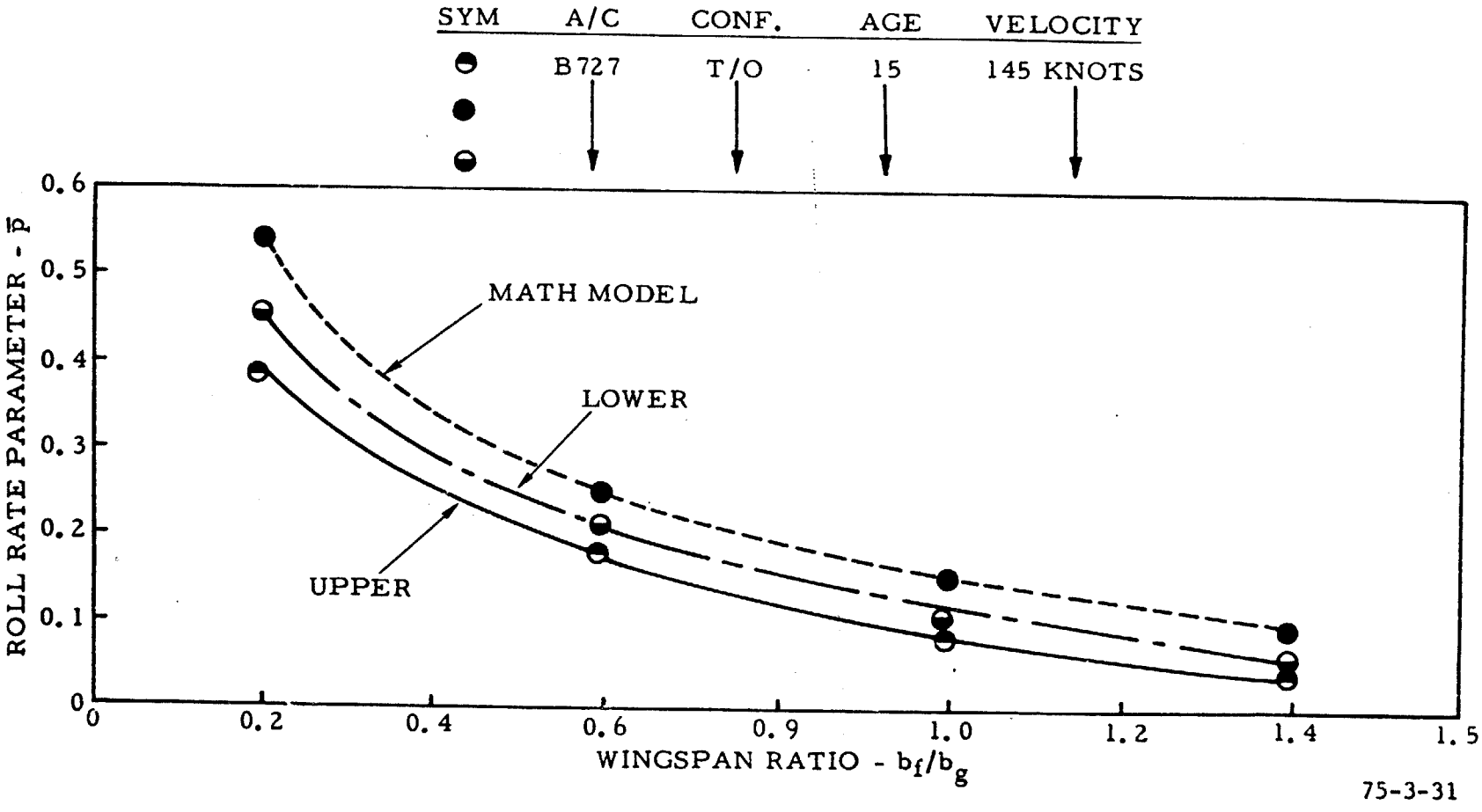

FIGURE 31. CALCULATION OF ROLL RATE PARAMETER USING NONUNIFORM VORTEX TOWER DATA, BOEING 727 AIRCRAFT GENERATING VORTEX

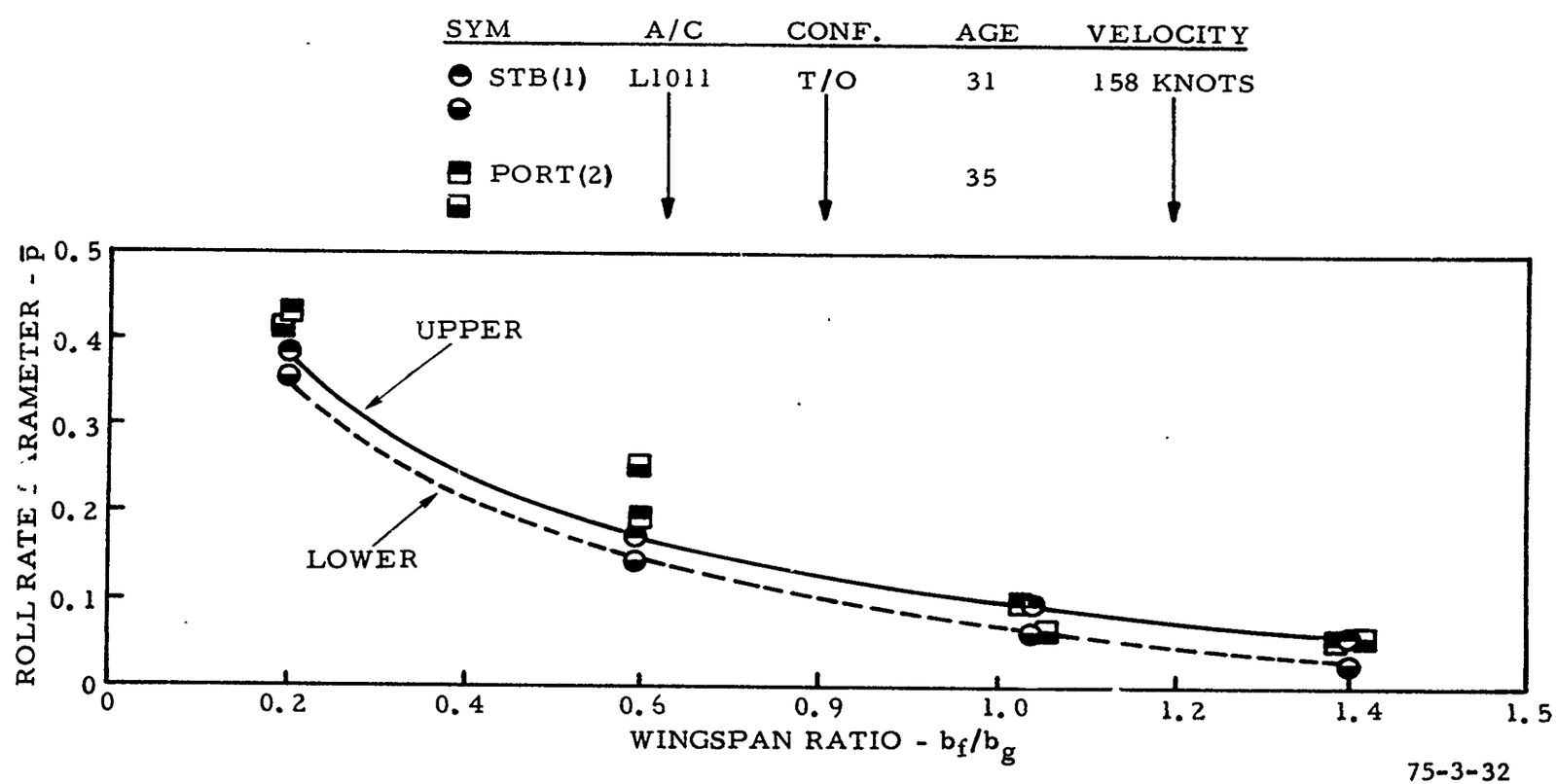

FIGURE 32. CALCULATION OF ROLL RATE PARAMETER USING NONUNIFORM VORTEX TOWER DATA, LOCKHEED L1011 AIRCRAFT

TABLE 7. LEARJET ROLL RATES FOLLOWING VARIOUS AIRCRAFT

Generating Aircraft	Config-uration	Vortex Age (sec)	Separation (nmi)	$\bar{p}$	$\dot{\phi}$ (deg/sec)	Velocity (kn)
DC9	T	21	.96	.17	159	165
		25	1.14	.17	159	
	L	19	.75	.13	104	142
		35	1.38	.28	225	
B727	T	15	.60	.30	247	145
		20	.80	.23	189	
		39	1.57	.14	115	
	L	20	.69	.32	225	124
		24	.83	.32	225	
	H	23	1.3	.07	81	205
		33	1.22	.15	175	
B707	T	22	.87	.18	148	145
		30	1.21	.18	148	
	L	32	1.30	.32	265	146
		81	3.28	.39	323	
		99	4.02	.31	257	
	H	24	1.43	.14	171	215
		40	2.39	.14	171	
		57	3.40	.08	98	
L1011	T	21	.92	.28	251	158
		31	1.36	.36	323	
		45	1.92	.38	341	
		67	2.94	.35	314	
	L	23	.91	.32	258	142
		30	1.18	.43	347	
		30	1.58	.44	355	
		60	2.37	.26	210	
L1011	H	37	3.13	.06	104	305
B727	T	11	.50	.18	167	163
		17	.77	.25	231	
	L	17	.68	.37	305	145
		26	1.05	.27	222	
		35	1.41	.13	107	
		68	2.73	.18	148	
		78	3.14	.29	239	
C5A	T	72	2.64	.48	360	132
	L	49	1.70	.21	149	125
		56	1.94	.28	199	
		64	2.22	.31	220	
	H	48	2.53	.41	442	190
DC7	T	17	.63	.2	152	134
		22	.82	.09	68	
		60	2.23	.07	53	
	L	19	.65	.2	141	124
		30	1.03	.48	338	
		40	1.38	.25	176	
	H	14	.54	.13	103	140
		21	.82	.16	127	
DC10	T	37	1.56	.32	276	152
	L	34	1.32	.31	246	140
		42	1.63	.27	214	
		50	1.94	.28	223	

Note:

T = Takeoff
H = Holding
L = Landing

The effect of generating aircraft configuration on the roll-rate parameter for the following aircraft is similar to the trend previously found for peak tangencial velocity; i.e., the landing and takeoff (figures D-1 through D-3 (appendix D) for the B707 aircraft) produce higher roll rates than for the aircraft in the clean configuration (figure D-2). A comparison of aircraft effects may be found in table 7. Shown on the table are the roll rate parameter p, and the roll rate $\dot{\phi}$, for the Learjet as the following aircraft. Also shown are the vortex ages and corresponding separation distances. This table was prepared using the wingspan data presented in table 8. As can be seen from table 7, separation distances ranged from 0.5 to 4.0 nautical mile (nmi). As was mentioned previously, for the short ages of vortex (also correspondingly small separation distances), the vortex has not decayed significantly (total energy has been redistributed) enough to affect the rolling moment imposed on the following Learjet. A comparison of test data roll rates from the vortex velocity profiles for the Learjet following the DC9 aircraft may be found in figure 33 (from reference 45). As can be seen p_{max} is very large for the short separation distances.

TABLE 8. WINGSPAN RATIOS FOR AIRCRAFT GENERATOR AND PENETRATOR (bf/bg)

		Penetrator Aircraft (Wingspan - Feet)					
Generator Aircraft	bg (ft)	Learjet (34.1)	CV990 (118)	F104 (21.9)	U3 (31)	B737 (93)	DC9 (99.4)
B747	195.7	.17	.60	.11	.19	.47	.46
C5A	222.8	.15	.53	.098	.17	.42	.40
B707	145.75	.23	.81	.15	.25	.63	.61
DC9	89.4	.38	1.31	.24	.41	1.04	1.00
L1011	155	.22	.76	.14	.24	.6	.58
B727	108	.32	1.09	.20	.34	.86	.83
B737	193	.37	1.27	.23	.40	1.00	.96
DC10	155.3	.22	.76	.14	.24	.60	.58
DC7	117.5	.29	1.00	.19	.31	.79	.76

It is to be pointed out that direct comparisons cannot be made since the data of reference 45 was obtained at 5,000 feet altitude.

A similar comparison of p_{max} for the Cessna 210 following the C5A and DC9 may be found in figure 34, (also from reference 45). Roll rates up to 160°/sec are noted for the Cessna 210 following the C5A at a separation distance of 2.2 nmi. For a DC9 following the C5A, the comparisons are seen in figure 35. p_{max} is essentially constant with separation distance from 1.7 to 2.2 nmi.

The effect of vortex age on rolling moment or $\bar{p}$ for the Learjet following various aircraft may be found in figures 36, 37, and 38. This data was

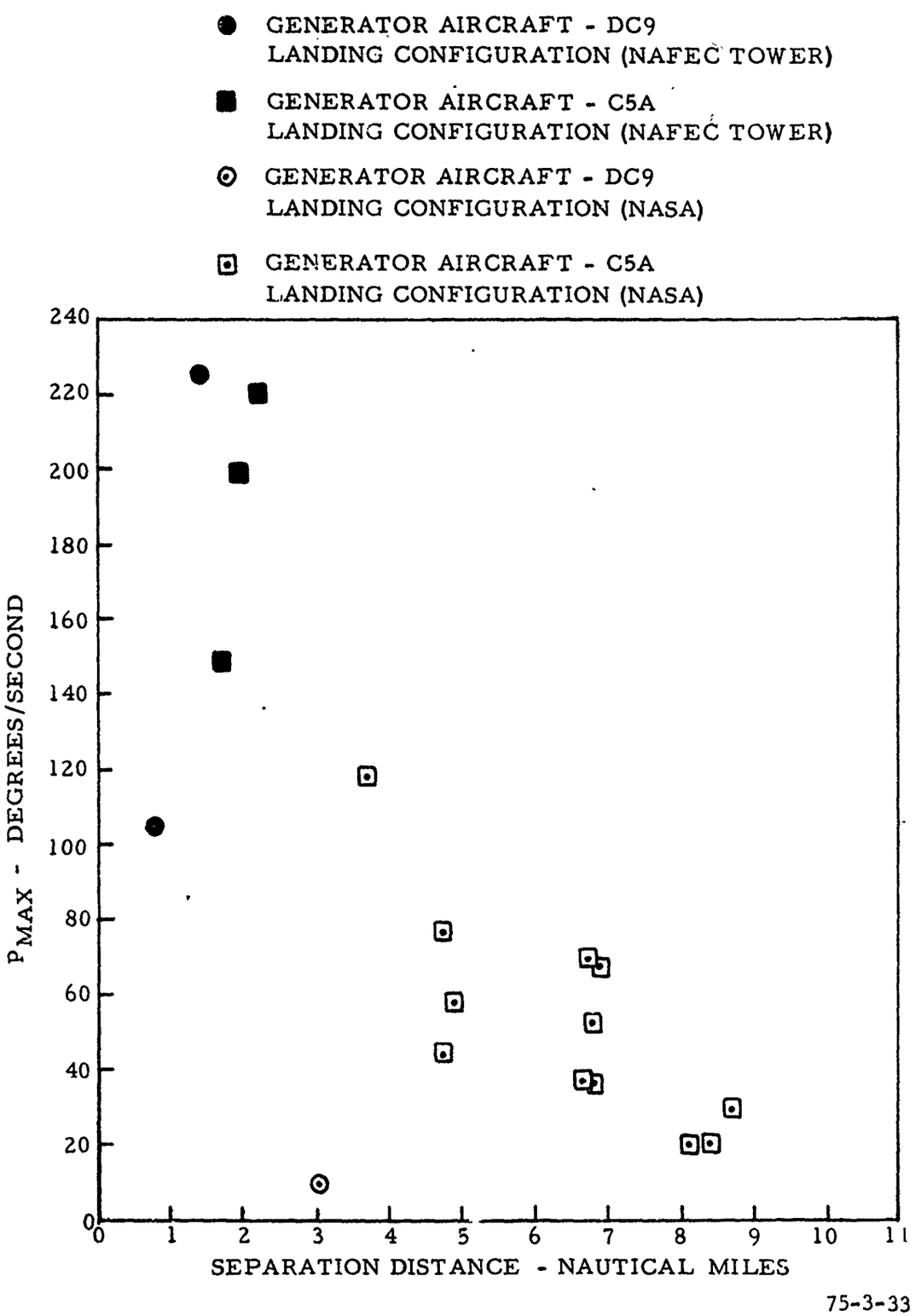

FIGURE 33. LEARJET MAXIMUM ROLL RESPONSE

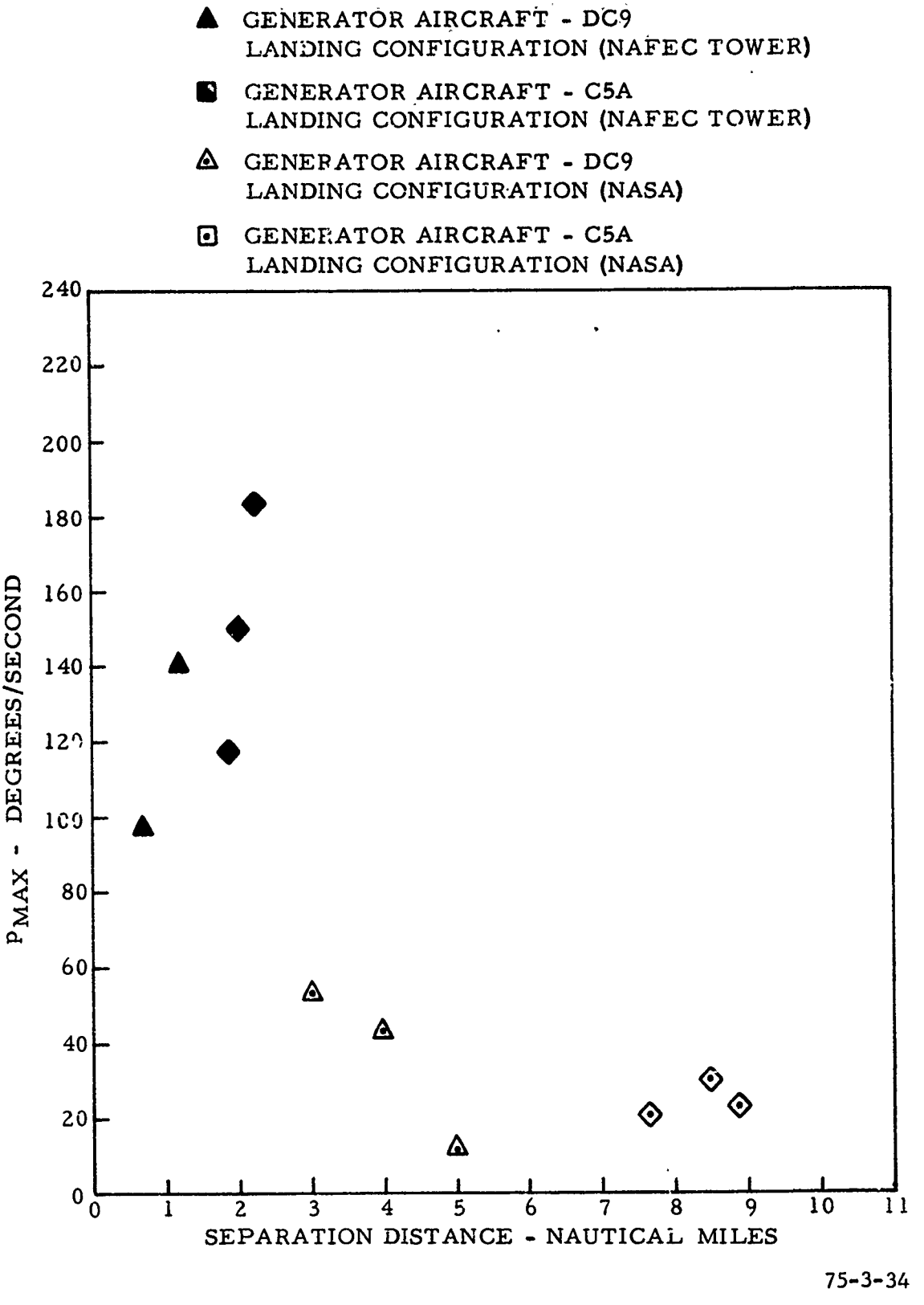

FIGURE 34. CESSNA 210 MAXIMUM ROLL RESPONSE

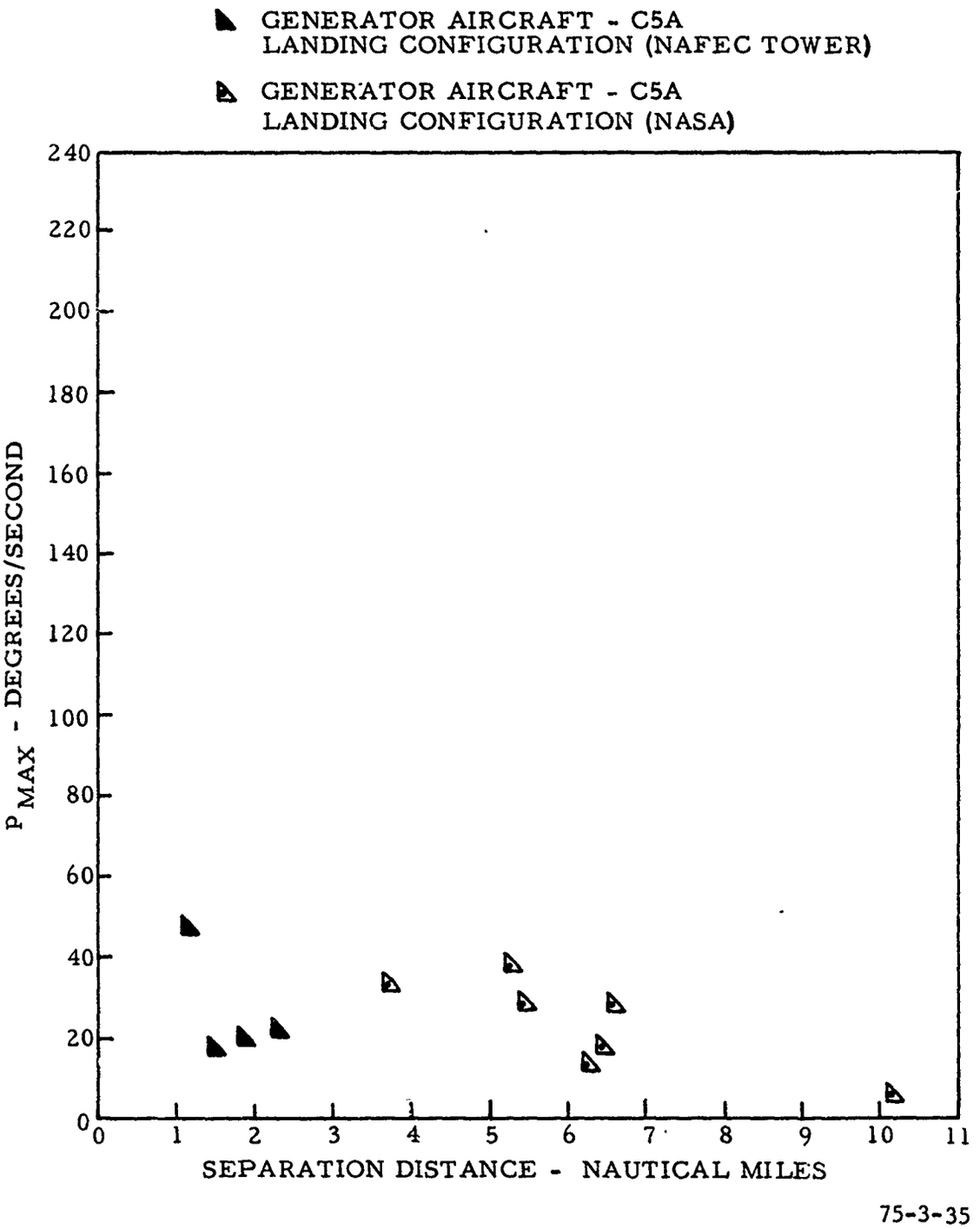

FIGURE 35. McDONNELL-DOUGLAS DC9 MAXIMUM ROLL RESPONSE

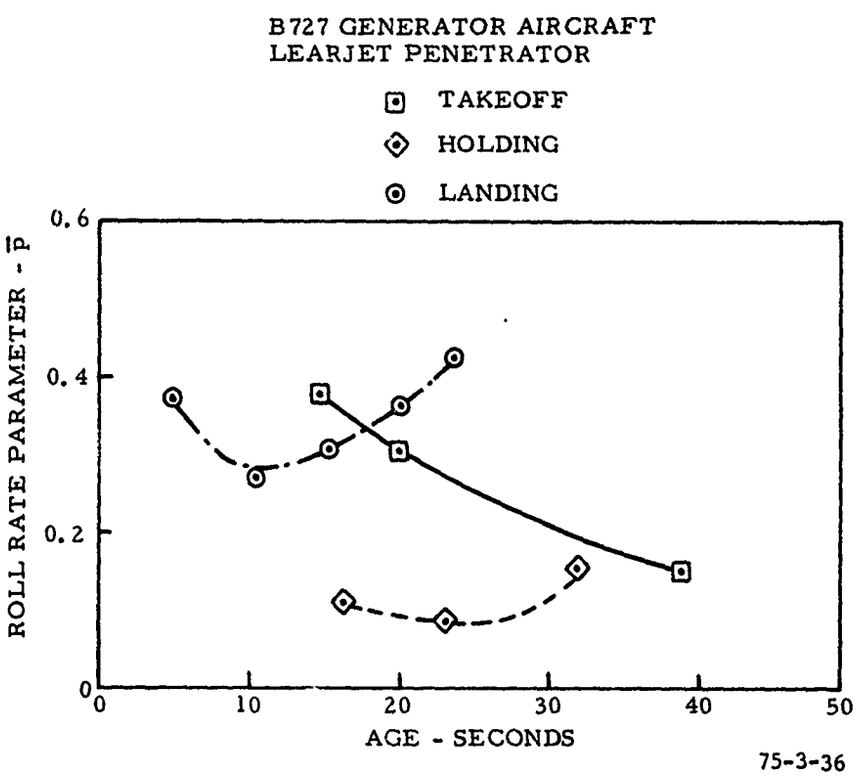

FIGURE 36. EFFECT OF VORTEX AGE ON LEARJET ROLL RATE FOR BOEING 727 VORTEX GENERATOR

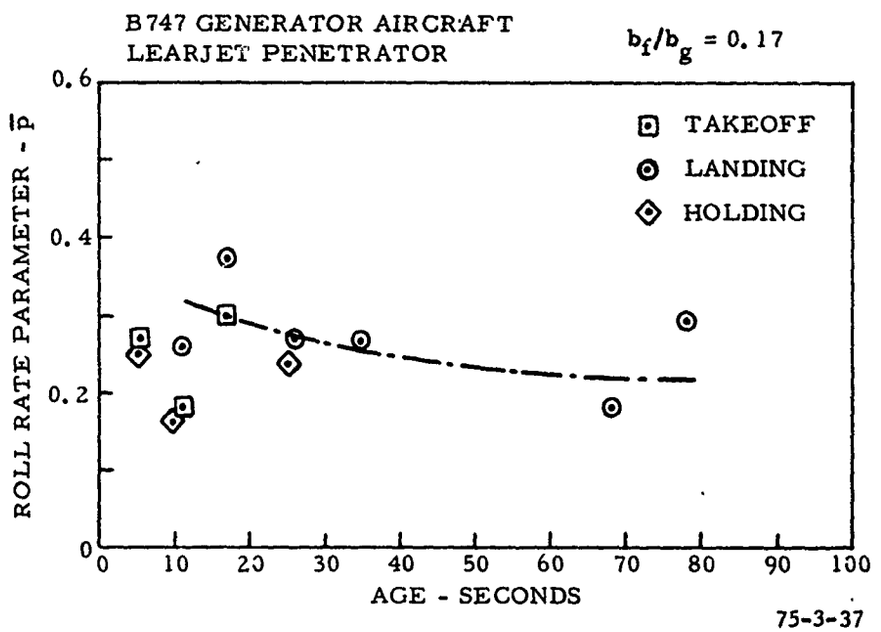

FIGURE 37. EFFECT OF VORTEX AGE ON LEARJET ROLL RATE FOR BOEING 747 VORTEX GENERATOR

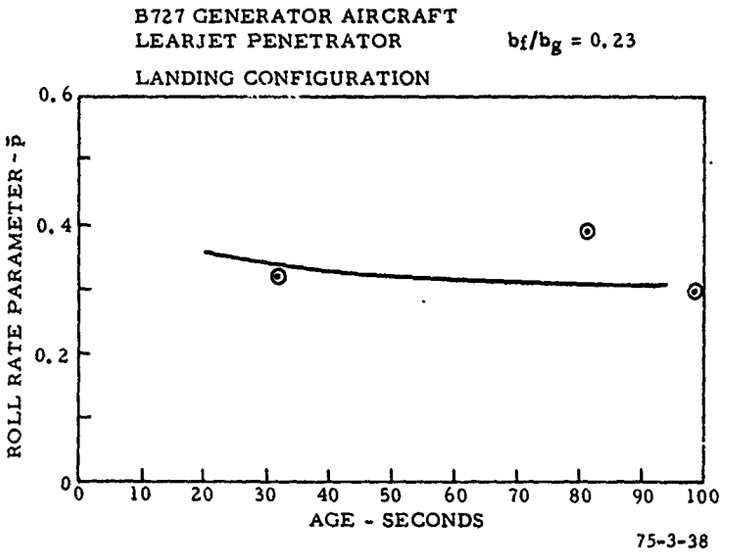

FIGURE 38. EFFECT OF VORTEX AGE ON LEARJET RESPONSE FOR BOEING 707 VORTEX GENERATOR

obtained by cross-plotting the appropriate data from figures 31 and 34 through 39. As can be seen from figure 36, a reduction of $\bar{p}$ with t is seen for a B727 generating aircraft in the takeoff configuration, while the reverse is seen for the landing configuration. Again, as was mentioned previously, the short ages (and separation distances) account for scatter in data, and at best, only an average $\bar{p}$ can be obtained for the short ages. This can be better seen in figures 37 and 38 for the Learjet following a B747 and a B707 aircraft.

A further comparison of the NAFEC tower-acquired data with that of reference 46, may be found in figure 39. The data falls within the range of test data acquired by NASA except for the F104 following the C5A which is most likely due to the small wing span of the F104 (21.9 feet) and the inability to encounter exactly centered on the vortex (which is assumed in all cases in the analysis presented in this report).

The results of the computer simulation (reference 34) of a vortex encounter are presented in figure 40. The penetrating aircraft is a DC9 and the generators are DC9, 727, and DC10 aircraft. The maximum roll angle is seen to be essentially constant for all combinations for separations from 2 to 3 miles. As was explained in reference 34, the insensitivity of ϕ with separation was due in part to the logarithmic math model used to describe the vortex which resulted in only a slight change in rolling moment coefficient with age (or separation distance). Shown also on figure 40 is the NAFEC data (for separation distances only up to 2 miles due to short vortex ages). The agreement is good considering that completely different methods of analysis were used.

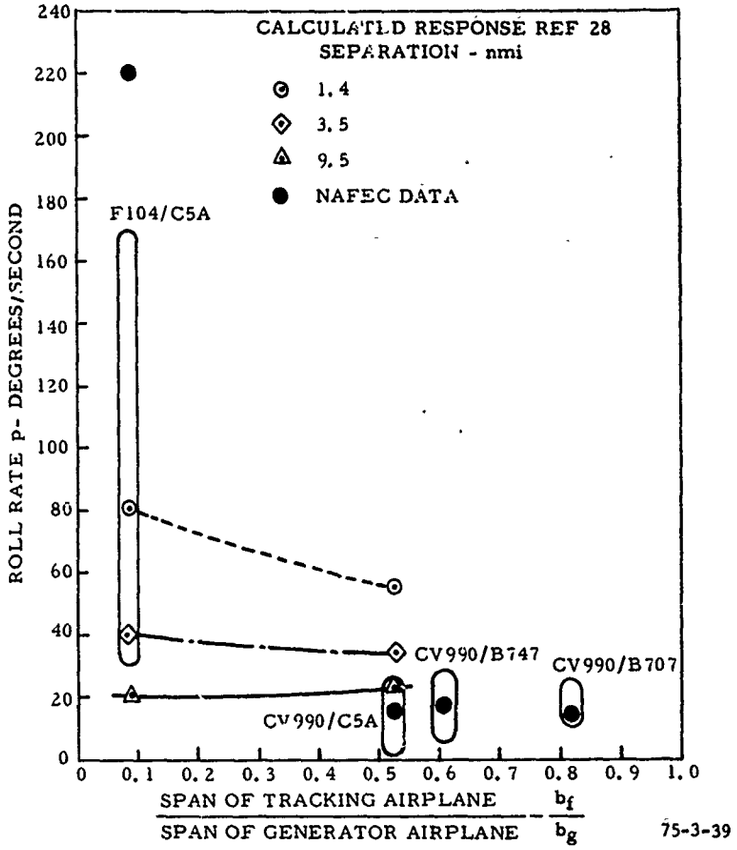

FIGURE 39. SUMMARY OF THE ROLL-RATE RESPONSE OF THE PROBE AIRCRAFT AS A FUNCTION OF WINGSPAN RATIO (FROM REFERENCE 44)

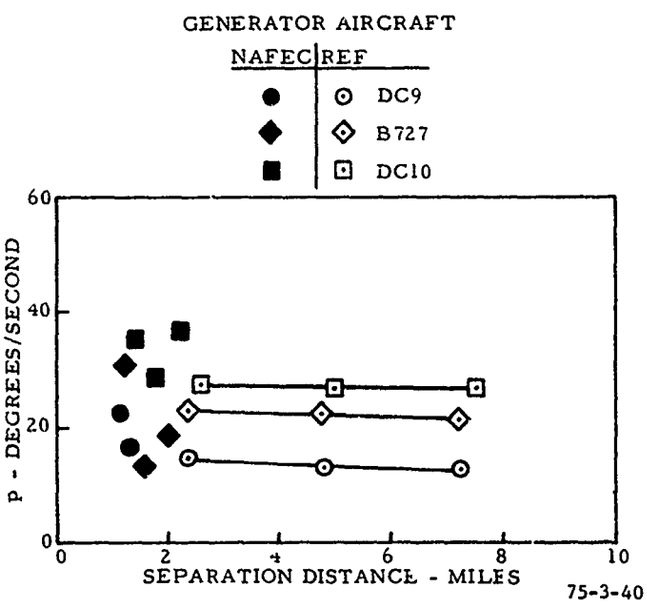

FIGURE 40. MAXIMUM ROLL ANGLE AND ROLL RATE OF A McDONNELL-DOUGLAS DC9 IN THE WAKE OF A McDONNELL-DOUGLAS DC9, BOEING 727, AND McDONNELL-DOUGLAS DC10

The effect of generating airplane gross weight on peak-induced roll rate may be found in figure 41 (from reference 2). The data of reference 2 shows little effect of gross weight on roll rate p; however the NAFEC tower data does show an increase in $\bar{p}$ with gross weight. It is to be noted however that during the calculation of $\bar{p}$, the increasing gross weight also includes effects of aircraft configuration from DC9, 707, DC10, C5A, whereas the data of reference 2 assumes constant aircraft configuration.

The strong effect of encountering airplane span on p is seen (as was noted in reference 2) in figure 42. The difference in the two curves is due in part to the fact that the aircraft gross weights differed from 534,000 pounds for the NAFEC data while 400,000 pounds was used in reference 2.

The results of correlation between kinetic energy and angular momentum (from equations (26) and (27)) with roll rate parameter, p, are found in figures 43 and 44. Shown on figure 43 for the B727 aircraft as the generator in various configurations is the almost direct relationship of $\bar{p}/KE$ for $bf/bg = 0.2$. Thus, one measure of aircraft roll appears to be connected with vortex wake energy.

Similarly, another measure of roll as seen in figure 44 is the wake momentum (also shown for B727 and DC9 aircraft in various configurations).

SEPARATION CRITERIA.

Each investigator who studies vortex behavior will define a vortex penetration hazard in a slightly different manner as was shown in table 7. In addition to defining closed analytic solutions, such as load factor, control moment exceedence, and critical area, there are other factors to be considered when determining safe separation criteria. The considerations presented in reference 25 are especially important and worth presenting here. They include:

1. Dependence of wake-encounter probability on time and location.

2. Vortex trajectory after generation.

3. Terrain in vicinity of runway.

4. Seasonal variations in wind.

5. Atmospheric conditions--turbulence level, inversions, wind shear.

6. Operational procedures.

7. Vortex instabilities--pinching, bursting, meandering, breakup.

8. Safety record.

9. Pilot and air traffic control training and awareness of vortex factors which minimize vortex encounter probability.

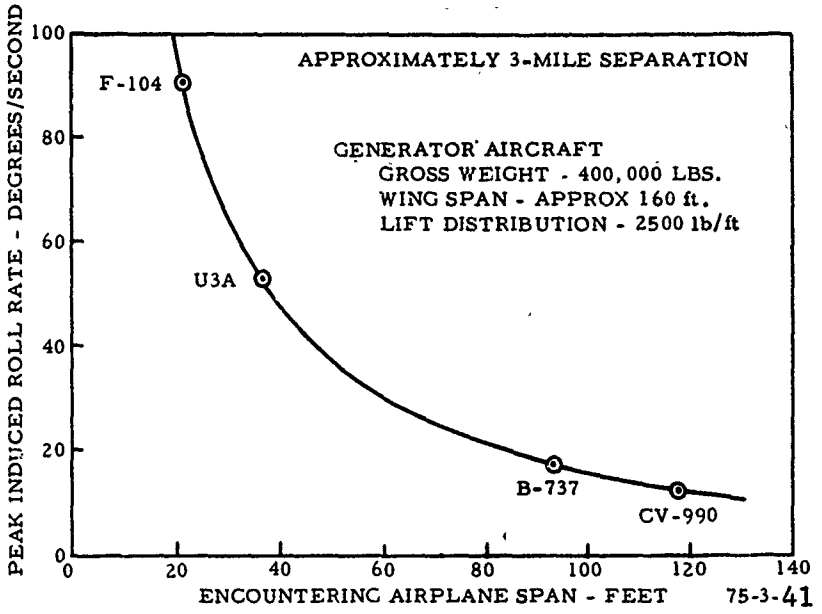

FIGURE 41. EFFECT OF ENCOUNTERING AIRPLANE WINGSPAN

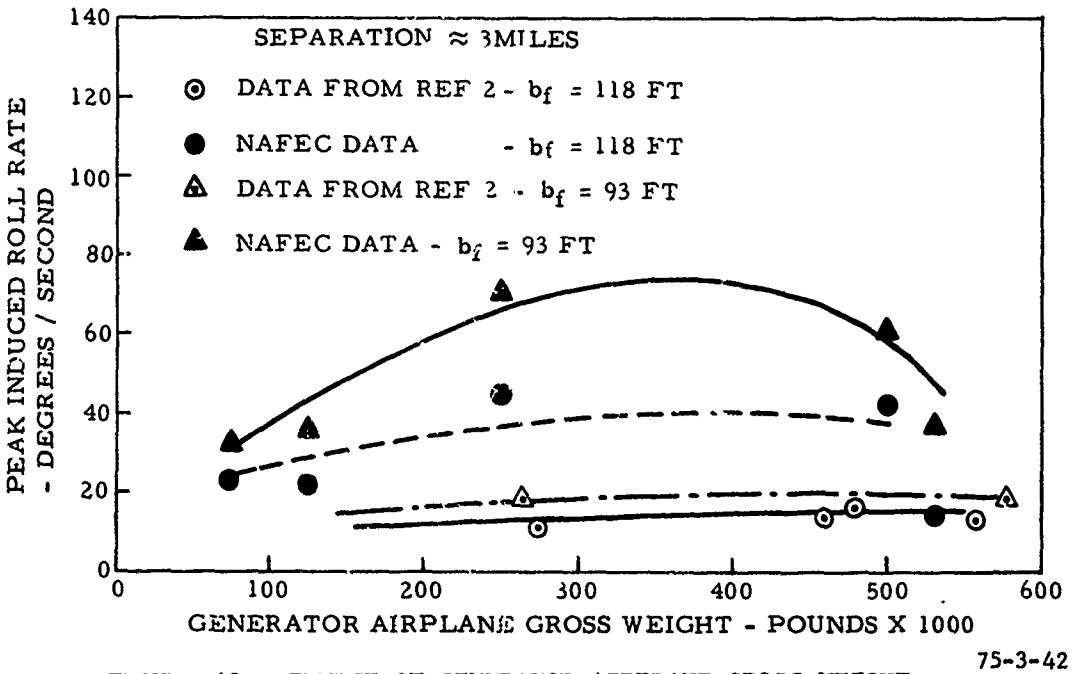

FIGURE 42. EFFECT OF GENERATOR AIRPLANE GROSS WEIGHT

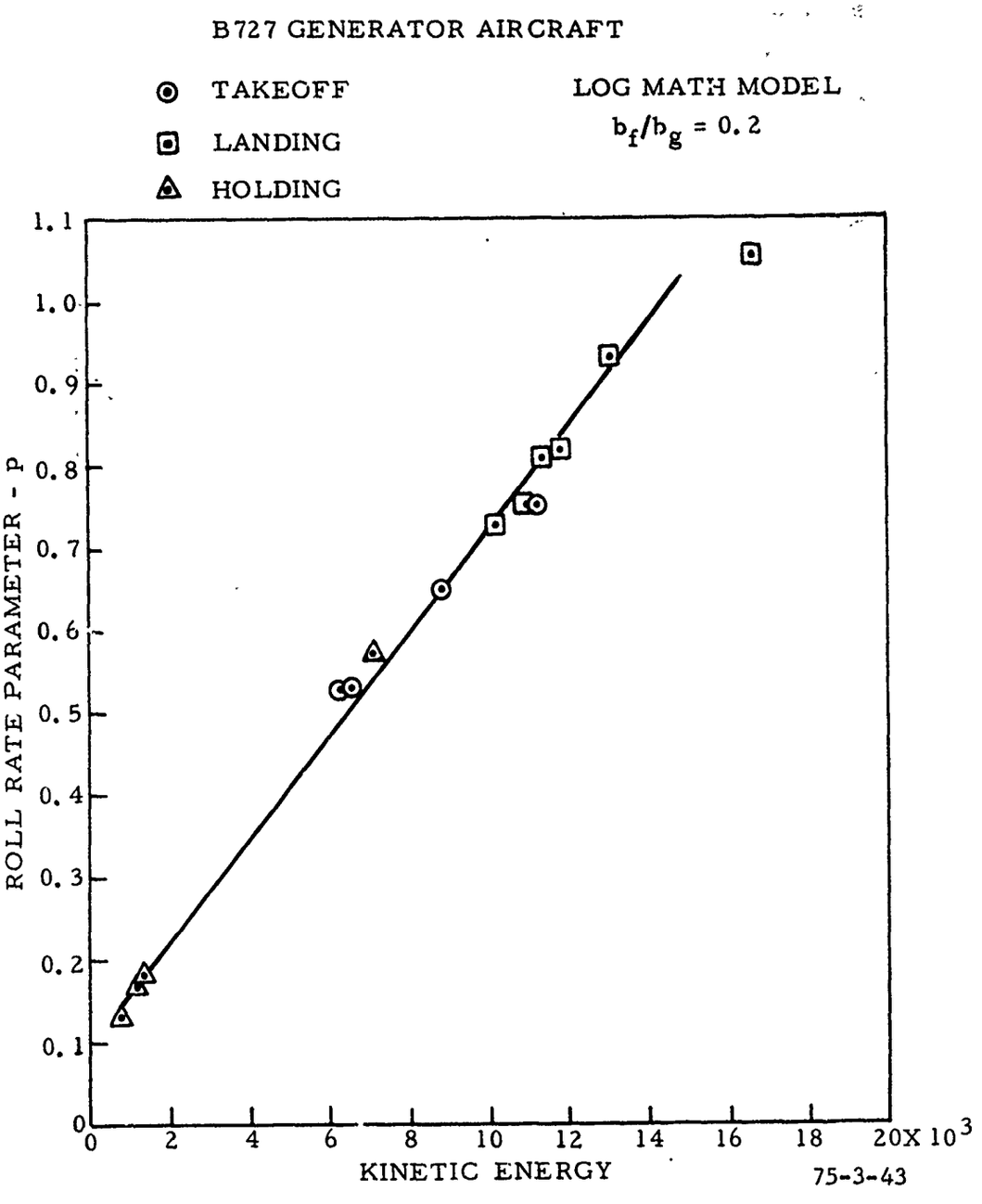

FIGURE 43. ROLL RESPONSE AS AFFECTED BY VORTEX KINETIC ENERGY

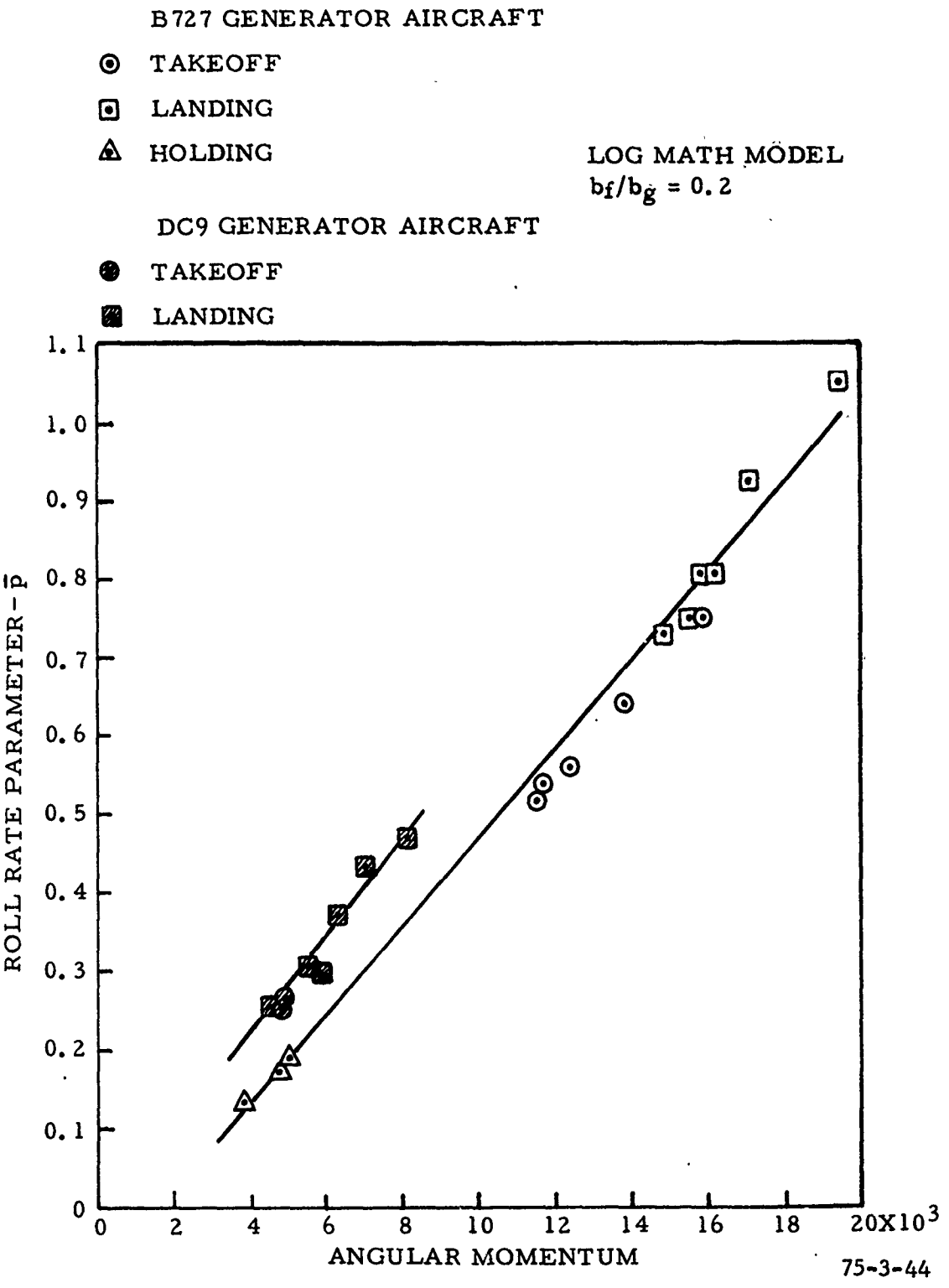

FIGURE 44. ROLL RESPONSE AS AFFECTED BY VORTEX ANGULAR MOMENTUM

One method of determining separation for air traffic control purposes was the concept of a vortex avoidance corridor as developed from the data of reference 30. In that work, consolidation of vortex data revealed wake breakup of approximately 2.6 minutes for flight above 5,000 feet and 2 minutes below 5,000 feet, thus establishing longitudinal separation. Consideration of vortex descent and crosswinds were utilized in that report to establish lateral and vertical separations. For the purpose of this report only the longitudinal separation is considered. As was mentioned in the previous section, one method to evaluate hazards was through roll-rate exceedance. The roll rates produced on a Learjet penetrating the wake of a B727 at various separations (in reality, various ages as the profiles measured on the NAFEC tower) is shown in figure 45.

The longest-lived B727 vortex (t = 78 seconds) measured on the tower would produce a roll rate of 230°/second on a following Learjet. Extrapolating the maximum data points, one can see a required separation distance of 7.3 nmi based on maximum roll capability established in reference 40. These results can be compared to those presented in reference 25 (figure 46). The criterion used in reference 25 is based on control power, $|\dot{p}|_{meas}/|\dot{p}|_{\delta_{max}} = 1$, which compares favorably with those obtained from figure 45.

SUMMARY--VORTEX PENETRATION EFFECTS.

Various methods have been used by investigators to classify the effects of vortex penetration. The method of calculating rolling moments on an airplane encountering the vortex system generated by a preceeding aircraft is the method selected in this report. The velocity profile data obtained from the NAFEC tower fly-bies was used with a logarithmic mathematical model to calculate the aircraft lift distribution, hence the rolling moment. The resulting roll rate parameter, $\bar{p}$, or pb/2v may then be compared with the aircrafts roll rate capability to determine the severity of the vortex encounter.

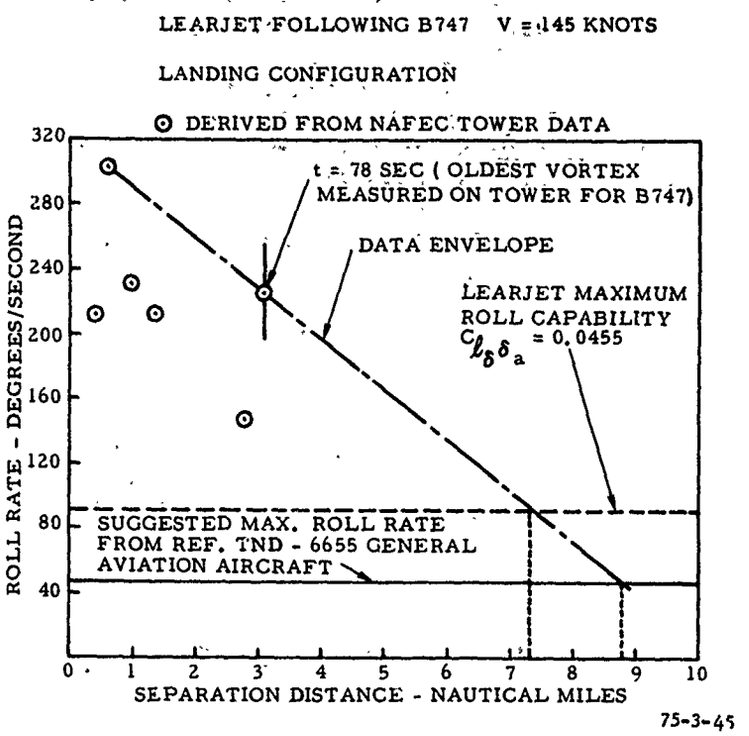

FIGURE 45. DEVELOPMENT OF SEPARATION CRITERIA BASED ON ROLL VELOCITY

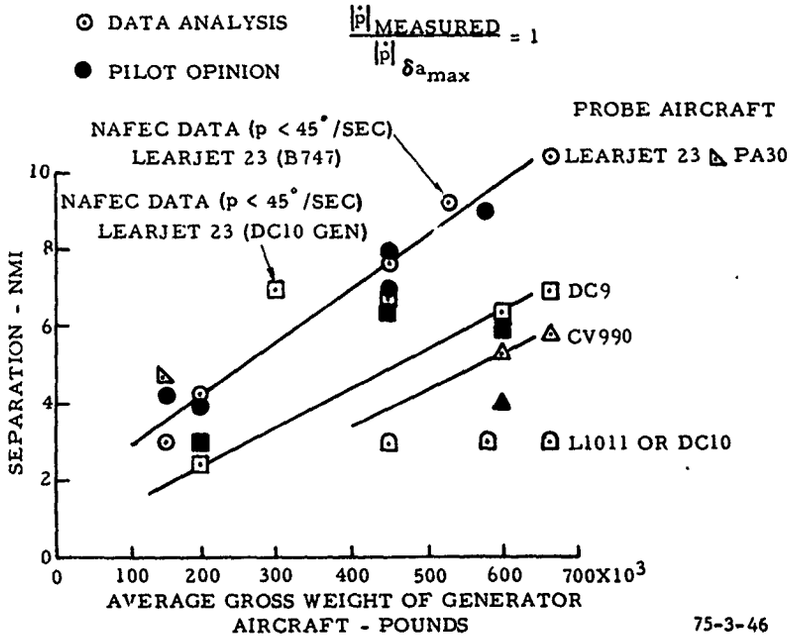

FIGURE 46. SEPARATION BASED ON ROLL CONTROL CRITERIA

CONCLUSIONS

1. Four-engine jet transports (with wing-mounted engines) produce small-core high-peak velocity vortices at zero and small (up to 10°) flap settings, and large-core low-peak velocity vortices at large flap settings (>25°).

2. Design configurations employing solely fuselage-mounted engines, or inboard wing-mounted engines far removed from the termination of the trailing edge flaps, consistently produce small-core, high-peak velocity vortices in all flight configurations.

3. Fully developed vortices with well-defined axial flow conform closely to the Hoffman-Joubert logarithmic circulation distribution.

$$\Gamma = \Gamma_o(\ln r/r_c + 1)$$

4. For altitudes below 5,000 feet, the maximum duration of a vortex system is approximately 2 minutes.

5. Previous work (reference 30) indicates that at higher altitudes (5,000 to 15,000 feet), the vortex life may be as long as 2.6 minutes.

6. Vortex duration is diminished by ambient wind, due to the associated turbulence.

7. In the earth's boundary layer, in the presence of a crosswind, the upwind vortex of a pair tends to be more persistent and intense than the downwind vortex.

8. In this test series, using the tower fly-by technique, the usual mechanism of vortex decay was the development of an unstable condition leading to vortex bursting.

9. Decay of vortices in the upper atmosphere also takes place through a form of instability -- either bursting or sinusoidal instability and linking.

10. Turning flight, up to 30° of bank, does not induce lateral separation between members of a vortex pair.

11. The wingspan ratio of following to generating aircraft is an important factor in determining following aircraft upset.

12. Based on a suggested roll capability of 45°/second, the study shows that a separation of 9 miles should be maintained for the Lear Jet following a B747.

13. Based on the Lear Jet's maximum roll capability, it should maintain a separation of seven miles behind a B747.

14. A simple relationship between separation and generating aircraft gross weight for various probe aircraft yields good results. The data obtained by the tower profile method agrees fairly well with that developed by flight test.

REFERENCES

1. Garodz, Leo J. Measurements of the Vortex Wake Characteristics of the Boeing 747, Lockheed C5A and Other Aircraft, Data Report, Project 177-621-03X (Special Task No. 1), April 1970.

2. Condit, Philip M. and Tracey, P. W., Results of the Boeing Wake Turbulence Test Program, Boeing Document No. D6-30851, April 1970.

3. Andrew, William H., Robinson, Glenn H., Krier, Gary E., and Drinkwater, Fred J., III, Flight Test Evaluation of the Wing Vortex Wake Generated by Large Jet Transport Aircraft, FWP-18, Edwards Flight Research Center, 1970.

4. Spreiter, John R. and Sacks, Alvin H., The Rolling Up of the Trailing Vortex Sheet and Its Effect on the Downwash Behind Wings, Journal of the Aerospace Sciences, Volume 18, No. 1, January 1951.

5. Eisenhuth, Joseph J., McCormick, B.W., Nelson, Robert C., Aero Engineering Associates, State College, Pa.; and Garodz, Leo J., FAA/NAFEC; Analysis of Experimental Measurements of Trailing Vortex Systems of Large Jet Transport Aircraft, NAECON, 1971 Record.

6. Garodz, Leo J., Lawrence, David M. and Miller, Nelson J., The Measurement of the Boeing 747 Trailing Vortex System Using the Tower Fly-By Technique, FAA/SRDS, FAA-RD-73-156, June 1974.

7. Garodz, Leo J., Miller, Nelson J., and Lawrence, David M., The Measurement of the Boeing 707 Trailing Vortex System Using the Tower Fly-By Technique, FAA/SRDS, FAA-RD-75-15, February 1975.

8. Garodz, L. J., Investigation of the Relatively Long Time-History Vortex Characteristics of the CV880 Airplane in Terminal Area-Type Flight Operations, Data Report, Project 504-303-03X (Special Task Number Three), FAA/NAFEC, November 1970.

9. Garodz, Leo J., Abbreviated Full Scale Flight Tests Investigation of the Lockheed L1011 Vortex System, FAA/SRDS-75 (in process).

10. Garodz, Leo J., Abbreviated Investigation of the McDonnell-Douglas DC10 Airplane Vortex Wake Characteristics in Terminal Area-Type Operations, FAA/SRDS-75- (in process).

11. Garodz, Leo J., Lawrence, David M., and Miller, Nelson J., The Measurement of the Boeing 727 Trailing Vortex System Using the Tower Fly-By Technique, FAA/SRDS, FAA-RD-74-90, August 1974.

12. Garodz, Leo J., Lawrence, David, Miller, Nelson, The Measurement of the McDonnell-Douglas DC9 Trailing Vortex System Using the Tower Fly-By Technique, FAA/SRDS, FAA-RD-74-173, November 1974.

13. Garodz, Leo J., Lawrence, David, Miller, Nelson, The Measurement of the DC7 Trailing Vortex System Using the Tower Fly-By Technique, FAA/SRDS, FAA-RD-73-141, November 1973.

14. Betz, A., Behavior of Vortex Systems, English translation published as Technical Memorandum 713, National Advisory Committee for Aeronautics, June 1933.

15. Donaldson, Coleman duPont, Snedeker, Richard S., and Sullivan, Roger D., A Method of Calculating Aircraft Wake Velocity Profiles and Comparison with Full-Scale Experimental Measurements, Aeronautical Research Associates of Princeton, Inc., Published as AIAA Paper No. 74-39, 1974.

16. Lamb, Sir Horace, Hydrodynamics, p. 592, 6th Edition, Dover Publications, New York, New York.

17. McCormick, Barnes W., Tangler, James L., and Sherrieb, Harold E., Structure of Trailing Vortices, AIAA Journal of Aircraft, Volume 5, No. 3, May-June 1968.

18. Bisgood, P. L., Maltby, R. L., and Dee, F. W., Some Work at the Royal Aircraft Establishment on the Behavior of Vortex Wakes, Presented at a symposium on Aircraft Wake Turbulence held in Seattle, Washington, September 1-3, 1970. Proceedings published as Aircraft Wake Turbulence and Its Detection, by Plenum Press, New York - London, 1971.

19. Hoffman, E. R. and Joubert, P. N., Turbulent Line Vortices, Journal of Fluid Mechanics, Volume 16, Part 3, p. 395-441, July 1963.

20. Squire, H. B., On the Growth of a Vortex on Turbulence Flow, Aeronautical Research Council, London, Paper No. 16,666, 1968.

21. Schlichting, H., Boundary Layer Theory, Fourth Edition, McGraw-Hill Book Company, New York, Chapter XIX, 1960.

22. Milne-Thomson, L. M., Theoretical Aerodynamics, Second Edition, Macmillan and Company, Ltd., London, p.206-207, 1952.

23. Crow, S. C., Stability Theory for a Pair of Trailing Vortices, Boeing Scientific Research Laboratories Document D1-82-0918 and AIAA Paper 70-53, January 1970.

24. Tombach, I., Observations of Atmospheric Effects on Vortex Wake Behavior, Journal of Aircraft, November 1973.

25. Tymczyszyn, J. J. (FAA), and Barber, Marvin R. (NASA-Flight Research Center), Recent Wake Turbulence Flight Test Programs, Presented at the 18th Annual Symposium of the Society of Experimental Test Pilots, Beverly Hills, California, September 26, 1974.

26. Chevalier, H., Flight Test Studies of the Formation and Dissipation of Trailing Vortices, SAE Paper 730295, Business Aircraft Meeting, Wichita, Kansas, April 3-6, 1973.

27. Garodz, L. J. and Miller, N. J., Investigation of the Vortex Wake Characteristics of Jet Transports During Climbout and Turning Flight, FAA Report AEQ-1 (FAA/NA-75-38), January 1975.

28. Kerr, T. H. and Dee, F. W., A Flight Investigation Into the Persistence of Trailing Vortices Behind Large Aircraft, Technical Note Aero 2649, Royal Aircraft Establishment, September 1959.

29. Lissaman, P. B. S., et al, Aircraft Vortex Descent and Decay Under Real Atmospheric Effects, FAA-RD-73-120, October 1973.

30. McGowan, W. A., Trailing Vortex Hazard, Paper presented at Business Aircraft Meeting, Wichita, Kansas, SAE-68-0220, April 3-5, 1968.

31. McGowan, W. A., Calculated Normal Load Factors on Light Airplanes Traversing the Trailing Vortices of Heavy Transport Airplanes, NASA TN-D-829, May 1961.

32. Funston, N. L. and Koeb, S. J., A Trailing Vortex Model and its Effect on A Penetrating Aircraft, NAECON 1971 Report.

33. Nelson, R. C. and McCormick, B. W., Aircraft Vortex Penetration, SAE Paper 730296

34. Nelson, R. C., The Response of Aircraft Encountering Aircraft Wake Turbulence, AFFDL-TR-74-29, Air Force Flight Dynamics Lab, June 1974.

35. Attwooll, V. W., The Effects of Trailing Vortices on the Safe Capacity of Air Routes and Airports, RAE TM Math 6702, 1967.

36. Iversen, J. D. and Bernstein, S., Trailing Vortex Effect on Following Aircraft, Journal of Aircraft, Vol. 11, No. 11, 1973.

37. Verstynen, H. A. and Dunham Jr., R. E., A Flight Investigation of the Trailing Vortices Generated By A Jumbo Jet Transport, NASA-TN-D-7172, April 1973.

38. Andrews, W. H., Robinson, G. H., and Larson, R. R., Exploratory Flight Investigation of Aircraft Response to the Wing Vortex Wake Generated by Jet Transport Aircraft, NASA-TND-6655, March 1972.

39. Robinson, G. H. and Larson, R. R., A Flight Evaluation of Methods for Predicting Vortex Wake Effects on Trailing Aircraft, NASA-TN-D-6904, November 1972.

40. Donaldson, C. duPont, et al., Vortex Wakes of Large Aircraft, Notebook, AIAA Professional Study Series, Vol. 2, June 1974.

41. Ramirez Jr., Rao, B. M. and Cronk, A. E., Longitudinal Response of an Aircraft Due to a Trailing Vortex Pair, Journal of Aircraft, Vol. 10, No. 10, 1973.

42. McCormick, B. W., Aircraft Wakes: A Survey of the Problem, Paper presented at FAA Symposium on Turbulence, Washington, D.C., March 1971.

43. El-Ramly, Z., Aircraft Trailing Vortices: A Survey of the Problem, Technical Report Faculty of Engineering, Carleton University, Ottawa, Report No. ME/A72-1, November 1972.

44. Harlan, R. and Madden Jr., S., Avoidance Hazard Definition for Wake Turbulence Encounters During Arrival Operations, MIT/MSL/RE 81, March 1973.

45. Anon, Vortex Wake Turbulence - Flight Tests Conducted During 1970, FAA/NASA/Boeing Report No. FAA-FS-71-1, February 1971.

46. Kobialka, E., TANFIV, Wakes and Vortices, NAFEC Memo 214-741-04X, May 1972.

47. Compilation of Work Papers Concerning Wake Turbulence Tests, Federal Aviation Administration, FSS, April 1970.

48. Donaldson, C. duPont, A Brief Review of the Aircraft Trailing Vortex Problem, AFOSR-TR-71-1910, May 1971.

49. Thelander, J., Separation Minimums for Aircraft Considering Disturbances Caused by Wake Turbulence, ATAB, FAA, January 1969.

APPENDIX A

TEST AIRPLANE SPECIFICATIONS AND THREE-VIEW DRAWINGS

LIST OF ILLUSTRATIONS

APPENDIX A

TEST AIRPLANE SPECIFICATIONS AND THREE-VIEW DRAWINGS

GROUP I

Boeing 747, Series 100

Wingspan	195 feet, 8 inches
Length	225 feet, 2 inches
Height	63 feet, 5 inches
Wing Area	5,500 square feet
Root Chord	54 feet, 4 inches
Tip Chord	13 feet, 4 inches
Aspect Ratio	5.8 (span + av. chd.)
Taper Ratio	.25
Wing Quarter-Chord Sweep Back	37.5 degrees
Maximum Takeoff Weight	710,000 pounds
Maximum Landing Weight	564,000 pounds
Powerplant	Pratt & Whitney JT9D-3A Turbofans (4)

The wings have full-span leading-edge flaps (variable camber outboard, Kreuger flaps inboard). Trailing-edge flaps are triple-slotted chord-extending, in two segments per side, with cut-outs at the fuselage and in line with the inboard engines. Low-speed control is by outboard ailerons, outboard spoilers (situated immediately ahead of the outboard flaps) and by inboard ailerons (situated in the cut-out between inboard and outboard flap segments). High-speed lateral control is by inboard ailerons only.

GROUP I

Boeing 707-320

Wingspan	145 feet, 9 inches
Length	152 feet, 11 inches
Height	42 feet, 5 inches
Wing Area	3,010 square feet
Root Chord	33 feet, 11 inches
Tip Chord	9 feet, 4 inches
Aspect Ratio	6.75 (span + av. chd.)
Taper Ratio	0.275
Wing Quarter-Chord Sweep Back	35 degrees
Maximum Takeoff Weight	332,000 pounds (320C)
Maximum Landing Weight	247,000 pounds (320C)
Powerplant	Pratt & Whitney JT3D-3 Turbofans (4)

The wings have full-span leading-edge flaps and Fowler-type trailing-edge flaps in two segments per side. A cut-out, between inboard and outboard flap segments,

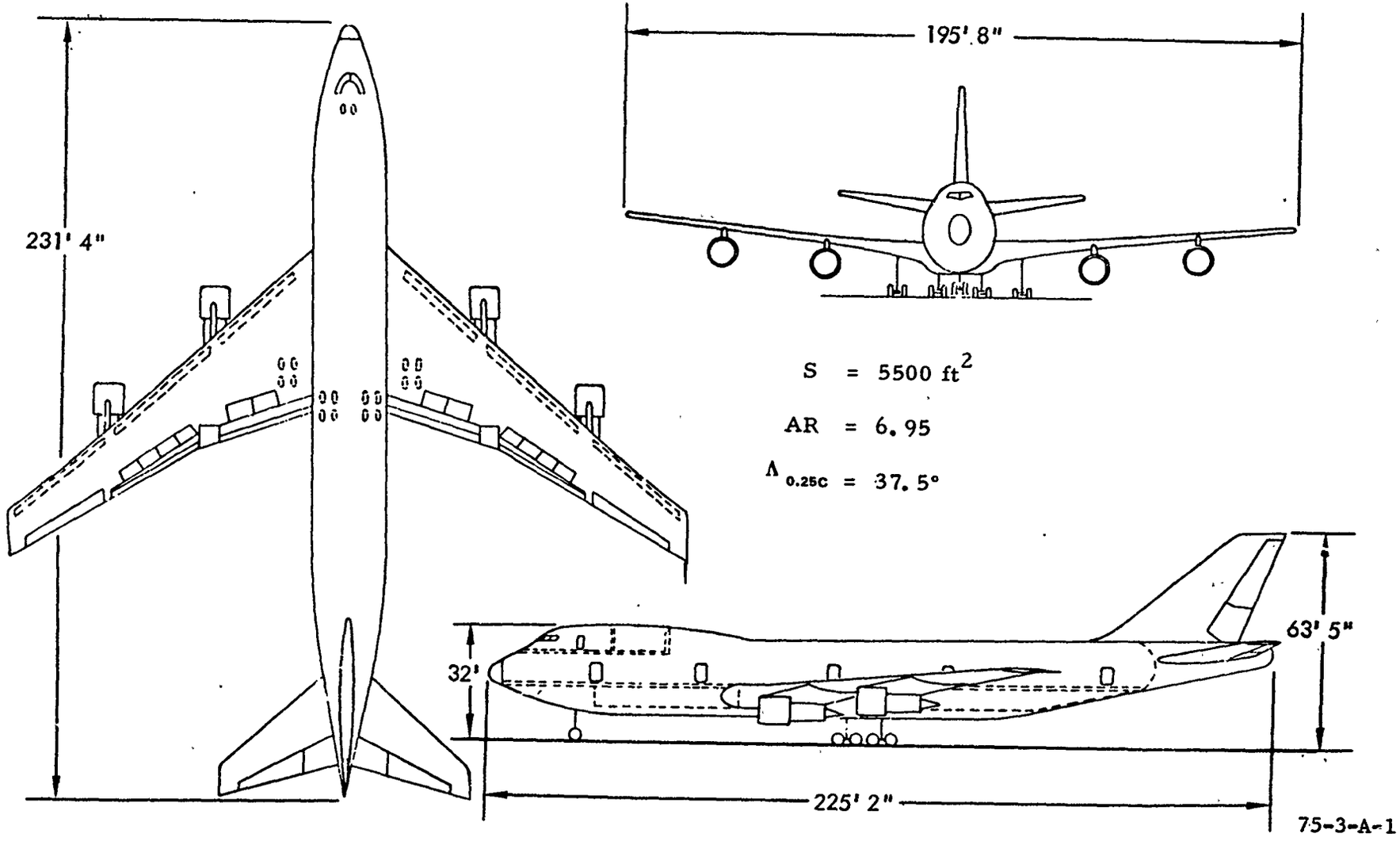

FIGURE A-1. THREE-VIEW SKETCH OF B747 AIRCRAFT

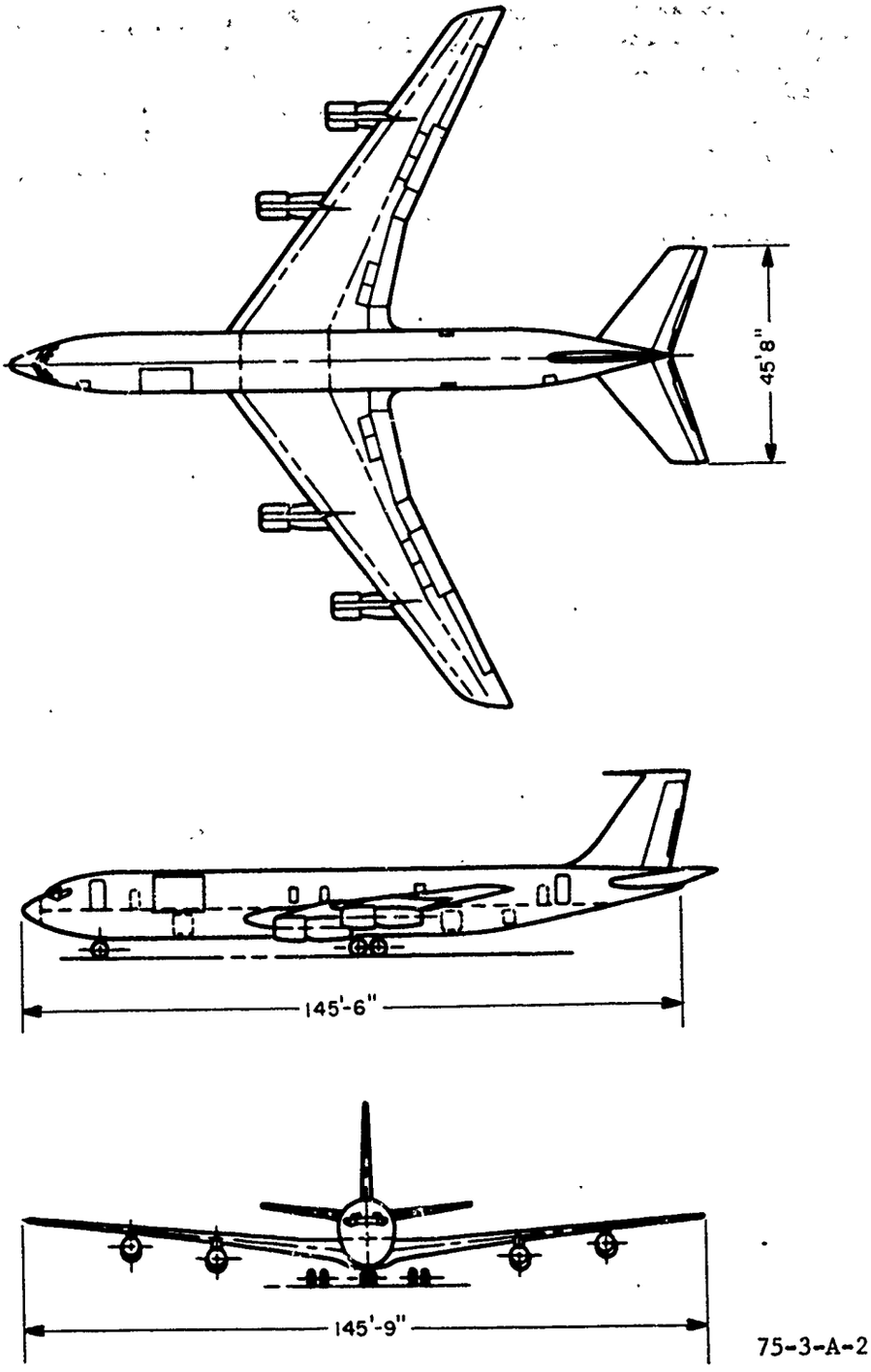

FIGURE A-2. THREE-VIEW SKETCH OF B707 AIRCRAFT

is situated in line with the inboard engines. Fillet flaps, occupying the space between the fuselage and the termination of the inboard main flap segment, are a simple split type. Low-speed lateral control is by outboard ailerons, spoilers and inboard ailerons. High-speed lateral control is by inboard ailerons only. The outboard ailerons are interlocked with the flaps so that they operate only when the flaps are deployed. At all other times, they are locked neutral. The inboard ailerons, situated in the cut-out between the inboard and outboard flap segments, function at all times. The spoilers may also be used symmetrically as speed brakes.

GROUP I

Convair 880, Model 22

Wingspan	120 feet
Length	129 feet, 4 inches
Height	36 feet, 4 inches
Wing Area	2,000 square feet
Root Chord	35 feet, 8 inches
Tip Chord	
Aspect Ratio	7.2 ($b^2 \div S$)
Taper Ratio	
Wing-Sweep Angle	35 degrees at 30 percent chord line
Maximum Takeoff Weight	184,500 pounds
Maximum Landing Weight	137,000 pounds
Powerplant	General Electric CJ-805-3 (4)

The CV-880 employs double-slotted trailing-edge flaps but no leading-edge high-lift devices. Lateral control is by conventional ailerons and differentially-operated spoilers.

GROUP II

Lockheed C141

Wingspan	160 feet
Length	145 feet
Height	39 feet, 3 inches
Wing Area	3,228 square feet (gross)
Root Chord	33 feet, 2 inches
Tip Chord	
Aspect Ratio	7.9 ($b^2 \div S$)
Taper Ratio	
Wing Quarter-Chord Sweep Back	25 degrees
Maximum Takeoff Weight	316,600 pounds
Maximum Landing Weight	257,700 pounds
Powerplant	Pratt & Whitney TF33-P-7 (4)

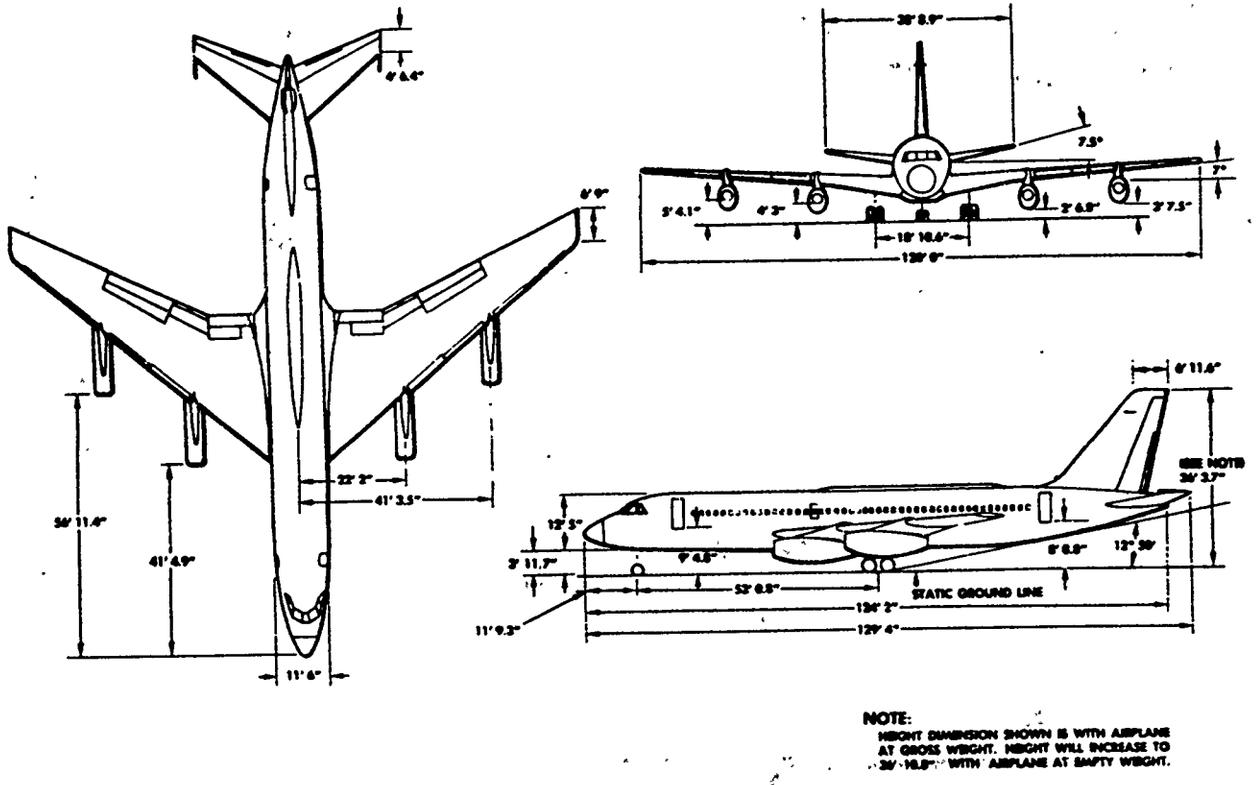

FIGURE A-3. THREE-VIEW SKETCH OF CV880 AIRCRAFT

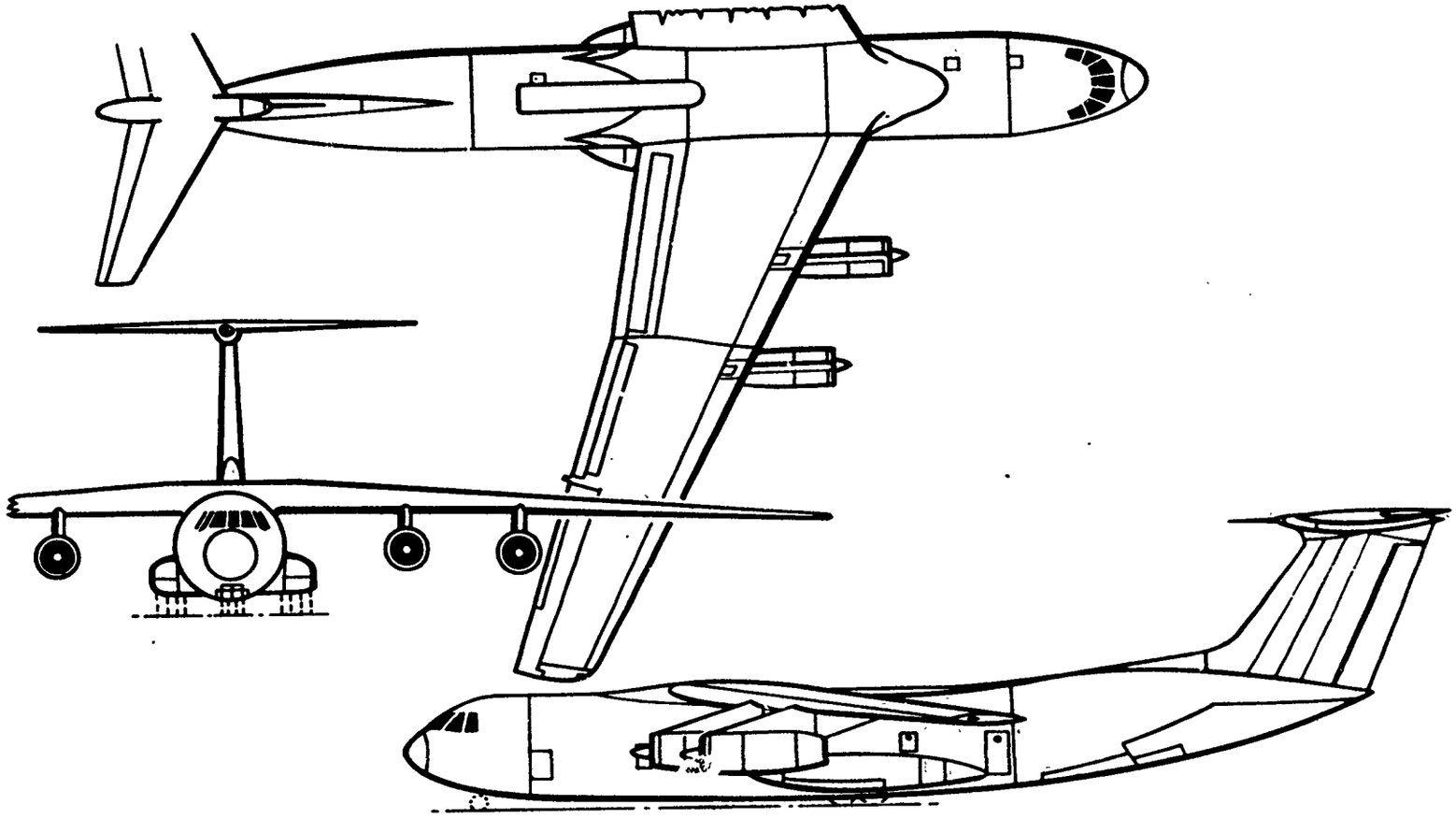

FIGURE A-4. THREE-VIEW SKETCH OF C141 AIRCRAFT

The lateral control system consists of conventional ailerons outboard and differentially-operated flight spoilers inboard. Fowler flaps extend over the complete trailing-edge inboard of the ailerons.

GROUP II

Lockheed C5A

Wingspan	222 feet, 8 inches
Length	247 feet, 11 inches
Height	65 feet, 1 inch
Wing Area	6,200 square feet
Root Chord	45 feet, 5 inches
Tip Chord	15 feet, 4 inches
Aspect Ratio	7.3 (Span/Av. Chd.)
Taper Ratio	.34
Wing Quarter-Chord Sweep Back	25 degrees
Maximum Takeoff Weight	764,500 pounds
Maximum Landing Weight	635,850 pounds
Powerplant	General Electric TF39-GE-1 Turbofan (4)

The C5A lateral control system consists of conventional ailerons outboard and differentially-operated flight spoilers inboard. High-lift devices are full-span leading-edge slats and Fowler flaps. There are no cut-outs in either of these two devices. The engines are placed low enough beneath the wing that flap cut-outs are not needed.

GROUP III

Lockheed L1011

Wingspan	155 feet, 4 inches
Length	178 feet, 8 inches
Height	55 feet, 4 inches
Wing Area	3,456 square feet (exposed)
Root Chord	34 feet, 4 inches
Tip Chord	10 feet, 3 inches
Aspect Ratio	6.95 (Span/Av. Chd.)
Taper Ratio	.30
Wing Quarter-Chord Sweep Back	35 degrees
Maximum Takeoff Weight	430,000 pounds
Maximum Landing Weight	358,000 pounds
Powerplant	Rolls-Royce RB 211-22B (3)

The L1011 uses outboard ailerons for low-speed lateral control, inboard ailerons at all speeds. Double-slotted Fowler flaps in two segments per side, the inboard ailerons occupying the gap between the inner and outer segments. Full-span leading-edge slats. The L1011 also has a direct lift control (DLC) system for glidepath control. Six spoilers are installed on the upper surface

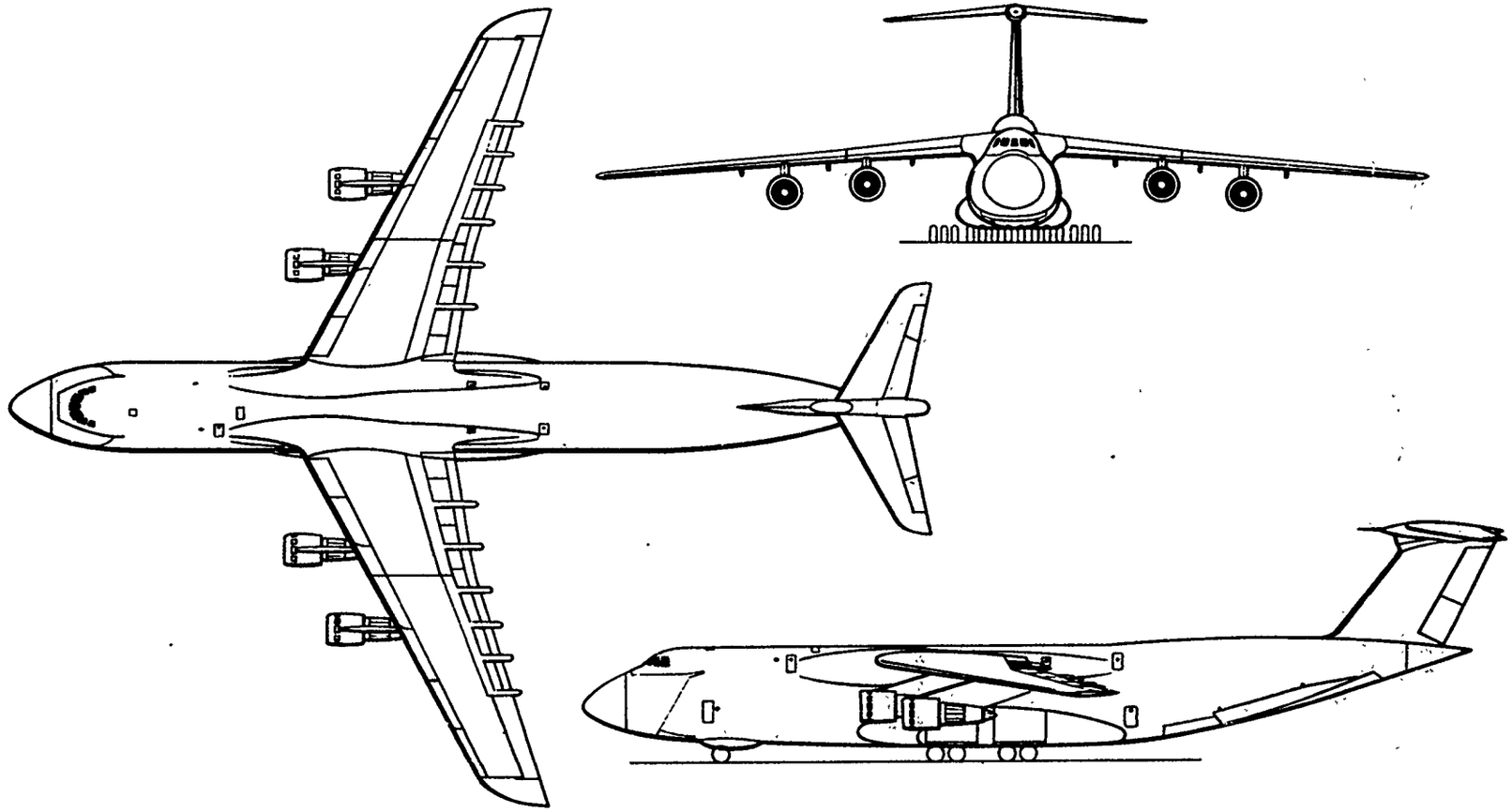

FIGURE A-5. THREE-VIEW SKETCH OF C5A AIRCRAFT

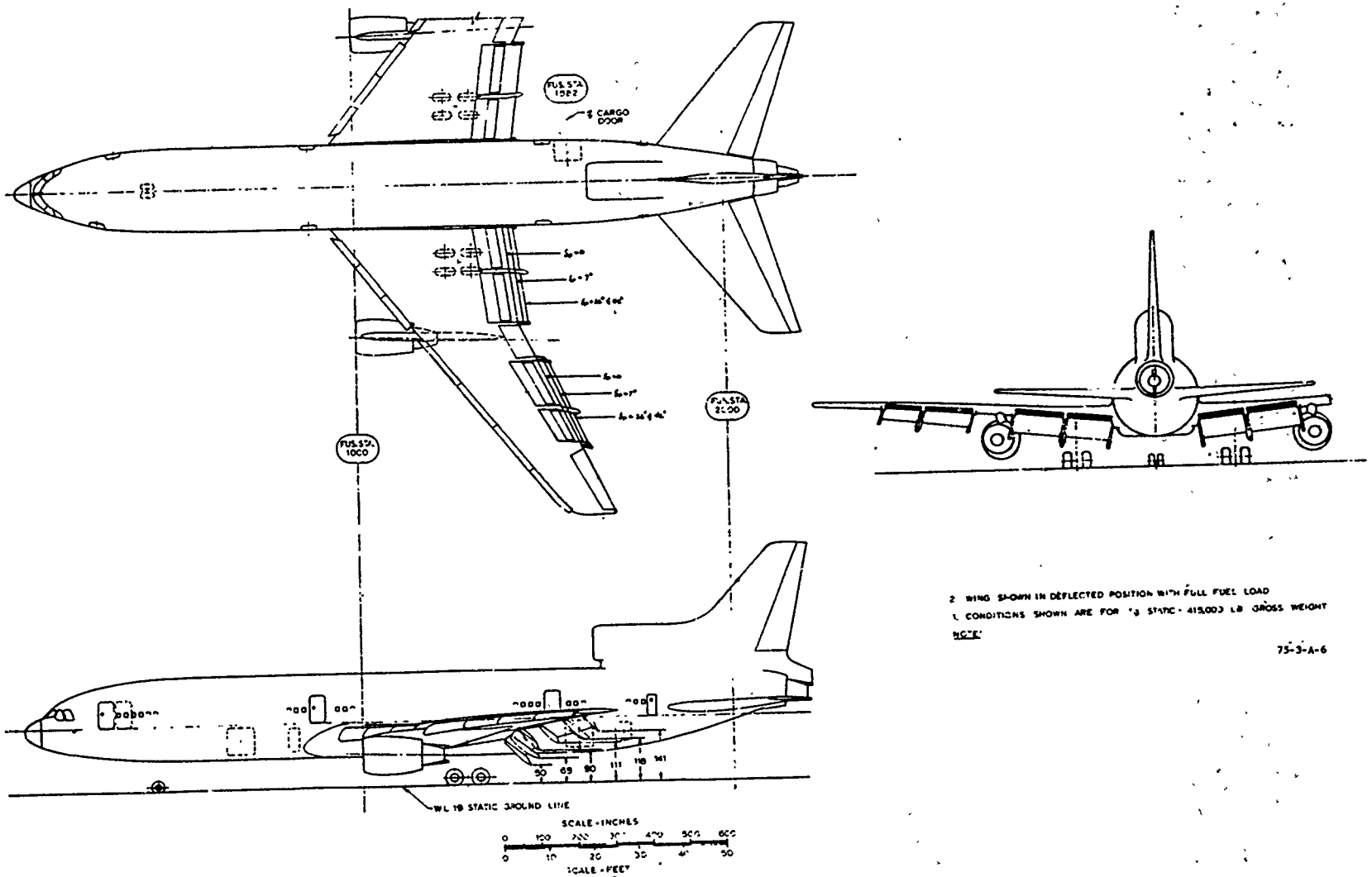

FIGURE A-6. THREE-VIEW SKETCH OF L1011 AIRCRAFT

of each wing, two inboard and four outboard of the high speed aileron. For landing approach at constant airspeed and pitch angle, DLC is accomplished by modulation of the flight spoilers about a null point and greatly improves glidepath control. The DLC function is only possible in the landing configuration. In addition, these upper surface spoilers ahead of the flaps operate differentially to augment the lateral control.

GROUP III

McDonnell-Douglas DC10, Series 10

Wingspan	155 feet, 4 inches
Length	181 feet, 5 inches
Height	58 feet
Wing Area	3,861 square feet (gross)
Root Chord	35 feet, 2 inches
Tip Chord	9 feet, 7 inches
Aspect Ratio	6.95 (Span/Av. Chd)
Taper Ratio	.27
Wing Quarter-Chord Sweep Back	35 degrees
Maximum Takeoff Weight	430,000 pounds
Maximum Landing Weight	363,500 pounds
Powerplant	General Electric CF6-6D Turbofans (3)

The lateral control system consists of outboard ailerons for low-speed operation (when leading-edge slats are deployed), inboard ailerons which are used at all times and spoilers used differentially. High-lift devices consist of full-span leading-edge slats and two-segment (inboard and outboard) double-slotted trailing-edge flaps. The inboard ailerons occupy the gap between the flap segments.

GROUP IV

Boeing 727, Series 100

Wingspan	108 feet
Length	133 feet
Height	34 feet
Wing Area	1,700 square feet
Root Chord	25 feet, 3 inches
Tip Chord	7 feet, 8 inches
Aspect Ratio	6.86 ($b^2 \div S$)

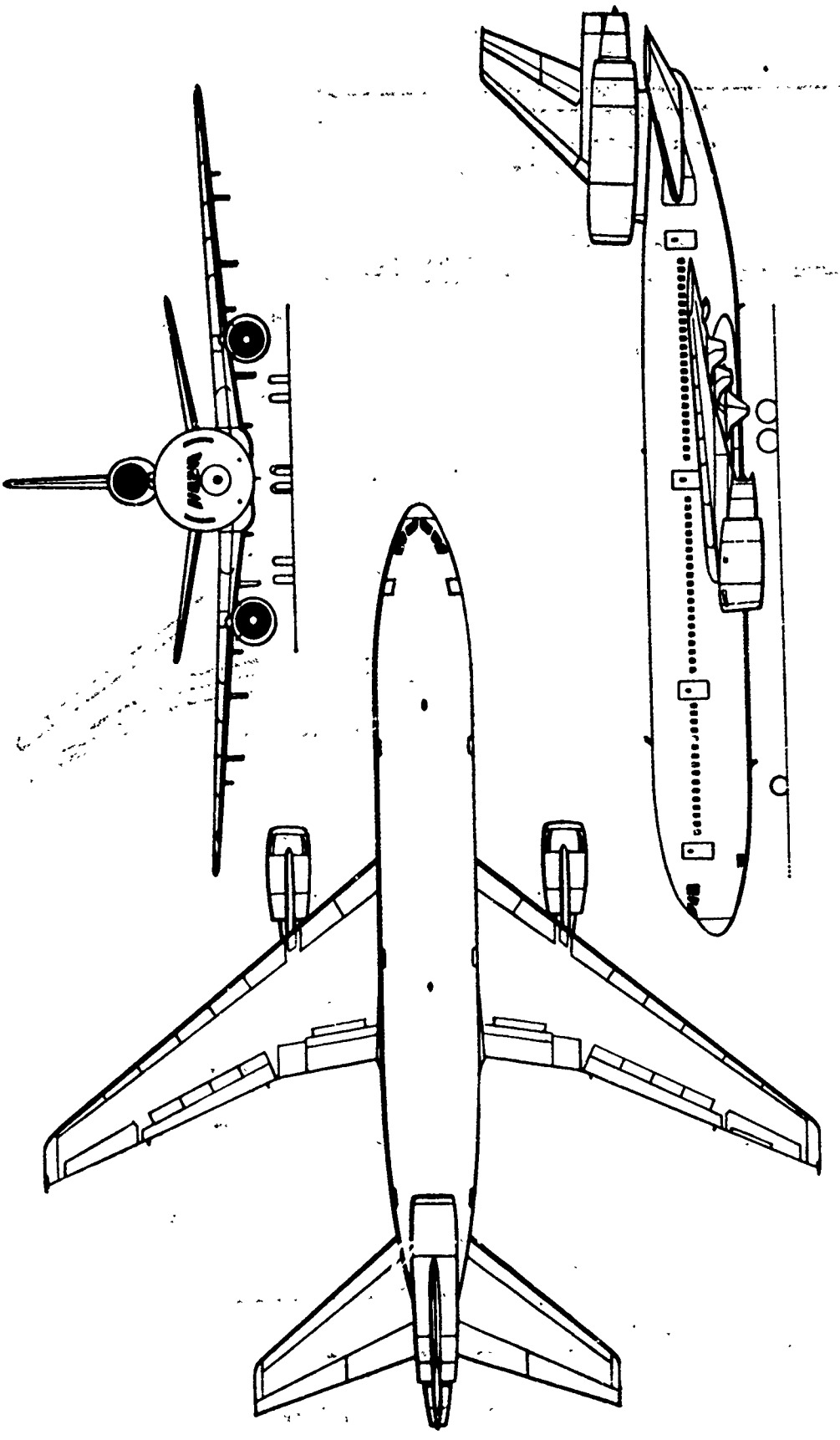

FIGURE A-7. THREE-VIEW SKETCH OF DC10 AIRCRAFT

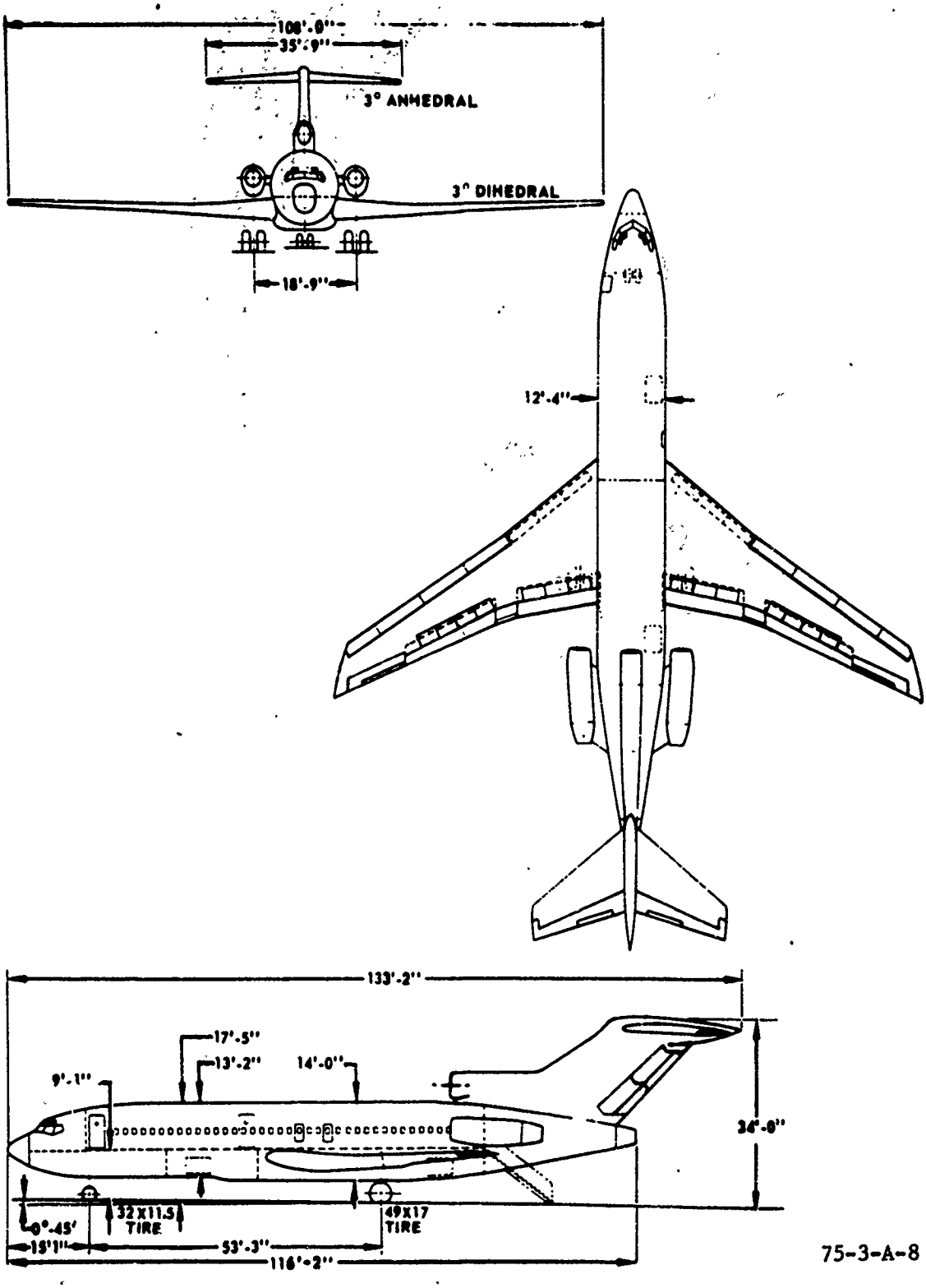

FIGURE A-8. THREE-VIEW SKETCH OF B727 AIRCRAFT

GROUP IV

Boeing 727, Series 100

Taper Ratio	.34
Wing Quarter-Chord Sweep Back	32 degrees
Maximum Takeoff Weight	142,000 pounds (100A)
Maximum Landing Weight	135,000 pounds (100A)
Powerplant	Pratt & Whitney JT8D-1

In cruising flight, the wing is essentially clean, with the exception of flap-track fairings and a few minor excrescences. The trailing-edge flaps are triple-slotted, chord-extending in two segments per side, with cut-outs at the fuselage and between inboard and outboard segments. Leading-edge high-lift devices extend from root to tip. Inboard, Kreuger flaps are fitted and outboard, slats are used. Outboard spoilers (immediately ahead of the outboard flap segment) are used in flight; inboard spoilers, ahead of the inboard flap segment, are used only on the ground. Low-speed lateral control is by outboard ailerons, spoilers and inboard ailerons. High-speed lateral control is by inboard ailerons only (these are situated in the cut-out between inboard and outboard flap segments). The outboard spoilers may also be used symmetrically as air brakes.

GROUP IV

McDonnell-Douglas DC9, Series 10

Wingspan	89 feet, 5 inches
Length	104 feet, 5 inches
Height	27 feet, 6 inches
Wing Area	930 square feet
Root Chord	15 feet, 4 inches (at fuselage junction)
Tip Chord	4 feet, 2 inches
Aspect Ratio	9.17 (Span/Av. Chd.)
Taper Ratio	.27
Wing Quarter-Chord Sweep Back	24 degrees
Maximum Takeoff Weight	90,500 pounds (Model 15)
Maximum Landing Weight	81,700 pounds (Model 15)
Powerplant	Pratt & Whitney JT8D-1

In cruising flight, the wing is essentially clean, with the exception of flap brackets and some minor excrescences. On series 10 airplanes (not later series), the leading edge is fixed. Lateral control, in both low- and high-speed flight is by conventional outboard ailerons. Trailing-edge flaps are a unique chord-extending type, in which the inboard segment, by use of a system of movable vanes, functions as single-slotted in takeoff position and triple-slotted in landing position, while the outboard segment functions as single-slotted for takeoff and double-slotted for landing. The inboard and outboard sections operate as a single section, with no gap between them.

WING SPAN	= 89.4 FEET
LENGTH	= 104.4 FEET
HEIGHT	= 27.5 FEET
WING AREA	= 930 SQUARE FEET
ASPECT RATIO	= 8.5:1
TAPER RATIO	= 0.25:1
WING QUARTER-CHORD SWEEP ANGLE	= 24 DEGREES
MAXIMUM T.O. WEIGHT	= 90,700 POUNDS (MODEL 15)
MAXIMUM LANDING GROSS WEIGHT	= 81,700 POUNDS (MODEL 15)
POWERPLANT:	PRATT & WHITNEY JT8D-1 (TWO)

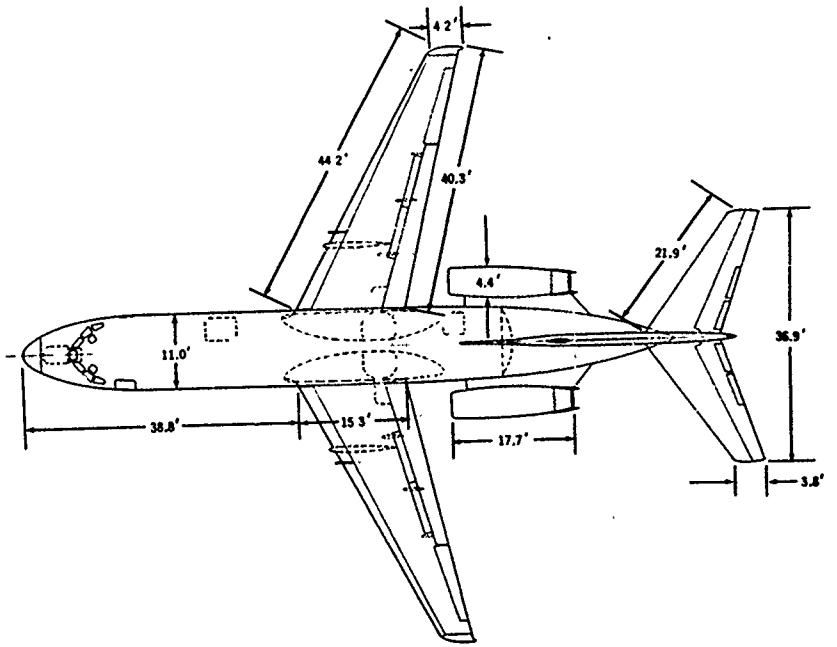

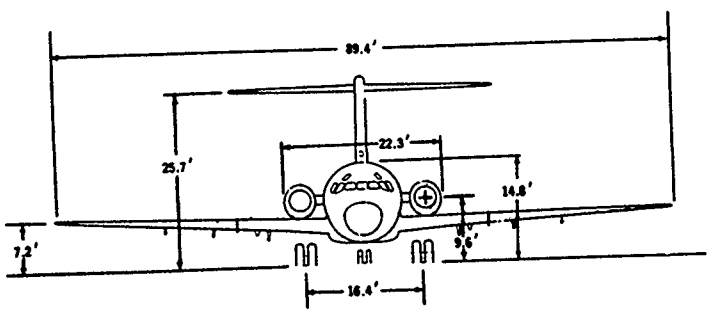

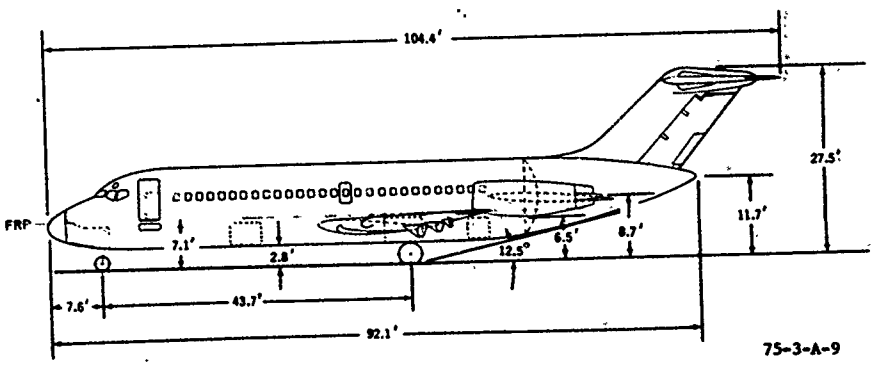

FIGURE A-9. THREE-VIEW SKETCH OF DC9 AIRCRAFT

GROUP V

Douglas DC7

Wingspan	117 feet, 6 inches
Length	108 feet, 11 inches
Height	28 feet, 9 inches
Wing Area	1,463 square feet
Root Chord	19 feet, 1 inch
Tip Chord	5 feet, 11 inches
Aspect Ratio	9.4 (Span/Av. Chd.)
Taper Ratio	.31
Wing 60 Percent Chord Line is Unswept	
Maximum Takeoff Weight	122,200 pounds
Maximum Landing Weight	95,000 pounds
Powerplant	Curtiss-Wright R3350 turbo-compound reciprocating engines
Propeller Diameter	13 feet, 6 inches

The DC7 wing is of conventional high aspect ratio unswept design. Lateral control is by outboard ailerons. The remainder of the wing trailing edge, inboard to the wing fuselage junction, is occupied by the trailing-edge flaps, which are in a single-segment per side. A cut-out in the flaps extends across the width of the fuselage.

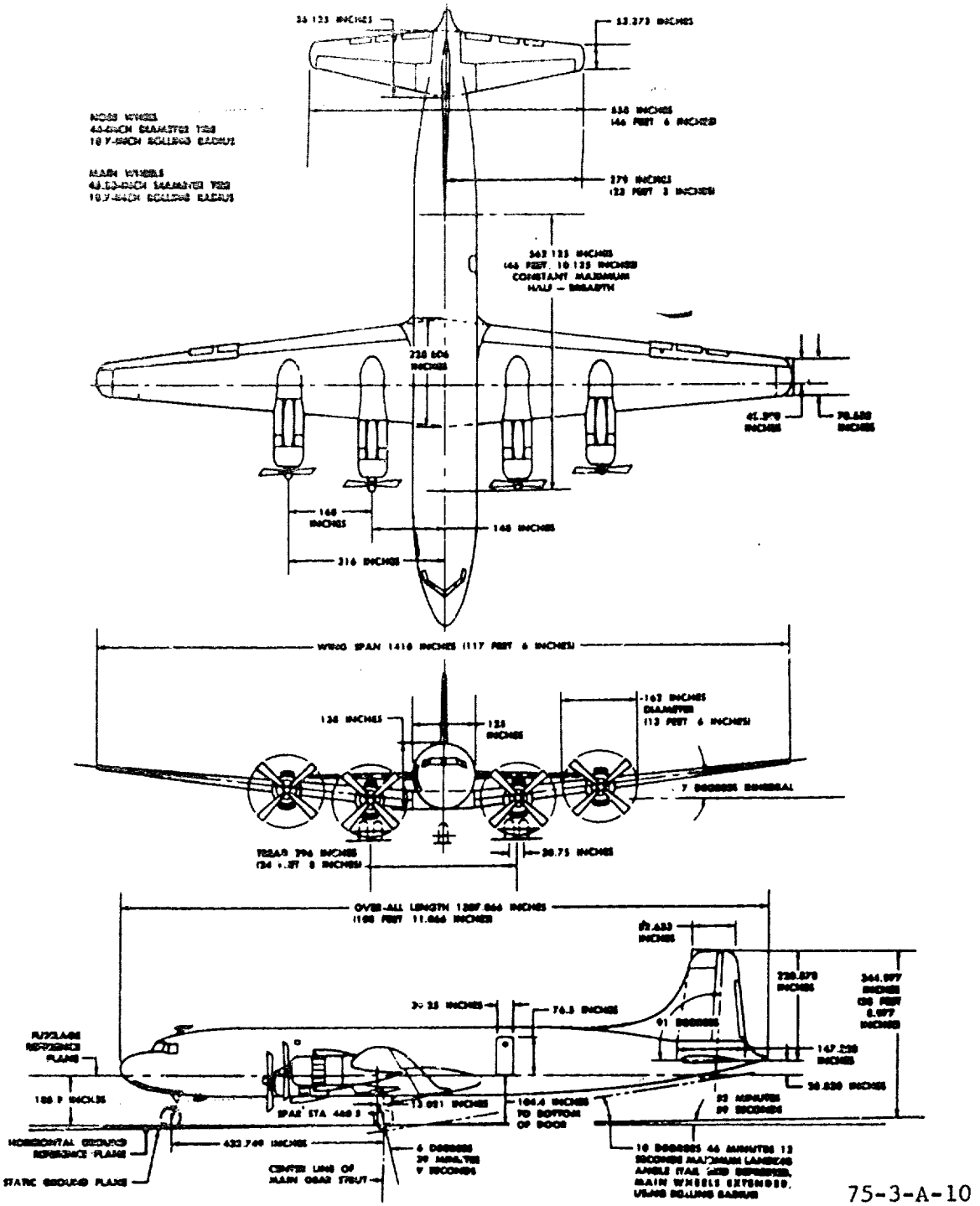

FIGURE A-10. THREE-VIEW SKETCH OF DC7 AIRCRAFT

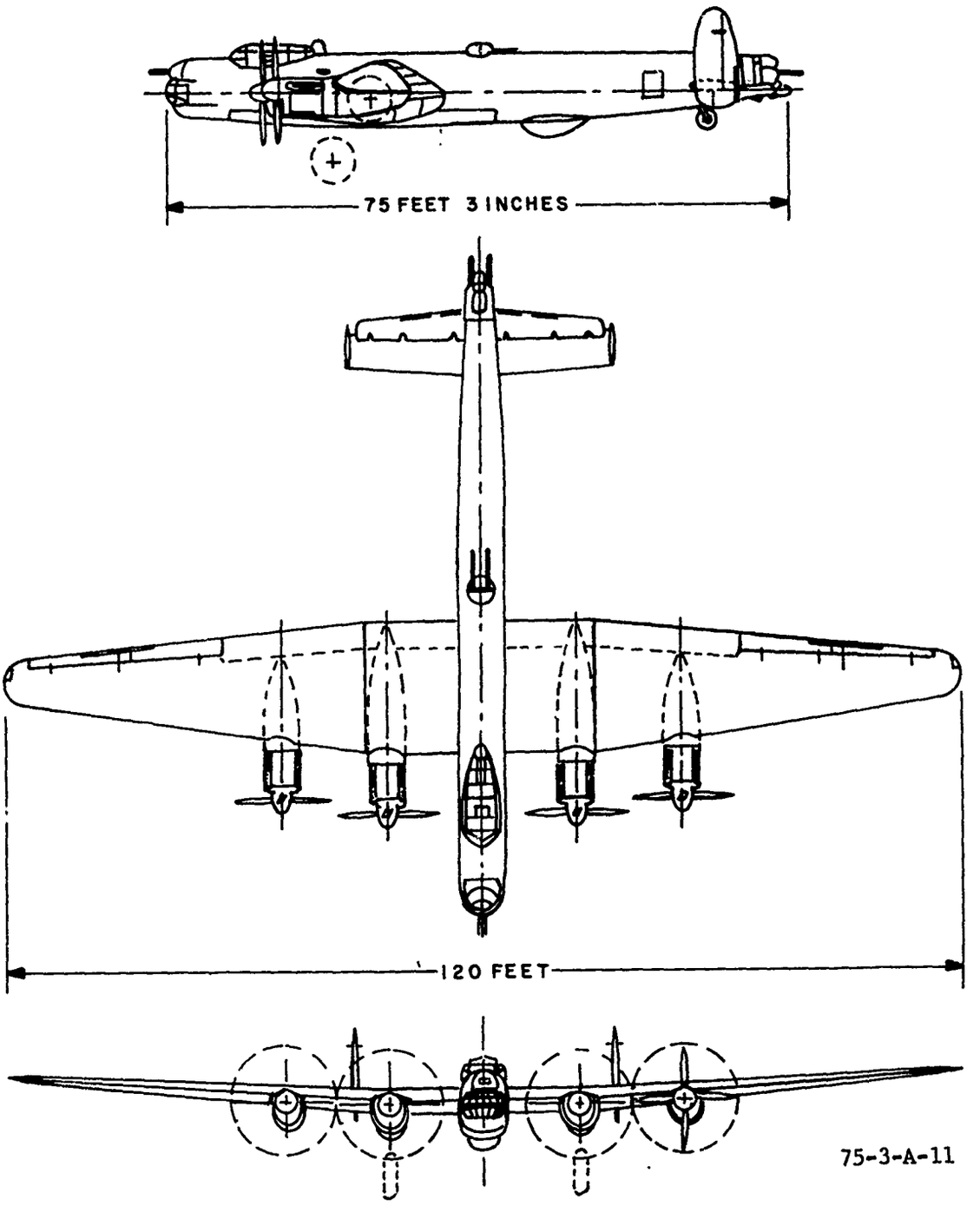

FIGURE A-11. THREE-VIEW SKETCH OF LINCOLN AIRCRAFT

APPENDIX B

TANGENTIAL VELOCITY DISTRIBUTIONS

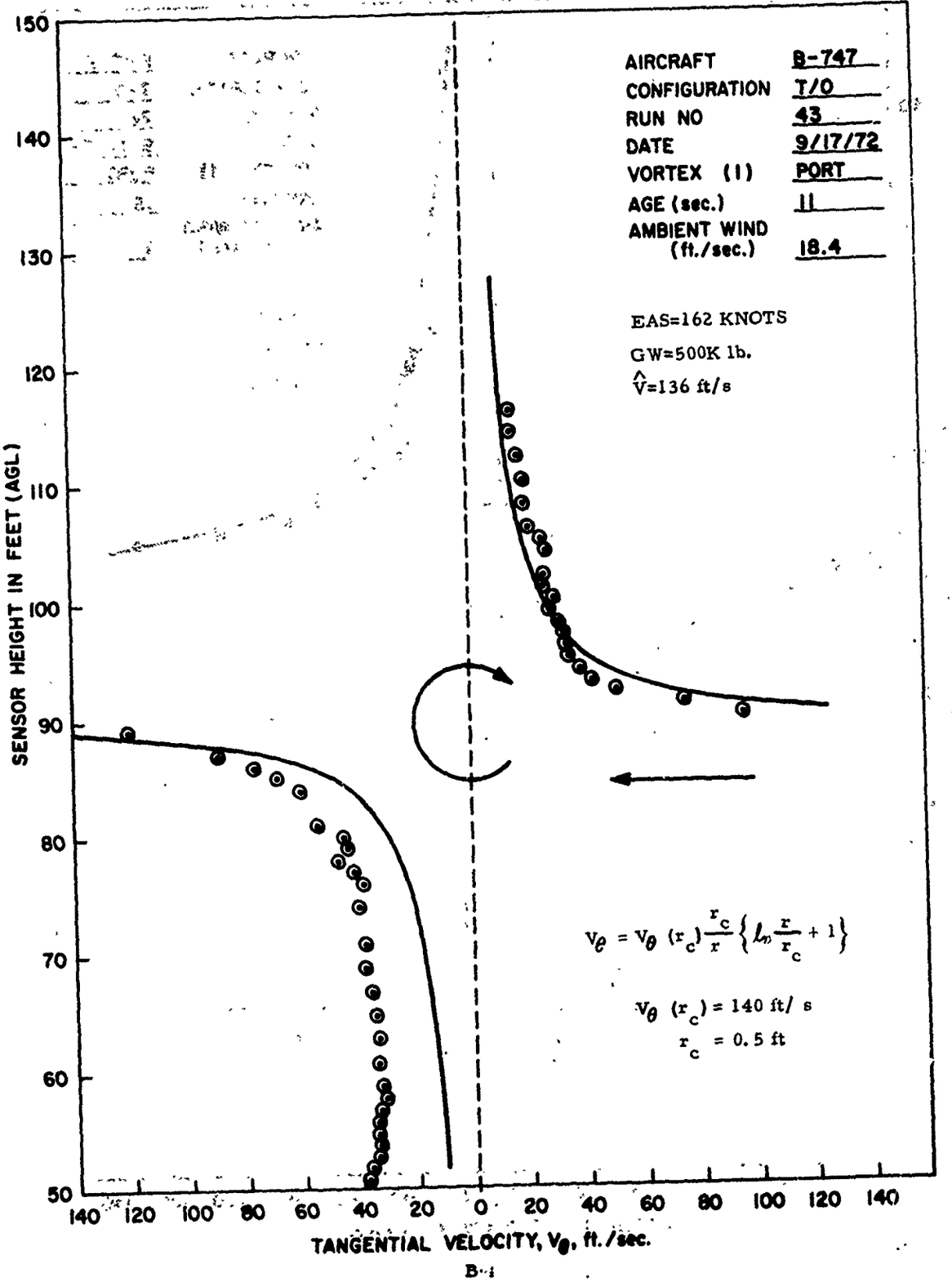
AIRCRAFT B-747
CONFIGURATION T/O
RUN NO 43
DATE 9/17/72
VORTEX (1) PORT
AGE (sec.) 11
AMBIENT WIND (ft./sec.) 18.4
EAS=162 KNOTS
GW=500K lb.
$\hat{V}$=136 ft/s
$V_\theta = V_\theta (r_c)\frac{r_c}{r}\left\{ln\frac{r}{r_c}+1\right\}$
$V_\theta (r_c)$ = 140 ft/ s
r_c = 0.5 ft
SENSOR HEIGHT IN FEET (AGL)
150
140
130
120
110
100
90
80
70
60
50
140 120 100 80 60 40 20 0 20 40 60 80 100 120 140
TANGENTIAL VELOCITY, V_θ, ft./sec.

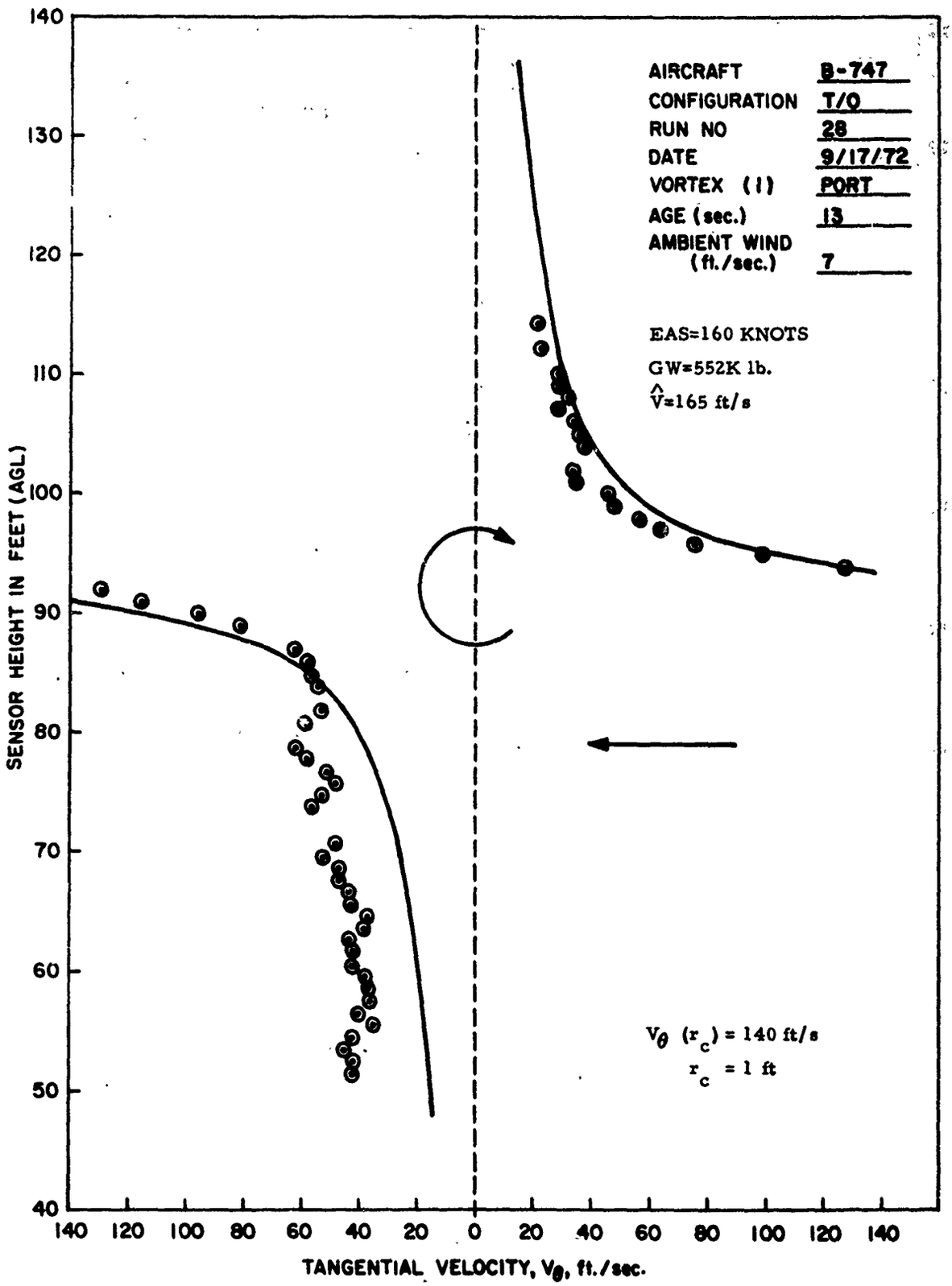
AIRCRAFT B-747
CONFIGURATION T/O
RUN NO 28
DATE 9/17/72
VORTEX (1) PORT
AGE (sec.) 13
AMBIENT WIND (ft./sec.) 7
EAS=160 KNOTS
GW=552K lb.
$\hat{V}$=165 ft/s
V_θ (r_c) = 140 ft/s
r_c = 1 ft
SENSOR HEIGHT IN FEET (AGL)
140
130
120
110
100
90
80
70
60
50
40
140 120 100 80 60 40 20 0 20 40 60 80 100 120 140
TANGENTIAL VELOCITY, V_θ, ft./sec.

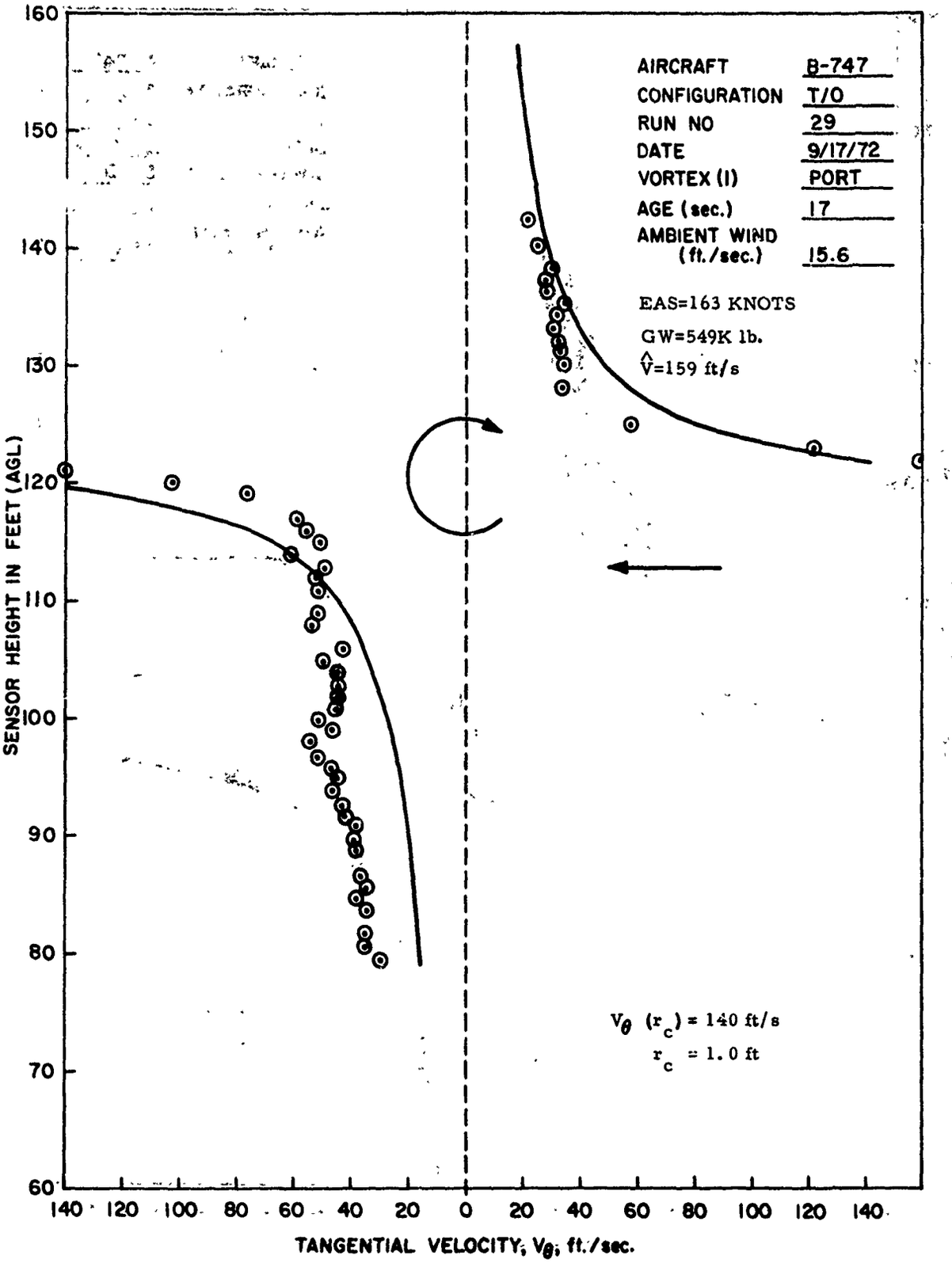
AIRCRAFT B-747
CONFIGURATION T/O
RUN NO 29
DATE 9/17/72
VORTEX (I) PORT
AGE (sec.) 17
AMBIENT WIND (ft./sec.) 15.6
EAS=163 KNOTS
GW=549K lb.
$\hat{V}$=159 ft/s
V_θ (r_c) = 140 ft/s
r_c = 1.0 ft
SENSOR HEIGHT IN FEET (AGL)
160
150
140
130
120
110
100
90
80
70
60
140 120 100 80 60 40 20 0 20 40 60 80 100 120 140
TANGENTIAL VELOCITY, V_θ, ft./sec.

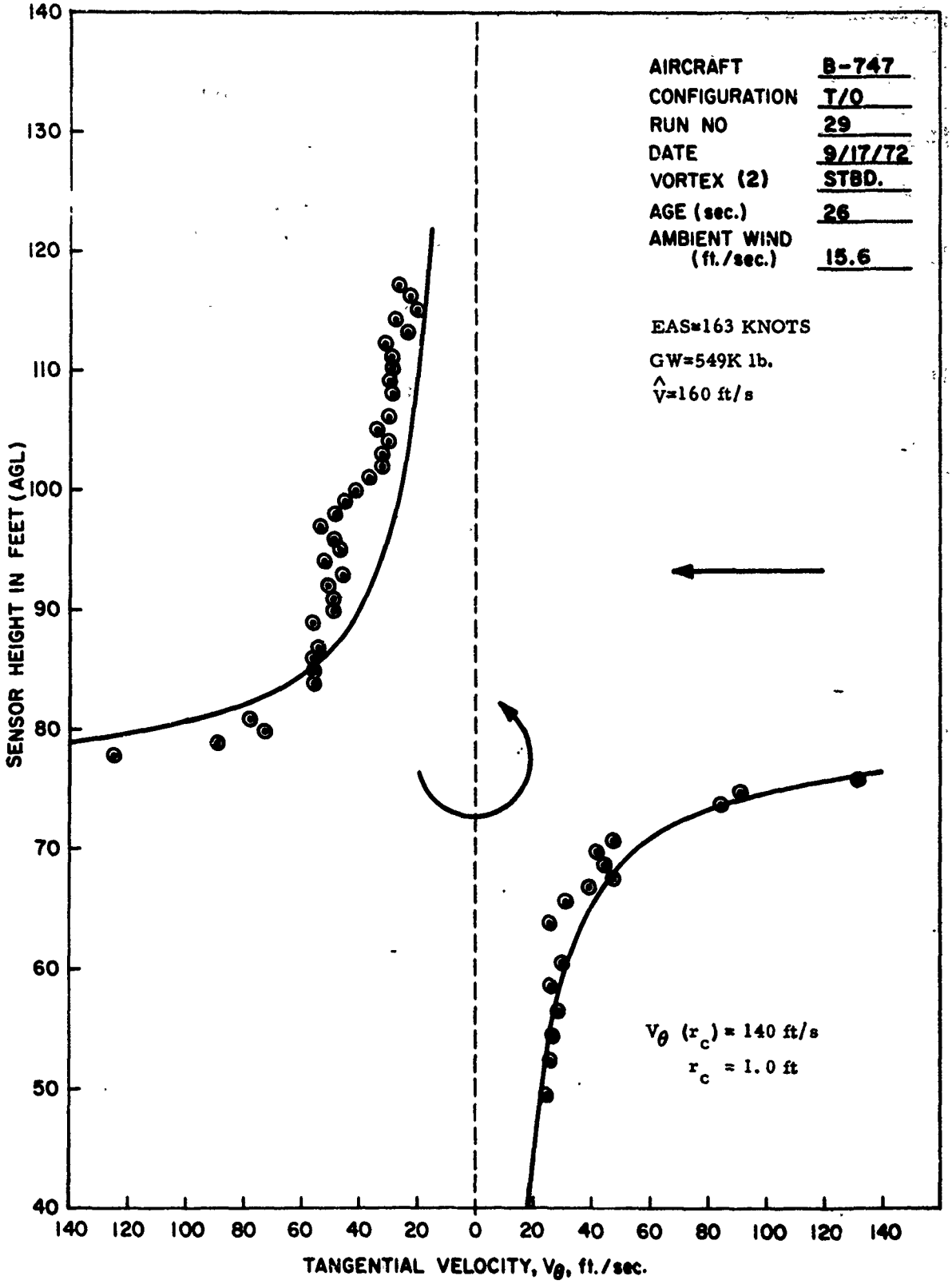
AIRCRAFT B-747
CONFIGURATION T/O
RUN NO 29
DATE 9/17/72
VORTEX (2) STBD.
AGE (sec.) 26
AMBIENT WIND (ft./sec.) 15.6
EAS=163 KNOTS
GW=549K lb.
$\hat{V}$=160 ft/s
V_θ (r_c) = 140 ft/s
r_c = 1.0 ft
SENSOR HEIGHT IN FEET (AGL)
140
130
120
110
100
90
80
70
60
50
40
140 120 100 80 60 40 20 0 20 40 60 80 100 120 140
TANGENTIAL VELOCITY, V_θ, ft./sec.

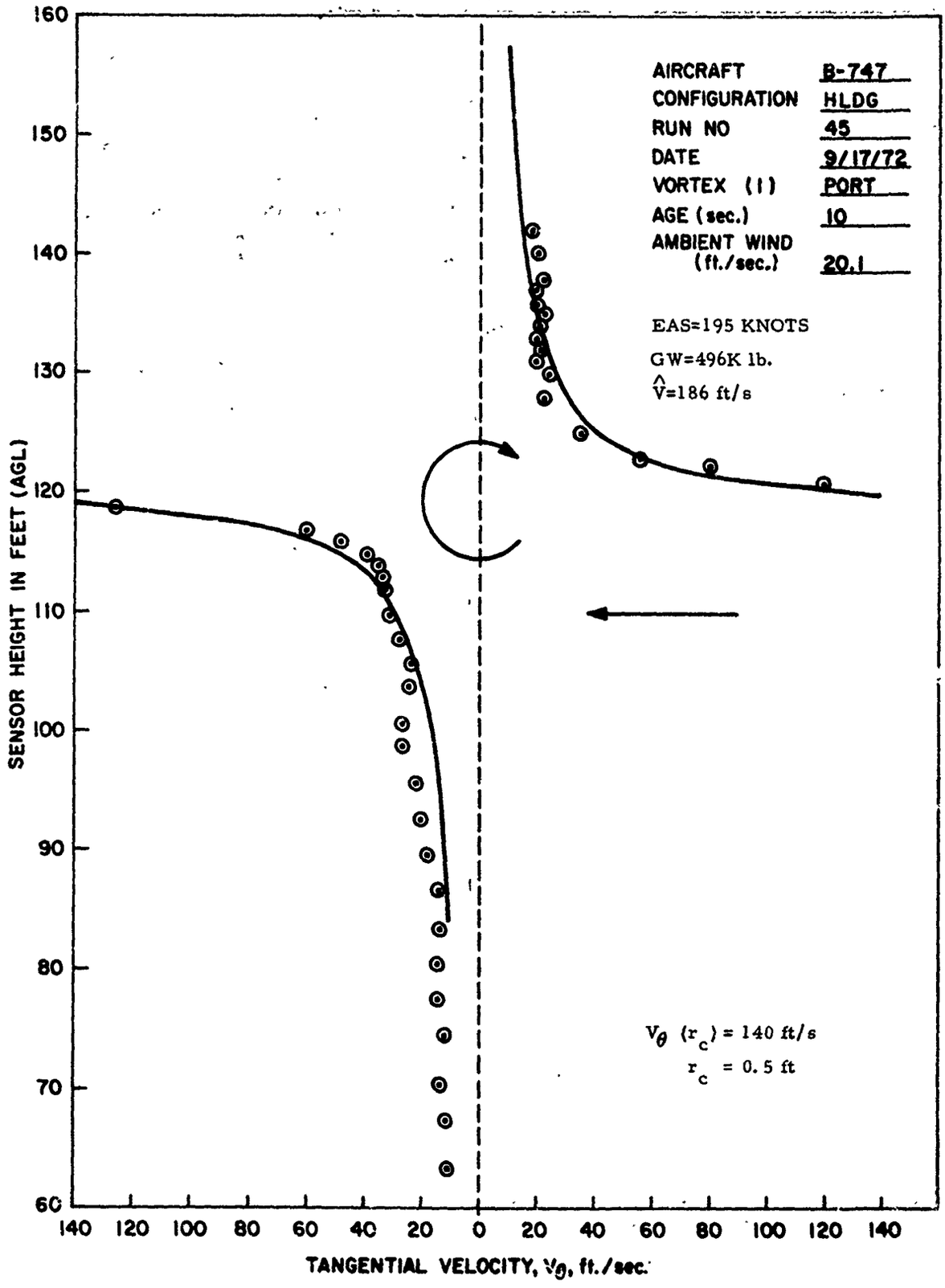
AIRCRAFT B-747
CONFIGURATION HLDG
RUN NO 45
DATE 9/17/72
VORTEX (1) PORT
AGE (sec.) 10
AMBIENT WIND (ft./sec.) 20.1
EAS=195 KNOTS
GW=496K lb.
$\hat{V}$=186 ft/s
V_θ (r_c) = 140 ft/s
r_c = 0.5 ft
SENSOR HEIGHT IN FEET (AGL)
160
150
140
130
120
110
100
90
80
70
60
140 120 100 80 60 40 20 0 20 40 60 80 100 120 140
TANGENTIAL VELOCITY, V_θ, ft./sec.

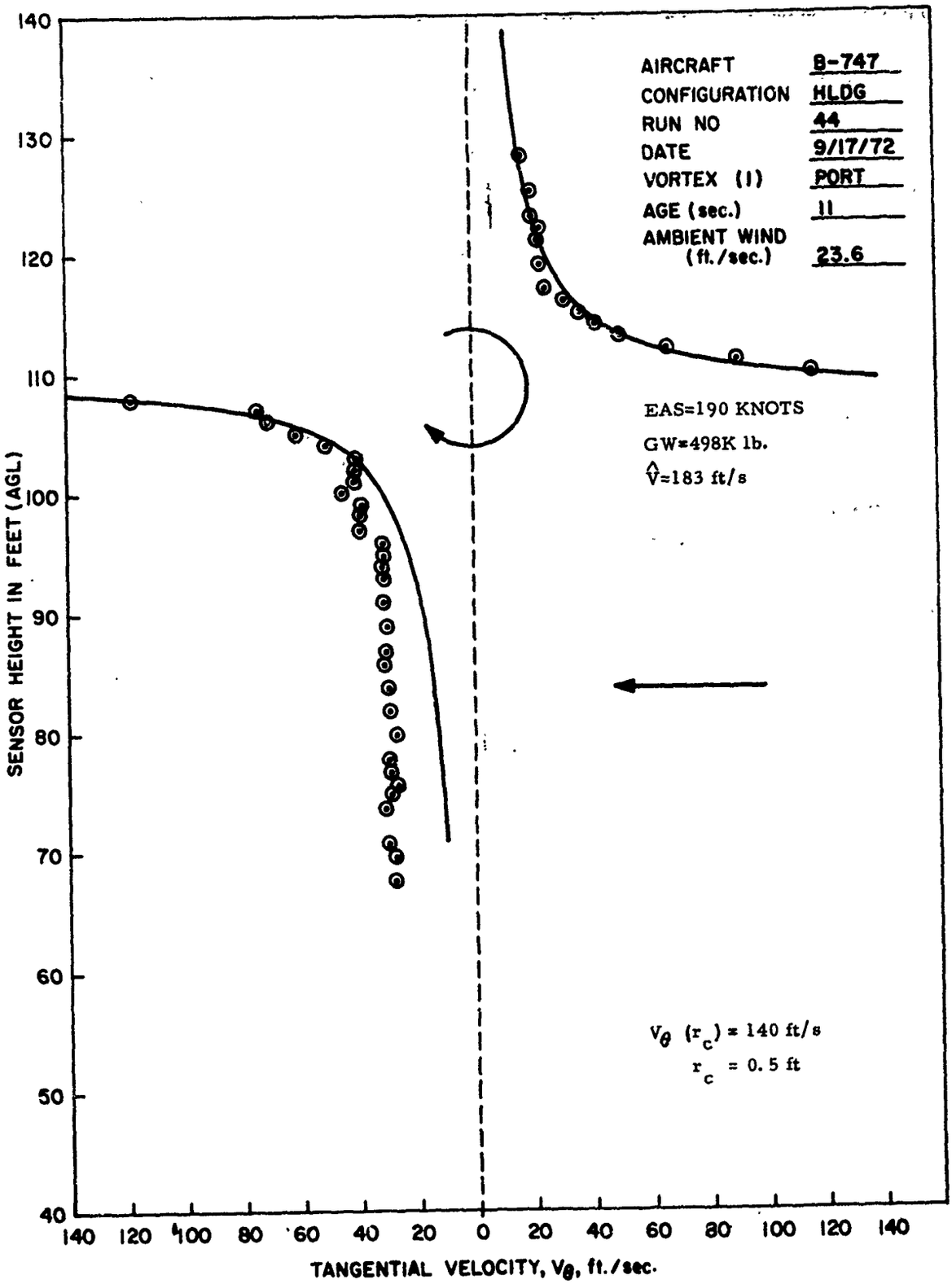
AIRCRAFT B-747
CONFIGURATION HLDG
RUN NO 44
DATE 9/17/72
VORTEX (1) PORT
AGE (sec.) 11
AMBIENT WIND (ft./sec.) 23.6
EAS=190 KNOTS
GW=498K lb.
$\hat{V}$=183 ft/s
V_θ (r_c) = 140 ft/s
r_c = 0.5 ft
SENSOR HEIGHT IN FEET (AGL)
140
130
120
110
100
90
80
70
60
50
40
140 120 100 80 60 40 20 0 20 40 60 80 100 120 140
TANGENTIAL VELOCITY, V_θ, ft./sec.

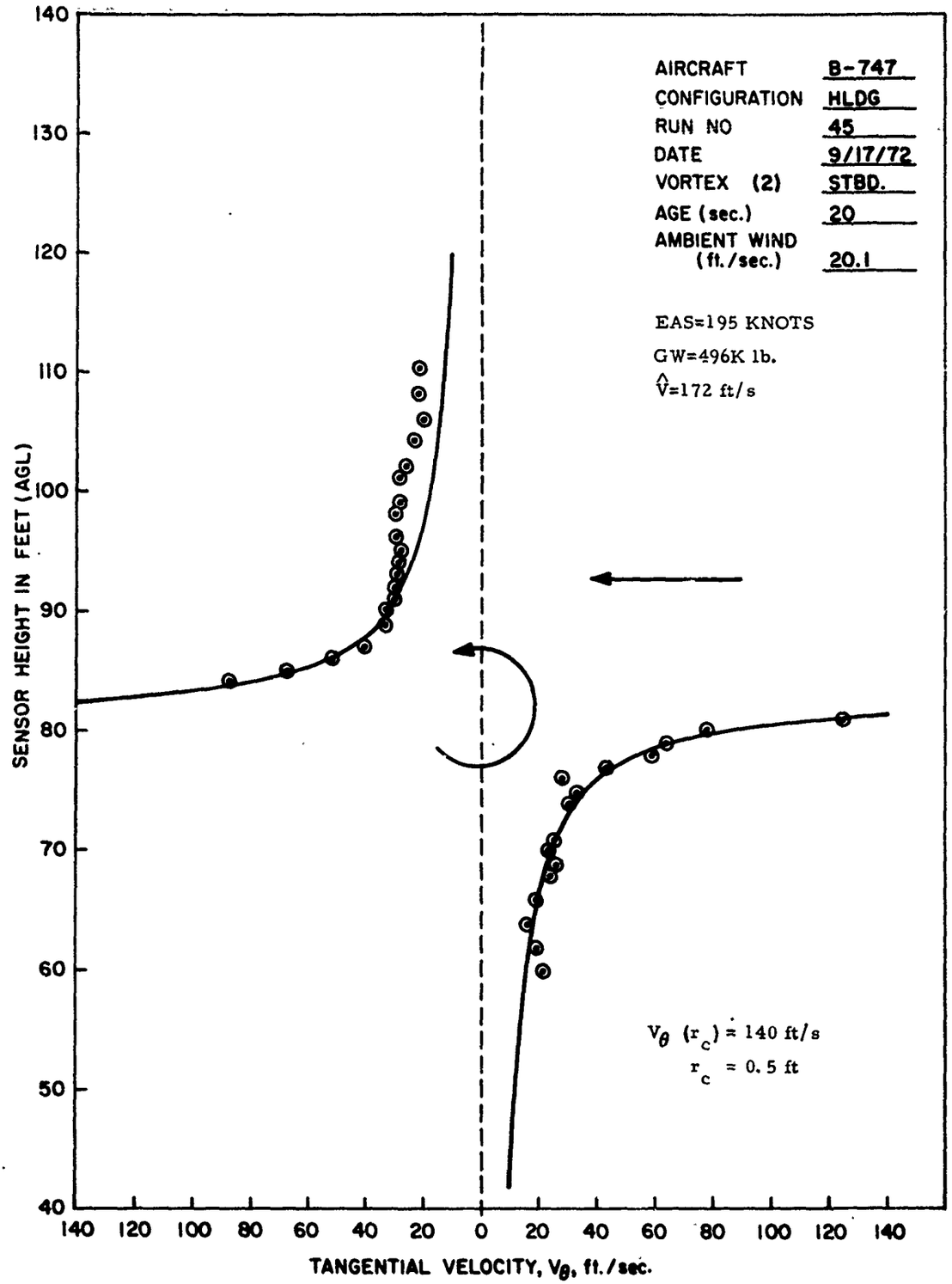
AIRCRAFT B-747
CONFIGURATION HLDG
RUN NO 45
DATE 9/17/72
VORTEX (2) STBD.
AGE (sec.) 20
AMBIENT WIND (ft./sec.) 20.1
EAS=195 KNOTS
GW=496K lb.
$\hat{V}$=172 ft/s
V_θ (r_c) = 140 ft/s
r_c = 0.5 ft
SENSOR HEIGHT IN FEET (AGL)
140
130
120
110
100
90
80
70
60
50
40
140 120 100 80 60 40 20 0 20 40 60 80 100 120 140
TANGENTIAL VELOCITY, V_θ, ft./sec.

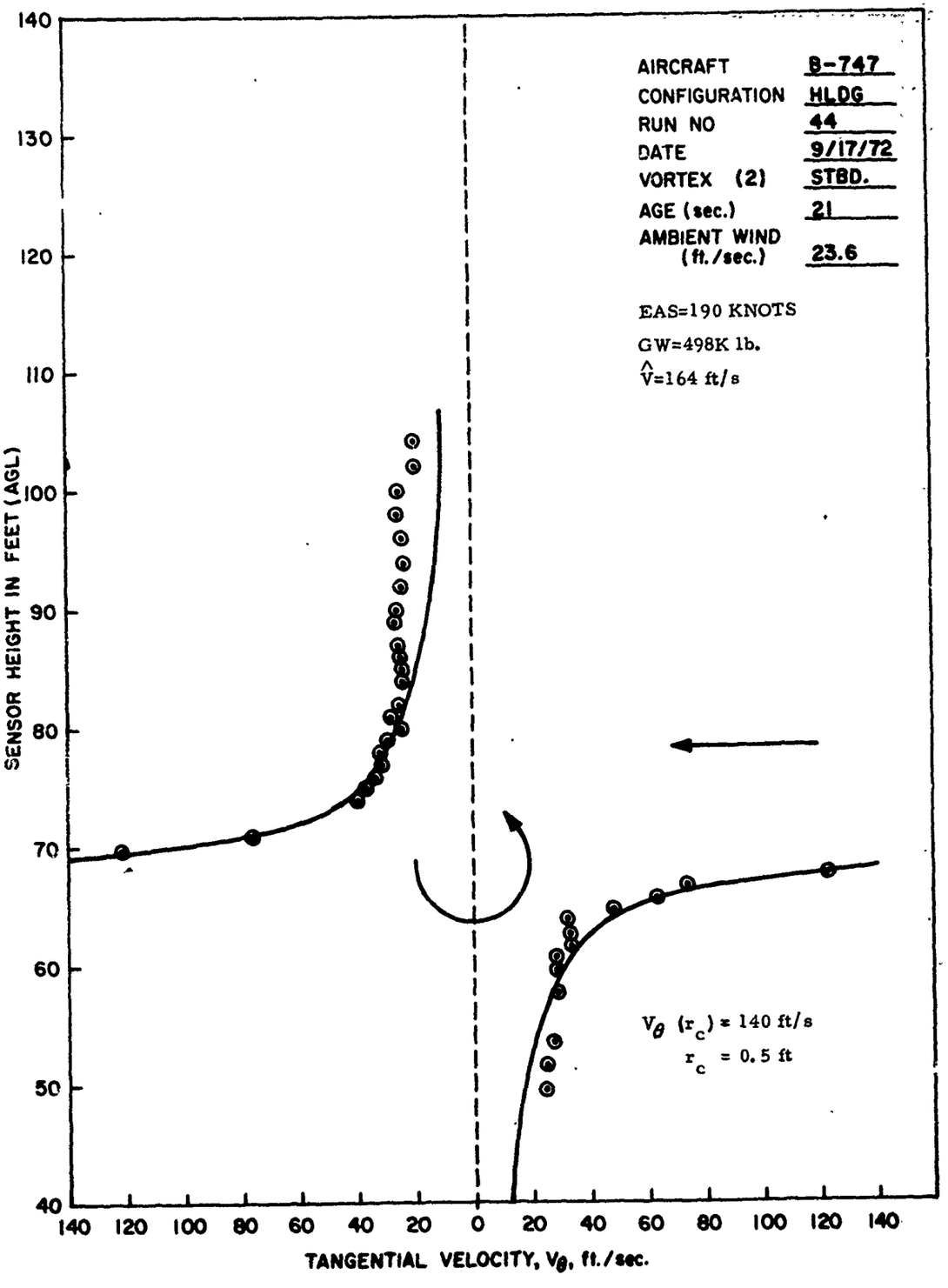
AIRCRAFT B-747
CONFIGURATION HLDG
RUN NO 44
DATE 9/17/72
VORTEX (2) STBD.
AGE (sec.) 21
AMBIENT WIND (ft./sec.) 23.6
EAS=190 KNOTS
GW=498K lb.
$\hat{V}$=164 ft/s
V_θ (r_c) = 140 ft/s
r_c = 0.5 ft
SENSOR HEIGHT IN FEET (AGL)
TANGENTIAL VELOCITY, V_θ, ft./sec.
140
130
120
110
100
90
80
70
60
50
40
140 120 100 80 60 40 20 0 20 40 60 80 100 120 140

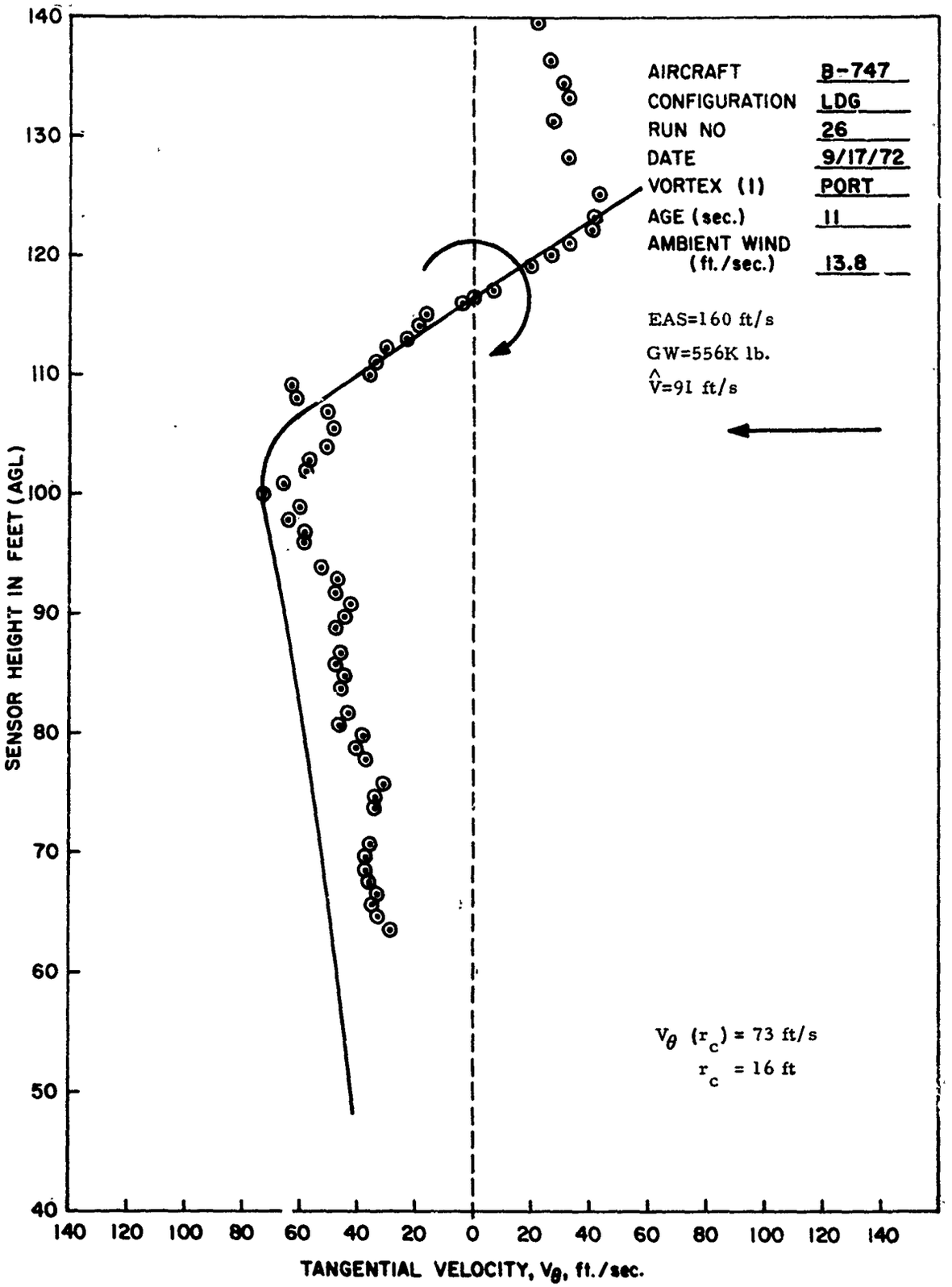
AIRCRAFT B-747
CONFIGURATION LDG
RUN NO 26
DATE 9/17/72
VORTEX (1) PORT
AGE (sec.) 11
AMBIENT WIND (ft./sec.) 13.8
EAS=160 ft/s
GW=556K lb.
$\hat{V}$=91 ft/s
V_θ (r_c) = 73 ft/s
r_c = 16 ft
SENSOR HEIGHT IN FEET (AGL)
140
130
120
110
100
90
80
70
60
50
40
140 120 100 80 60 40 20 0 20 40 60 80 100 120 140
TANGENTIAL VELOCITY, V_θ, ft./sec.

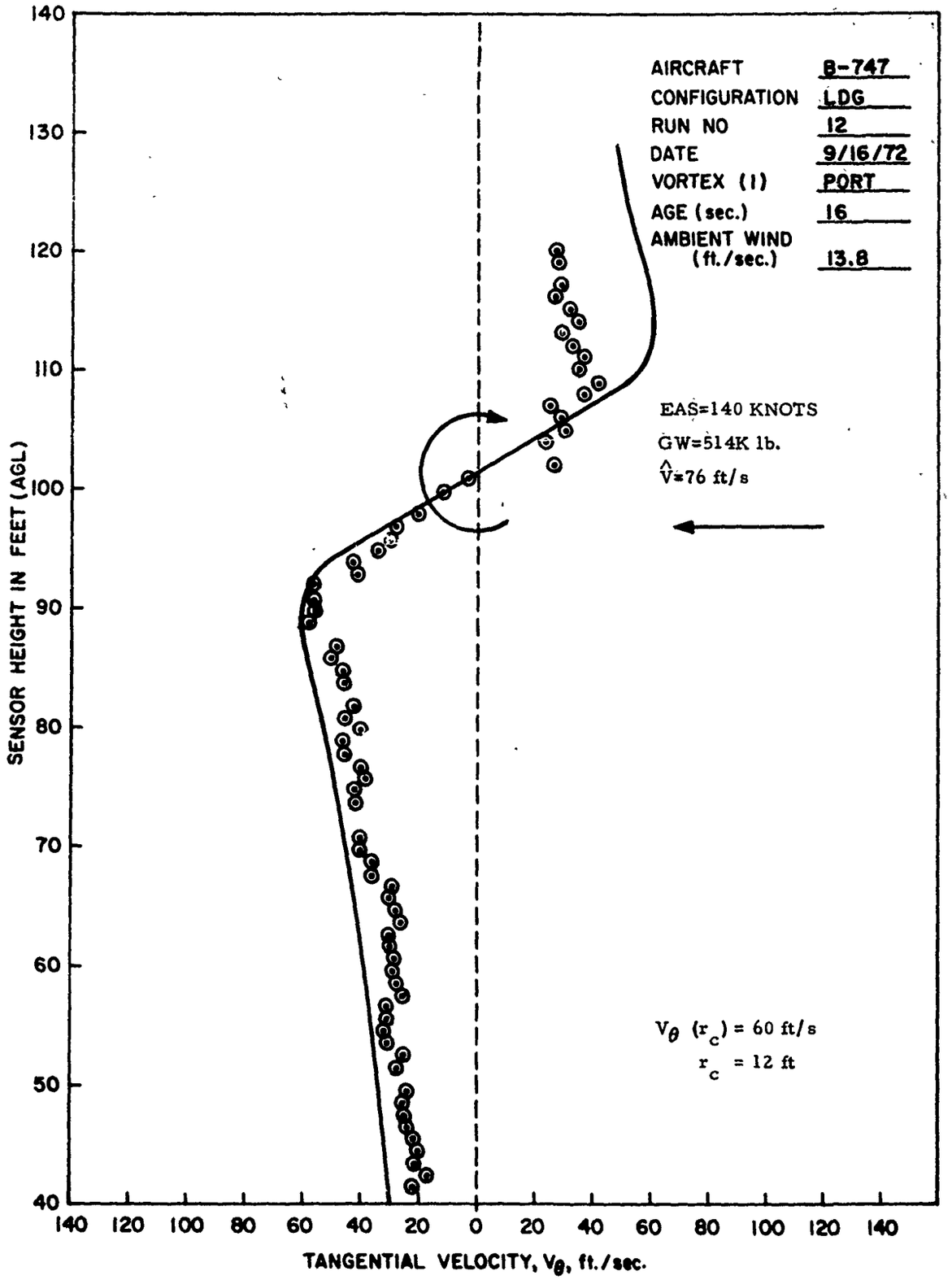
AIRCRAFT B-747
CONFIGURATION LDG
RUN NO 12
DATE 9/16/72
VORTEX (1) PORT
AGE (sec.) 16
AMBIENT WIND (ft./sec.) 13.8
EAS=140 KNOTS
GW=514K lb.
$\hat{V}$=76 ft/s
V_θ (r_c) = 60 ft/s
r_c = 12 ft
SENSOR HEIGHT IN FEET (AGL)
TANGENTIAL VELOCITY, V_θ, ft./sec.
140
130
120
110
100
90
80
70
60
50
40
140 120 100 80 60 40 20 0 20 40 60 80 100 120 140

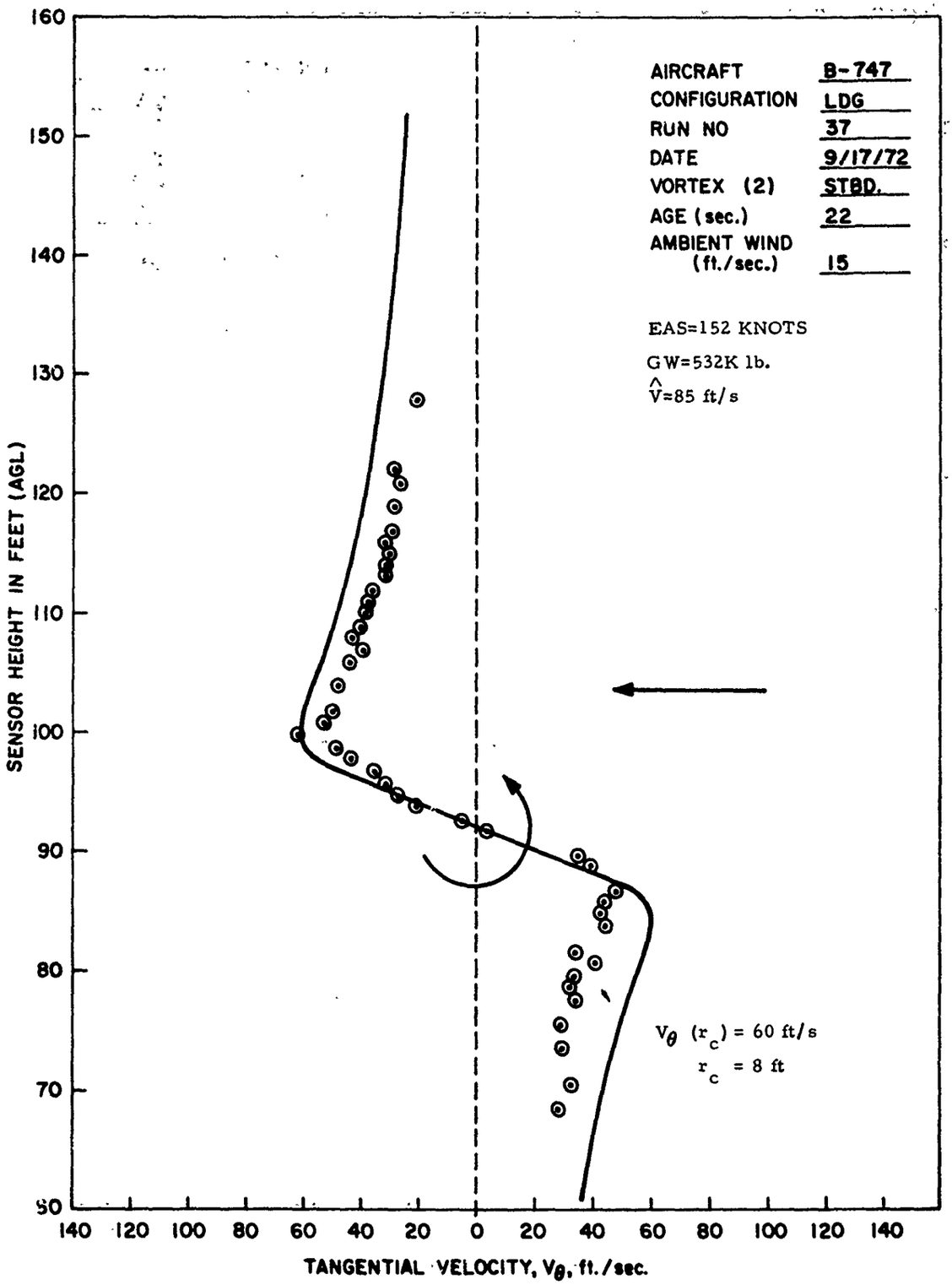
AIRCRAFT B-747
CONFIGURATION LDG
RUN NO 37
DATE 9/17/72
VORTEX (2) STBD.
AGE (sec.) 22
AMBIENT WIND (ft./sec.) 15
EAS=152 KNOTS
GW=532K lb.
$\hat{V}$=85 ft/s
V_θ (r_c) = 60 ft/s
r_c = 8 ft
SENSOR HEIGHT IN FEET (AGL)
160
150
140
130
120
110
100
90
80
70
60
140 120 100 80 60 40 20 0 20 40 60 80 100 120 140
TANGENTIAL VELOCITY, V_θ, ft./sec.

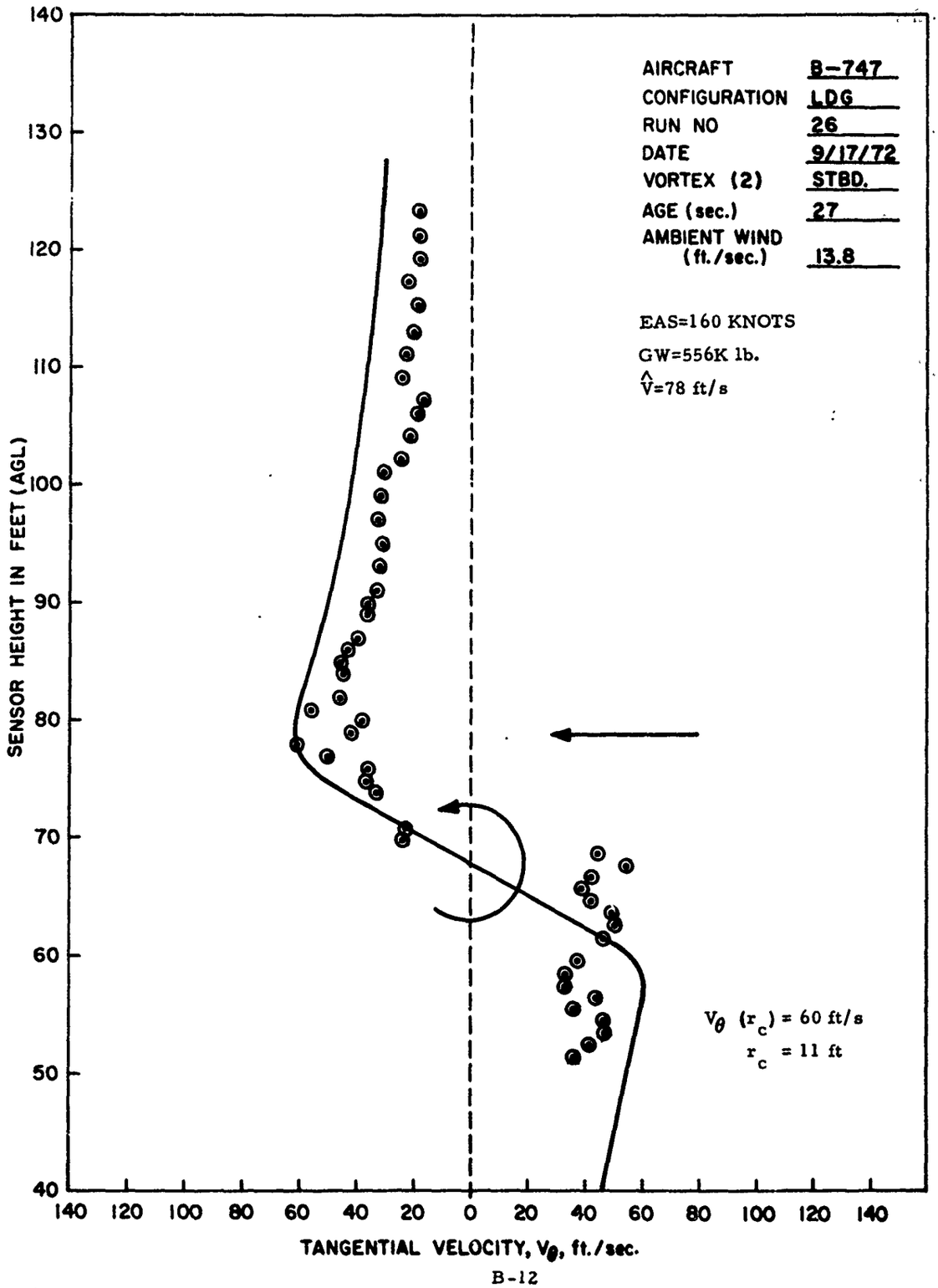
AIRCRAFT B-747
CONFIGURATION LDG
RUN NO 26
DATE 9/17/72
VORTEX (2) STBD.
AGE (sec.) 27
AMBIENT WIND (ft./sec.) 13.8
EAS=160 KNOTS
GW=556K lb.
V̂=78 ft/s
V_θ (r_c) = 60 ft/s
r_c = 11 ft
SENSOR HEIGHT IN FEET (AGL)
140
130
120
110
100
90
80
70
60
50
40
140 120 100 80 60 40 20 0 20 40 60 80 100 120 140
TANGENTIAL VELOCITY, V_θ, ft./sec.

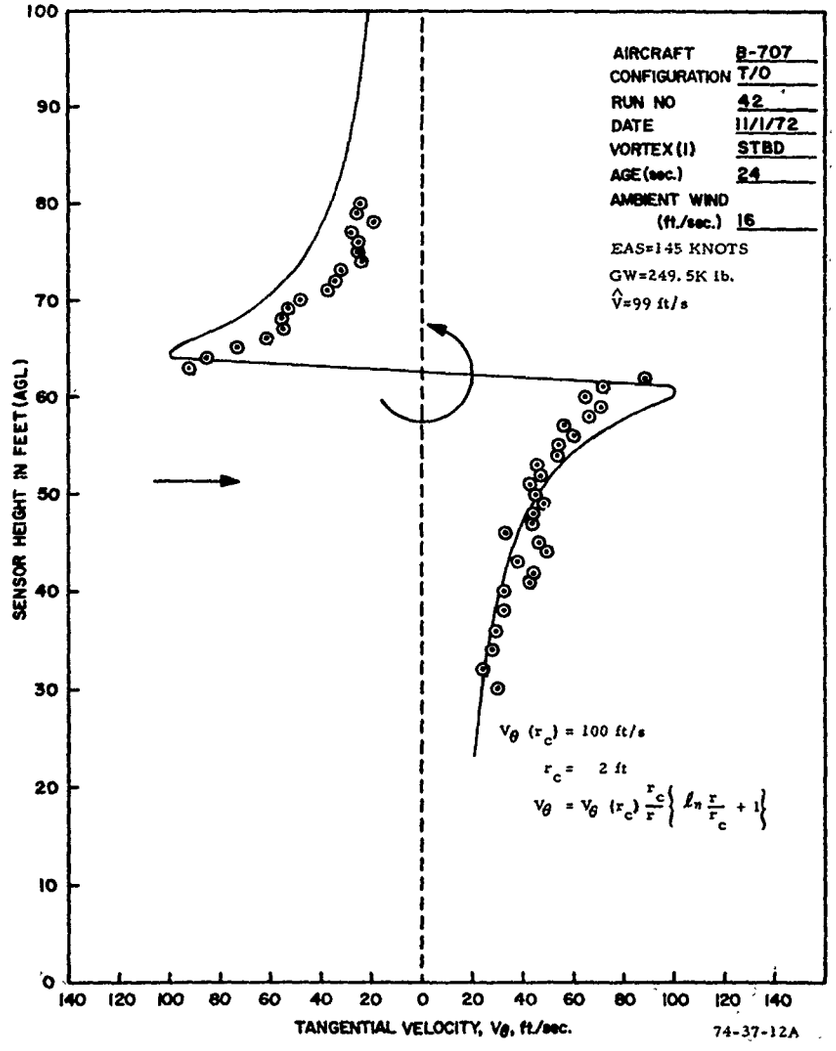
AIRCRAFT B-707
CONFIGURATION T/O
RUN NO 42
DATE 11/1/72
VORTEX (I) STBD
AGE (sec.) 24
AMBIENT WIND (ft./sec.) 16
EAS=145 KNOTS
GW=249.5K lb.
$\hat{V}$=99 ft/s
$V_\theta (r_c)$ = 100 ft/s
r_c = 2 ft
$V_\theta = V_\theta (r_c) \frac{r_c}{r} \left\{ \ell n \frac{r}{r_c} + 1 \right\}$
SENSOR HEIGHT IN FEET (AGL)
TANGENTIAL VELOCITY, V_θ, ft./sec.
74-37-12A

13 A

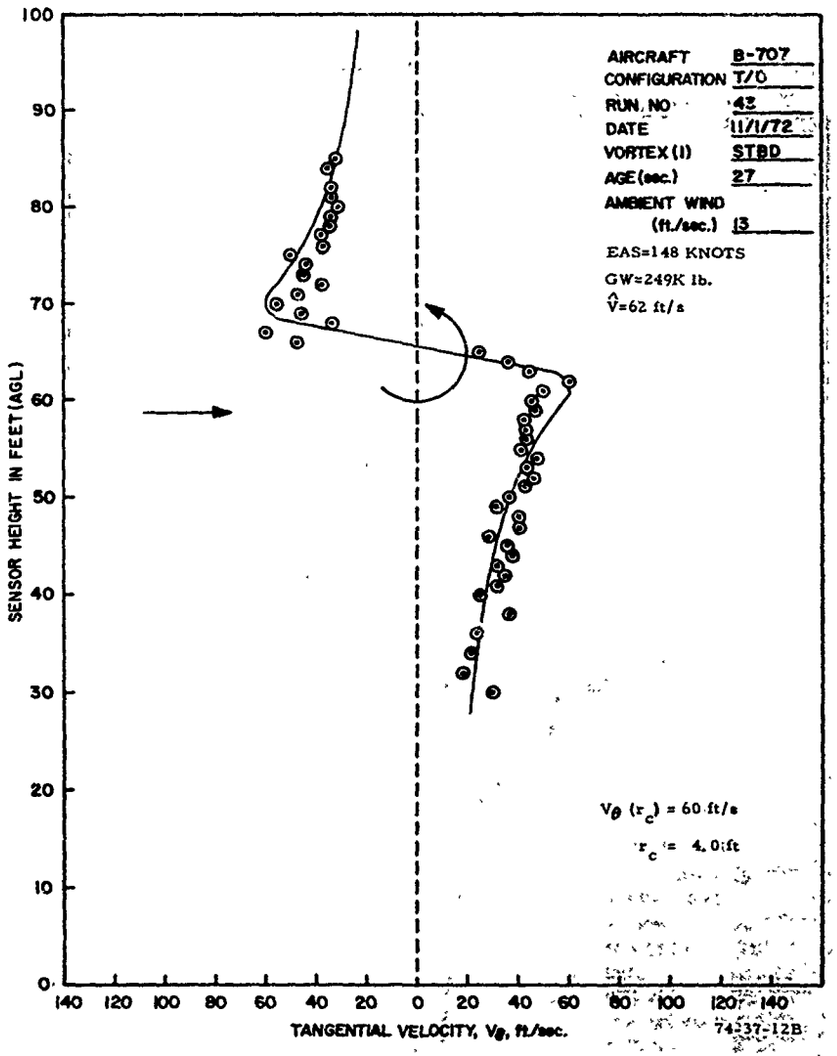
AIRCRAFT B-707
CONFIGURATION T/O
RUN NO 43
DATE 11/1/72
VORTEX (I) STBD
AGE (sec.) 27
AMBIENT WIND (ft./sec.) 13
EAS=148 KNOTS
GW=249K lb.
$\hat{V}$=62 ft/s
$V_\theta (r_c)$ = 60 ft/s
r_c = 4.0 ft
SENSOR HEIGHT IN FEET (AGL)
TANGENTIAL VELOCITY, V_θ, ft./sec.
74-37-12B

13 B

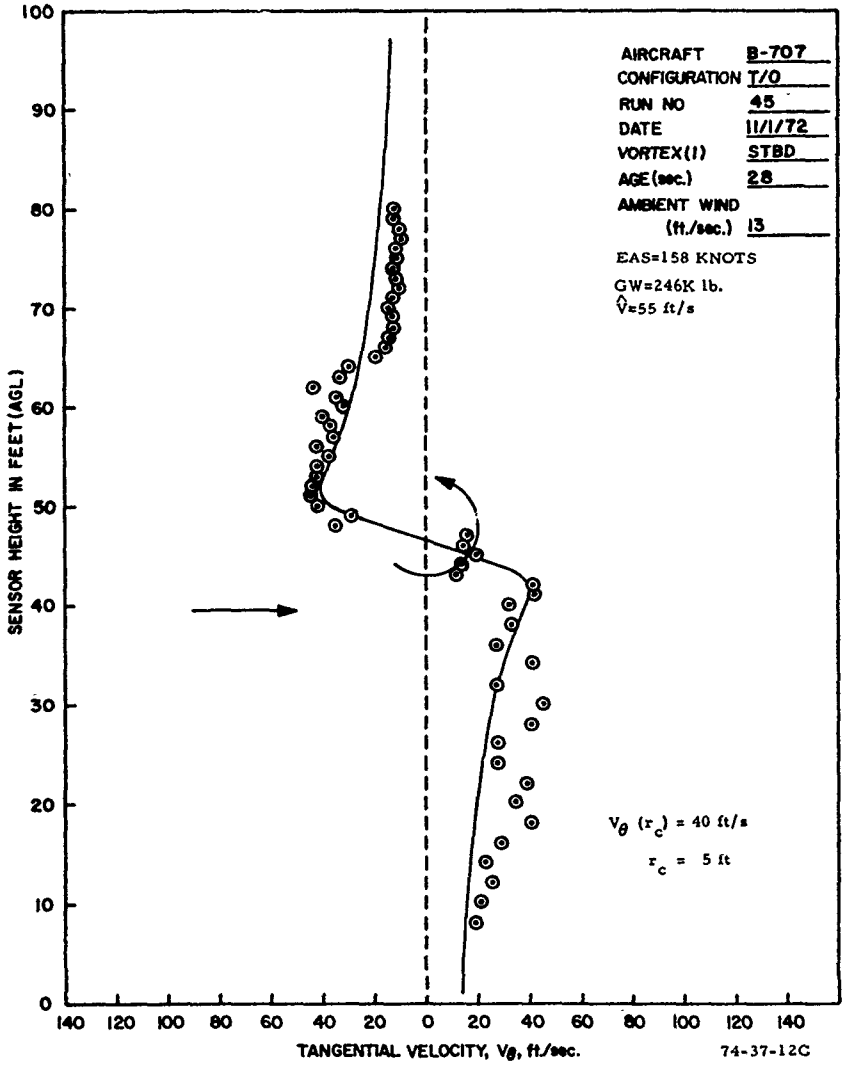
AIRCRAFT B-707
CONFIGURATION T/O
RUN NO 45
DATE 11/1/72
VORTEX(1) STBD
AGE(sec.) 28
AMBIENT WIND (ft./sec.) 13
EAS=158 KNOTS
GW=246K lb.
V̂=55 ft/s
V_θ (r_c) = 40 ft/s
r_c = 5 ft
SENSOR HEIGHT IN FEET (AGL)
TANGENTIAL VELOCITY, V_θ, ft./sec.
74-37-12C

14A

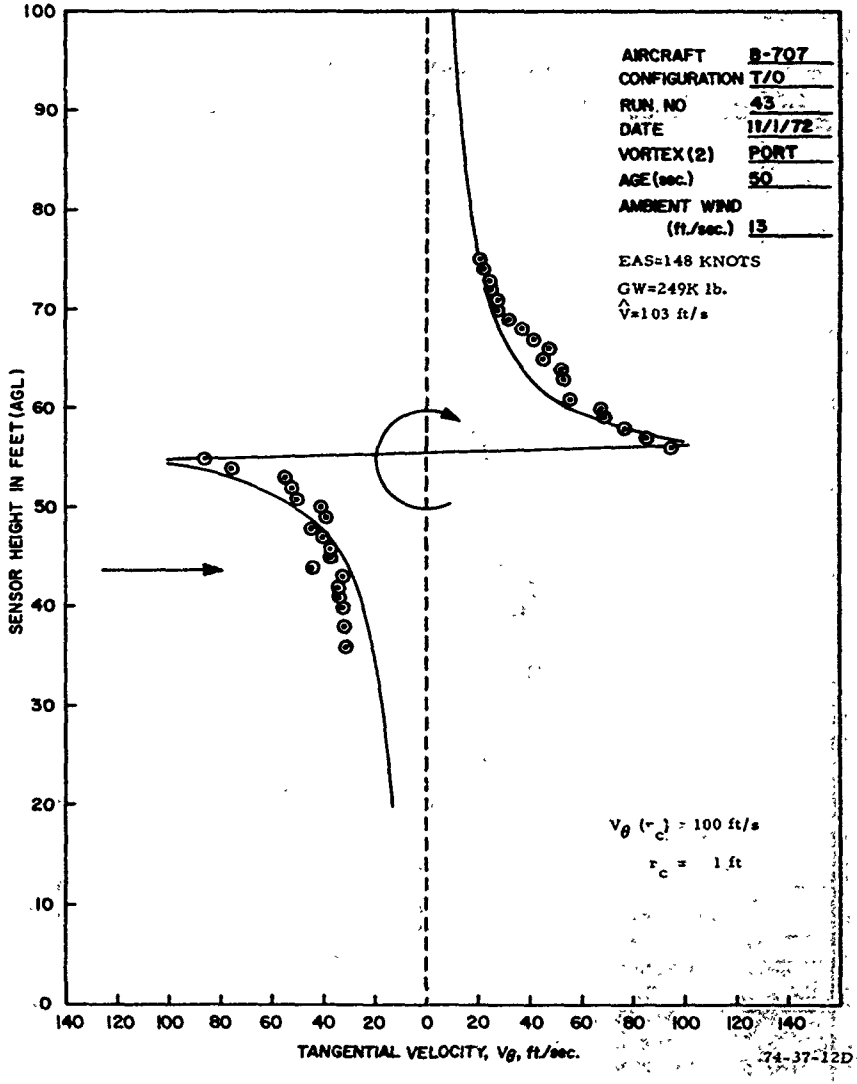
AIRCRAFT B-707
CONFIGURATION T/O
RUN NO 43
DATE 11/1/72
VORTEX(2) PORT
AGE(sec.) 50
AMBIENT WIND (ft./sec.) 13
EAS=148 KNOTS
GW=249K lb.
V̂=103 ft/s
V_θ (r_c) = 100 ft/s
r_c = 1 ft
SENSOR HEIGHT IN FEET (AGL)
TANGENTIAL VELOCITY, V_θ, ft./sec.
74-37-12D

14B

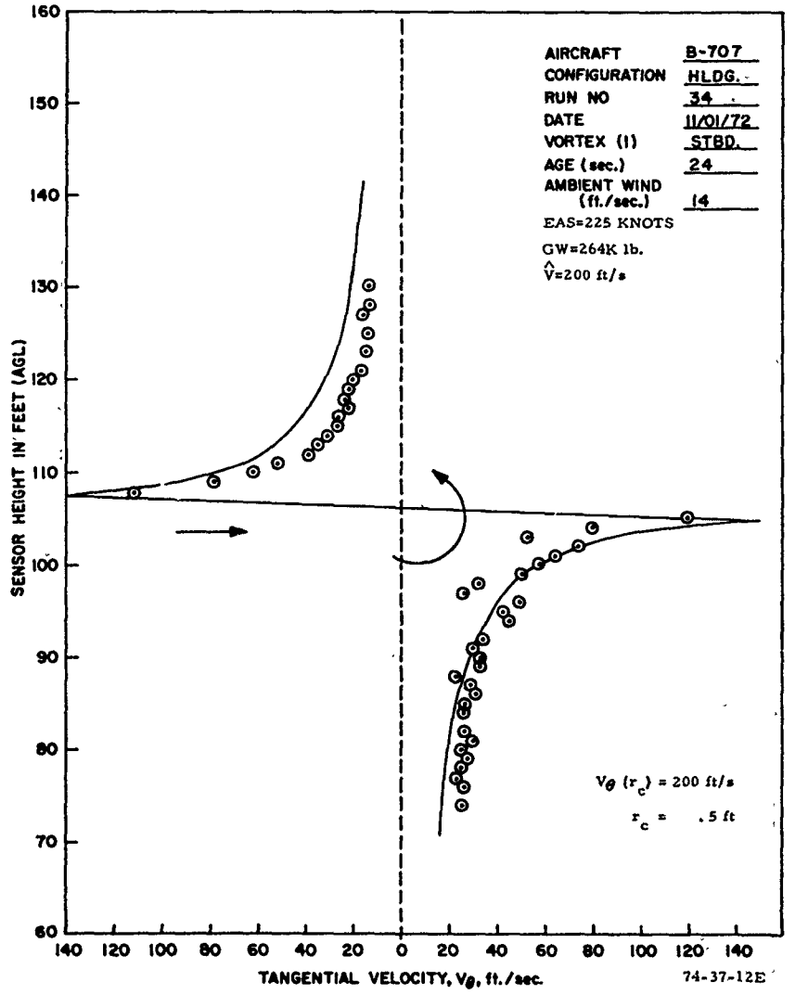
AIRCRAFT B-707
CONFIGURATION HLDG.
RUN NO 34
DATE 11/01/72
VORTEX (1) STBD.
AGE (sec.) 24
AMBIENT WIND (ft./sec.) 14
EAS=225 KNOTS
GW=264K lb.
$\hat{V}$=200 ft/s
V_θ (r_c) = 200 ft/s
r_c = .5 ft
SENSOR HEIGHT IN FEET (AGL)
TANGENTIAL VELOCITY, V_θ, ft./sec.
74-37-12E

15A

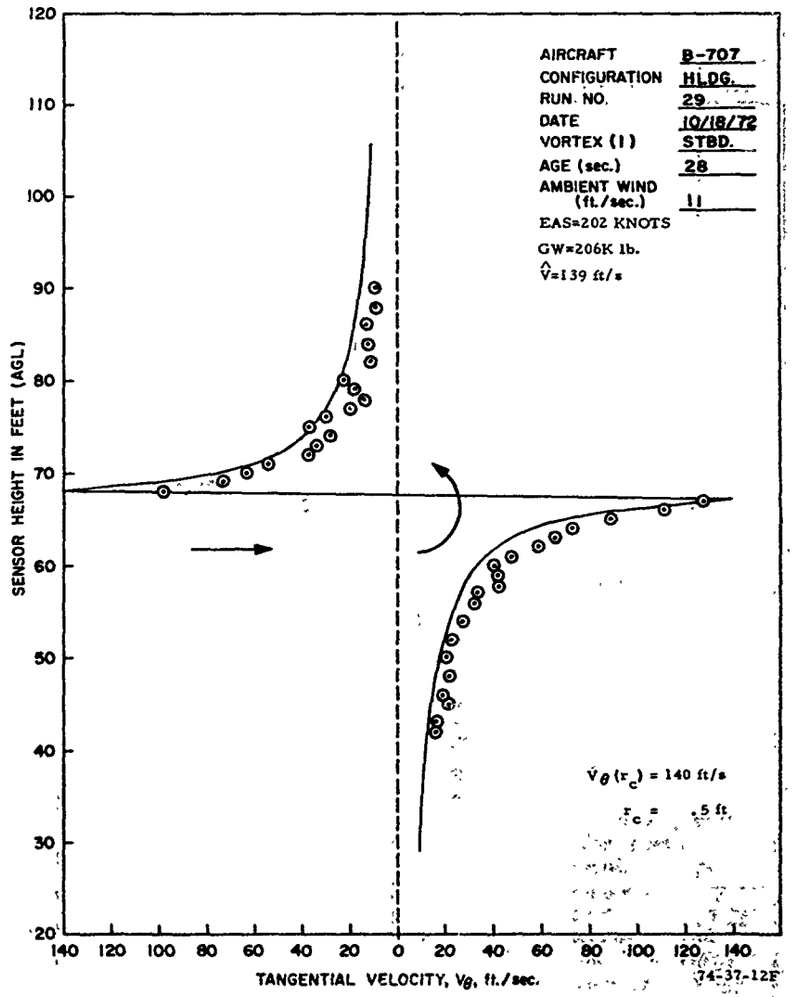
AIRCRAFT B-707
CONFIGURATION HLDG.
RUN NO. 29
DATE 10/18/72
VORTEX (1) STBD.
AGE (sec.) 28
AMBIENT WIND (ft./sec.) 11
EAS=202 KNOTS
GW=206K lb.
$\hat{V}$=139 ft/s
V_θ (r_c) = 140 ft/s
r_c = .5 ft
SENSOR HEIGHT IN FEET (AGL)
TANGENTIAL VELOCITY, V_θ, ft./sec.
74-37-12E

15B

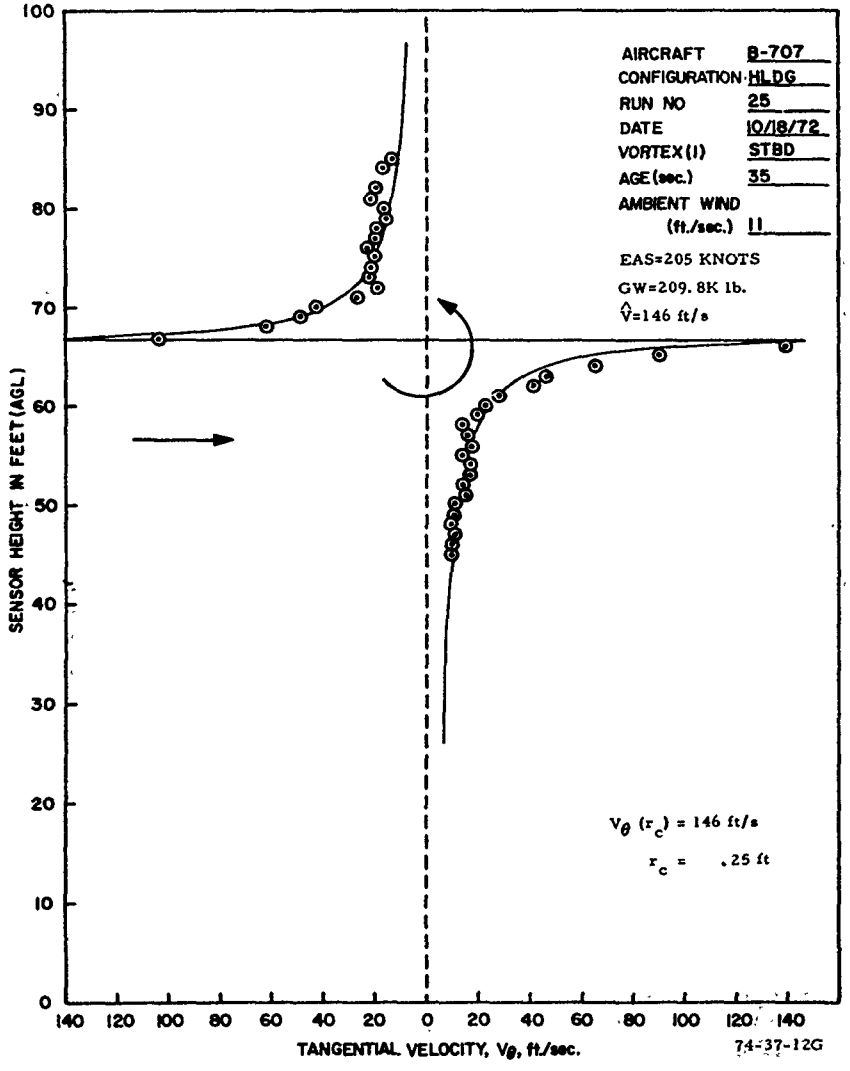
AIRCRAFT B-707
CONFIGURATION HLDG
RUN NO 25
DATE 10/18/72
VORTEX (1) STBD
AGE (sec.) 35
AMBIENT WIND (ft./sec.) 11
EAS=205 KNOTS
GW=209.8K lb.
$\hat{V}$=146 ft/s
$V_\theta (r_c)$ = 146 ft/s
r_c = .25 ft
SENSOR HEIGHT IN FEET (AGL)
TANGENTIAL VELOCITY, V_θ, ft./sec.
74-37-12G

16A

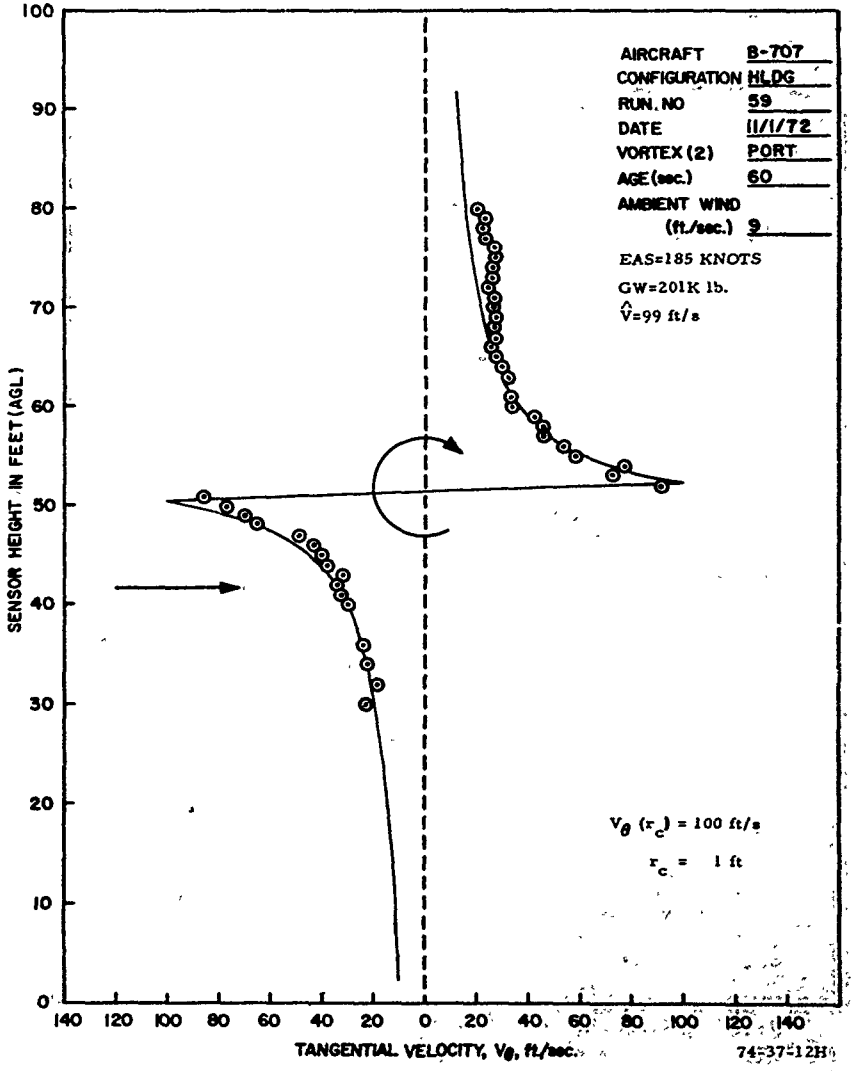
AIRCRAFT B-707
CONFIGURATION HLDG
RUN. NO 59
DATE 11/1/72
VORTEX (2) PORT
AGE (sec.) 60
AMBIENT WIND (ft./sec.) 9
EAS=185 KNOTS
GW=201K lb.
$\hat{V}$=99 ft/s
$V_\theta (r_c)$ = 100 ft/s
r_c = 1 ft
SENSOR HEIGHT IN FEET (AGL)
TANGENTIAL VELOCITY, V_θ, ft./sec.
74-37-12H

16B

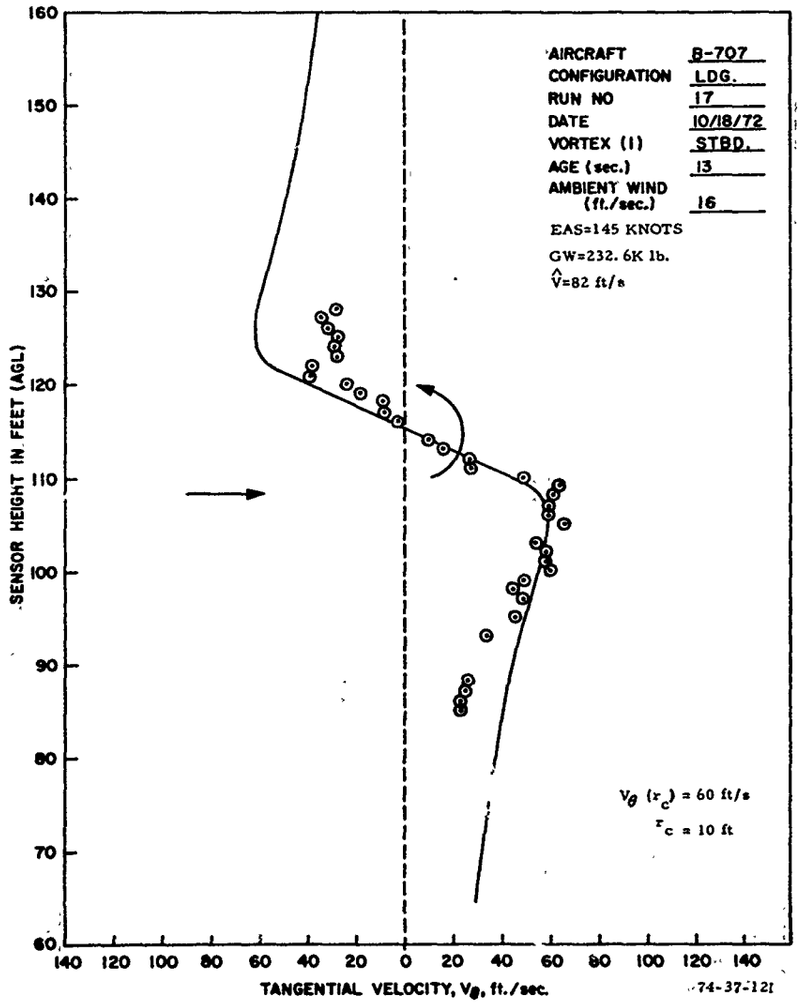
AIRCRAFT B-707
CONFIGURATION LDG.
RUN NO 17
DATE 10/18/72
VORTEX (I) STBD.
AGE (sec.) 13
AMBIENT WIND (ft./sec.) 16
EAS=145 KNOTS
GW=232. 6K lb.
$\hat{V}$=82 ft/s
V_θ (r_c) = 60 ft/s
r_c = 10 ft
SENSOR HEIGHT IN FEET (AGL)
TANGENTIAL VELOCITY, V_θ, ft./sec.
74-37-12I

17A

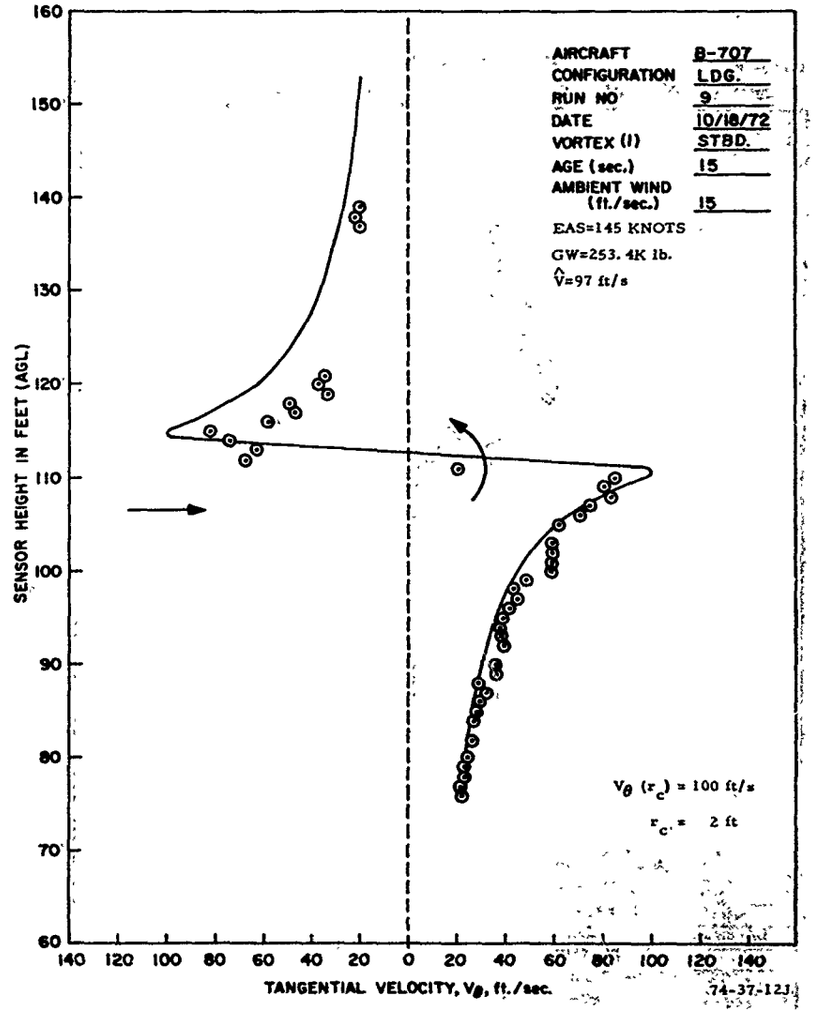
AIRCRAFT B-707
CONFIGURATION LDG.
RUN NO 9
DATE 10/18/72
VORTEX (I) STBD.
AGE (sec.) 15
AMBIENT WIND (ft./sec.) 15
EAS=145 KNOTS
GW=253. 4K lb.
$\hat{V}$=97 ft/s
V_θ (r_c) = 100 ft/s
r_c = 2 ft
SENSOR HEIGHT IN FEET (AGL)
TANGENTIAL VELOCITY, V_θ, ft./sec.
74-37-12J

17B

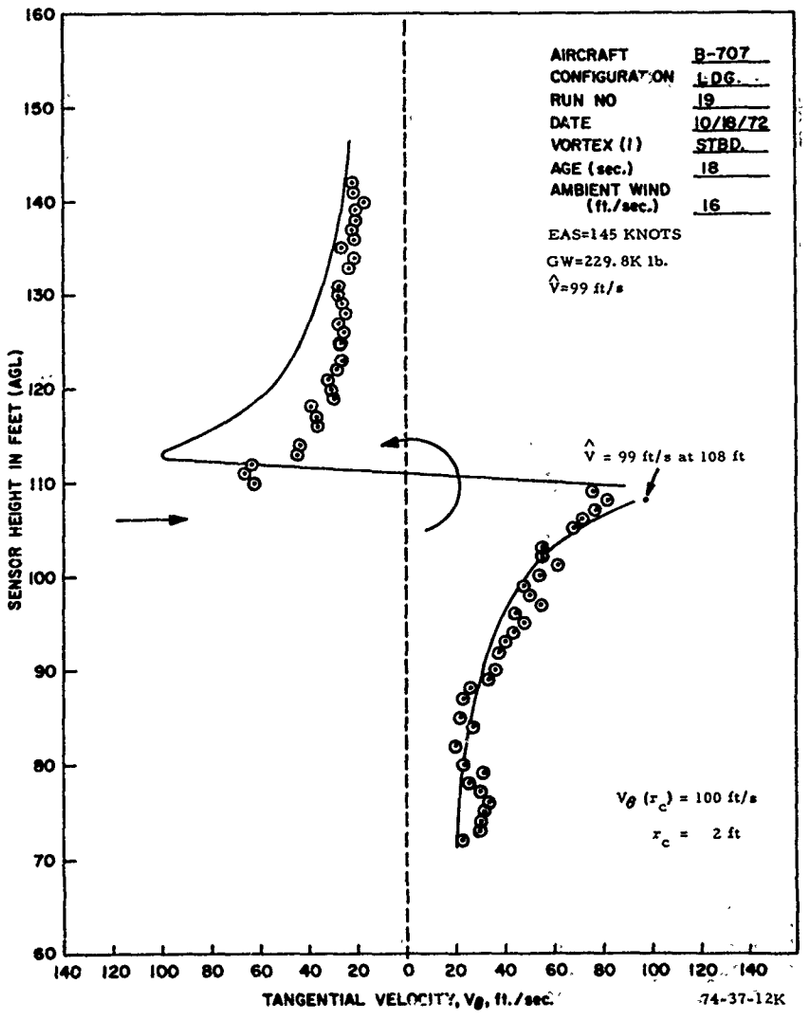
AIRCRAFT B-707
CONFIGURATION LDG.
RUN NO 19
DATE 10/18/72
VORTEX (1) STBD.
AGE (sec.) 18
AMBIENT WIND (ft./sec.) 16
EAS=145 KNOTS
GW=229.8K lb.
$\hat{V}$=99 ft/s
$\hat{V}$ = 99 ft/s at 108 ft
V_θ (r_c) = 100 ft/s
r_c = 2 ft
SENSOR HEIGHT IN FEET (AGL)
TANGENTIAL VELOCITY, V_θ, ft./sec.
74-37-12K

18A

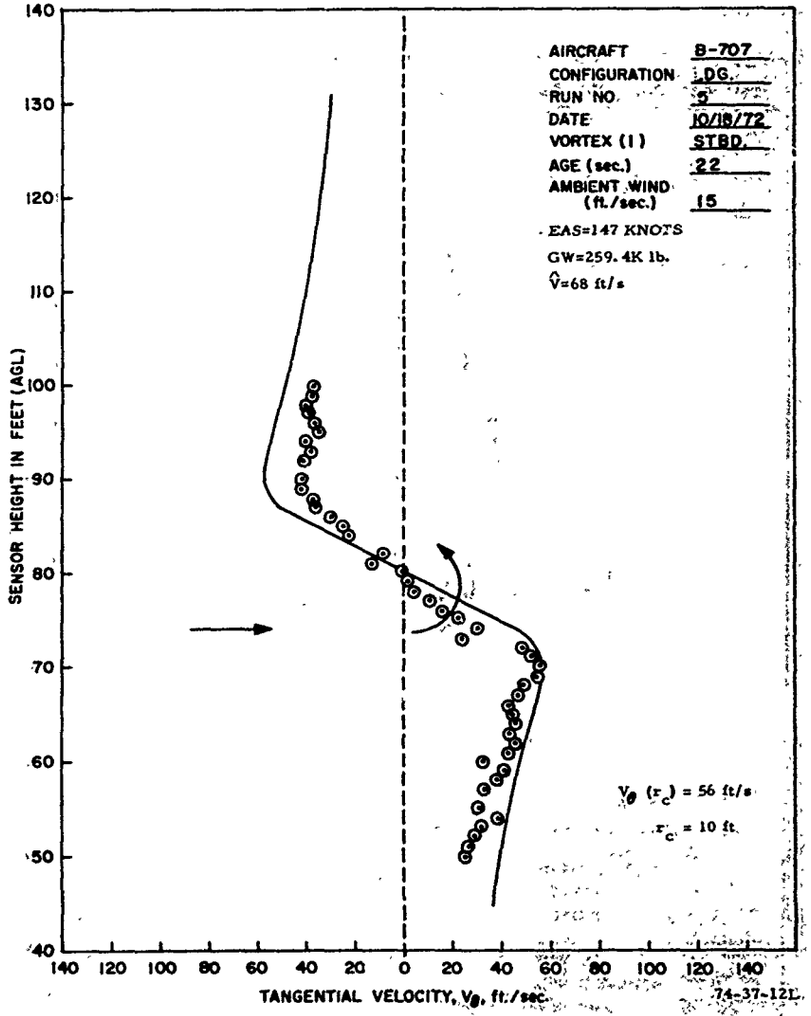
AIRCRAFT B-707
CONFIGURATION LDG.
RUN NO. 5
DATE 10/18/72
VORTEX (1) STBD.
AGE (sec.) 22
AMBIENT WIND (ft./sec.) 15
EAS=147 KNOTS
GW=259.4K lb.
$\hat{V}$=68 ft/s
V_θ (r_c) = 56 ft/s
r_c = 10 ft.
SENSOR HEIGHT IN FEET (AGL)
TANGENTIAL VELOCITY, V_θ, ft./sec.
74-37-12L

18B

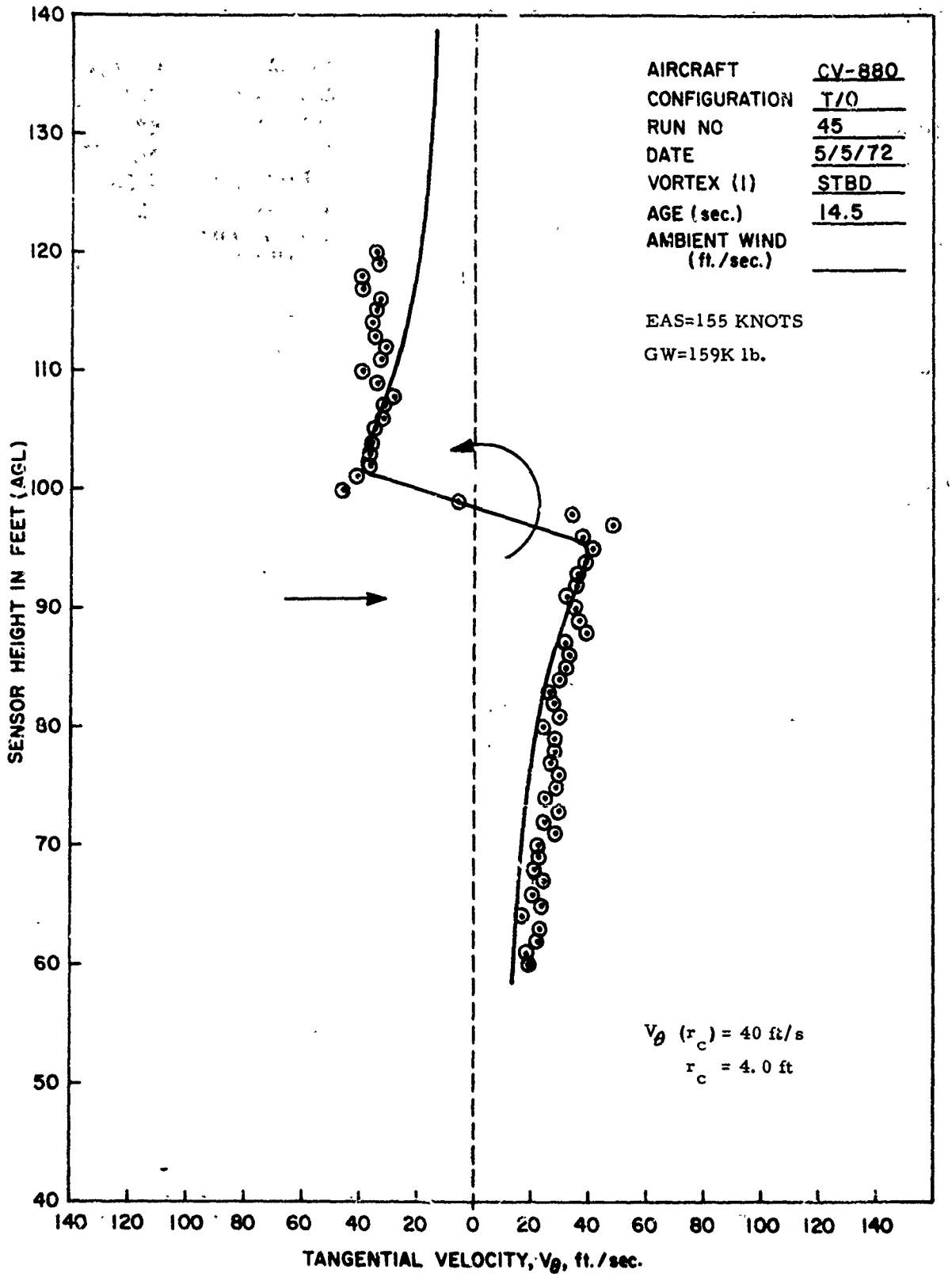
AIRCRAFT CV-880
CONFIGURATION T/O
RUN NO 45
DATE 5/5/72
VORTEX (1) STBD
AGE (sec.) 14.5
AMBIENT WIND (ft./sec.)
EAS=155 KNOTS
GW=159K lb.
V_θ (r_c) = 40 ft/s
r_c = 4.0 ft
SENSOR HEIGHT IN FEET (AGL)
140
130
120
110
100
90
80
70
60
50
40
140 120 100 80 60 40 20 0 20 40 60 80 100 120 140
TANGENTIAL VELOCITY, V_θ, ft./sec.

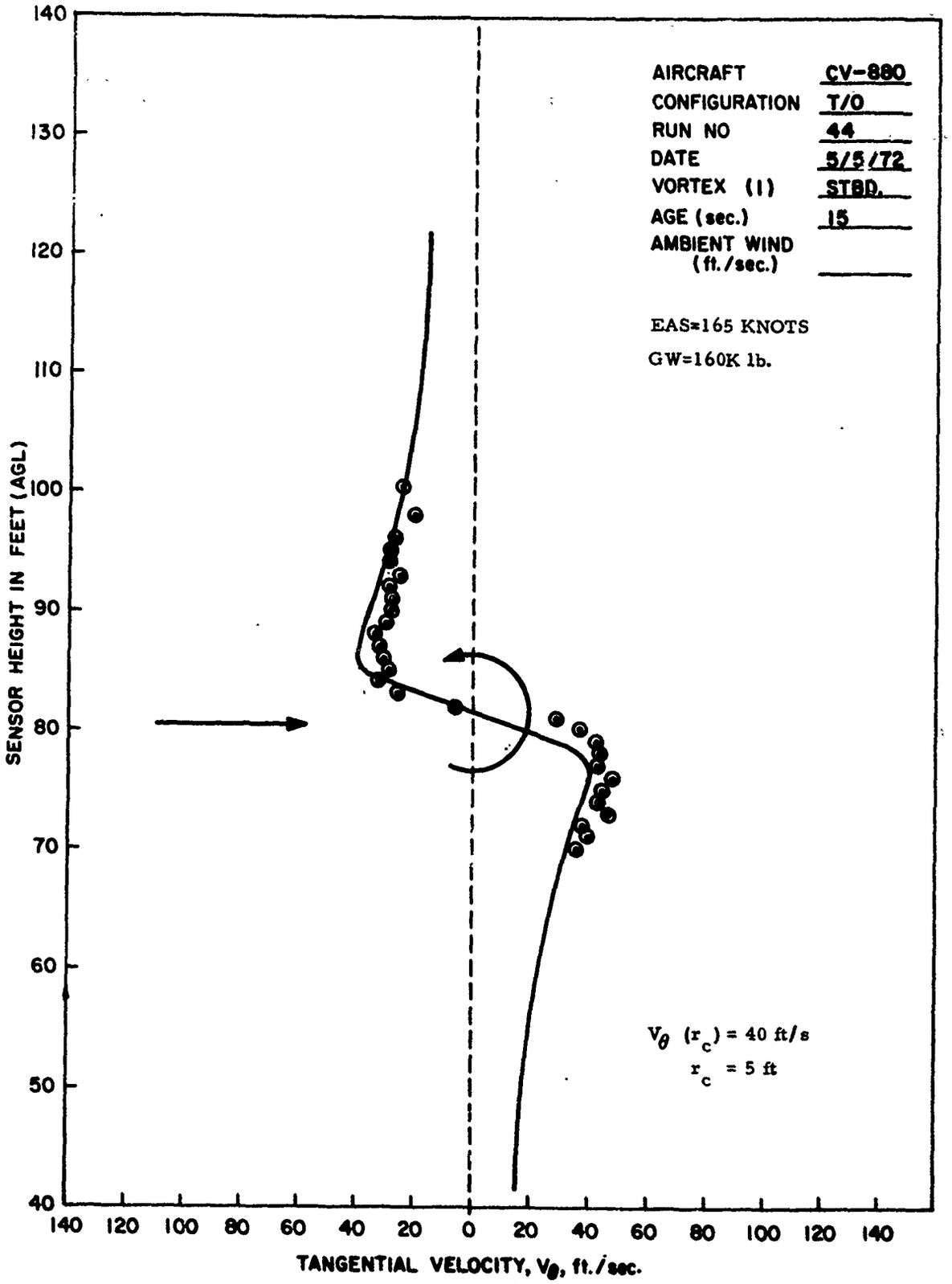
AIRCRAFT CV-880
CONFIGURATION T/O
RUN NO 44
DATE 5/5/72
VORTEX (1) STBD.
AGE (sec.) 15
AMBIENT WIND (ft./sec.)
EAS=165 KNOTS
GW=160K lb.
V_θ (r_c) = 40 ft/s
r_c = 5 ft
SENSOR HEIGHT IN FEET (AGL)
140
130
120
110
100
90
80
70
60
50
40
140 120 100 80 60 40 20 0 20 40 60 80 100 120 140
TANGENTIAL VELOCITY, V_θ, ft./sec.

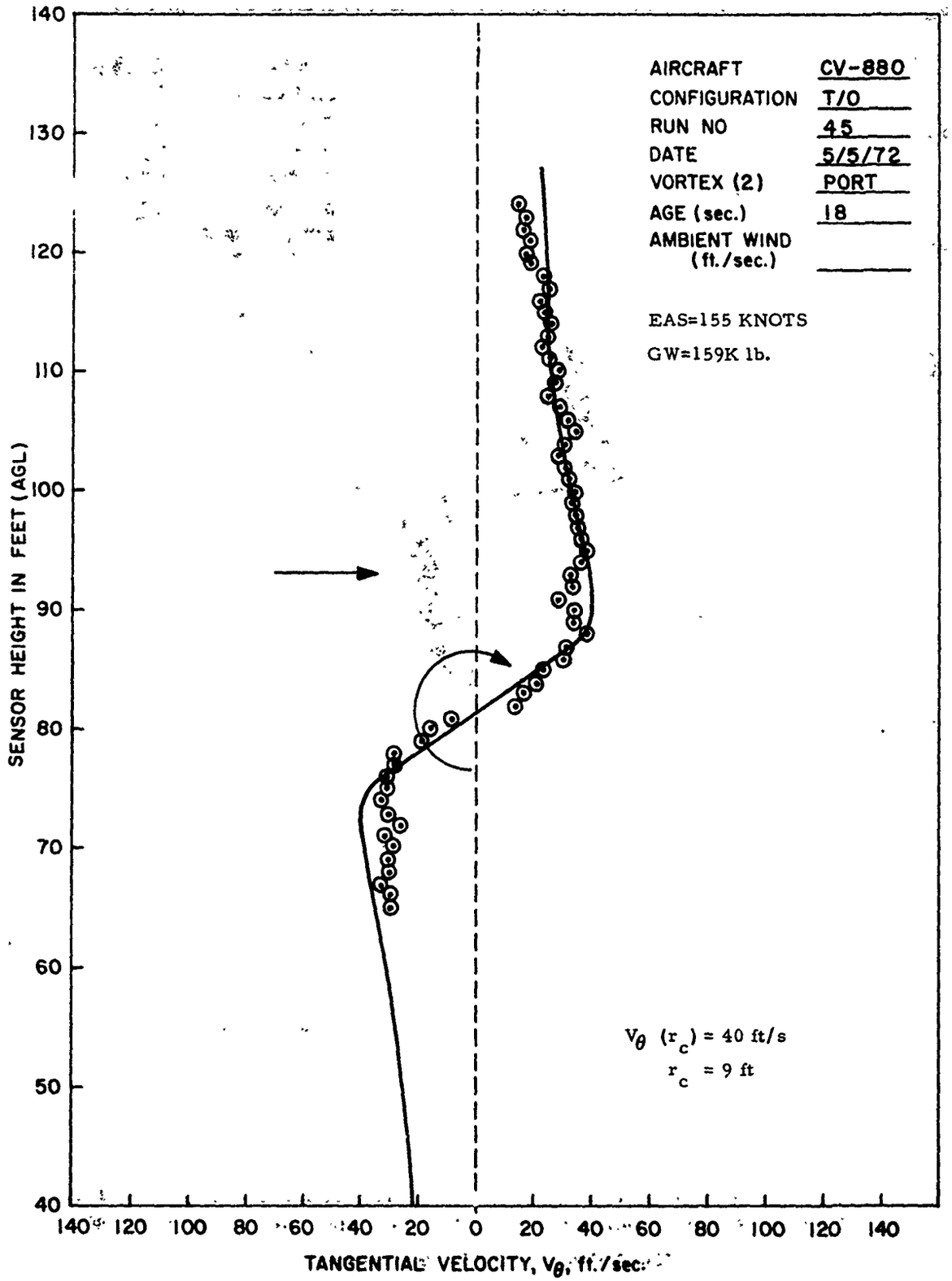
AIRCRAFT CV-880
CONFIGURATION T/O
RUN NO 45
DATE 5/5/72
VORTEX (2) PORT
AGE (sec.) 18
AMBIENT WIND (ft./sec.)
EAS=155 KNOTS
GW=159K lb.
V_θ (r_c) = 40 ft/s
r_c = 9 ft
SENSOR HEIGHT IN FEET (AGL)
140
130
120
110
100
90
80
70
60
50
40
140 120 100 80 60 40 20 0 20 40 60 80 100 120 140
TANGENTIAL VELOCITY, V_θ, ft./sec.

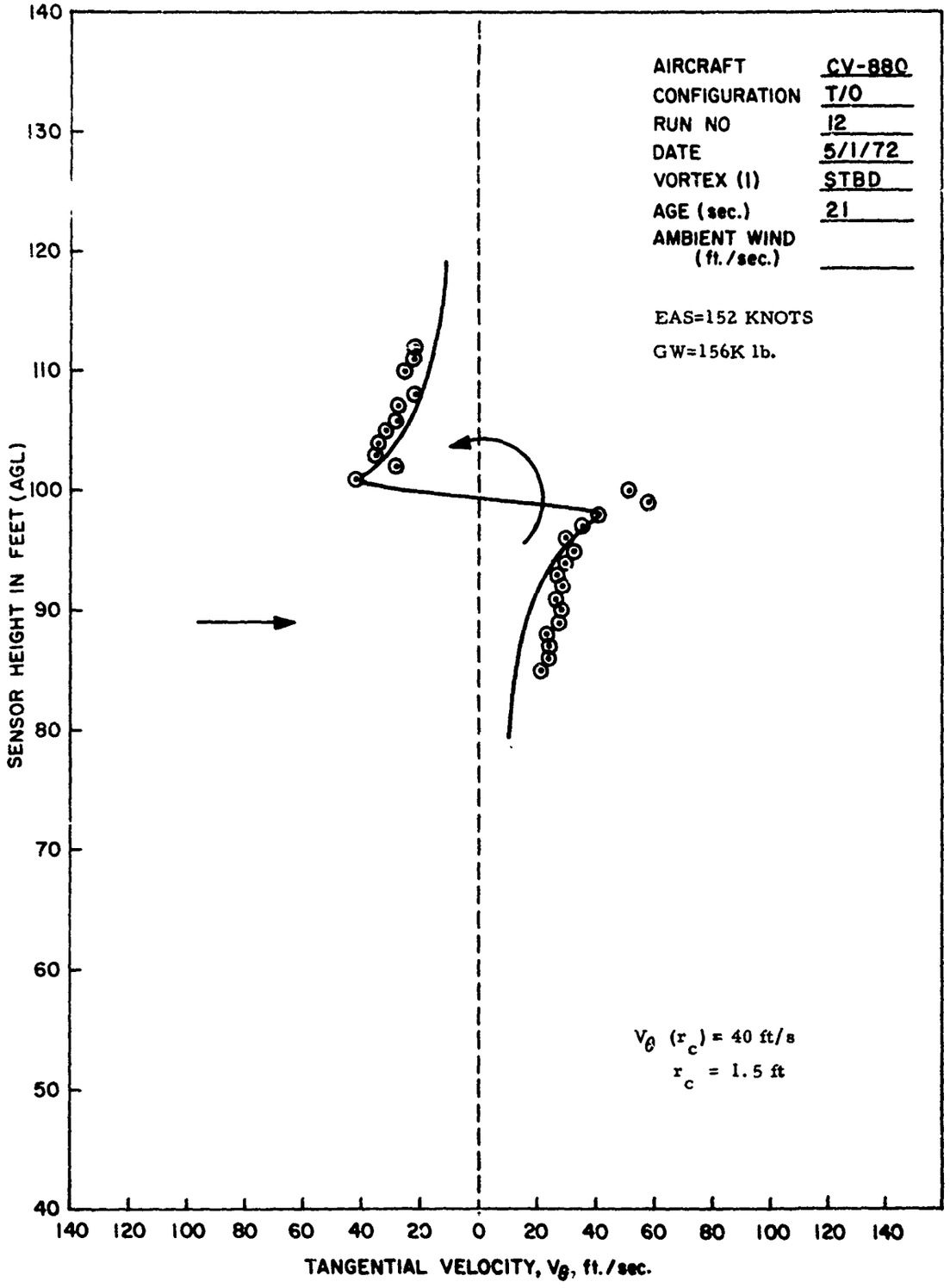
AIRCRAFT CV-880
CONFIGURATION T/O
RUN NO 12
DATE 5/1/72
VORTEX (1) STBD
AGE (sec.) 21
AMBIENT WIND (ft./sec.)
EAS=152 KNOTS
GW=156K lb.
V_θ (r_c) = 40 ft/s
r_c = 1.5 ft
SENSOR HEIGHT IN FEET (AGL)
140
130
120
110
100
90
80
70
60
50
40
140 120 100 80 60 40 20 0 20 40 60 80 100 120 140
TANGENTIAL VELOCITY, V_θ, ft./sec.

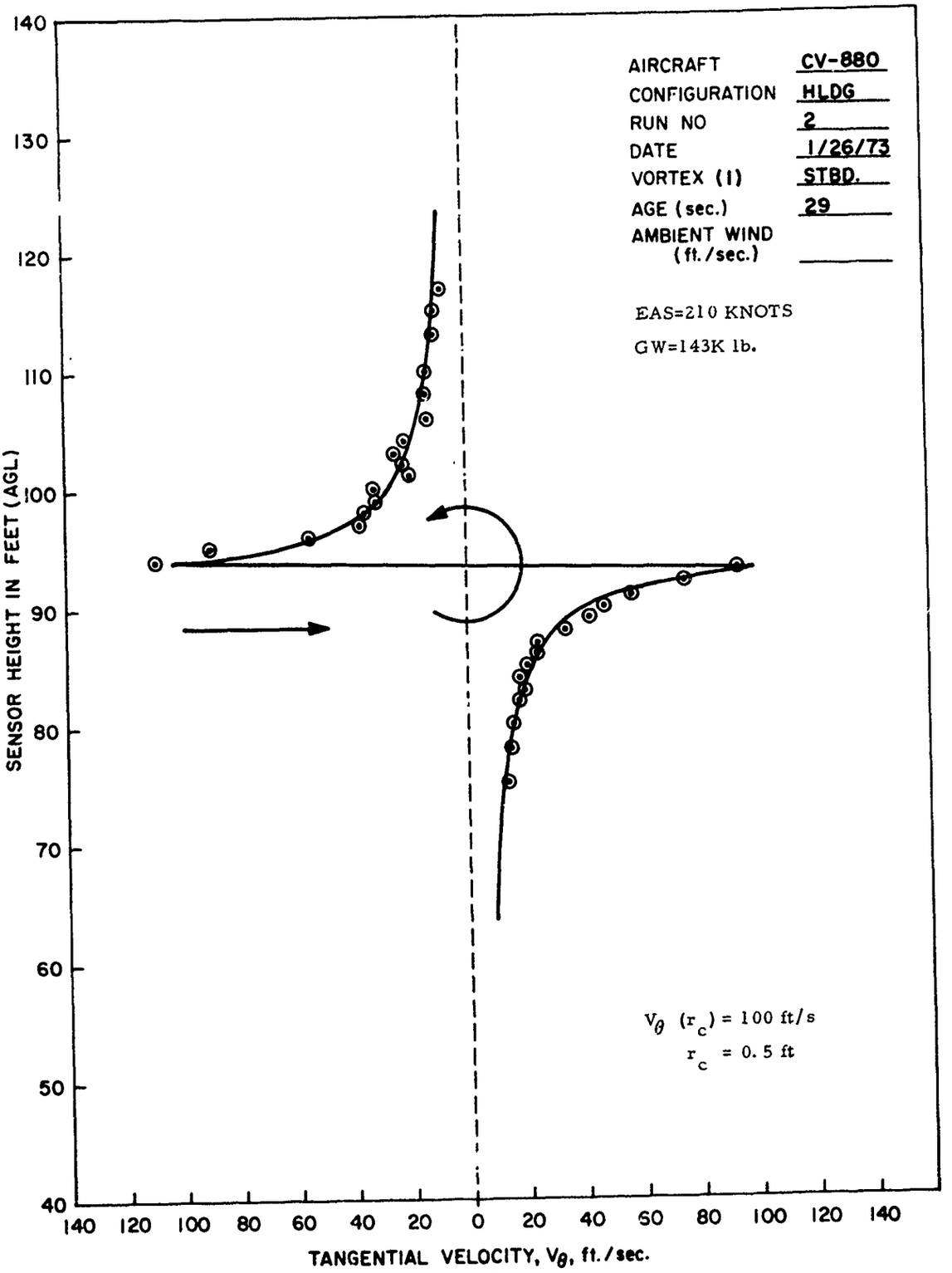
AIRCRAFT CV-880
CONFIGURATION HLDG
RUN NO 2
DATE 1/26/73
VORTEX (1) STBD.
AGE (sec.) 29
AMBIENT WIND (ft./sec.)
EAS=210 KNOTS
GW=143K lb.
V_θ (r_c) = 100 ft/s
r_c = 0.5 ft
SENSOR HEIGHT IN FEET (AGL)
140
130
120
110
100
90
80
70
60
50
40
140 120 100 80 60 40 20 0 20 40 60 80 100 120 140
TANGENTIAL VELOCITY, V_θ, ft./sec.

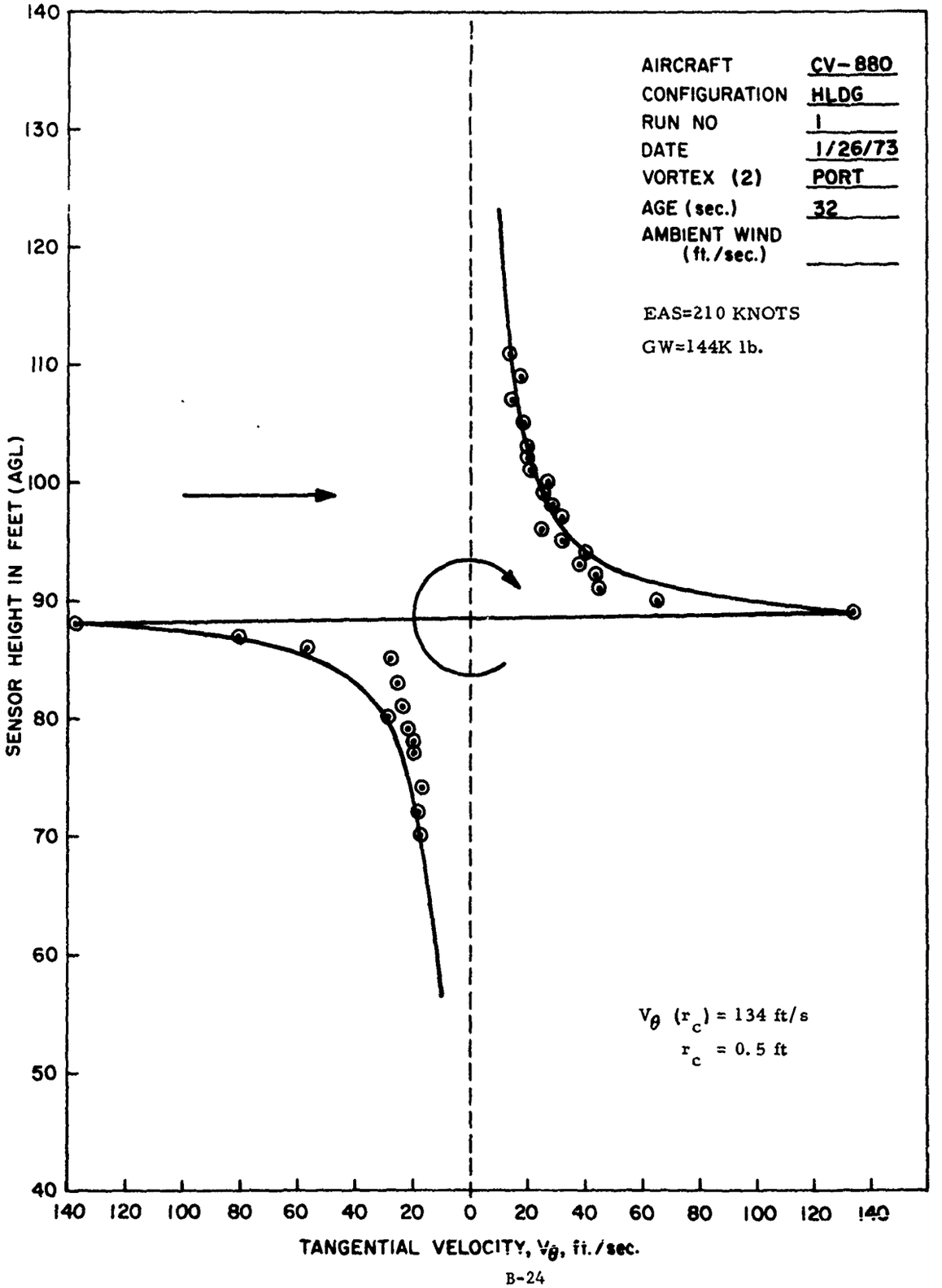
AIRCRAFT CV-880
CONFIGURATION HLDG
RUN NO 1
DATE 1/26/73
VORTEX (2) PORT
AGE (sec.) 32
AMBIENT WIND (ft./sec.)
EAS=210 KNOTS
GW=144K lb.
V_θ (r_c) = 134 ft/s
r_c = 0.5 ft
SENSOR HEIGHT IN FEET (AGL)
140
130
120
110
100
90
80
70
60
50
40
140 120 100 80 60 40 20 0 20 40 60 80 100 120 140
TANGENTIAL VELOCITY, V_θ, ft./sec.

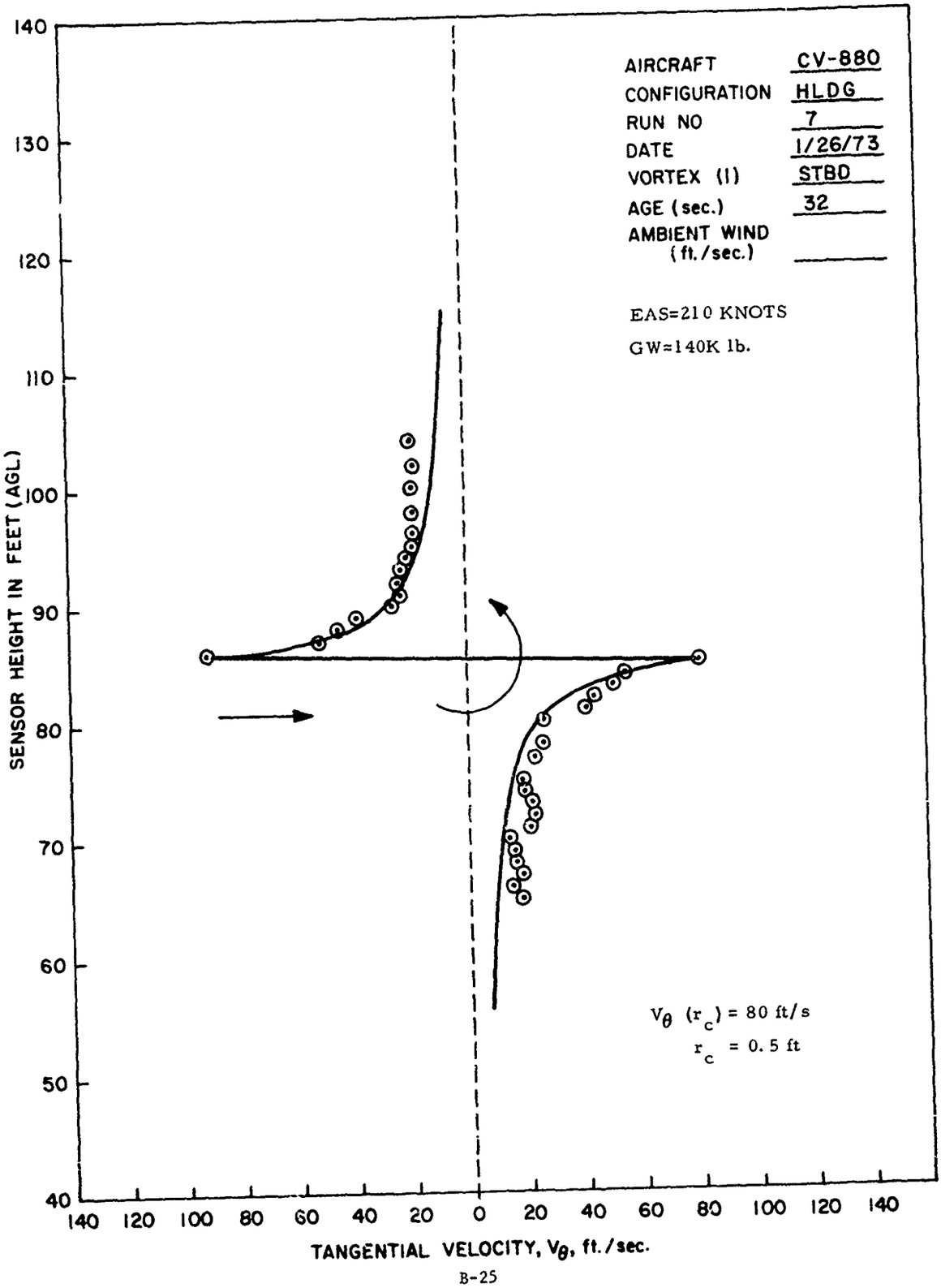
AIRCRAFT CV-880
CONFIGURATION HLDG
RUN NO 7
DATE 1/26/73
VORTEX (1) STBD
AGE (sec.) 32
AMBIENT WIND (ft./sec.)
EAS=210 KNOTS
GW=140K lb.
V_θ (r_c) = 80 ft/s
r_c = 0.5 ft
SENSOR HEIGHT IN FEET (AGL)
TANGENTIAL VELOCITY, V_θ, ft./sec.
140
130
120
110
100
90
80
70
60
50
40
140 120 100 80 60 40 20 0 20 40 60 80 100 120 140

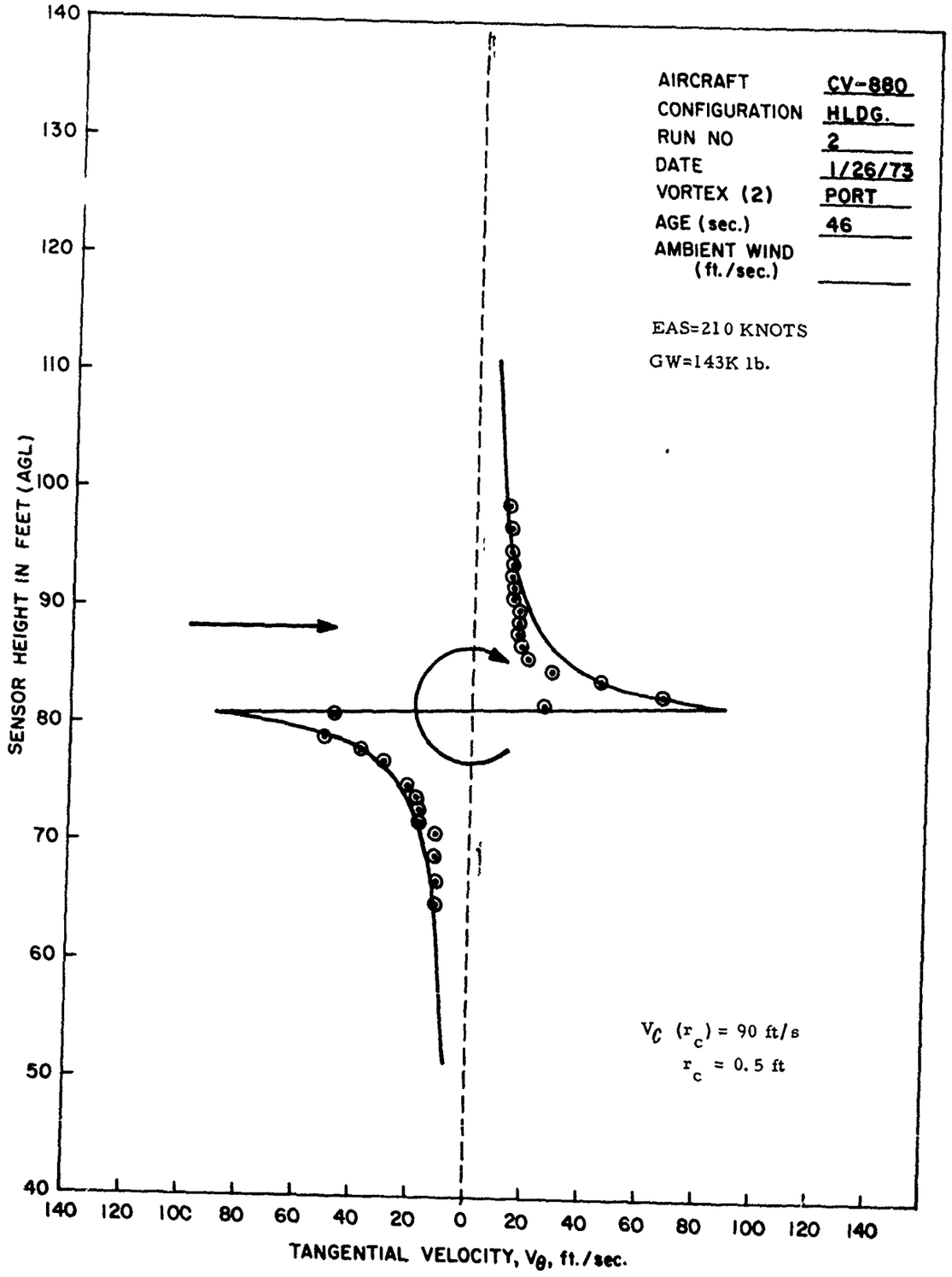
AIRCRAFT CV-880
CONFIGURATION HLDG.
RUN NO 2
DATE 1/26/73
VORTEX (2) PORT
AGE (sec.) 46
AMBIENT WIND (ft./sec.)
EAS=210 KNOTS
GW=143K lb.
V_C (r_c) = 90 ft/s
r_c = 0.5 ft
SENSOR HEIGHT IN FEET (AGL)
140
130
120
110
100
90
80
70
60
50
40
140 120 100 80 60 40 20 0 20 40 60 80 100 120 140
TANGENTIAL VELOCITY, V_θ, ft./sec.

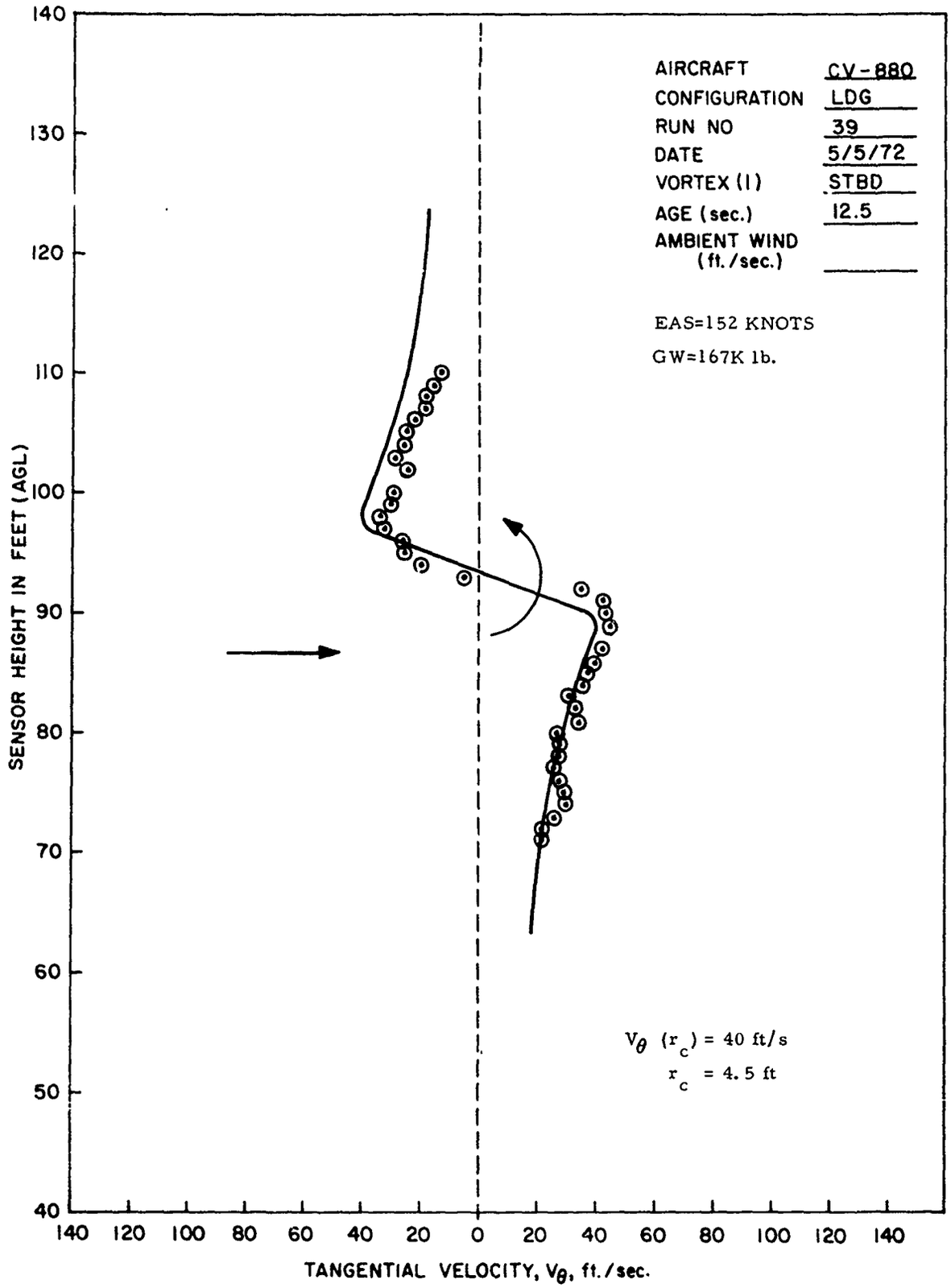
AIRCRAFT CV-880
CONFIGURATION LDG
RUN NO 39
DATE 5/5/72
VORTEX (1) STBD
AGE (sec.) 12.5
AMBIENT WIND (ft./sec.)
EAS=152 KNOTS
GW=167K lb.
V_θ (r_c) = 40 ft/s
r_c = 4.5 ft
SENSOR HEIGHT IN FEET (AGL)
140
130
120
110
100
90
80
70
60
50
40
140 120 100 80 60 40 20 0 20 40 60 80 100 120 140
TANGENTIAL VELOCITY, V_θ, ft./sec.

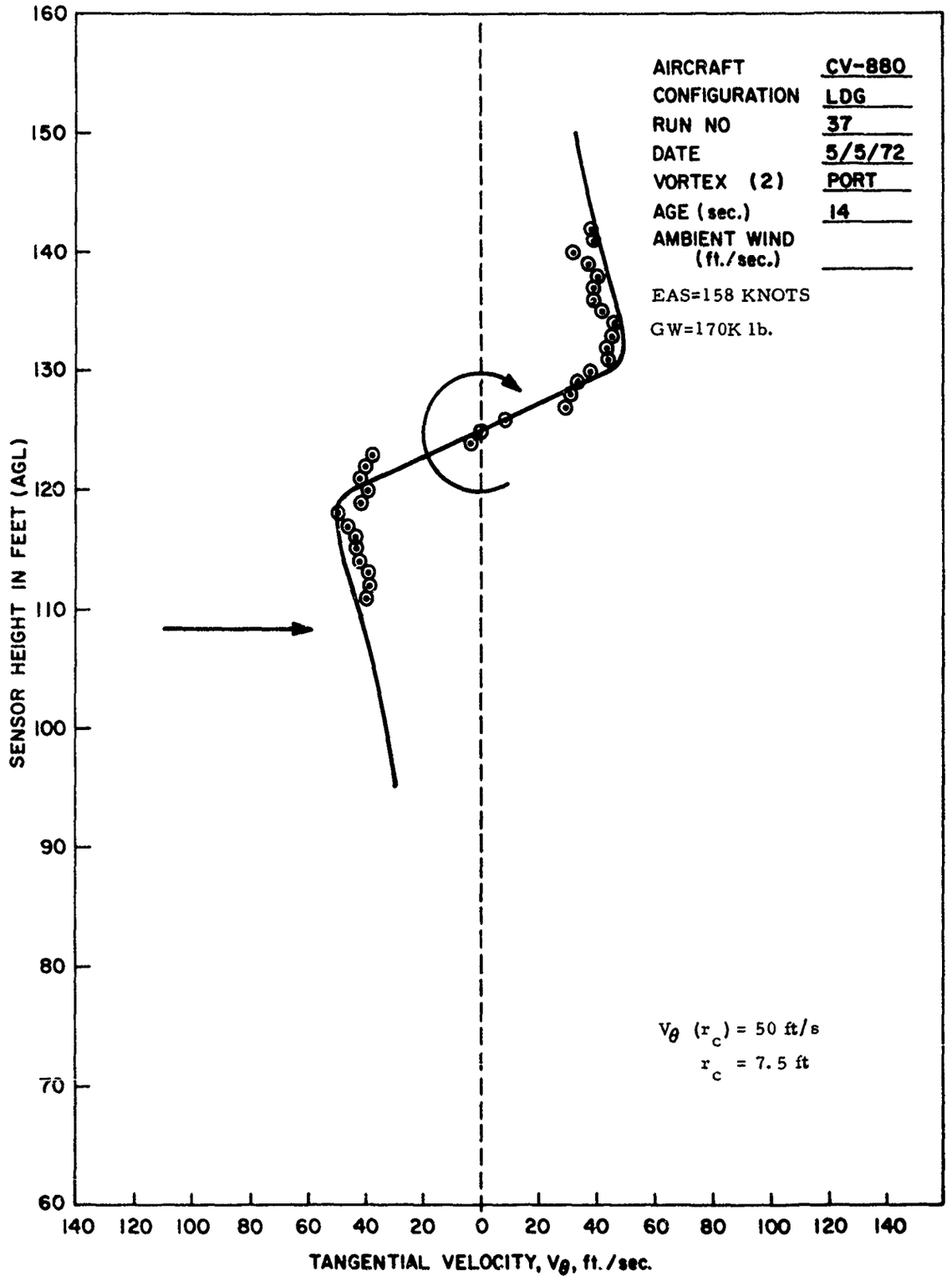
AIRCRAFT CV-880
CONFIGURATION LDG
RUN NO 37
DATE 5/5/72
VORTEX (2) PORT
AGE (sec.) 14
AMBIENT WIND (ft./sec.)
EAS=158 KNOTS
GW=170K lb.
V_θ (r_c) = 50 ft/s
r_c = 7.5 ft
SENSOR HEIGHT IN FEET (AGL)
160
150
140
130
120
110
100
90
80
70
60
140 120 100 80 60 40 20 0 20 40 60 80 100 120 140
TANGENTIAL VELOCITY, V_θ, ft./sec.

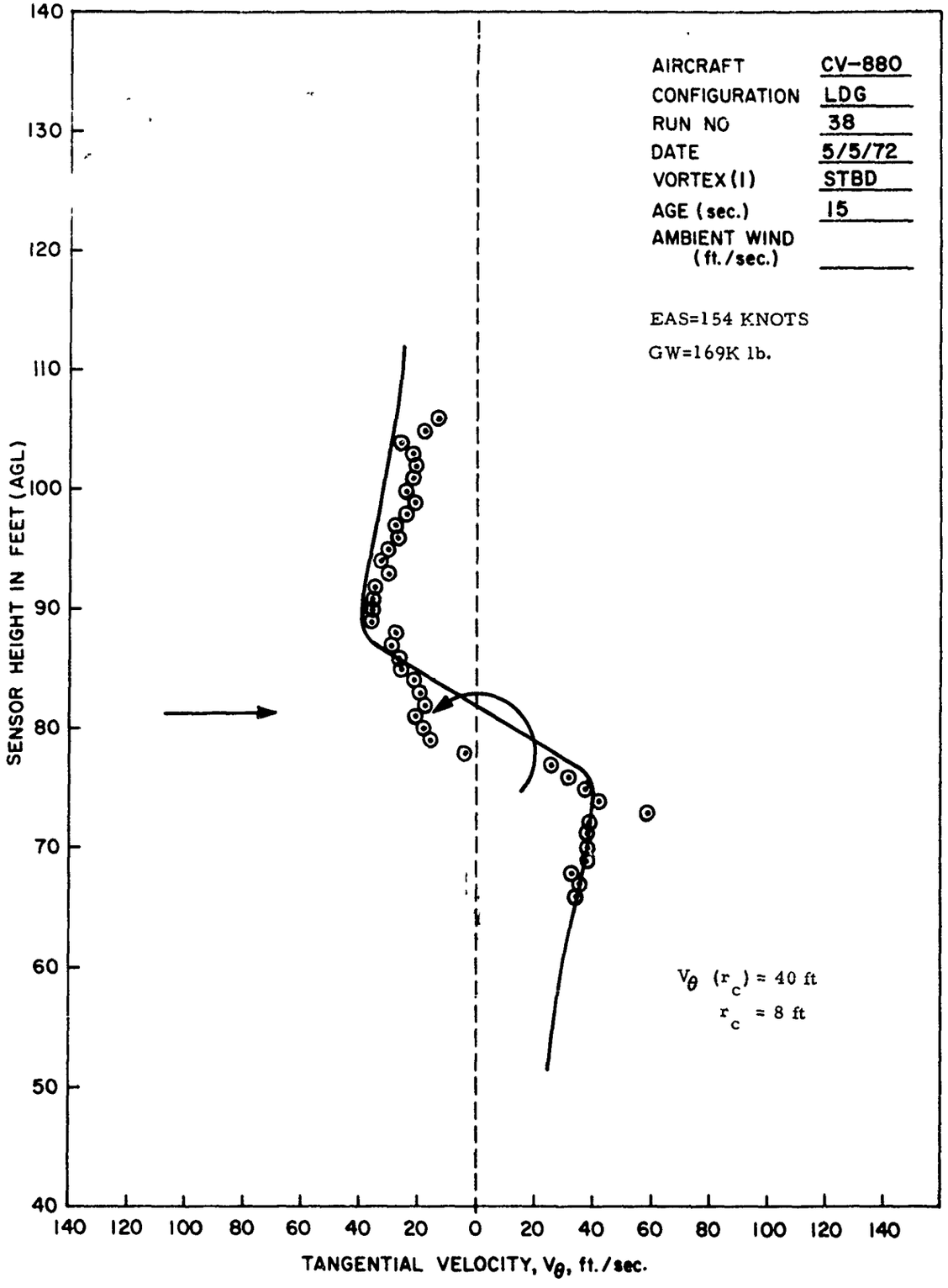
AIRCRAFT CV-880
CONFIGURATION LDG
RUN NO 38
DATE 5/5/72
VORTEX (1) STBD
AGE (sec.) 15
AMBIENT WIND (ft./sec.)
EAS=154 KNOTS
GW=169K lb.
V_θ (r_c) = 40 ft
r_c = 8 ft
SENSOR HEIGHT IN FEET (AGL)
140
130
120
110
100
90
80
70
60
50
40
140 120 100 80 60 40 20 0 20 40 60 80 100 120 140
TANGENTIAL VELOCITY, V_θ, ft./sec.

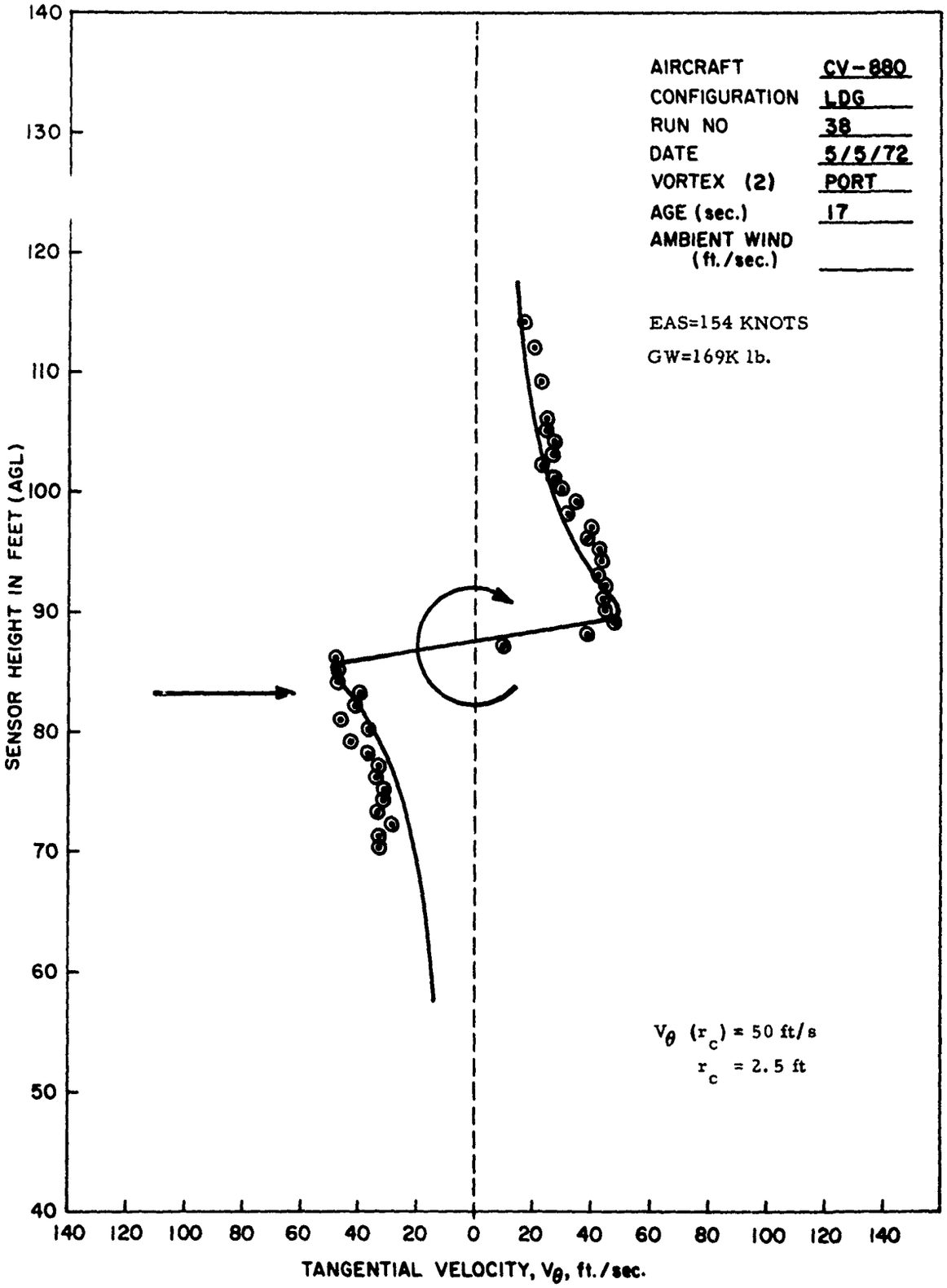
AIRCRAFT CV-880
CONFIGURATION LDG
RUN NO 38
DATE 5/5/72
VORTEX (2) PORT
AGE (sec.) 17
AMBIENT WIND (ft./sec.)
EAS=154 KNOTS
GW=169K lb.
V_θ (r_c) = 50 ft/s
r_c = 2.5 ft
SENSOR HEIGHT IN FEET (AGL)
140
130
120
110
100
90
80
70
60
50
40
140 120 100 80 60 40 20 0 20 40 60 80 100 120 140
TANGENTIAL VELOCITY, V_θ, ft./sec.

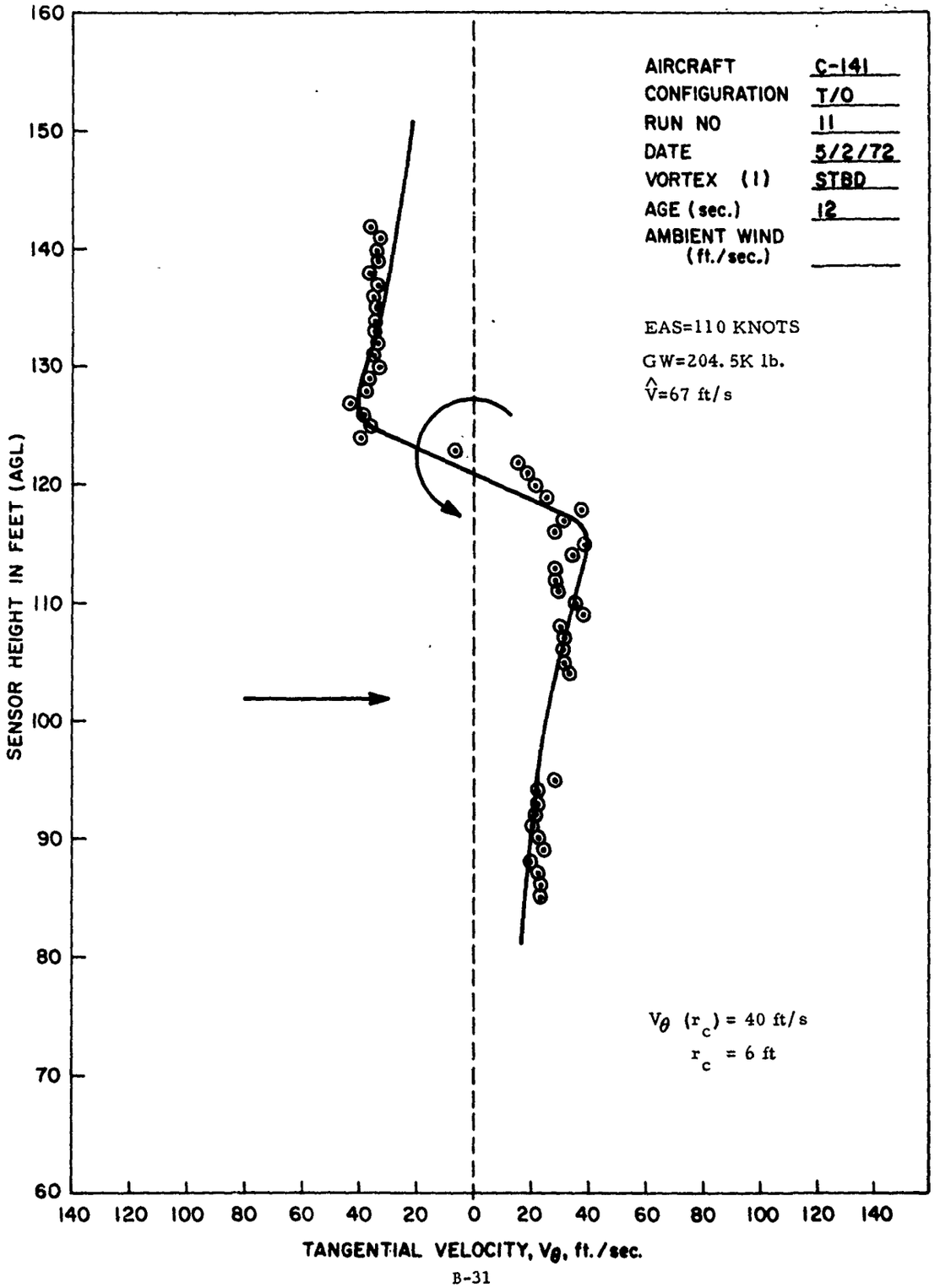
AIRCRAFT C-141
CONFIGURATION T/O
RUN NO 11
DATE 5/2/72
VORTEX (1) STBD
AGE (sec.) 12
AMBIENT WIND (ft./sec.)
EAS=110 KNOTS
GW=204.5K lb.
$\hat{V}$=67 ft/s
V_θ (r_c) = 40 ft/s
r_c = 6 ft
SENSOR HEIGHT IN FEET (AGL)
160
150
140
130
120
110
100
90
80
70
60
140 120 100 80 60 40 20 0 20 40 60 80 100 120 140
TANGENTIAL VELOCITY, V_θ, ft./sec.

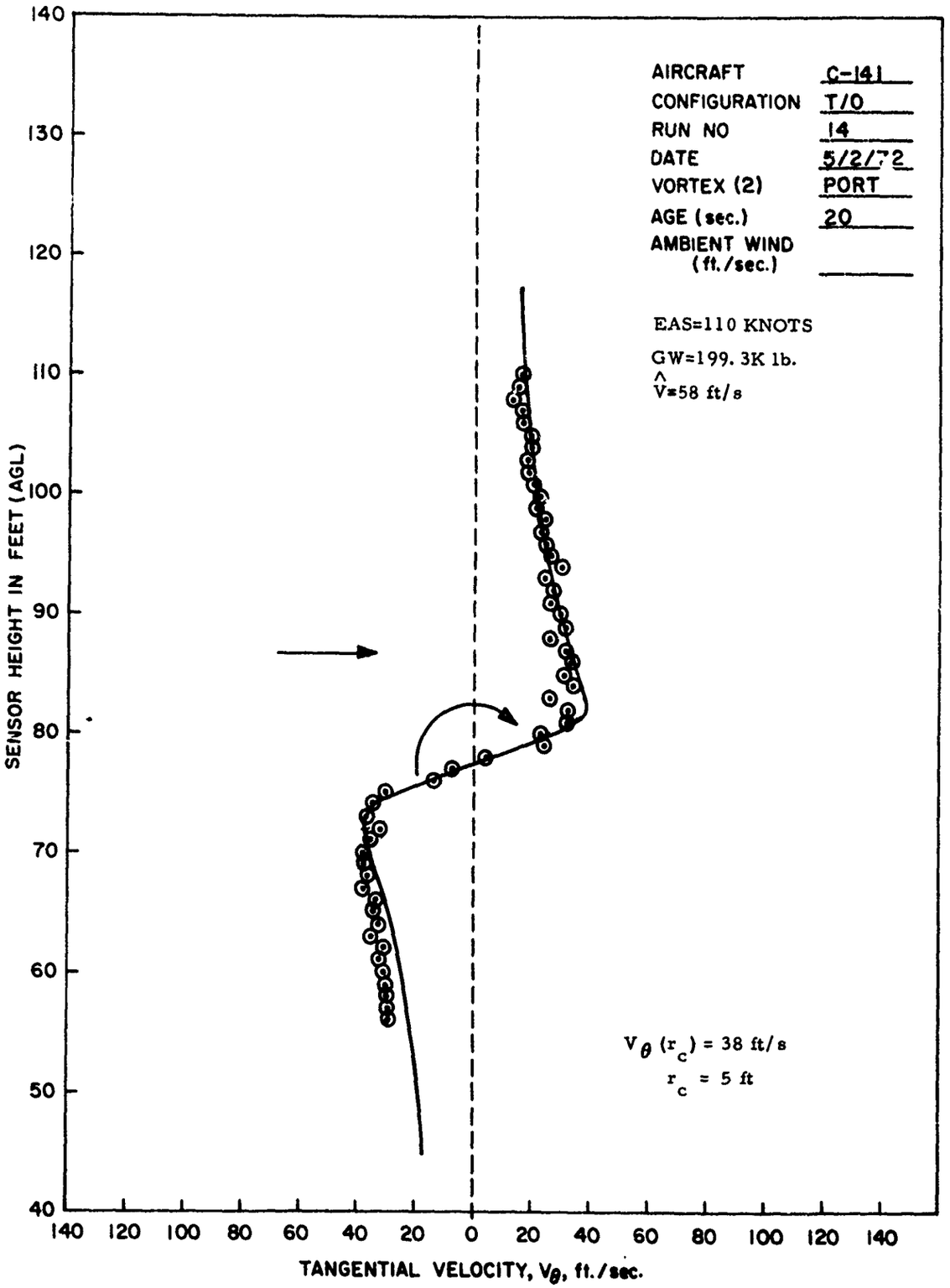
AIRCRAFT C-141
CONFIGURATION T/O
RUN NO 14
DATE 5/2/72
VORTEX (2) PORT
AGE (sec.) 20
AMBIENT WIND (ft./sec.)
EAS=110 KNOTS
GW=199.3K lb.
$\hat{V}$=58 ft/s
$V_\theta (r_c)$ = 38 ft/s
r_c = 5 ft
SENSOR HEIGHT IN FEET (AGL)
140
130
120
110
100
90
80
70
60
50
40
140 120 100 80 60 40 20 0 20 40 60 80 100 120 140
TANGENTIAL VELOCITY, V_θ, ft./sec.

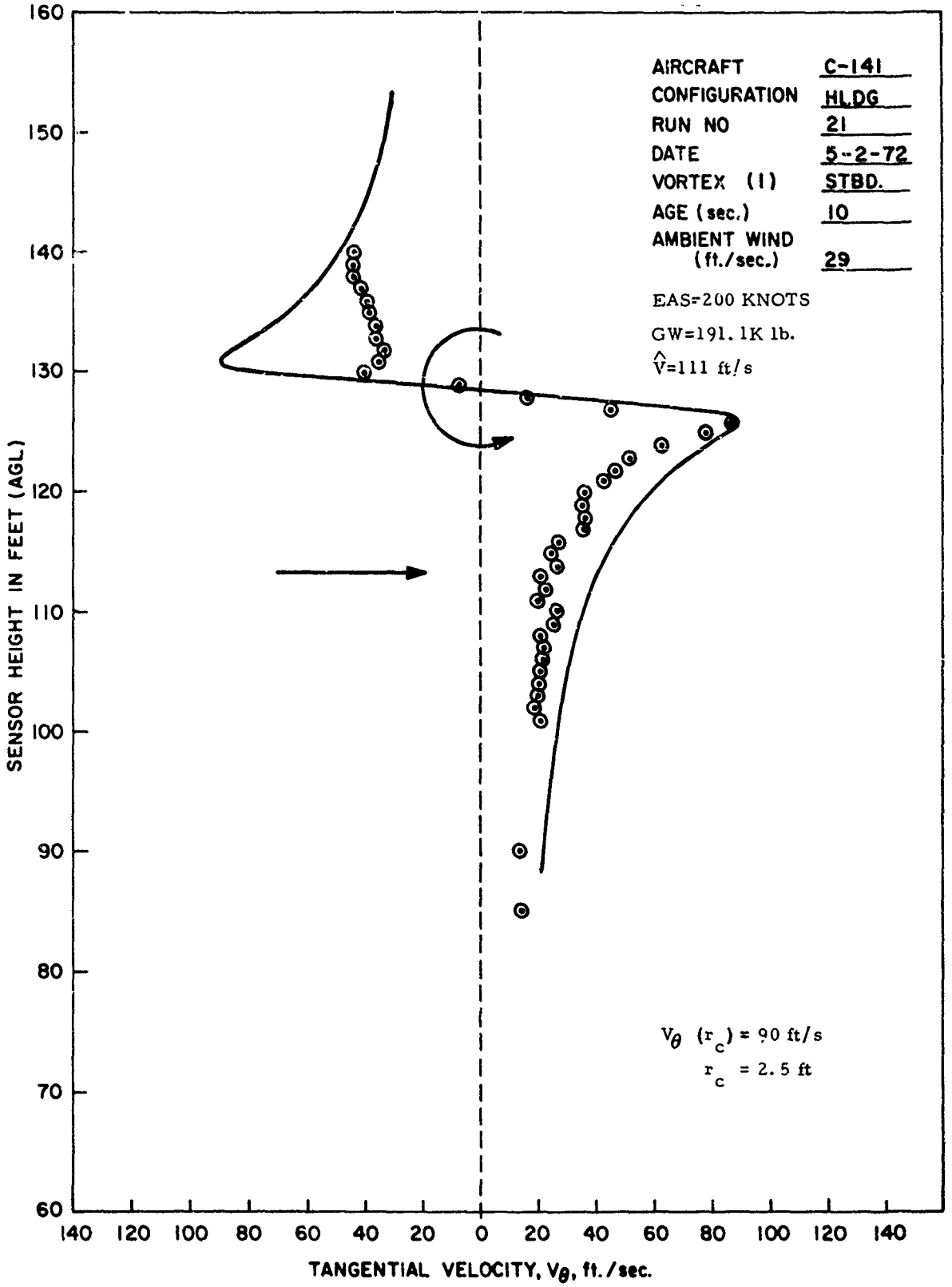
AIRCRAFT C-141
CONFIGURATION HLDG
RUN NO 21
DATE 5-2-72
VORTEX (1) STBD.
AGE (sec.) 10
AMBIENT WIND (ft./sec.) 29
EAS=200 KNOTS
GW=191.1K lb.
$\hat{V}$=111 ft/s
V_θ (r_c) = 90 ft/s
r_c = 2.5 ft
SENSOR HEIGHT IN FEET (AGL)
160
150
140
130
120
110
100
90
80
70
60
140 120 100 80 60 40 20 0 20 40 60 80 100 120 140
TANGENTIAL VELOCITY, V_θ, ft./sec.

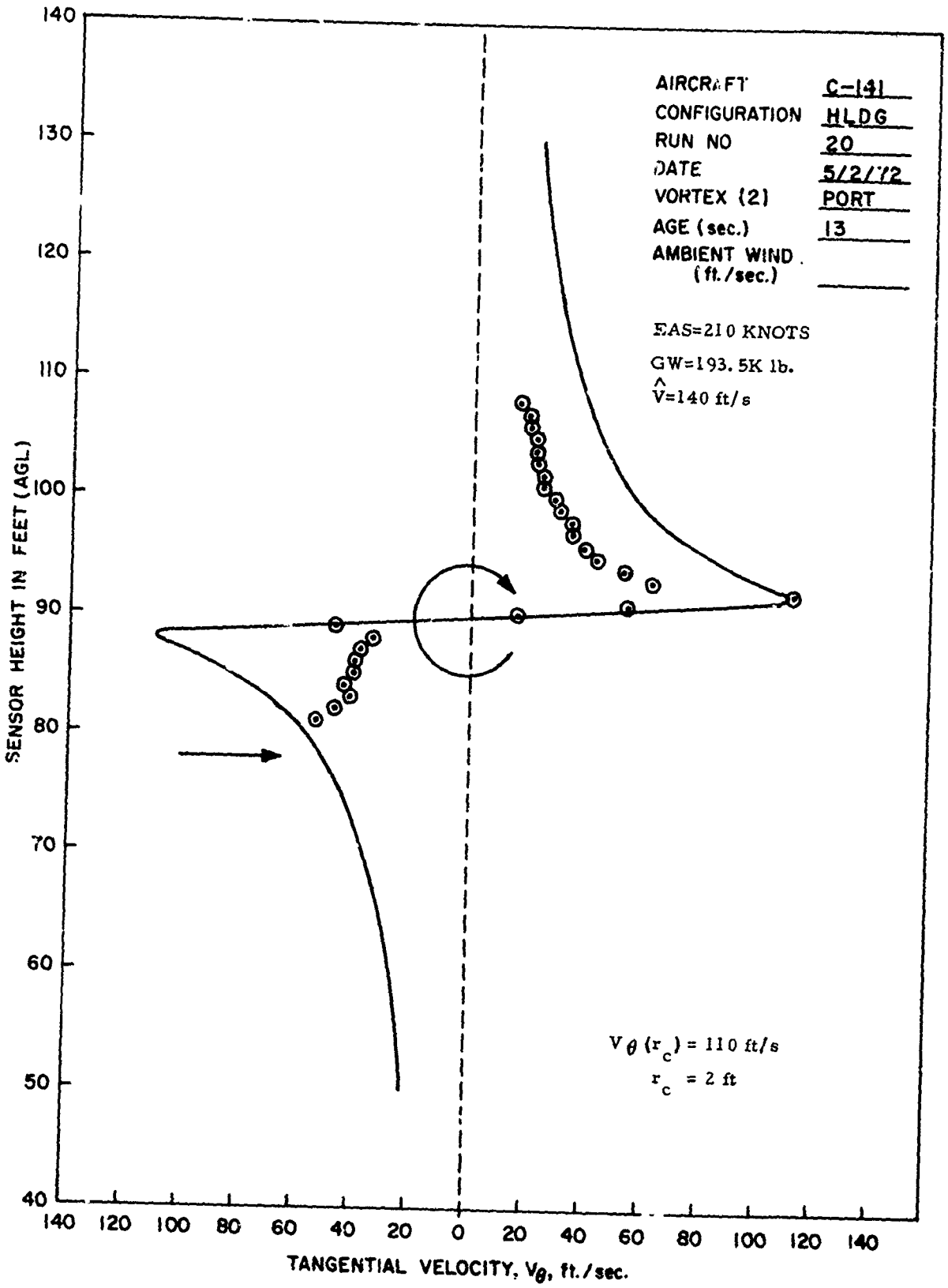
AIRCRAFT C-141
CONFIGURATION HLDG
RUN NO 20
DATE 5/2/72
VORTEX (2) PORT
AGE (sec.) 13
AMBIENT WIND (ft./sec.)
EAS=210 KNOTS
GW=193.5K lb.
V̂=140 ft/s
Vθ (rc) = 110 ft/s
rc = 2 ft
SENSOR HEIGHT IN FEET (AGL)
140
130
120
110
100
90
80
70
60
50
40
140 120 100 80 60 40 20 0 20 40 60 80 100 120 140
TANGENTIAL VELOCITY, Vθ, ft./sec.

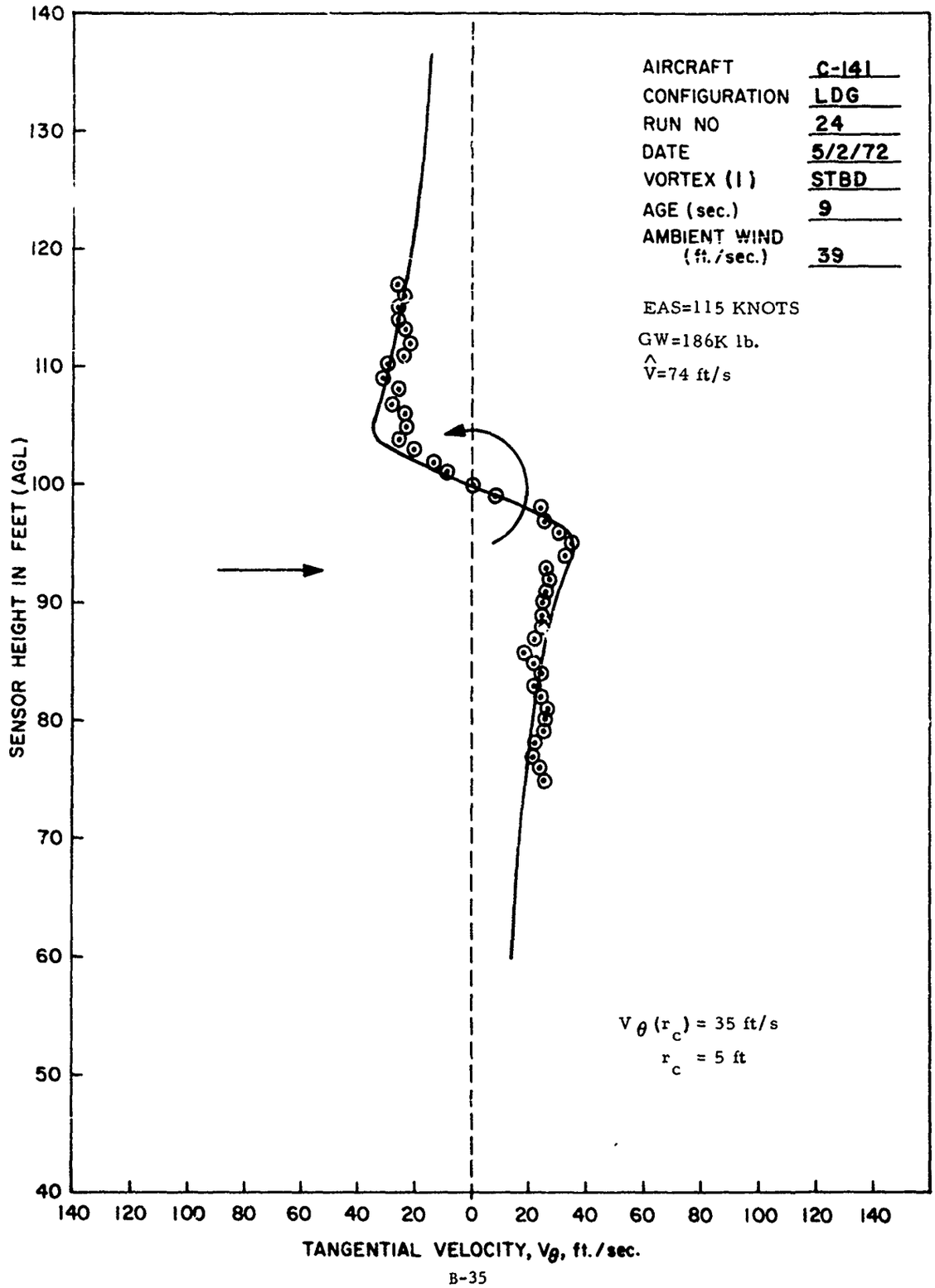
AIRCRAFT C-141
CONFIGURATION LDG
RUN NO 24
DATE 5/2/72
VORTEX (1) STBD
AGE (sec.) 9
AMBIENT WIND (ft./sec.) 39
EAS=115 KNOTS
GW=186K lb.
$\hat{V}$=74 ft/s
$V_\theta(r_c)$ = 35 ft/s
r_c = 5 ft
SENSOR HEIGHT IN FEET (AGL)
140
130
120
110
100
90
80
70
60
50
40
140 120 100 80 60 40 20 0 20 40 60 80 100 120 140
TANGENTIAL VELOCITY, V_θ, ft./sec.

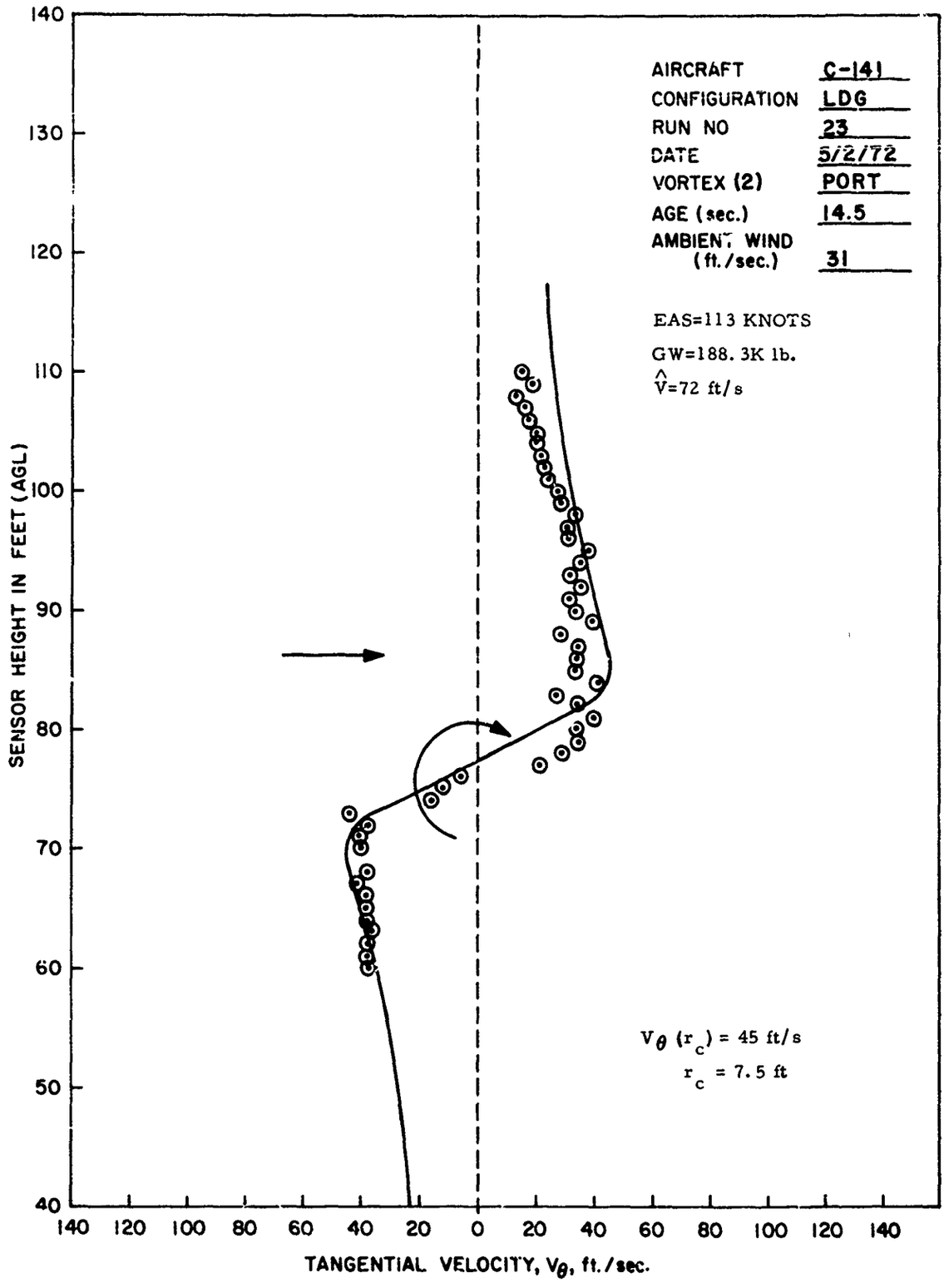
AIRCRAFT C-141
CONFIGURATION LDG
RUN NO 23
DATE 5/2/72
VORTEX (2) PORT
AGE (sec.) 14.5
AMBIENT WIND (ft./sec.) 31
EAS=113 KNOTS
GW=188.3K lb.
$\hat{V}$=72 ft/s
V_θ (r_c) = 45 ft/s
r_c = 7.5 ft
SENSOR HEIGHT IN FEET (AGL)
140
130
120
110
100
90
80
70
60
50
40
140 120 100 80 60 40 20 0 20 40 60 80 100 120 140
TANGENTIAL VELOCITY, V_θ, ft./sec.

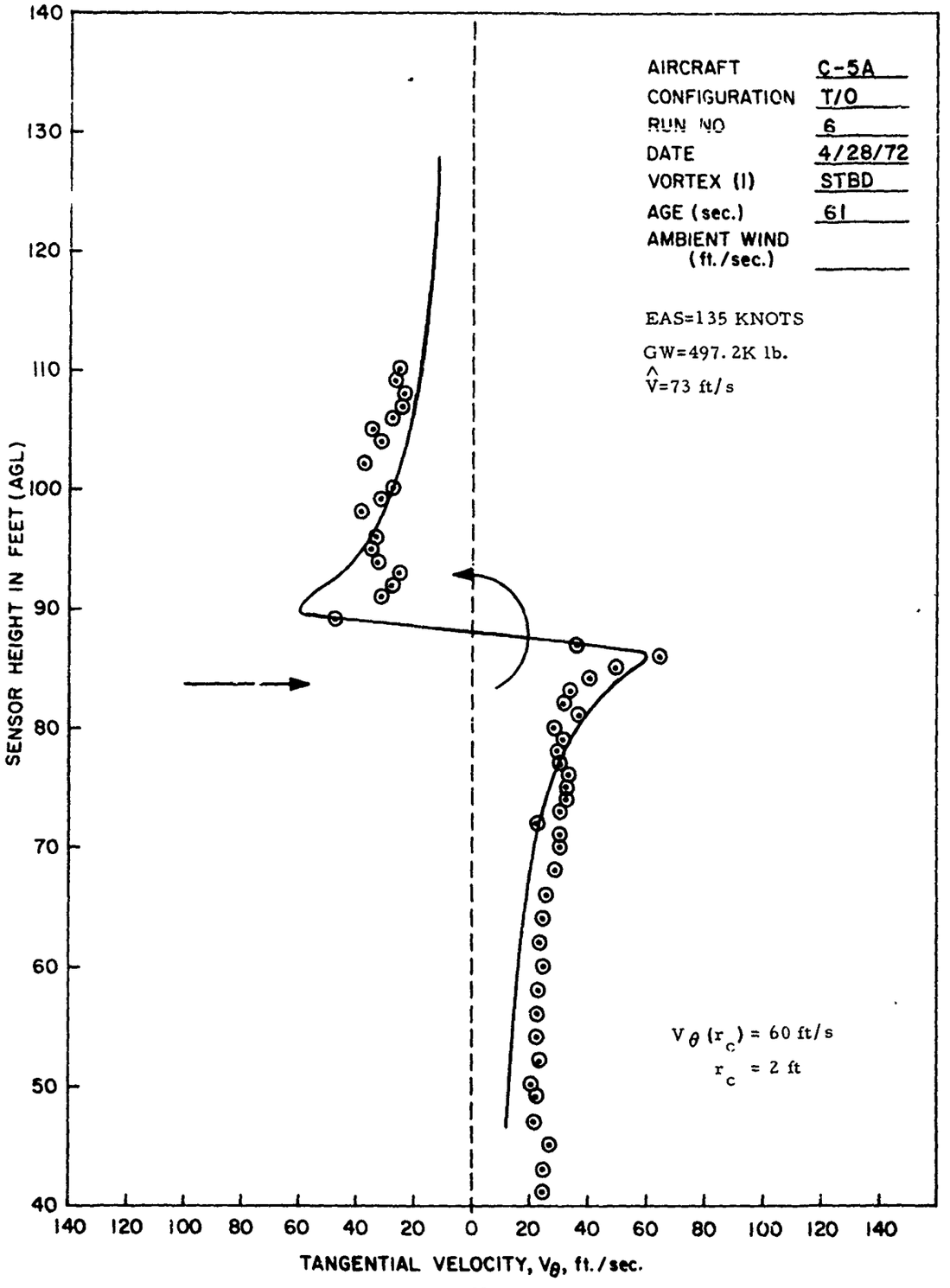
AIRCRAFT C-5A
CONFIGURATION T/O
RUN NO 6
DATE 4/28/72
VORTEX (I) STBD
AGE (sec.) 61
AMBIENT WIND (ft./sec.)
EAS=135 KNOTS
GW=497.2K lb.
V̂=73 ft/s
$V_\theta (r_c)$ = 60 ft/s
r_c = 2 ft
SENSOR HEIGHT IN FEET (AGL)
140
130
120
110
100
90
80
70
60
50
40
140 120 100 80 60 40 20 0 20 40 60 80 100 120 140
TANGENTIAL VELOCITY, V_θ, ft./sec.

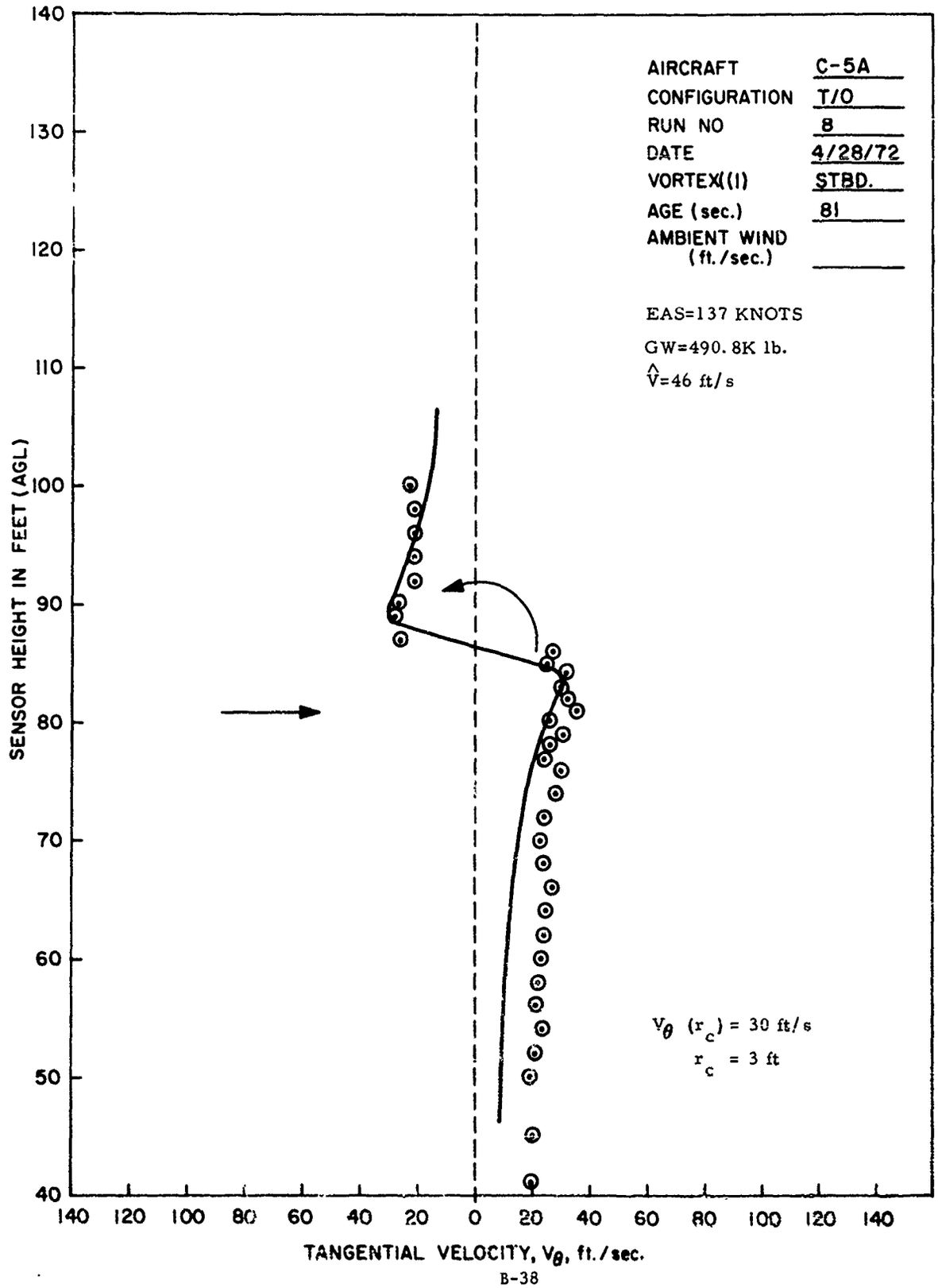
AIRCRAFT C-5A
CONFIGURATION T/O
RUN NO 8
DATE 4/28/72
VORTEX(1) STBD.
AGE (sec.) 81
AMBIENT WIND (ft./sec.)
EAS=137 KNOTS
GW=490.8K lb.
V̂=46 ft/s
V_θ (r_c) = 30 ft/s
r_c = 3 ft
SENSOR HEIGHT IN FEET (AGL)
140
130
120
110
100
90
80
70
60
50
40
140 120 100 80 60 40 20 0 20 40 60 80 100 120 140
TANGENTIAL VELOCITY, V_θ, ft./sec.

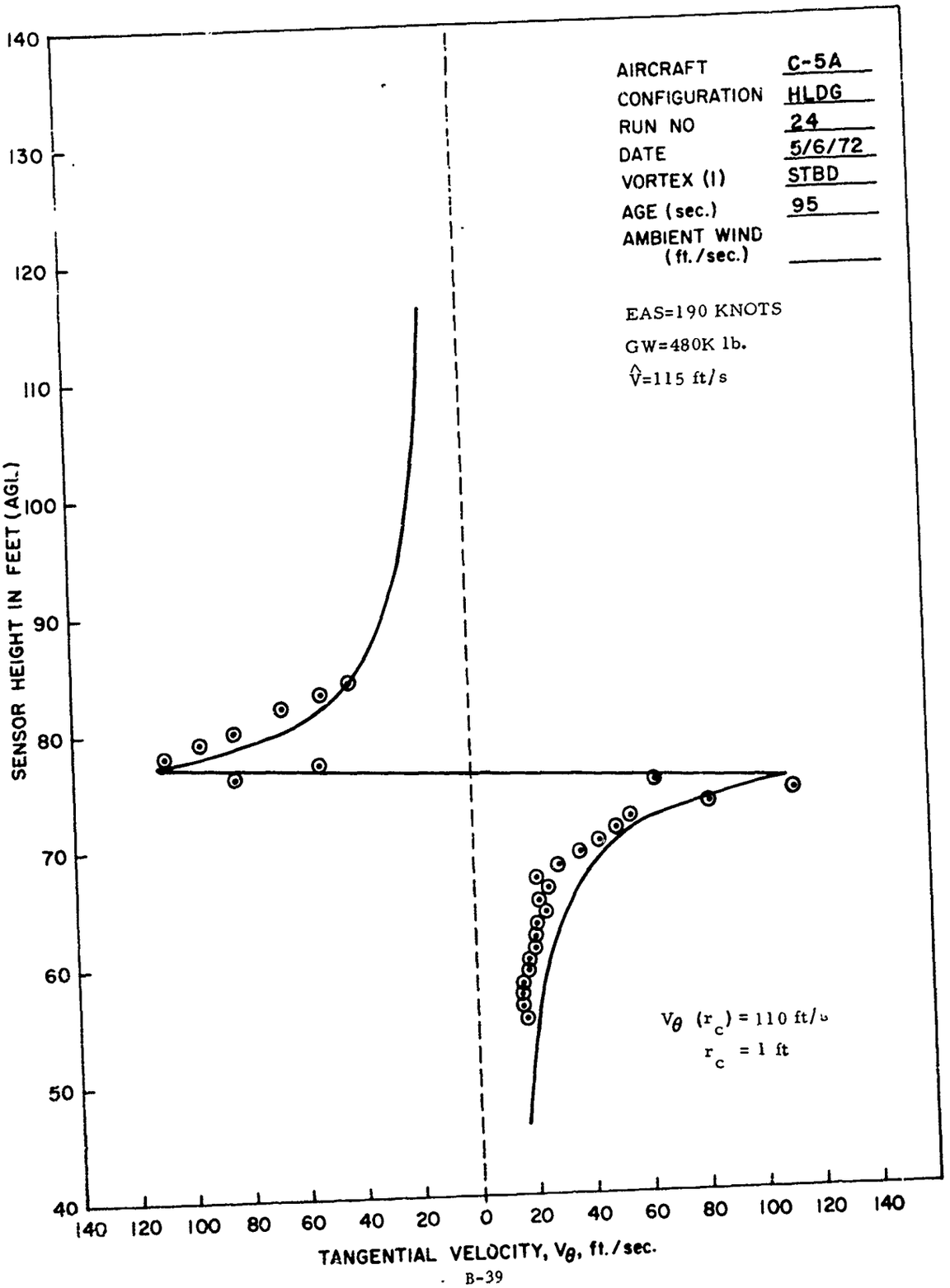
AIRCRAFT C-5A
CONFIGURATION HLDG
RUN NO 24
DATE 5/6/72
VORTEX (1) STBD
AGE (sec.) 95
AMBIENT WIND (ft./sec.)
EAS=190 KNOTS
GW=480K lb.
$\hat{V}$=115 ft/s
V_θ (r_c) = 110 ft/s
r_c = 1 ft
SENSOR HEIGHT IN FEET (AGL.)
TANGENTIAL VELOCITY, V_θ, ft./sec.
140
130
120
110
100
90
80
70
60
50
40
140 120 100 80 60 40 20 0 20 40 60 80 100 120 140

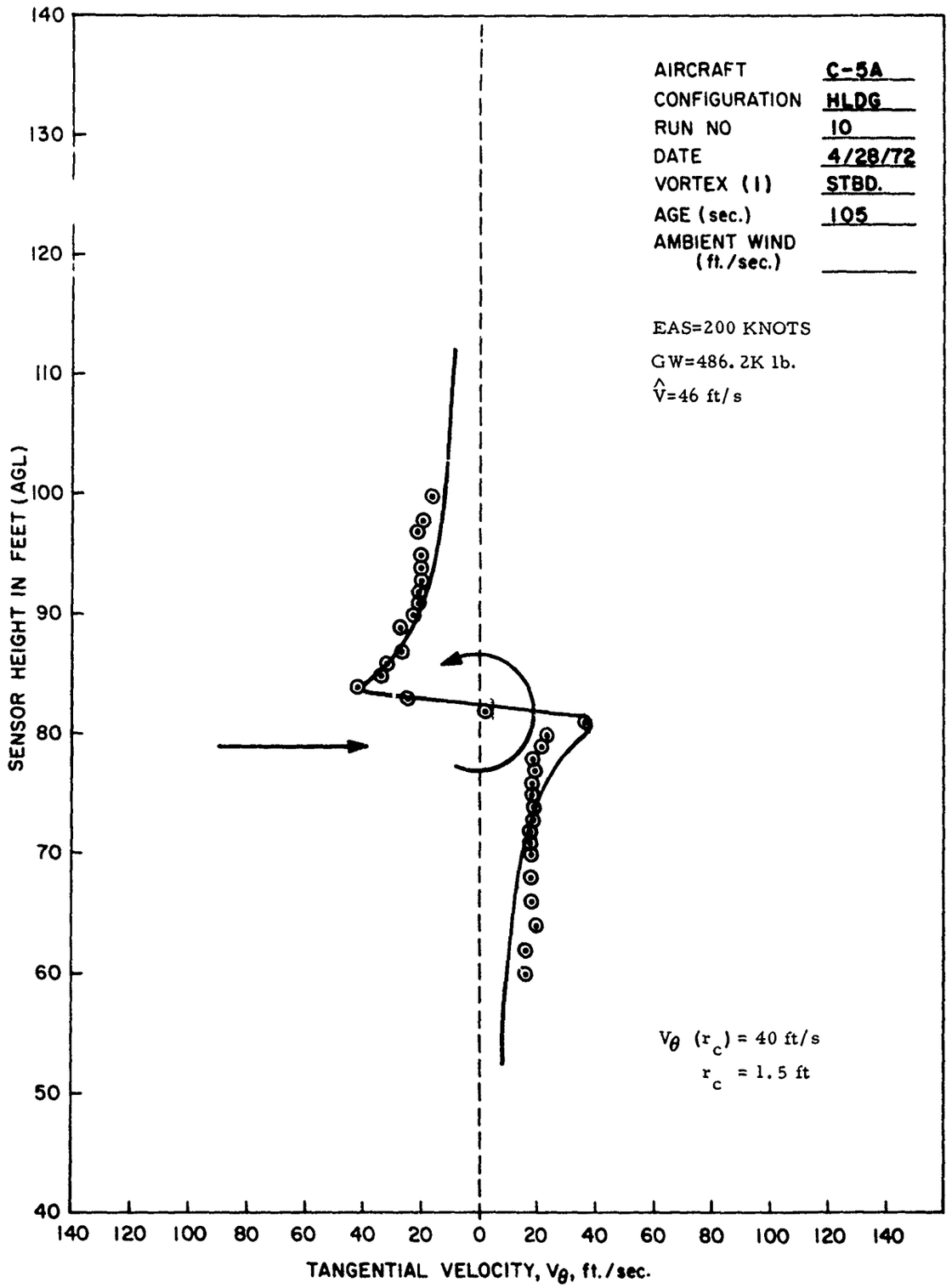
AIRCRAFT C-5A
CONFIGURATION HLDG
RUN NO 10
DATE 4/28/72
VORTEX (1) STBD.
AGE (sec.) 105
AMBIENT WIND (ft./sec.)
EAS=200 KNOTS
GW=486.2K lb.
$\hat{V}$=46 ft/s
V_θ (r_c) = 40 ft/s
r_c = 1.5 ft
SENSOR HEIGHT IN FEET (AGL)
140
130
120
110
100
90
80
70
60
50
40
140 120 100 80 60 40 20 0 20 40 60 80 100 120 140
TANGENTIAL VELOCITY, V_θ, ft./sec.

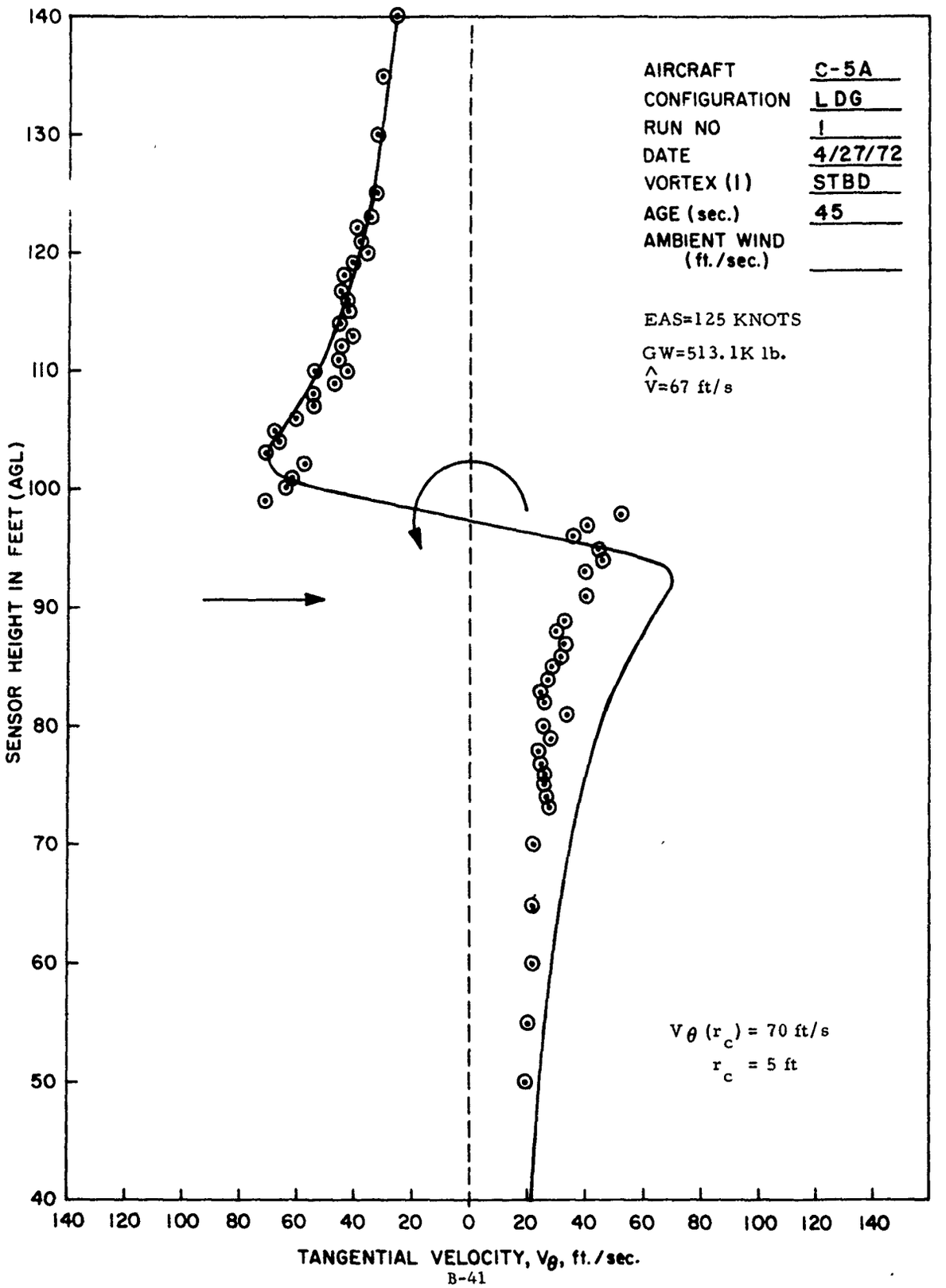
AIRCRAFT C-5A
CONFIGURATION LDG
RUN NO 1
DATE 4/27/72
VORTEX (1) STBD
AGE (sec.) 45
AMBIENT WIND (ft./sec.)
EAS=125 KNOTS
GW=513.1K lb.
V=67 ft/s
Vθ (rc) = 70 ft/s
rc = 5 ft
SENSOR HEIGHT IN FEET (AGL)
140
130
120
110
100
90
80
70
60
50
40
140 120 100 80 60 40 20 0 20 40 60 80 100 120 140
TANGENTIAL VELOCITY, Vθ, ft./sec.

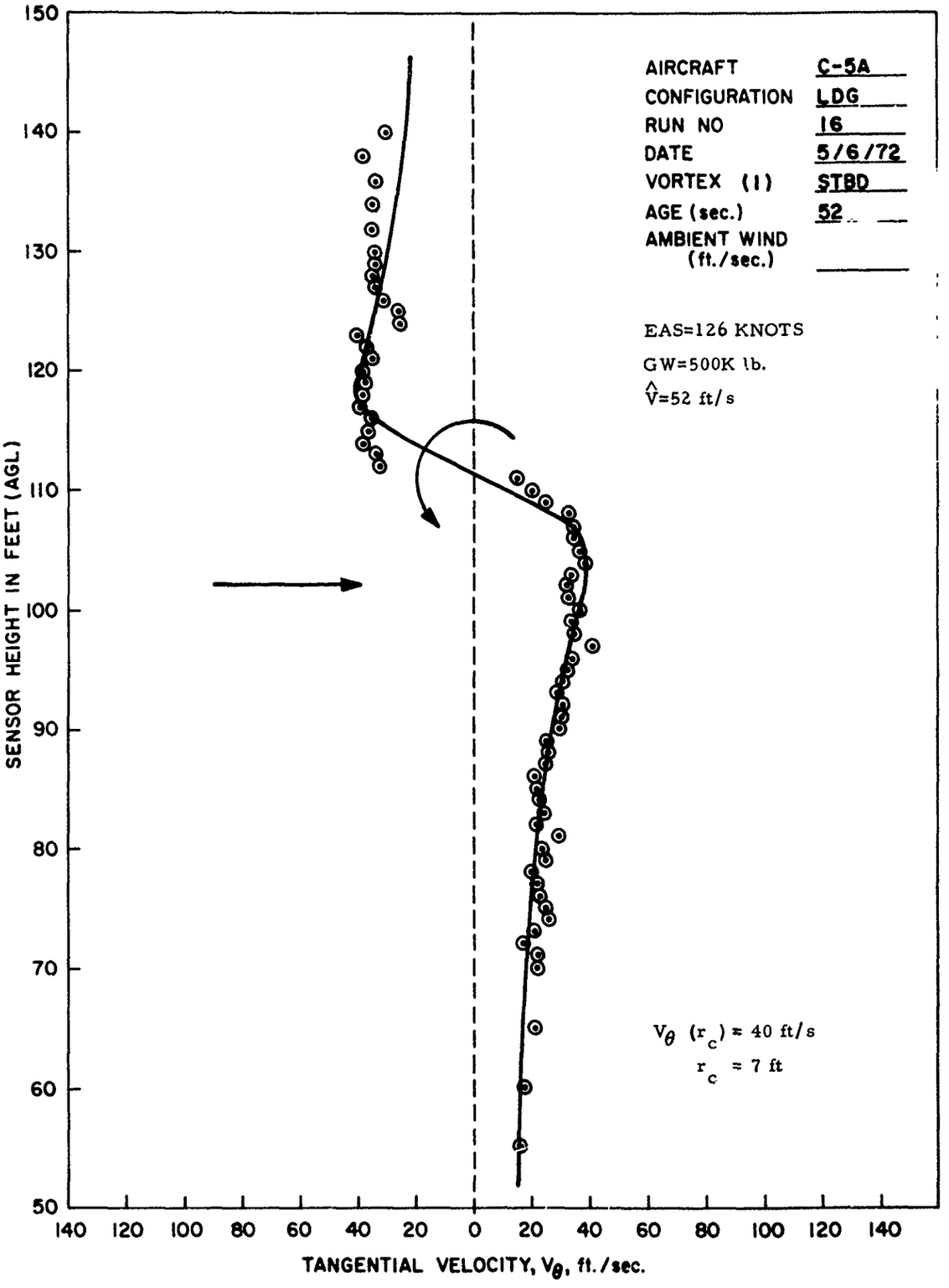
AIRCRAFT C-5A
CONFIGURATION LDG
RUN NO 16
DATE 5/6/72
VORTEX (1) STBD
AGE (sec.) 52
AMBIENT WIND (ft./sec.)
EAS=126 KNOTS
GW=500K lb.
$\hat{V}$=52 ft/s
V_θ (r_c) = 40 ft/s
r_c = 7 ft
SENSOR HEIGHT IN FEET (AGL)
150
140
130
120
110
100
90
80
70
60
50
140 120 100 80 60 40 20 0 20 40 60 80 100 120 140
TANGENTIAL VELOCITY, V_θ, ft./sec.

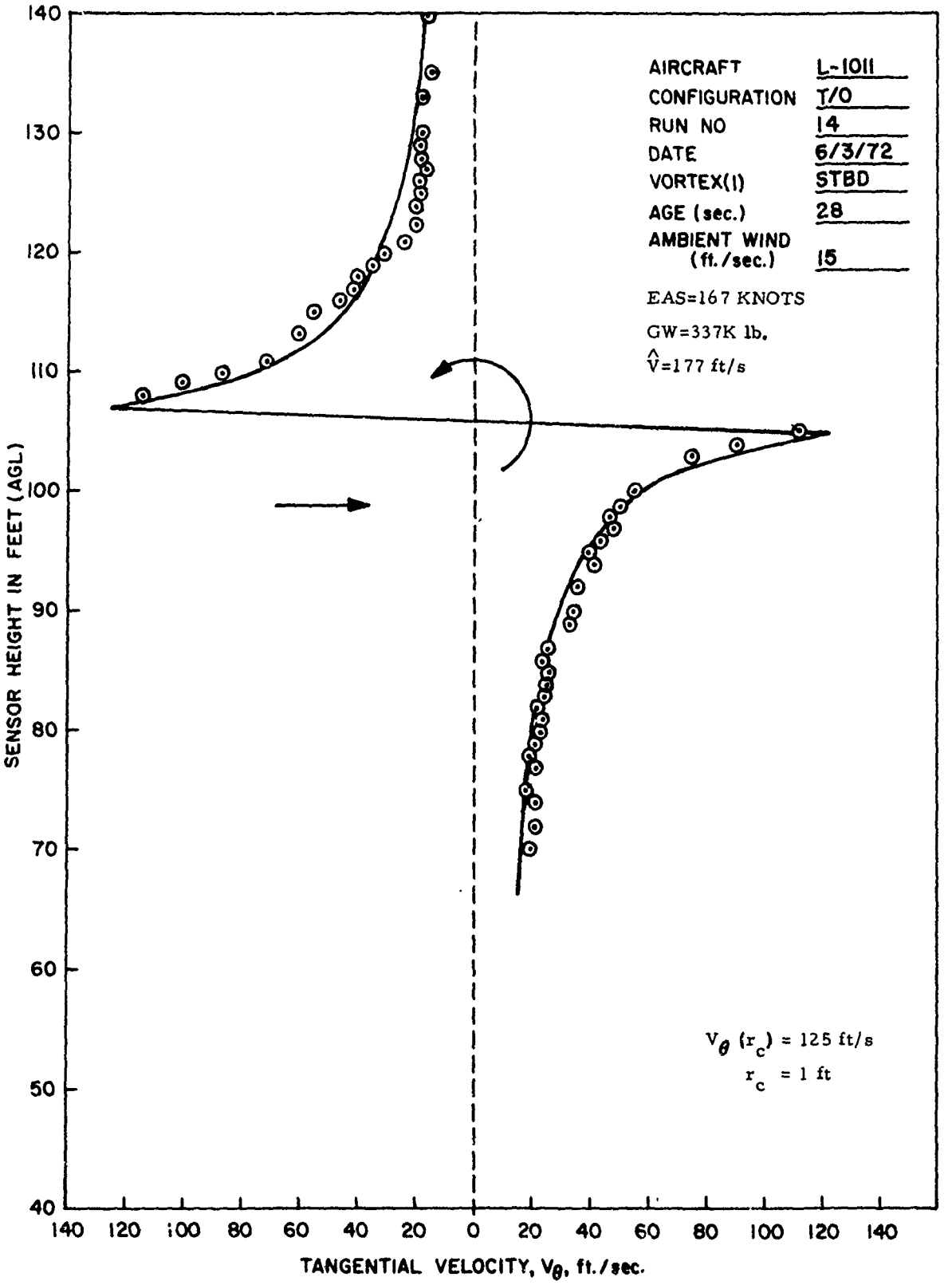
AIRCRAFT L-1011
CONFIGURATION T/O
RUN NO 14
DATE 6/3/72
VORTEX(I) STBD
AGE (sec.) 28
AMBIENT WIND (ft./sec.) 15
EAS=167 KNOTS
GW=337K lb.
$\hat{V}$=177 ft/s
V_θ (r_c) = 125 ft/s
r_c = 1 ft
SENSOR HEIGHT IN FEET (AGL.)
140
130
120
110
100
90
80
70
60
50
40
140 120 100 80 60 40 20 0 20 40 60 80 100 120 140
TANGENTIAL VELOCITY, V_θ, ft./sec.

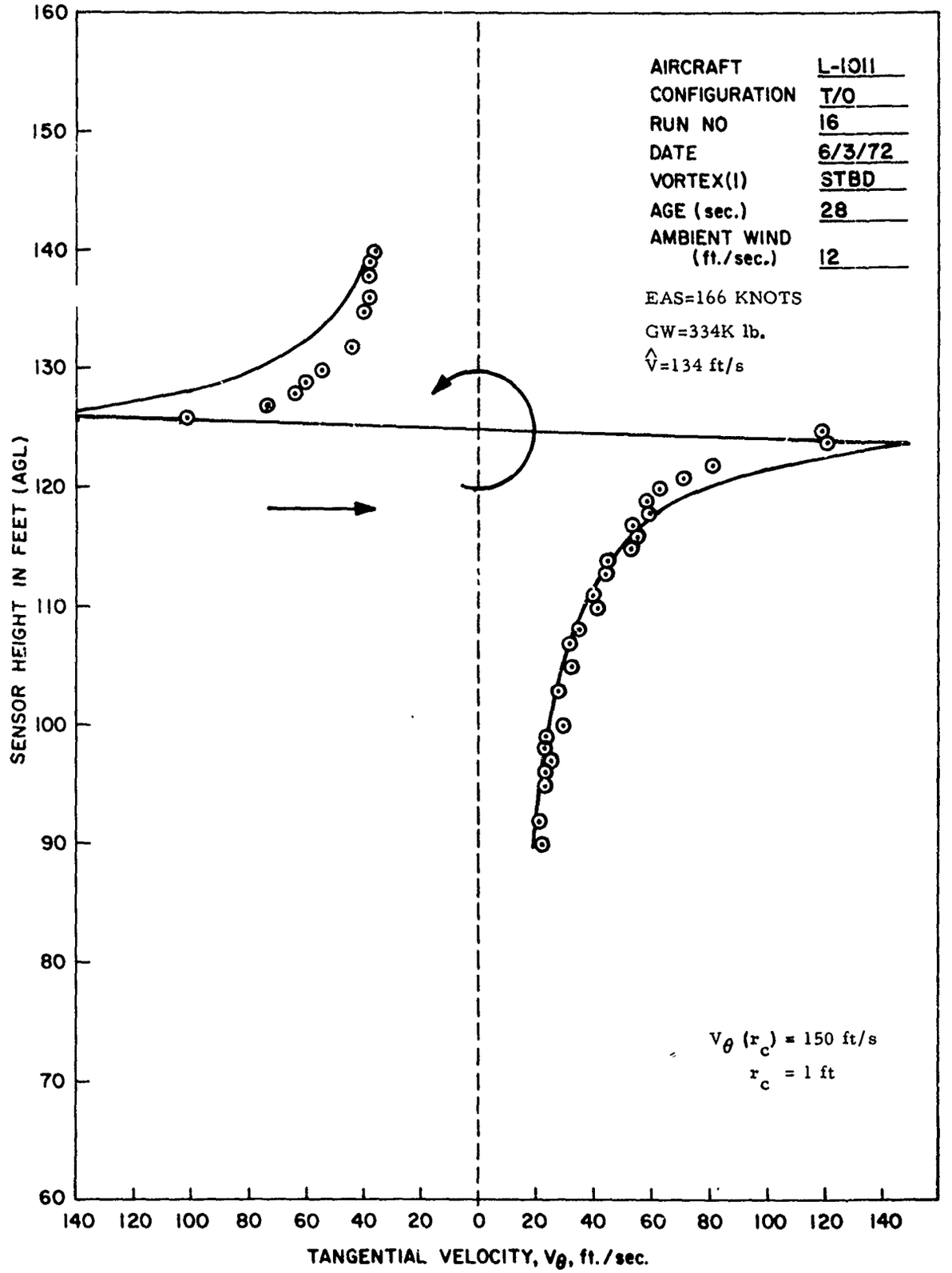
AIRCRAFT L-1011
CONFIGURATION T/O
RUN NO 16
DATE 6/3/72
VORTEX(I) STBD
AGE (sec.) 28
AMBIENT WIND (ft./sec.) 12
EAS=166 KNOTS
GW=334K lb.
$\hat{V}$=134 ft/s
$V_\theta (r_c)$ = 150 ft/s
r_c = 1 ft
SENSOR HEIGHT IN FEET (AGL)
160
150
140
130
120
110
100
90
80
70
60
140 120 100 80 60 40 20 0 20 40 60 80 100 120 140
TANGENTIAL VELOCITY, V_θ, ft./sec.

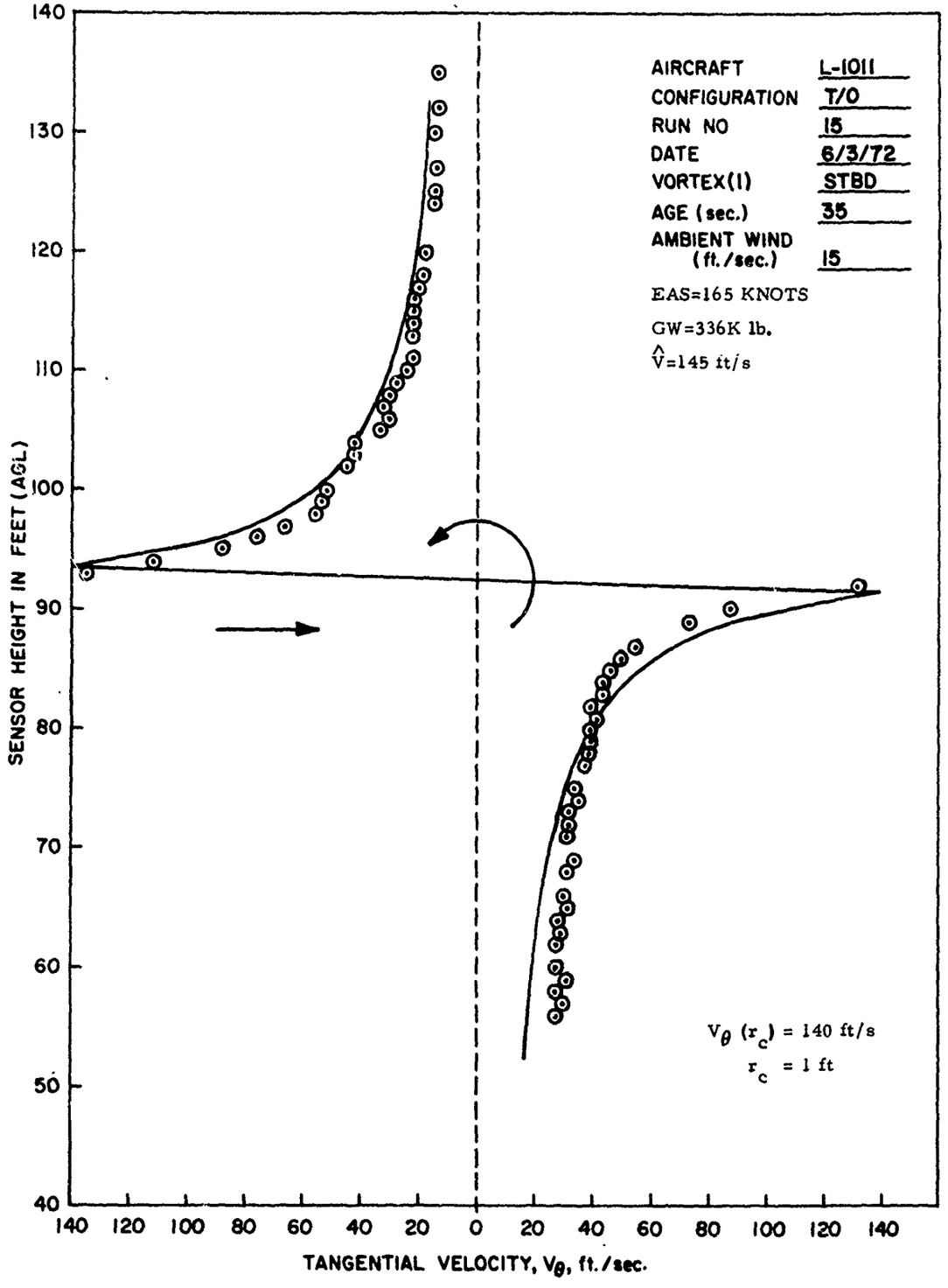
AIRCRAFT L-1011
CONFIGURATION T/O
RUN NO 15
DATE 6/3/72
VORTEX(1) STBD
AGE (sec.) 35
AMBIENT WIND (ft./sec.) 15
EAS=165 KNOTS
GW=336K lb.
$\hat{V}$=145 ft/s
V_θ (r_c) = 140 ft/s
r_c = 1 ft
SENSOR HEIGHT IN FEET (AGL)
TANGENTIAL VELOCITY, V_θ, ft./sec.
140
130
120
110
100
90
80
70
60
50
40
140 120 100 80 60 40 20 0 20 40 60 80 100 120 140

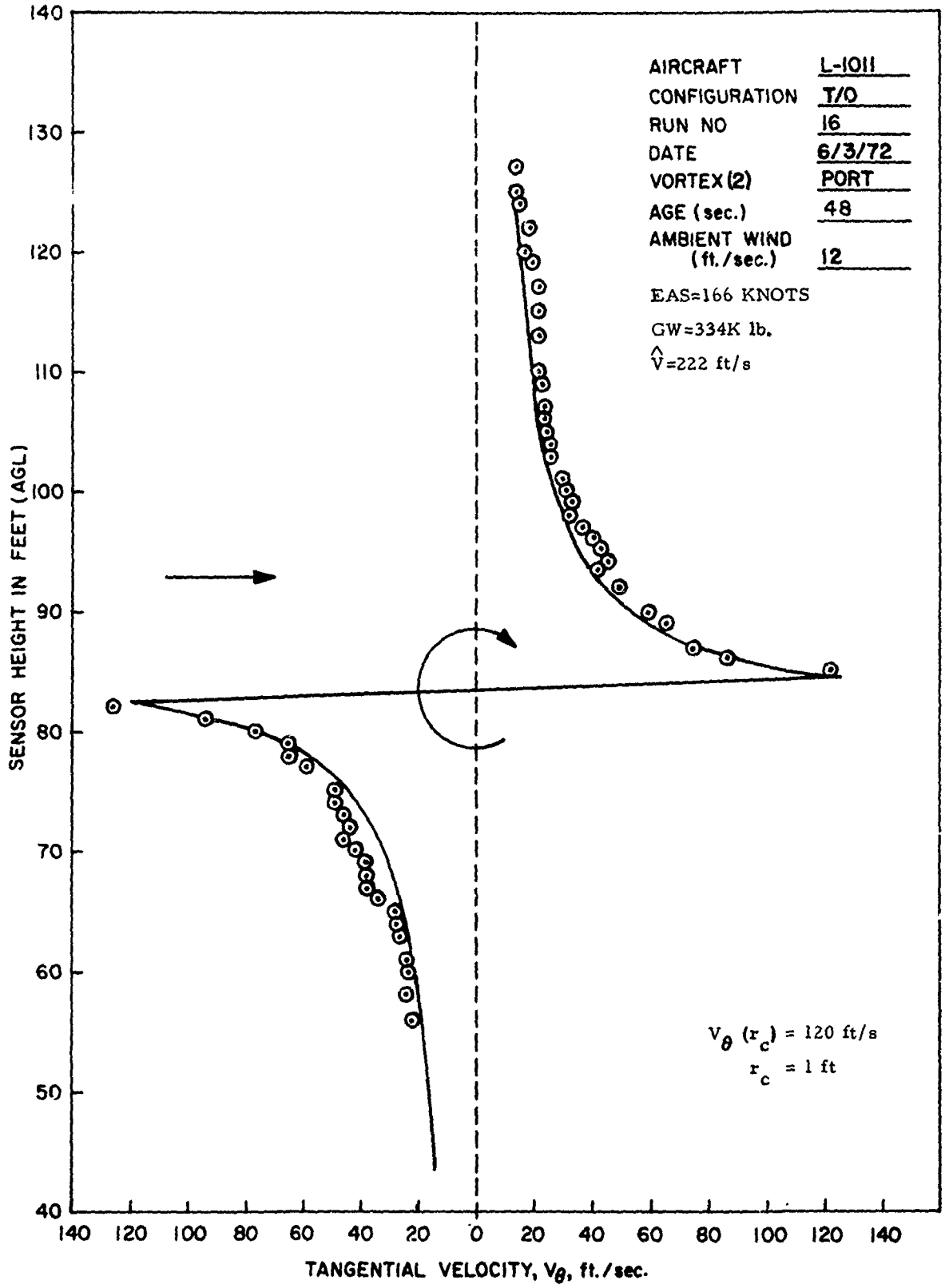
AIRCRAFT L-1011
CONFIGURATION T/O
RUN NO 16
DATE 6/3/72
VORTEX (2) PORT
AGE (sec.) 48
AMBIENT WIND (ft./sec.) 12
EAS=166 KNOTS
GW=334K lb.
$\hat{V}$=222 ft/s
V_θ (r_c) = 120 ft/s
r_c = 1 ft
SENSOR HEIGHT IN FEET (AGL)
140
130
120
110
100
90
80
70
60
50
40
140 120 100 80 60 40 20 0 20 40 60 80 100 120 140
TANGENTIAL VELOCITY, V_θ, ft./sec.

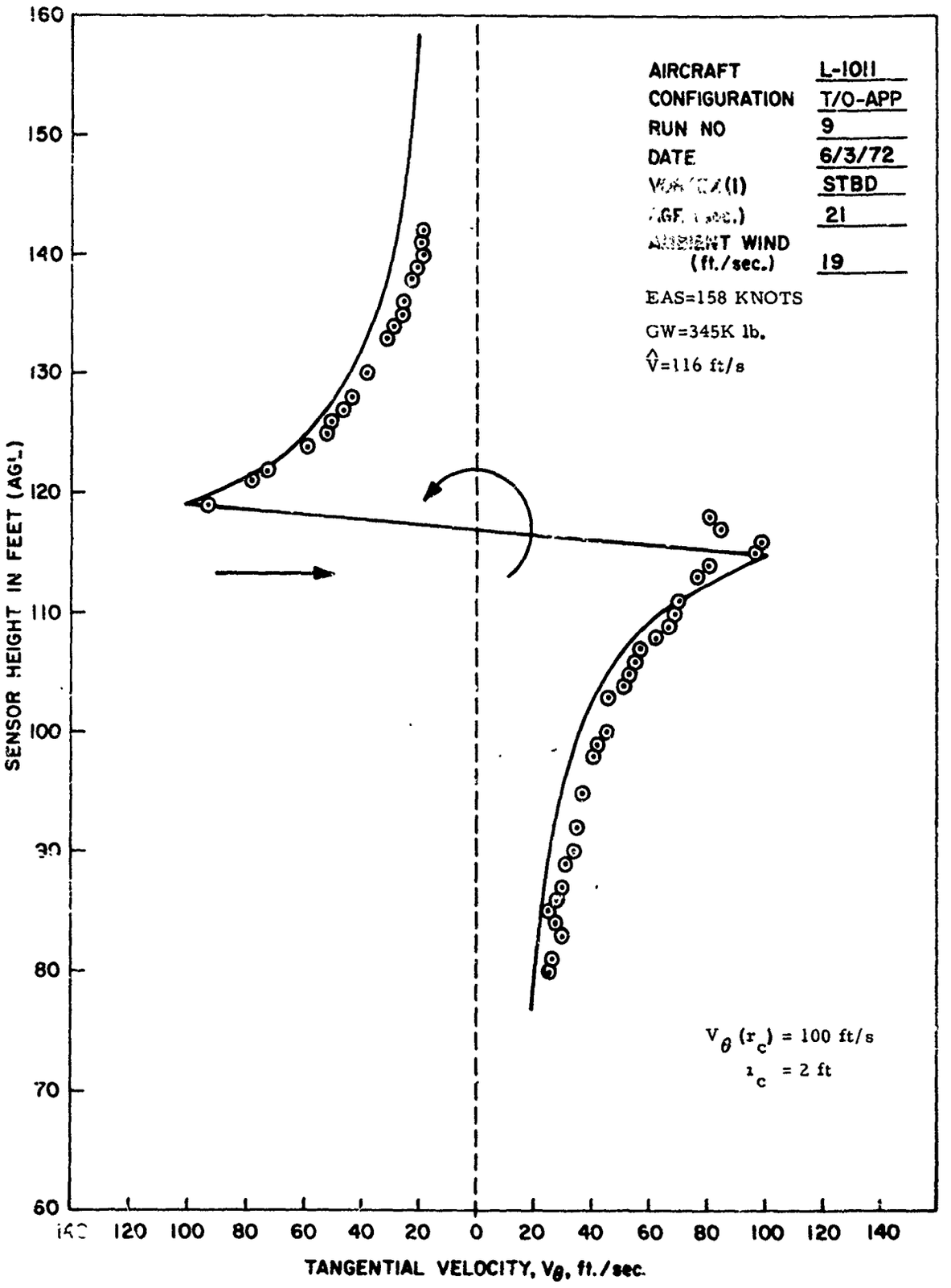
AIRCRAFT L-1011
CONFIGURATION T/O-APP
RUN NO 9
DATE 6/3/72
VORTEX(1) STBD
AGE (sec.) 21
AMBIENT WIND (ft./sec.) 19
EAS=158 KNOTS
GW=345K lb.
$\hat{V}$=116 ft/s
$V_\theta (r_c)$ = 100 ft/s
r_c = 2 ft
SENSOR HEIGHT IN FEET (AGL)
160
150
140
130
120
110
100
90
80
70
60
140 120 100 80 60 40 20 0 20 40 60 80 100 120 140
TANGENTIAL VELOCITY, V_θ, ft./sec.

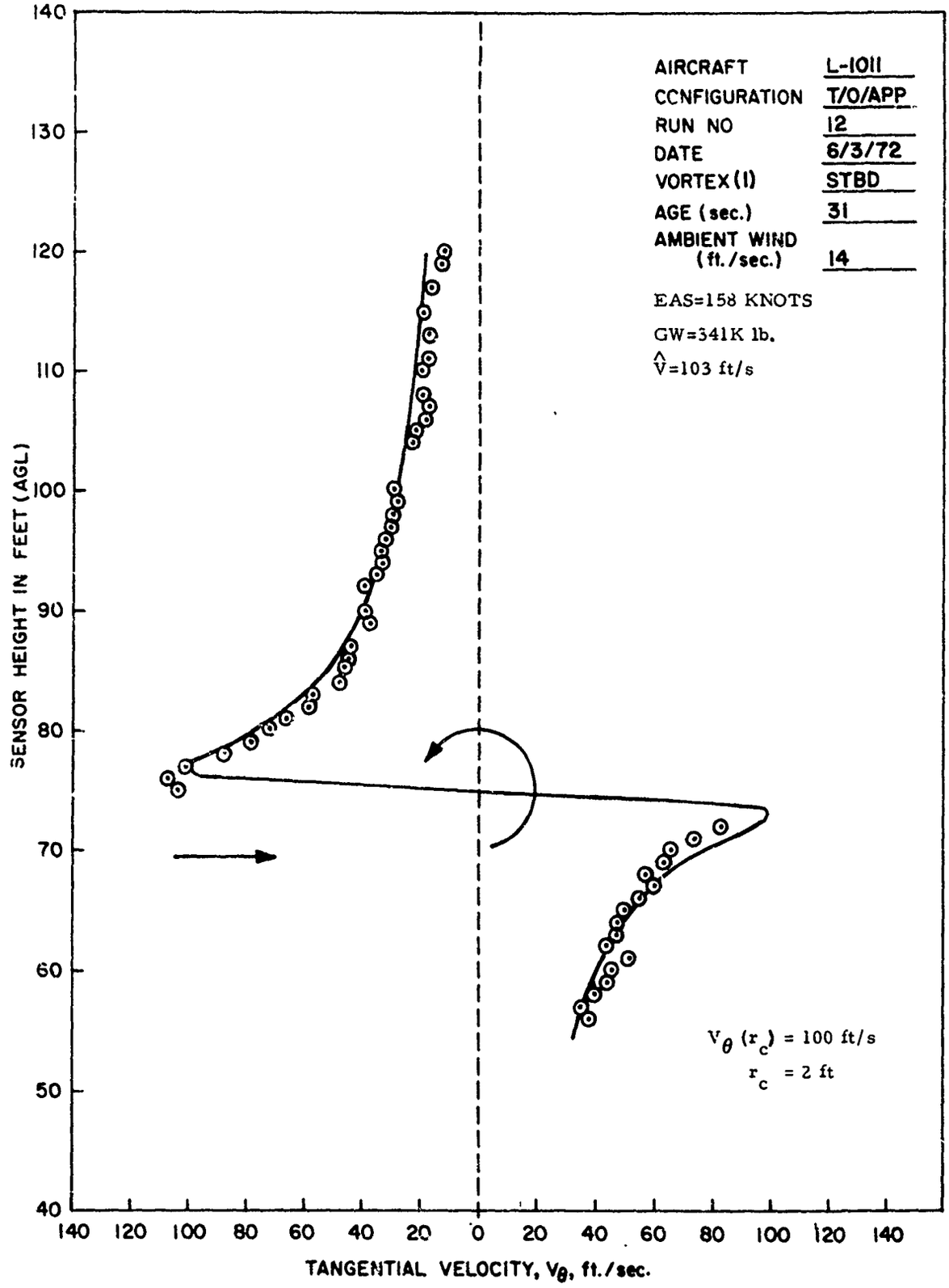
AIRCRAFT L-1011
CONFIGURATION T/O/APP
RUN NO 12
DATE 6/3/72
VORTEX (1) STBD
AGE (sec.) 31
AMBIENT WIND (ft./sec.) 14
EAS=158 KNOTS
GW=341K lb.
$\hat{V}$=103 ft/s
$V_\theta (r_c)$ = 100 ft/s
r_c = 2 ft
SENSOR HEIGHT IN FEET (AGL)
140
130
120
110
100
90
80
70
60
50
40
140 120 100 80 60 40 20 0 20 40 60 80 100 120 140
TANGENTIAL VELOCITY, V_θ, ft./sec.

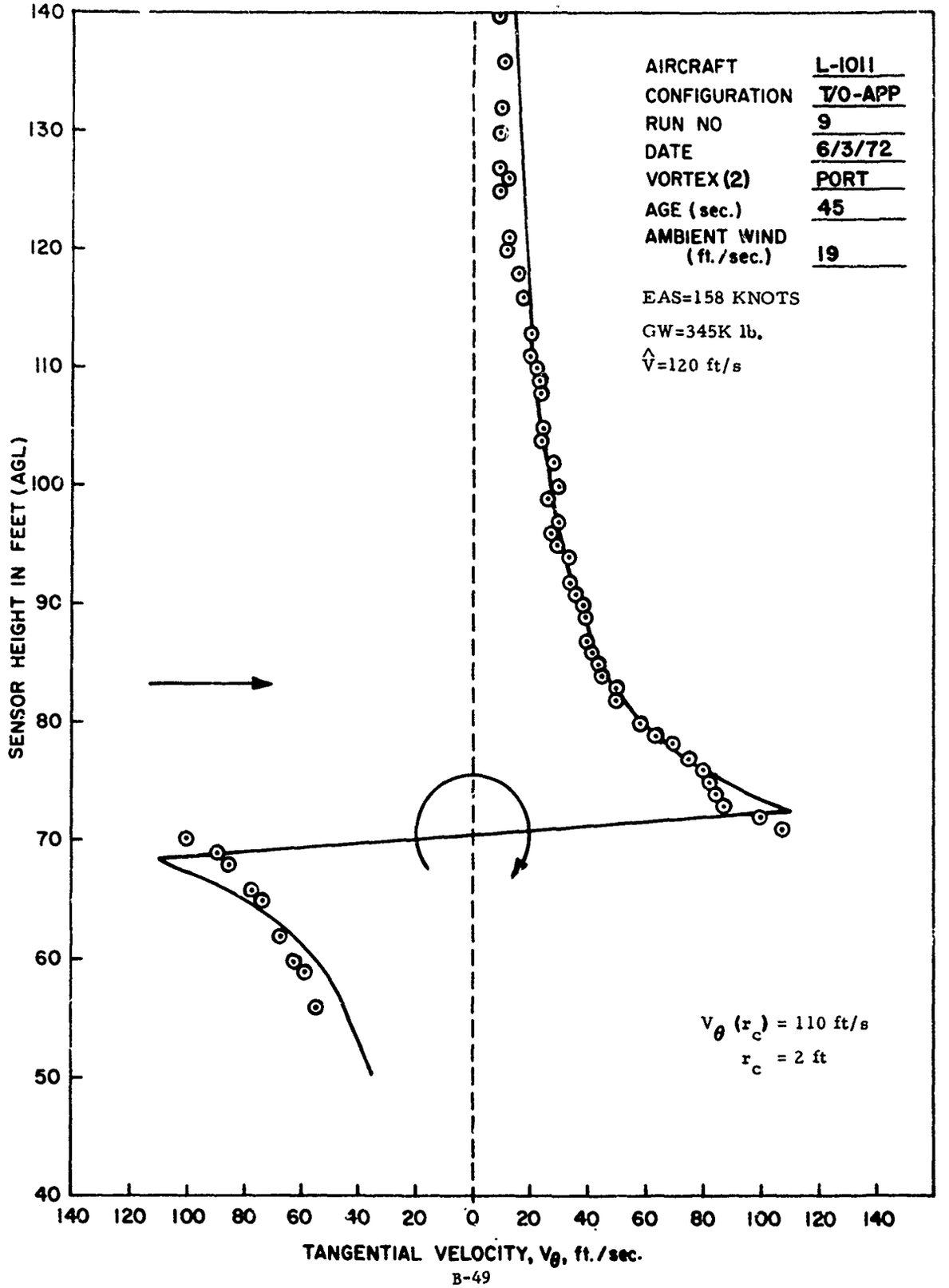
AIRCRAFT L-1011
CONFIGURATION T/O-APP
RUN NO 9
DATE 6/3/72
VORTEX (2) PORT
AGE (sec.) 45
AMBIENT WIND (ft./sec.) 19
EAS=158 KNOTS
GW=345K lb.
$\hat{V}$=120 ft/s
$V_\theta (r_c)$ = 110 ft/s
r_c = 2 ft
SENSOR HEIGHT IN FEET (AGL)
140
130
120
110
100
90
80
70
60
50
40
140 120 100 80 60 40 20 0 20 40 60 80 100 120 140
TANGENTIAL VELOCITY, V_θ, ft./sec.

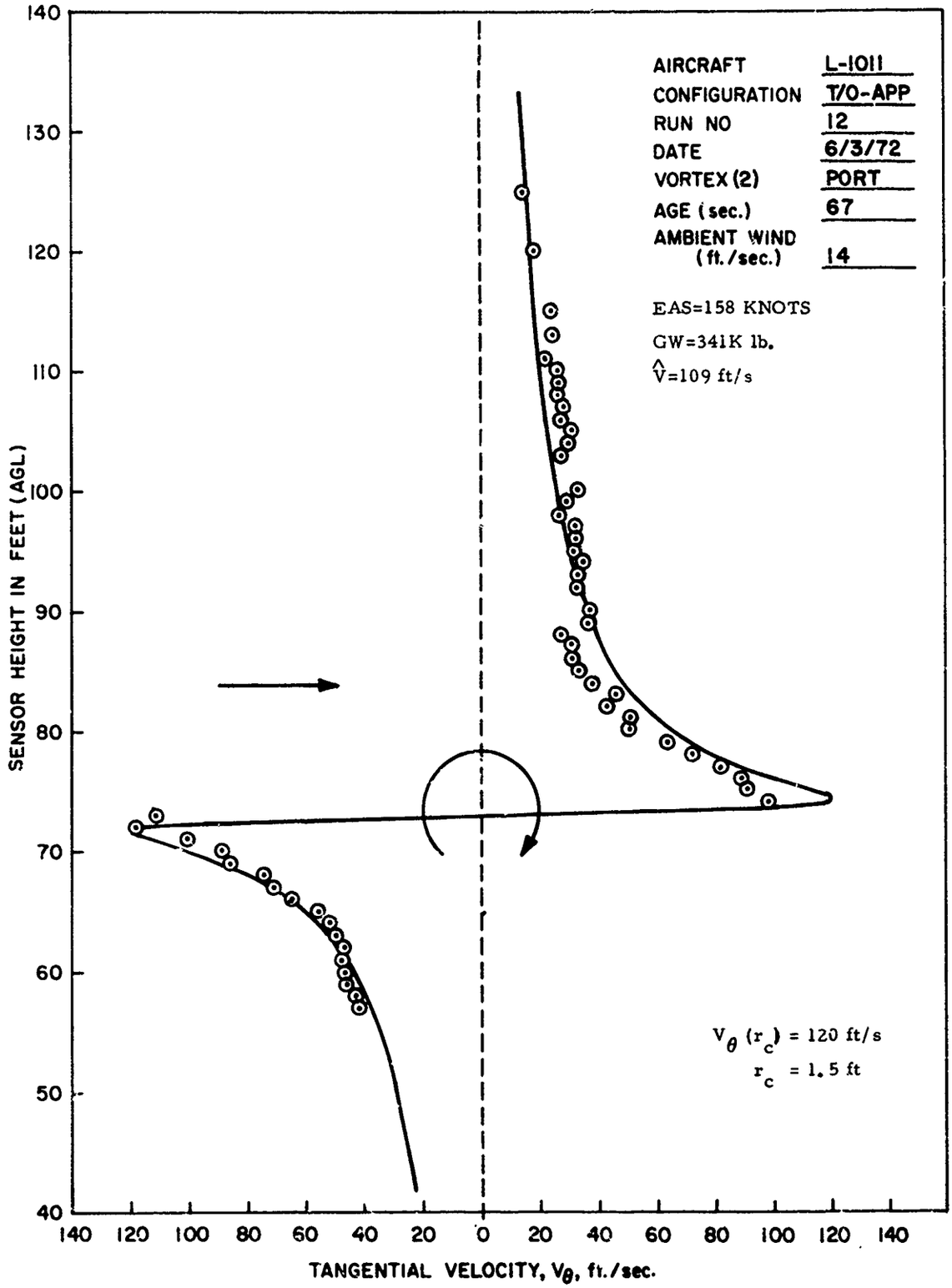
AIRCRAFT L-1011
CONFIGURATION T/O-APP
RUN NO 12
DATE 6/3/72
VORTEX (2) PORT
AGE (sec.) 67
AMBIENT WIND (ft./sec.) 14
EAS=158 KNOTS
GW=341K lb.
$\hat{V}$=109 ft/s
$V_\theta (r_c)$ = 120 ft/s
r_c = 1.5 ft
SENSOR HEIGHT IN FEET (AGL)
140
130
120
110
100
90
80
70
60
50
40
140 120 100 80 60 40 20 0 20 40 60 80 100 120 140
TANGENTIAL VELOCITY, V_θ, ft./sec.

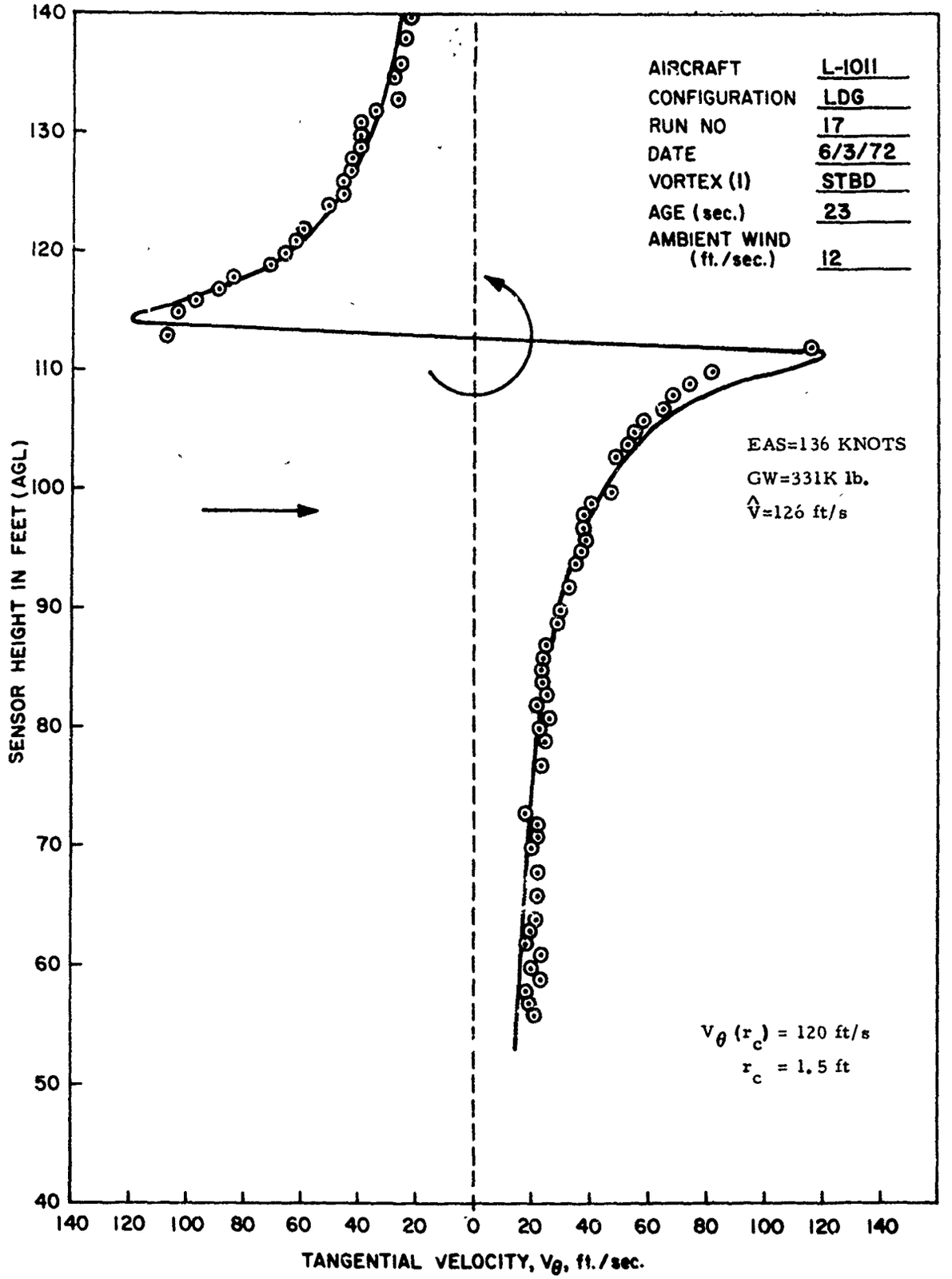
AIRCRAFT L-1011
CONFIGURATION LDG
RUN NO 17
DATE 6/3/72
VORTEX (I) STBD
AGE (sec.) 23
AMBIENT WIND (ft./sec.) 12
EAS=136 KNOTS
GW=331K lb.
$\hat{V}$=126 ft/s
$V_\theta (r_c)$ = 120 ft/s
r_c = 1.5 ft
SENSOR HEIGHT IN FEET (AGL)
140
130
120
110
100
90
80
70
60
50
40
140 120 100 80 60 40 20 0 20 40 60 80 100 120 140
TANGENTIAL VELOCITY, V_θ, ft./sec.

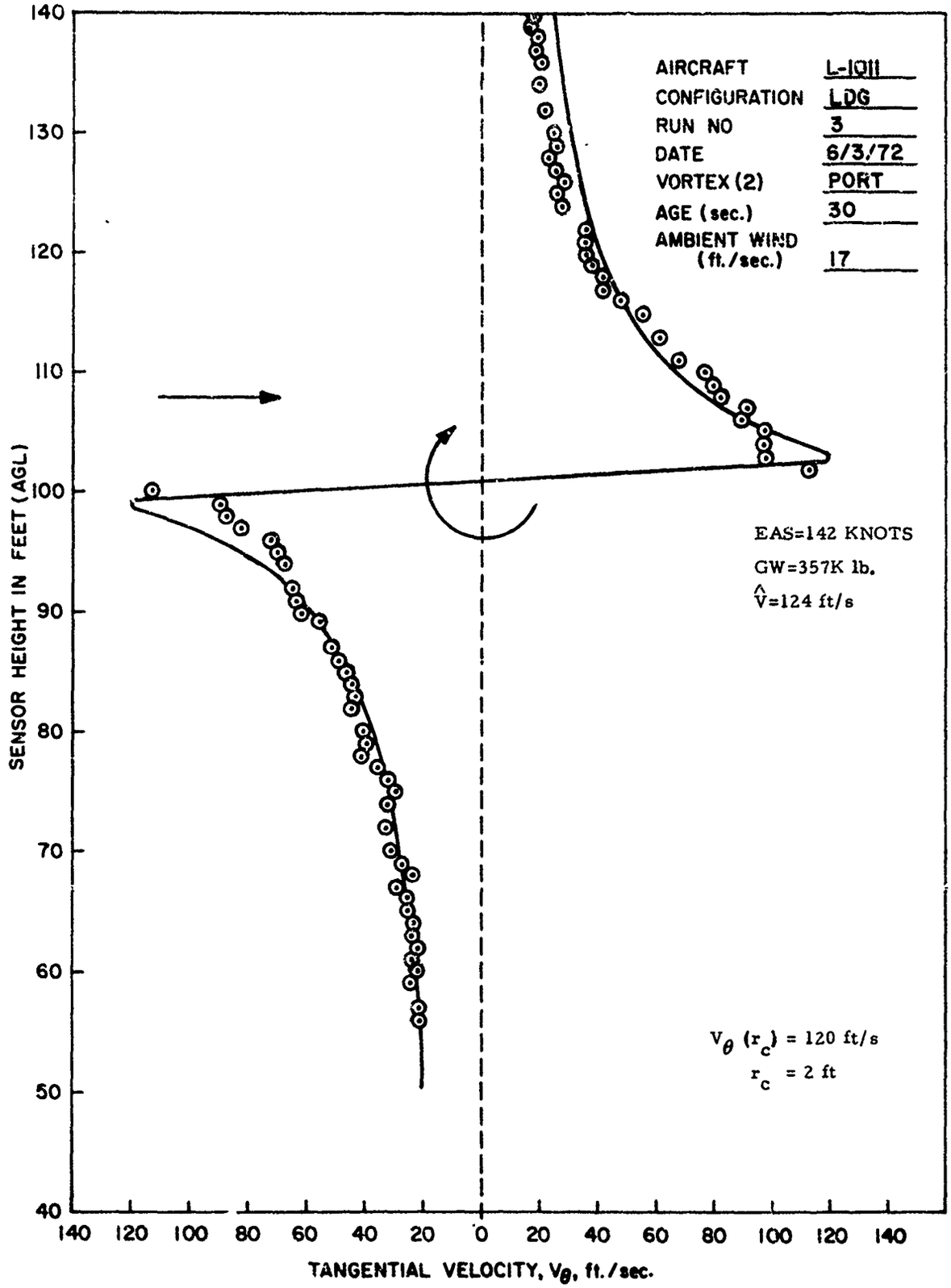
AIRCRAFT L-1011
CONFIGURATION LDG
RUN NO 3
DATE 6/3/72
VORTEX (2) PORT
AGE (sec.) 30
AMBIENT WIND (ft./sec.) 17
EAS=142 KNOTS
GW=357K lb.
$\hat{V}$=124 ft/s
$V_\theta (r_c)$ = 120 ft/s
r_c = 2 ft
SENSOR HEIGHT IN FEET (AGL)
TANGENTIAL VELOCITY, V_θ, ft./sec.
140
130
120
110
100
90
80
70
60
50
40
140 120 100 80 60 40 20 0 20 40 60 80 100 120 140

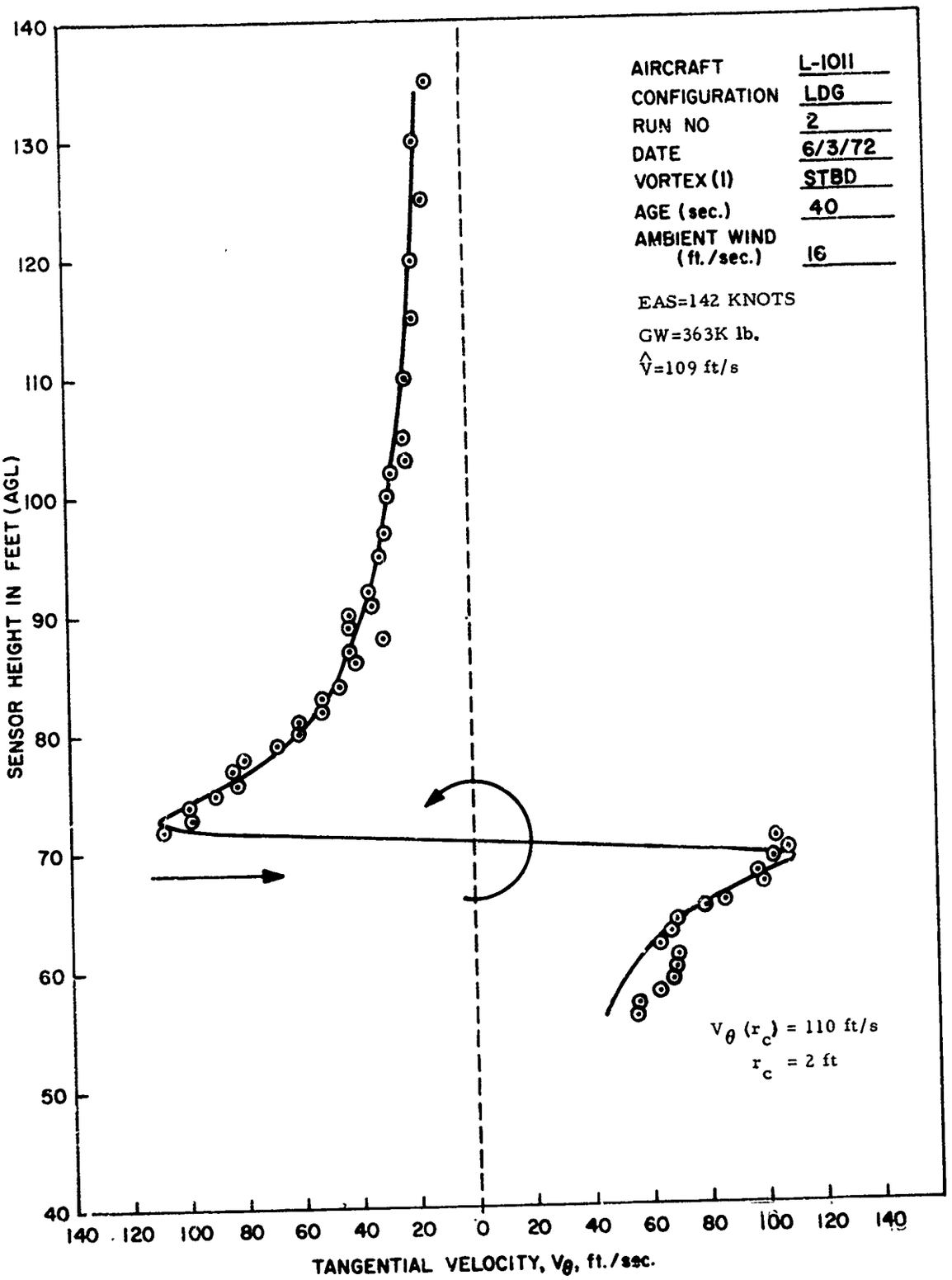
AIRCRAFT L-1011
CONFIGURATION LDG
RUN NO 2
DATE 6/3/72
VORTEX (I) STBD
AGE (sec.) 40
AMBIENT WIND (ft./sec.) 16
EAS=142 KNOTS
GW=363K lb.
$\hat{V}$=109 ft/s
$V_\theta (r_c)$ = 110 ft/s
r_c = 2 ft
SENSOR HEIGHT IN FEET (AGL)
TANGENTIAL VELOCITY, V_θ, ft./sec.
140
130
120
110
100
90
80
70
60
50
40
140 120 100 80 60 40 20 0 20 40 60 80 100 120 140

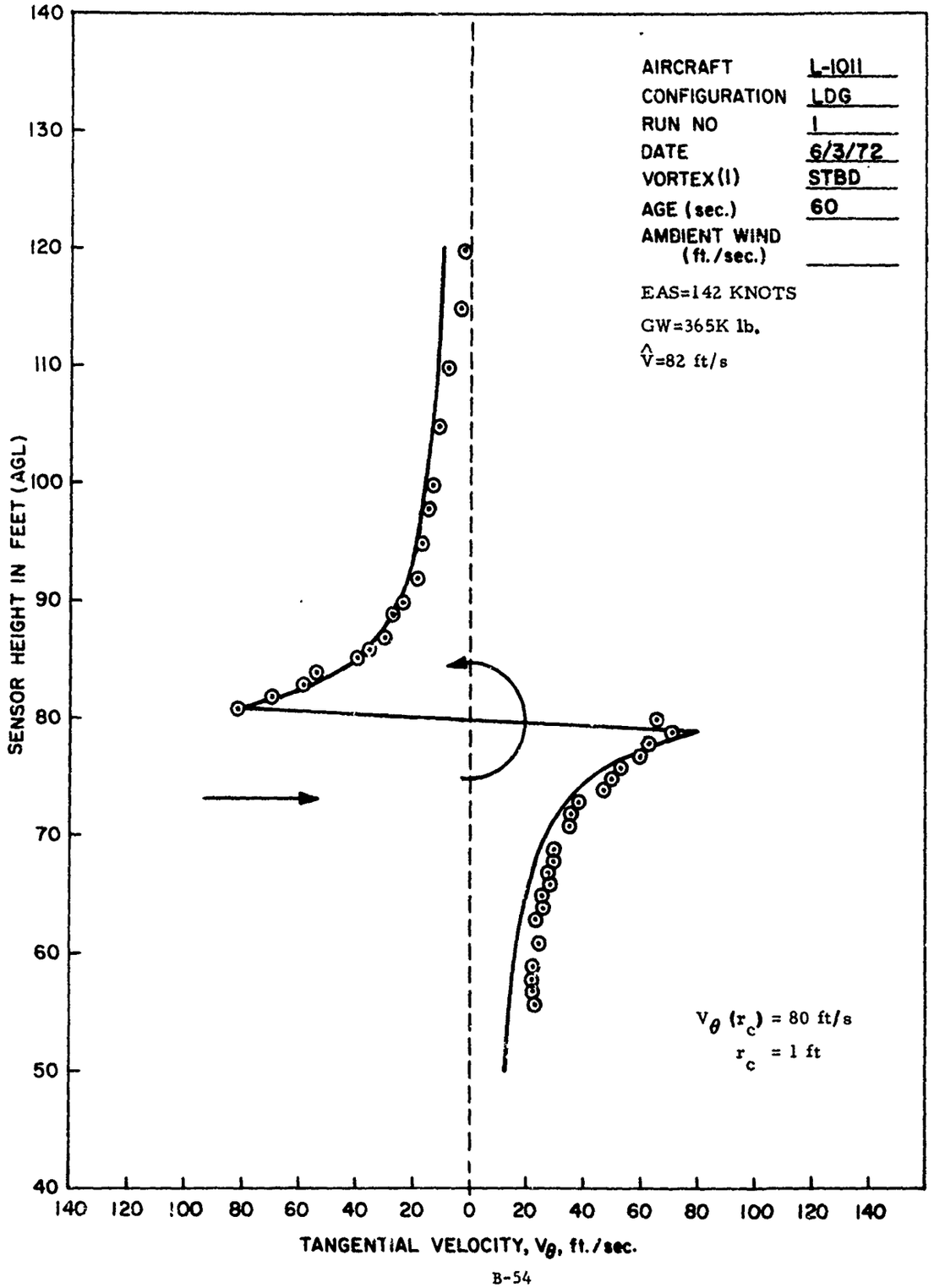
AIRCRAFT L-1011
CONFIGURATION LDG
RUN NO 1
DATE 6/3/72
VORTEX (1) STBD
AGE (sec.) 60
AMBIENT WIND (ft./sec.)
EAS=142 KNOTS
GW=365K lb.
$\hat{V}$=82 ft/s
$V_\theta (r_c)$ = 80 ft/s
r_c = 1 ft
SENSOR HEIGHT IN FEET (AGL)
140
130
120
110
100
90
80
70
60
50
40
140 120 100 80 60 40 20 0 20 40 60 80 100 120 140
TANGENTIAL VELOCITY, V_θ, ft./sec.

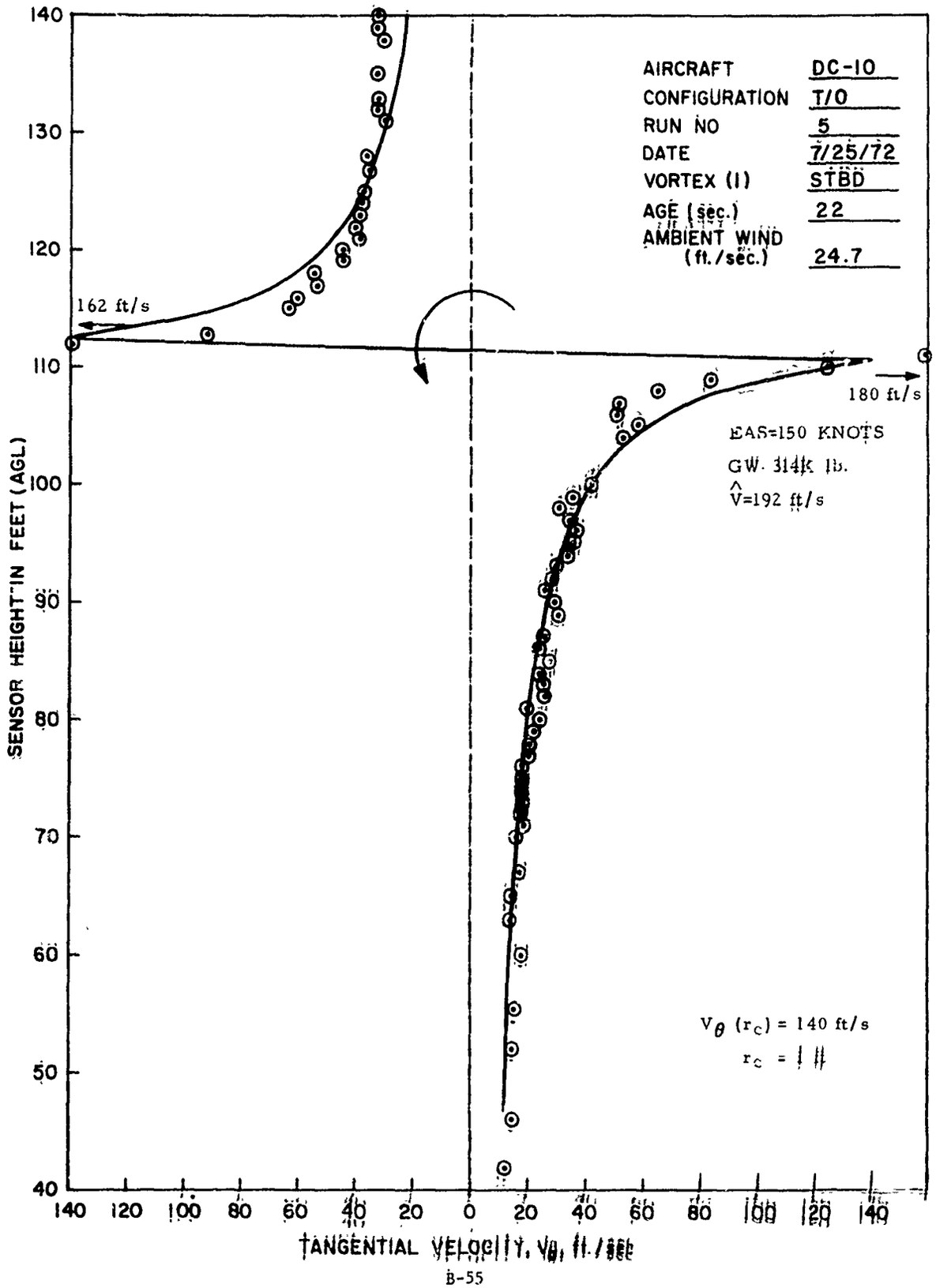
AIRCRAFT DC-10
CONFIGURATION T/O
RUN NO 5
DATE 7/25/72
VORTEX (1) STBD
AGE (sec.) 22
AMBIENT WIND (ft./sec.) 24.7
162 ft/s
180 ft/s
EAS=150 KNOTS
GW. 314K lb.
V̂=192 ft/s
V_θ (r_c) = 140 ft/s
r_c = 1 ft
SENSOR HEIGHT IN FEET (AGL)
TANGENTIAL VELOCITY, V_θ, ft./sec
140 130 120 110 100 90 80 70 60 50 40
140 120 100 80 60 40 20 0 20 40 60 80 100 120 140

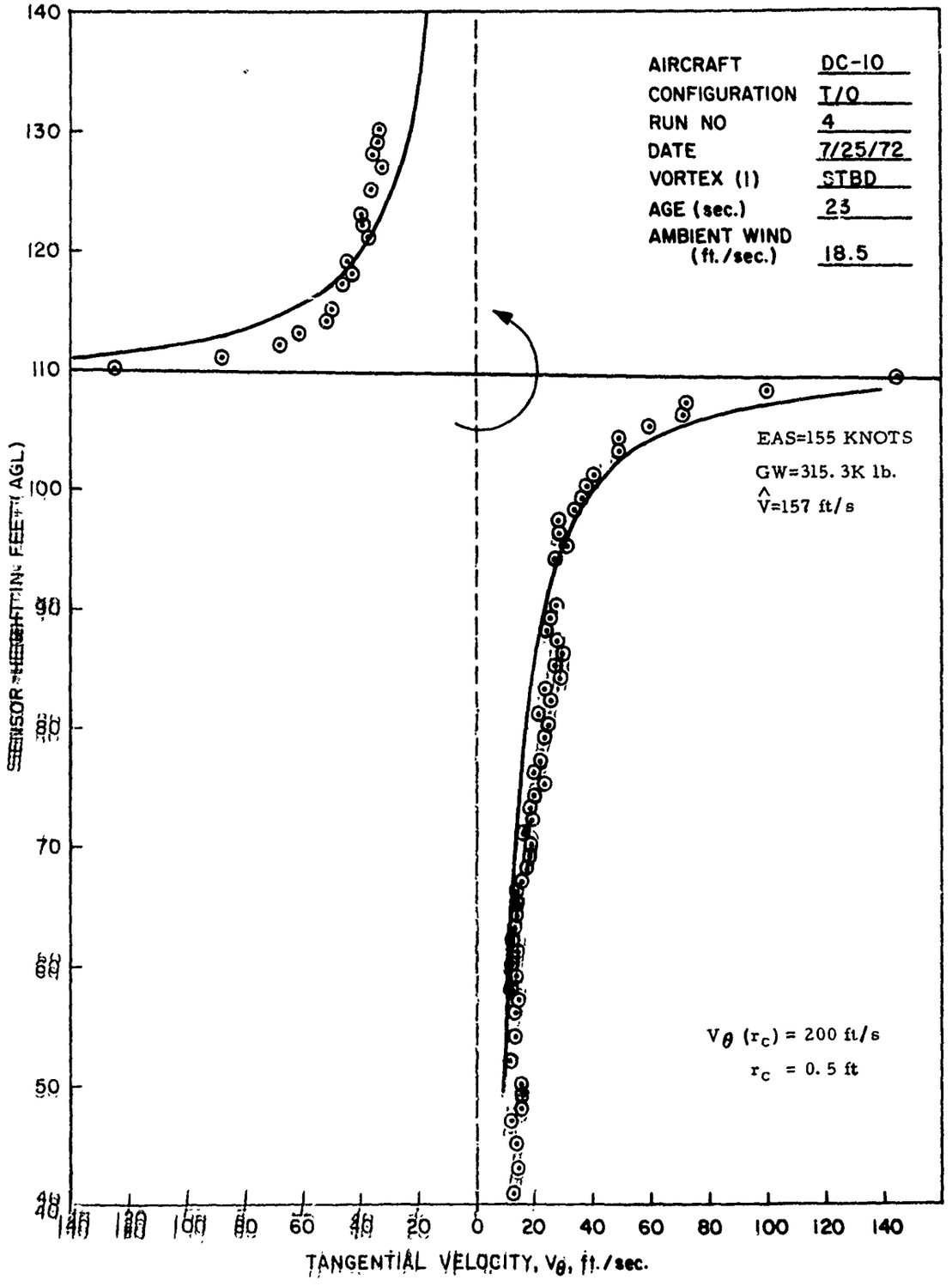
AIRCRAFT DC-10
CONFIGURATION T/O
RUN NO 4
DATE 7/25/72
VORTEX (1) STBD
AGE (sec.) 23
AMBIENT WIND (ft./sec.) 18.5
EAS=155 KNOTS
GW=315. 3K lb.
V̂=157 ft/s
Vθ (rc) = 200 ft/s
rc = 0. 5 ft
SENSOR HEIGHT IN FEET (AGL)
140
130
120
110
100
90
80
70
60
50
40
140 120 100 80 60 40 20 0 20 40 60 80 100 120 140
TANGENTIAL VELOCITY, Vθ, ft./sec.

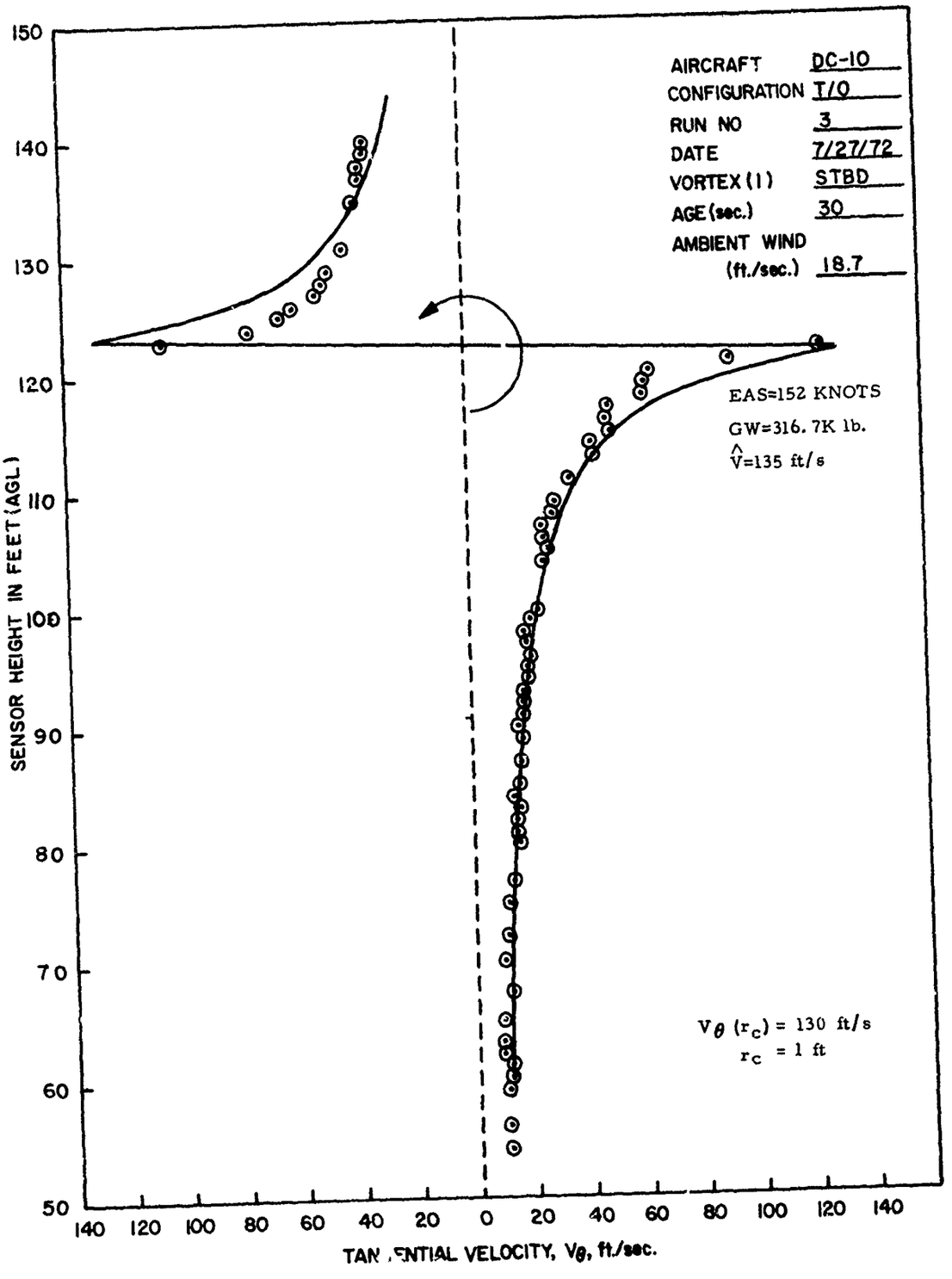
AIRCRAFT DC-10
CONFIGURATION T/O
RUN NO 3
DATE 7/27/72
VORTEX (1) STBD
AGE (sec.) 30
AMBIENT WIND (ft./sec.) 18.7
EAS=152 KNOTS
GW=316.7K lb.
$\hat{V}$=135 ft/s
$V\theta\ (r_c)$ = 130 ft/s
r_c = 1 ft
SENSOR HEIGHT IN FEET (AGL)
150
140
130
120
110
100
90
80
70
60
50
140 120 100 80 60 40 20 0 20 40 60 80 100 120 140
TANGENTIAL VELOCITY, $V\theta$, ft./sec.

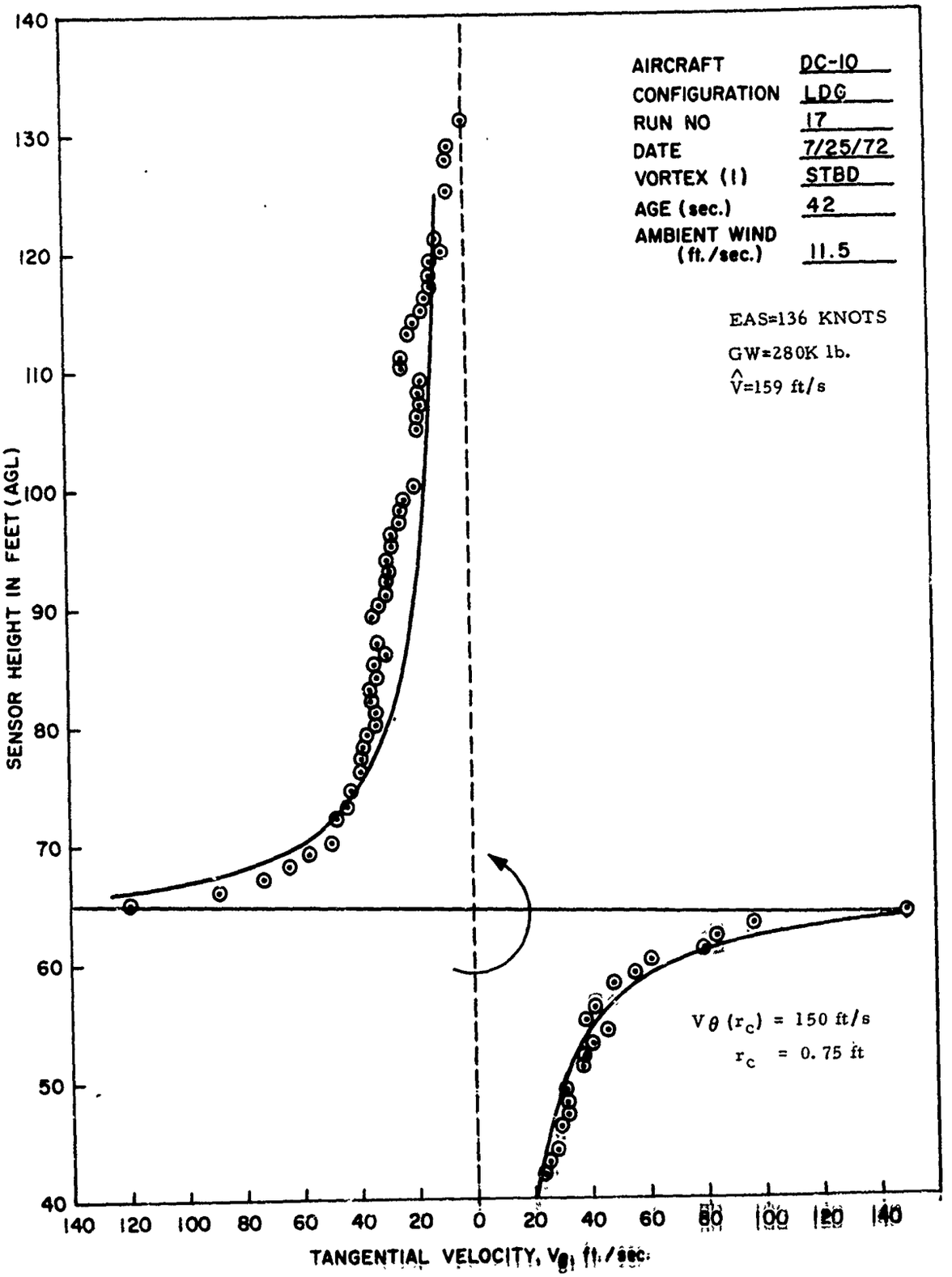
AIRCRAFT DC-10
CONFIGURATION LDG
RUN NO 17
DATE 7/25/72
VORTEX (1) STBD
AGE (sec.) 42
AMBIENT WIND (ft./sec.) 11.5
EAS=136 KNOTS
GW=280K lb.
$\hat{V}$=159 ft/s
$V\theta\ (r_c)$ = 150 ft/s
r_c = 0.75 ft
SENSOR HEIGHT IN FEET (AGL)
TANGENTIAL VELOCITY, V_θ, ft./sec.
140
130
120
110
100
90
80
70
60
50
40
140 120 100 80 60 40 20 0 20 40 60 80 100 120 140

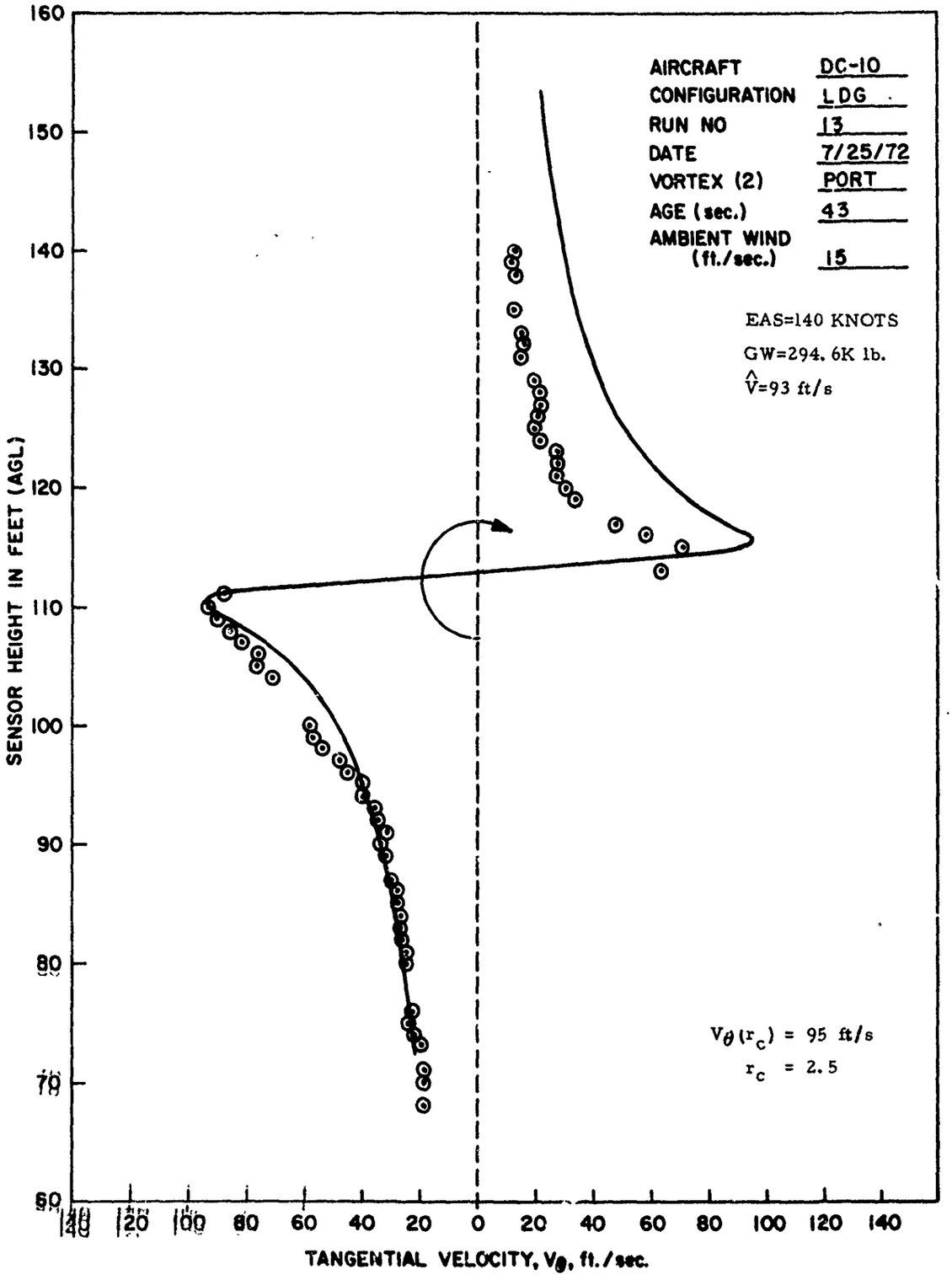
AIRCRAFT DC-10
CONFIGURATION LDG
RUN NO 13
DATE 7/25/72
VORTEX (2) PORT
AGE (sec.) 43
AMBIENT WIND (ft./sec.) 15
EAS=140 KNOTS
GW=294.6K lb.
$\hat{V}$=93 ft/s
$V_\theta(r_c)$ = 95 ft/s
r_c = 2.5
SENSOR HEIGHT IN FEET (AGL)
TANGENTIAL VELOCITY, V_θ, ft./sec.
160
150
140
130
120
110
100
90
80
70
60
40
20
0
20
40
60
80
100
120
140

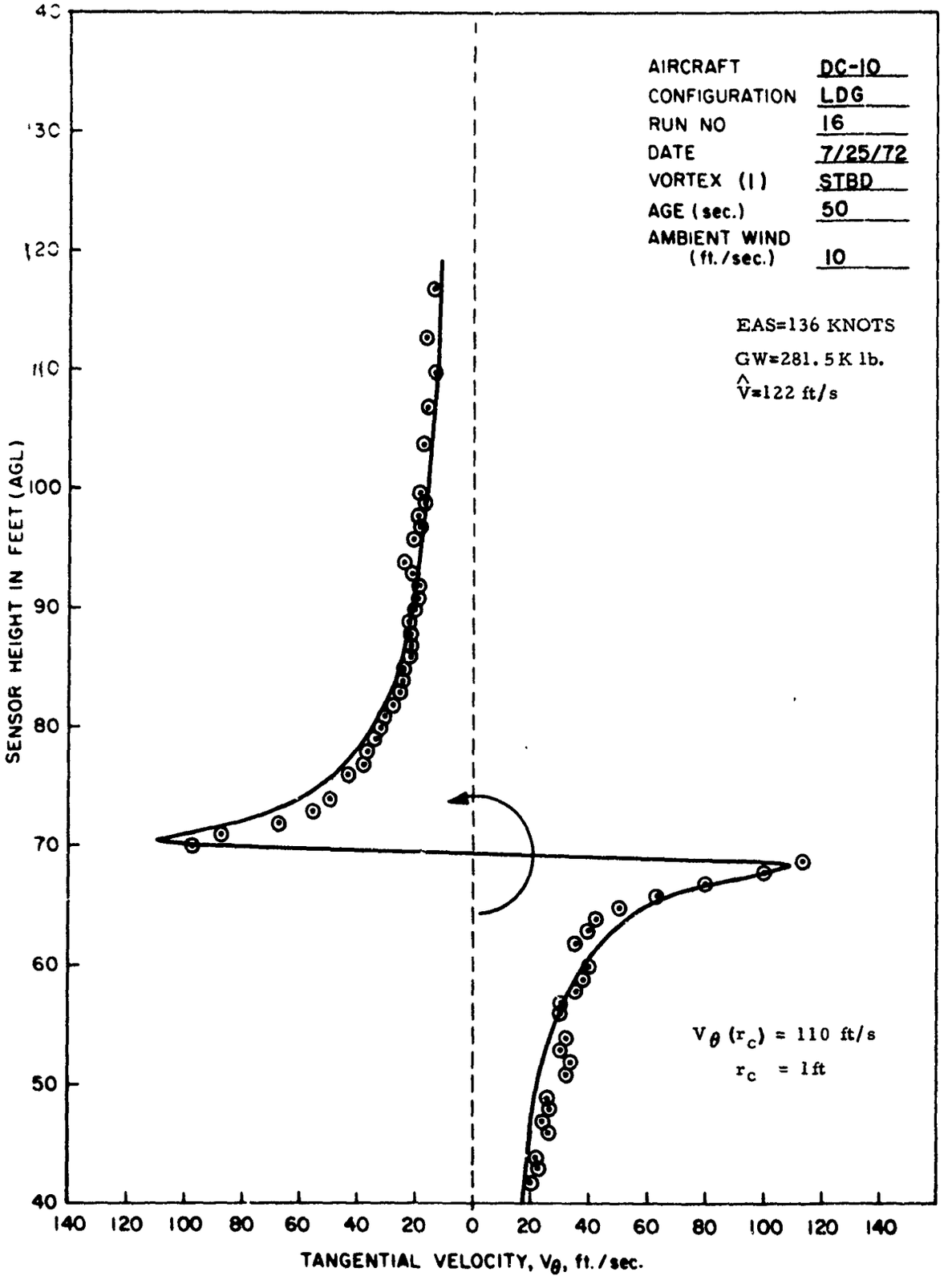
AIRCRAFT DC-10
CONFIGURATION LDG
RUN NO 16
DATE 7/25/72
VORTEX (1) STBD
AGE (sec.) 50
AMBIENT WIND (ft./sec.) 10
EAS=136 KNOTS
GW=281.5K lb.
$\hat{V}$=122 ft/s
$V_\theta (r_c)$ = 110 ft/s
r_c = 1ft
SENSOR HEIGHT IN FEET (AGL)
TANGENTIAL VELOCITY, V_θ, ft./sec.
140 120 100 80 60 40 20 0 20 40 60 80 100 120 140
40 50 60 70 80 90 100 110 120 130

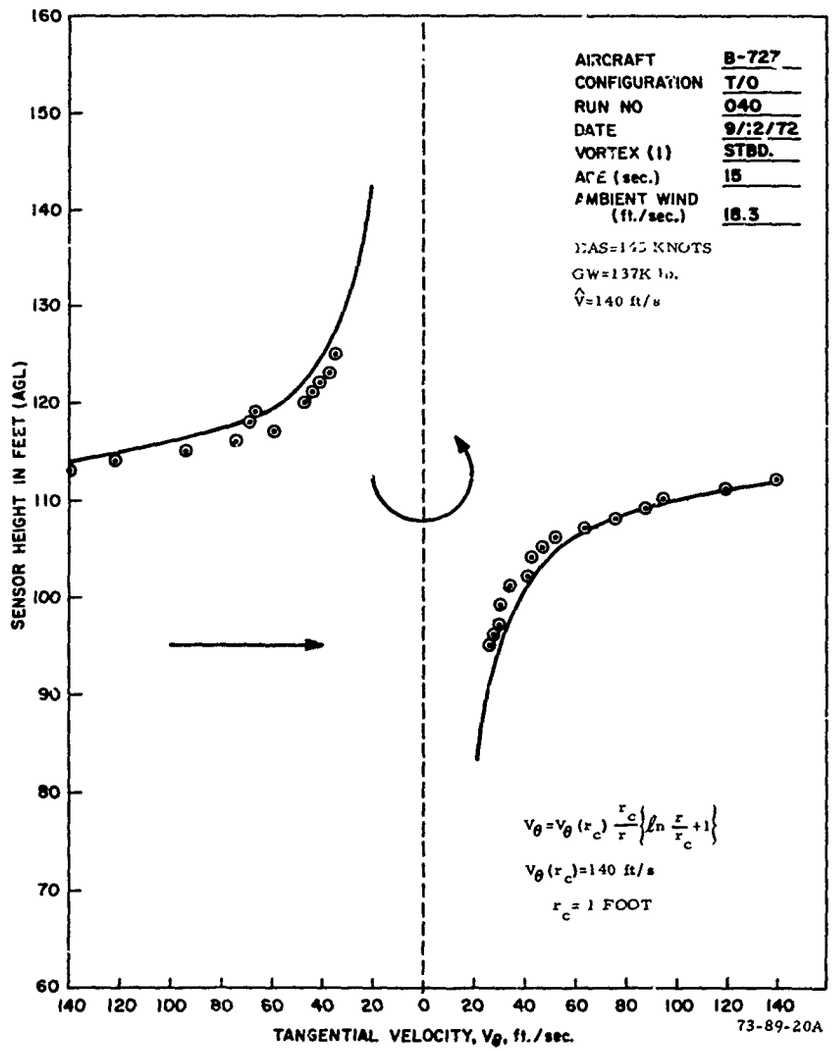
AIRCRAFT B-727
CONFIGURATION T/O
RUN NO 040
DATE 9/:2/72
VORTEX (1) STBD.
AGE (sec.) 15
AMBIENT WIND (ft./sec.) 18.3
EAS=145 KNOTS
GW=137K lb.
$\hat{V}$=140 ft/s
$V_\theta = V_\theta(r_c)\frac{r_c}{r}\left\{\ln\frac{r}{r_c}+1\right\}$
$V_\theta(r_c)$=140 ft/s
r_c= 1 FOOT
SENSOR HEIGHT IN FEET (AGL)
TANGENTIAL VELOCITY, V_θ, ft./sec.
73-89-20A

61A

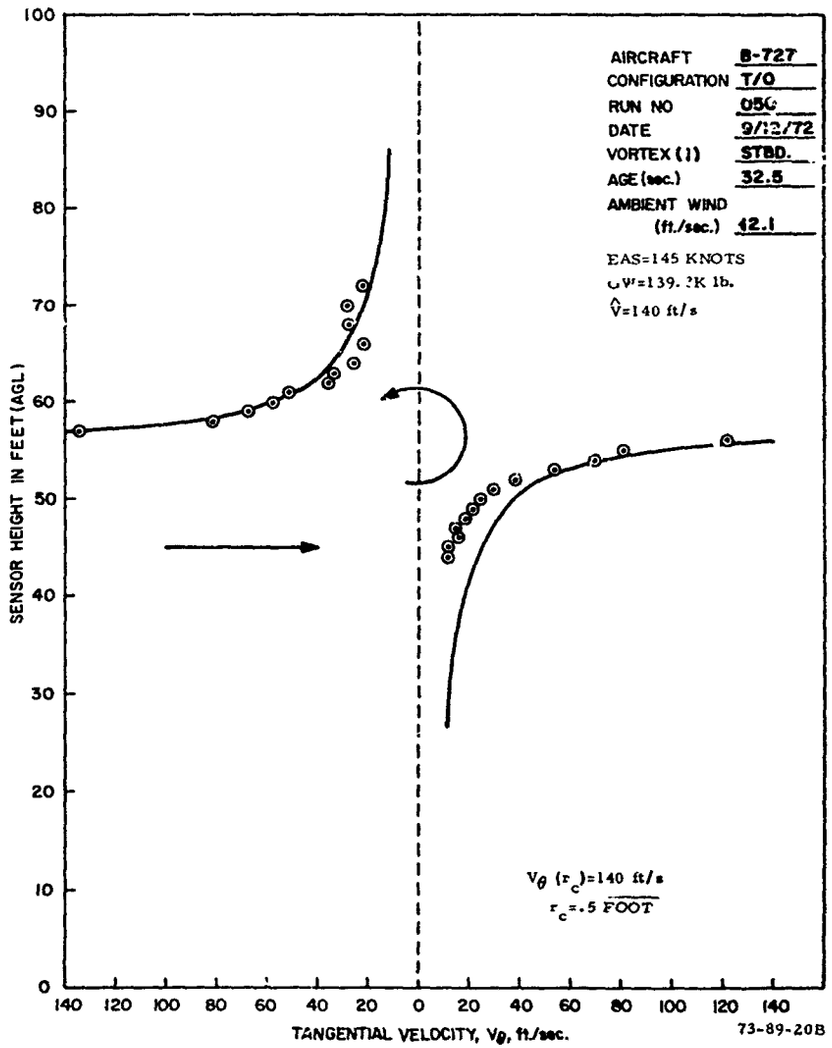
AIRCRAFT B-727
CONFIGURATION T/O
RUN NO 05C
DATE 9/12/72
VORTEX (1) STBD.
AGE (sec.) 32.5
AMBIENT WIND (ft./sec.) 12.1
EAS=145 KNOTS
GW=139. ?K lb.
$\hat{V}$=140 ft/s
$V_\theta(r_c)$=140 ft/s
r_c=.5 FOOT
SENSOR HEIGHT IN FEET (AGL)
TANGENTIAL VELOCITY, V_θ, ft./sec.
73-89-20B

61B

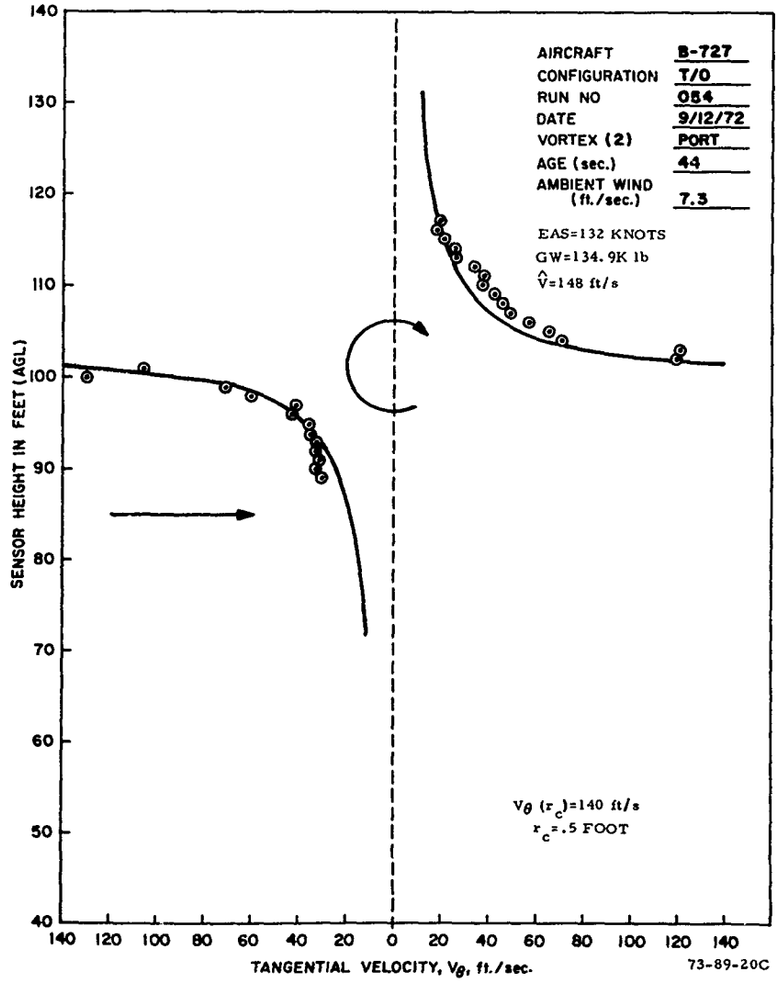
AIRCRAFT B-727
CONFIGURATION T/O
RUN NO 084
DATE 9/12/72
VORTEX (2) PORT
AGE (sec.) 44
AMBIENT WIND (ft./sec.) 7.3
EAS=132 KNOTS
GW=134.9K lb
$\hat{V}$=148 ft/s
V_θ (r_c)=140 ft/s
r_c=.5 FOOT
SENSOR HEIGHT IN FEET (AGL)
TANGENTIAL VELOCITY, V_θ, ft./sec.
73-89-20C

62A

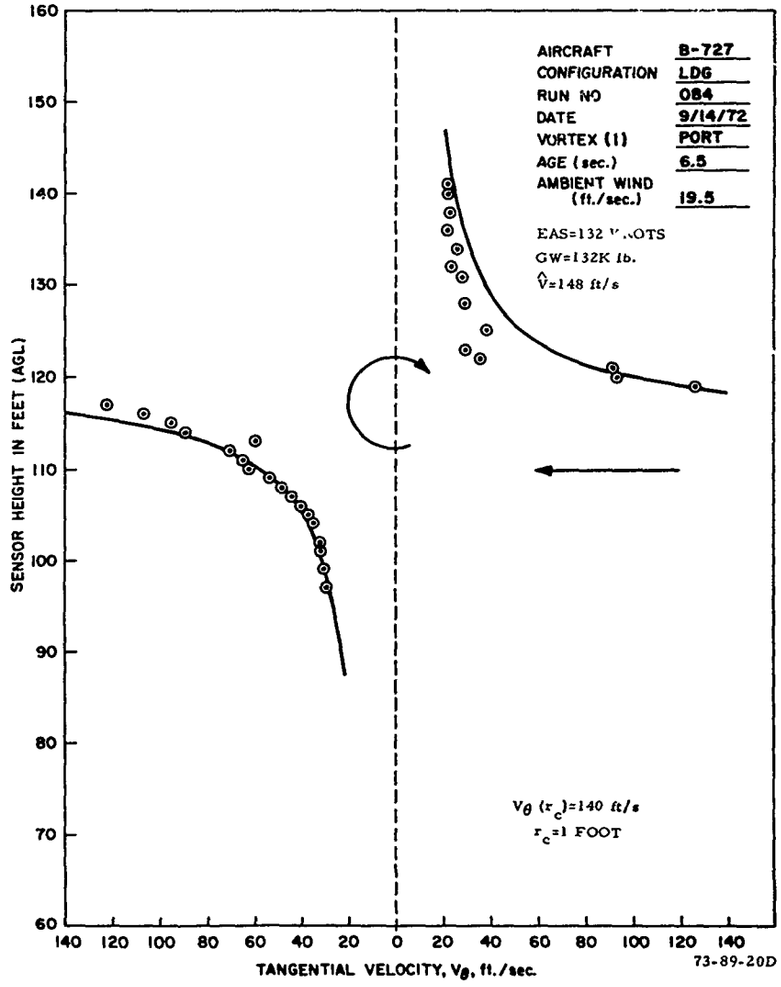
AIRCRAFT B-727
CONFIGURATION LDG
RUN NO 084
DATE 9/14/72
VORTEX (1) PORT
AGE (sec.) 6.5
AMBIENT WIND (ft./sec.) 19.5
EAS=132 KNOTS
GW=132K lb.
$\hat{V}$=148 ft/s
V_θ (r_c)=140 ft/s
r_c=1 FOOT
SENSOR HEIGHT IN FEET (AGL)
TANGENTIAL VELOCITY, V_θ, ft./sec.
73-89-20D

62B

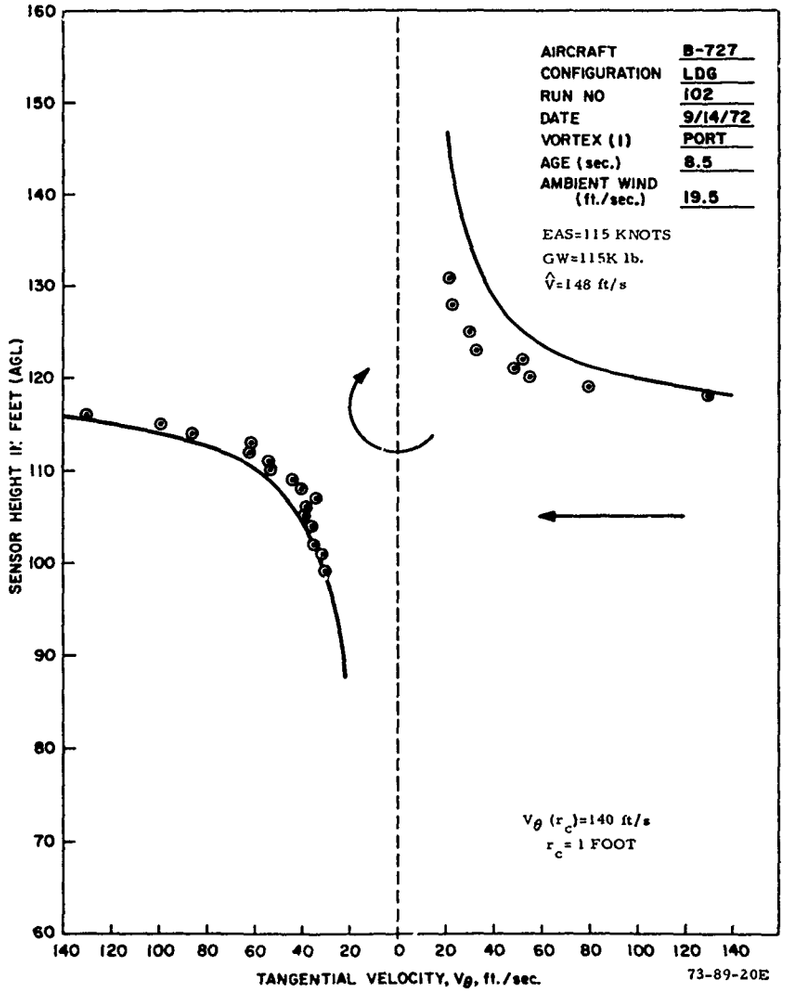
AIRCRAFT B-727
CONFIGURATION LDG
RUN NO 102
DATE 9/14/72
VORTEX (1) PORT
AGE (sec.) 8.5
AMBIENT WIND (ft./sec.) 19.5
EAS=115 KNOTS
GW=115K lb.
$\hat{V}$=148 ft/s
V_θ (r_c)=140 ft/s
r_c = 1 FOOT
SENSOR HEIGHT IN FEET (AGL)
TANGENTIAL VELOCITY, V_θ, ft./sec.
73-89-20E

63A

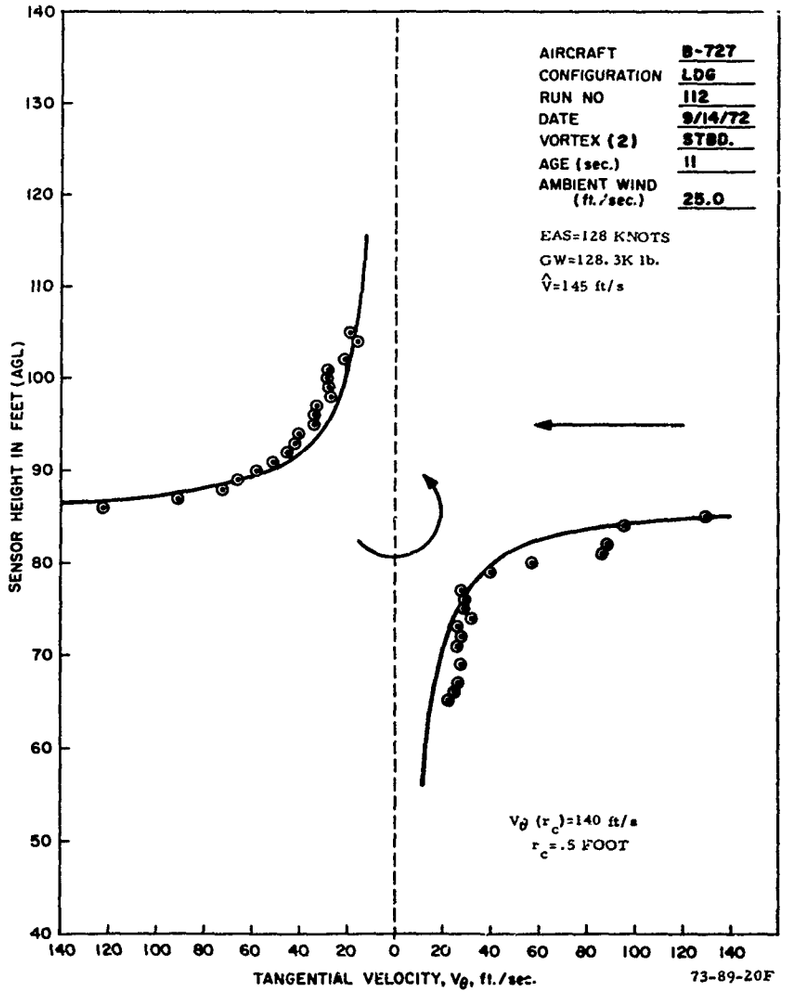
AIRCRAFT B-727
CONFIGURATION LDG
RUN NO 112
DATE 9/14/72
VORTEX (2) STBD.
AGE (sec.) 11
AMBIENT WIND (ft./sec.) 25.0
EAS=128 KNOTS
GW=128.3K lb.
$\hat{V}$=145 ft/s
V_θ (r_c)=140 ft/s
r_c = .5 FOOT
SENSOR HEIGHT IN FEET (AGL)
TANGENTIAL VELOCITY, V_θ, ft./sec.
73-89-20F

63B

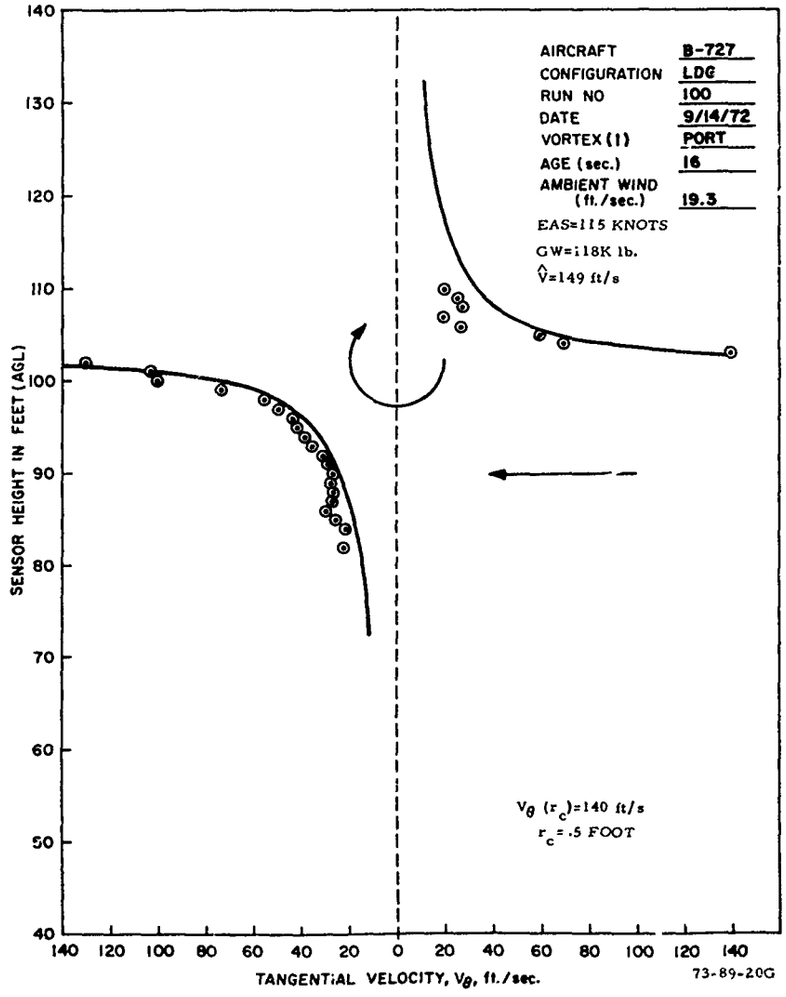
AIRCRAFT B-727
CONFIGURATION LDG
RUN NO 100
DATE 9/14/72
VORTEX (1) PORT
AGE (sec.) 16
AMBIENT WIND (ft./sec.) 19.3
EAS=115 KNOTS
GW=118K lb.
◊=149 ft/s
V_θ (r_c)=140 ft/s
r_c=.5 FOOT
SENSOR HEIGHT IN FEET (AGL)
TANGENTIAL VELOCITY, V_θ, ft./sec.
73-89-20G

64A

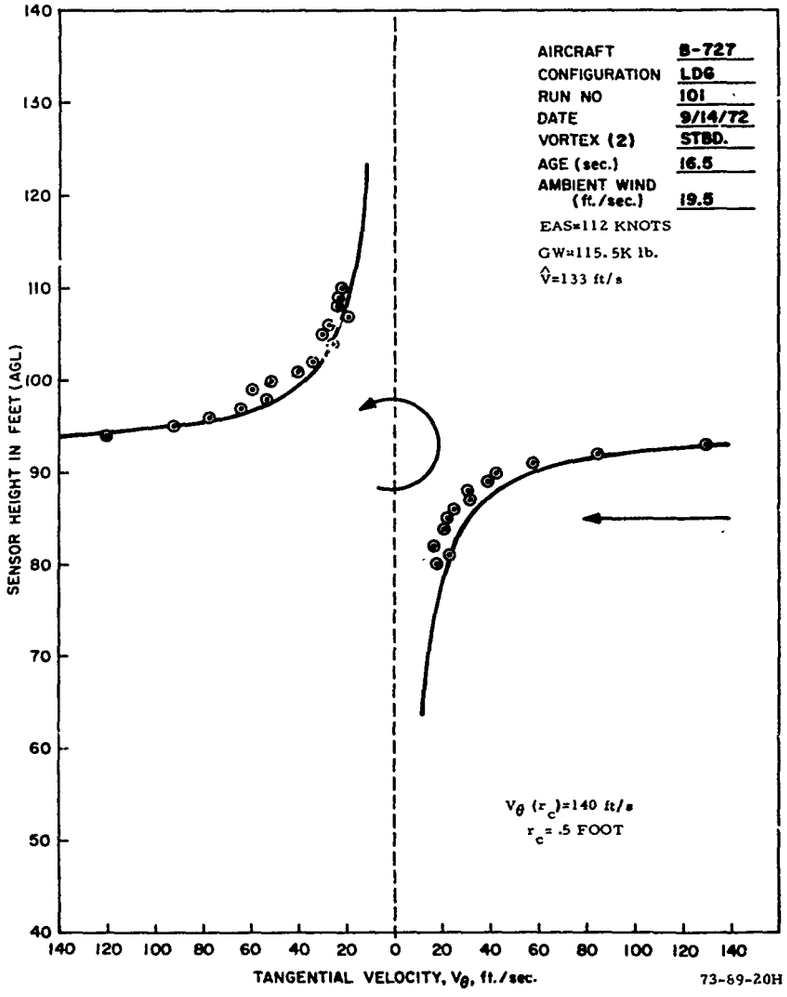
AIRCRAFT B-727
CONFIGURATION LDG
RUN NO 101
DATE 9/14/72
VORTEX (2) STBD.
AGE (sec.) 16.5
AMBIENT WIND (ft./sec.) 19.5
EAS=112 KNOTS
GW=115.5K lb.
◊=133 ft/s
V_θ (r_c)=140 ft/s
r_c=.5 FOOT
SENSOR HEIGHT IN FEET (AGL)
TANGENTIAL VELOCITY, V_θ, ft./sec.
73-89-20H

64B

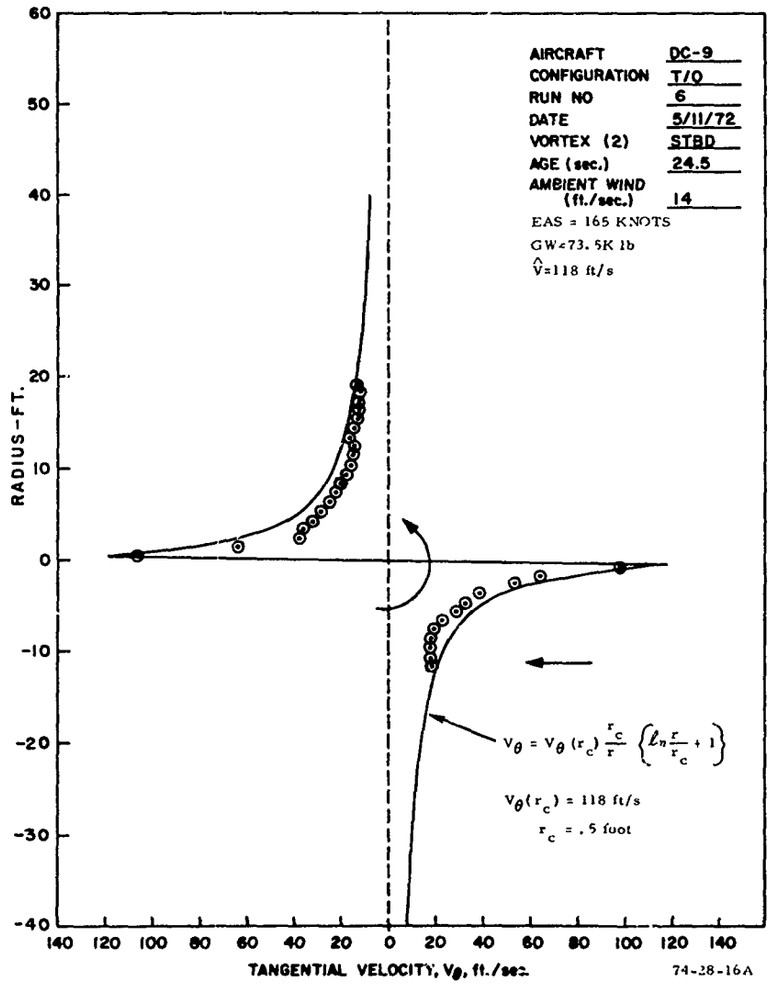
AIRCRAFT DC-9
CONFIGURATION T/O
RUN NO 6
DATE 5/11/72
VORTEX (2) STBD
AGE (sec.) 24.5
AMBIENT WIND (ft./sec.) 14
EAS = 165 KNOTS
GW=73.5K lb
$\hat{V}$=118 ft/s
$V_\theta = V_\theta(r_c)\frac{r_c}{r}\left\{\ell_n\frac{r}{r_c}+1\right\}$
$V_\theta(r_c)$ = 118 ft/s
r_c = .5 foot
RADIUS-FT.
TANGENTIAL VELOCITY, V_θ, ft./sec.
74-28-16A

65A

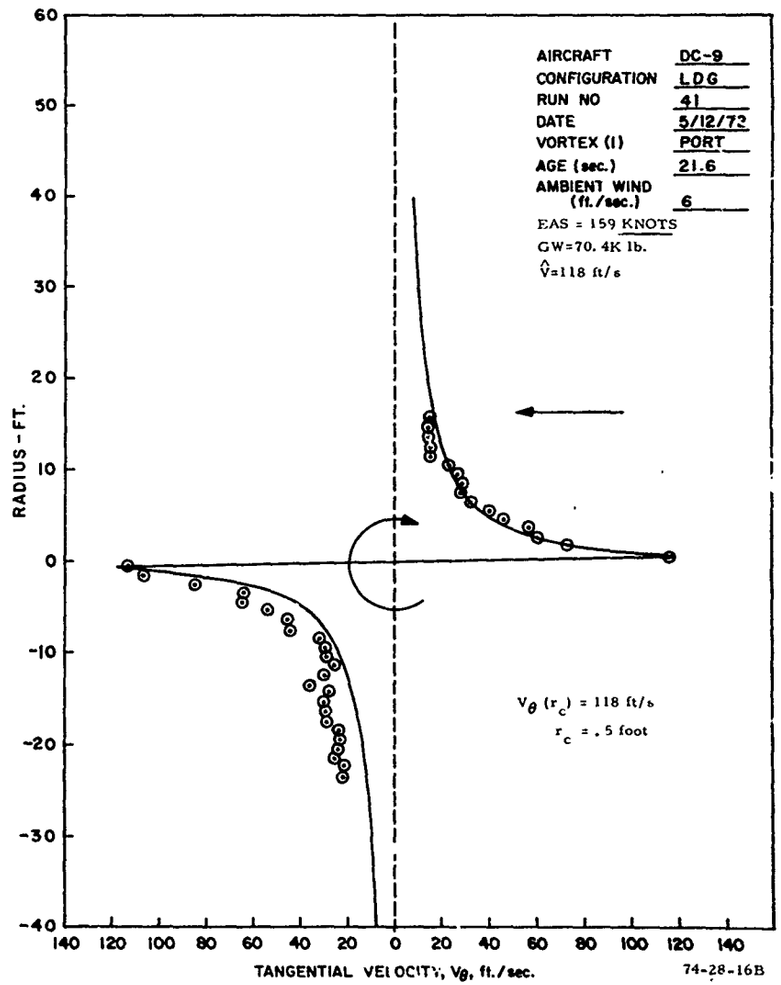
AIRCRAFT DC-9
CONFIGURATION LDG
RUN NO 41
DATE 5/12/72
VORTEX (1) PORT
AGE (sec.) 21.6
AMBIENT WIND (ft./sec.) 6
EAS = 159 KNOTS
GW=70.4K lb.
$\hat{V}$=118 ft/s
$V_\theta(r_c)$ = 118 ft/s
r_c = .5 foot
RADIUS-FT.
TANGENTIAL VELOCITY, V_θ, ft./sec.
74-28-16B

65B

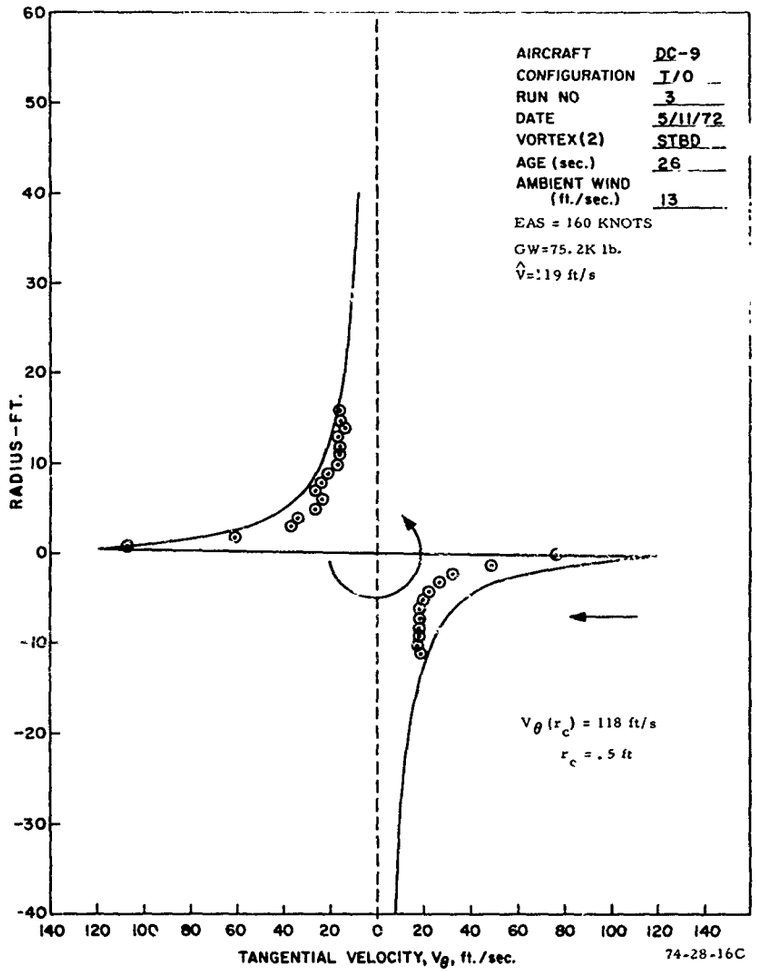
AIRCRAFT DC-9
CONFIGURATION T/O
RUN NO 3
DATE 5/11/72
VORTEX(2) STBD
AGE (sec.) 26
AMBIENT WIND (ft./sec.) 13
EAS = 160 KNOTS
GW=75.2K lb.
$\hat{V}$=119 ft/s
$V_\theta (r_c)$ = 118 ft/s
r_c = .5 ft
RADIUS - FT.
TANGENTIAL VELOCITY, V_θ, ft./sec.
74-28-16C

66A

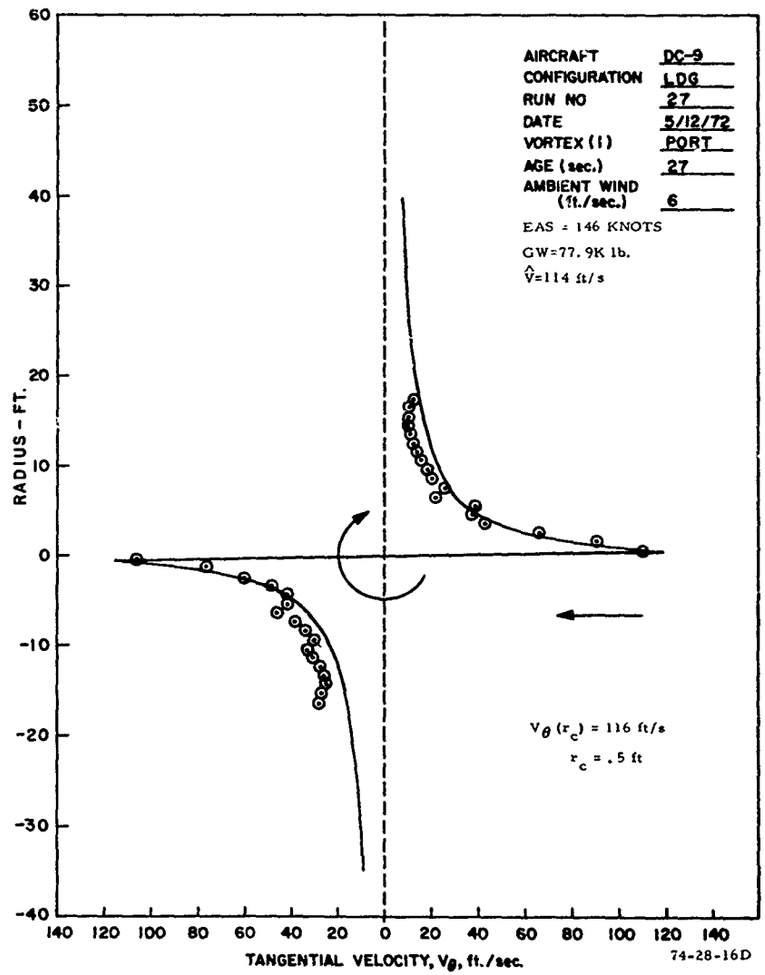
AIRCRAFT DC-9
CONFIGURATION LDG
RUN NO 27
DATE 5/12/72
VORTEX (1) PORT
AGE (sec.) 27
AMBIENT WIND (ft./sec.) 6
EAS = 146 KNOTS
GW=77.9K lb.
$\hat{V}$=114 ft/s
$V_\theta (r_c)$ = 116 ft/s
r_c = .5 ft
RADIUS - FT.
TANGENTIAL VELOCITY, V_θ, ft./sec.
74-28-16D

66B

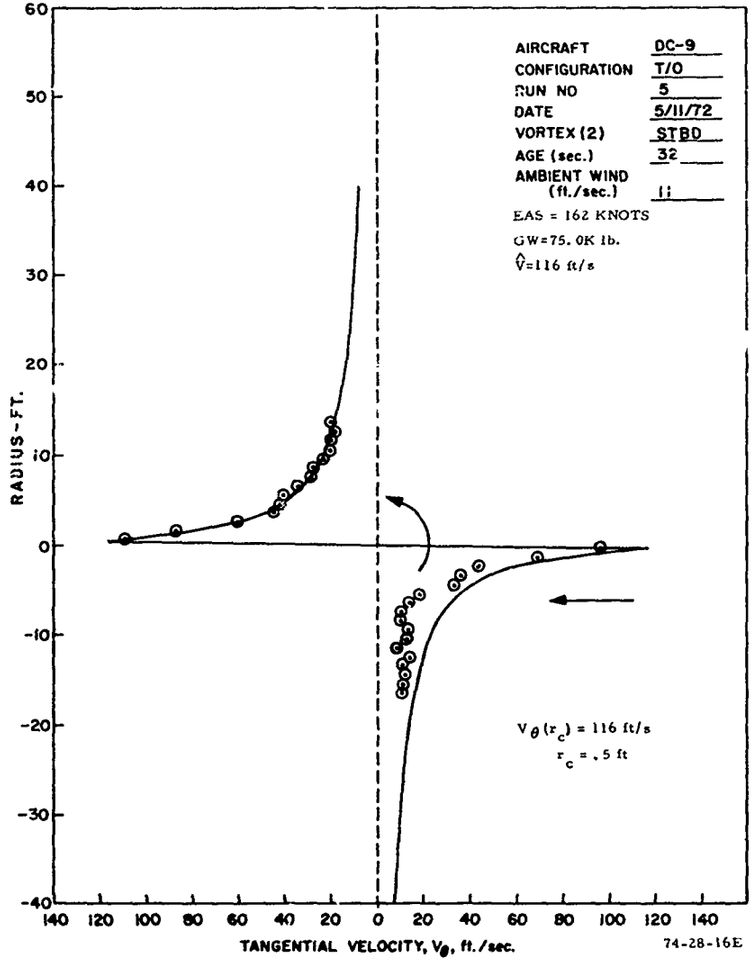
AIRCRAFT DC-9
CONFIGURATION T/O
RUN NO 5
DATE 5/11/72
VORTEX (2) STBD
AGE (sec.) 32
AMBIENT WIND (ft./sec.) 1
EAS = 162 KNOTS
GW=75.0K lb.
$\hat{V}$=116 ft/s
$V_\theta(r_c)$ = 116 ft/s
r_c = .5 ft
RADIUS - FT.
TANGENTIAL VELOCITY, V_θ, ft./sec.
74-28-16E

67A

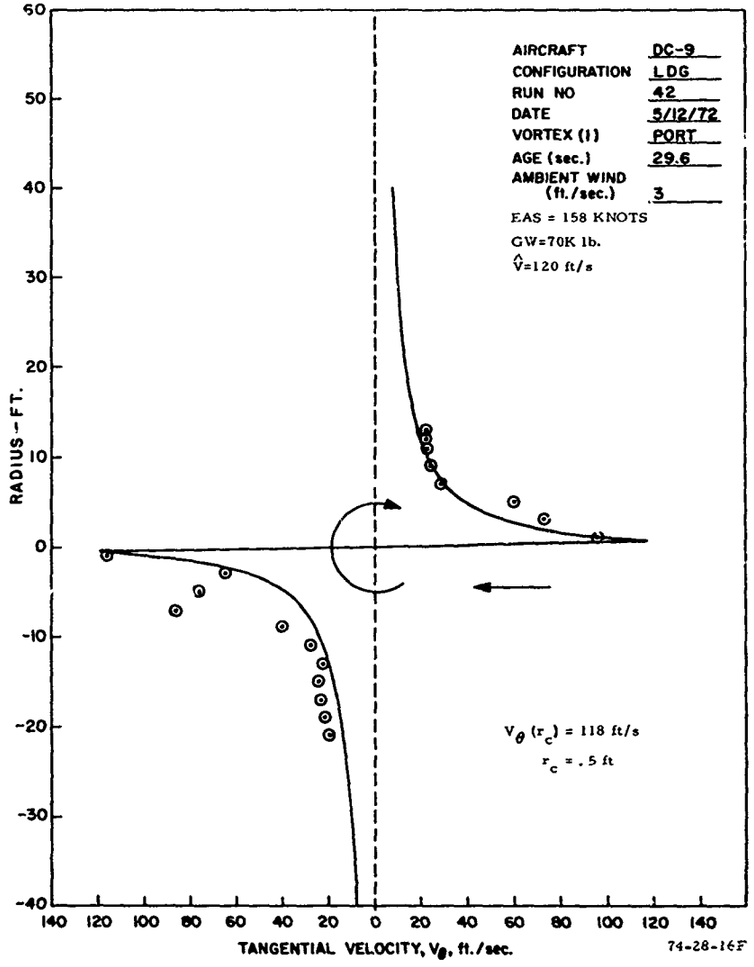
AIRCRAFT DC-9
CONFIGURATION LDG
RUN NO 42
DATE 5/12/72
VORTEX (1) PORT
AGE (sec.) 29.6
AMBIENT WIND (ft./sec.) 3
EAS = 158 KNOTS
GW=70K lb.
$\hat{V}$=120 ft/s
$V_\theta(r_c)$ = 118 ft/s
r_c = .5 ft
RADIUS - FT.
TANGENTIAL VELOCITY, V_θ, ft./sec.
74-28-16F

67B

APPENDIX C

HIGH ALTITUDE FLOW VISUALIZATION

LIST OF ILLUSTRATIONS

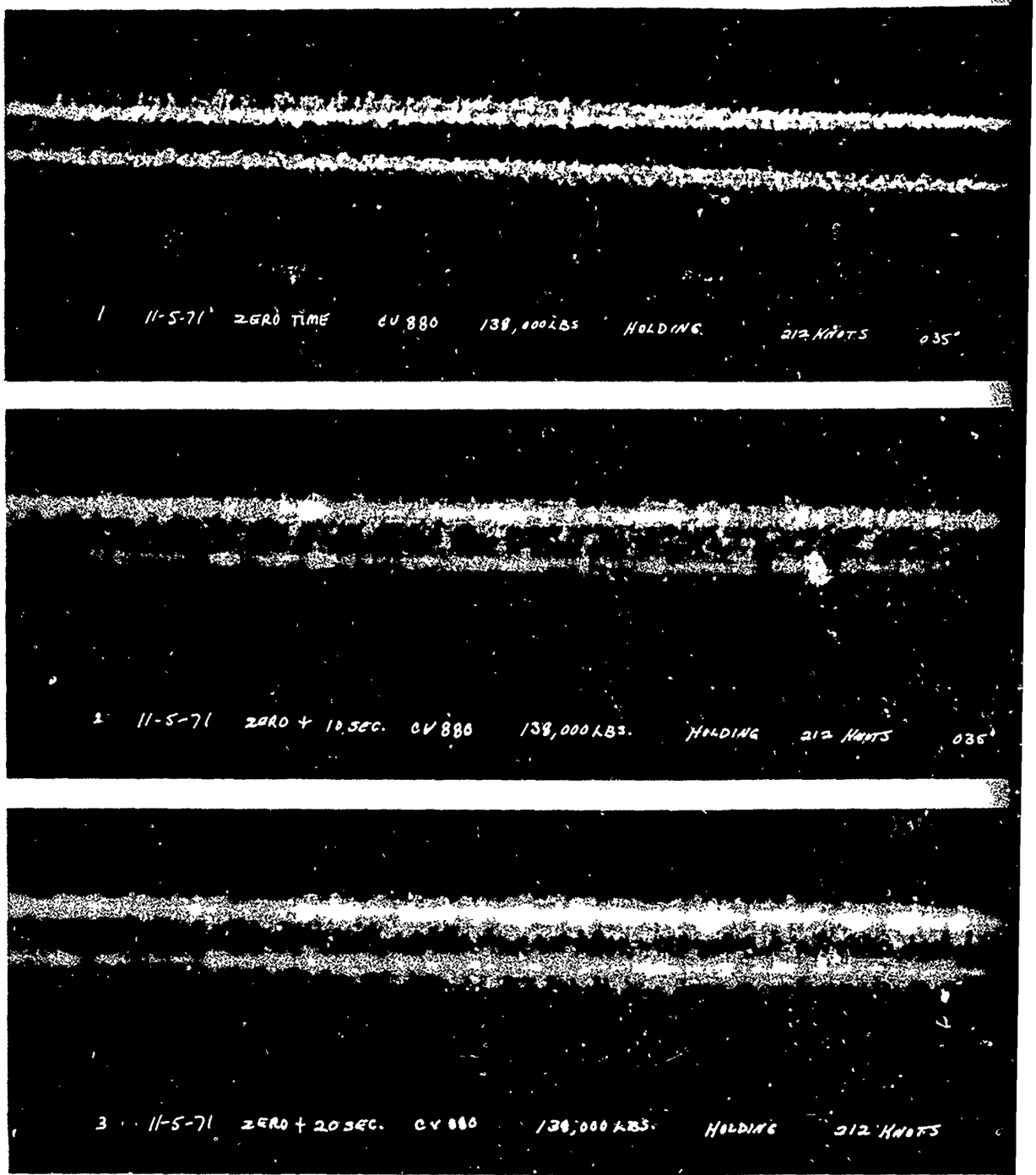

FIGURE C-1. UPPER AIR FLOW VISUALIZATION (K-38). CO
CONFIGURATION. H_p = 5,000 FEET (Sheet 1

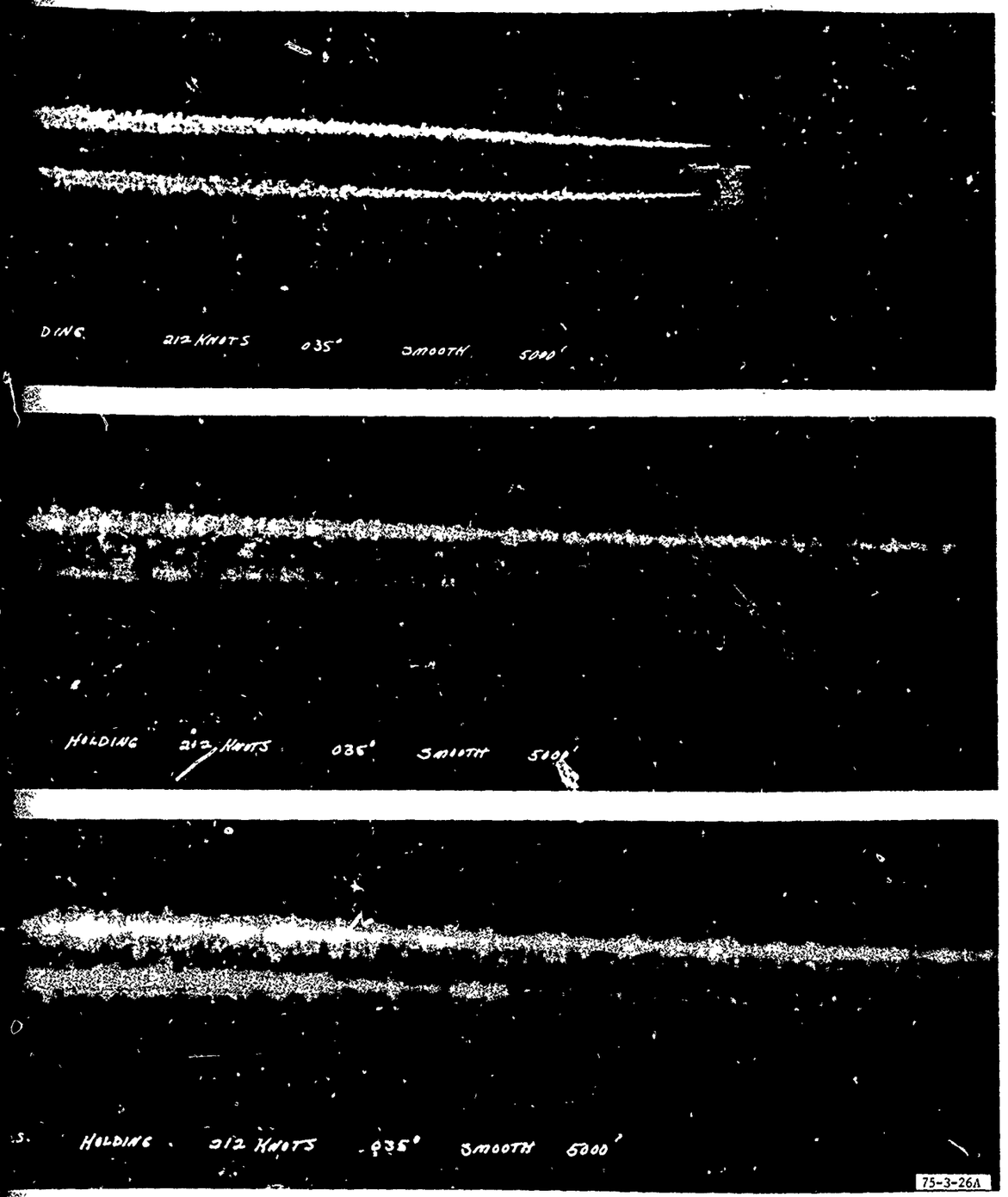

AIR FLOW VISUALIZATION (K-38). CONVAIR 880, HOLDING
GURATION. H_p = 5,000 FEET (Sheet 1 of 4)

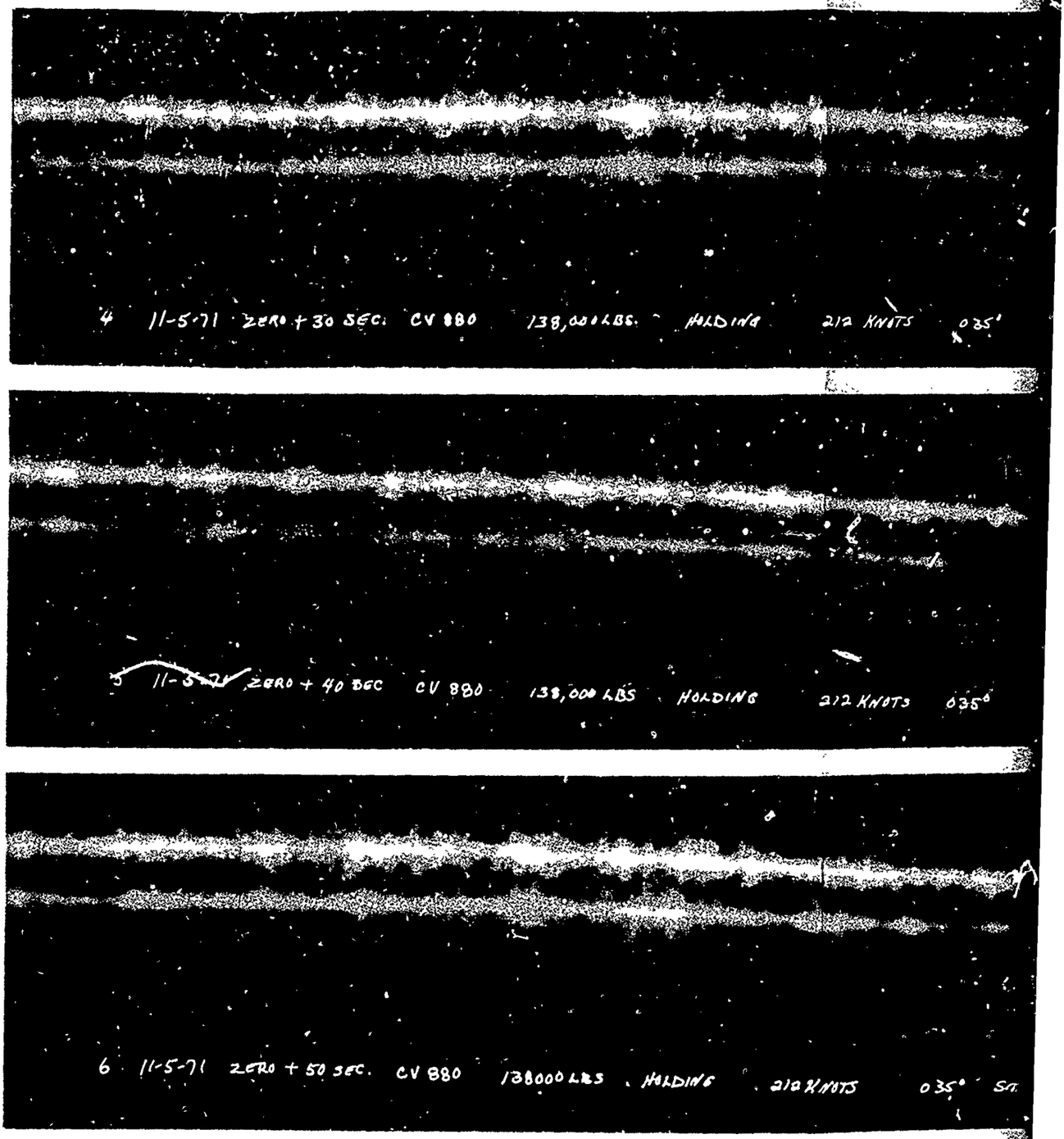

FIGURE C-1. UPPER AIR FLOW VISUALIZATION (K-38). CONVAIR CONFIGURATION. H_p = 5,000 FEET (Sheet 2 of

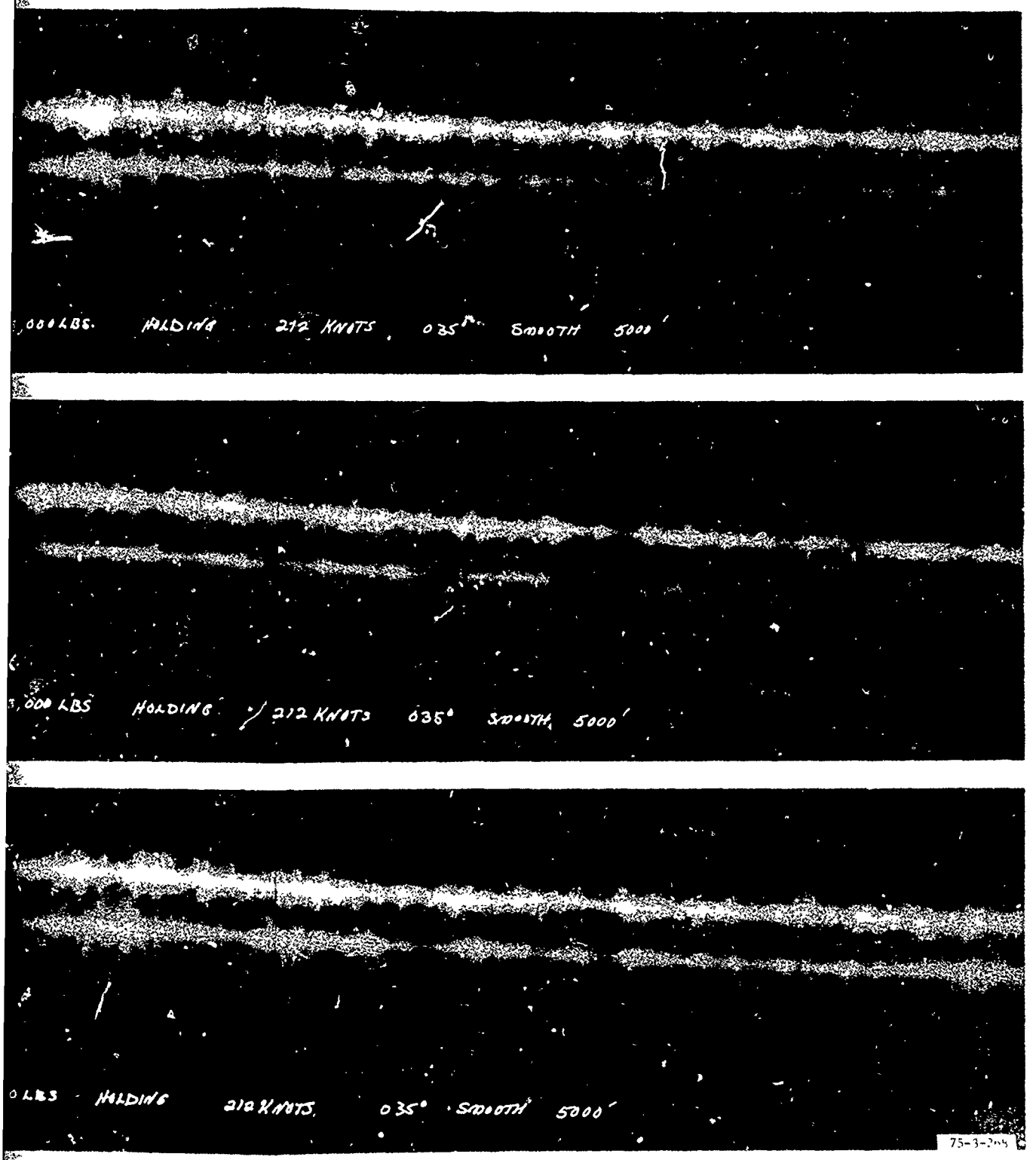

UPPER AIR FLOW VISUALIZATION (K-38). CONVAIR 880, HOLDING CONFIGURATION. H_p = 5,000 FEET (Sheet 2 of 4)

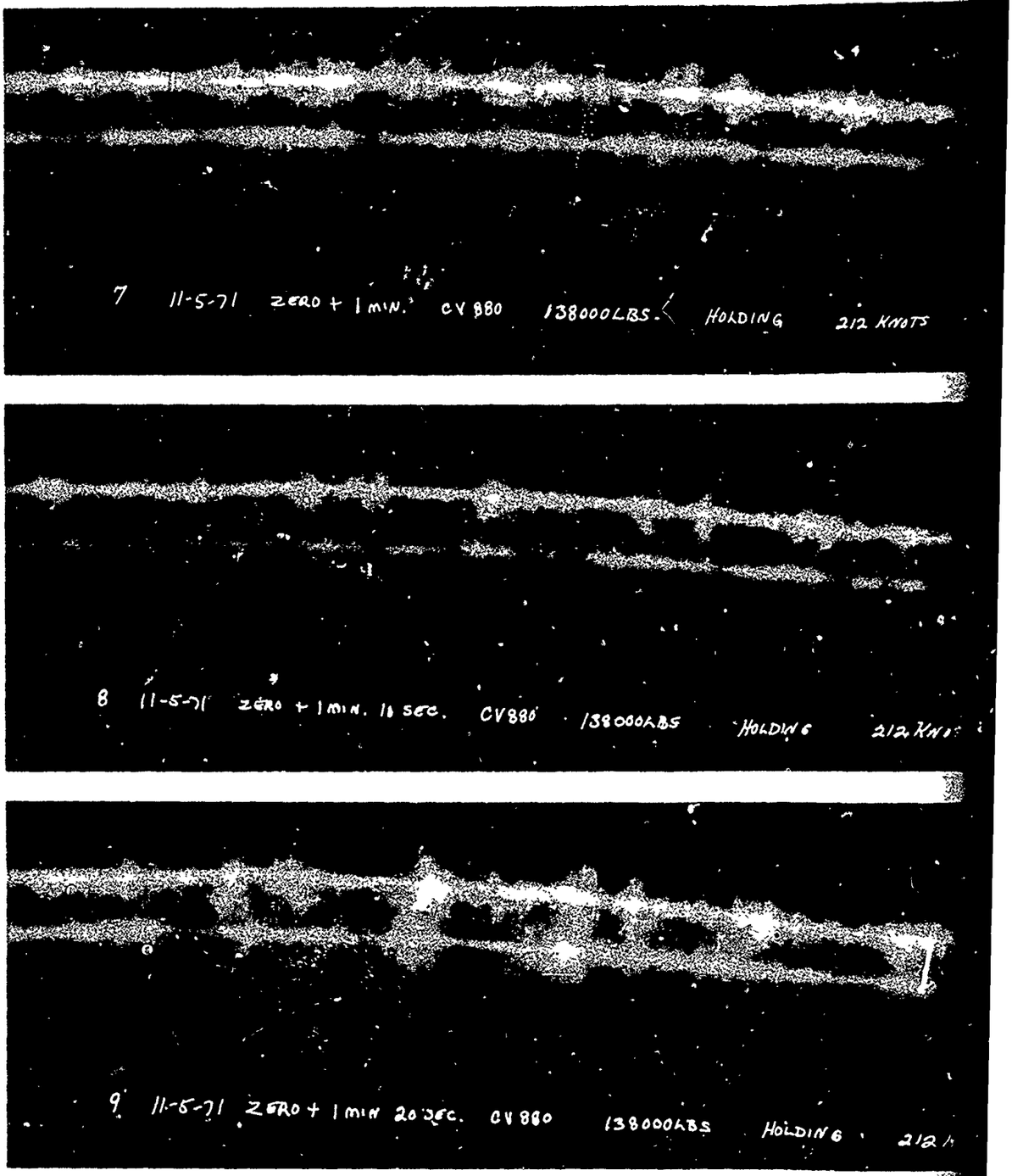

FIGURE C-1. UPPER AIR FLOW VISUALIZATION (K-38). CONFIGURATION. H_p = 5,000 FEET (Sh

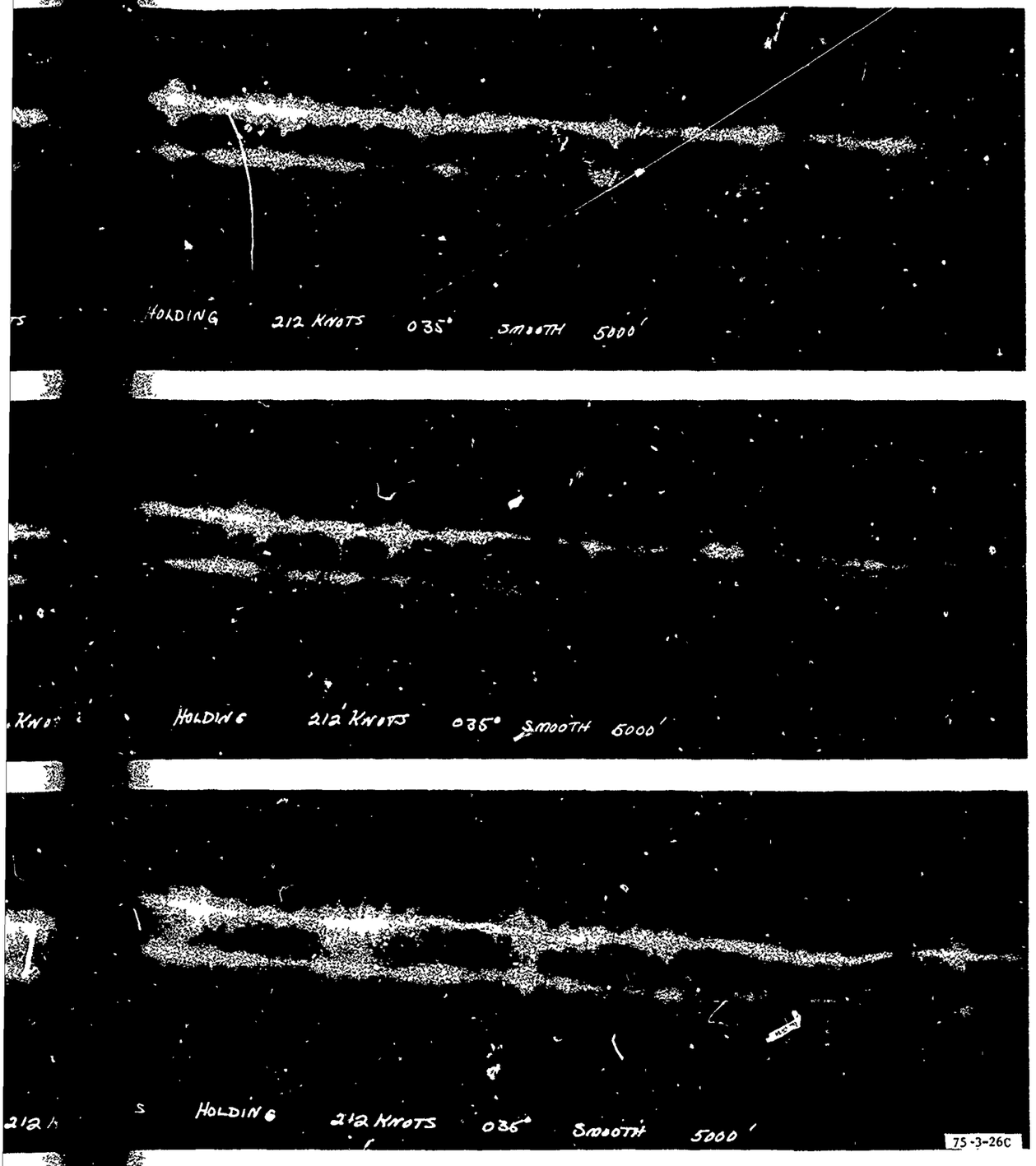

...OW VISUALIZATION (K-38). CONVAIR 880, HOLDING
...N. H_p = 5,000 FEET (Sheet 3 of 4)

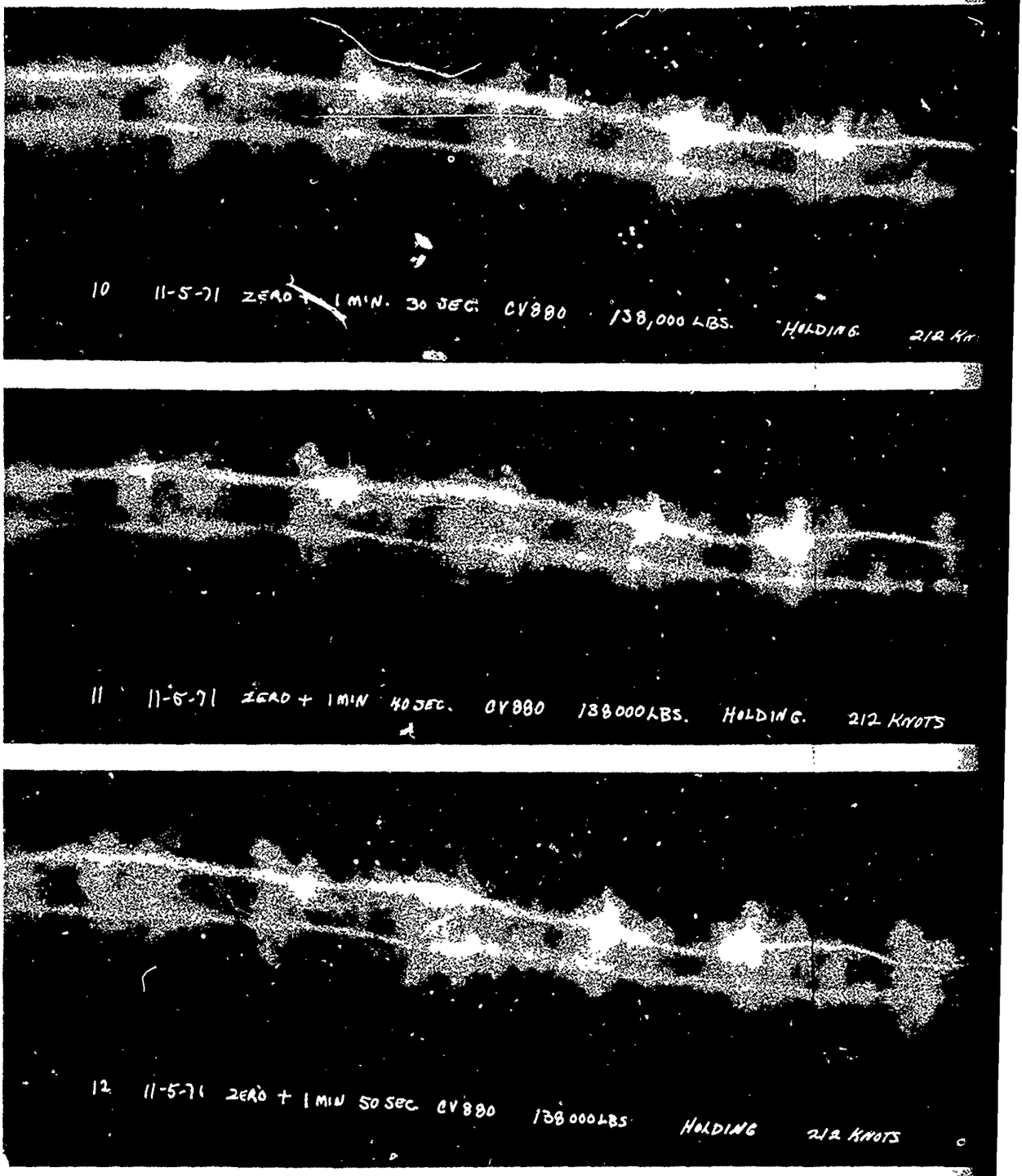

FIGURE C-1. UPPER AIR FLOW VISUALIZATION (K-38). CON
CONFIGURATION. H_p = 5,000 FEET (Sheet 4

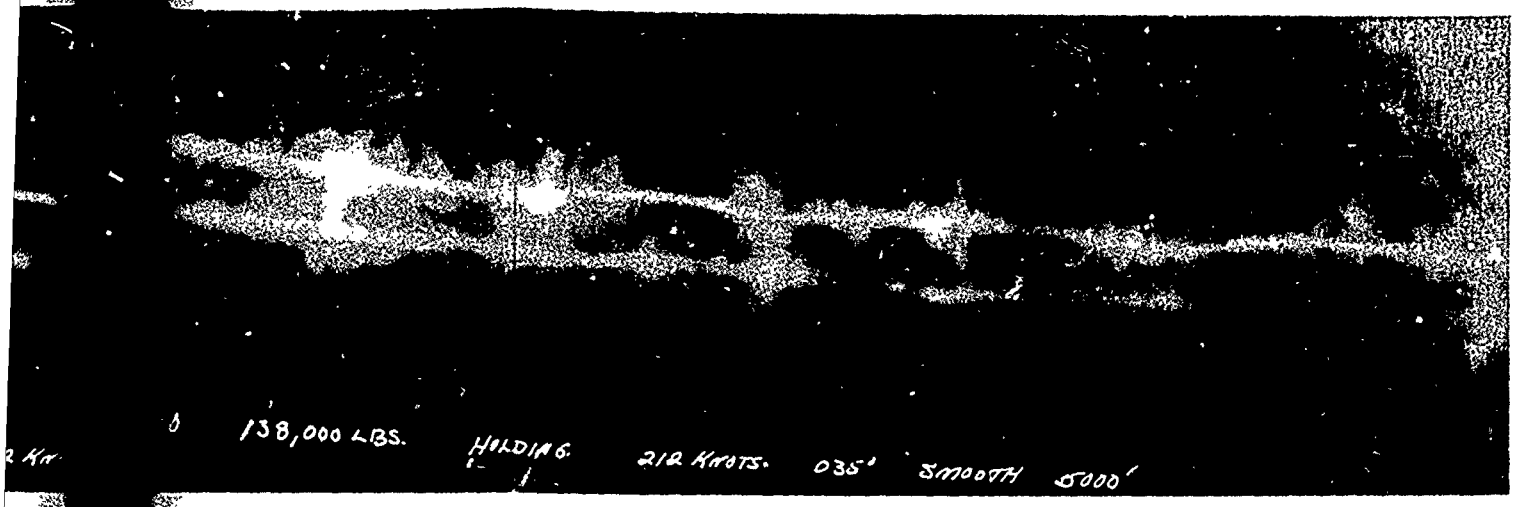

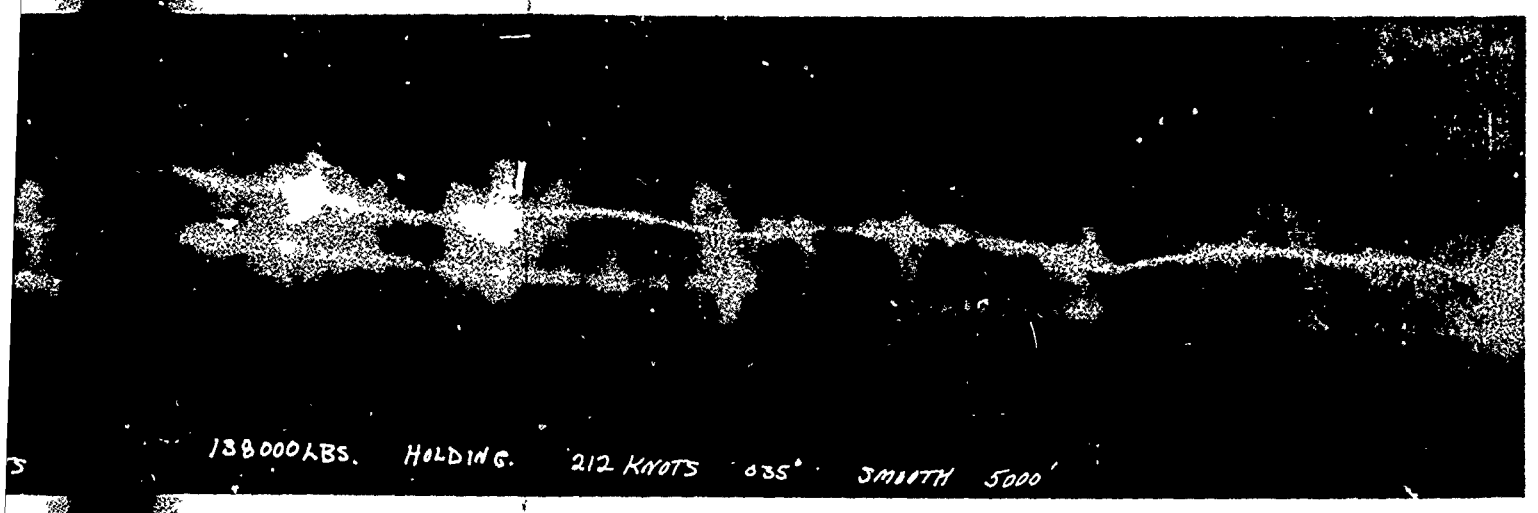

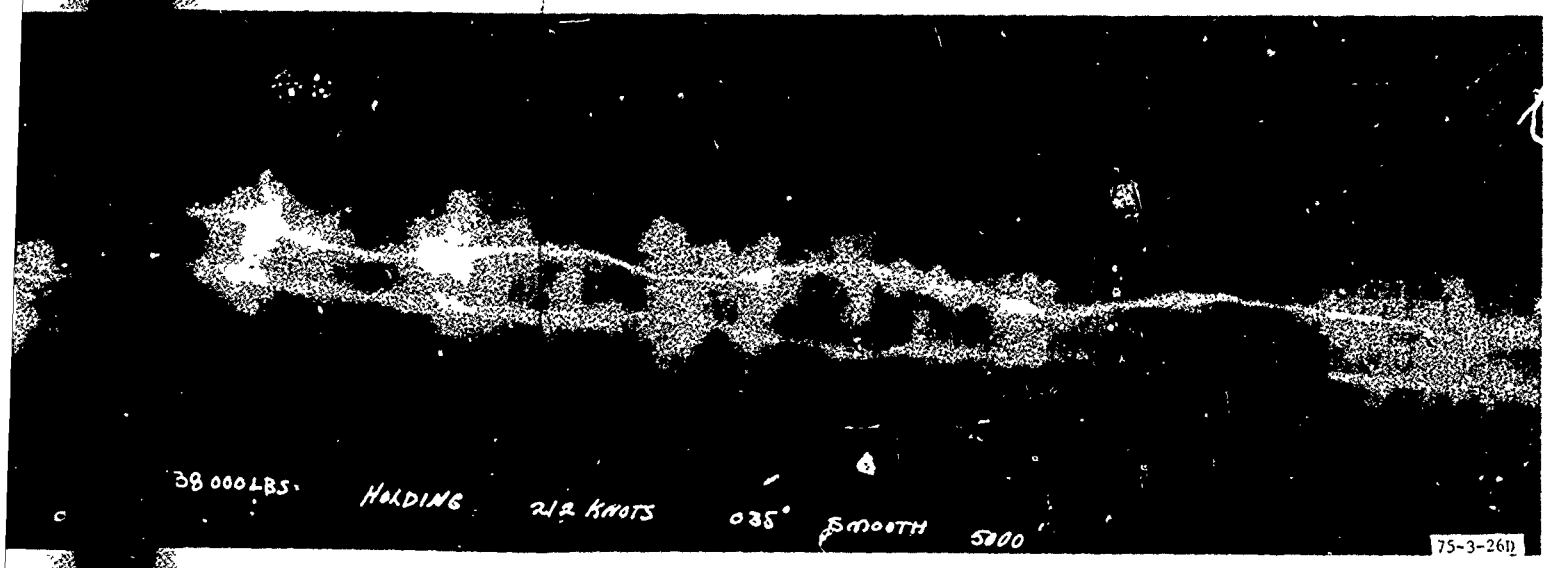

UPPER AIR FLOW VISUALIZATION (K-38). CONVAIR 880, HOLDING CONFIGURATION. H_p = 5,000 FEET (Sheet 4 of 4)

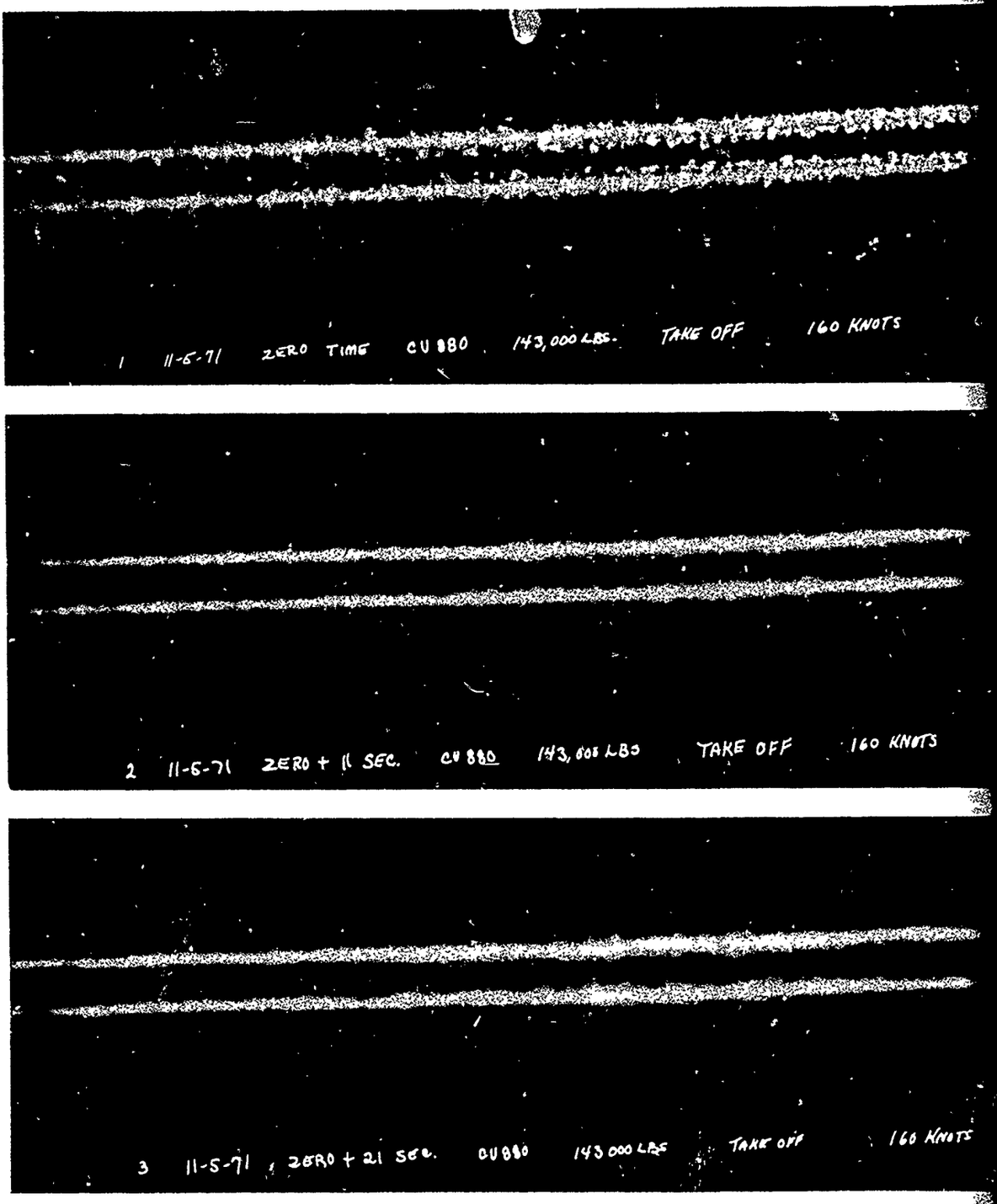

FIGURE C-2. UPPER AIR FLOW VISUALIZATION (K-38).
CONFIGURATION. H_p = 5,000 FEET (She

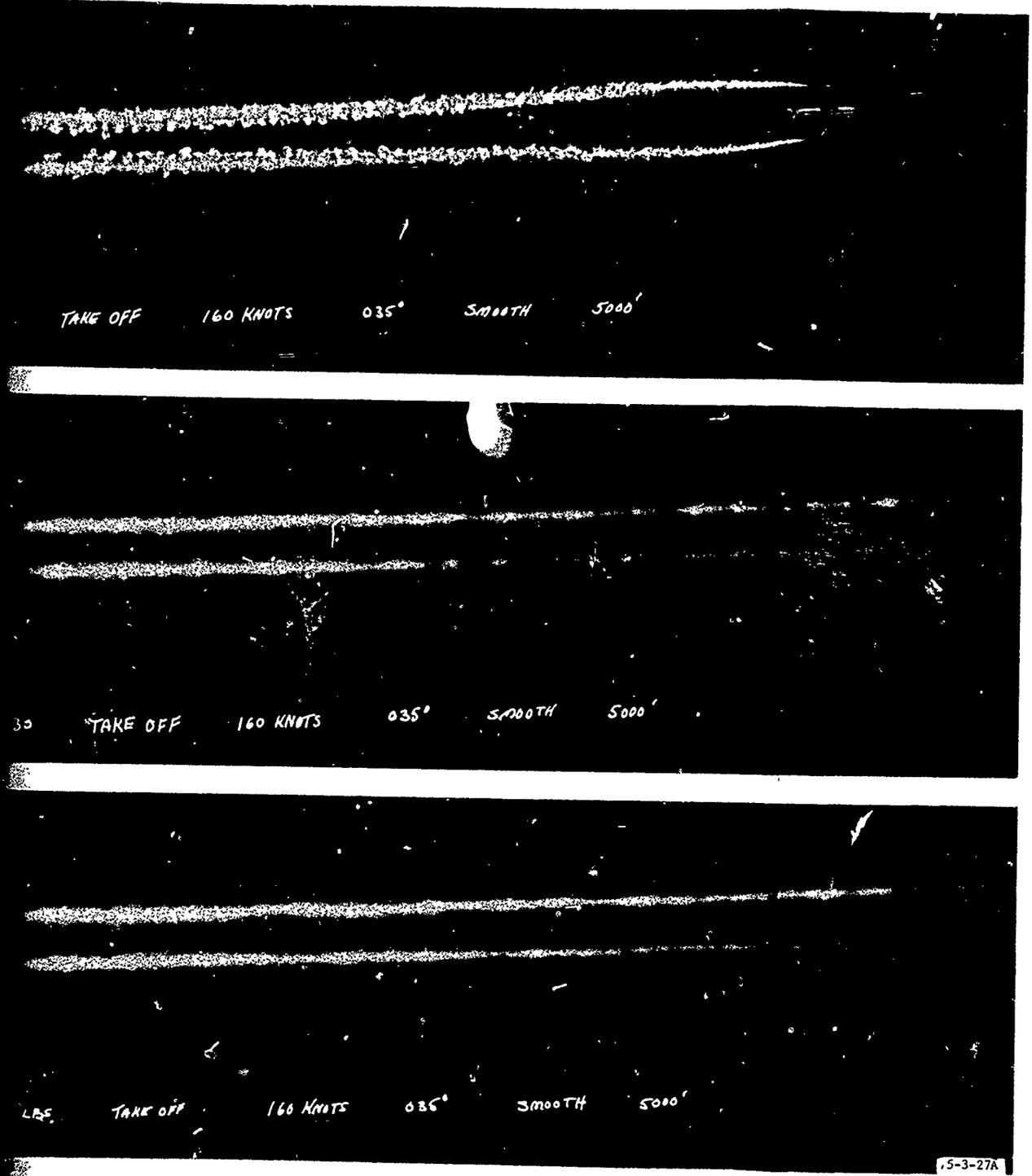

R AIR FLOW VISUALIZATION (K-38). CONVAIR 880, TAKEOFF
IGURATION. H_p = 5,000 FEET (Sheet 1 of 4)

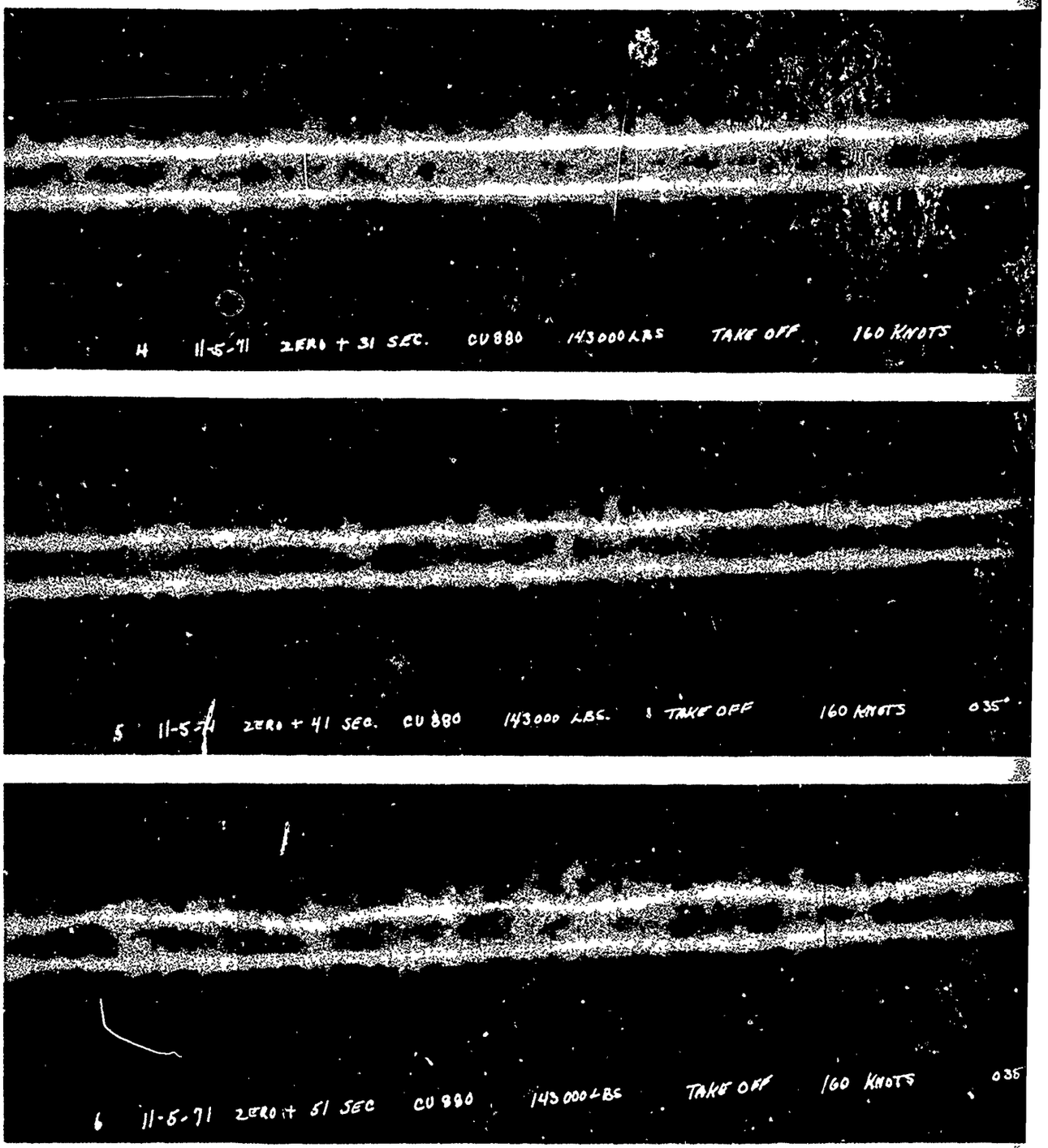

FIGURE C-2. UPPER AIR FLOW VISUALIZATION (K-38). CONVAIR CONFIGURATION. H_p = 5,000 FEET (Sheet 2 of 4

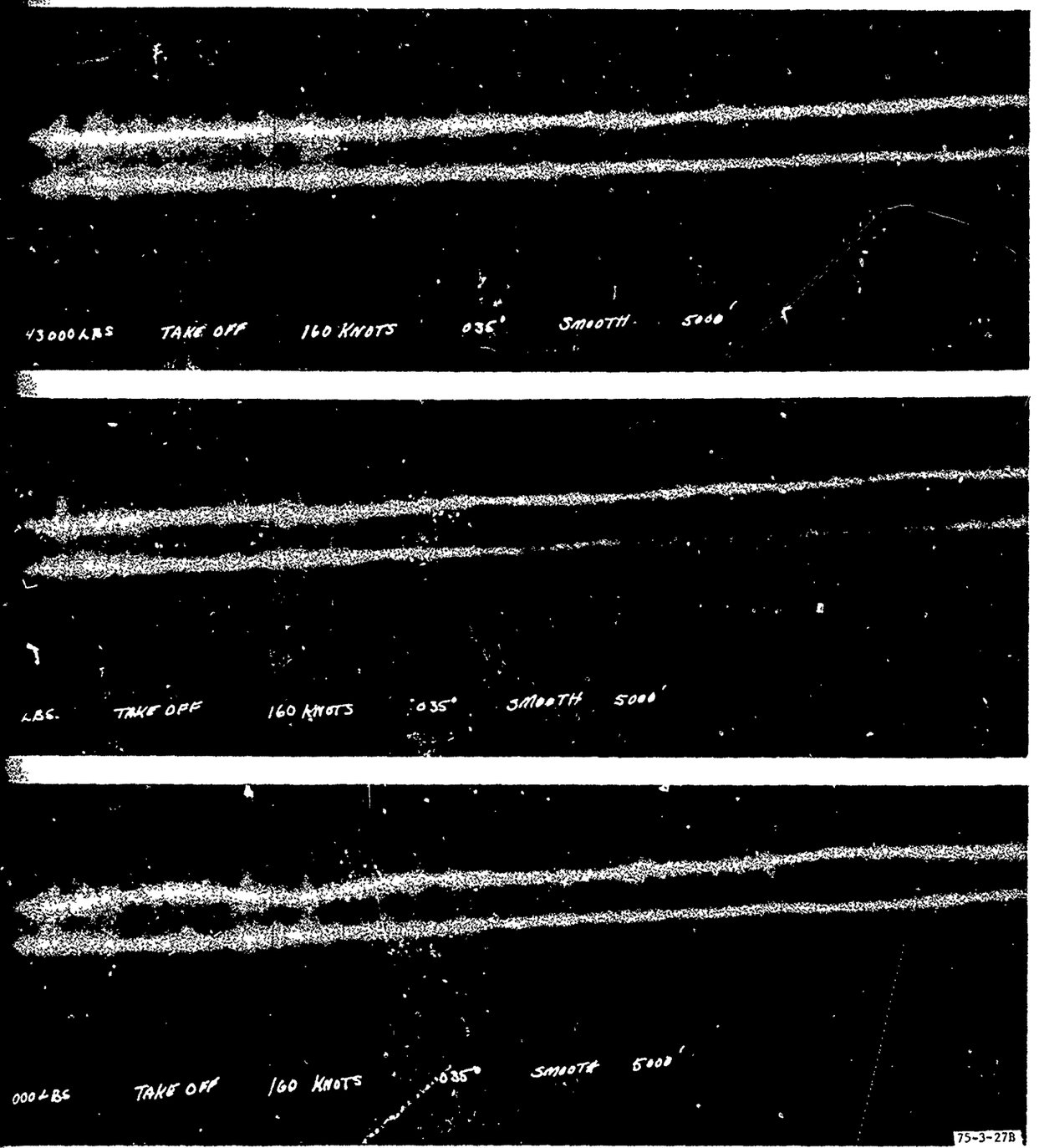

UPPER AIR FLOW VISUALIZATION (K-38). CONVAIR 880, TAKEOFF CONFIGURATION. H_p = 5,000 FEET (Sheet 2 of 4)

2

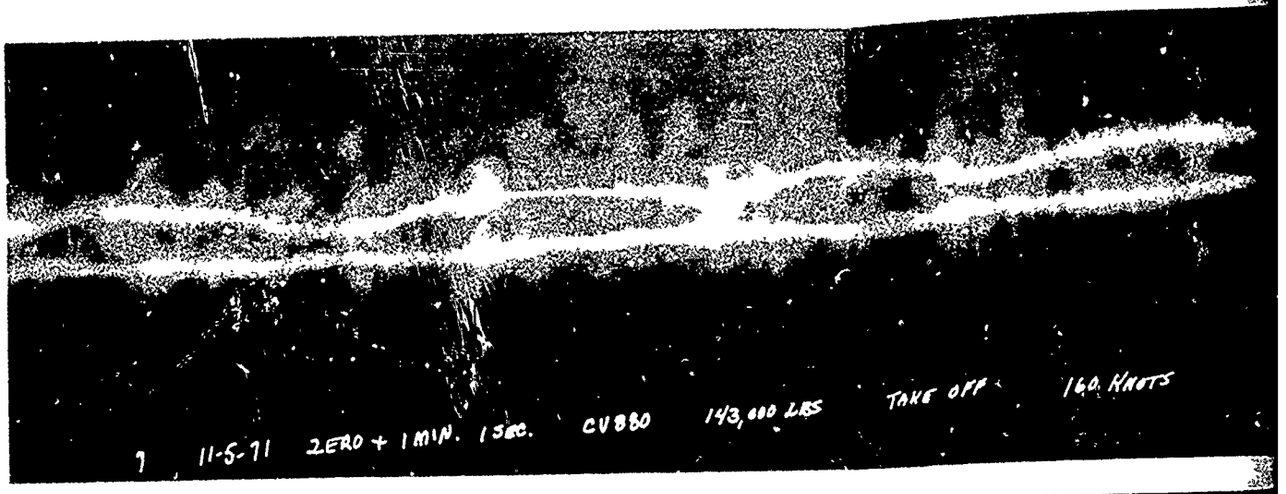

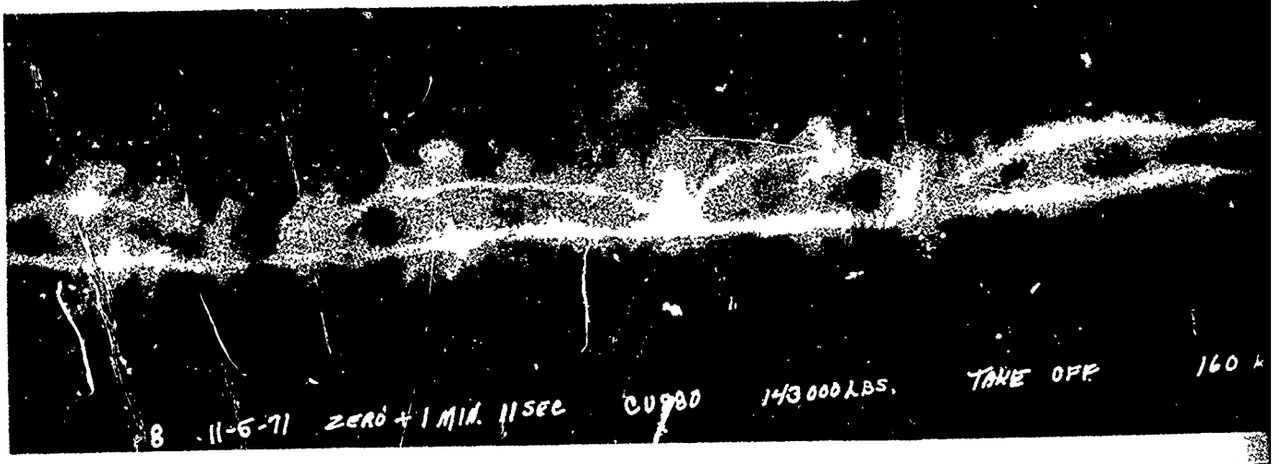

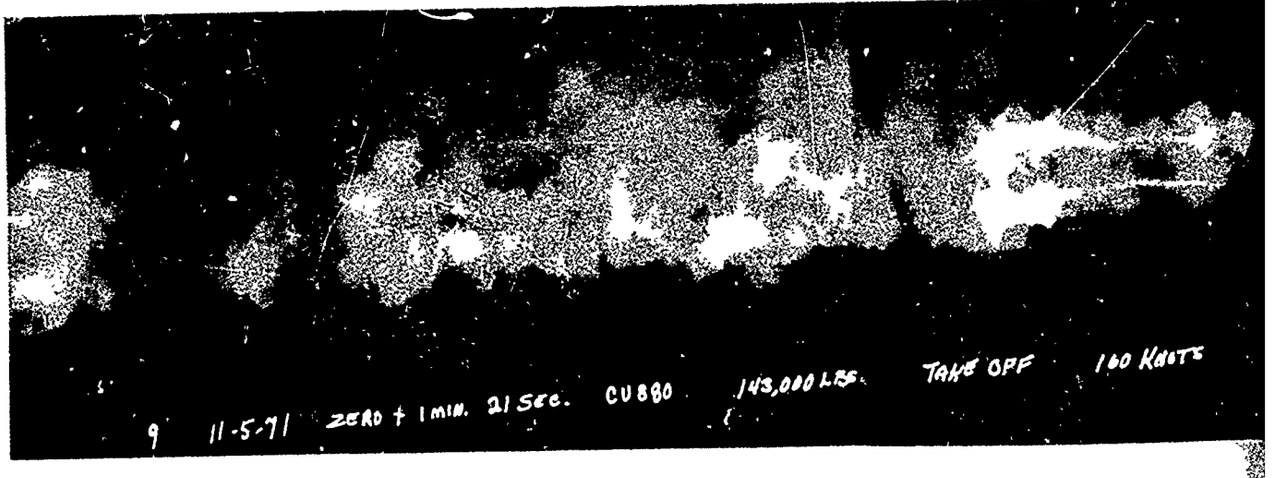

FIGURE C-2. UPPER AIR FLOW VISUALIZATION (K-38). CONVAIR CONFIGURATION. H_p = 5,000 FEET (Sheet 3 of

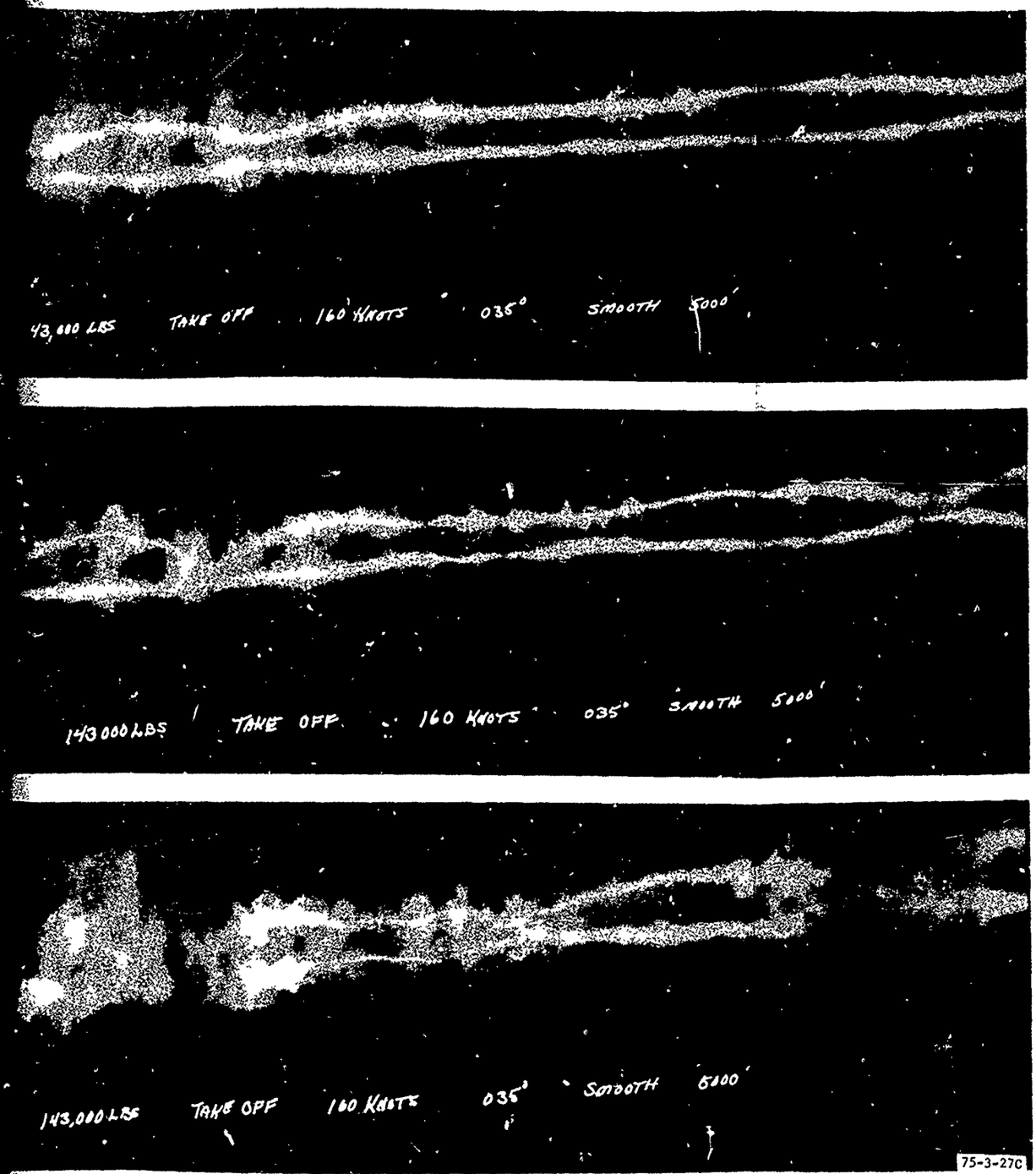

UPPER AIR FLOW VISUALIZATION (K-38). CONVAIR 880, TAKEOFF CONFIGURATION. H_p = 5,000 FEET (Sheet 3 of 4)

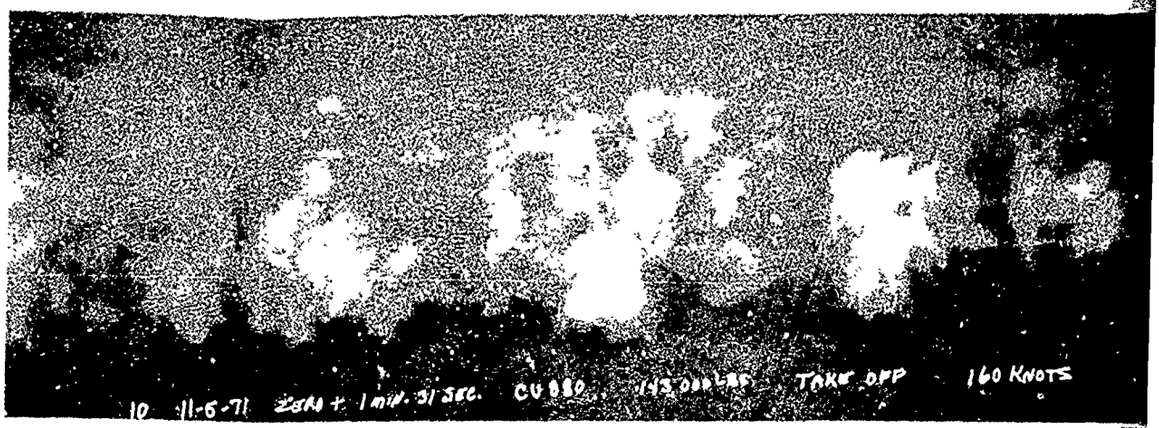

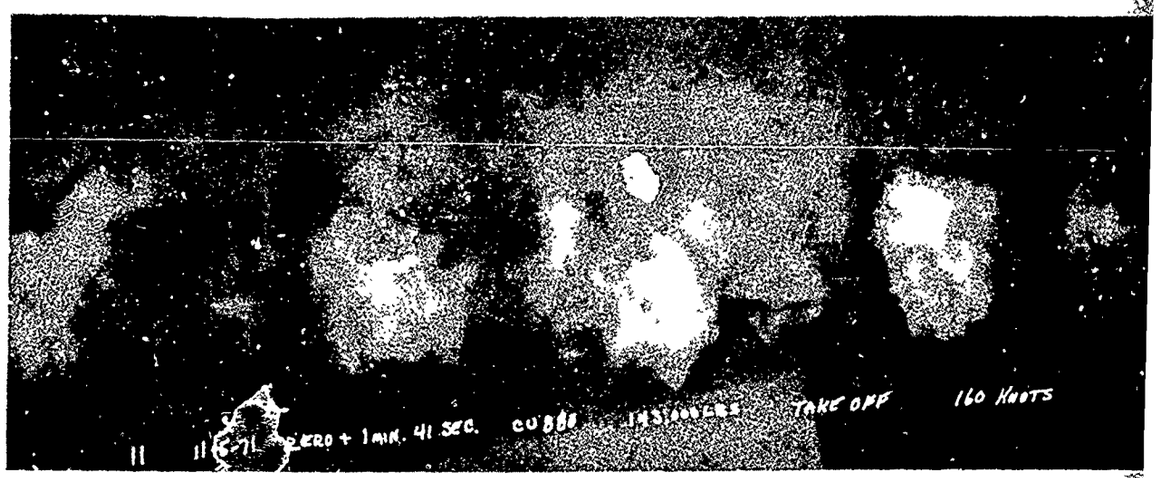

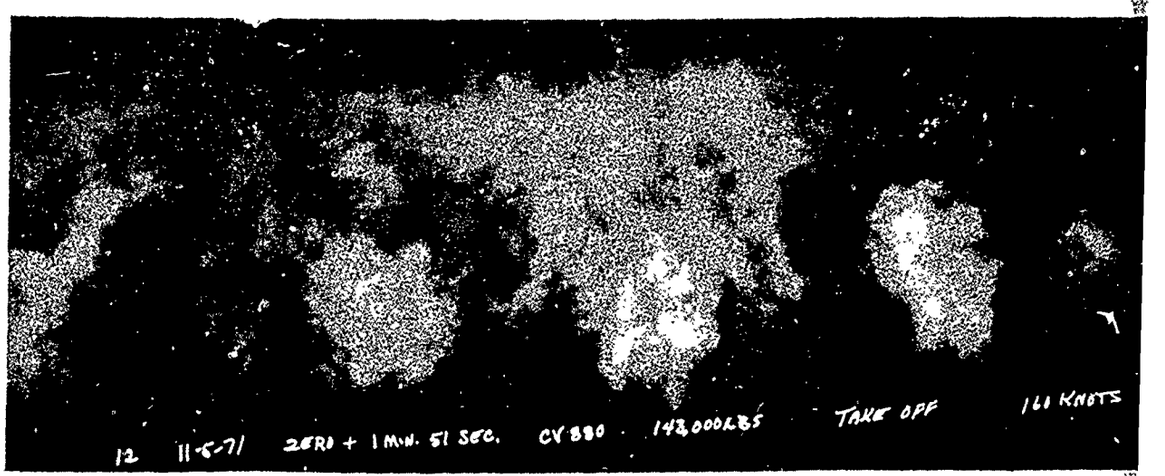

FIGURE C-2. UPPER AIR FLOW VISUALIZATION (K-38). CONV
CONFIGURATION. H_p = 5,000 FEET (Sheet 4 o

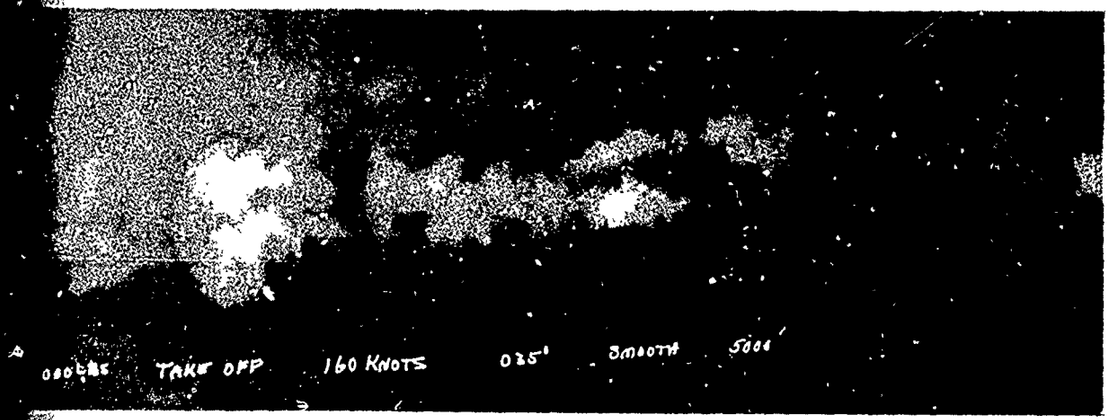

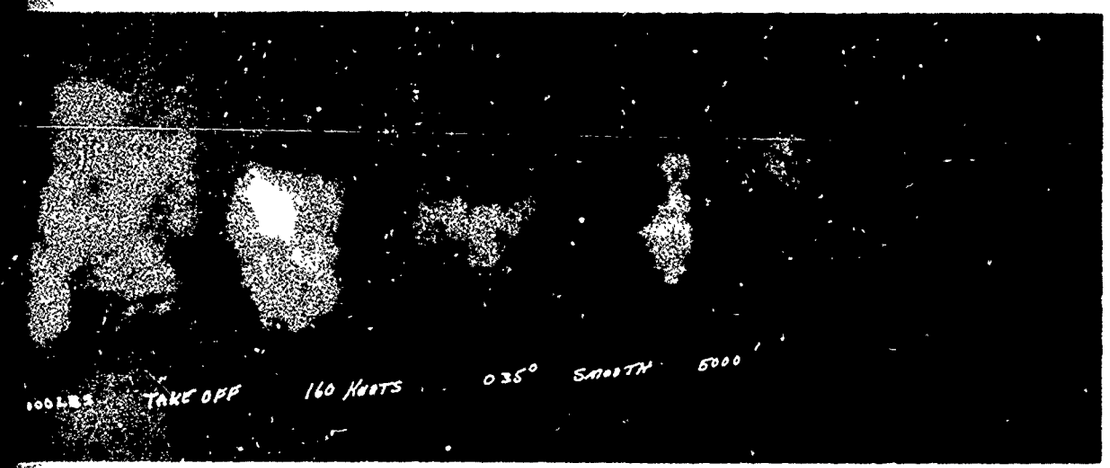

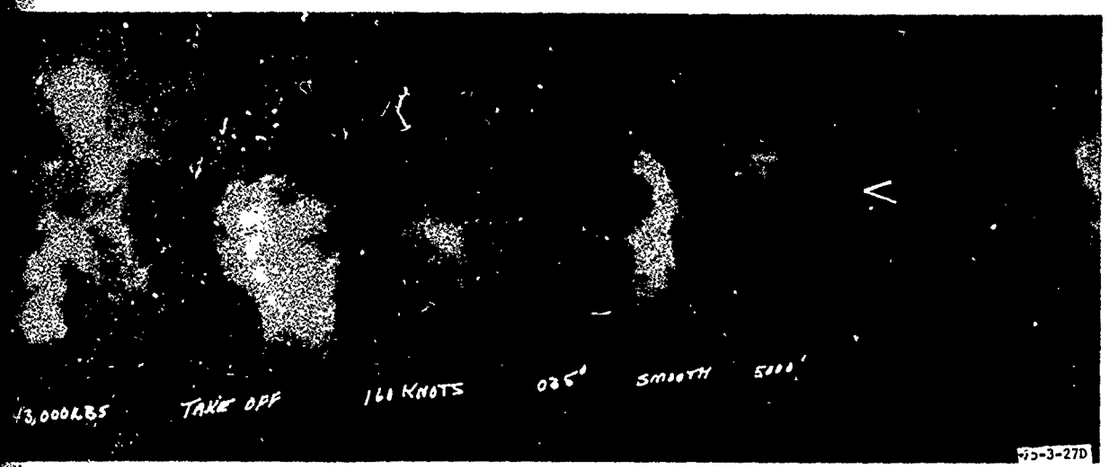

FD-3-27D

). CONV
heet 4 o

AIR FLOW VISUALIZATION (K-38). CONVAIR 880. TAKEOFF
IGURATION. H_p = 5,000 FEET (Sheet 4 of 4)

C-8

C-8

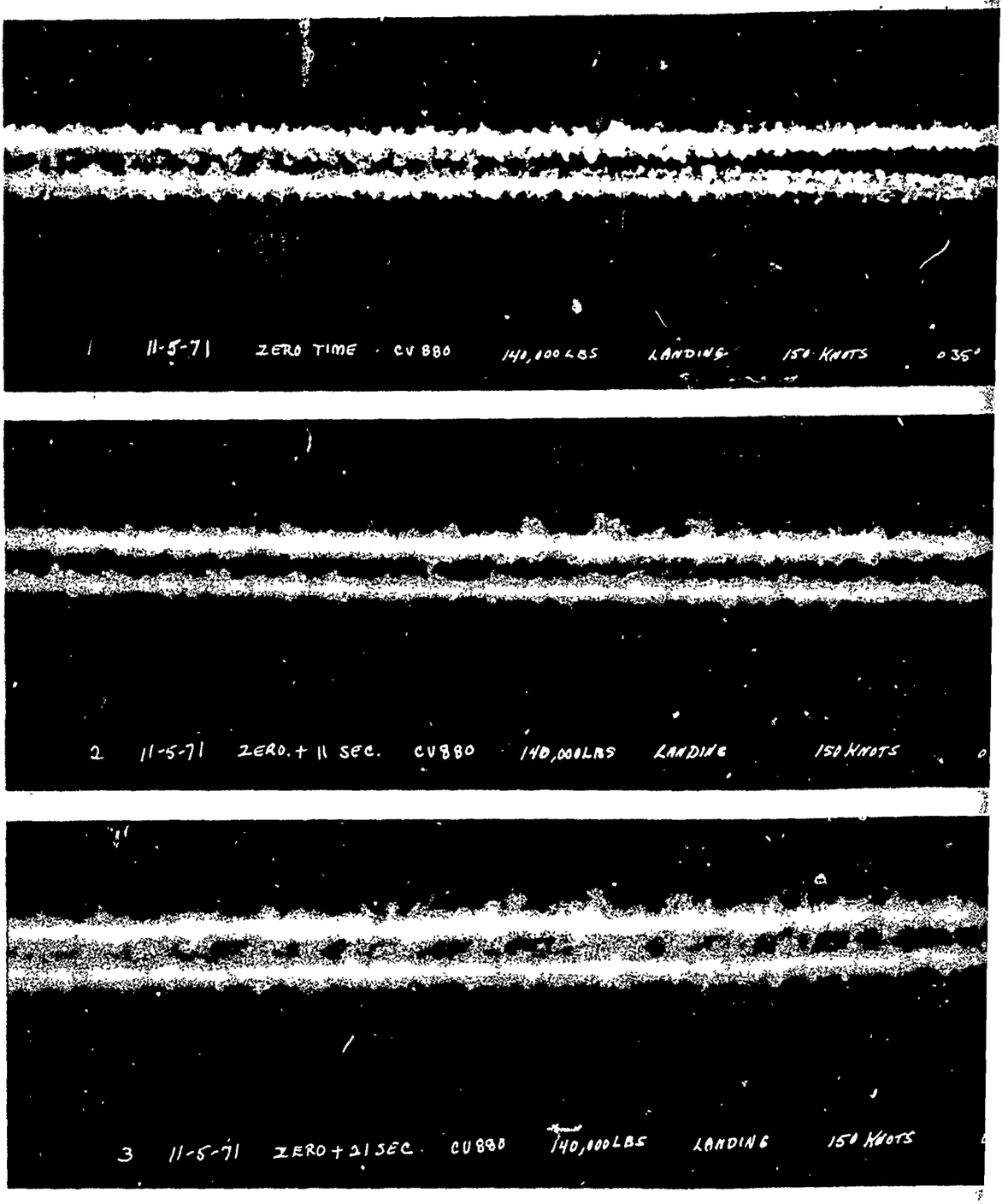

FIGURE C-3. UPPER AIR FLOW VISUALIZATION (K-38). CONFIGURATION. H_p = 5,000 FEET (Sheet

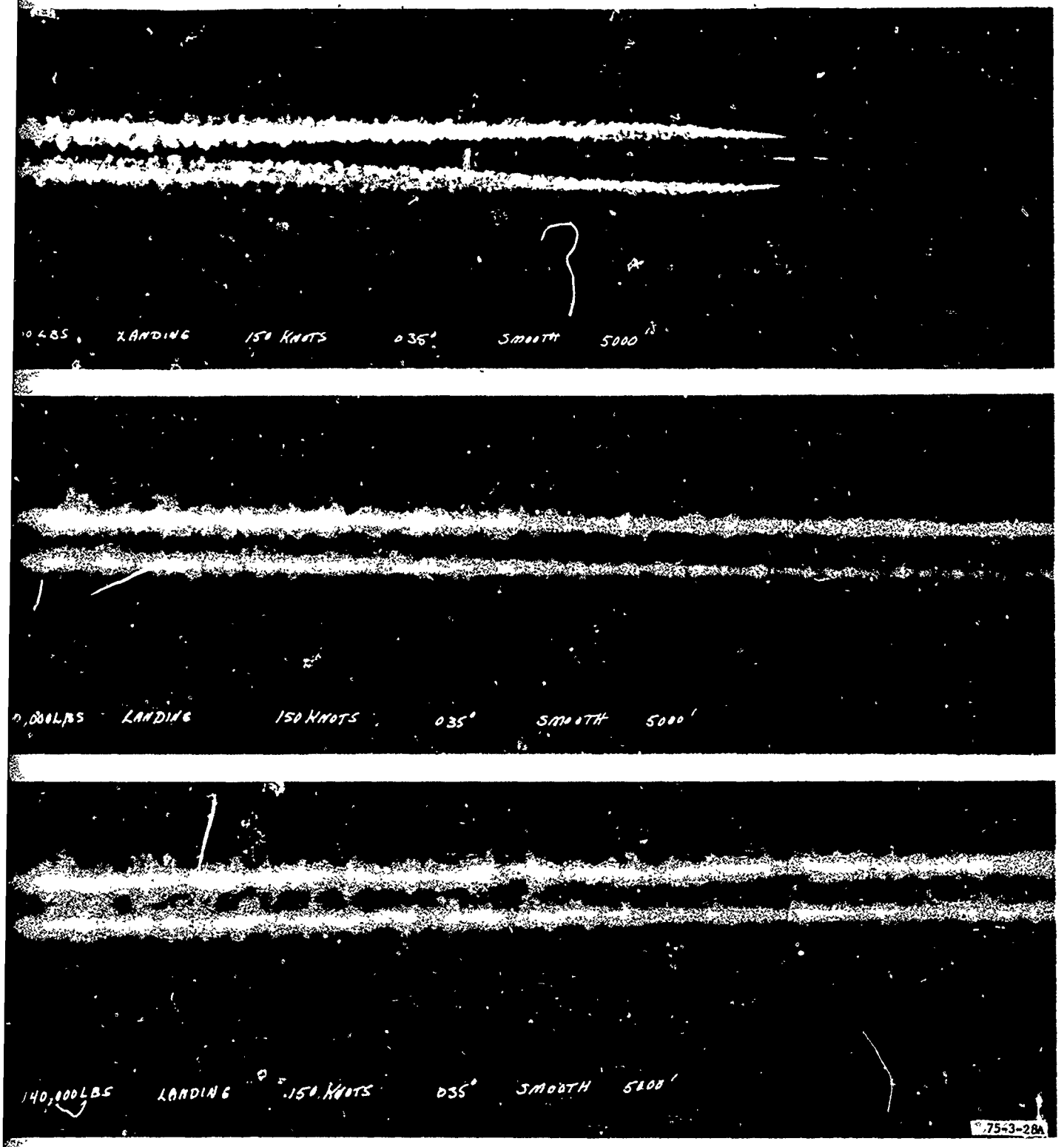

3. UPPER AIR FLOW VISUALIZATION (K-38). CONVAIR 880, LANDING CONFIGURATION. H_p = 5,000 FEET (Sheet 1 of 4)

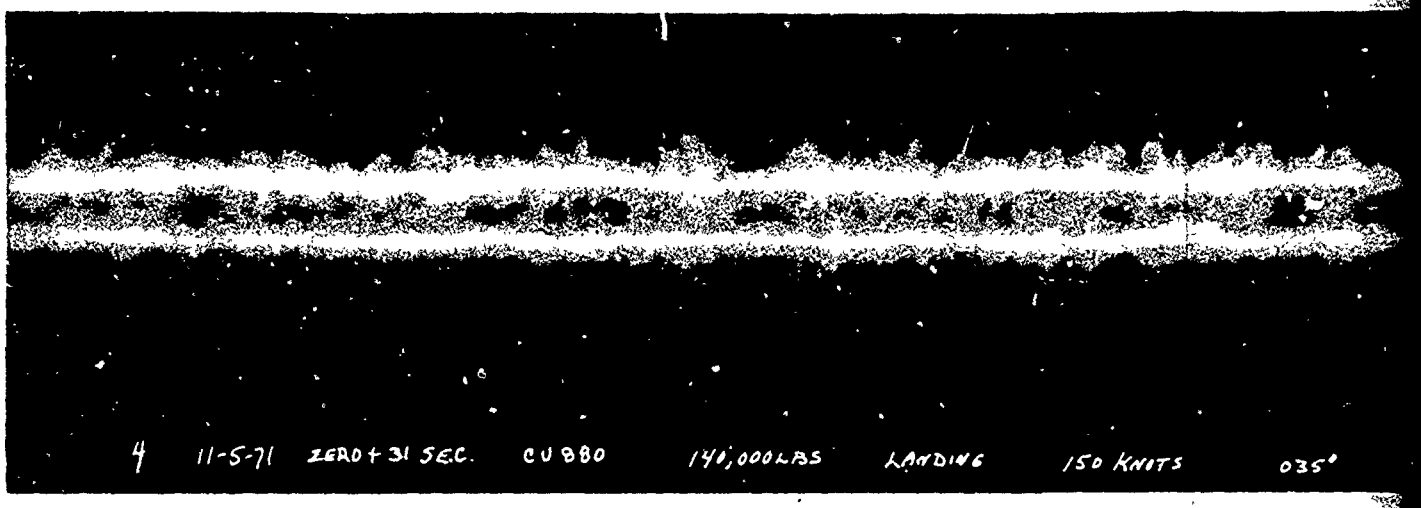

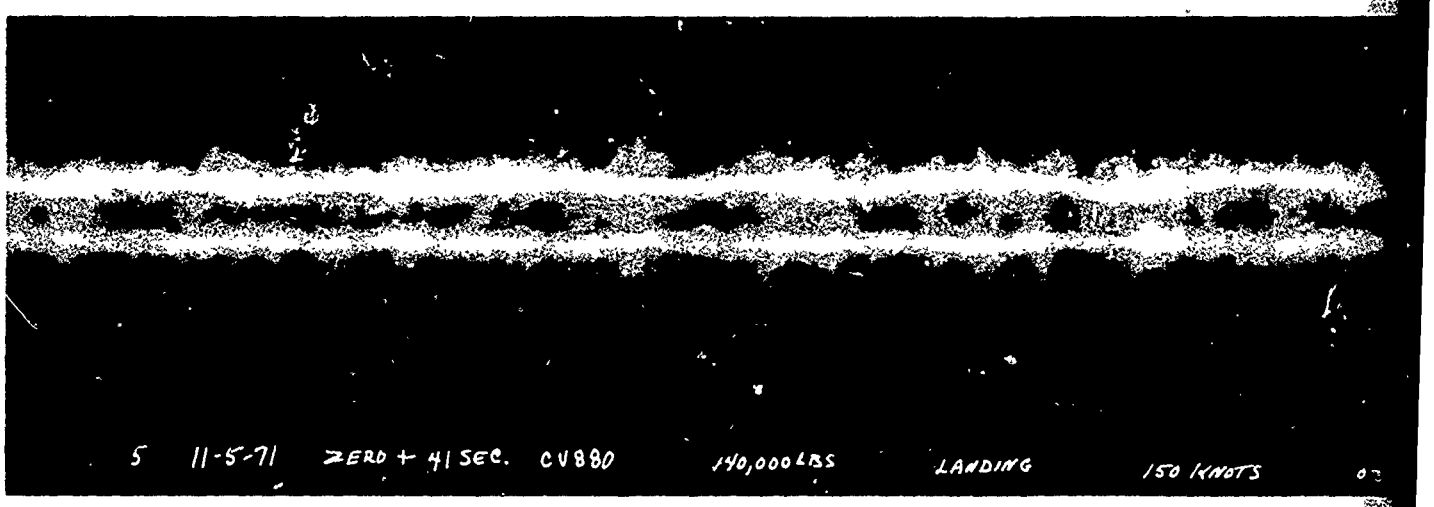

FIGURE C-3. UPPER AIR FLOW VISUALIZATION (K-38). CONVAIR CONFIGURATION. H_p = 5,000 FEET (Sheet 2 of

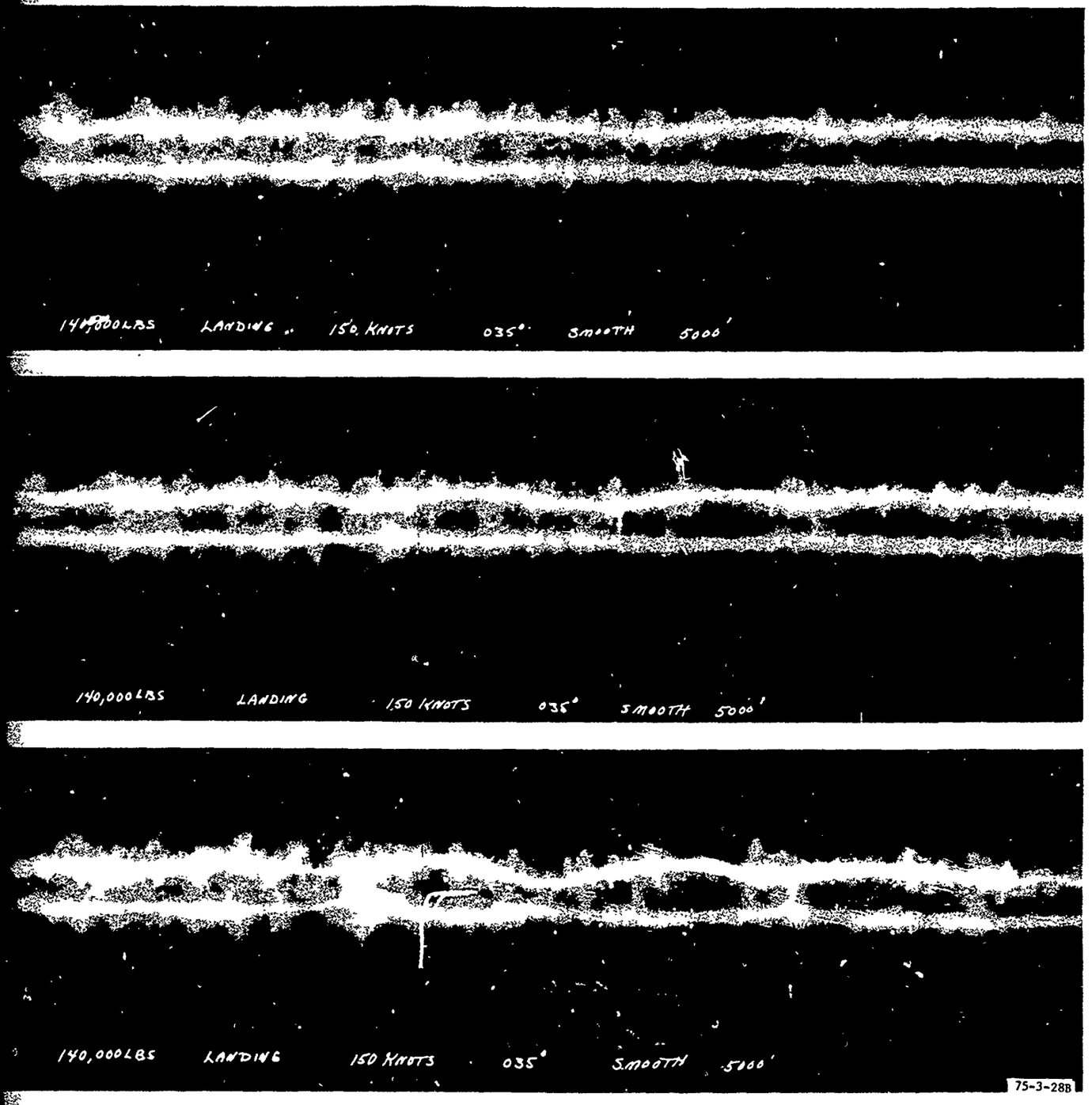

URE C-3. UPPER AIR FLOW VISUALIZATION (K-38). CONVAIR 880, LANDING CONFIGURATION. H_p = 5,000 FEET (Sheet 2 of 4)

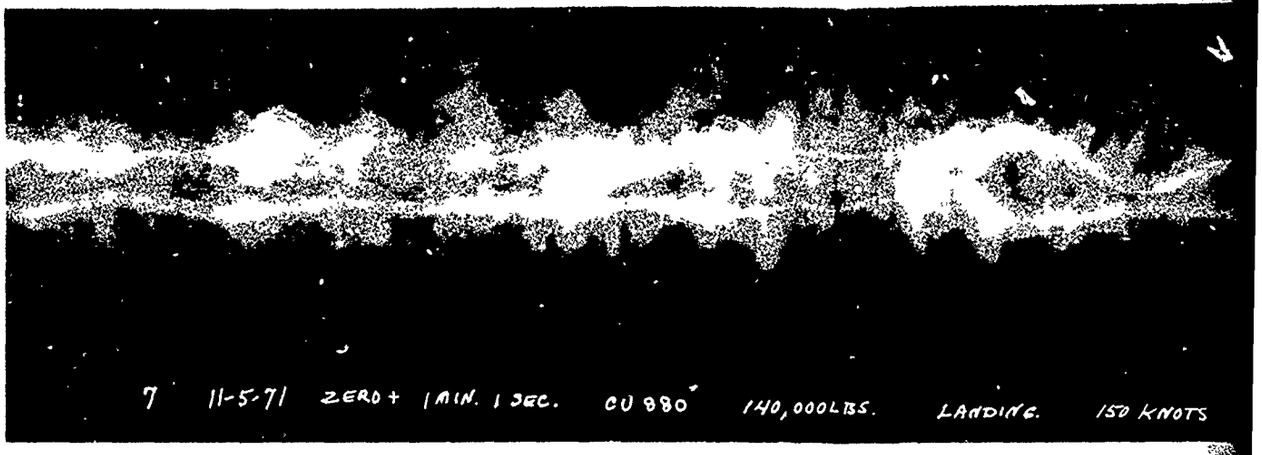

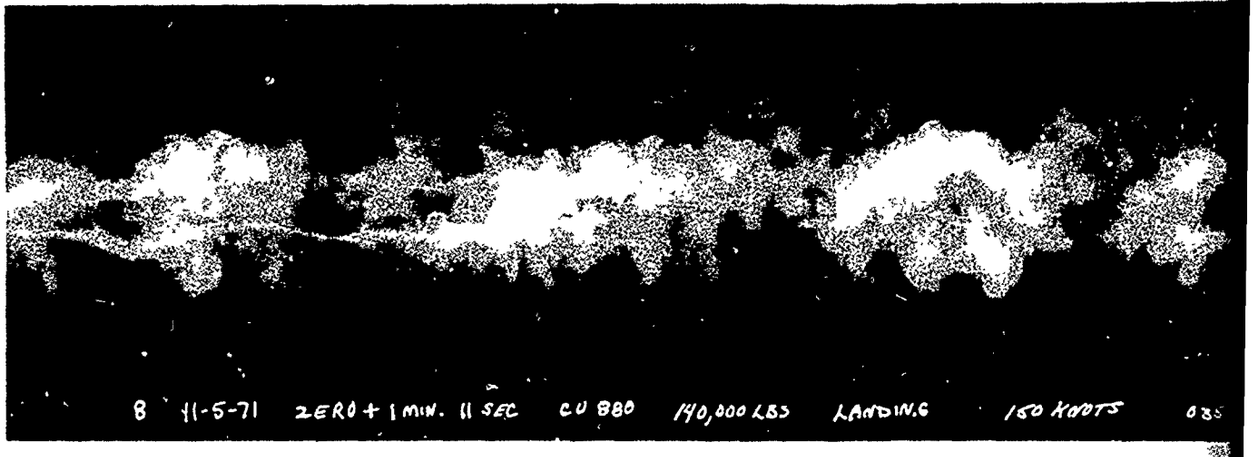

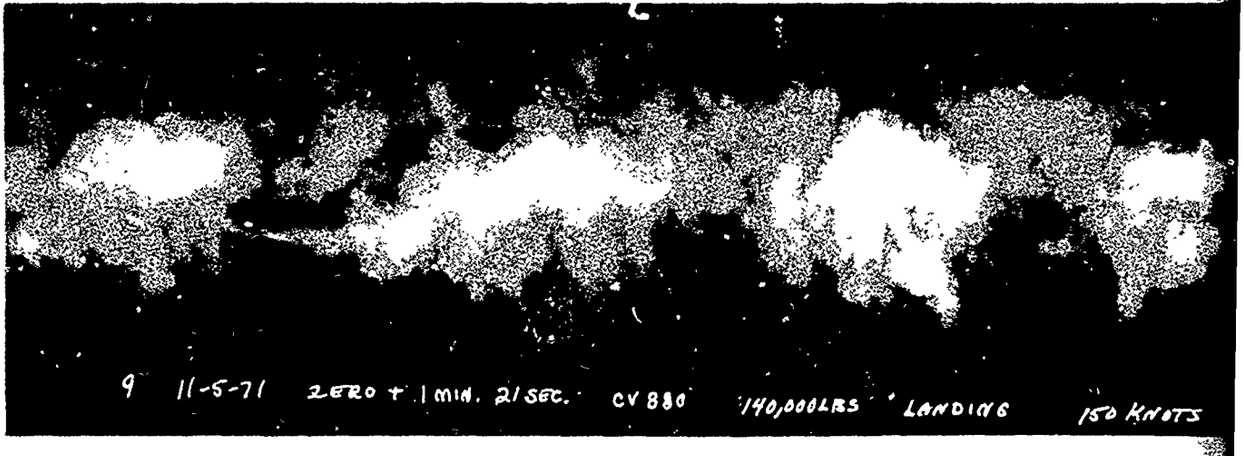

FIGURE C-3. UPPER AIR FLOW VISUALIZATION (K-38). CONV
CONFIGURATION. H_p = 5,000 FEET (Sheet 3 o

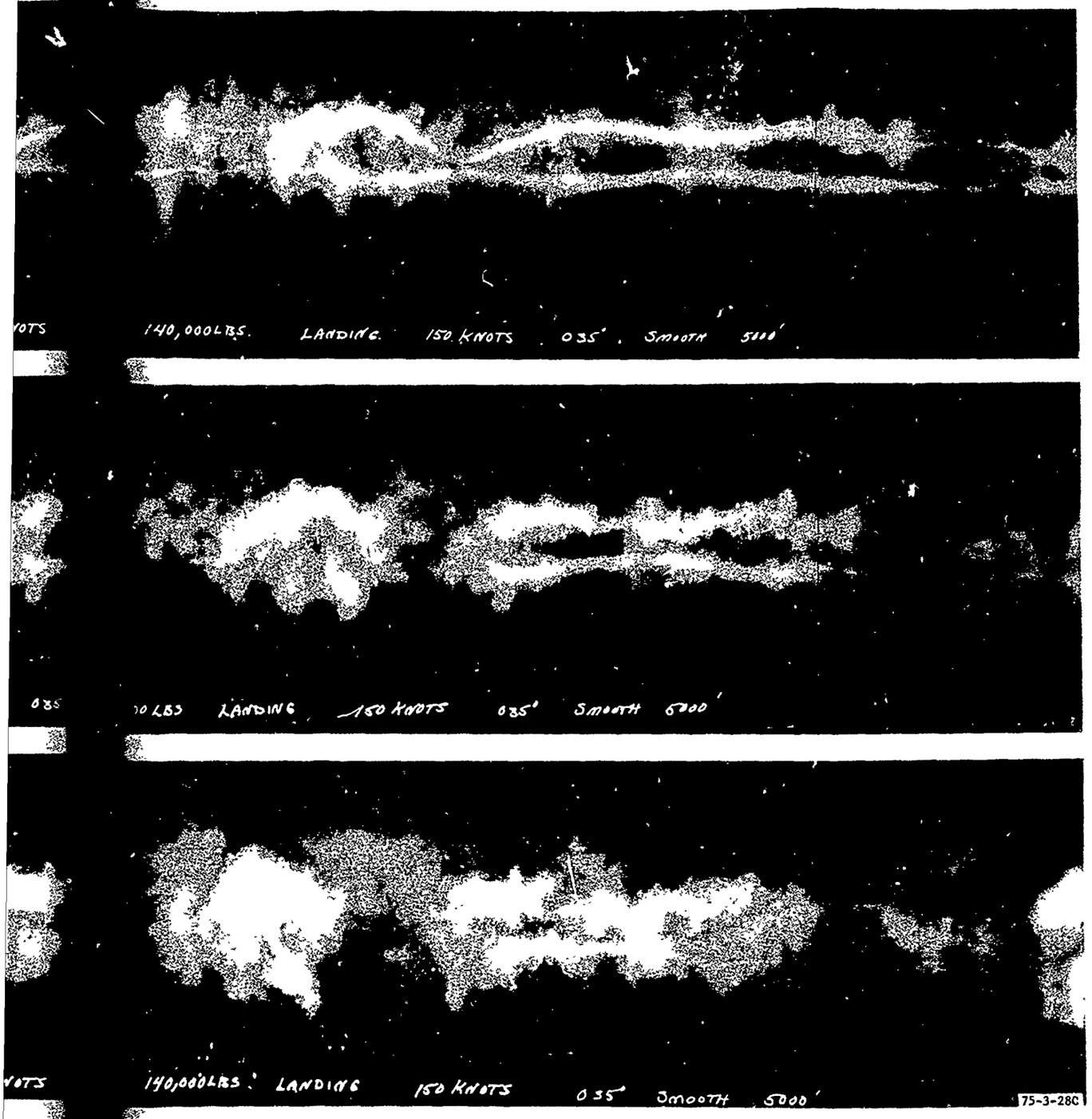

ER AIR FLOW VISUALIZATION (K-38). CONVAIR 880, LANDING
FIGURATION. H_p = 5,000 FEET (Sheet 3 of 4)

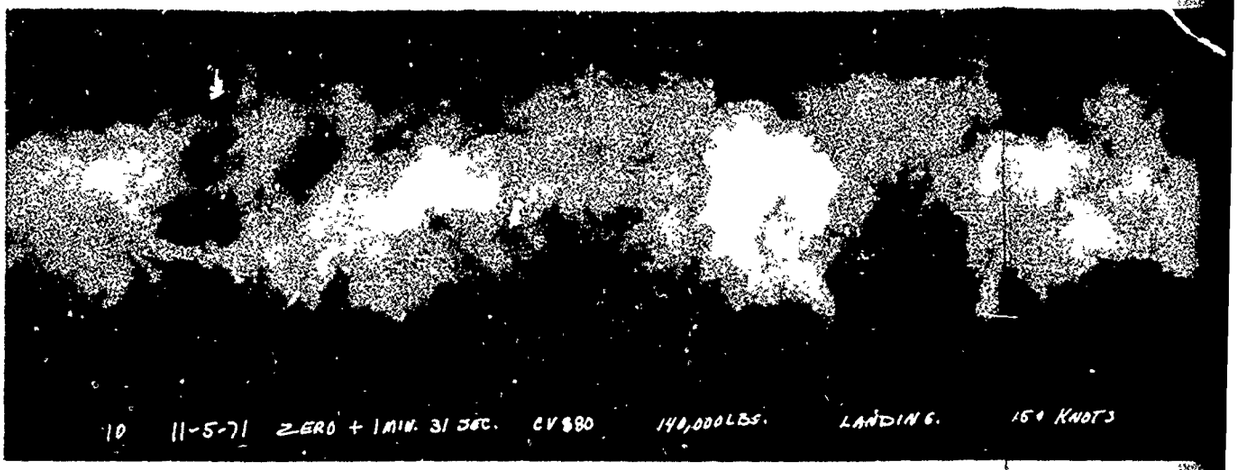

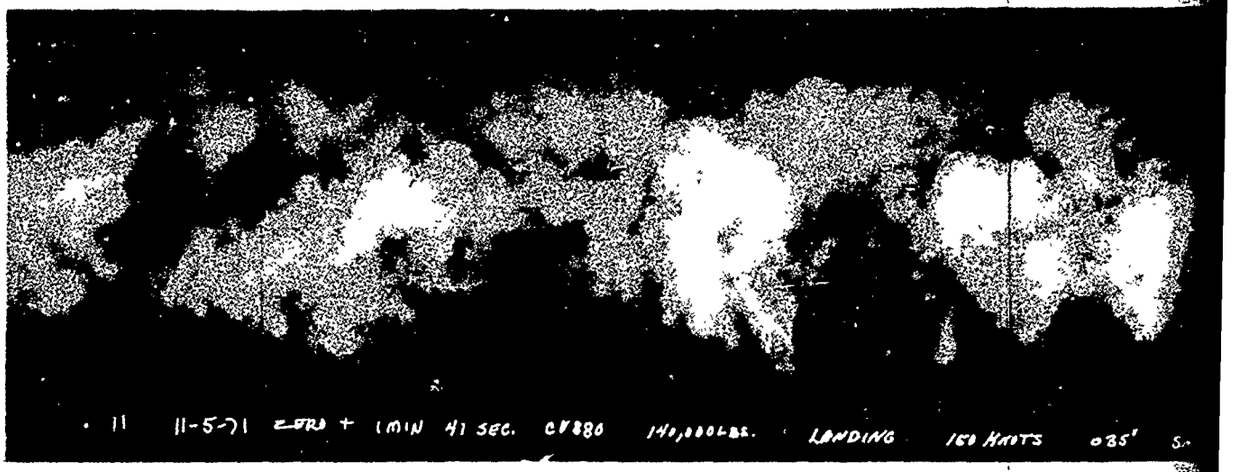

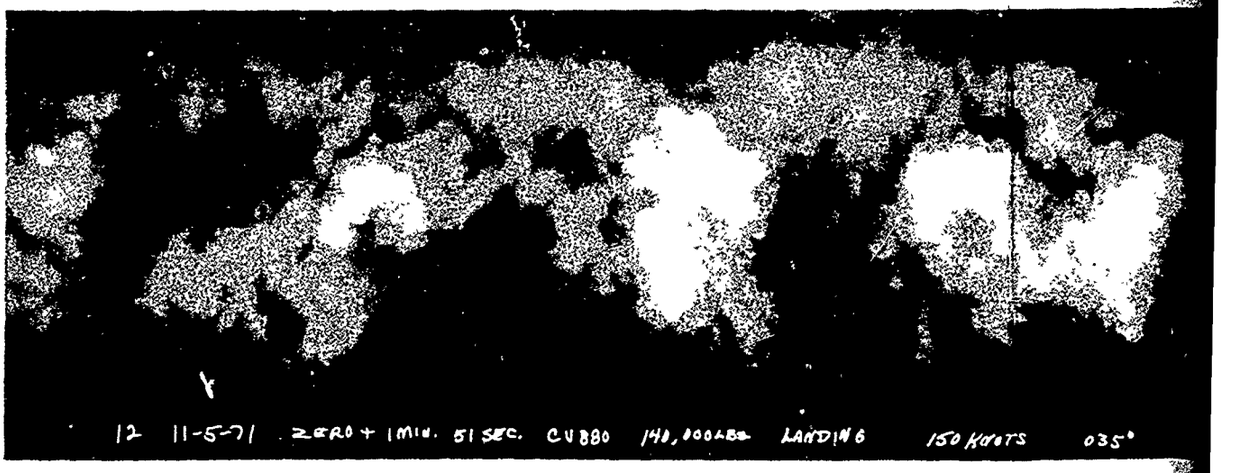

FIGURE C-3. UPPER AIR FLOW VISUALIZATION (K-38). CONVAIR CONFIGURATION. H_p = 5,000 FEET (Sheet 4 of 4)

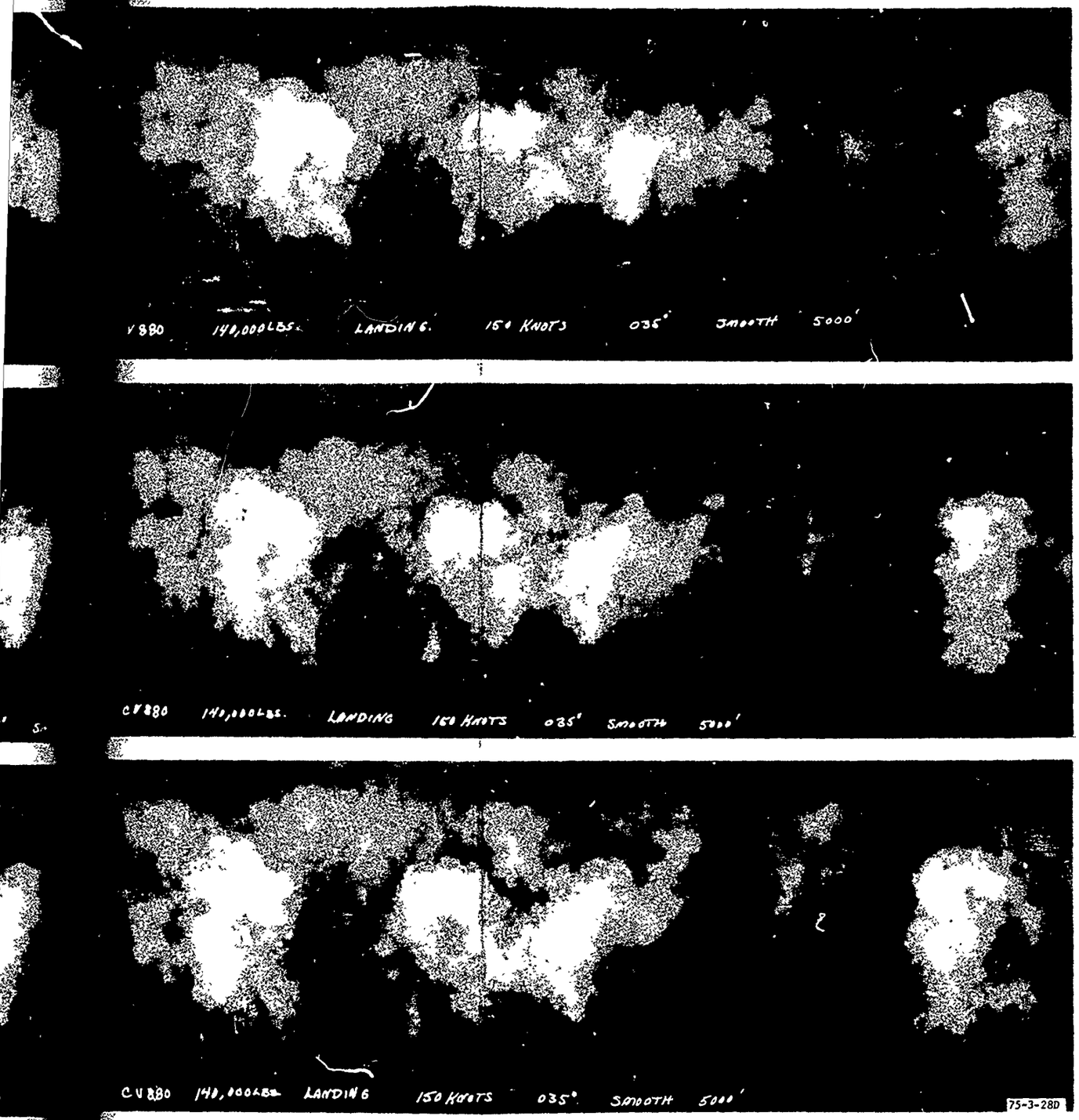

C-3. UPPER AIR FLOW VISUALIZATION (K-38). CONVAIR 880, LANDING CONFIGURATION. H_p = 5,000 FEET (Sheet 4 of 4)

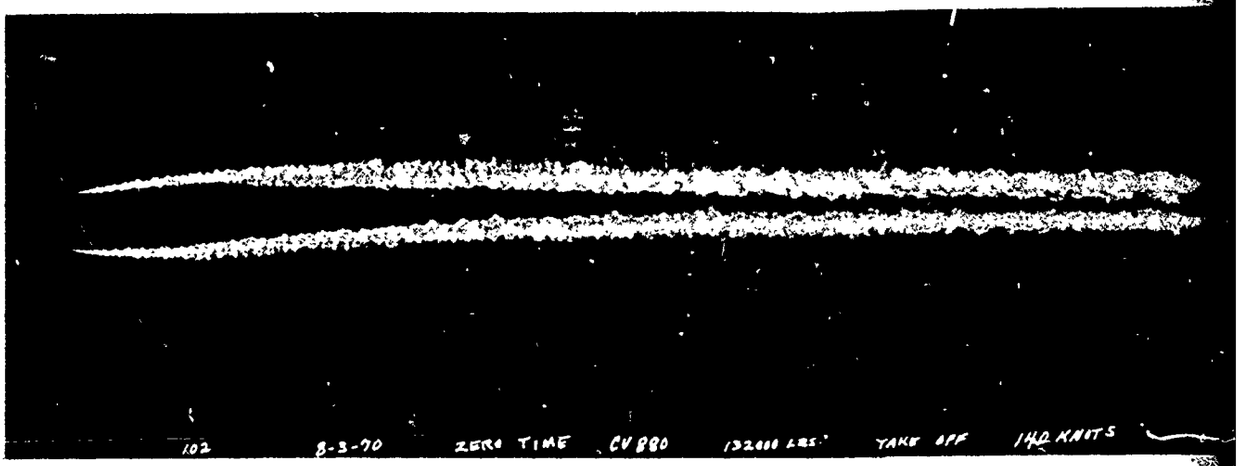

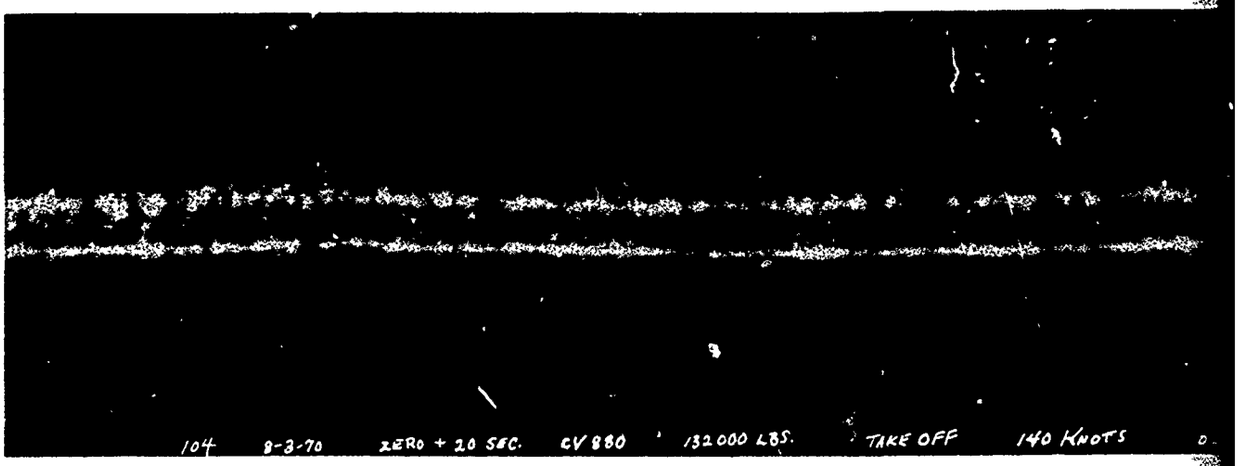

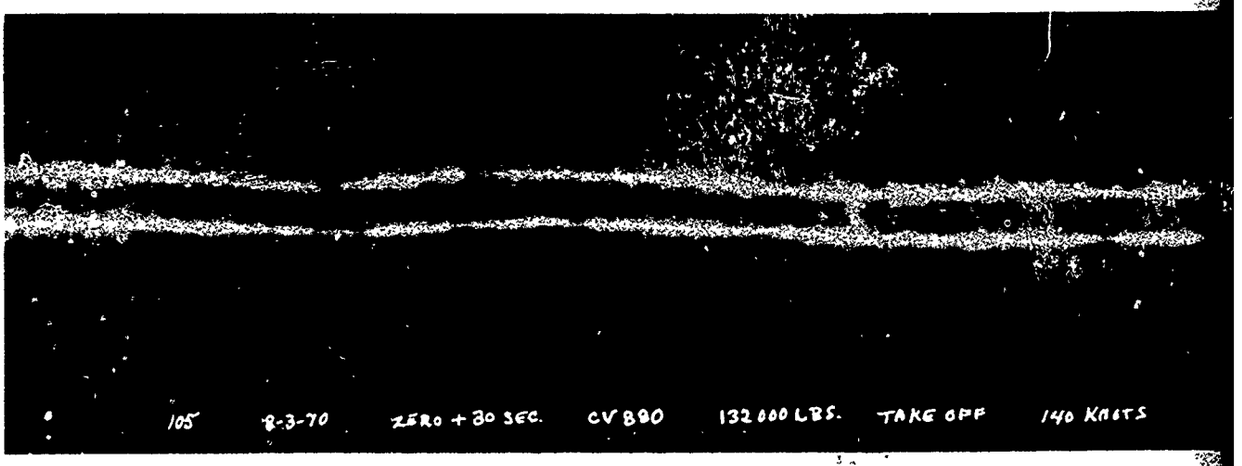

FIGURE C-4. UPPER AIR FLOW VISUALIZATION. CONVAIR 880. H_p = 5,000 FEET (Sheet 1 of 3)

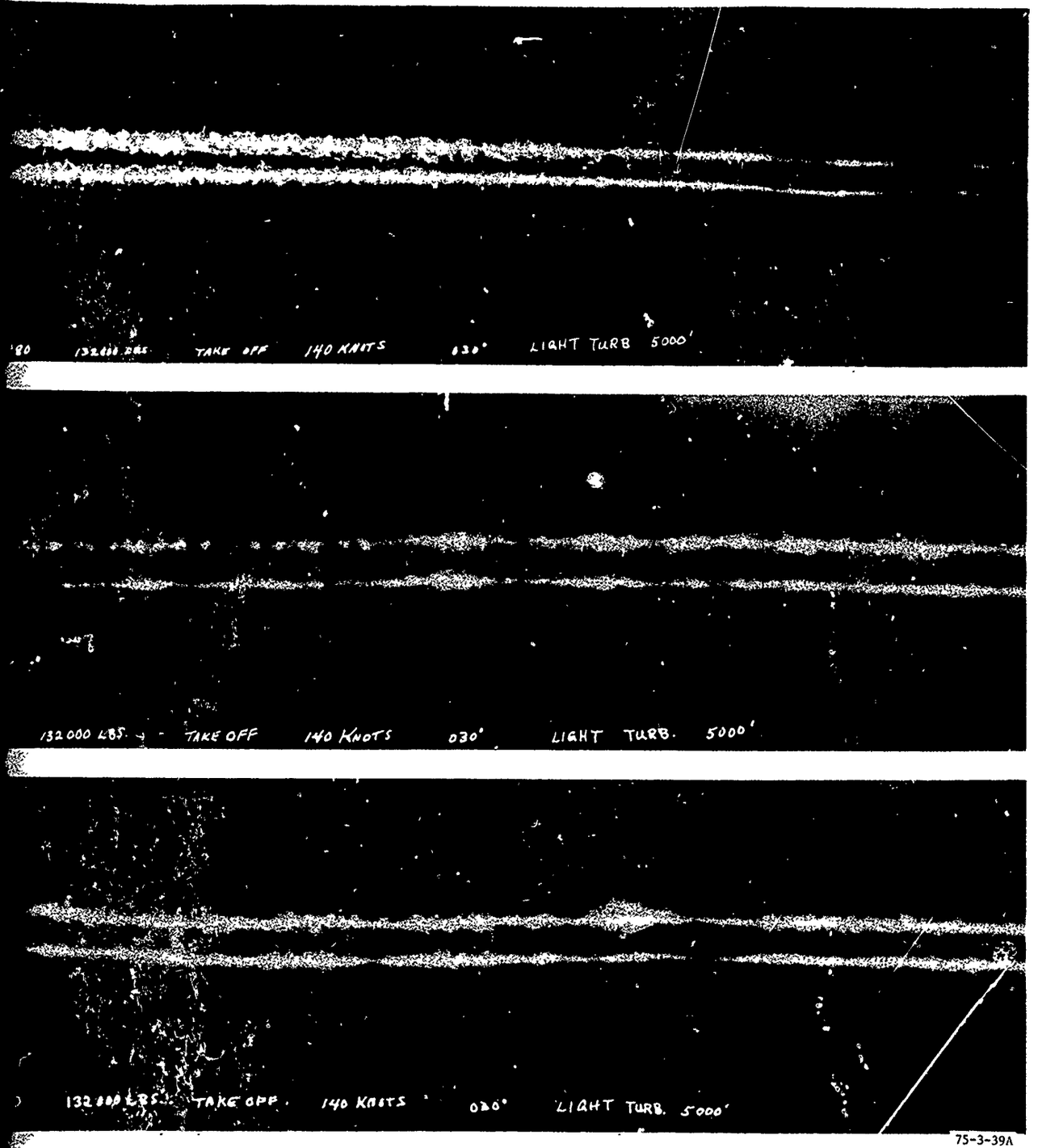

75-3-39A

UPPER AIR FLOW VISUALIZATION. CONVAIR 880, TAKEOFF CONFIGURATION.
H_p = 5,000 FEET (Sheet 1 of 3)

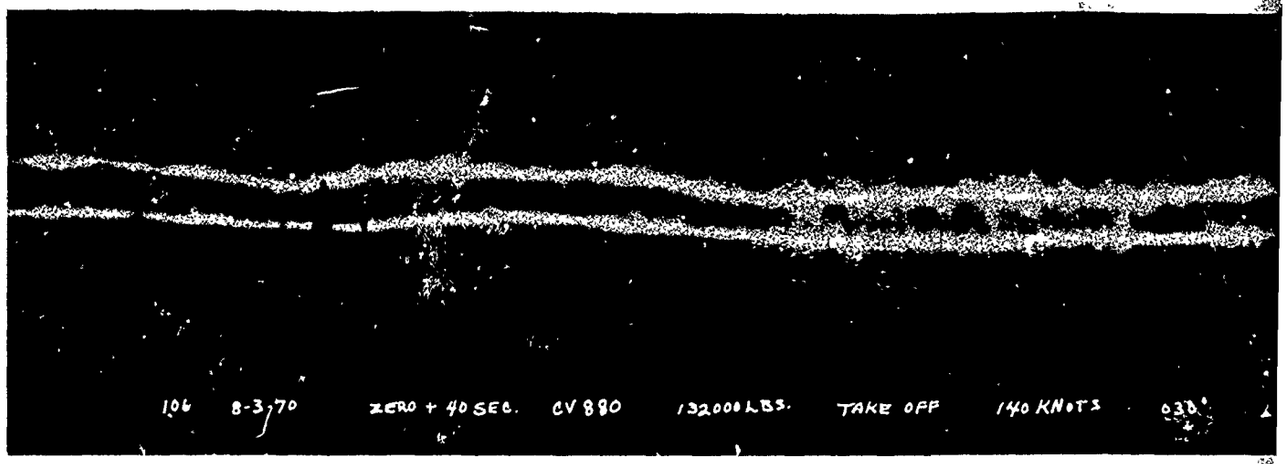

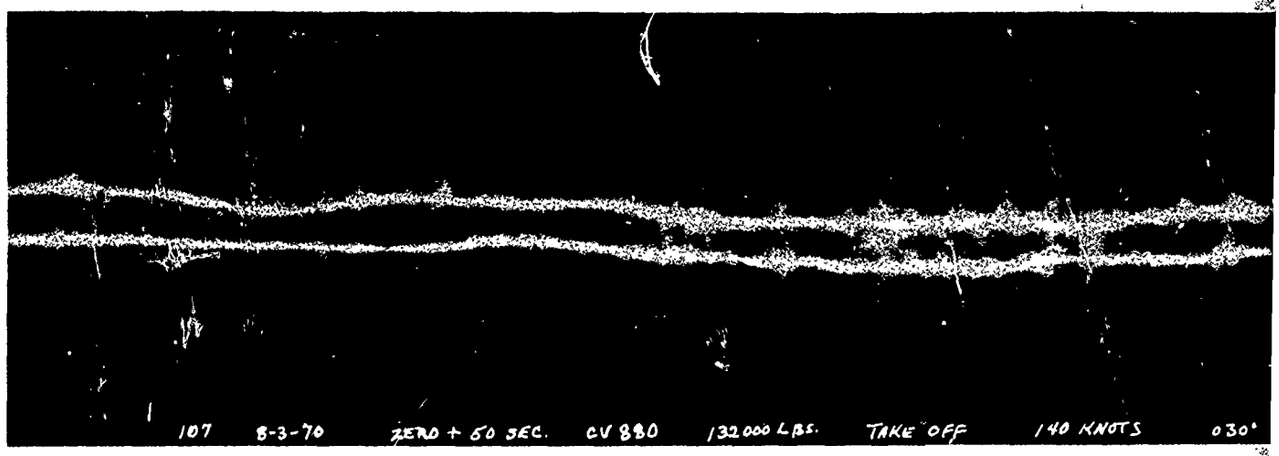

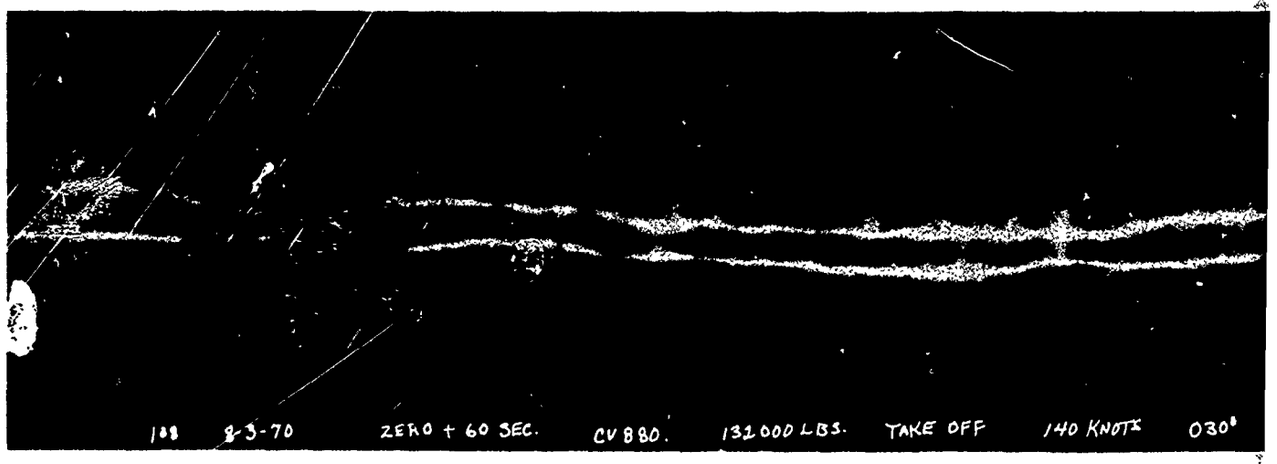

FIGURE C-4. UPPER AIR FLOW VISUALIZATION. CONVAIR 880, TAK
H_p = 5,000 FEET (Sheet 2 of 3)

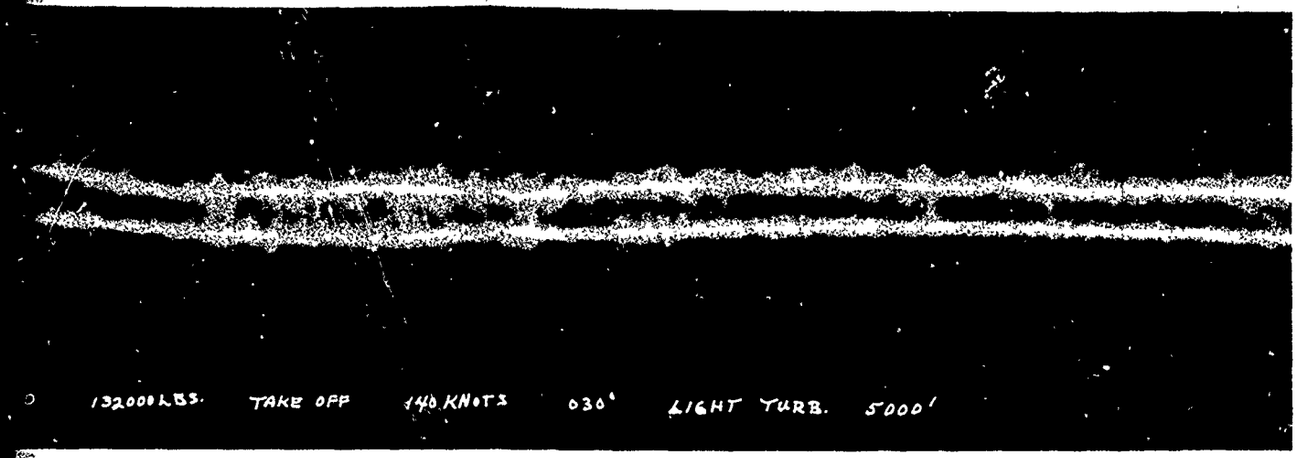

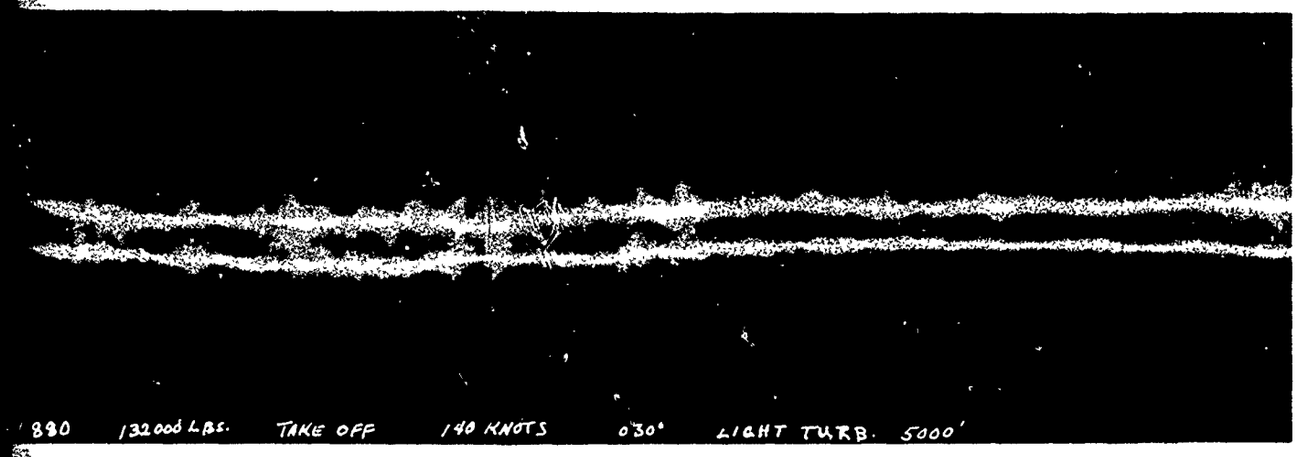

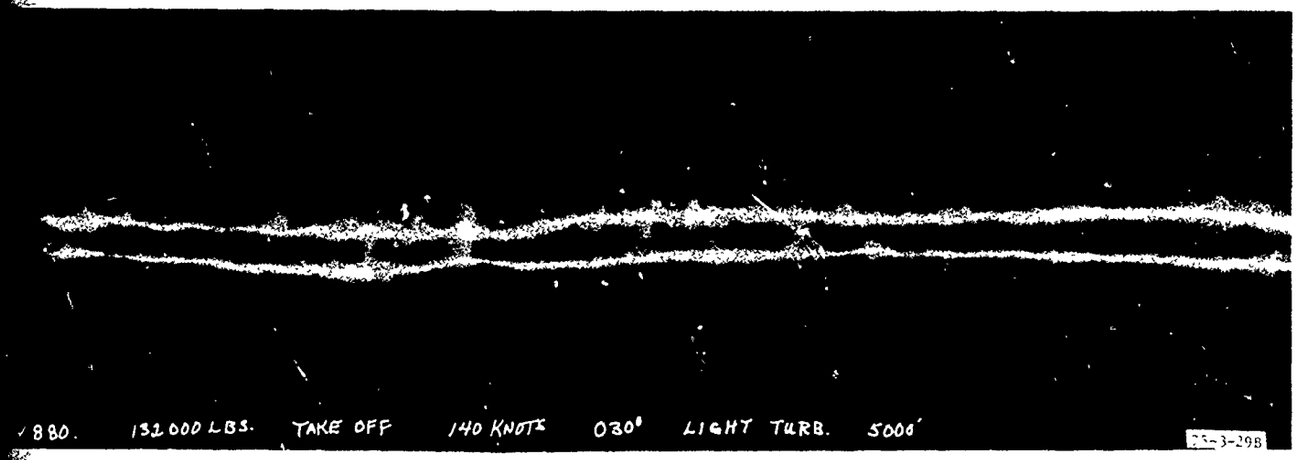

4. UPPER AIR FLOW VISUALIZATION. CONVAIR 880, TAKEOFF CONFIGURATION. H_p = 5,000 FEET (Sheet 2 of 3)

2

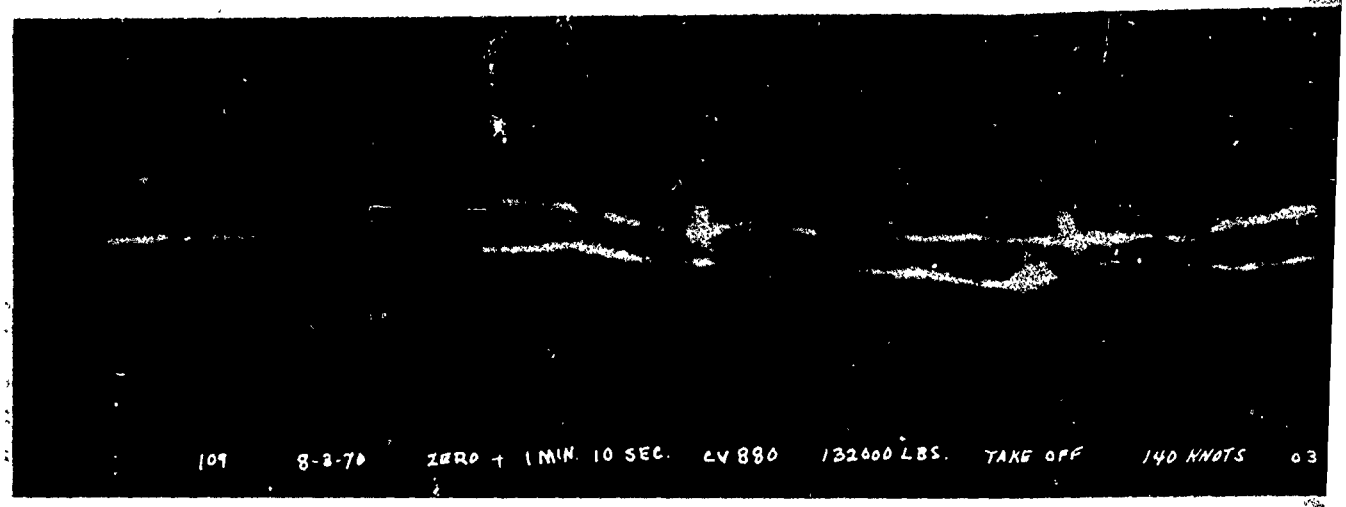

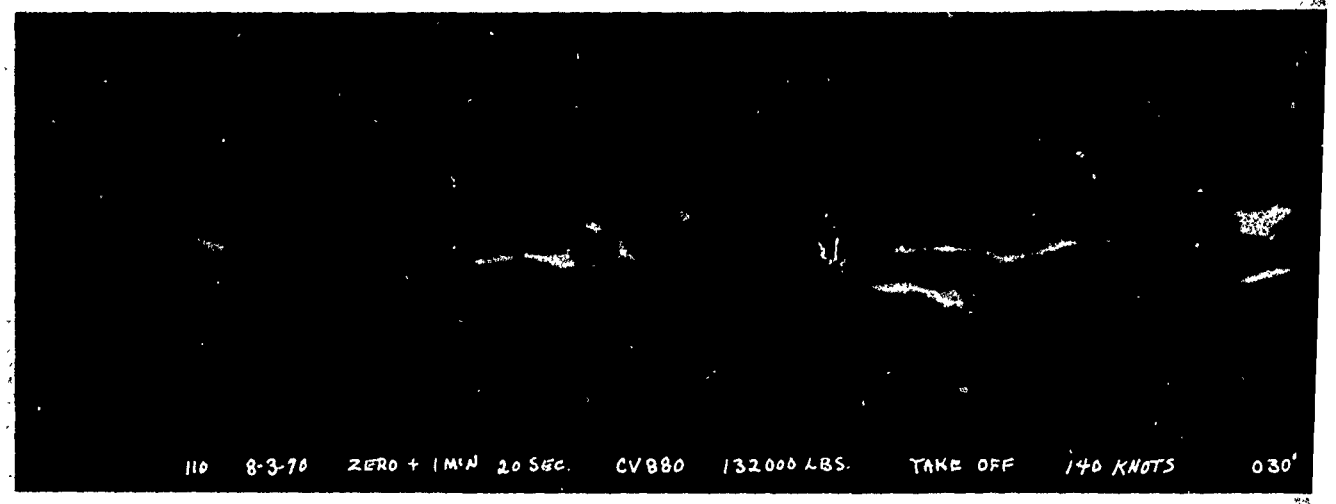

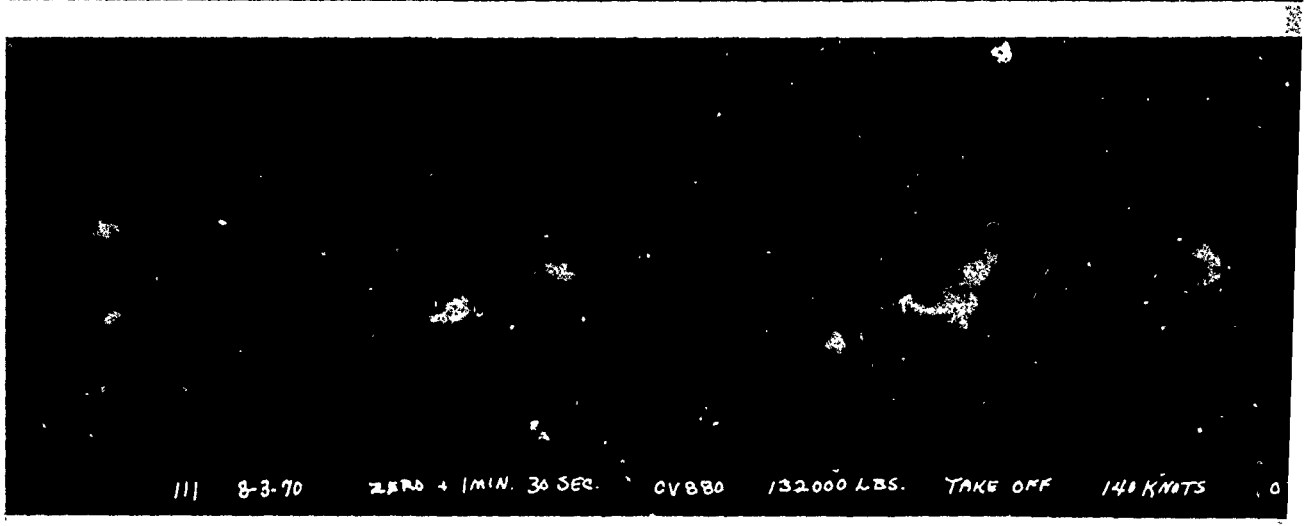

FIGURE C-4. UPPER AIR FLOW VISUALIZATION. CONVAIR 8
H_p = 5,000 FEET (Sheet 3 of 3)

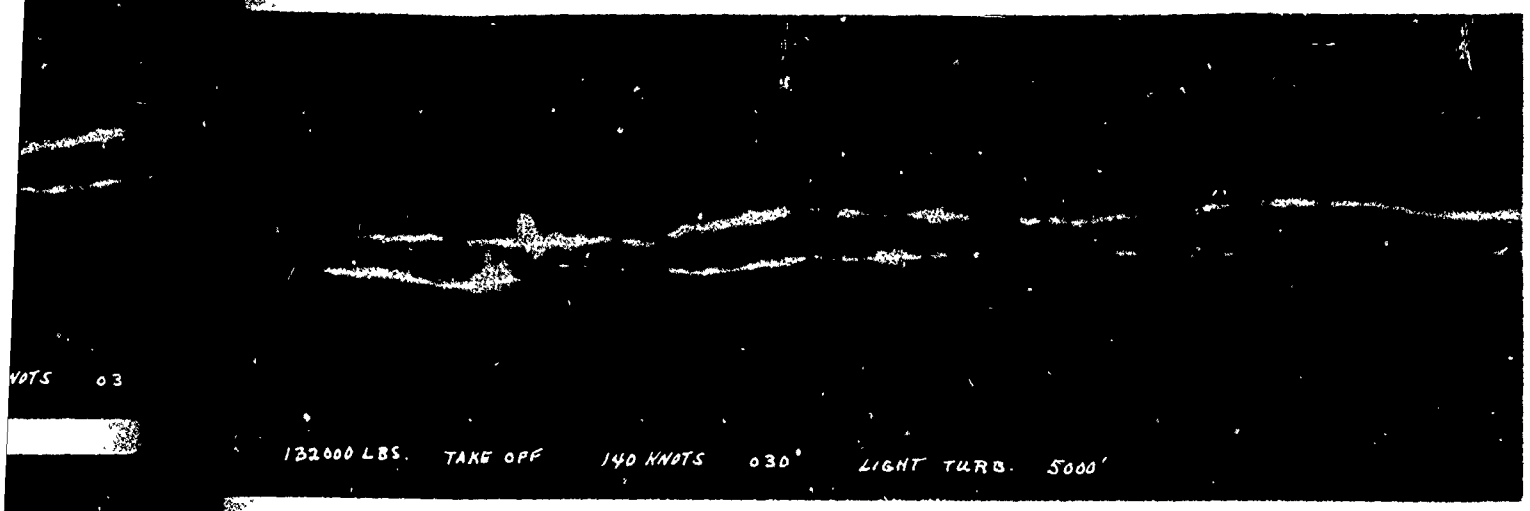

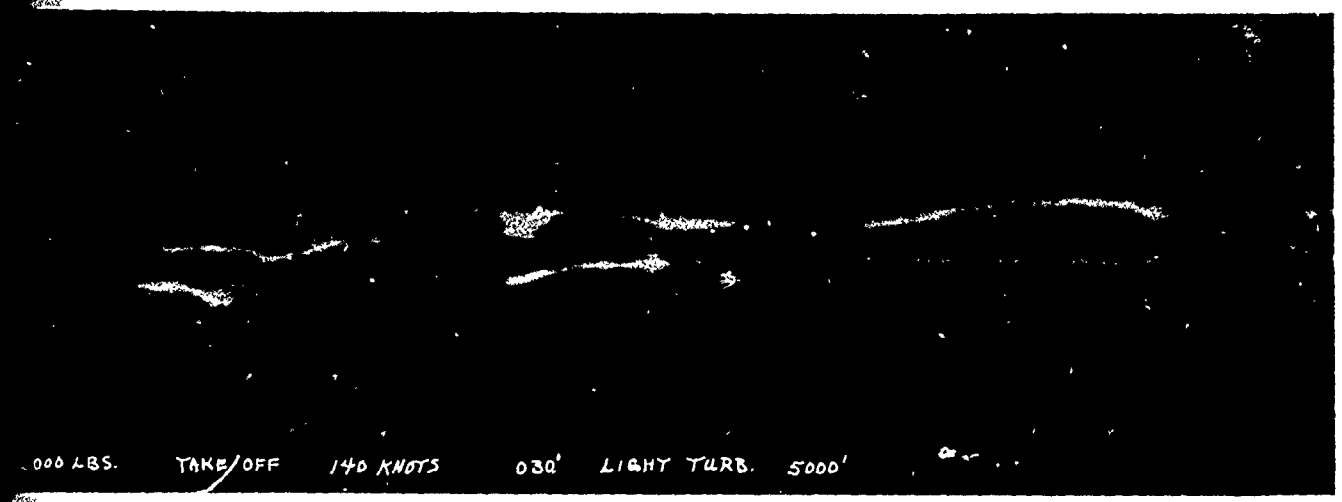

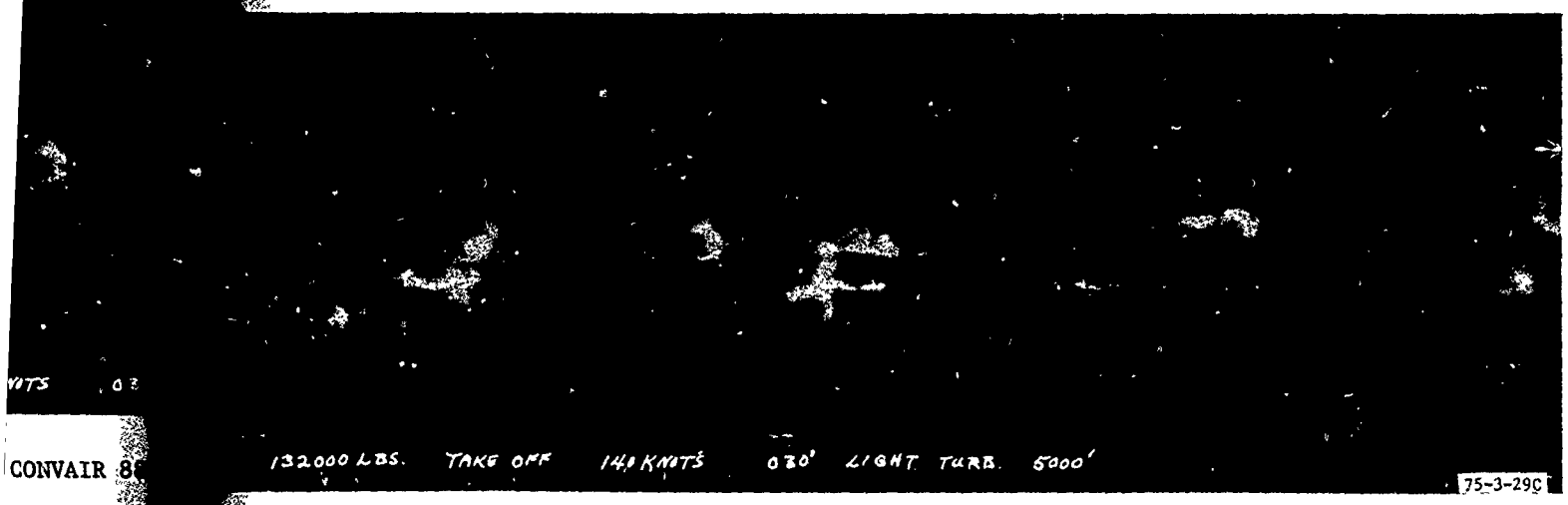

UPPER AIR FLOW VISUALIZATION. CONVAIR 880, TAKEOFF CONFIGURATION.
H_p = 5,000 FEET (Sheet 3 of 3)

2

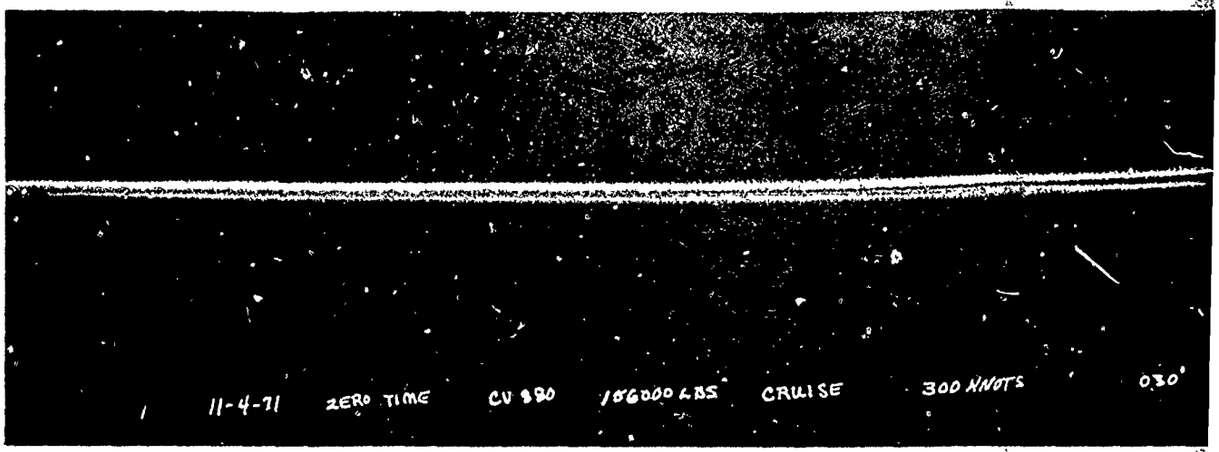

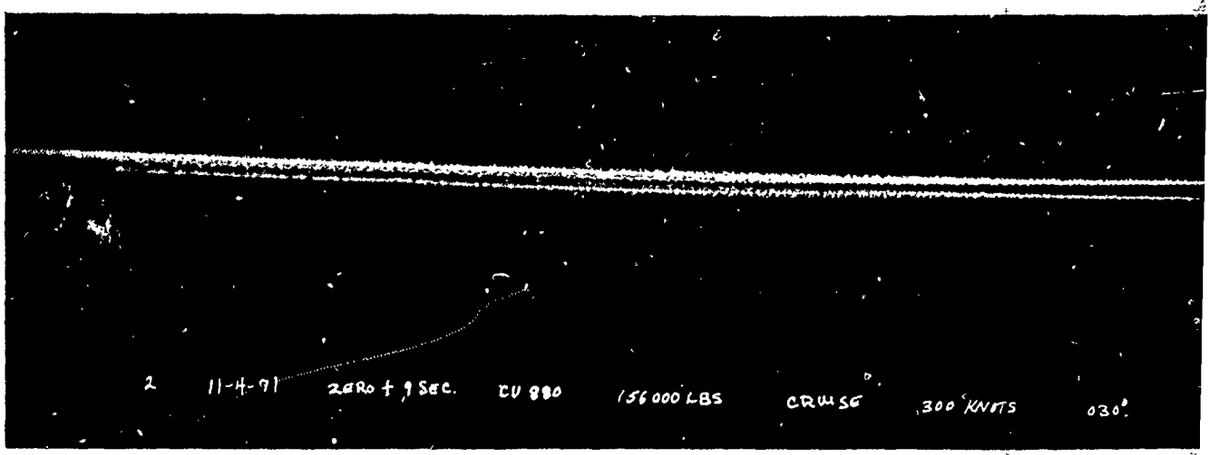

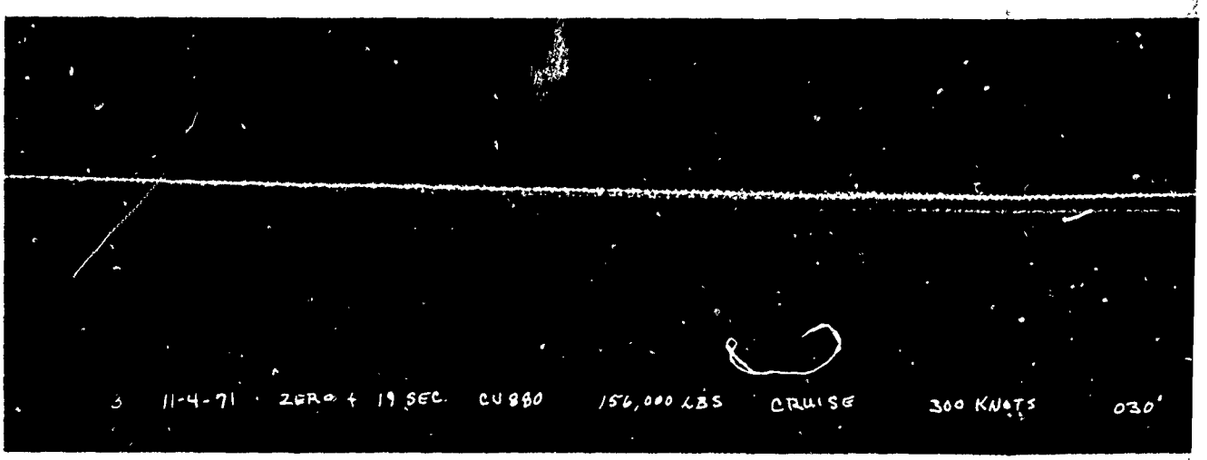

FIGURE C-5. CV880 VORTEX PAIR, HOLDING CONFIGURATION (H_p = 20,000 FEET (Sheet 1 of 3)

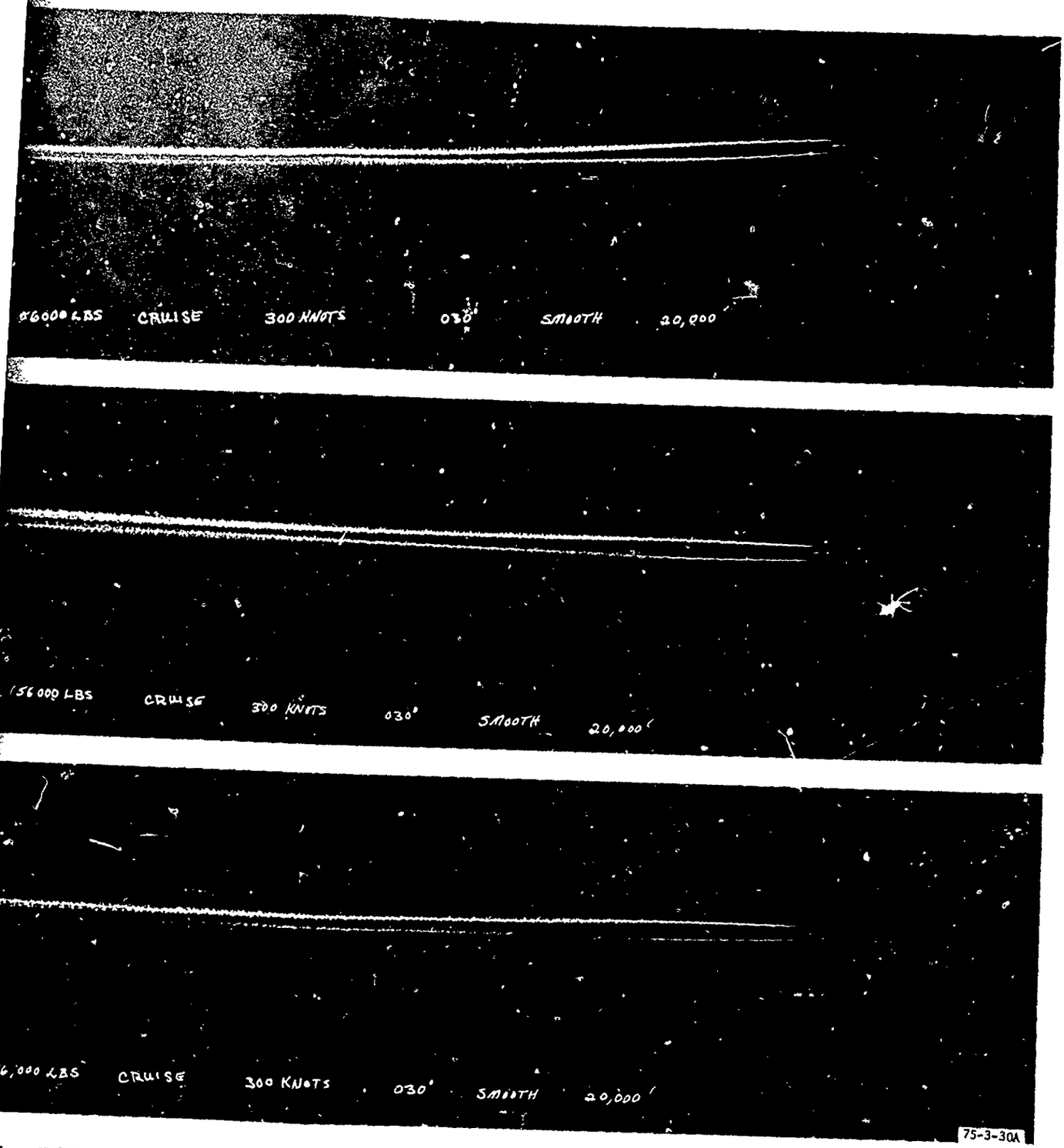

C-5. CV880 VORTEX PAIR, HOLDING CONFIGURATION (ZERO DEGREE FLAPS)
H_p = 20,000 FEET (Sheet 1 of 3)

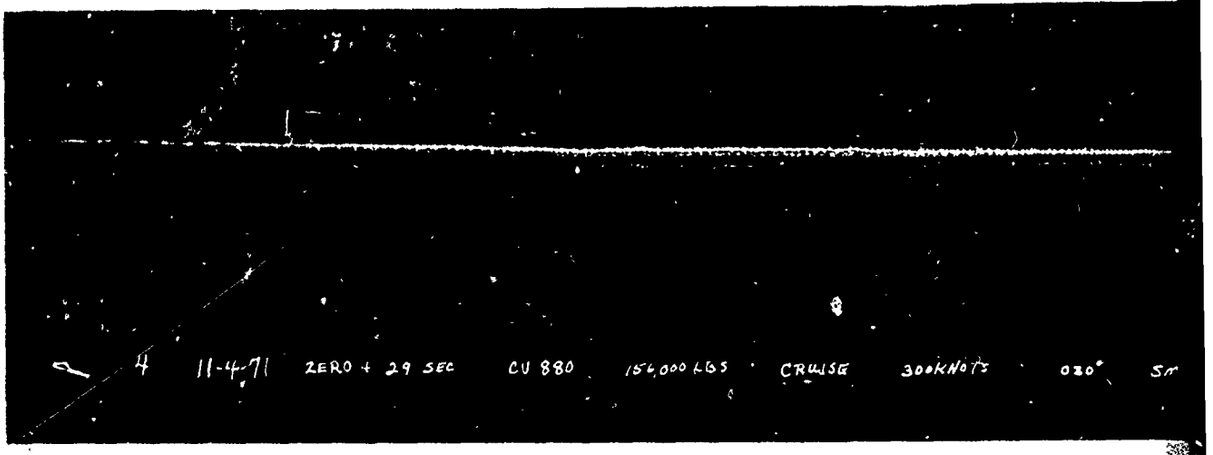

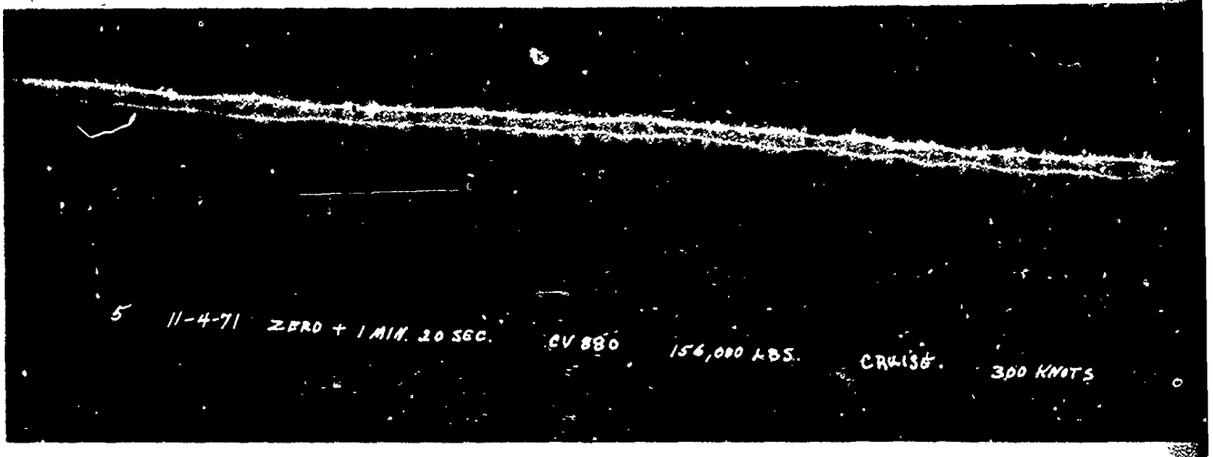

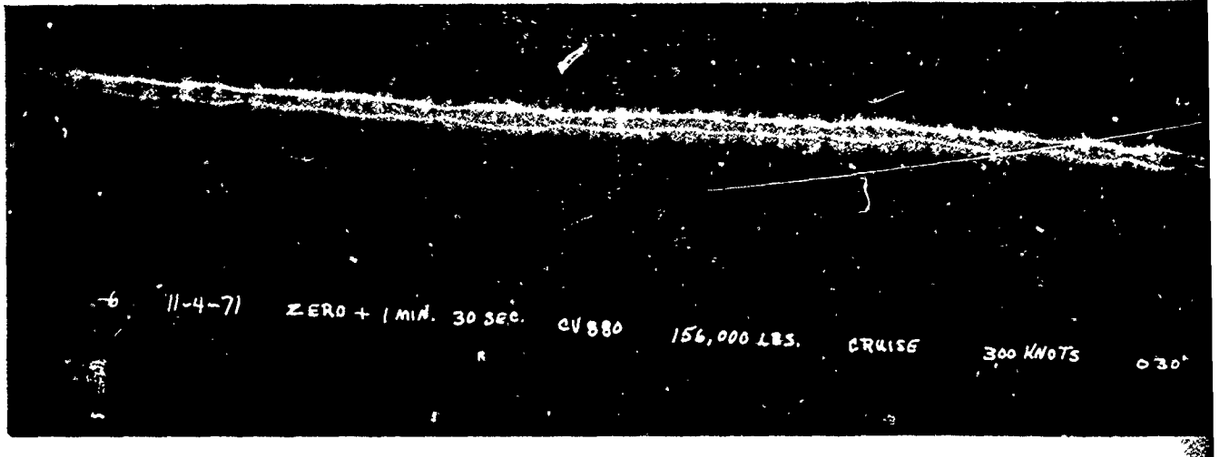

FIGURE C-5. CV880 VORTEX PAIR, HOLDING CONFIGURATION (H_p = 20,000 FEET (Sheet 2 of 3)

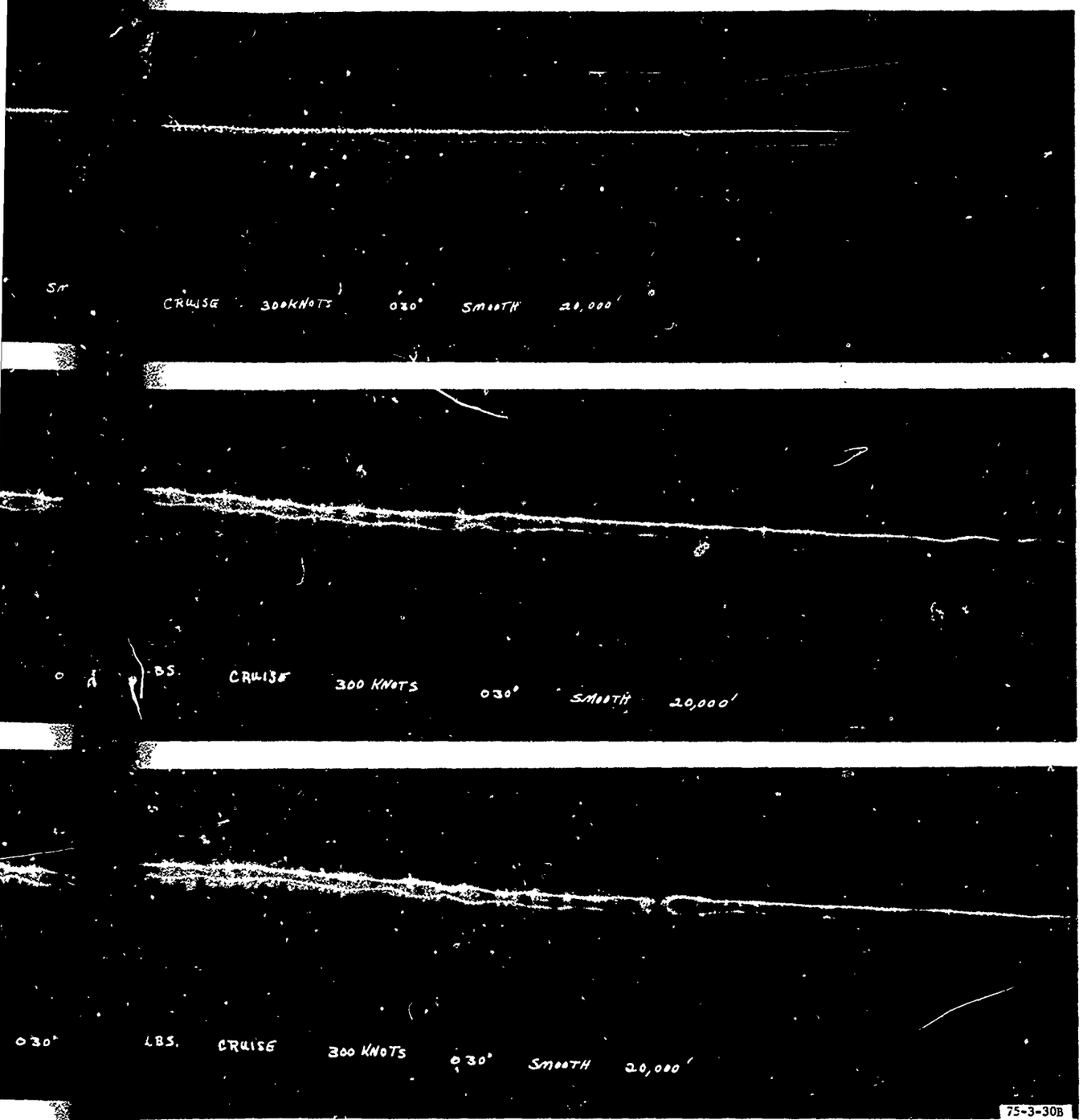

VORTEX PAIR, FOLDING CONFIGURATION (ZERO DEGREE FLAPS)
0,000 FEET (Sheet 2 of 3)

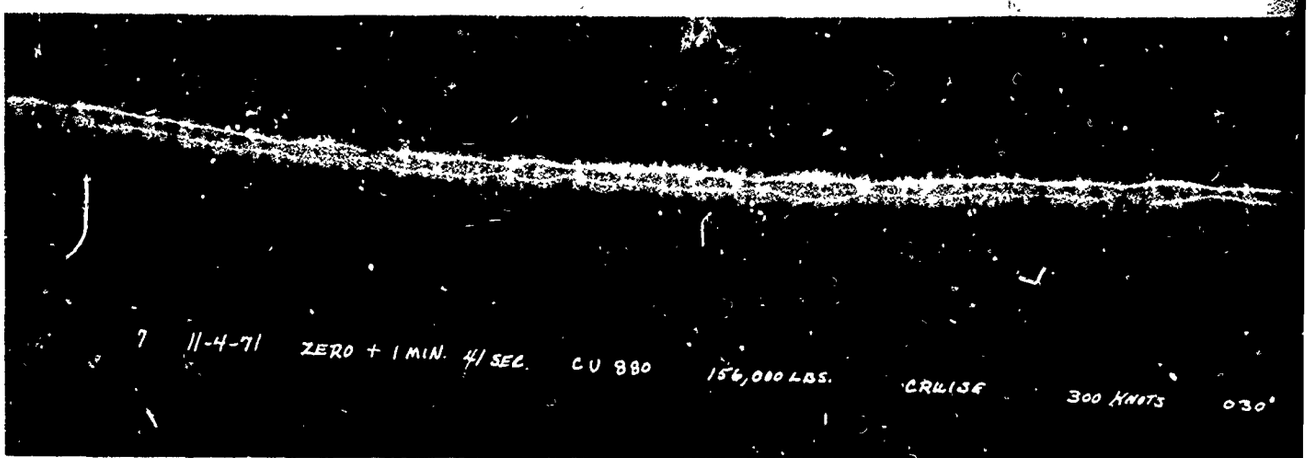

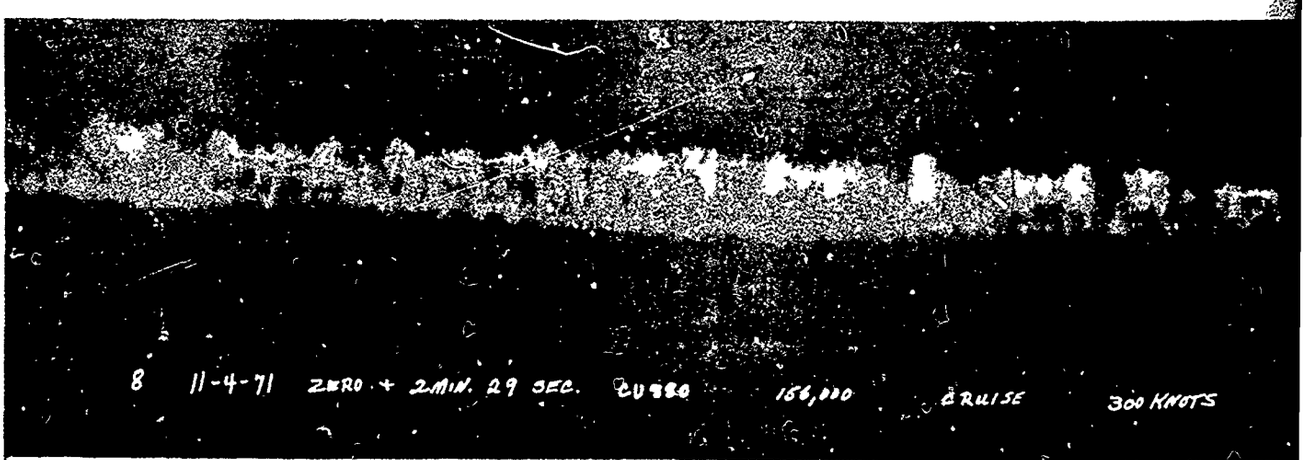

FIGURE C-5. CV880 VORTEX PAIR, HOLDING CONFIGURATION (ZERO D
H_p = 20,000 FEET (Sheet 3 of 3)

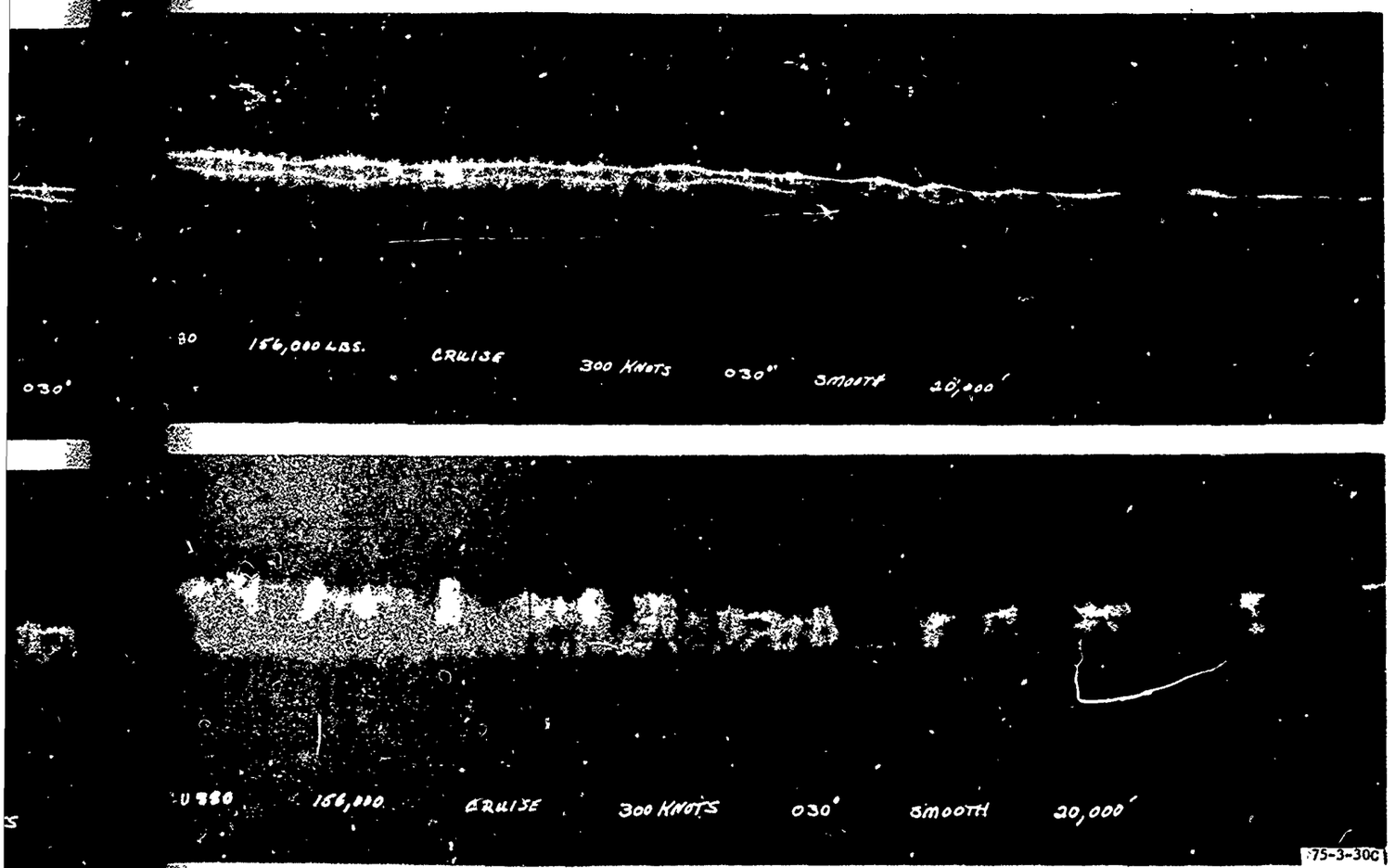

5. CV880 VORTEX PAIR, HOLDING CONFIGURATION (ZERO DEGREE FLAPS)
H_p = 20,000 FEET (Sheet 3 of 3)

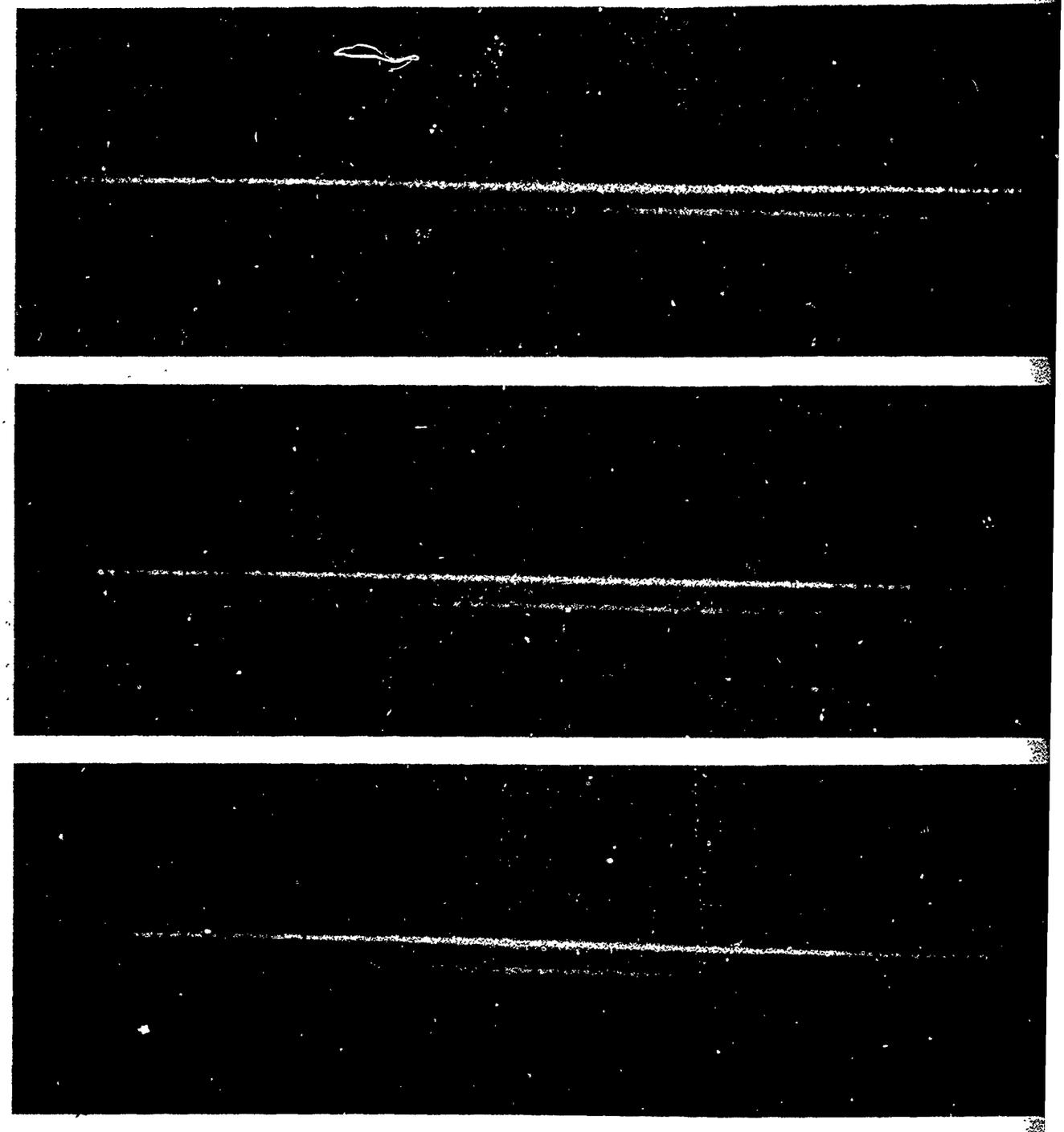

FIGURE C-6. CV880 VORTEX PAIR, HOLDING CONFIGURATION (ZERO DE
H_p = 10,000 FEET (Sheet 1 of 2)

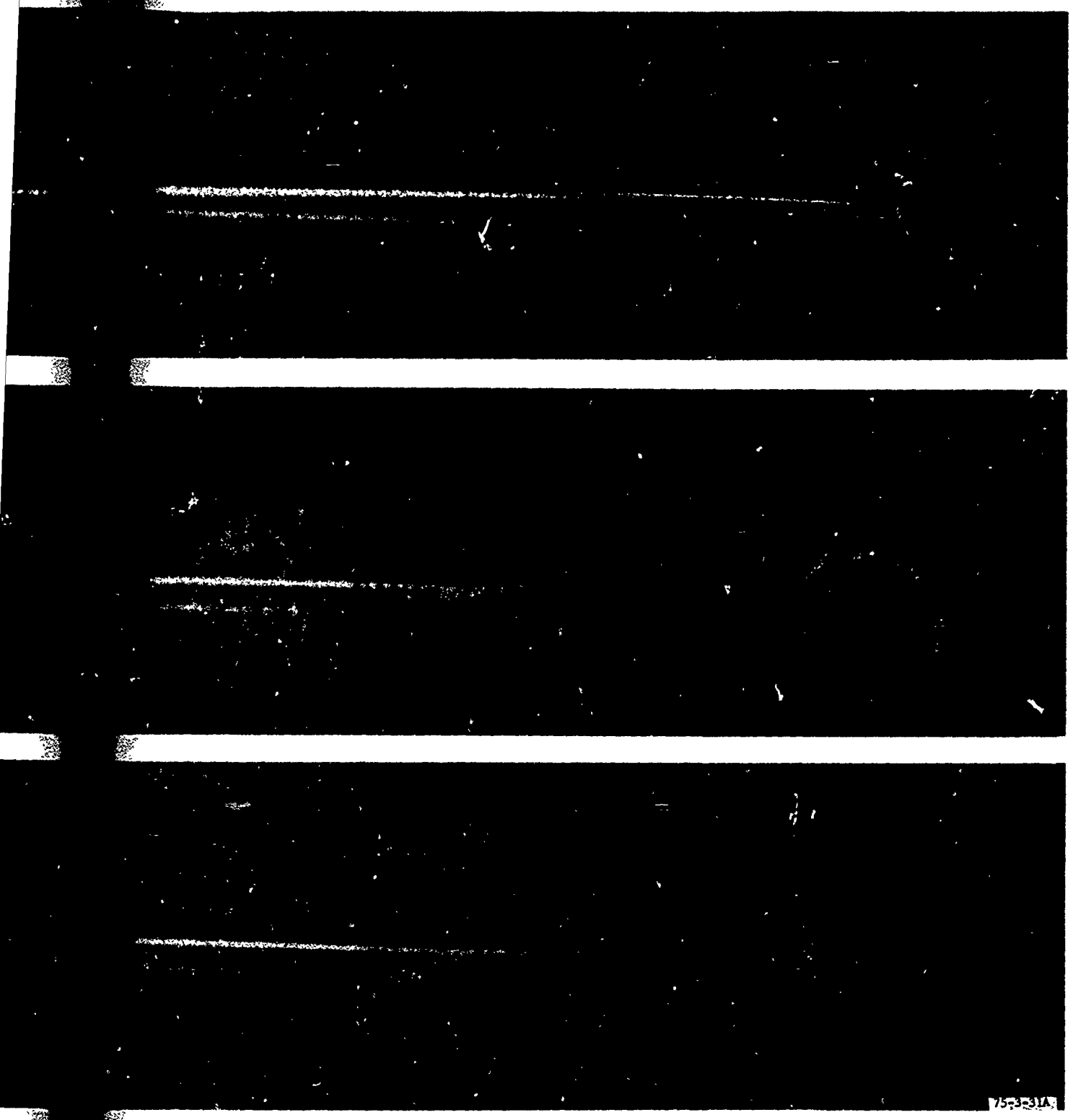

ZERO D... ...O VORTEX PAIR, HOLDING CONFIGURATION (ZERO DEGREE FLAPS)
...10,000 FEET (Sheet 1 of 2)

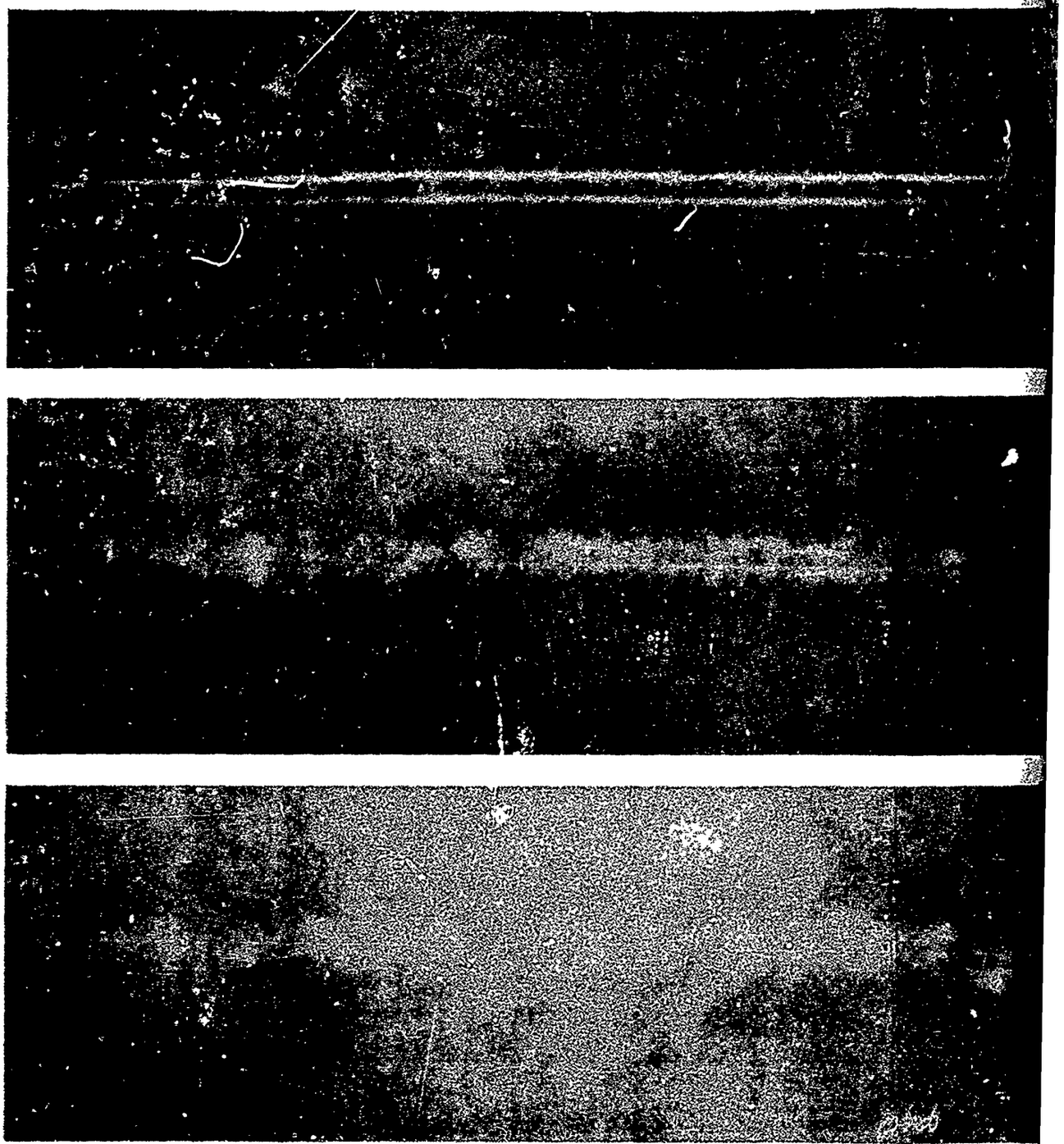

FIGURE C-6. CV880 VORTEX PAIR, HOLDING CONFIGURATION (ZERO H_p = 10,000 FEET (Sheet 2 of 2)

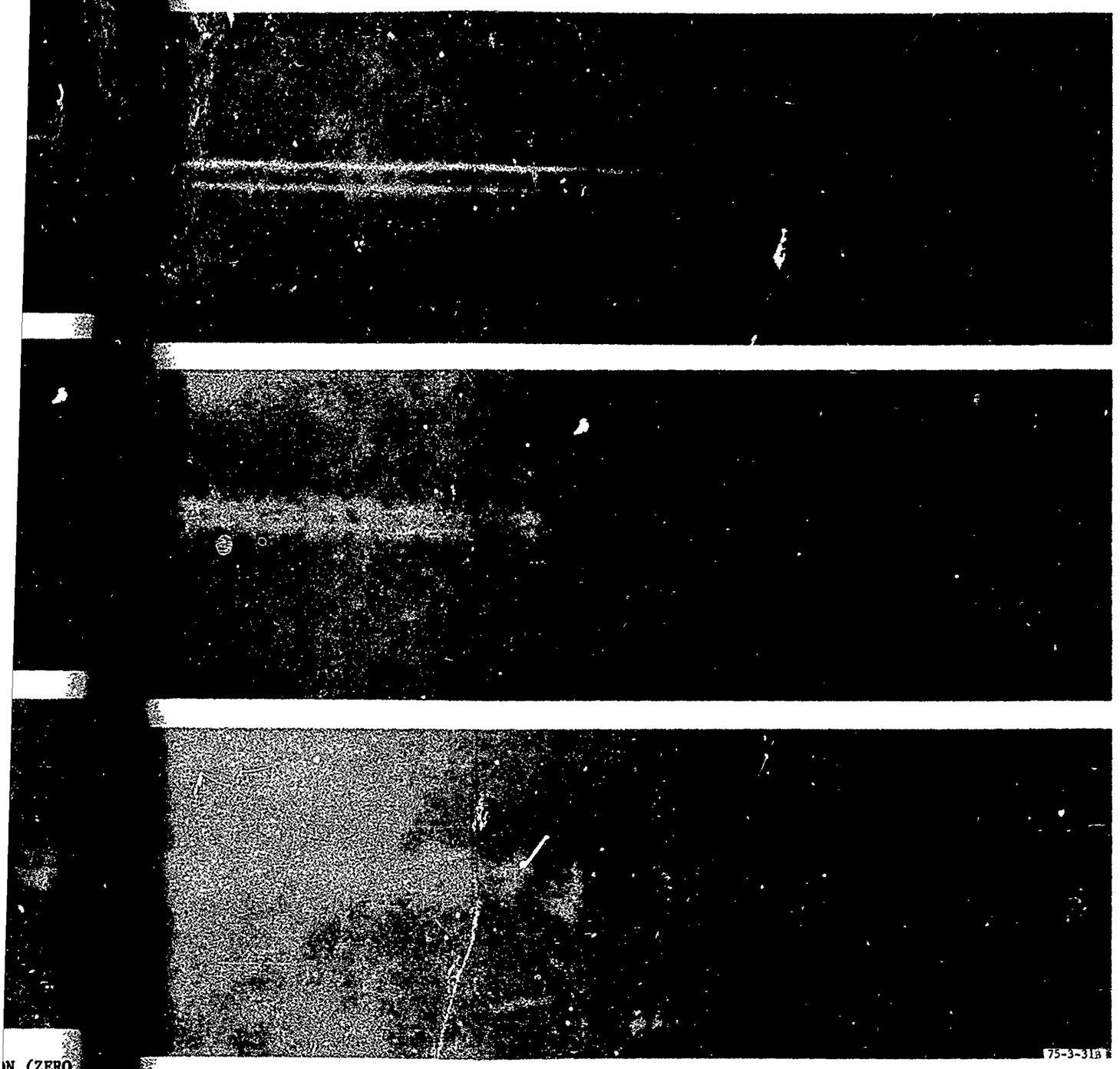

CV880 VORTEX PAIR, HOLDING CONFIGURATION (ZERO DEGREE FLAPS)
H_p = 10,000 FEET (Sheet 2 of 2)

FLIGHT 11-1 (t = -10 SECOND), δ_f =

FIGURE C-7A. BOEING 727-200 EDWARDS
(t = ZERO SECOND, δ_f =
δ_f = ZERO DEGREE) AND

D), δ_f=

10 SECOND), δ_f=15°, 5-MILE TURN

75-3-32A

EDWARDS'
ND, δ_f = 1
EE) AND 11

ING 727-200 EDWARDS' TEST SERIES, FLIGHTS 10-1
= ZERO SECOND, δ_f = 15°), 10-2 (t = ZERO SECOND,
= ZERO DEGREE) AND 11-1 (t = -10 SECONDS, δ_f = 15°)

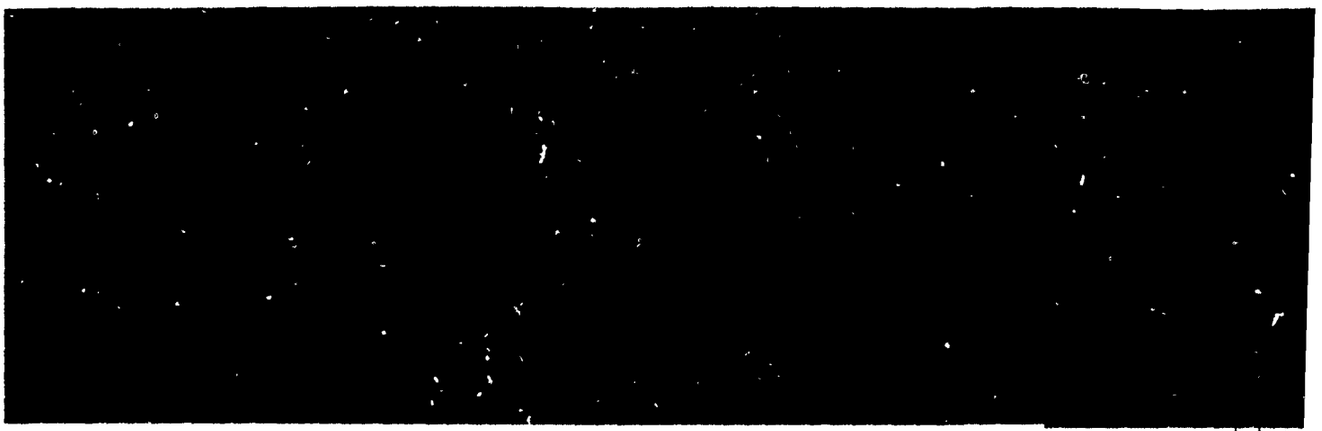

FLIGHT 11-1 (t =

FLIGHT 11-1 (t =

FIGURE C-7B. BOEING 727-200 EDW/
(t = 0, 10, 20 SEC(

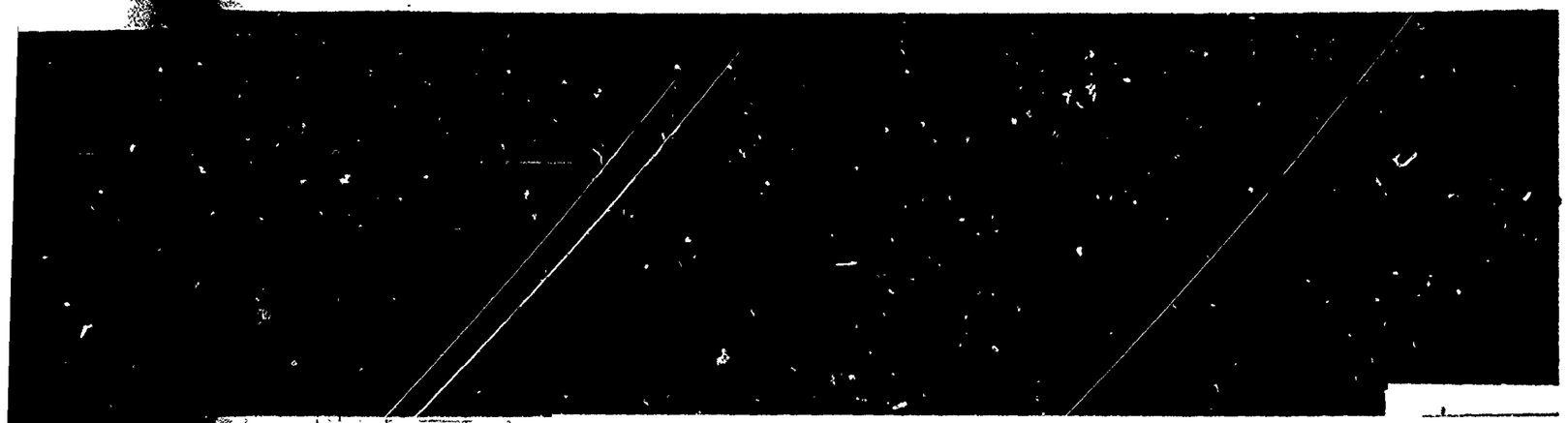

HT 11-1 (t = 10 SECONDS)

HT 11-1 (t = 20 SECONDS)

75-3-32B

G 727-200 EDWARDS' TEST SERIES, FLIGHT 11-1
0, 10, 20 SECONDS, δ_f = 15°)

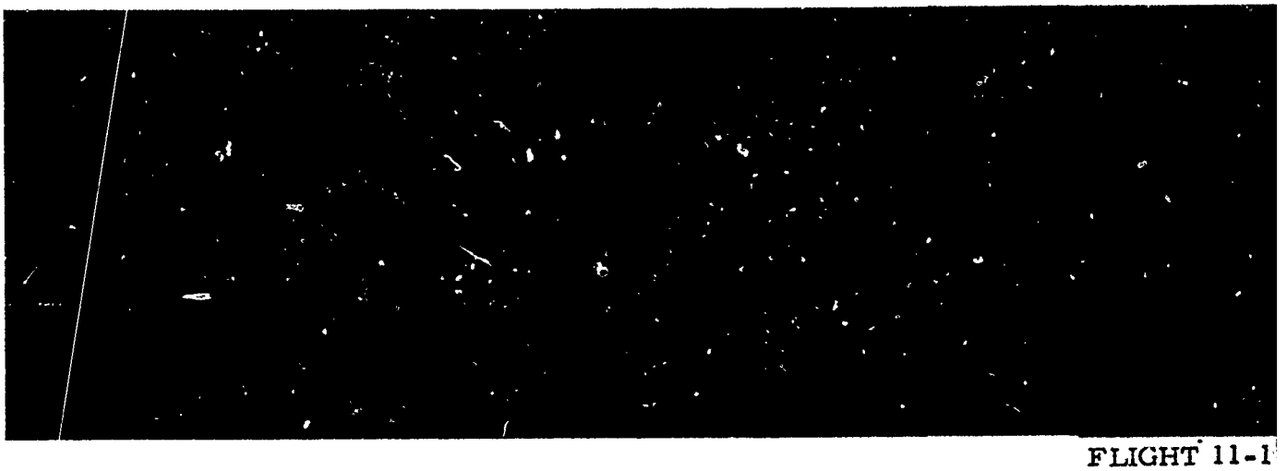

FLIGHT 11-1

FLIGHT 11-1

FLIGHT 11-1

FIGURE C-8A. BOEING 727-200
(t = 30, 40, 5

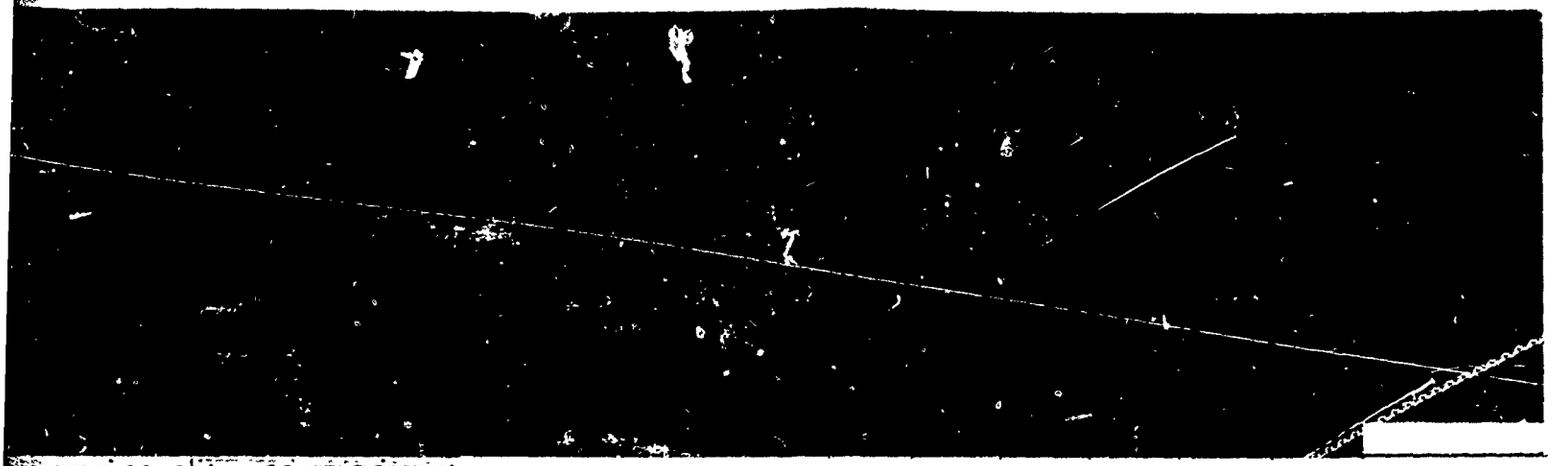

FLIGHT 11-1 (t = 30 SECONDS)

FLIGHT 11-1 (t = 40 SECONDS)

FLIGHT 11-1 (t = 50 SECONDS)

75-3-33A

BOEING 727-200 EDWARDS' TEST SERIES, FLIGHT 11-1
(t = 30, 40, 50 SECONDS, δ_f = 15°)

FLIGHT 12-1 (t=0 SECOND),

FLIGHT 12-1 (t=20

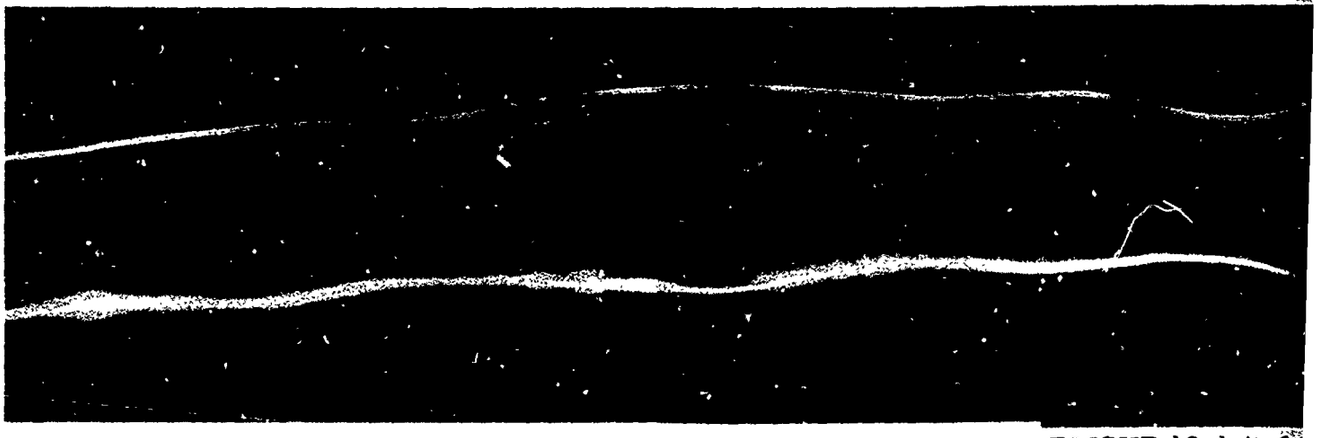

FLIGHT 12-1 (t=3

FIGURE C-8B. BOEING 727-200 EDWA
(t = 0, 20, 30 SECO

3A

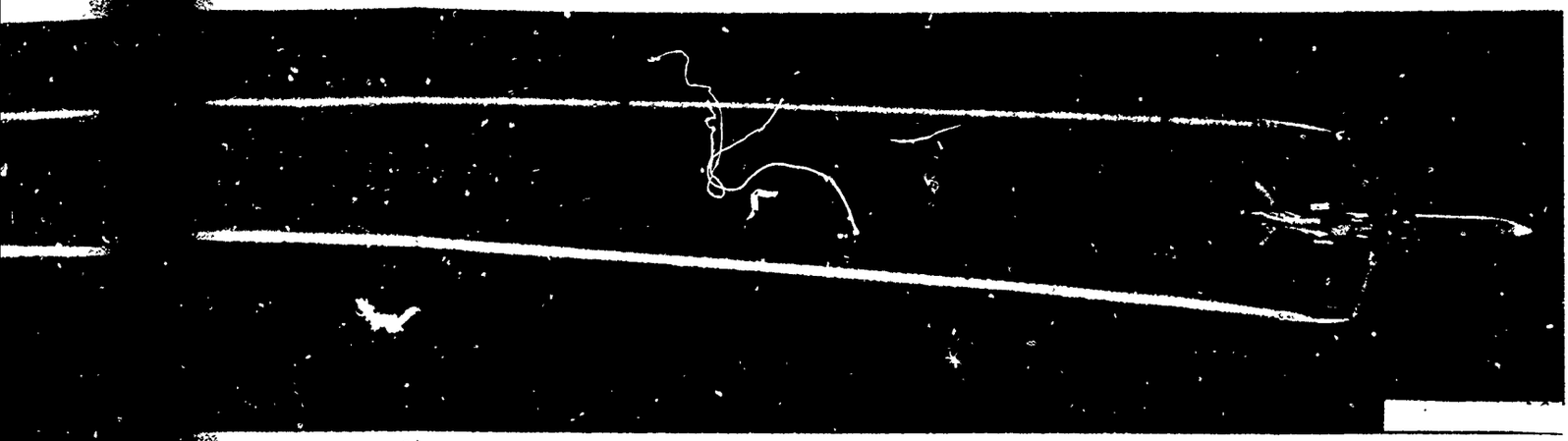

ECOND), $\delta_f = 0°$; 5 - MILE TURN

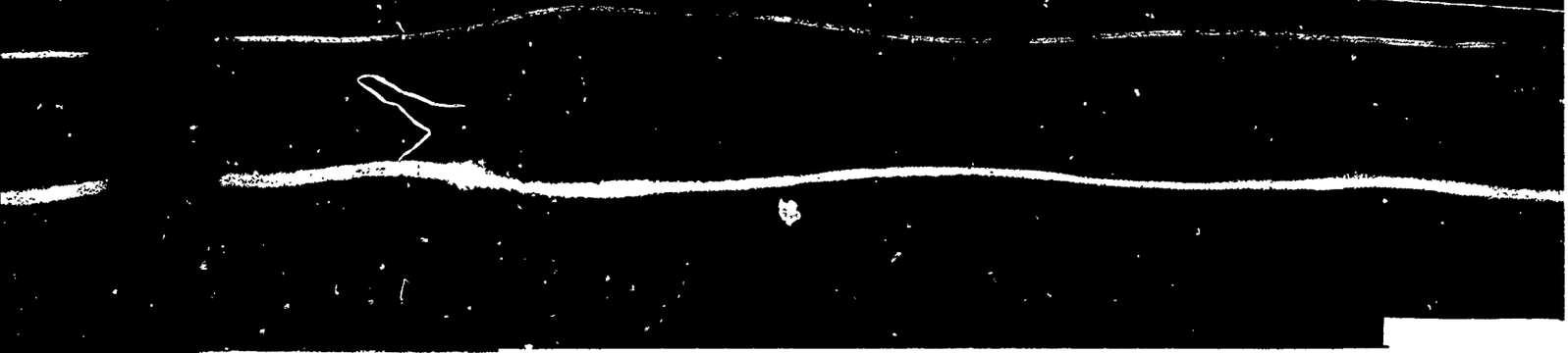

12-1 (t=20 SECONDS)

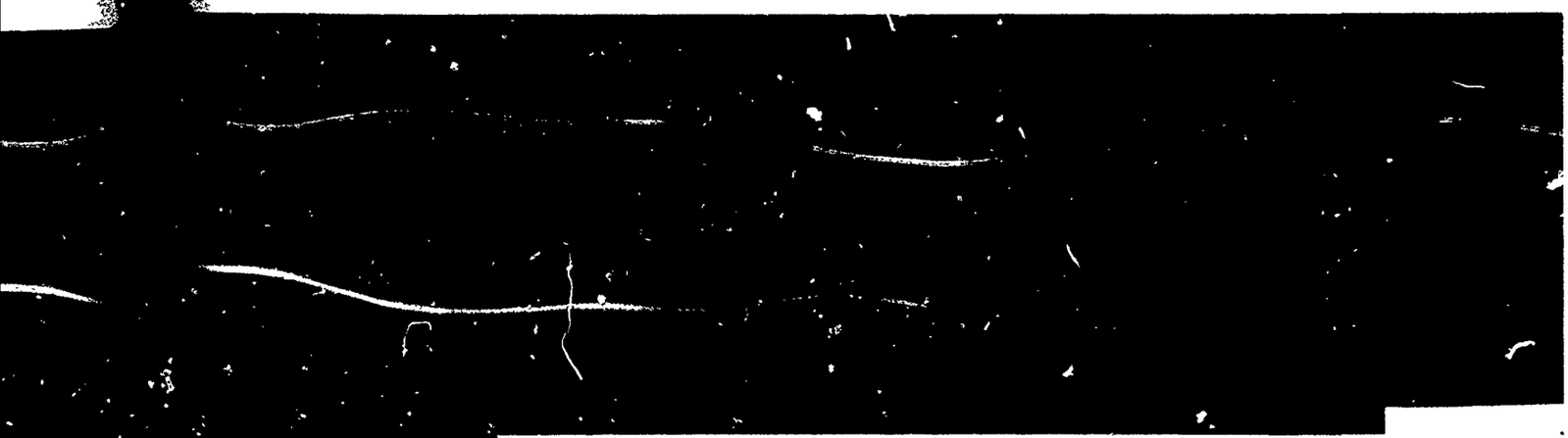

12-1 (t=30 SECONDS)

75-3-33B

7-200 EDWARDS' TEST SERIES, FLIGHT 12-1
0, 30 SECONDS, δ_f = ZERO DEGREE)

FLIGHT 12-1 (t=

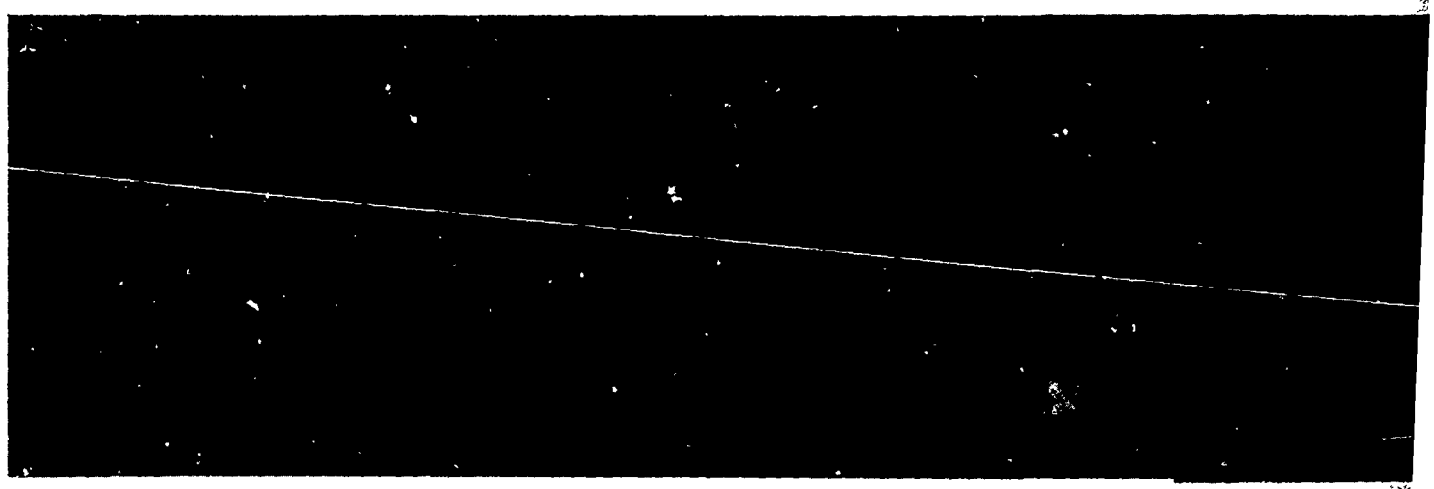

FLIGHT 12-1 (t

FLIGHT 12-1

FIGURE C-8C. BOEING 727-200
(t = 40, 50, 60

2-1 (t= IGHT 12-1 (t=40 SECONDS)

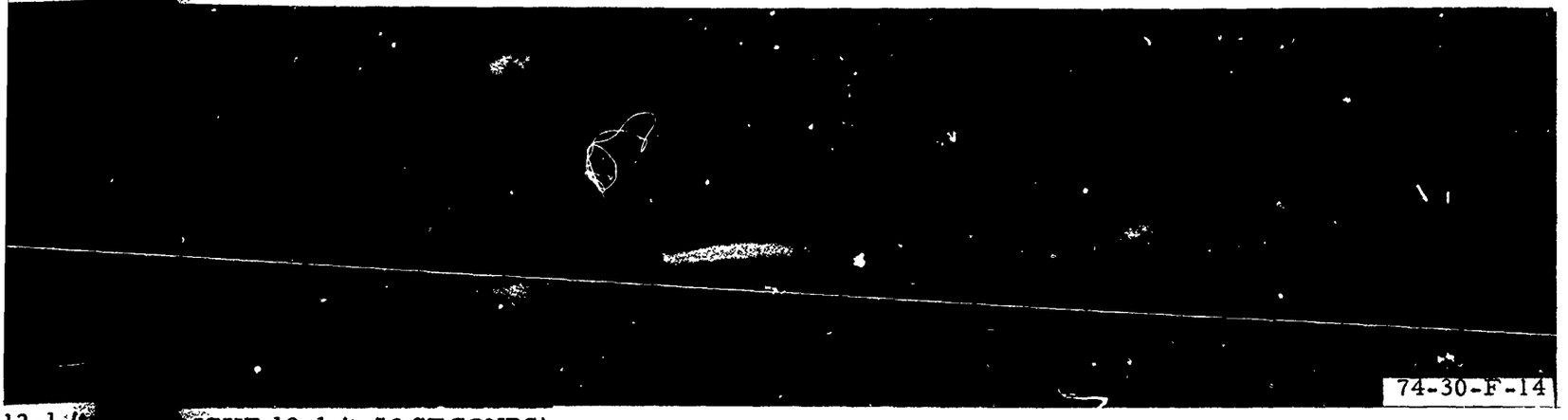

12-1 (t IGHT 12-1 (t=50 SECONDS)

12-1 (LIGHT 12-1 (t=60 SECONDS)

727-200 E , 50, 60 OEING 727-200 EDWARDS' TEST SERIES, FLIGHT 12-1
= 40, 50, 60 SECONDS, δ_f = ZERO DEGREE)

APPENDIX D

ROLL RATE DATA FOR VARIOUS GENERATOR AIRCRAFT

APPENDIX D

Illustration List

APPENDIX D

Illustration List (Continued)

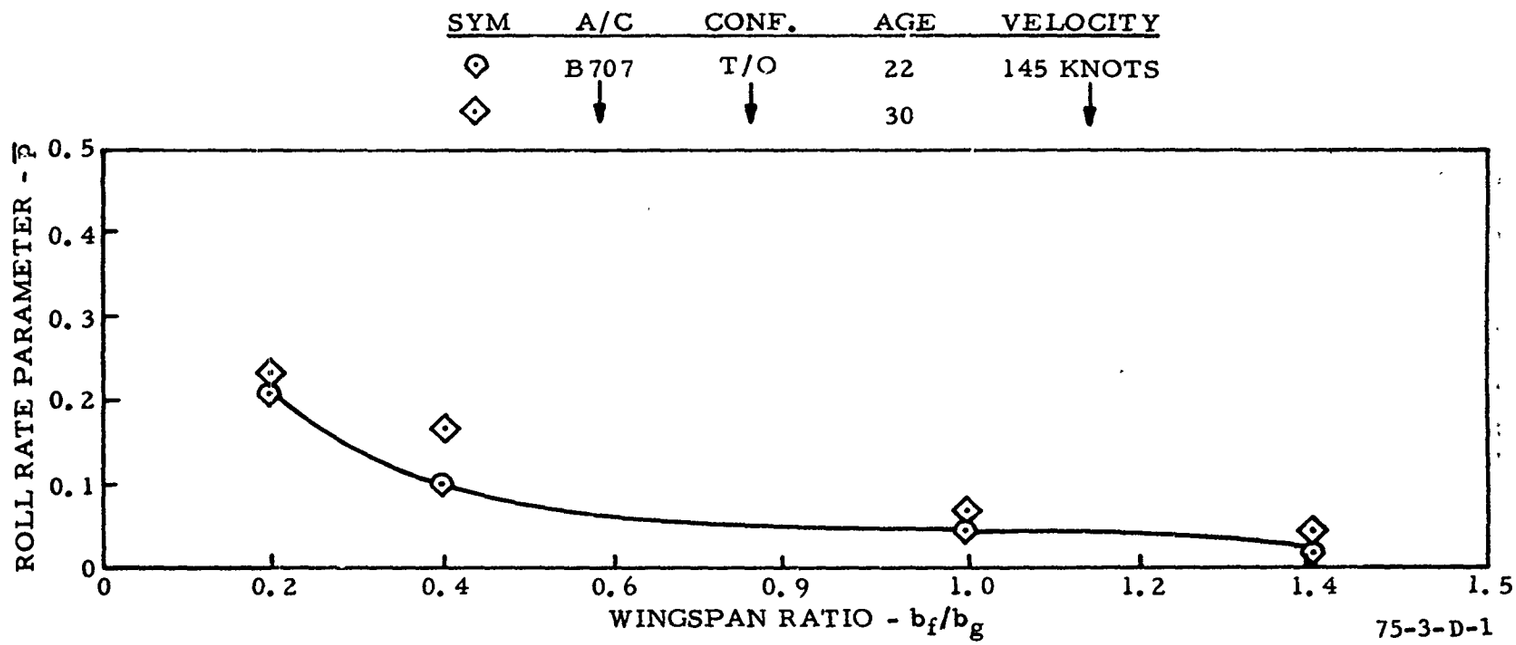

FIGURE D-1. EFFECT OF WINGSPAN RATIO ON ROLL RATE FOR BOEING 707 GENERATOR AIRCRAFT, TAKEOFF CONFIGURATION

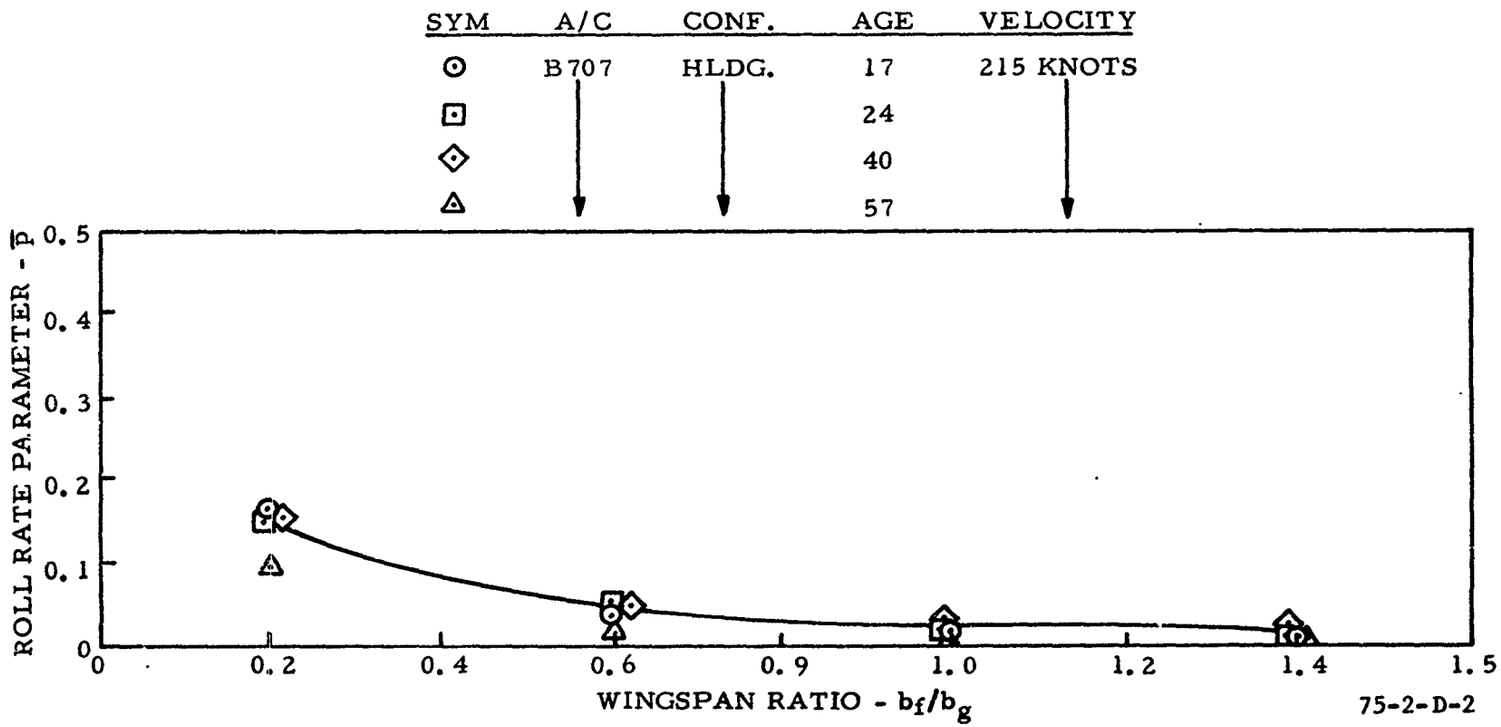

FIGURE D-2. EFFECT OF WINGSPAN RATIO ON ROLL RATE FOR BOEING 707 GENERATOR AIRCRAFT, HOLDING CONFIGURATION

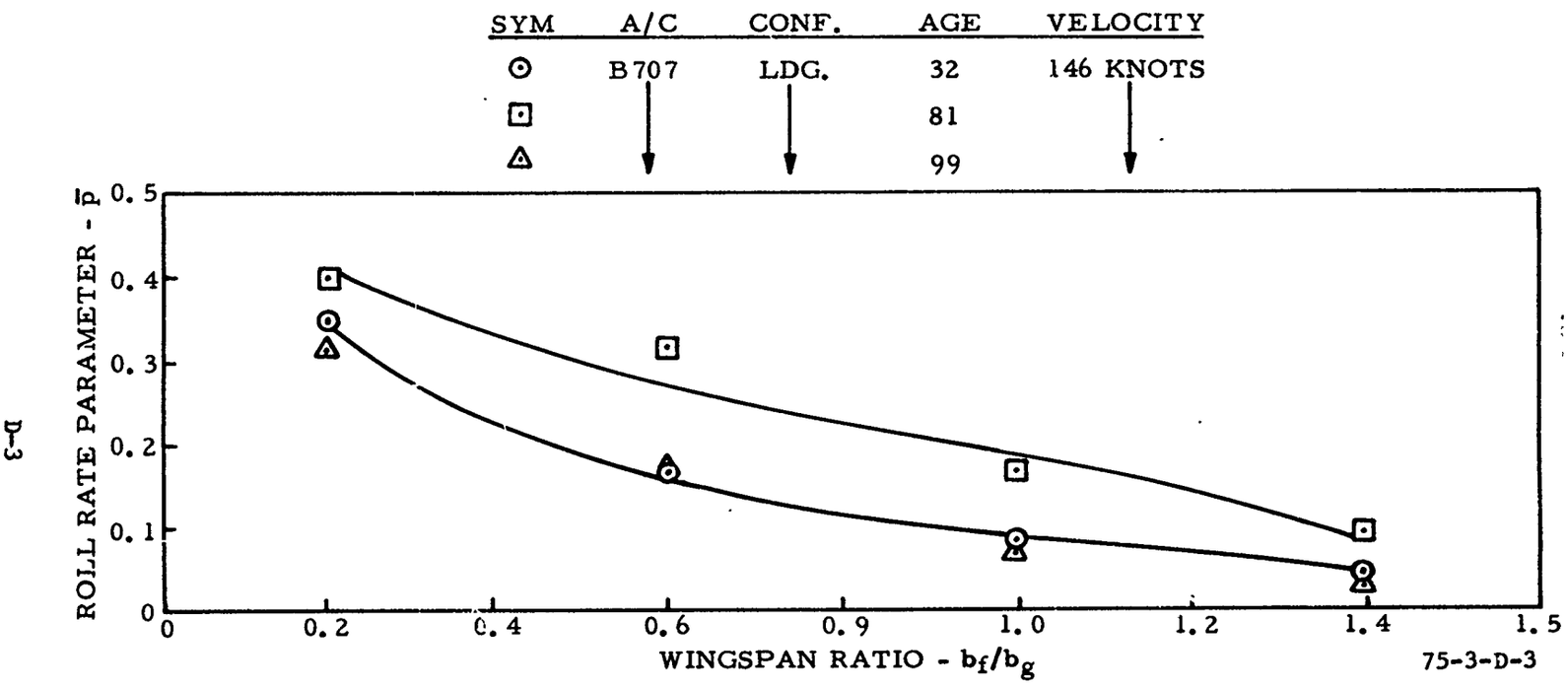

FIGURE D-3. EFFECT OF WINGSPAN RATIO ON ROLL RATE FOR BOEING 707 GENERATOR AIRCRAFT, LANDING CONFIGURATION

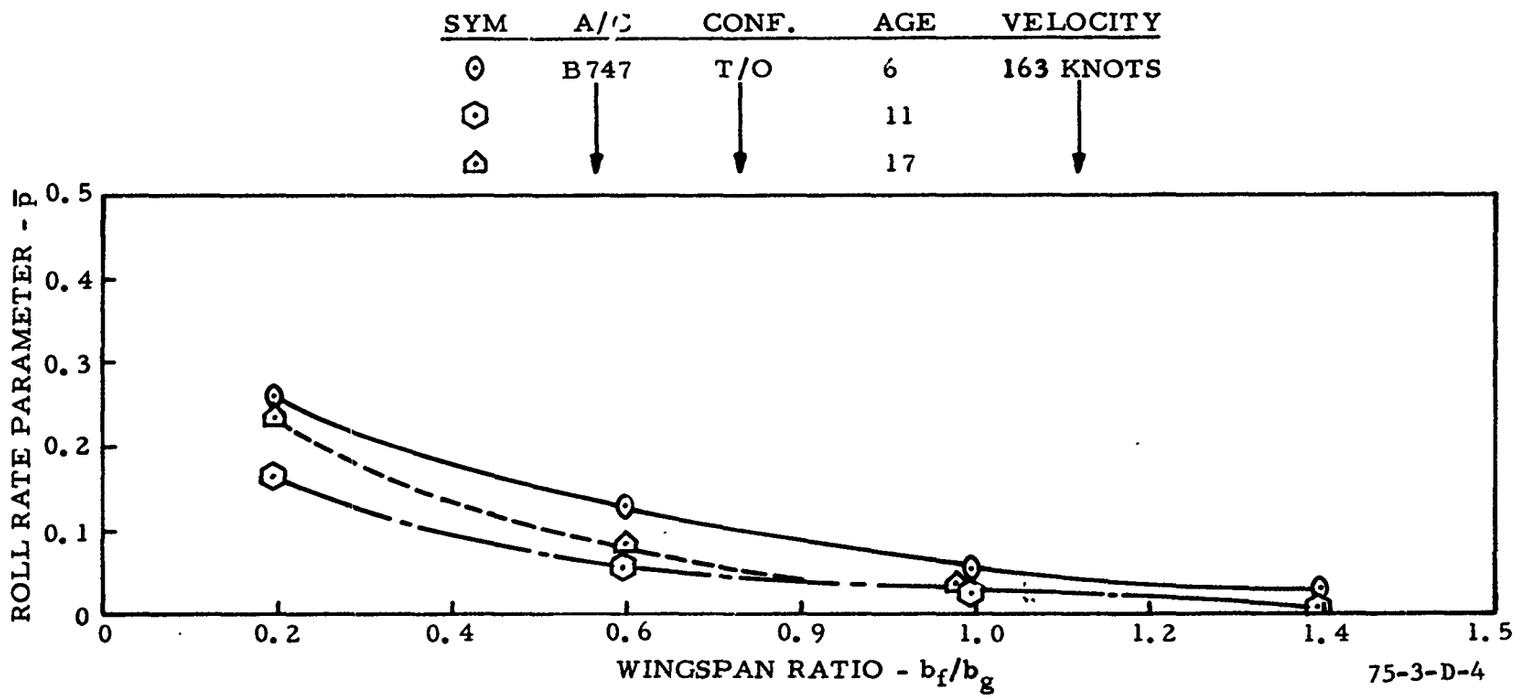

FIGURE D-4. EFFECT OF WINGSPAN RATIO ON ROLL RATE FOR BOEING 747 GENERATOR AIRCRAFT, TAKEOFF CONFIGURATION

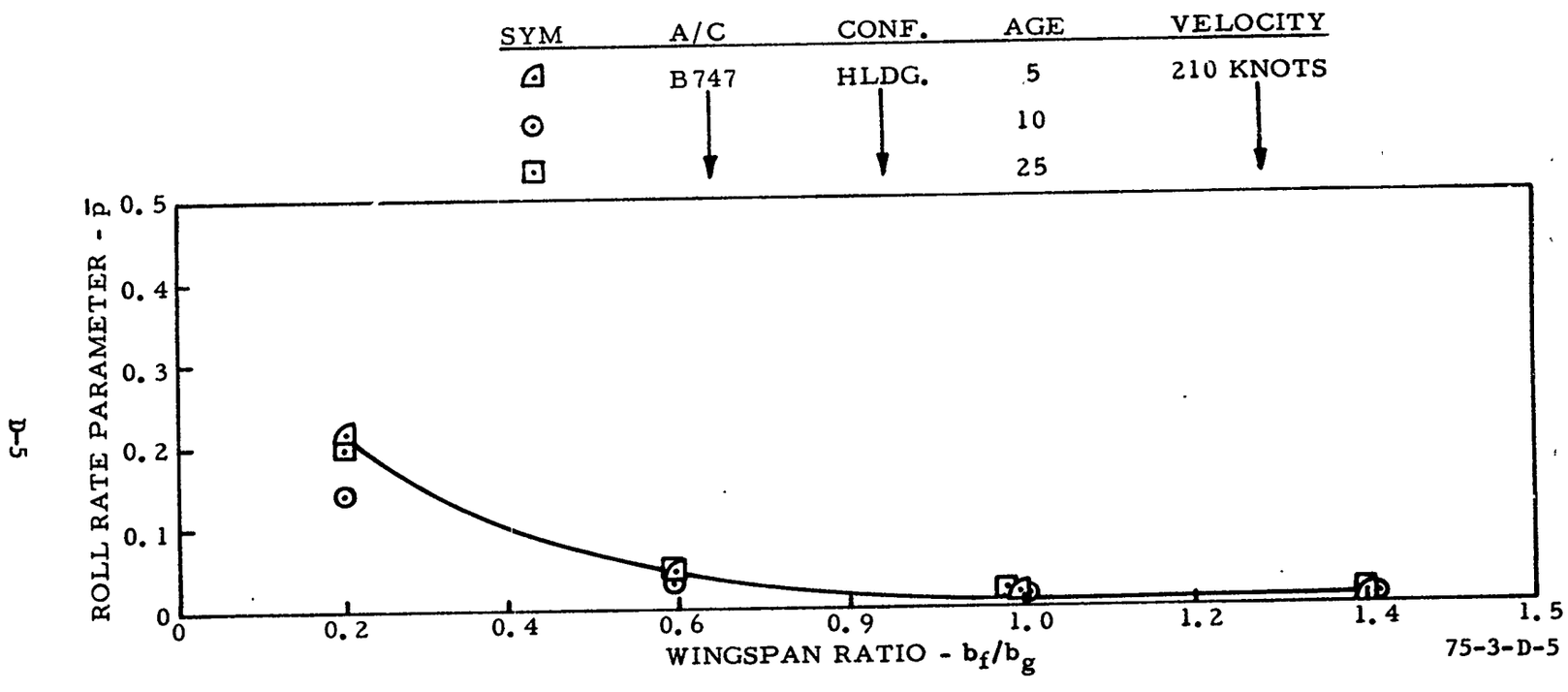

FIGURE D-5. EFFECT OF WINGSPAN RATIO ON ROLL RATE FOR BOEING 747 GENERATOR AIRCRAFT, HOLDING CONFIGURATION

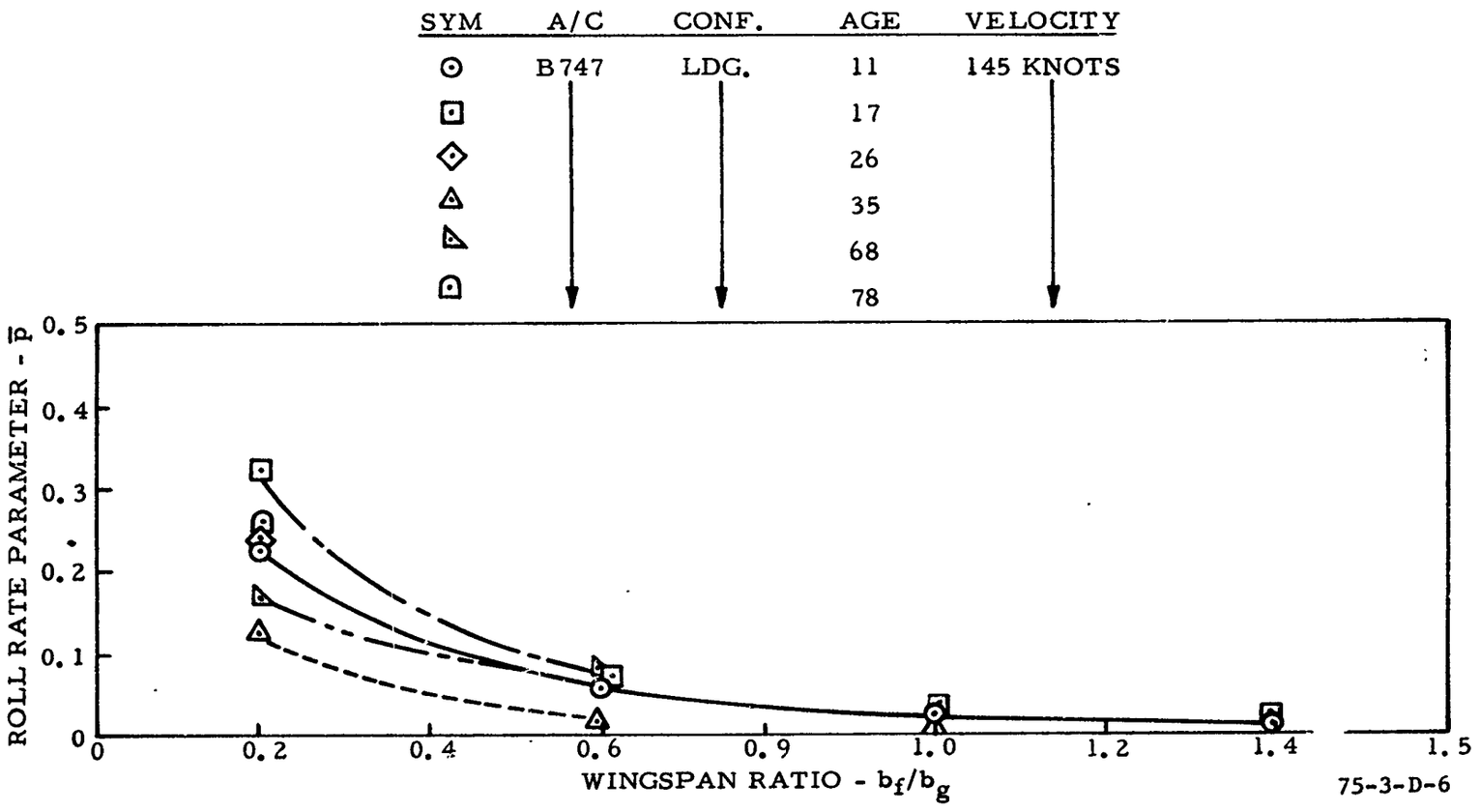

FIGURE D-6. EFFECT OF WINGSPAN RATIO ON ROLL RATE FOR BOEING 747 GENERATOR AIRCRAFT, LANDING CONFIGURATION

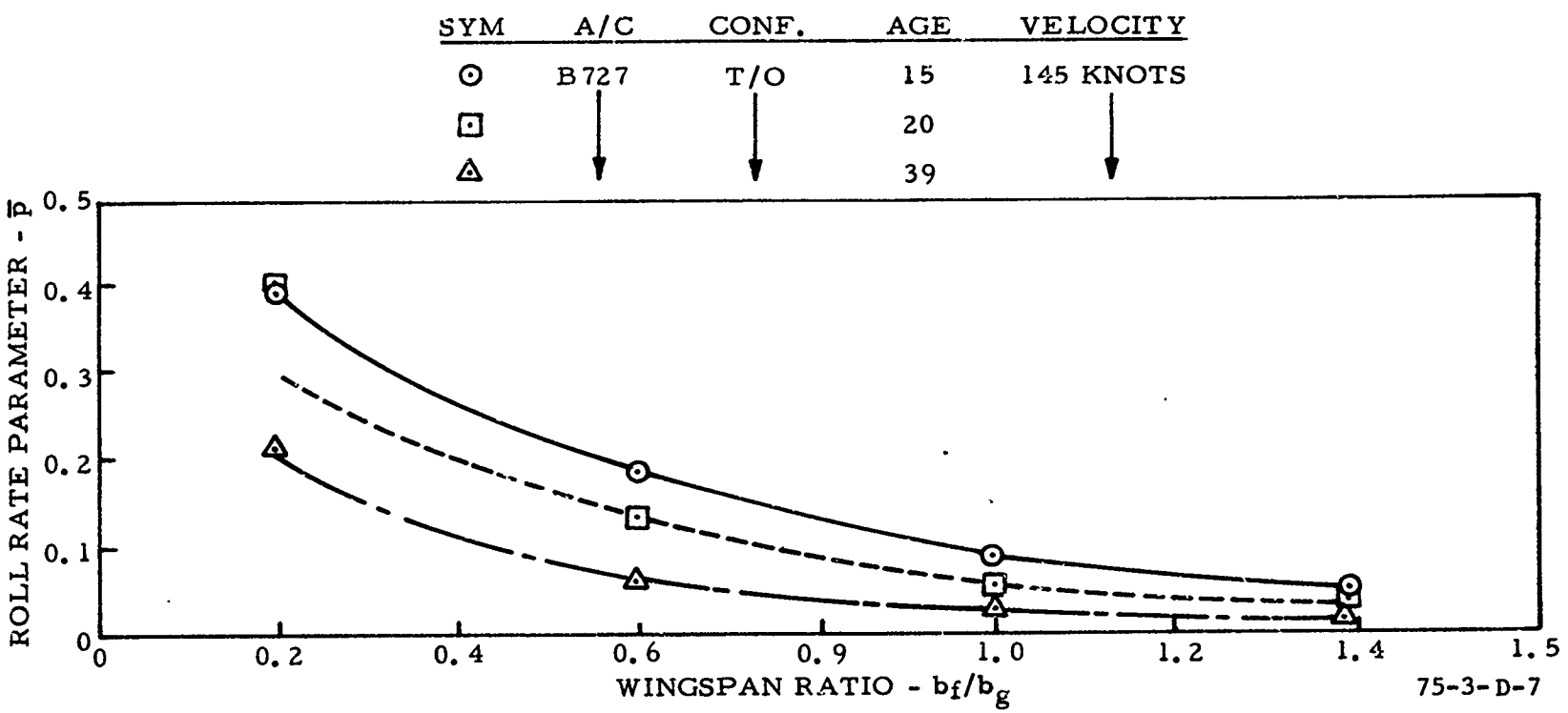

FIGURE D-7. EFFECT OF WINGSPAN RATIO ON ROLL RATE FOR BOEING 727 GENERATOR AIRCRAFT, TAKEOFF CONFIGURATION

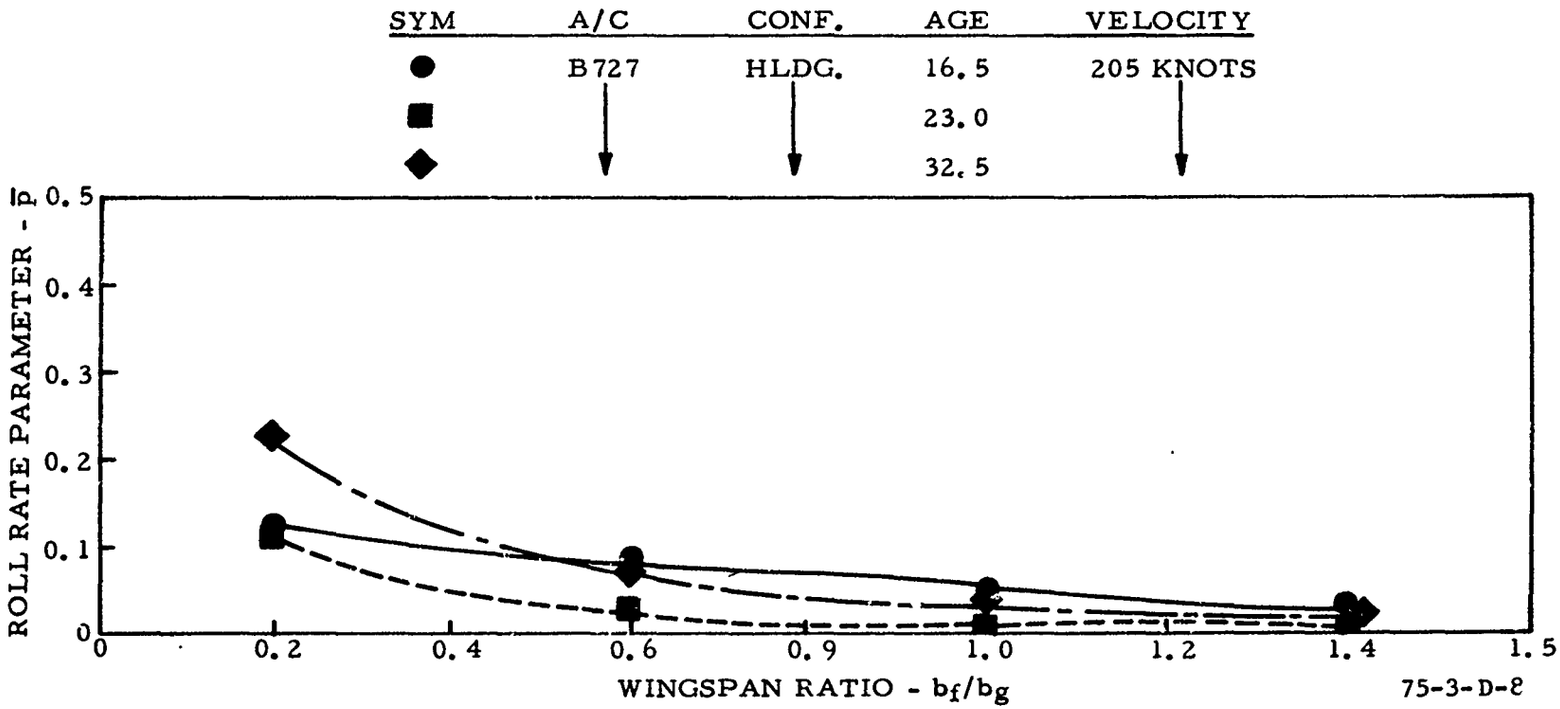

FIGURE D-8. EFFECT OF WINGSPAN RATIO ON ROLL RATE FOR BOEING 727 GENERATOR AIRCRAFT, HOLDING CONFIGURATION

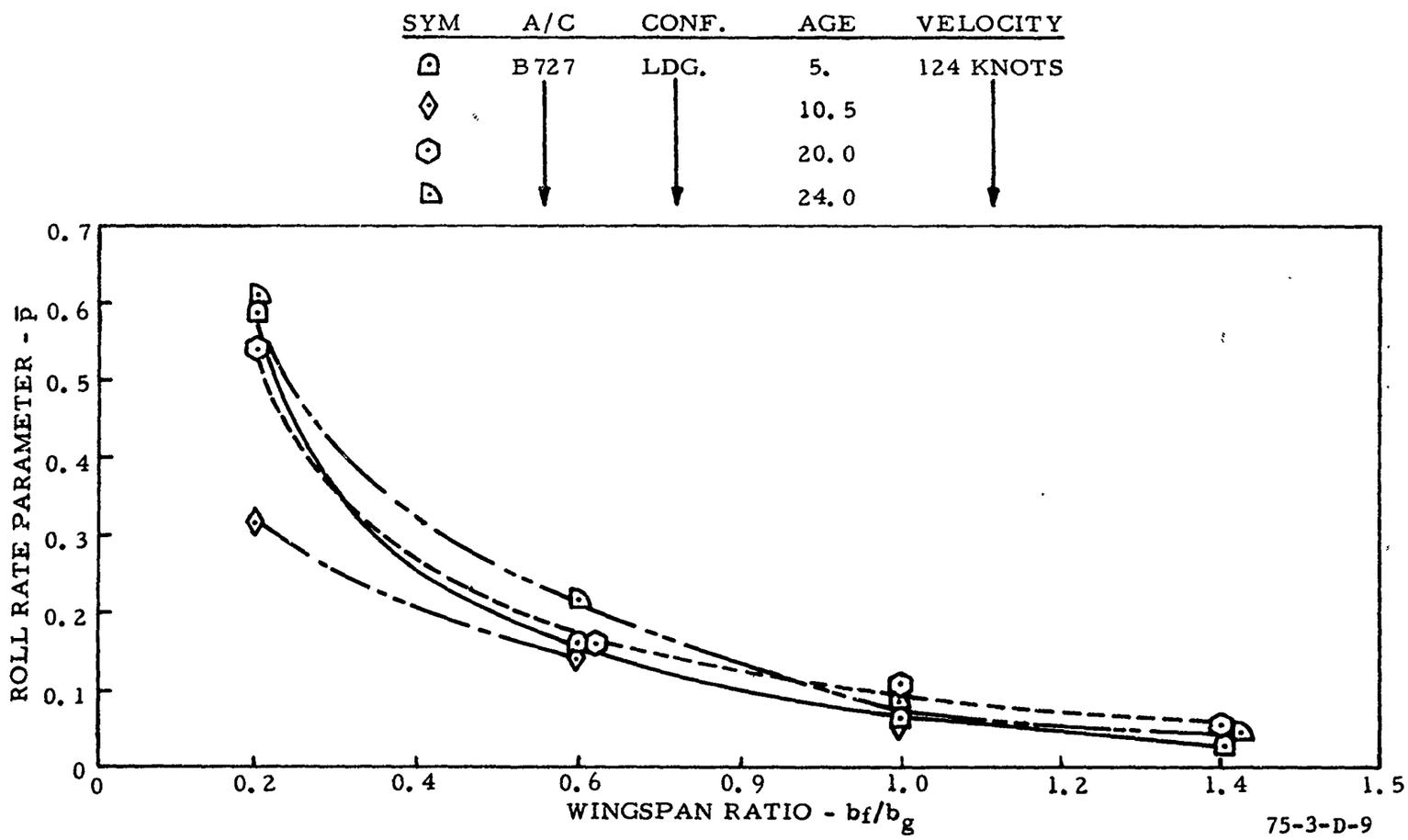

FIGURE D-9. EFFECT OF WINGSPAN RATIO ON ROLL RATE FOR BOEING 727 GENERATOR AIRCRAFT, LANDING CONFIGURATION

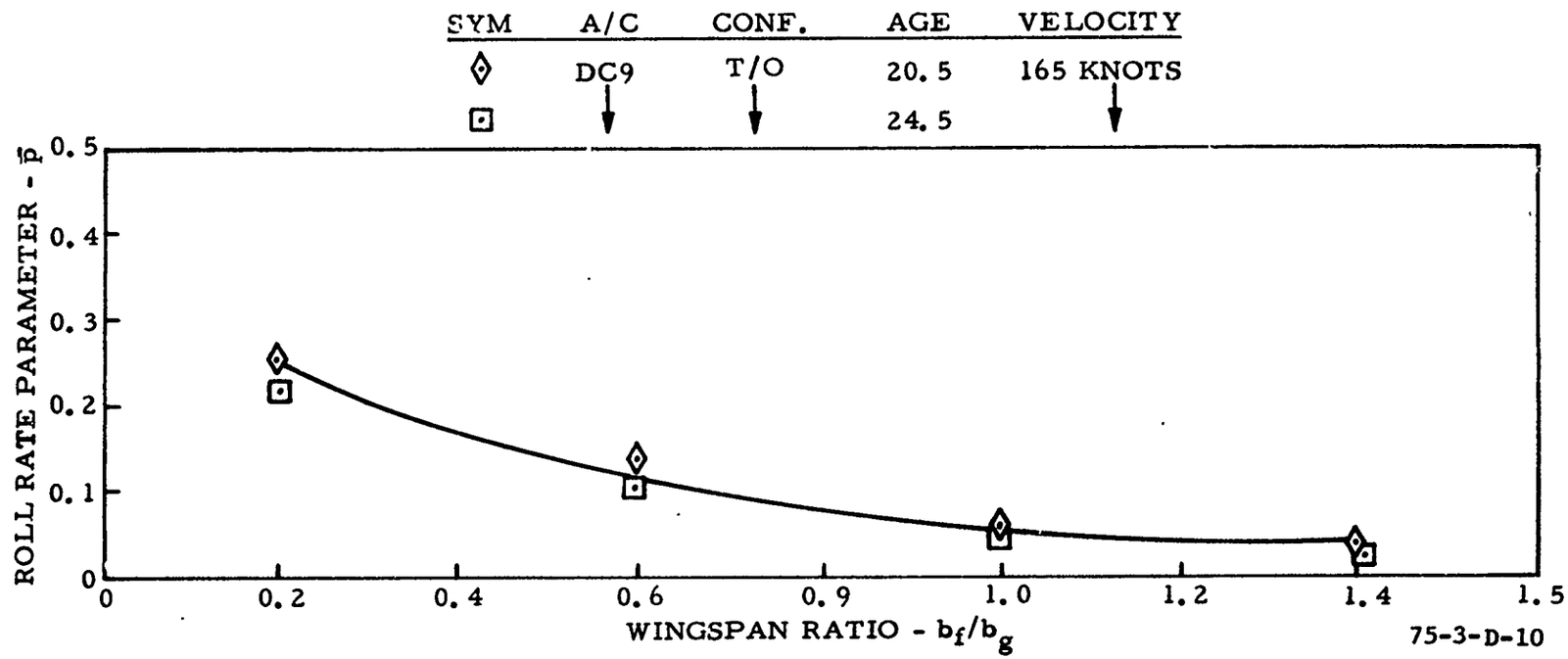

FIGURE D-10. EFFECT OF WINGSPAN RATIO ON ROLL RATE FOR McDONNELL-DOUGLAS DC9 GENERATOR AIRCRAFT, TAKEOFF CONFIGURATION

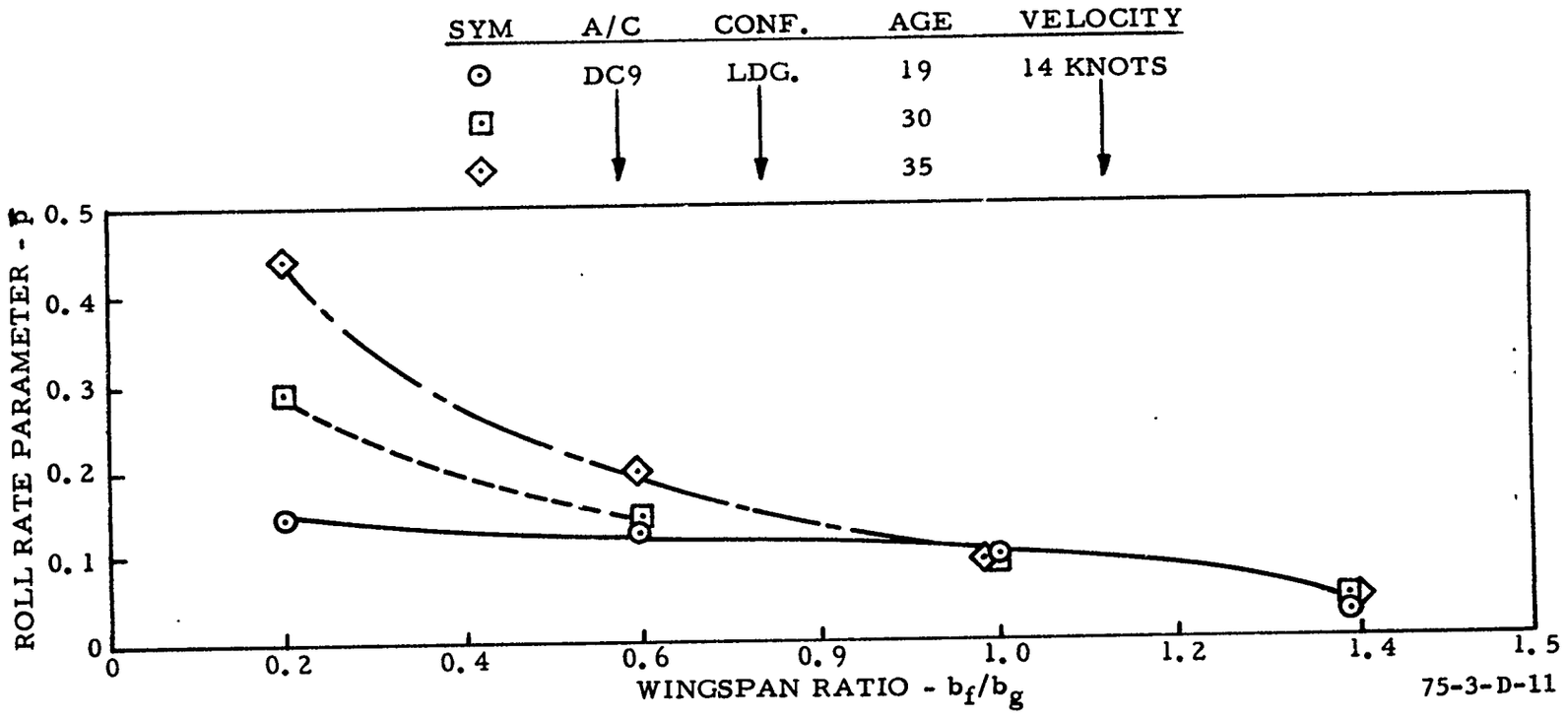

FIGURE D-11. EFFECT OF WINGSPAN RATIO ON ROLL RATE FOR McDONNELL-DOUGLAS DC9 GENERATOR AIRCRAFT, LANDING CONFIGURATION

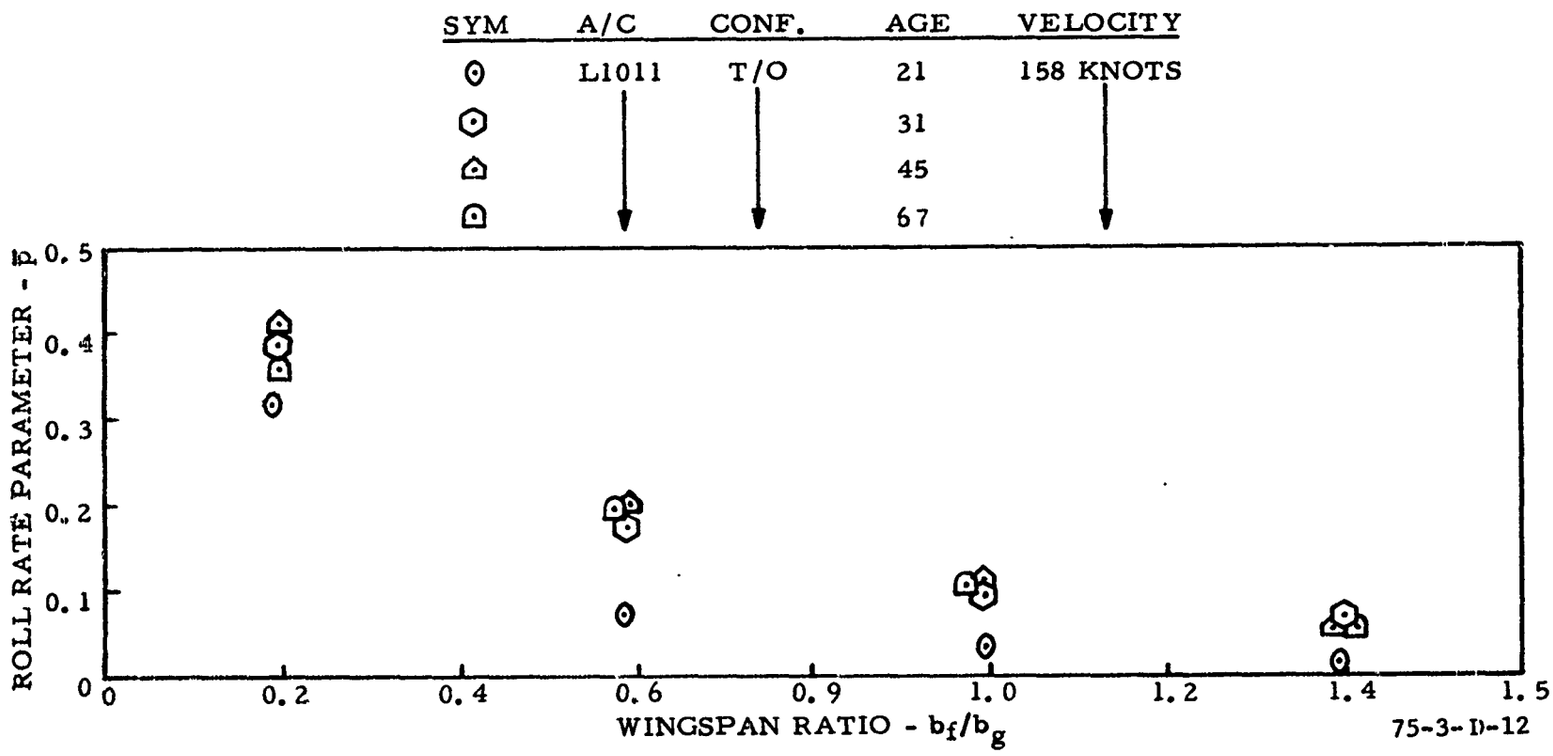

FIGURE D-12. EFFECT OF WINGSPAN RATIO ON ROLL RATE FOR LOCKHEED L1011 GENERATOR AIRCRAFT, TAKEOFF CONFIGURATION

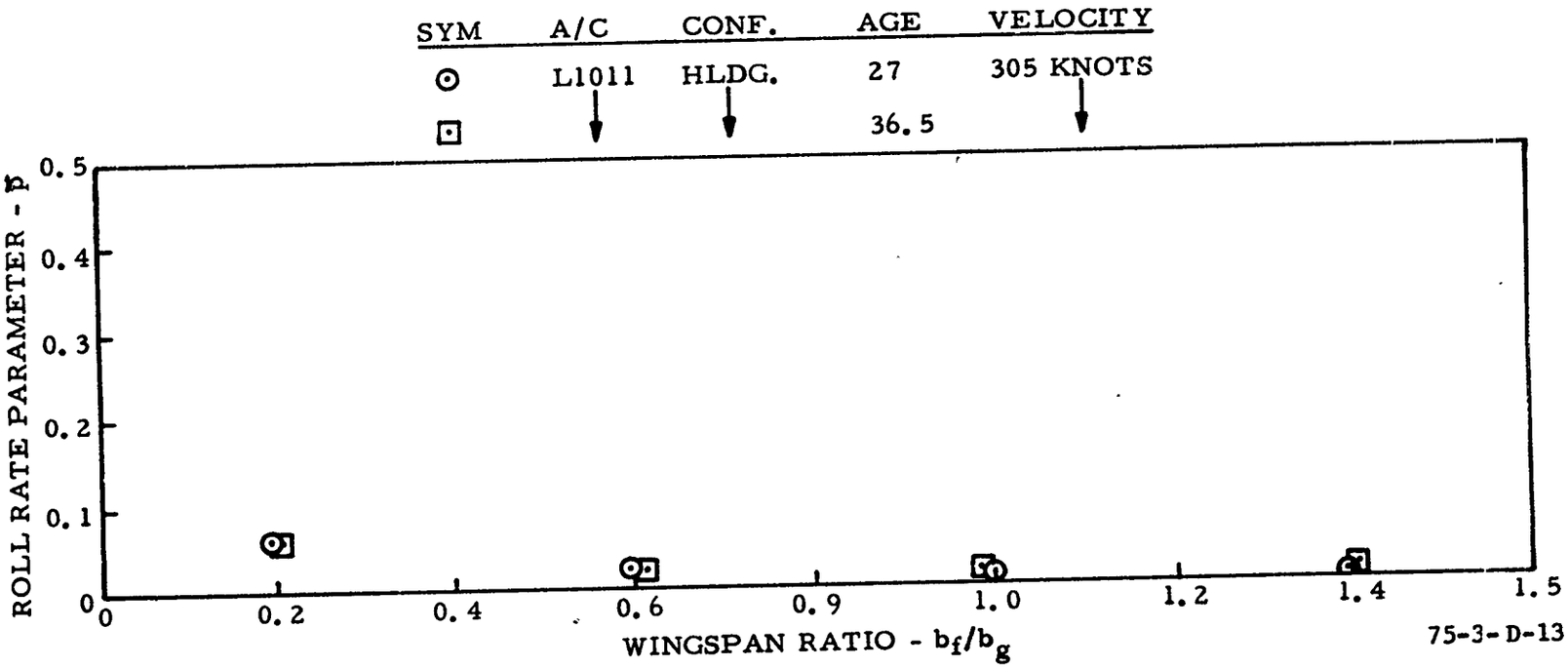

FIGURE D-13. EFFECT OF WINGSPAN RATIO ON ROLL RATE FOR LOCKHEED L1011 GENERATOR AIRCRAFT, HOLDING CONFIGURATION

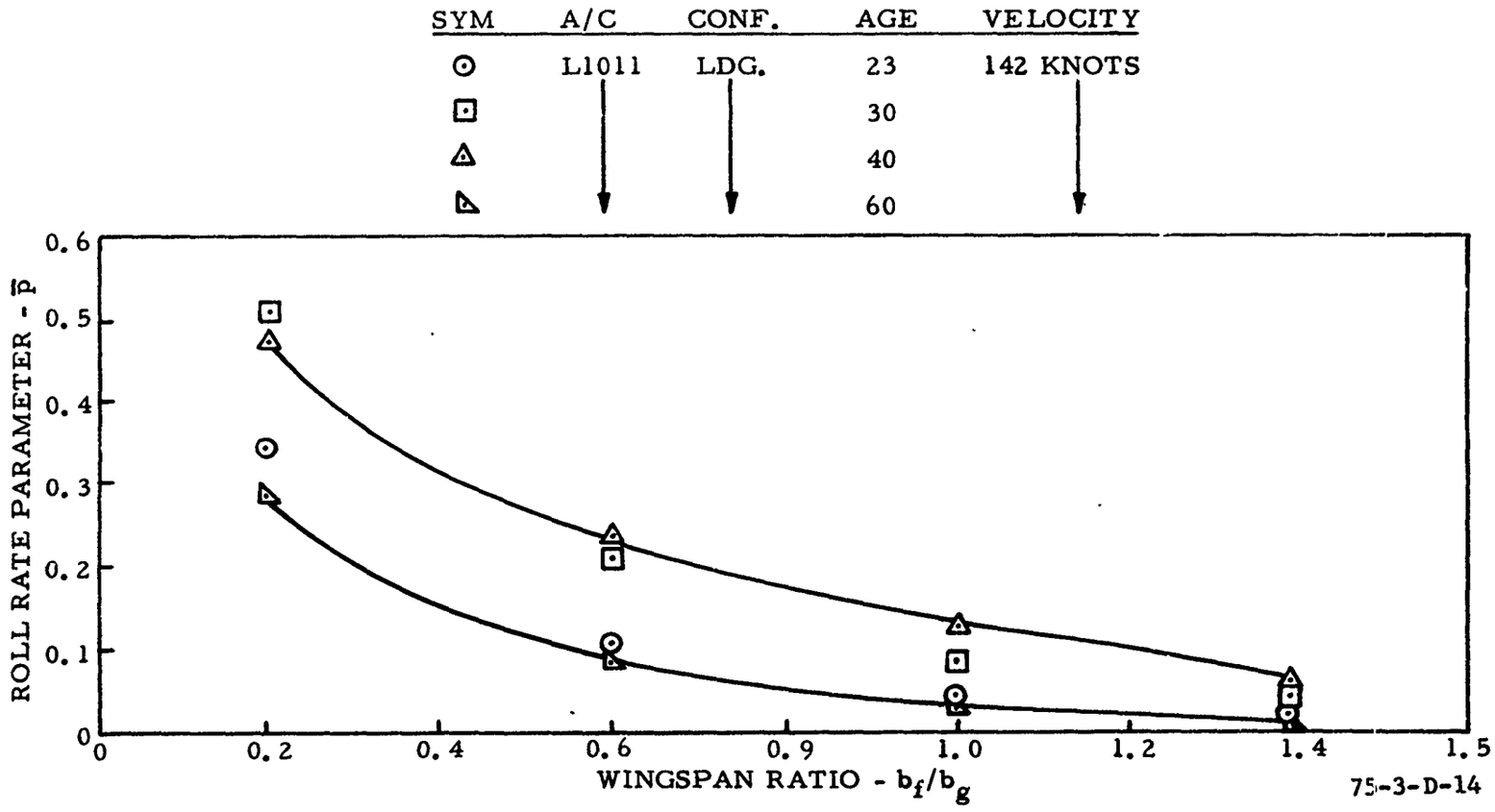

FIGURE D-14. EFFECT OF WINGSPAN RATIO ON ROLL RATE FOR LOCKHEED L1011 GENERATOR AIRCRAFT, LANDING CONFIGURATION

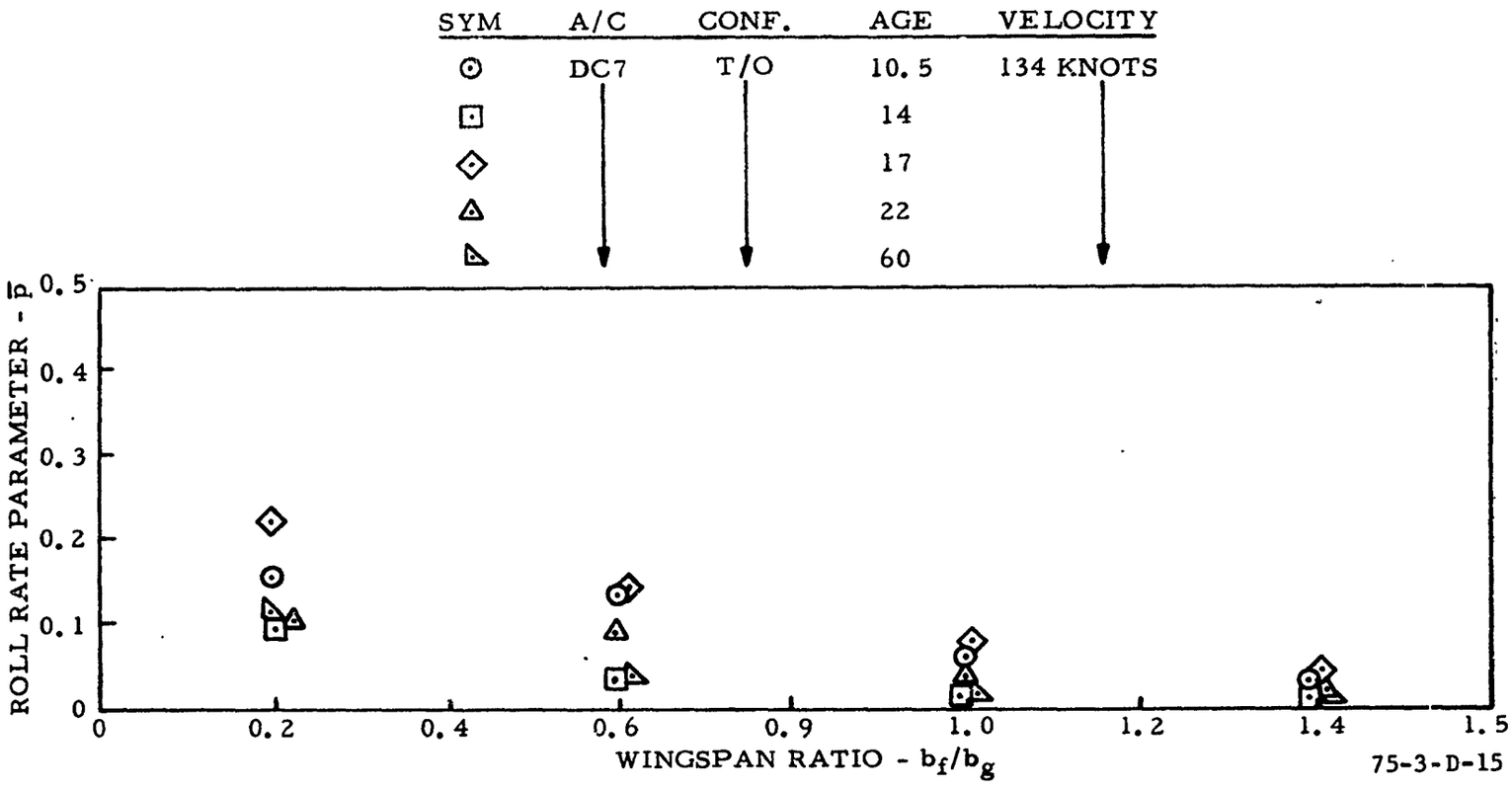

FIGURE D-15. EFFECT OF WINGSPAN RATIO ON ROLL RATE FOR DOUGLAS DC7 GENERATOR AIRCRAFT, TAKEOFF CONFIGURATION

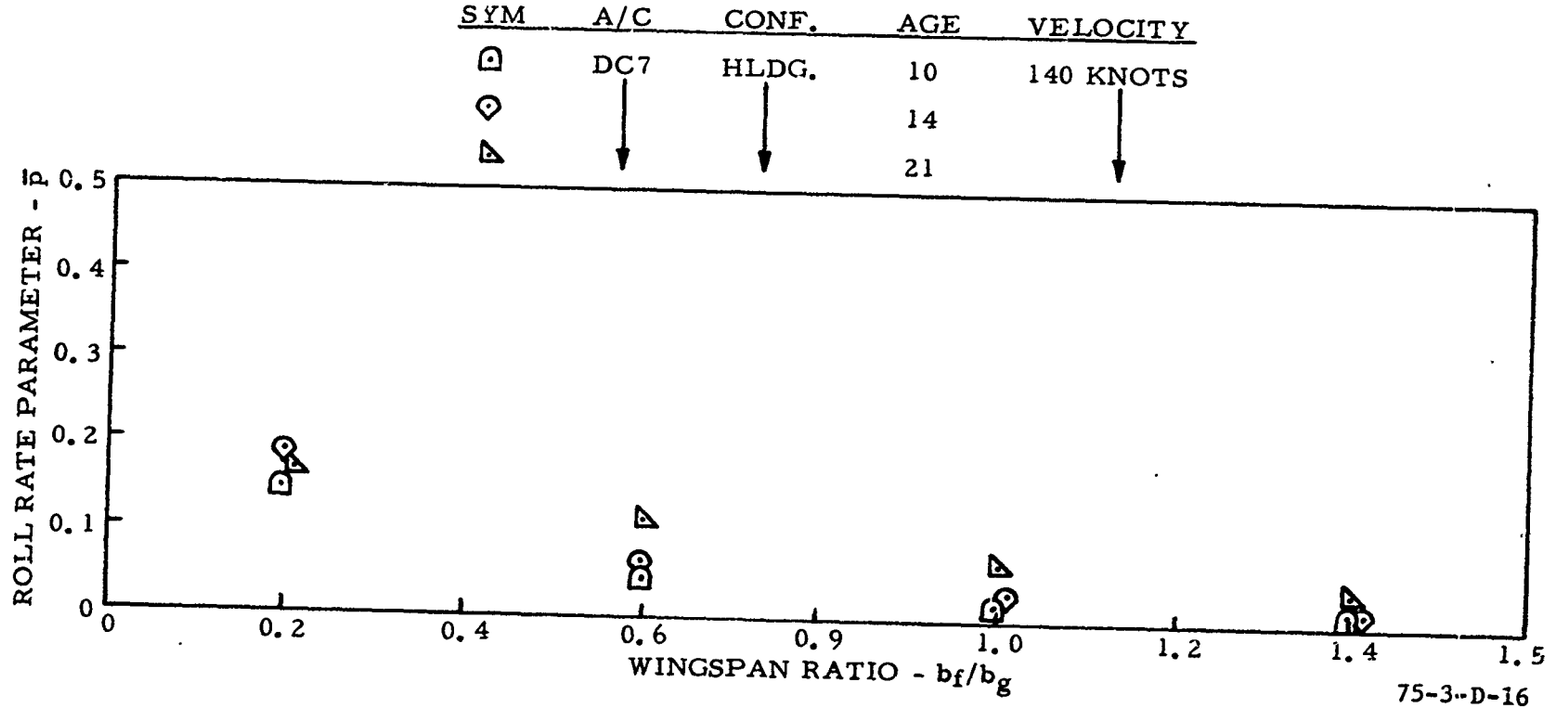

FIGURE D-16. EFFECT OF WINGSPAN RATIO ON ROLL RATE FOR DOUGLAS DC7 GENERATOR AIRCRAFT, HOLDING CONFIGURATION

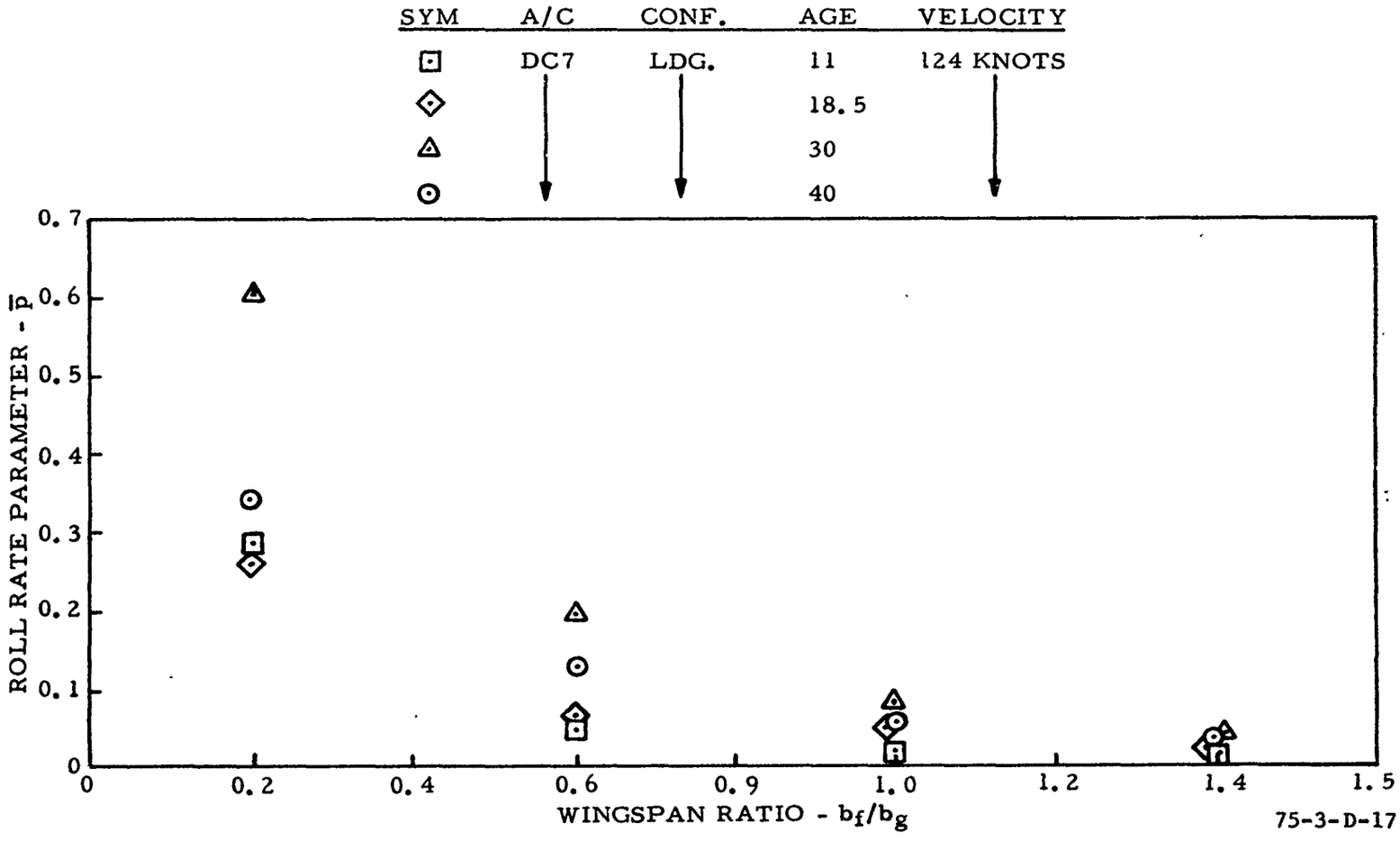

FIGURE D-17. EFFECT OF WINGSPAN RATIO ON ROLL RATE FOR DOUGLAS DC7 GENERATOR AIRCRAFT, LANDING CONFIGURATION

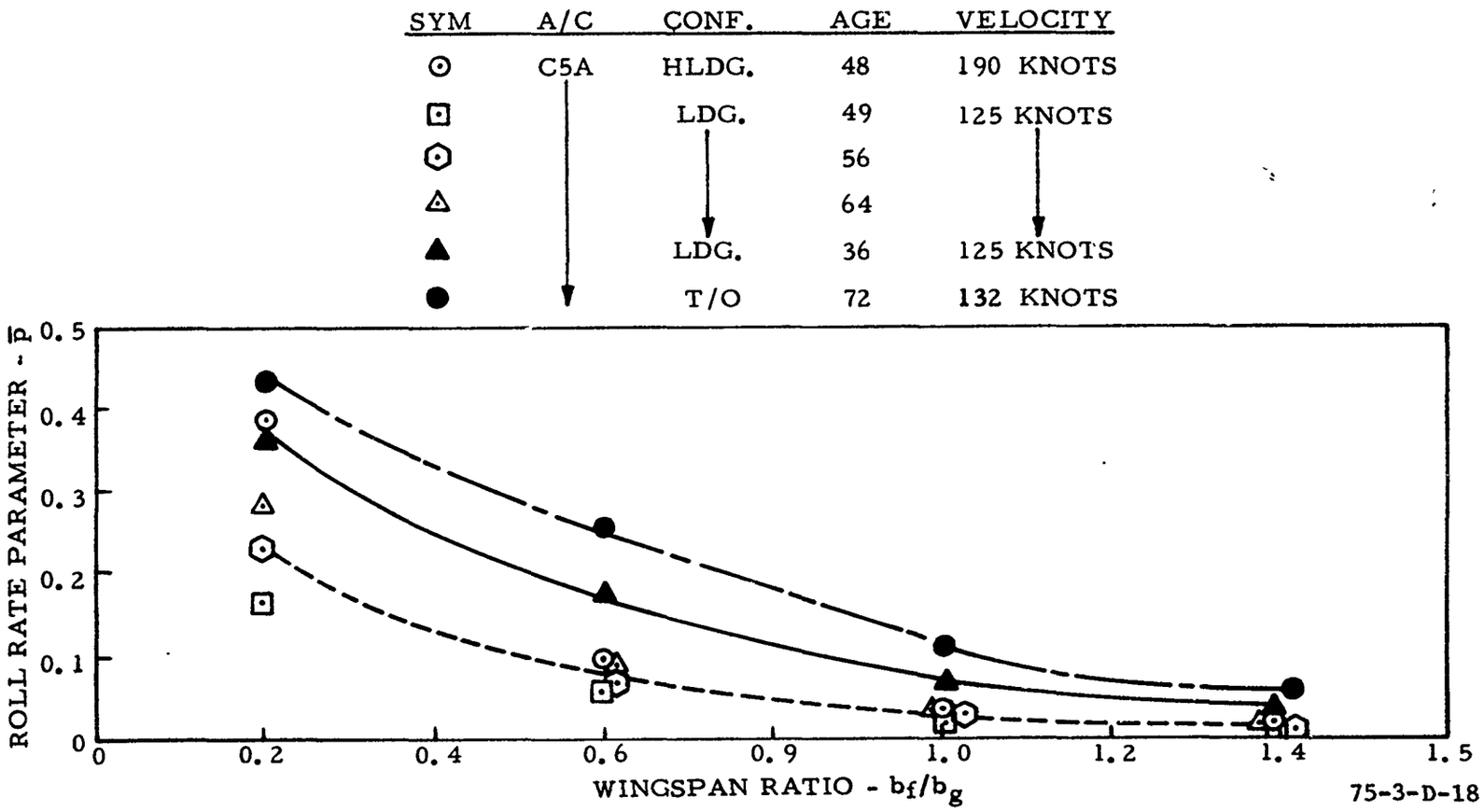

FIGURE D-18. EFFECT OF WINGSPAN RATIO ON ROLL RATE FOR LOCKHEED C5A GENERATOR AIRCRAFT, HOLDING, LANDING AND TAKEOFF CONFIGURATION

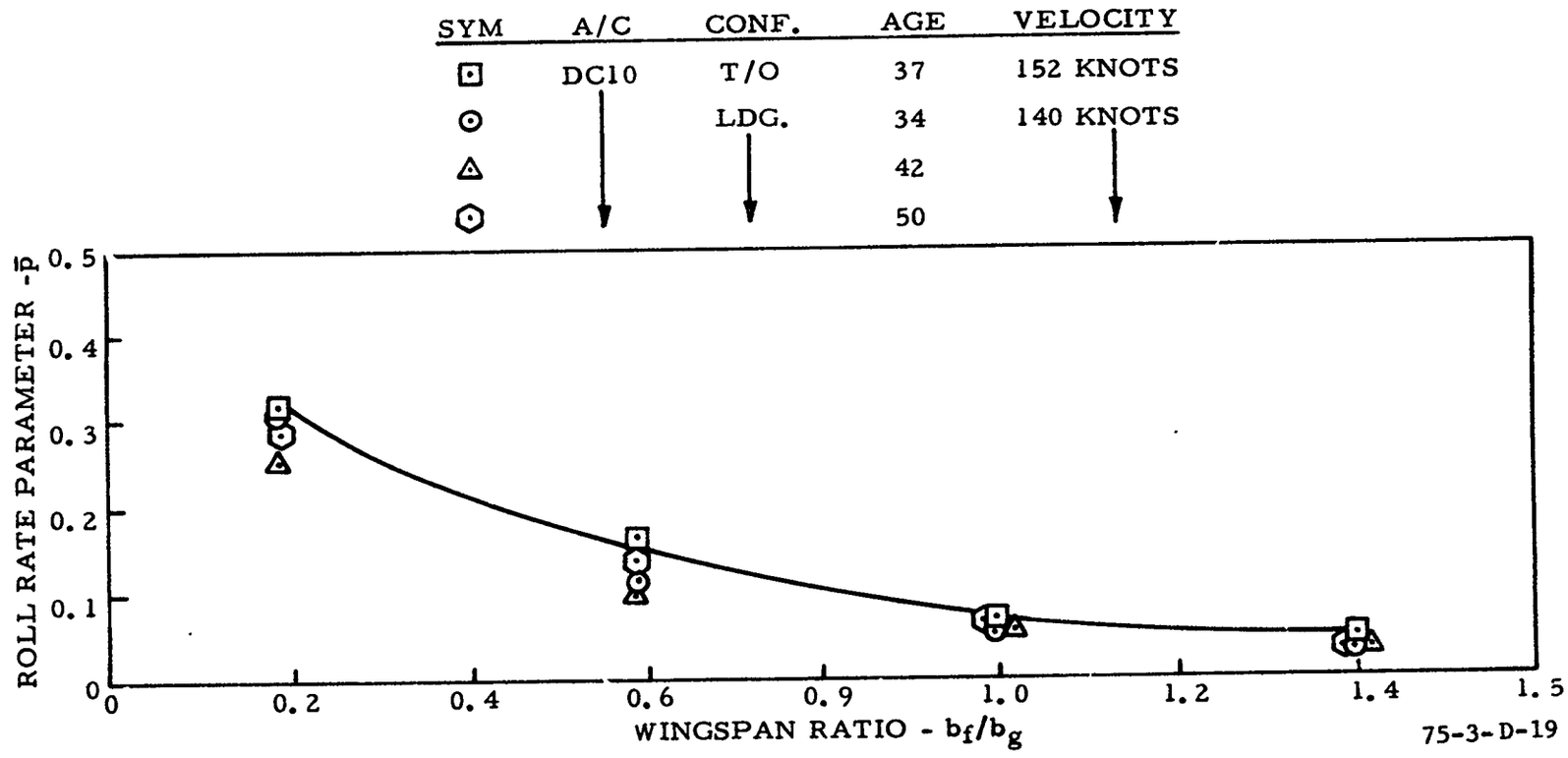

FIGURE D-19. EFFECT OF WINGSPAN RATIO ON ROLL RATE FOR McDONNELL-DOUGLAS DC10 GENERATOR AIRCRAFT, LANDING AND TAKEOFF CONFIGURATION